AB

AD 675443

# USAAVLABS TECHNICAL REPORT 67-58

# 16H-1A FLIGHT TEST RESEARCH PROGRAM

By

B. N. Meyers

L. V. Tompkins

J. H. Goldberg



August 1968

U. S. ARMY AVIATION MATERIEL LABORATORIES
FORT EUSTIS, VIRGINIA

CONTRACT DA-44-177-AMC-154(T)
PIASECKI AIRCRAFT CORPORATION
PHILADELPHIA, PENNSYLVANIA

DEPARTMENT OF THE ARMY
U. S. ARMY AVIATION MATERIEL LABORATORIES
FORT EUSTIS, VIRGINIA 23604

The 16H-1A flight test research effort was conducted as part of the exploratory development program in support of AAFSS (Advanced Aerial Fire Support System). This effort was initiated in May 1964, and flights of the 16H-1A aircraft were ended in July 1966. The objective of the program was to obtain flight test data at speeds up to 200 knots for future high-performance rotary-wing aircraft designs. The 16H-1A attained a maximum true airspeed in level flight of 160 knots at sea-level standard-day conditions and at a gross weight of approximately 6200 pounds. This speed performance was less than anticipated; consequently, use of the program results for high-speed design criteria is limited.

This report is published to release the data obtained under the contract. Further analysis or interpretation of the results contained in this report is subject to the limitations and scatter of the data obtained under the program. The analyses, conclusions, and recommendations contained herein are those of the investigator and are not confirmed or endorsed by the Government through the publication of this report.

## Disclaimers

When Government drawings, specifications, or other data are used for any purpose other than in connection with a definitely related Government procurement operation, the United States Government thereby incurs no responsibility nor any obligation whatsoever; and the fact that the Government may have formulated, furnished, or in any way supplied the said drawings, specifications, or other data is not to be regarded by implication or otherwise as in any manner licensing the holder or any other person or corporation, or conveying any rights or permission, to manufacture, use, or sell any patented invention that may in any way be related thereto.

Trade names cited in this report do not constitute an official endorsement or approval of the use of such commercial hardware or software.

## Disposition Instructions

Destroy this report when no longer needed. Do not return it to originator.

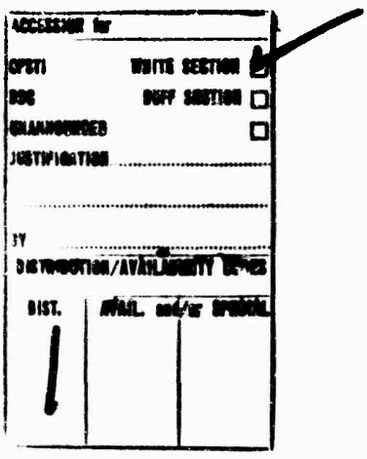

# DISCLAIMER NOTICE

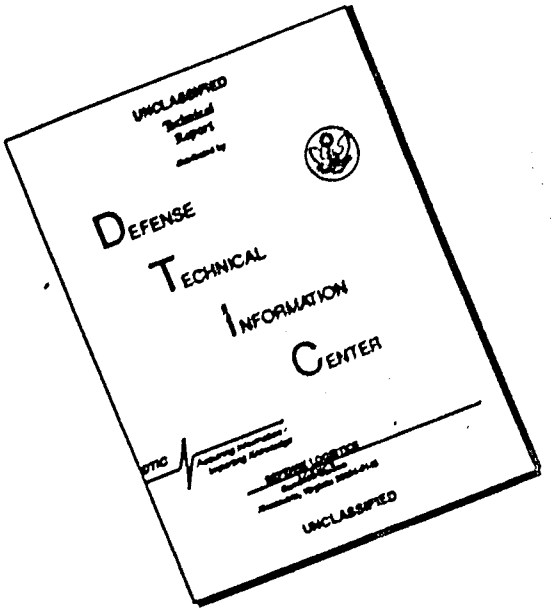


THIS DOCUMENT IS BEST QUALITY AVAILABLE. THE COPY FURNISHED TO DTIC CONTAINED A SIGNIFICANT NUMBER OF PAGES WHICH DO NOT REPRODUCE LEGIBLY.

Task 1F162203A14311

Contract DA-44-177-AMC-154(T)

USAAVLABS Technical Report 67-58

August 1968

# 16H-1A FLIGHT TEST RESEARCH PROGRAM

Final Report

by

D.N. Meyers, L.V. Tompkins, J.H. Goldberg

Prepared by

Piasecki Aircraft Corporation

Philadelphia, Pennsylvania

for

U. S. ARMY AVIATION MATERIEL LABORATORIES

FORT EUSTIS, VIRGINIA

## SUMMARY

This report presents the results of a flight test program conducted by Piasecki Aircraft Corporation of the Piasecki Model 16H-1A shaft-driven compound helicopter. The flying qualities and performance of the 16H-1A aircraft were investigated over a level-flight speed range of 0 to 167 knots and dive speeds up to 195 knots. These tests resulted in a better understanding of the independent design parameters in the compound helicopter, such as the tail propeller/main rotor power distribution and the distribution of lift between the wing and main rotor.

The interrelationship of the axes of lift, thrust, drag, and angular attitudes of the wing, fuselage, and rotor axis had been investigated previously during more than 100 hours of ground and flight testing of Model 16H-1. The Model 16H-1A test program has provided recorded measurements of these parameters. In obtaining these data, the 16H-1A made 171 flights and accumulated 56-1/2 hours of flight time, in addition to 66 hours of ground testing.

Lift sharing between main rotor and wing was investigated over a broad range of the flight envelope. It was determined that maximum speed performance required lower collective pitch settings with the resultant unloading of the main rotor. Rotor lift loading was reduced to a minumum of 54 percent of the gross weight in level flight.

Flying quality and performance data were obtained through comprehensive instrumentation of the aircraft and by external photo coverage from the ground and from a chase plane.

Throughout the entire test speed range, and in all tested flight regimes, the 16H-1A proved to have suitable controllability with the two exceptions noted below, both of which could be eliminated by incorporating conventional aileron roll control. The aircraft possesses a high degree of positive dynamic stability about all axes at forward flight speeds above 35 knots. Positive overall longitudinal static stability is evident from approximately 70 knots to maximum speed attained. The lateral cyclic control was intentionally made sensitive because it was anticipated that, without ailerons, it would be needed in high-speed unloaded flight. At speeds above 150 knots and collective pitch settings of 3 degrees or less, the lateral control response decreased because of the low rotor loading. Compensation for this decrease in control response could be obtained by connecting the existing ailerons (flaperons) to the cyclic stick. In hovering, although the pilot at no time had any difficulty with the lateral control because of

this cyclic rigging, it was found to be more sensitive than permitted by MIL-H-8501A. Ailerons would permit the lateral cyclic to be reduced to the allowable sensitivity.

The ring-tail method of counteracting main rotor torque by deflecting the airflow at the tail propeller duct proved to be entirely adequate in taxiing, in hovering, and in sideward, backward, and transition flight.

Flight handling qualities of the Model 16H-1A during STOL tests were considered by the pilot to be similar to those of conventional fixed-wing aircraft. Ground run speeds as high as 55 knots were experienced during takeoff with no tendency to swerve. Forward speed landings with partial power proved equally conventional and controllable.

The maximum true airspeed demonstrated was 195 knots, which was achieved in a 10-degree dive. One major factor which limited extension of the speed envelope during this flight test program was the inadequacy of the inlet air duct to the buried engine installation. The air inlet used for these tests precluded full engine horsepower due to air starvation at high powers.

Vibration was not a limiting factor up to the maximum speeds attained in exploring the performance and flying qualities of the 16H-1A. A three-per-revolution vibration component limited operation in the earlier stage of the program. However, a stiffening of the control system alleviated this condition.

All the measured stresses in the dynamic components permit unlimited fatigue life. Bearings and other wear-limited components were operating at loads which would permit at least 420 hours of service at the highest speeds tested.

## FOREWORD

This report summarizes the results of an exploratory flight test research program to determine high speed aspects of rotary-wing aircraft utilizing the 16H-1A shaft driven, compound helicopter. The program was conducted by Piasecki Aircraft Corporation under USAAVLABS Contract DA 44-177-AMC-154(T).

The vehicle described herein, the 16H-1A, is an outgrowth of the 16H-1, previously built and tested by the contractor in a company-funded program.

All flights were conducted in accordance with FAA Experimental Certificate of Airworthiness No. N616H dated 10 September 1965, and took place between November 1965 and July 1966.

CONTENTS

## LIST OF ILLUSTRATIONS

## LIST OF TABLES

## LIST OF SYMBOLS

| | |
|---|---|
| $A$ | rotor or propeller disc area, square feet |
| $C$ | mean aerodynamic wing chord, feet |
| $C_P$ | power coefficient $\frac{P}{\rho A V_T^3}$ |
| $C_T$ | thrust coefficient $\frac{T}{\rho A V_T^2}$ |

Sub-subscript P refers to propeller; sub-subscript R (or none) refers to rotor.

| | |
|---|---|
| $D(\ )$ | $\frac{d(\ )}{dt}$ |
| $D^2(\ )$ | $\frac{d^2(\ )}{dt^2}$ |
| $D\psi$ | yaw rate, radian per second |
| $ESHP$ | engine shaft horsepower |
| $ESHP_{CORR}$ | corrected engine shaft horsepower |
| $F_H$ | calculated horizontal force on rotor shaft at rotor hub, pounds |
| $g$ | acceleration due to gravity, 32.2 feet per second per second |
| $H$ | pressure altitude, feet |
| $I_X$ | moment of inertia in roll, slug-feet$^2$ |
| $I_Y$ | moment of inertia in pitch, slug-feet$^2$ |
| $I_Z$ | moment of inertia in yaw, slug-feet$^2$ |
| $K_P$ | specific heat correction factor to power |
| $K_W$ | specific heat correction factor to fuel flow |
| $k$ | ratio of propeller plus rotor horsepower to rotor induced power |
| $k_1$ | correction factor accounting for variation from uniform induced velocity profile |
| $L_e$ | engine exhaust pressure loss |

| | |
|---|---|
| $L_i$ | engine inlet pressure loss |
| $L_p$ | rolling moment derivative with roll rate, foot-pound-seconds per radian |
| $L_V$ | lift derivative with speed, pounds per foot per second |
| $L_\alpha$ | lift derivative with angle of attack change, pounds per radian |
| $L_\delta$ | lift derivative with longitudinal stick displacement, pounds per inch |
| | or |
| | rolling moment derivative with lateral stick displacement, foot-pounds per inch |
| M | Mach number |
| $M_H$ | calculated moment in rotor shaft at rotor hub, inch-pounds |
| $M_{LG}$ | measured moment in rotor shaft at lower strain gage location, inch-pounds |
| $M_q$ | pitching moment derivative with pitch rate, foot-pound-seconds per radian |
| $M_{UB}$ | calculated moment in rotor shaft at upper bearing location, inch-pounds |
| $M_{UG}$ | measured moment in rotor shaft at upper strain gage location, inch-pounds |
| $M_V$ | pitching moment derivative with velocity change (velocity stability), foot-pound-seconds per foot |
| $M_\alpha$ | pitching moment derivative with angle of attack change (angle of attack stability), foot-pounds per radian |
| $M_\delta$ | pitching moment derivative with longitudinal stick displacement, foot-pounds per inch |
| m | aircraft mass, slugs |
| N | engine output shaft RPM |

| | |
|---|---|
| $N_{REF}$ | referred engine output shaft RPM |
| $N_r$ | yaw moment derivative with yaw rate, foot-pound-seconds per radian |
| $N_\beta$ | yawing moment with sideslip derivative, foot-pounds per radian |
| $N_\delta$ | yaw moment derivative with pedal displacement, foot-pounds per inch |
| n | blip number; also load factor |
| $n_o$ | stick-fixed neutral point, fraction of C |
| $n_t$ | total number of blips in a flight |
| OAT | outside air temperature, degrees centigrade |
| P | period of oscillation, seconds |
| $P_E$ | engine torquemeter pressure, pounds per square inch |
| PSHP | propeller shaft horsepower |
| $P_{t_2}/P_2$ | ram pressure ratio |
| $P_{t_2}/P_{s_6}$ | total engine pressure ratio |
| $Q_P$ | propeller torque, inch-pounds |
| $Q_R$ | rotor torque, inch-pounds |
| R | radius, feet (subscript P refers to propeller; subscript R (or none) refers to main rotor) |
| RSHP | rotor shaft horsepower |
| $R_L$ | calculated horizontal reaction at lower bearing supporting rotor shaft, pounds |
| $R_U$ | calculated horizontal reaction at upper bearing supporting rotor shaft, pounds |
| s | Laplace variable |
| $T_{sp}$ | longitudinal short period mode time constant, seconds |

| | |
|---|---|
| $T_{t_2}$ | temperature at engine compressor inlet, degrees centigrade |
| $T_{t_2}/T_2$ | ram temperature ratio |
| $V$ | longitudinal velocity, feet per second |
| $V_o$ | trim flight speed, feet per second |
| $V_C$ | rate of climb, feet per minute |
| $V_{CAL}$ | calibrated airspeed, knots |
| $V_{CORR}$ | corrected airspeed, knots |
| $V_{C_{OBS}}$ | observed rate of climb, feet per minute |
| $V_{C_{REF}}$ | referred rate of climb, feet per minute |
| $V_{C_{STD}}$ | standard rate of climb, feet per minute |
| $V_T$ | tip speed, feet per second (sub-subscript P refers to propeller; sub-subscript R (or none) refers to rotor) |
| $V_{TRUE}$ | true airspeed, knots |
| $W$ | gross weight, pounds |
| $W_{REF}$ | referred gross weight, pounds |
| $W_{STD}$ | standard gross weight, pounds |
| $W_{TO}$ | takeoff gross weight, pounds |
| $W_f$ | fuel flow, pounds per hour |
| $W_{f_{CORR}}$ | corrected fuel flow, pounds per hour |
| $X_{CG}$ | center-of-gravity location, fraction of C |
| $X_V$ | longitudinal force derivative with velocity, pound-seconds per foot |
| $X_\delta$ | longitudinal force derivative with longitudinal stick displacement, pounds per inch |
| $\alpha$ | change in aircraft angle of attack from trim, radians |

| | |
|---|---|
| $\beta$ | aircraft sideslip angle, radians |
| $\Delta SHP_{(R/C)}$ | increment in horsepower due to vertical speed |
| $\Delta V_C$ | increment in rate of climb due to horsepower discrepancy |
| $\delta$ | control position (stick or pedal), inches |
| $\delta_o$ | ambient pressure ratio |
| $\delta(t)$ | stick or pedal displacement from trim input time function, inches |
| $\zeta$ | critical damping ratio |
| $\eta$ | overall efficiency |
| $\eta_T$ | rotor transmission loss |
| $\theta$ | change in aircraft pitch angle from trim, radians |
| $\theta_2$ | temperature ratio at engine compressor inlet |
| $\mu$ | rotor tip speed ratio |
| $\rho$ | ambient density |
| $\rho_o$ | mass air density at sea level - $\frac{lb\text{-}sec^2}{ft^4}$ |
| $\sigma$ | density ratio |
| $\phi$ | roll angle |
| $\psi$ | yaw angle |
| $\omega_o$ | undamped natural frequency, radians per second |

## INTRODUCTION

This report presents the flight test results of the Piasecki 16H-1A, shaft-driven compound helicopter. This program was conducted under Contract DA 44-177-AMC-154(T) awarded by the Government in May 1964 to obtain test data relative to the high-speed aspects of rotary-wing aircraft.

The main objective of the flight test program was to investigate the flying qualities and performance of the 16H-1A over the speed range of hover to $V_{max}$. A secondary objective was to gain a better understanding of the interdependent design parameters in the compound helicopter, such as the propeller/main rotor power distribution and the distribution of lift between the wing and main rotor.

## DESIGN BACKGROUND

In order to accomplish the objectives, it was necessary to modify the existing Piasecki 16H-1 Compound Helicopter (see Figure 1) to the model designated 16H-1A. Principal modifications required for the high-speed regime included: installation of a General Electric T58 turbine; incorporation of H-21 rotor and controls; design, fabrication, and installation of a new transmission system; a lengthening of the fuselage; development of a new propeller; and beef-up of various structural components.

Following modifications, the 16H-1A completed 66 hours of ground testing that included the following:

1. Component Testing
   a. Tail Propeller and Tail Rudders
   b. Transfer and Main Transmissions

2. Tie-Down Testing
   a. Airframe Shake Test
   b. Wing Proof Load
   c. Control Proof Load
   d. Landing Gear Stress
   e. Test Summary and Results
   f. Tear-Down Inspection

Information on the ground test phase of the contract is given in Appendix I.

## FLIGHT TESTING

Flight testing was conducted from 13 November 1965 to 6 July 1966 under Federal Aviation Agency Experimental Air-

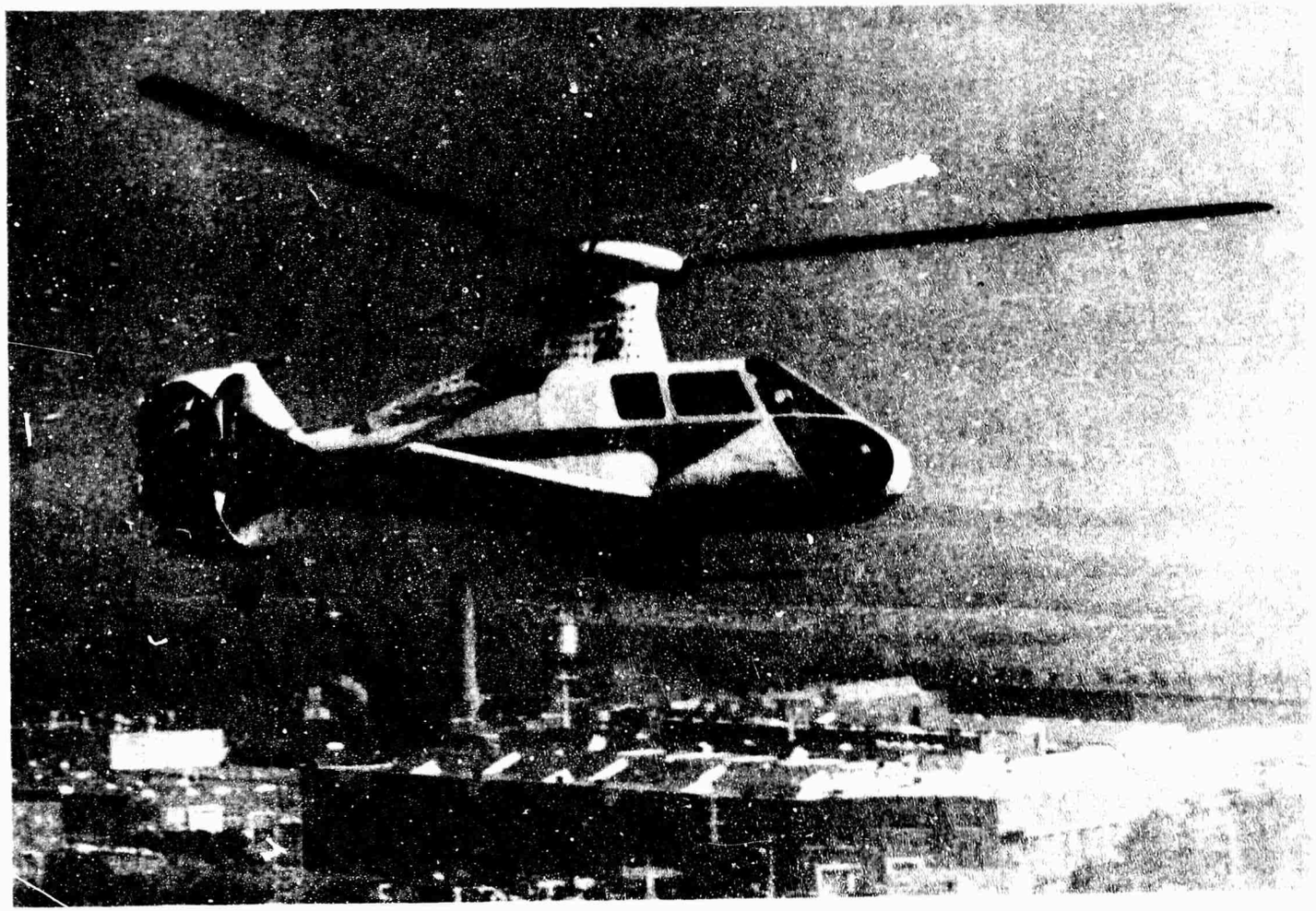

Figure 1. 16H-1 in Flight.

worthiness Certificate N616H dated 10 September 1965, in accordance with the objectives set forth in the Flight Test Agenda, PiAC Report 16-Y-13. The test phases were as follows:

1. Taxi
2. Hovering In and Out of Ground Effect
3. Sideward and Backward Flight
4. Transition From Hover to Forward Flight and Back to Hover
5. Forward Speed Climb
6. Autorotation
7. Vertical Climb
8. Level Flight
9. Maneuverability
10. Dynamic Stability
11. STOL Performance

In this report each phase of testing is discussed in independent sections that include description of tests, test data and results, and analysis of results.

The flight conditions have been assembled into one section and presented in Table XIX.

Stresses and load data were obtained from many of the test phases and have been presented in a separate section.

## DESCRIPTION OF TEST ARTICLE

The 16H-1A is a low-wing, single-engine, shaft-turbine-powered compound helicopter (see Figure 2). At the fuselage aft end, the aircraft is equipped with a ducted pusher propeller and with a set of vertical and horizontal tail surfaces. The vertical tail surfaces (rudder vanes) placed behind the propeller serve to control the aircraft in yaw, both in hovering and in forward flight regimes. They are also used to produce side, antitorque force in hovering. The horizontal tail surface is composed of a fixed stabilizer and a trim elevator.

The engine drives both the main rotor and the propeller mechanically, through an overrunning clutch which allows the rotor to drive the propeller, or vice versa, when the engine is slowed down or stopped (in autorotation). The engine output speed is controlled by a conventional turbine governor, and its power distribution between the rotor and the propeller depends on the power demanded by the blade pitch setting of each.

The rotor system consists of Model H21-C metal rotor blades and hub assembly. It is a three-bladed, fully articulated system, using tension/torsion straps for the blade retention.

The three-bladed pusher propeller consists of the blades, designed and manufactured by Piasecki Aircraft Corporation, and the hub, which is of standard airplane manufacture, modified to accept mechanical blade-pitch control in lieu of the hydraulic control system normally used.

As a test vehicle, the aircraft was equipped with two seats: one for the pilot on the right side and one for the flight test engineer on the left side. The remaining portion of the cabin was used to house the instrumentation, ballast, etc.

The wing consists of the center portion and of the outer panels. The center portion is of two-spar construction and houses the bladder-type main fuel tank. The outer wing panels are of double skin honeycomb construction and are sealed to form integral fuel tanks The aft portion of each outer wing panel forms a full span flaperon.

The landing gear is of conventional, main wheel/tail design and it uses air-oil shock absorbers. The main wheels are attached to the center wing panel and retract inboard, into wells on the underside of the fuselage, by means of electrically operated screw jacks. Emergency operation is by mech-

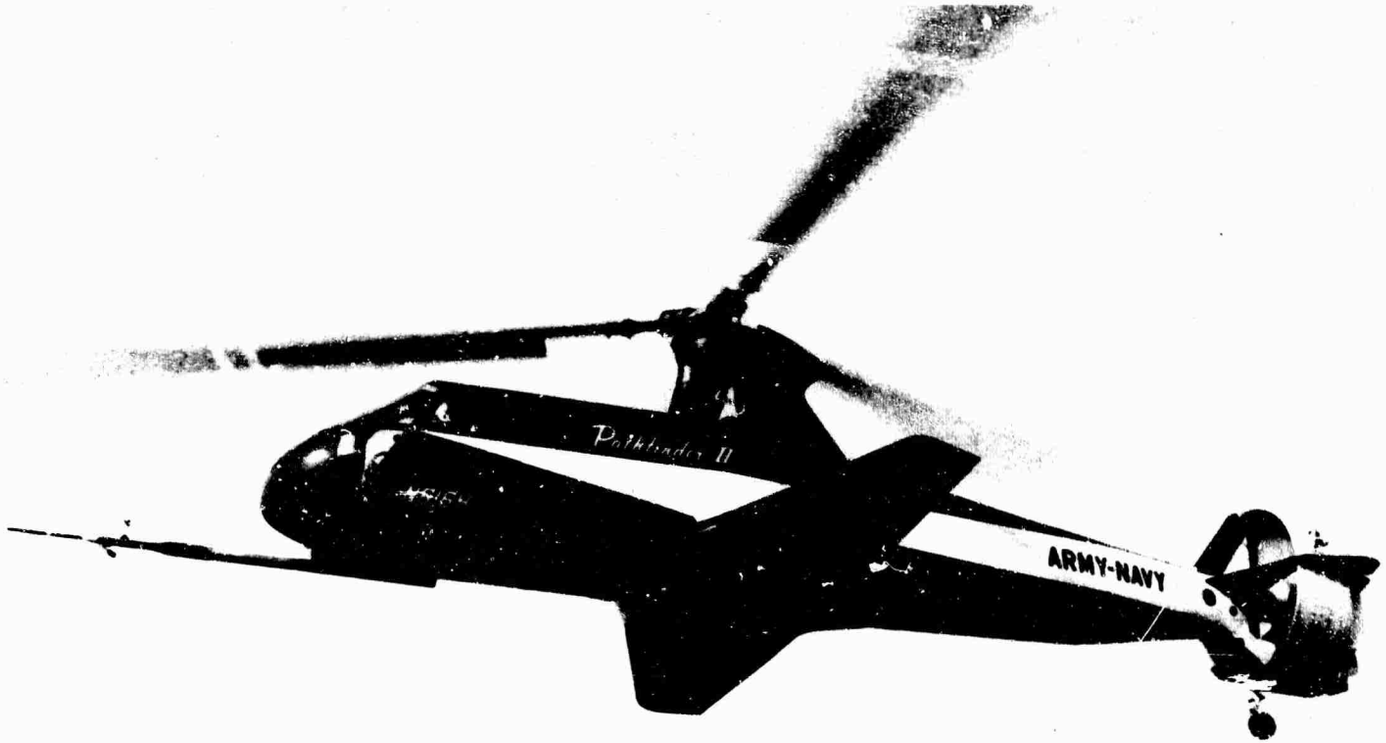


Figure 2. 16H-1A Pathfinder.

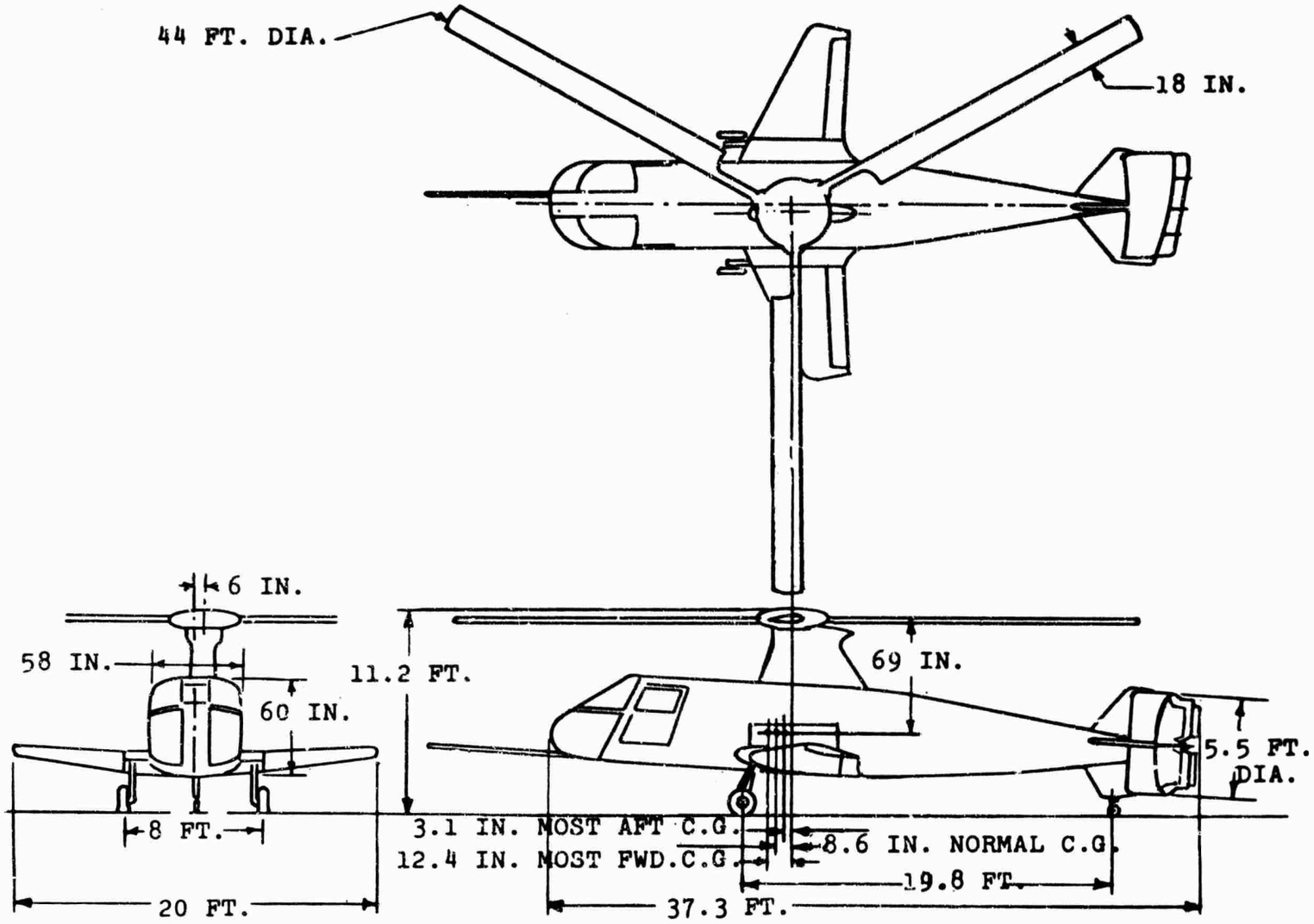


Figure 3. Three-view Drawing of 16H-1A, Showing C.G. Envelope.

anical crank drive in the cockpit. The nonretractable tail wheel is fully swivelling and can be locked.

The primary flight controls in the cockpit consist of conventional collective and cyclic stick levers, rudder pedals, and two (primary and emergency) beeper switches which permit the flight test engineer to control the aircraft in an emergency.

The secondary flight controls in the cockpit consist of trim beeper switches: one for the flaperons and one for the elevator trim.

The main rotor cyclic and collective pitch are controlled through dual irreversible hydraulic servo actuators mounted in the rotor pylon under the swash plate.

The General Electric T-58-GE-8 free-shaft turbine is installed in the fuselage, aft of the main rotor. Mounted on it is a General Electric speed reduction gearbox. Power is delivered from the rear of the engine and is shafted forward to the aircraft drive system. The engine has its governor ($N_2$ speed) controlled from the cockpit by means of a beeper switch which operates an electric actuator located on the engine and connected to the engine fuel-control arm. It also has its emergency shutoff mechanically controlled from the cockpit by a lever. Engine starting is by an electric starter located on the nose of the engine. The engine air-intake and exhaust are both on the starboard side of the aircraft.

The drive system consists of a transfer case, rotor transmission, mast assembly, propeller shaft bearing box, and shafting. The spur-gear-type transfer transmission receives power from the engine at 6000 RPM and distributes it to the rotor transmission and to the propeller drive shaft. The rotor transmission, a modified H-21 gearbox, consists of a set of spiral bevel gears and a single-stage planetary reduction system. The transfer and the rotor transmission are bolted rigidly together and have a common lubrication system. The propeller shaft bearing box supports the propeller shaft and also houses the mechanical yoke and levers of the propeller pitch control. It is self-lubricated by the wet sump system.

The fuel system is of conventional design. It consists of two booster pumps located in the main tank which supply the fuel under pressure through a filter to the engine. The tank is vented overboard and has a float-type quantity gage indicator. In the test vehicle, the outer wing tanks were not used and were disconnected.

TABLE I. DESCRIPTION OF TEST ARTICLE

| General | Units | |
|---|---|---|
| Design Gross Weight | lb | 5,782 to 8135* |
| Fuel Capacity (41 gals. plus 60 gals.) | lb | 279 + 409 |
| Normal Crew | no. | 2 |
| Empty Weight | lb | 4415 |
| Overall Length - blades extended | ft | 44 |
| Overall Length - blades folded | ft | 37.3 |
| Height | ft | 11.2 |
| Landing Gear Type | -- | Retractable main wheels - nonretractable tail wheel |
| Wheel Base | ft-in. | 19-9 |
| Number of Rotors (Location & Type) | -- | One main rotor One pusher prop |
| Structure | -- | Alum. alloy semimonocoque and honeycomb |
| **Main Rotor** | | |
| Type | -- | Fully articulated (H-21) with tension torsion straps |
| Diameter | ft | 44 |
| Blades | no. | 3 (metal) |
| Blade Chord | in. | 18 |

*Various components were designed to different limits. Test weight was limited by strength of fuselage and landing gear.

TABLE I. - Continued

| Main Rotor (Cont'd) | Units | |
|---|---|---|
| Airfoil Section | -- | NACA 0012 |
| Blade Taper | -- | Constant chord |
| Blade Twist (Root Airfoil to Tip Airfoil) | deg | 7.3 |
| Rotational Axis Tilt to Fuse Axis | deg | 3 |
| Disc Area | sq ft | 1520 |
| Total Blade Area | sq ft | 99 |
| Disc Loading (based on 6500 pounds gross weight) | lb/sq ft | 4.28 |
| Normal Operation Speed | RPM | 279 |
| Normal Tip Speed | ft/sec | 643 |
| **Tail Group** | | |
| The tail group consists of a propeller and a ring or shroud surrounding the propeller, supported in front by horizontal and vertical stators and, in turn, supporting an elevator surface and an assembly of rudder surfaces in the propeller slipstream. | | |
| Ring-Tail Span | ft | 6.4 |
| Ring Surface Area (Outside) | sq ft | 47.5 |
| Arm to Rotor Centerline from Vertical Surface Center of Pressure | ft | 20.5 |
| Rudder Area | sq ft | 20.3 |
| Elevator Area | sq ft | 3.7 |
| Horizontal Stabilizer Area | sq ft | 4.9 |
| **Tail Propeller** | | |
| Diameter | ft | 5.5 |

TABLE I. - Continued

| Tail Propeller (Cont'd) | Units | |
|---|---|---|
| Blades | no. | 3 |
| Airfoil Section | -- | NACA 16 Series |
| Blade Twist | deg | 32 |
| Chord | in. | 9 |
| Blade Pitch Range | deg | -5 to +35 |
| Normal Operation Speed | RPM | 2700 |
| Normal Tip Speed | ft/sec | 778 |
| **Wing** | | |
| Type - Aluminum alloy honeycomb sandwich structure; flaperons full length of outer panels; left & right panels interchangeable and fold upwards | | |
| Span | ft | 20 |
| Wing Loading @ 6500 lb. Gross Wt. | lb/sq ft | 75 |
| Taper Ratio | in./in. | 82.6/27.5 |
| Area | sq ft | 86 |
| Aspect Ratio (Effective) | -- | 4.65 |
| Chord (MAC) | in. | 59 |
| Dihedral | deg | 1-1/2 |
| Sweepback (leading edge) | deg | 25 |
| Airfoil | -- | NACA 0012 |
| Incidence (fixed with respect to rotor disc) | deg | 9-1/2 |
| Flaperon Area (each) | sq ft | 7.2 |

TABLE I. - Continued.

| Wing (Cont'd) | Units | |
|---|---|---|
| Flap Deflection | deg | 40 |
| **Powerplant** | | |
| Type | -- | One GE Free Shaft turbine T-58-8 |
| Maximum Power (takeoff & 30 Min) | SHP | 1250 @ Sea Level |
| Normal Power | SHP | 1050 @ Sea Level |
| Fuel Type | -- | JP-4 |
| RPM (at output of speed decreaser gears) | RPM | 6000 |
| **Drive System** | | |
| Ratio - Engine to Main Rotor | -- | 69.89 to 1 |
| Ratio - Engine to Prop | -- | 7.22 to 1 |
| **Controls** | | |
| Upper - Swashplate controlling rotor blade pitch through pitch links | | |
| Lower - Stainless steel cables; pulleys; push-pull rods; rotor control dual servo units | | |

## TEST INSTRUMENTATION

### GENERAL DESCRIPTION

Key points in the drive system distributing the power to the rotor and to the propeller were selected in order to measure properly the power going to these two components as well as the total power developed by the turbine.

In order to determine flight loads and to insure structural integrity with safety margins in the high speed flight regimes, one metal rotor blade was instrumented. The rotor hinge assembly was completely instrumented for motions about all axes, and one pitch link force measurement gave the pitching moment of the blade. Similarly the pilot control motions were measured in the cockpit and the attitude of the aircraft throughout all flight conditions was measured about all axes. Parameters which would not vary significantly in short time intervals (less than one-half second), such as speed, RPM, altitude, flap setting, etc., were taken from the photopanel located inside the cabin. The rest of the information was recorded on three 18-channel oscillographs. Locations of the various transducers and recorders are shown on the perspective drawing, Figure 4.

The highest quality instrumentation was used throughout. However, wherever rewiring was necessary, a larger gage wire was used, as the initial light gage wire installed was difficult to maintain.

Many of the parameters were checked by photographic coverage from the ground and/or chase plane during flight trim attitude tests. Five camera positions were built on the aircraft to record local conditions of operation in addition to the ground and chase plane photographic coverage. Several of these cameras were high-speed gun cameras capable of 64 frames per second. One of them was capable of over 1000 frames per second. Such photographic coverage aided correlation between effect and cause, especially during the vibration part of the program.

A considerable number of strain gages had to be replaced in order to improve their readability, and constant maintenance was required for the instrumentation wiring which was affected by fatigue conditions.

The primary recording system consisted of three oscillographs with 18 channels each, providing a total of 54 channels. The use of three oscillographs permitted recording at three different speeds so that the necessary frequency response could be recorded with a minimum of exposed footage.

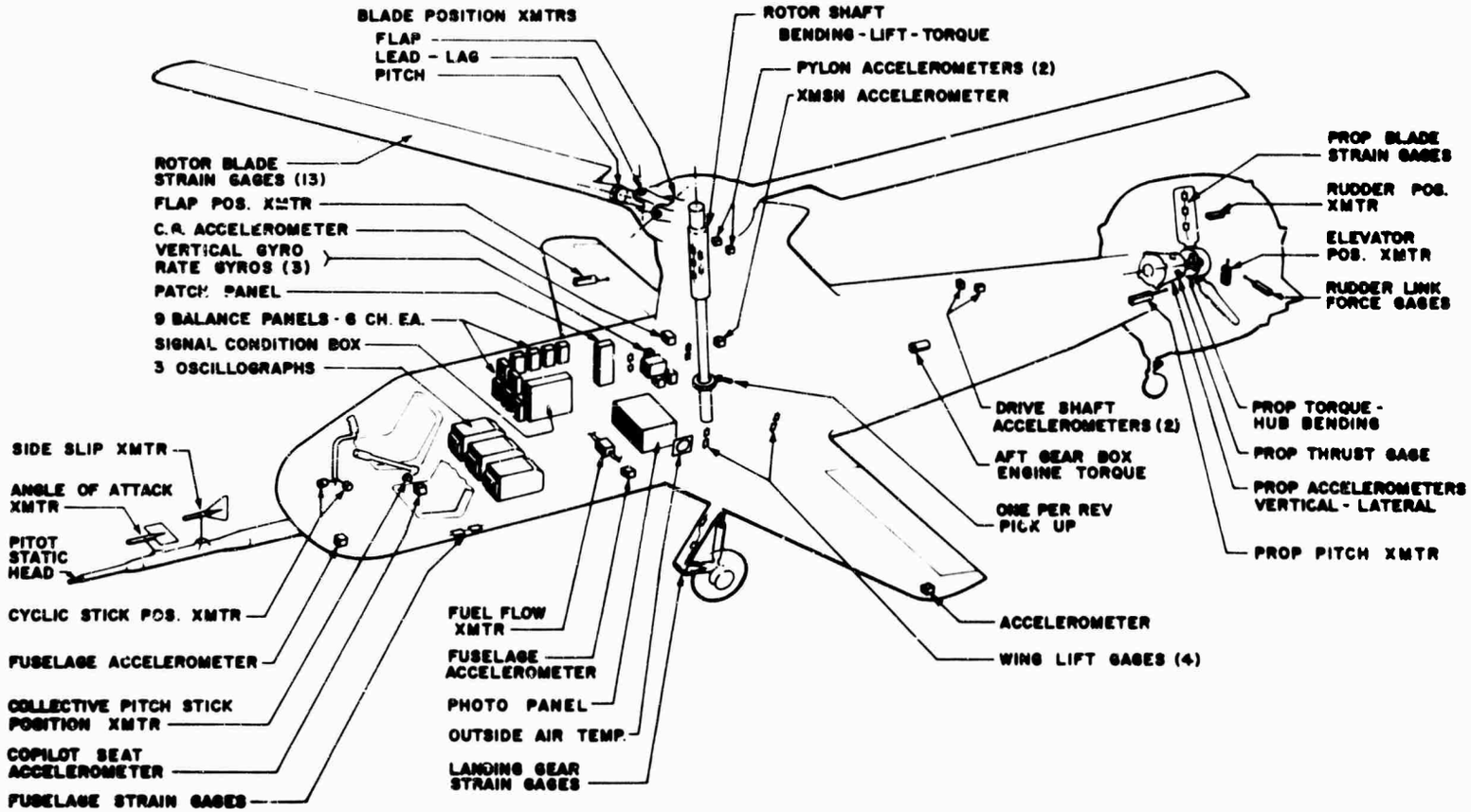


Figure 4. 16H-1A Instrumentation Locations.

In addition to the above-mentioned automatic recorders, a large amount of observed data was collected by manually recording cockpit instrument readings. Some of the cockpit instruments were duplicated either in the photo panel or by recording on one of the three oscillographs. This redundancy provided a quick look at the aircraft's performance immediately after the flight.

Three basic types of transducers were used to drive the galvanometers and indicators in the 16H-1A: 350-ohm strain gages, linear and rotary potentiometers, and autosyn transmitters.

In-flight loads were measured by means of 350-ohm, foil-type strain gages bonded to the load-carrying members. Vibration and accelerations were measured by means of seismic type strain gage accelerometers mounted on the appropriate portions of the aircraft. Signal-conditioning for both the bonded and seismic strain gage bridges was accomplished by means of nine 6-channel balance panels. These units provide a means of balancing the strain gage transducer to zero output at any load within the range of the instrument. They also provide a gain control to give the desired galvanometer deflection at the maximum load expected in flight. Provision is also made for a shunt-type calibration resistor so that sensitivity of each channel can be checked before and after each flight, and for correlating the flight data with the latest load calibration. Calibration resistors are ±1% film- or wire-wound with a 50-PPM. temperature coefficient.

Position transducers were generally of the potentiometer type in which a variable resistor is displaced in proportion to the motion of some component on the aircraft. To facilitate mechanical installation, a rotary type was chosen in some cases and a linear type in others, but electrically they are considered interchangeable. For those channels that could be moved through full travel before and after each flight, signal conditioning was provided for by the Piasecki signal conditioning box. This provides a balance potentiometer which permits adjustment of circuit output to zero at the desired reference position and fixed resistors to adjust circuit sensitivity and galvanometer damping. Pre- and postflight sensitivity checks were performed by recording while moving the aircraft component through full travel from stop to stop.

Those potentiometers which could not be conveniently run through full travel before and after each flight to check sensitivity were handled in the same manner as the strain gage channels. In these cases (rate and attitude gyros) the potentiometer was connected across two legs of a 350-ohm dummy

bridge fabricated from fixed precision resistors with a low temperature coefficient of resistance. This provided a four-arm bridge which could be connected into one of the balance panels. As in the case of the strain gage transducers, the balance panels provided sensitivity adjustment, balance adjustment and shunt resistance calibration capability for pre- and postflight sensitivity checks.

Excitation voltage for all transducers discussed so far was provided by a 24-volt lead-acid battery which was completely separate from the aircraft electrical system. This battery was tapped at 6, 12, 18, and 24 volts so that the desired sensitivity of each channel was within the range of the gain adjustment on the balance panels. The battery was ungrounded and was not charged in flight, but was charged on a normal battery charger at night and reinstalled in a fully-charged condition each morning. The voltage of the battery was monitored on the oscillographs in flight by impressing the 24-volt output on the rotor one-per-revolution traces of Number 2 and Number 3 oscillographs, thus permitting the recording of battery voltage with no loss in data channels. This voltage-monitor system was a backup for the shunt calibration, since any change in battery voltage was reflected in the galvanometer deflection during the shunt calibration and full throw recordings that were taken before and after each flight.

The above mentioned potentiometer systems are unsuitable for certain parameters which have repeated cyclic motion and thus tend to wear at a rapid rate, particularly in the case of the rotor-blade position transmitters (pitch, lead-lag, and flap angles). In these channels, autosyn transmitters were used, since they have virtually no wear and have excellent repeatability. Excitation power was provided by a static-type inverter that converts 28 volts D.C. to 115 volts, 400-cps, A.C., a voltage regulation accuracy of $\pm 1\%$. The output of one phase of the autosyn is rectified, filtered, and attenuated in the signal-conditioning box to provide a D.C. voltage to the galvanometer proportional to transmitter angle. This same system was used for angle of attack, since it provided minimum drag on the vane and therefore minimum hysteresis.

## DISCUSSION OF ACCURACY

All performance parameters (torque of rotor, tail propeller, and engine, all tachometers, airspeed, altitude and outside air temperature together with the combined values of turbine, rotor and propeller powers, true airspeed, and density altitude) had errors of 5 percent or less. In addition, 85 percent of the remaining data submitted has probable instrumentation errors less than 5 percent.

The fact that the probable error for each channel is usually based on maximum value presented results in a high percentage number for the error, since flight data were always significantly lower than the critical value. For example, the rotor pitch link force data have an absolute maximum error of only 43.5 pounds; but since pitch link loads in flight never exceeded 345 pounds, the conversion to a percentage results in a misleading, high figure for the error. For this reason the absolute errors should be considered more significant than the percentage errors.

As the data were reduced and plotted, it became apparent that certain channels were providing inconsistent data and were not as accurate as desired. These channels were modified to increase their accuracy during the tests; as a result, the overall accuracy of the system was improved throughout the program. For instance, the original method of checking sensitivity of the attitude and rate gyros proved to be inadequate. These circuits were redesigned to provide for sensitivity checks before and after each flight.

The wing lift circuits were particularly troublesome from the start. Ground tests at varying ambient temperatures indicated large amounts of drift due to expansion of the structure on which the gages were bonded. A modified temperature compensating system was installed which solved the drift problem, but lift data in flight still proved to be inconsistent, even though ground calibrations appeared to be excellent. It is possible that the errors in these channels were due to the different stress patterns experienced in flight with the wings loaded aerodynamically as compared to the concentrated loads experienced during ground calibration. On the other hand, the rotor lift measurements were determined to be consistent, and these were used in the determination of rotor/wing lift distribution.

In other cases, large errors were uncovered during a normal recalibration when the failure to repeat the previous calibration within the desired accuracy indicated a transducer failure. In these cases the transducer was replaced before the next flight.

Specific accuracies for each channel are indicated in the data presented in Appendix II.

## DESCRIPTION OF FLIGHT TESTS

Prior to flight testing the basic aircraft was weighed, and the empty weight was determined at 4415 pounds. Gross weight was then calculated for each flight, and exact weights were calculated for crew, fuel, and ballast.

Instrumentation was set up so that the oscillographs recorded control positions, fuselage angle of attack, attitude, angular acceleration, and loads and stresses from critical static and dynamic locations on the aircraft. They also recorded the lead-lag angle of the instrumented rotor blade, its pitch angle and its azimuth position, accelerations on the aircraft, and the landing gear loads. Blade motions, blade stresses, rotor and propeller torque, and vertical drive shaft stresses were recorded for all flights; other data were recorded only as needed to meet the objectives of the specific tests.

The photo panel recorded airspeed, altitude, time, gas generator RPM, power-turbine RPM, engine torque, air temperature, fuel flow, vertical rate of climb, and sideslip angle.

Before and after each flight test, an instrumentation sensitivity check was conducted. This procedure, popularly called "R cal", was accomplished by the flight test instrumentation group after preflight inspection and servicing (prior to the flight) and before postflight inspection and servicing (after the flight).

All taxi, hover, sideward and backward flight, and vertical climb tests were conducted over the concrete mat areas adjacent to the Piasecki facilities at Philadelphia International Airport. The remainder of the tests were generally conducted within autorotation distance of the airport.

Use of the gross weight/density altitude ratio system required data to be gathered at specific altitudes which are dependent upon takeoff weight, the ambient temperature, and the gross weight to which the data were to be referred. Since conditions might vary between flights, a graph (Figure 5) was constructed (similar to the example given in Reference 5) for the weight range of the 16H-1A that enabled the pilot to determine the proper altitude for any test. Entering the graph with the 16H-1A actual gross weight (less estimated fuel used before reaching test altitude), the proper pressure altitude can be found for the required referred weight. Flights were made at gross weights ranging from 5689 to 7500 pounds, and at combinations of altitude and temperature which produced weight/density ratios ranging from 5370 to 8040 pounds.

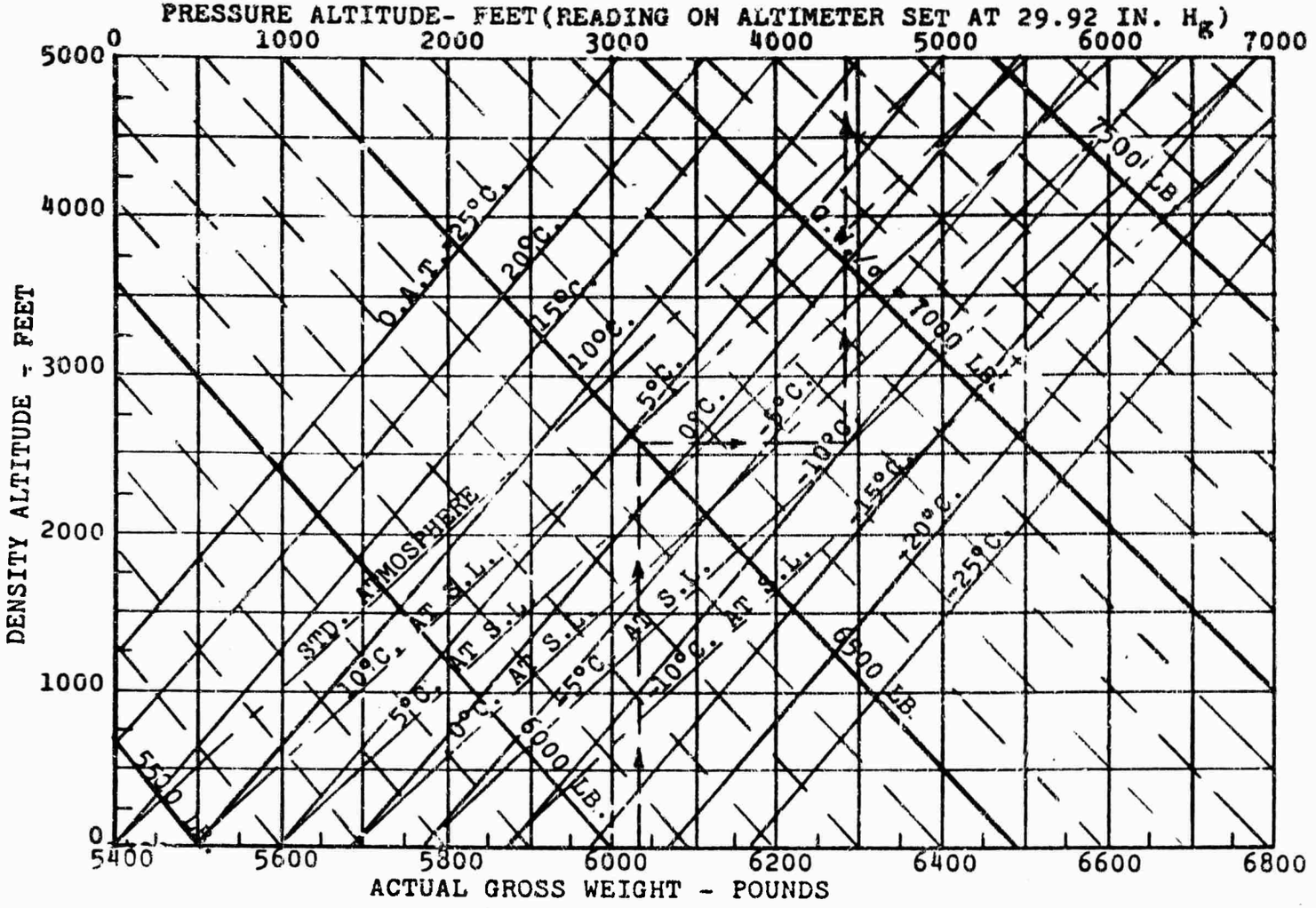


Figure 5. 16H-1A Altitude Planning Chart.

The vulnerability of the propeller and duct to foreign object damage was monitored throughout the test program. While tests involving deliberate injection of various kinds and sizes of materials were not made, the amount and degree of foreign object damage were continually observed under normal flight operations. Except for an emergency power-off landing in a rough field with tall reeds (see "Technical Problems"), only occasional minor nicks and abrasions were found; these never interfered with scheduled flight operations.

TAXI

This phase of testing was devised to determine the ability of the 16H-1A to perform taxi maneuvers with and without brakes in varying wind conditions and velocities up to 35 knots. The following maneuvers were established as the taxi requirements:

1. Taxi upwind, cross wind, and downwind without brakes at ground speeds up to 20 knots.

2. Execute figure eights without the use of brakes.

3. Determine main rotor blade to duct clearance with 100% rotor RPM and minimum collective pitch while taxiing downwind in 35-knot winds.

4. Demonstrate the ability to stop the aircraft at any time while performing these maneuvers by the application of brakes and/or cyclic control.

HOVER

These tests cover the investigation of performance, flying qualities, and stresses encountered in the 16H-1A during hover, both in ground effect and out of ground effect.

Total power required and power distribution were determined as a function of gross weight. Tail propeller power required was determined as a function of vane deflection and gross weight. Data were recorded when the aircraft was stabilized with the desired rotor RPM and tail propeller pitch in calm winds. Data were gathered at least three separate, nonconsecutive times for each height (in ground effect and out of ground effect) over a range of actual gross weights from 5700 to 7500 pounds.

Flying qualities were investigated by establishing control positions and response rates when making 360-degree

hovering turns in winds of 0 to 20 knots (gusting to 30 knots), including turns in winds in ground effect at the most critical center of gravity. Static stability and control motions were investigated while hovering in winds of less than 3 knots. Variations in center-of-gravity location of 9.3 inches were investigated, and control positions were determined as related to gross weight, horizontal trim setting, and tail propeller pitch. Time histories of control positions and angular accelerations were obtained about all three axes individually for abrupt pulse inputs of pitch, roll, and yaw. Tests for response rates were conducted from a stabilized hover with the most critical combination of rudder deflection and propeller pitch. The most critical combination was selected such that a 1-inch left-pedal displacement from trim (to turn to the left) brought the pedal to full travel.

In order to use consistent heights for in-ground-effect and out-of-ground-effect hovering, a calibrated weighted line of 6 feet and 60 feet (as measured from the main landing gear wheels) was used for the respective test categories. This line was on a reel and was lowered only after the aircraft was airborne. A ground observer stationed to one side of the aircraft would convey to the pilot the exact height of his hover, allowing a tolerance of 1 to 2 feet. The hover tests were all conducted with the aircraft facing into the wind.

In obtaining a data point, the pilot would hover and adjust his collective pitch and cyclic stick settings until the aircraft was stable; then the flight engineer would take a blip of at least 3 seconds' duration. The pilot would then change the attitude of the aircraft by means of elevator trim and stabilize; then the flight engineer would take another blip.

The ducted pusher-propeller deflected-vane arrangement in the tail for antitorque yaw control presents an approach that combines the functions of the conventional helicopter tail rotor and propulsion propeller. To provide antitorque force and directional control, the propeller and the vanes work together. That is, directional control in hover can be maintained by keeping a relatively high propeller pitch setting and a moderate vane deflection angle, or by keeping a higher vane angle but lower propeller pitch setting. Tests were conducted to investigate both extremes.

The effect of the horizontal trim position and propeller pitch was measured in hovering. The trimmable elevator, because of its position behind the ducted propeller, is effective in all regimes of flight, including hover, and can be used to adjust for nose-up or nose-down aircraft attitudes. This

was evaluated as to its effect on total power requirements and allowable center-of-gravity travel.

SIDEWARD AND BACKWARD FLIGHT TESTS

These tests cover the investigation of performance, flying qualities, and stresses encountered in the 16H-1A aircraft during sideward and backward flight at speeds up to 30 knots.

Total power required and power distribution both in and out of ground effect were recorded in 10-knot increments up to 30 knots, in sideward flight, in calm air. The same data were recorded for backward flight.

The flying qualities were investigated by determining control positions as a function of speed in both sideward and backward flight. Response rates and the effect of rapid control inputs were also evaluated. The control power available was determined for each control at 30 knots in each direction. The flying qualities were determined with the aircraft gross weight varying from 6000 to 6382 pounds and with the center of gravity 3.1, 5.1, and 12.4 inches forward of the rotor axis.

Sideward and backward flight tests of the aircraft were all performed at the Piasecki ramp area. A pace car with a calibrated speedometer was used to establish speed. A windmeter, suspended outside the car during the run, was used to verify speeds and to check wind correction. The pace car accelerated to, and held, the desired speed. When the appropriate speed had been reached, a card was displayed from the car notifying the pilot and flight test engineer to maintain this speed and to take a blip.

From a hover, the aircraft was rotated 90° to the wind and was flown laterally into the wind. After being stabilized long enough for a blip to be taken by the flight engineer, the aircraft could be rotated into backward flight and stabilized for another blip. The following excerpt from Flight 263 Test Report indicates one pilot technique used in gathering data for this portion of the program.

"...The third maneuver was right sideward flight of 20 knots, with full left rudder and then varying tail prop pitch to bring the aircraft around to the position 180° out of the wind and continuing at 20 knots rearward flight ..."

The procedure was repeated until the required data points had been achieved and verified as needed.

Figure 6 shows the 16H-1A performing rearward flight.

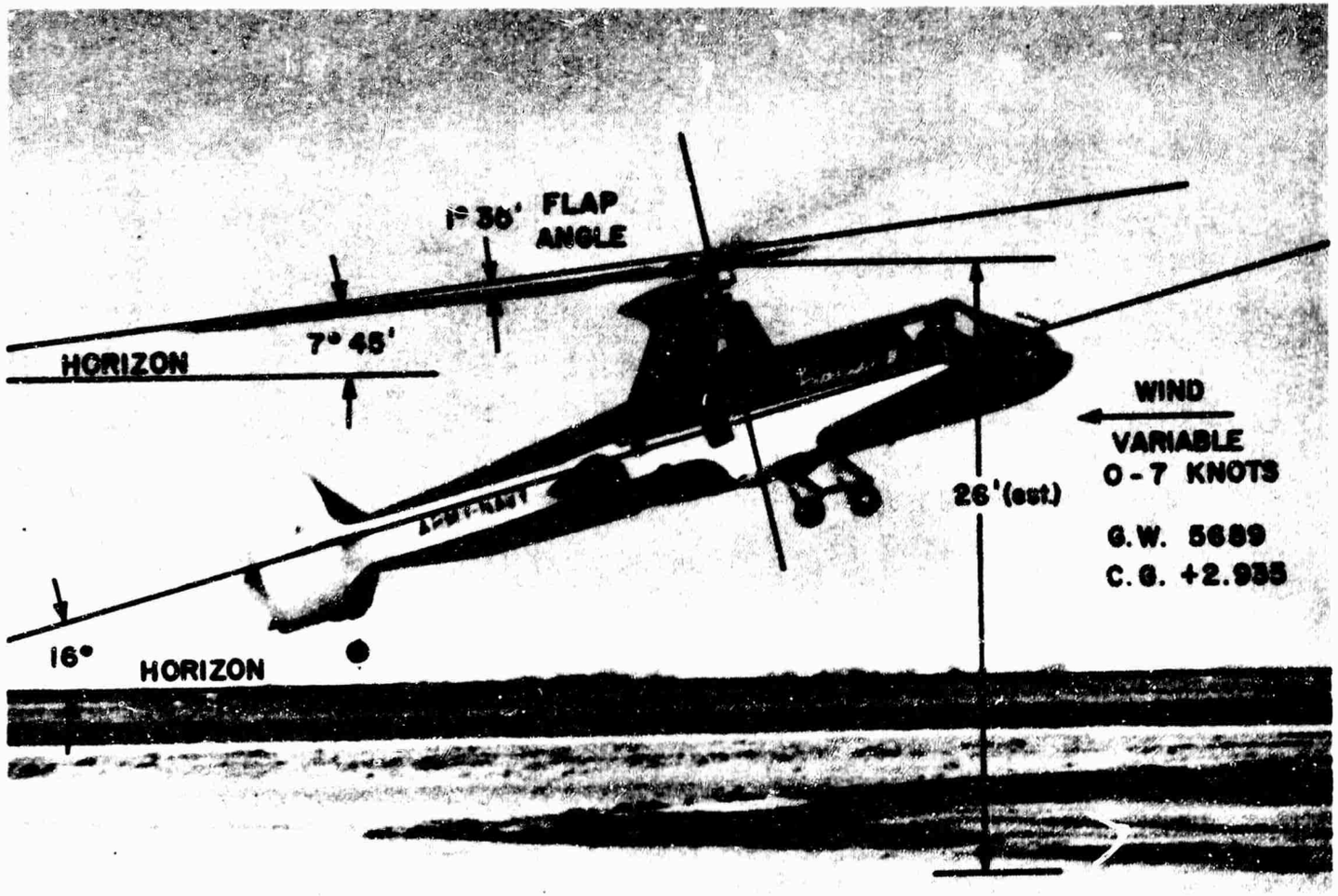


Figure 6. Rearward Flight - 10 Knots.

## TRANSITION TESTS

Transition represents the flight regimes of acceleration from hover to forward flight and deceleration from forward flight back to hover.

The flying qualities of the aircraft during transition were established by determining the positions of all controls (longitudinal and lateral cyclic, collective, rudder pedal, longitudinal trim vane, and tail propeller pitch) as the aircraft accelerated and decelerated through the 0 to 70-knot speed range.

Level flight accelerations and quick stops were performed between the airspeeds of 0 to 70 knots at center-of-gravity locations 4.8 inches and 12.4 inches forward of the rotor axis.

The following verbal time history describes an acceleration from hover through transition and back to hover using a technique where the tail propeller provides the required thrust for translation. Acceleration in this manner results in a much smaller pitch change and somewhat slower acceleration than would occur using the rotor to provide the aft component of thrust. The technique used was:

1. Hover with excessive tail propeller pitch and hold aft longitudinal cyclic.

2. Start oscillograph recordings.

3. Add tail propeller pitch while maintaining attitude with longitudinal cyclic and direction with rudder.

4. Decrease collective pitch as necessary while adding tail propeller pitch (within torque limits).

5. At 70 knots forward speed, decrease tail propeller pitch to minimum.

6. Decrease collective pitch to minimum.

7. Flare with aft cyclic while maintaining constant altitude.

8. Reduce turbine speed control to keep the engine RPM constant (required due to 8% engine governor droop).

9. Add necessary tail propeller pitch for hover.

10. Stabilize hover.

11. Turn off oscillographs.

The procedure used when maximum acceleration is desired and attitude change is unimportant follows:

1. Hover using a high vane deflection with a low propeller pitch setting.

2. Start oscillograph recordings.

3. Apply forward cyclic and collective as required for forward motion.

4. Increase propeller pitch and gradually lower collective, smoothly bringing the aircraft to a level flight attitude at about 70 knots.

5. Slow-up and flare are as previously described.

FORWARD-SPEED CLIMB

These tests cover the investigation of the performance, flying qualities, and stresses encountered in the 16H-1A during forward-speed climb at true airspeeds between 42 and 141 knots.

The rates of climb were determined as a function of airspeed, power distribution, and flap setting. Rate-of-climb tests were conducted between a speed range of 42 to 141 knots in nominal 20-knot increments at normal rated power with a nominal gross weight and center of gravity. The saw-tooth technique was utilized for determining the performance of the 16H-1A in forward-speed climb tests. During these tests, the aircraft alternately performed stabilized climb and then stabilized level flight or descent to record rate of climb as a function of airspeed, power, and flap setting. Each climb was maintained through at least 1000 feet of altitude.

Flying qualities in climb were established by determining control positions as a function of airspeed, flap deflection, and center of gravity. The tests were conducted with centers of gravity of 8.6 and 3.1 inches forward of the rotor axis, with retracted flaps at the nominal gross weight. Tests were repeated with flaps fully extended at airspeeds of 50 to 90 knots.

## AUTOROTATION

Procedure was established whereby the Philadelphia International Airport runways or other adjacent clear areas were selected for autorotative approaches. Normally, at a predetermined altitude, a power recovery was executed. A procedure was established whereby many test flights that were conducted in other phases of testing ended with an intentional autorotation.

The first autorotation in the 16H-1A became an emergency when power could not be applied because of a malfunction in the turbine speed selector system (see "Technical Problems"). Although this was the first autorotation attempted with this aircraft, the pilot was able to complete a successful autorotation to touch down into a selected clear area. During the flare just prior to touchdown, the height over a ground protrusion adjacent to the clearing was misjudged and the ring-tail was dragged, shearing the tail wheel and damaging the bottom of the trailing edge of the rudder vanes. It is significant that the ring-tail protected the tail propeller and prevented a quick stoppage of the drive system and the serious damage that is common to such an occurrence.

The pilot technique in autorotation was similar to the technique used in conventional helicopters. To illustrate this, the following excerpt from the Flight Report for Flight 276 is presented:

"...The aircraft was trimmed out at 60 knots with 11° tail prop pitch. Collective was lowered and the throttle was reduced at 5800 RPM. The needles split and the aircraft entered autorotation without any difficulty at all. The tail prop pitch was at minimum throughout the flight.... Pitch attitude control of the aircraft, power off, requires more longitudinal cyclic movement than it does with power on. 60 knots in autorotation was established; we then went to 80 knots and then approximately 90 to 100 knots. Throughout this time the rate of descent (indicated) was pegged at 2000 feet per minute."

"...The collective pitch was then confirmed to be completely bottomed. I reduced to 60 knots which let my rotor RPM increase to about 5900 RPM (rotor RPM equivalent to 5900 engine RPM) and the only thing I concentrated on was first avoiding a ditch and a cement culvert in order to reach a clear area of what looked like gravel. A flare was then entered and the tail wheel was felt to hit the ground prior to the time that I thought it would. We still had 30 to 40 knots forward airspeed and I had not pulled any collective yet, so

flare was continued and collective pitch was applied and the tail wheel bounced once or twice. We were very close to zero airspeed when I finally let the front gear come down to the ground. In the final landing, there was plenty of rotor inertia and the final landing of the aircraft was very smooth and like a normal landing..."

VERTICAL CLIMB

These tests cover the investigation of the 16H-1A performance, flying qualities, and stresses in vertical climb.

Power required and rotor/tail propeller power distribution were determined as a function of gross weight and vertical rate of climb. Vertical climb tests were conducted at 100% main rotor RPM at referred gross weights of 6200 and 7000 pounds and referred power varying from 1044 to 1226 horsepower.

The aircraft flying qualities in vertical climb were established by showing control positions as a function of vertical rate of climb.

A standard pilot technique was used for all vertical rate-of-climb data acquisition. From a stabilized hover over the Piasecki ramp area, the power was increased to a predetermined level and the aircraft climbed vertically. When the rate of climb had stabilized, three blips were taken at 500-foot intervals.

LEVEL FLIGHT

This portion of the test program covers the investigation of the performance, flying qualities, and structural integrity of the 16H-1A in level flight.

Total power required and power distribution between the main rotor and the tail propeller were determined for stabilized flight by the weight/density ratio method mentioned earlier. In order to determine the optimum (least power) points, power distribution at a given speed was varied by appropriate changes in propeller and rotor collective pitch. For each combination, airspeed was maintained with longitudinal stick, which also produced a specific attitude.

Static, directional and longitudinal control-fixed stability were investigated at various aircraft speeds, angles of attack, and centers of gravity. The margin of control available was investigated for various centers of gravity.

As the data were to be acquired using the weight/density method, it was necessary to fly at the proper density altitude to achieve the desired referred gross weight (w/σ). The method of establishing the proper density altitude and a chart used for altitude selection are discussed at the beginning of this section.

Normal procedure was to climb to the required density altitude, stabilize at the first speed point, and take a 3- to 5-second instrumentation record. Pertinent cockpit instruments were recorded manually on the flight card as a backup for the automatic recorders and to provide a quick look at the aircraft's performance immediately after the flight. Records were taken over a true airspeed range from 30 to 167 knots in level flight and to 195 knots in dives up to 10 degrees. Angle of attack was varied by means of the elevator trim vane and by using different combinations of rotor and tail propeller pitch.

Longitudinal static stability was investigated over the speed range by determining stick position as a function of speed in level flight, climb, and autorotation. In addition, the aircraft was trimmed at a specific speed, and the changes in stick position were determined which would produce speed changes from trim of ±10 knots and ±20 knots.

Dynamic stability was investigated at trim speeds of 0, 50, and 150 knots at two centers of gravity (8.6 to 9.7 inches, and 3.1 inches forward of rotor axis) and at a nominal gross weight of 6100 pounds, with flaps retracted. The test procedure was to record on oscillographs a time history of the control motions and aircraft responses from which the period and damping characteristics of the aircraft were derived. At no time was it necessary for the pilot to use an abnormal control recovery procedure, and he has reported that the aircraft appeared to have a very high degree of positive dynamic stability.

It was found that originally planned stick-free stability tests were not feasible because the 16H-1A cockpit controls act through irreversible hydraulic servos and are not equipped with centering bungees of any kind. Thus the stick will stay in any position in which it is placed, regardless of the force at the output end of the system. In the beginning of the program, the servos were located under the cockpit floor, and friction was so low that the stick would fall off in any direction of its own weight. After the servos were relocated in the pylon (see "Technical Problems"), there was enough friction to prevent this falling off, but stick-free stability was still without significance.

The phugoid or long-period oscillation characteristics were obtained by holding controls essentially fixed and allowing the aircraft to deviate from its trim speed and pitch attitude and by recording the time history of the ensuing long-period oscillation.

For purposes of airspeed calibration, the position error affecting the pitot-static system was determined by the Ground Speed Course Method. Several speed courses were laid out adjacent to runways at the Philadelphia International Airport. The 16H-1A was flown over these courses of known distance in both directions at an altitude of less than 200 feet so that transit times could be accurately measured ($\pm$.1 second). The selection of the particular course was on the basis of minimum crosswind. True airspeed was determined from the resultant time/distance data.

Figure 7 gives the results of the level flight calibration of the airspeed indicating system. Since the instrument reliability below the speed of 30 knots is low, the calibration is only useful for speeds above this value.

The calibration curve was constructed in two stages, coinciding with the speeds concurrently being tested. The first series of tests covered an indicated airspeed up to 129 knots, and the second series covered the speed range above this speed. For the first series, the curve was drawn as shown by a dotted line, since at that time the points from flights 402 and 411 had not yet been obtained. It was subsequently corrected as shown by a solid line. It was extrapolated as shown in phantom lines for speeds above 160 knots (indicated) because power limitations prevented calibration at higher speed by the method used. Maximum deviation of measured points from the final calibration curve is less than 5 knots, and average deviation is less than 3 knots.

STOL

This portion of the test program covers the investigation of the STOL performance of the 16H-1A and the stresses encountered during simulated STOL operations.

STOL performance was evaluated by conducting forward velocity takeoffs and landings over a measured concrete operating strip. STOL operations were conducted at various gross weights and with different flap settings. In addition to recording power and flight data, landing loads on the landing gear shock strut were measured and recorded. Since the 16H-1A landing gear was not designed for STOL weights, the tests were actually conducted at weights for which VTOL operation would

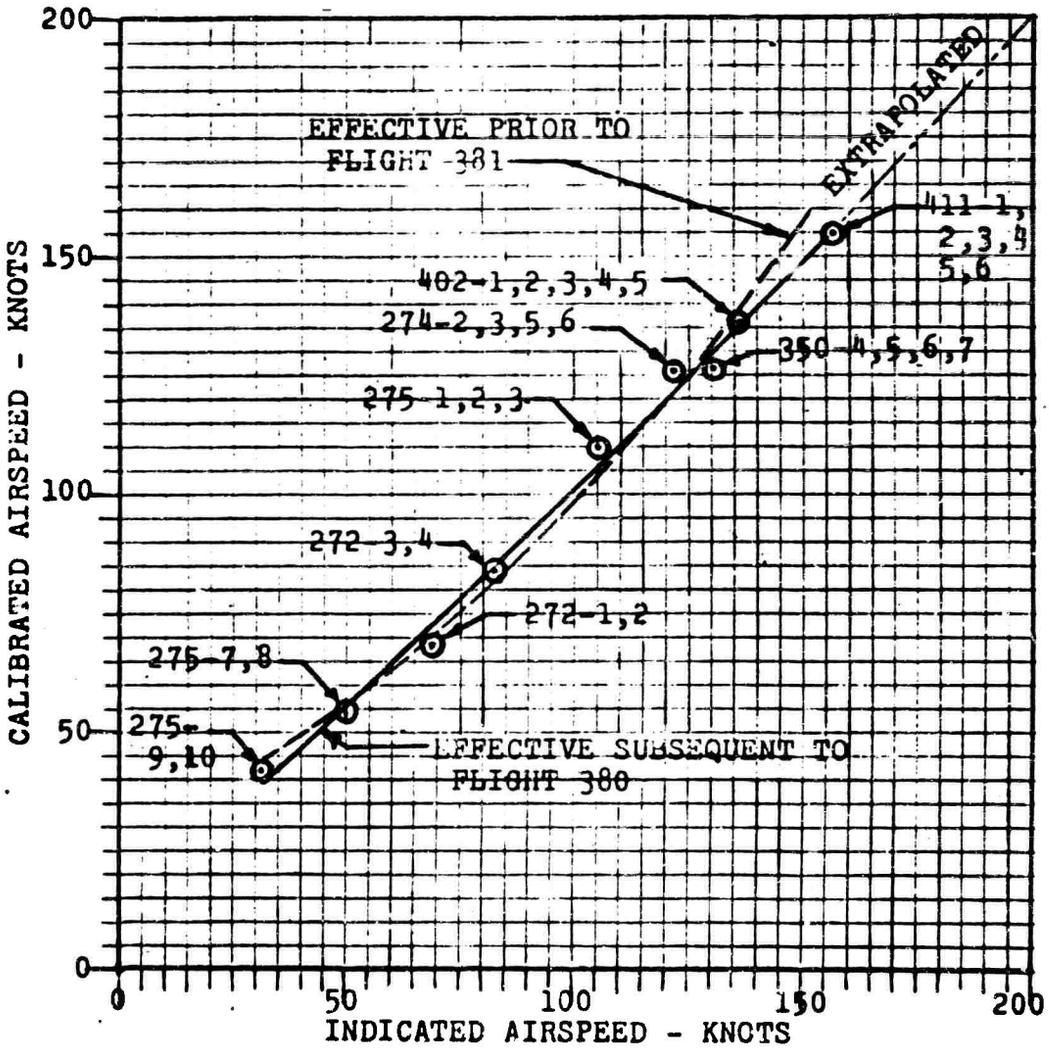


Figure 7. 16H-1A Level Flight Airspeed Calibration.

have been possible. STOL operation was simulated by maintaining reduced collective pitch settings throughout the takeoff run.

Maximum static tail-propeller horsepower within brake holding power was set prior to the start of the takeoff run. After brake release, the pilot increased propeller pitch in order to obtain maximum thrust. The aircraft was allowed to fly off without a takeoff rotation. The collective pitch setting was held constant during the entire takeoff run. This procedure did not permit the minimum takeoff distance capability to be achieved, since utilization of the forward component of rotor thrust could have increased the forward acceleration considerably.

STOL approaches and landings were also performed with a constant collective pitch setting. The propeller pitch was varied to control the rate of descent and was reduced to minimum just prior to touchdown. Longitudinal cyclic control was used to control airspeed, which was maintained at 60 knots during the approach and was then reduced by a flare to 45 knots just prior to touchdown.

## DATA REDUCTION METHODS

All performance data have been reduced to standard sea level (59 degrees Fahrenheit, 29.92 inches of mercury), constant gross weight, and constant rotor RPM. Methods of correction to these standards followed those in Reference 5, and included corrections for pressure altitude, ambient temperature, and airspeed calibration errors. For level flight data, correction in power was made for incidental rate of climb or descent. For constant-power climb data, correction for rate of climb was made for minor variations from standard power.

The specific equations employed in the data reduction program are described below.

For the purpose of computing instantaneous weight for a test blip, the fuel flow during any one flight has been assumed constant from takeoff to landing. Therefore, the vehicle weight for any blip is

$$W = W_{TO} - \left[(n+1)\ \left(\frac{W_f}{n_t+2}\right)\right] \qquad (1)$$

where the fuel comsumption in takeoff and landing portions of the flight has been accounted for in the proportion.

The ambient pressure and density ratios are given as

$$\delta_o = [1-(6.88\,H \times 10^{-6})]^{5.25} \qquad (2a)$$

and

$$\sigma = \delta_o \left[\frac{288}{OAT + 273}\right] \qquad (2b)$$

respectively.

Equation (2a) yields the pressure ratio of the standard atmosphere to better than three significant figures, to higher than 10,000 feet.

Calibrated airspeeed in forward flight is obtained from indicated airspeed as read from the photo panel by means of calibration curves. True airspeed can be calculated as

$$V_{TRUE} = \frac{V_{CAL}}{\sqrt{\sigma}} \qquad (3)$$

Turbine power is calculated directly from engine torquemeter pressure as read from photo panel instrumentation.

$$ESHP = 2.714\ (P_E)\left(\frac{N}{1000}\right) \qquad (4)$$

Rotor and propeller shaft power are determined from oscillograph strain gage instrumentation as

$$RSHP = Q_R \times \frac{N}{21.5 \times 63{,}000} \qquad (5)$$

$$PSHP = \frac{Q_P \times N}{2.22 \times 63{,}000} \qquad (6)$$

where the constants 21.5 and 2.22 are the respective gear ratios between engine and rotor and between engine and propeller.

The following correction is applied to weight to account for ambient air density.

$$W_{STD} = \frac{W}{\sigma} \qquad (7)$$

Rotor and propeller tip speed and thrust and power coefficients are obtained from equations (8) through (12), where the final subscripts R and P refer to rotor and propeller, respectively.

$$V_{T_R} = \frac{\pi R_R N}{30 \times 21.5} \qquad (8)$$

$$V_{T_P} = \frac{\pi R_P N}{30 \times 2.22} \qquad (9)$$

$$C_{T_R} = \frac{W_{STD}}{\rho_o A_R V_{T_R}^2} \qquad (10)$$

$$C_{P_R} = \frac{550\ RSHP}{\rho_o \sigma A_R V_{T_R}^3} \qquad (11)$$

$$C_{P_P} = \frac{550\ PSHP}{\rho_o \sigma A_P V_{T_P}^3} \qquad (12)$$

## Mechanical Efficiency

Turbine shaft torque, rotor shaft torque, and propeller shaft torque were all measured independently by three separate torquemeters. Thus, ESHP, RSHP, and PSHP, computed from equations (4), (5), and (6), respectively, represent independent determinations of these quantities. The mechanical losses in the drive system can be ascribed to three separate sources: (1) accessories, such as pumps, generator, and oil-cooler fan, which are relatively constant; (2) losses in the transmission system between turbine and propeller shaft, which are a function of propeller power; and (3) losses in the transmission system between turbine and rotor, which are a function of rotor power. Functions (2) and (3) are not the same, since different gear trains are involved. Hence, the overall losses depend not only upon the total useful power but also upon its distribution. Accordingly, plots were made of efficiency versus combined power (rotor plus propeller), for different ratios of rotor power to combined power, from measurements taken during the various types of steady-state flight (hover, vertical climb, forward climb, level flight). These plots are shown in Figure 8: (a, b, c, d) and a summary of all four is shown in Figure 8 (e).

In the presentation of final curves for hover, vertical climb, and level flight, rotor power and propeller power are derived from their respective plotted power coefficients.

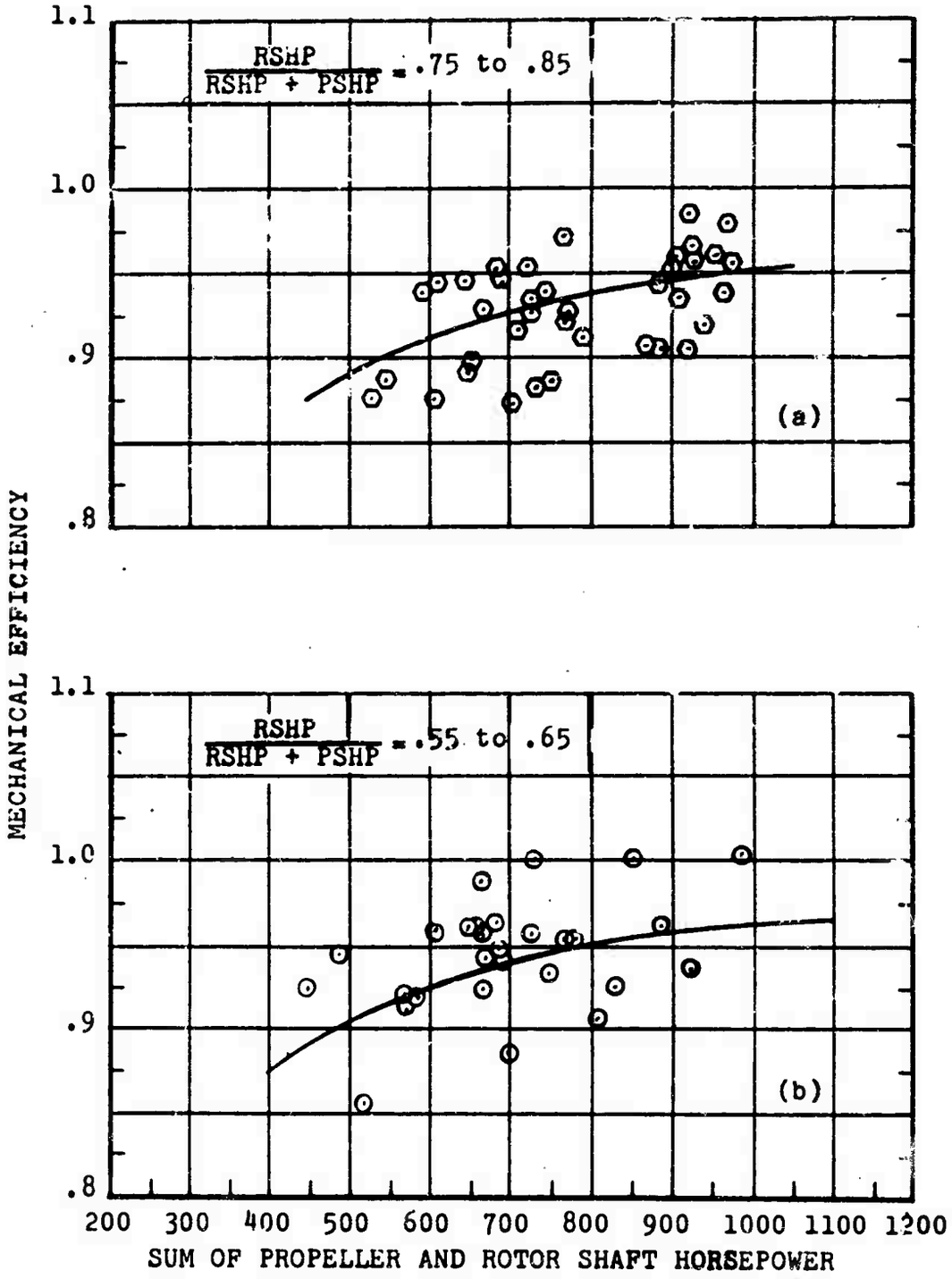


Figure 8. Mechanical Efficiency of Drive System versus Combined Rotor and Propeller Power for Given Ratios of Rotor Power to Combined Power.

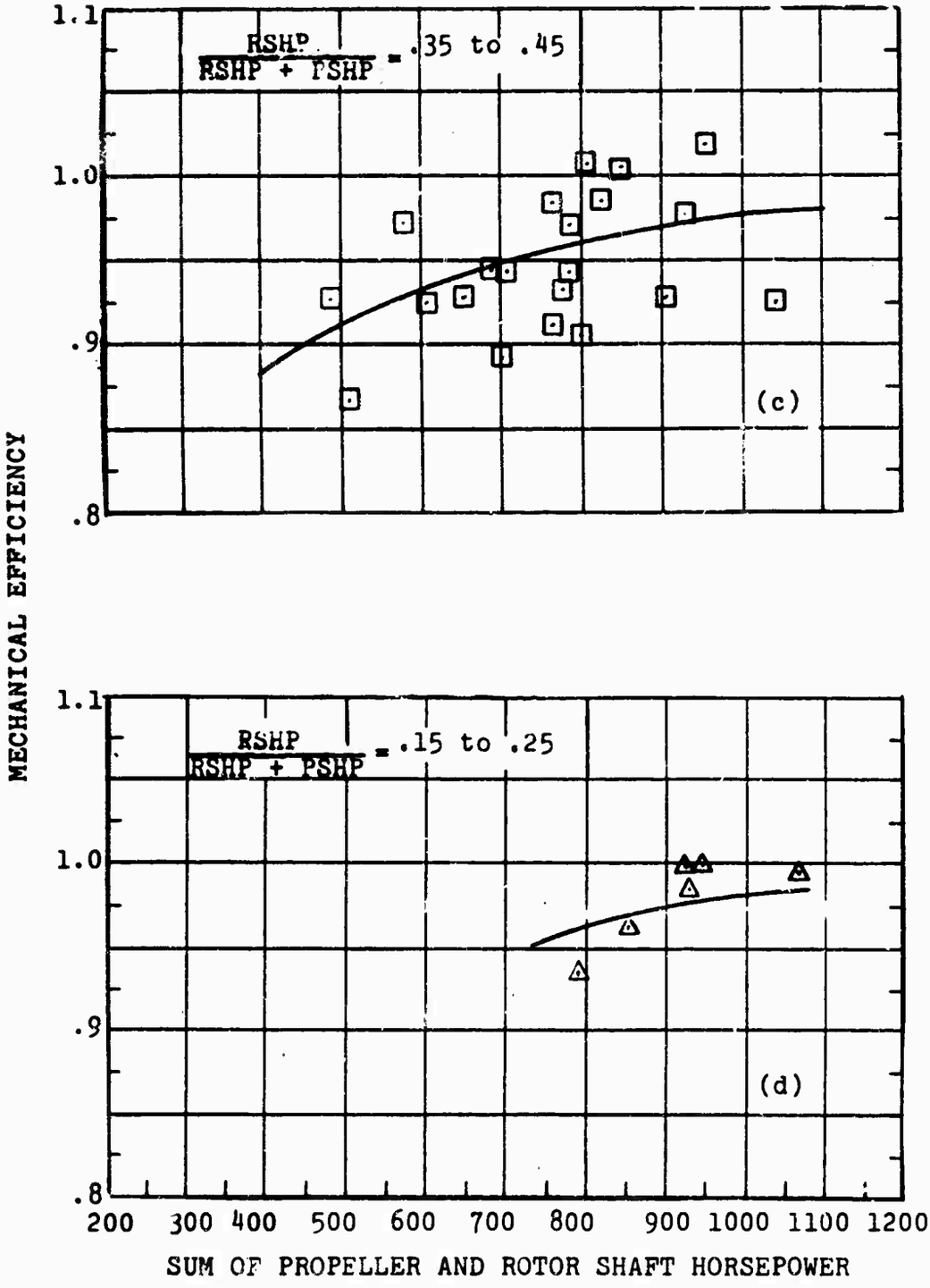


Figure 8. Continued.

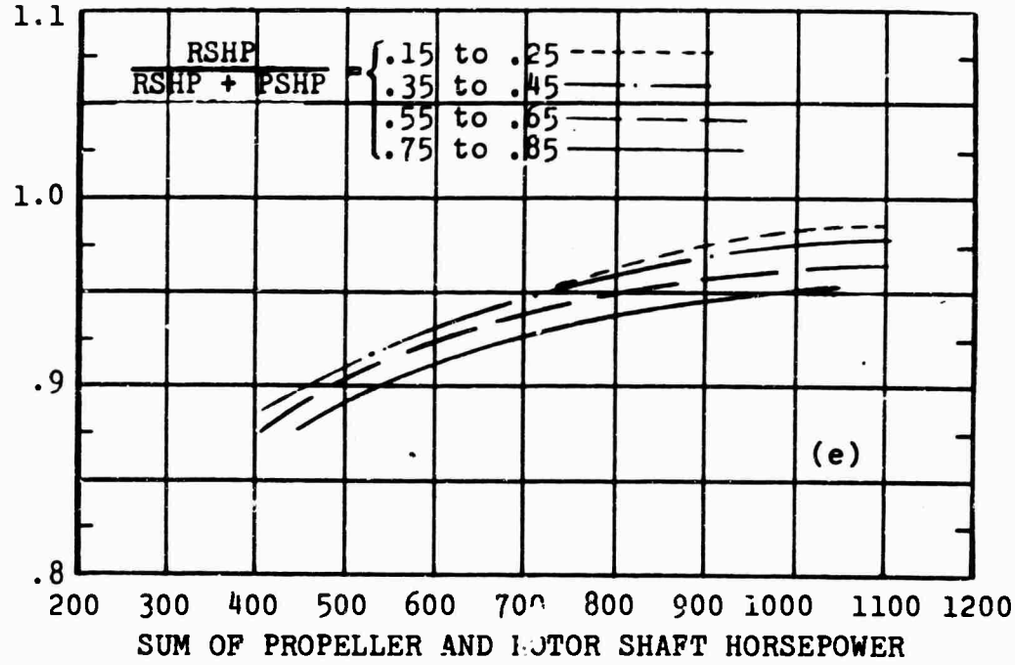


NOTE: See Table II for list of Flight and Blip numbers plotted in this figure.

Figure 8.-Continued.

Turbine power is derived from the appropriate combination of rotor and propeller power, using the efficiencies of Figure 8.

TABLE II. FLIGHT AND BLIP NUMBERS FOR DATA USED IN MECHANICAL EFFICIENCY CURVES (FIGURE 8)

| FLIGHT | BLIPS | FLIGHT | BLIPS | FLIGHT | BLIPS |
|---|---|---|---|---|---|
| 255 | 5 | 296 | 2 | 350 | 4,6,8 |
| 257 | 6 | 301 | 1,2 | 355 | 7 |
| 259 | 2 | 302 | 4 | 357 | 1,2 |
| 261 | 5,8 | 304 | 2,3 | 399 | 6 |
| 264 | 1,2,3,4, 7,10,11, 15,16,18, 19 | 305 | 1 | 401 | 1,4,6,7 |
| | | 306 | 5,6 | 402 | 2,3 |
| | | 307 | 2 | 408 | 5,6 |
| | | 308 | 1,6 | 409 | 2 |
| 274 | 1,2,7 | 309 | 5 | 412 | 1,2,3,5, 8 |
| 290 | 1,2,3,7, 9 | 317 | 2,5,6,9, 10 | 413 | 2 |
| 291 | 3 | 332 | 2,3 | 416 | 3,7 |
| 292 | 4,6,7,8, 11 | 333 | 1 | 420 | 7,8,9 |
| | | 337 | 3,4 | 421 | 2,3 |
| 295 | 2,4,7,9 | 344 | 3,4,7,8, 9,10 | 423 | 1 |
| | | | | 438 | 1,2,3 |

The following methods employed in the data reduction program are presented with reference to the applicable flight maneuver.

## Level Flight

Having derived the power components (ESHP, RSHP, PSHP) as a function of gross weight and speed, the horsepower correction due to an incidental rate of climb is

$$\Delta SHP_{(R/C)} = - \frac{V_{C_{STD}} \left( W_{STD} \right)}{33{,}000 \times \eta} \qquad (13)$$

With the exception of three blips at speeds in excess of 175 knots, which were in dives (10 degrees maximum), the mean rate of climb (absolute value) for all other blips used for plotting was ±150 feet per minute, so that this correction was normally quite small, of the order of 35 horsepower.

Except for the three blips just mentioned, the corrected powers are

$$ESHP = ESHP + \Delta SHP_{(R/C)} \tag{14}$$

$$RSHP = \left(\frac{RSHP}{ESHP}\right) ESHP \tag{15}$$

$$PSHP = \left(\frac{PSHP}{ESHP}\right) ESHP \tag{16}$$

For the three exceptional blips, the departure of the flight path from horizontal was considered sufficiently large (up to 10 degrees) that the power distribution would be significantly distorted by the corrections of equations (15) and (16). Since the primary effect in these cases was for gravity to produce a component of propulsive force along the flight path, the corrections were applied as

$$\Delta RSHP = \Delta ESHP \sin^2 \gamma \tag{17}$$

and

$$\Delta PSHP = \Delta ESHP \cos^2 \gamma \tag{18}$$

when

$\gamma$ = flight path angle to horizontal (positive downward)

$$= \sin^{-1} \frac{V_{C_{OBS}}}{1.69 \times 60\ V_{TRUE}} \tag{19}$$

Power coefficients for the rotor and propeller are then calculated from equations (11) and (12).

In order to present engine fuel flow performance the following corrections have been applied to the data.

Calibrated airspeed becomes

$$V_{CORR} = \frac{V_{CAL}}{\sqrt{\delta_o}} \tag{20}$$

from which Mach number is determined:

$$M = \frac{V_{CORR}}{49.0\ \sqrt{1.8(OAT) + 492}} \tag{21}$$

The ram temperature and pressure are calculated as

$$T_{t_2}/T_2 = 1 + .2M^2 \tag{22}$$

and

$$P_{t_2}/P_2 = (T_{t_2}\ T_2)^{3.5} \tag{23}$$

The overall engine pressure ratio is

$$P_{t_2}/P_{s_6} = P_{t_2}/P_2\ (1-L_i)(1-L_e) \tag{24}$$

The pressure and temperature ratios at the compressor inlet are

$$\delta_2 = \delta_o\ (1-L_1) \tag{25}$$

$$\theta_2 = \left(\frac{278+OAT}{288}\right)\theta_{RAM}$$

Specific heat corrections to shaft horsepower and fuel flow are included and arise due to variations in compressor inlet total temperature

$$T_2 = 288\ \theta_2 - 273 \tag{26}$$

The correction factors are

$$K_W = .001025\ T_2 + 0.986 \tag{27}$$

and

$$K_P = .99 + 7.5 \times 10^{-4}\ T_2 \tag{28}$$

Finally we obtain corrected fuel flow:

$$W_{f_{CORR}} = \frac{W_f}{K_W \delta_2 \sqrt{\theta_2}} \tag{29}$$

and corrected engine shaft power as:

$$ESHP_{CORR} = \frac{ESHP}{K_P \delta_2 \sqrt{\theta_2}} \tag{30}$$

Forward Climb

Test data reduction involves corrections to rate of climb due to variations from programmed power level. Data are presented at a constant altitude - sea level standard.

The increment due to variation in power level is

$$\Delta V_C = \frac{33{,}000(1050 - \frac{ESHP}{\sqrt{\sigma}})\eta}{W_{REF}} \tag{31}$$

where 1050 represents sea-level normal rated power.

Then referred rate of climb is

$$V_{C_{REF}} = \frac{V_C}{\sqrt{\sigma}} + \Delta V_C \tag{32}$$

Hover

$W_{STD}$, RSHP, and PSHP were computed by means of equations (7), (5), and (6). $C_P$ and $C_T$ for the rotor were obtained by using equations (11) and (13), and $C_P$ was plotted against $(C_T)^{3/2}$ (Figure 11). A straight line, which is the proper functional relationship according to momentum theory, was then fitted to the data points. The plots of rotor horsepower versus gross weight (Figures 9 and 10) for standard sea level were then constructed from these $C_P$ - $C_T$ plots.

The tail propeller thrust ($T_{PROP}$) in hover is directly proportional to rotor torque, and it is easily shown that the tail propeller thrust coefficient $C_T$ is proportional to the rotor power coefficient $C_{P_R}$.

$$T_{PROP} = K_1 Q_R$$

Where $K_1$ is a constant determined by aircraft geometry.

$$T_{PROP} = K_1 \frac{550RSHP}{V_T} \times R \tag{33}$$

Substituting the expressions for $T_{PROP}$ and RSHP in terms of their coefficients in equation (33), we obtain

$$C_{T_P} \rho A_{PROP} V_{T^2} = K_1 \times 550 \frac{C_{P_R} \rho A_{ROTOR} V_{T^3} R}{V_T} \quad (34)$$

$$C_{T_P} = C_{P_R} \left[ K_1 \times 550 \times R\left(\frac{A_{ROTOR}}{A_{PROP}}\right) \left(\frac{V_T}{V_{T_P}}\right)^2 \right] \quad (35)$$

All quantities within the square brackets are constant. Hence,

$$C_{T_P} = K_2 C_{P_R} \quad (36)$$

From momentum theory, a linear relationship exists between $C_{P_P}$ and $(C_{T_P})^{3/2}$, and hence also between $C_{P_P}$ and $(C_{P_R})^{3/2}$. The tail propeller data points were plotted in this manner, and the faired straight line was then used to construct propeller power versus gross weight (Figure 12).

## PERFORMANCE AND POWER DISTRIBUTION

### HOVER

Power required is plotted against gross weight in ground effect (Figure 9) and out of ground effect (Figure 10). These figures show the total turbine power required, as well as the components of rotor and propeller power. Rotor and propeller power were derived from the faired lines of Figures 11 and 12, respectively. Shown for reference on Figure 11 are flight test results (per rotor) on an H-21B and an H-21C helicopter obtained from data in References 6 and 3, respectively. The power was measured in the tests of References 6 and 3 by reading, in the cockpit, manifold pressure and RPM and by obtaining engine brake horsepower from engine performance curves corrected for ambient temperature and pressure. The 16H-1A rotor power was obtained from torque measurements at the rotor shaft. Considering these different measurement techniques, the rotor power measured on the 16H-1A is in good agreement with the H-21 data (in general within 3 percent).

An attempt was made to find trends in power required as affected by elevator trim. The points show no distinguishable trend, however, and only a single set of curves has been drawn through the points in Figures 11 and 12. Note that Figure 12 (propeller power coefficient) shows points obtained in vertical climb as well as hover. Since the propeller is operating in essentially the same environment during vertical climb, the points fall on the same curve, except for a bit more scatter, which is probably attributable to the difficulty of maintaining zero airspeed during a protracted climb.

Propeller power in hover is used to generate side force for antitorque and for yaw control. Figure 13 shows how the power required for antitorque varies with rudder-vane angle. As expected, the power and propeller pitch decrease with increasing vane deflection. For maximum hover performance, pilot technique was to hold full left rudder pedal and make minor yaw corrections by means of the propeller-pitch-control beep switch located on the collective pitch handle. For normal operation, however, the technique was to use enough propeller pitch to provide at least a 1-inch margin of left pedal, which was equivalent to 34 degrees of vane deflection. In a side wind, when power is not a limiting factor, more propeller pitch and less left rudder can be used for antitorque, leaving more left rudder available for yaw control.

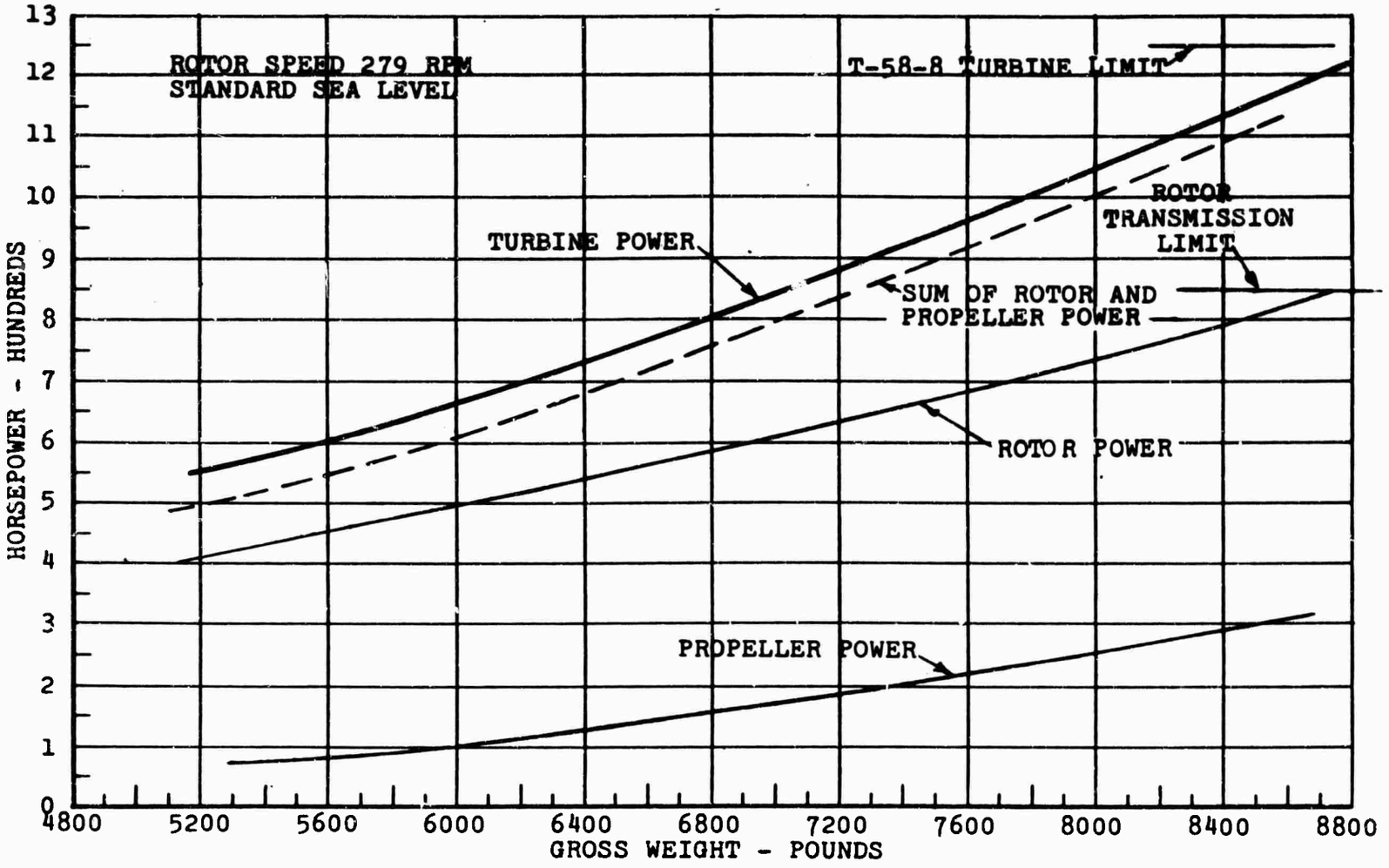


Figure 9. Hover Power versus Gross Weight, in Ground Effect.

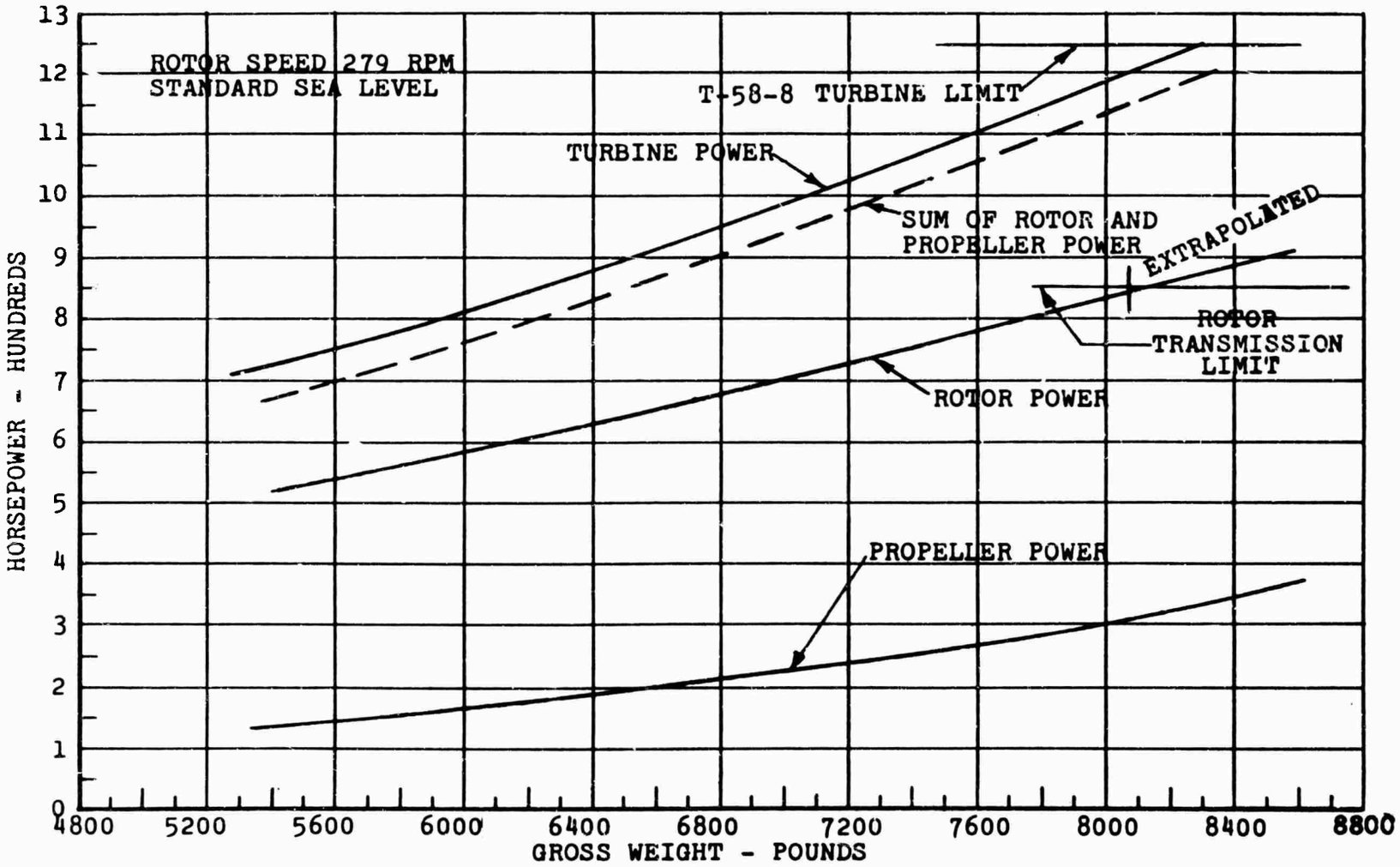


Figure 10. Hover Power versus Gross Weight, out of Ground Effect.

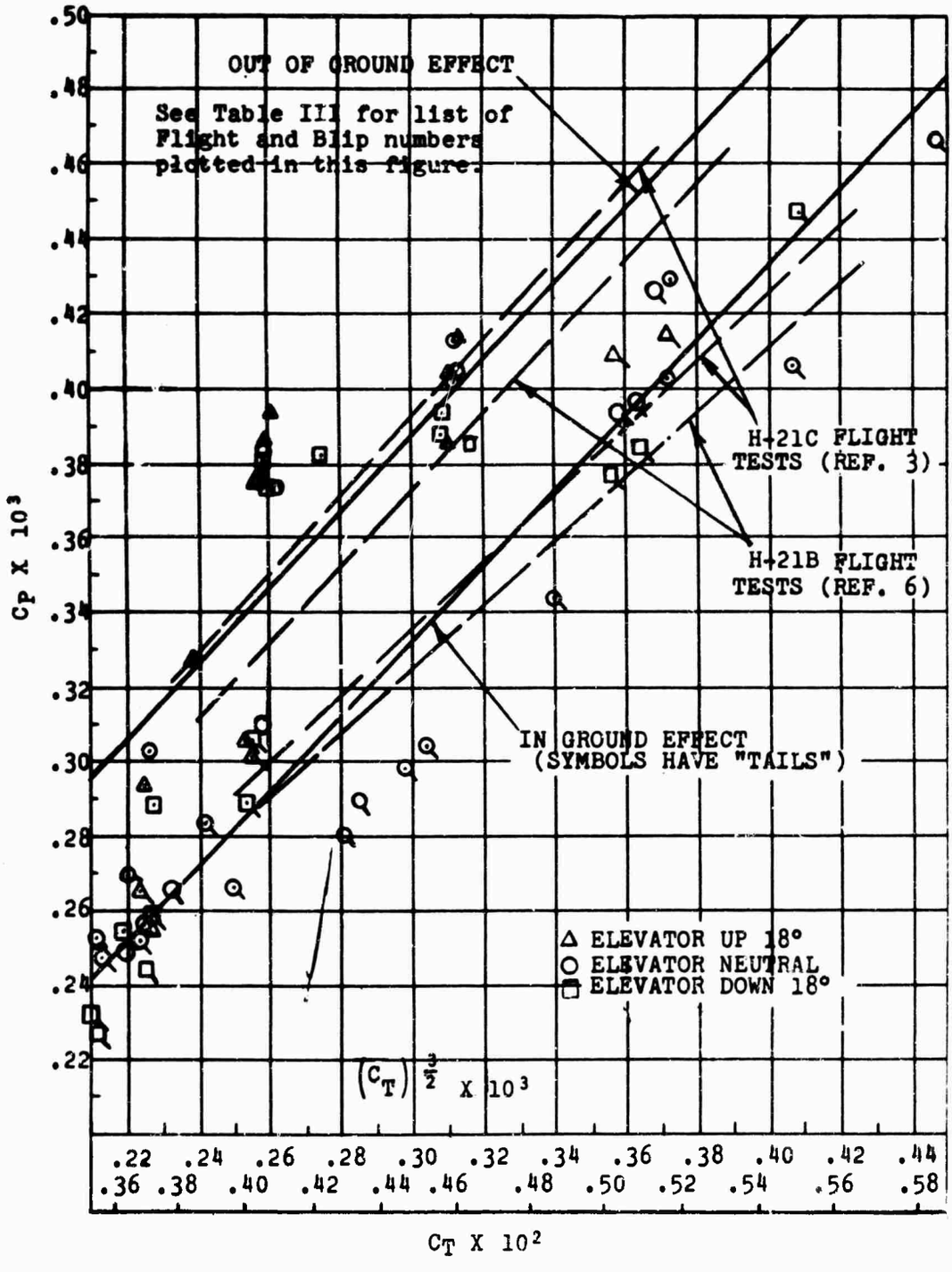


Figure 11. Rotor Hover Performance, $C_P$ versus $C_T$.

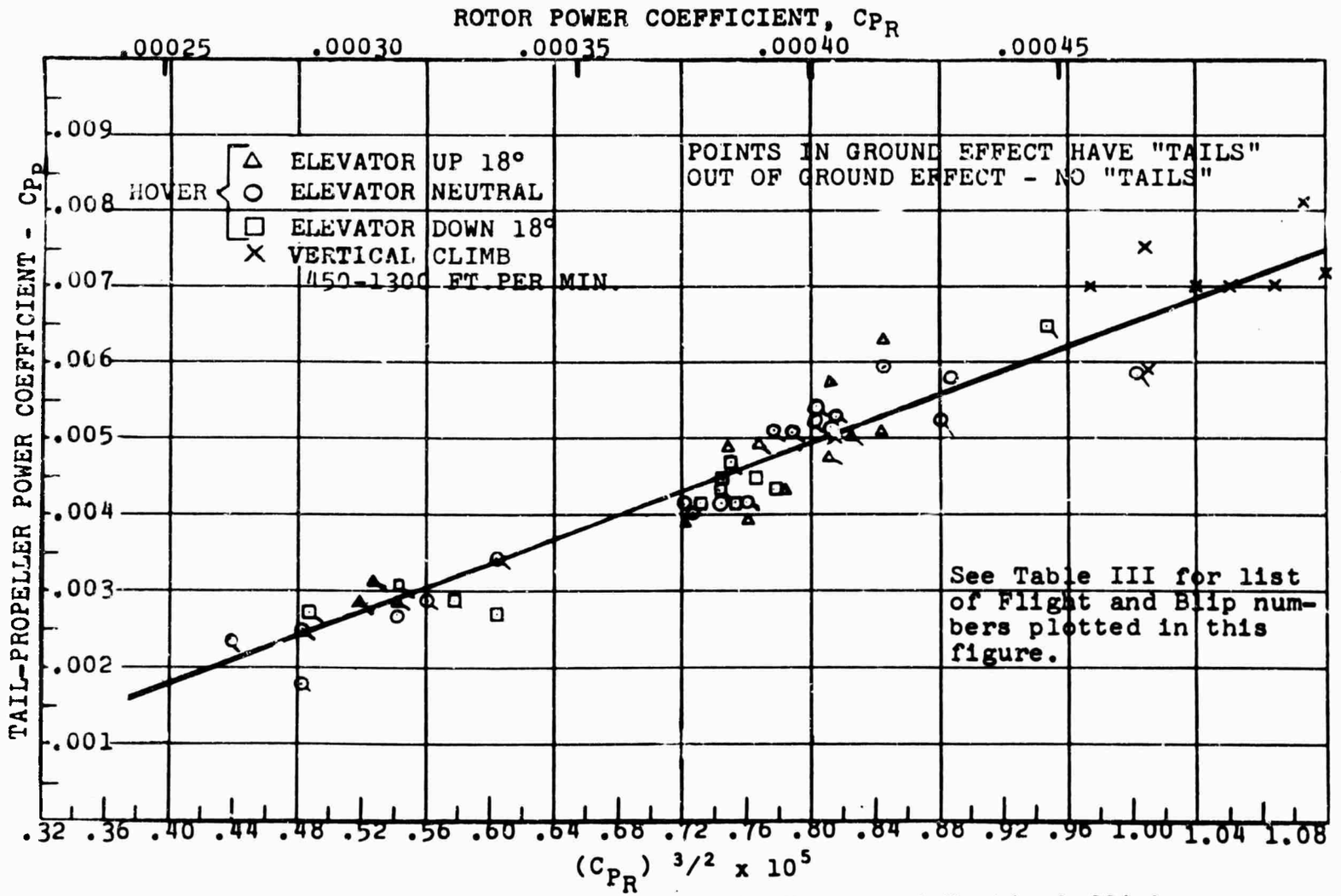


Figure 12. Tail Propeller Performance in Hover and Vertical Climb- Propeller Power Coefficient versus Rotor Power Coefficient.

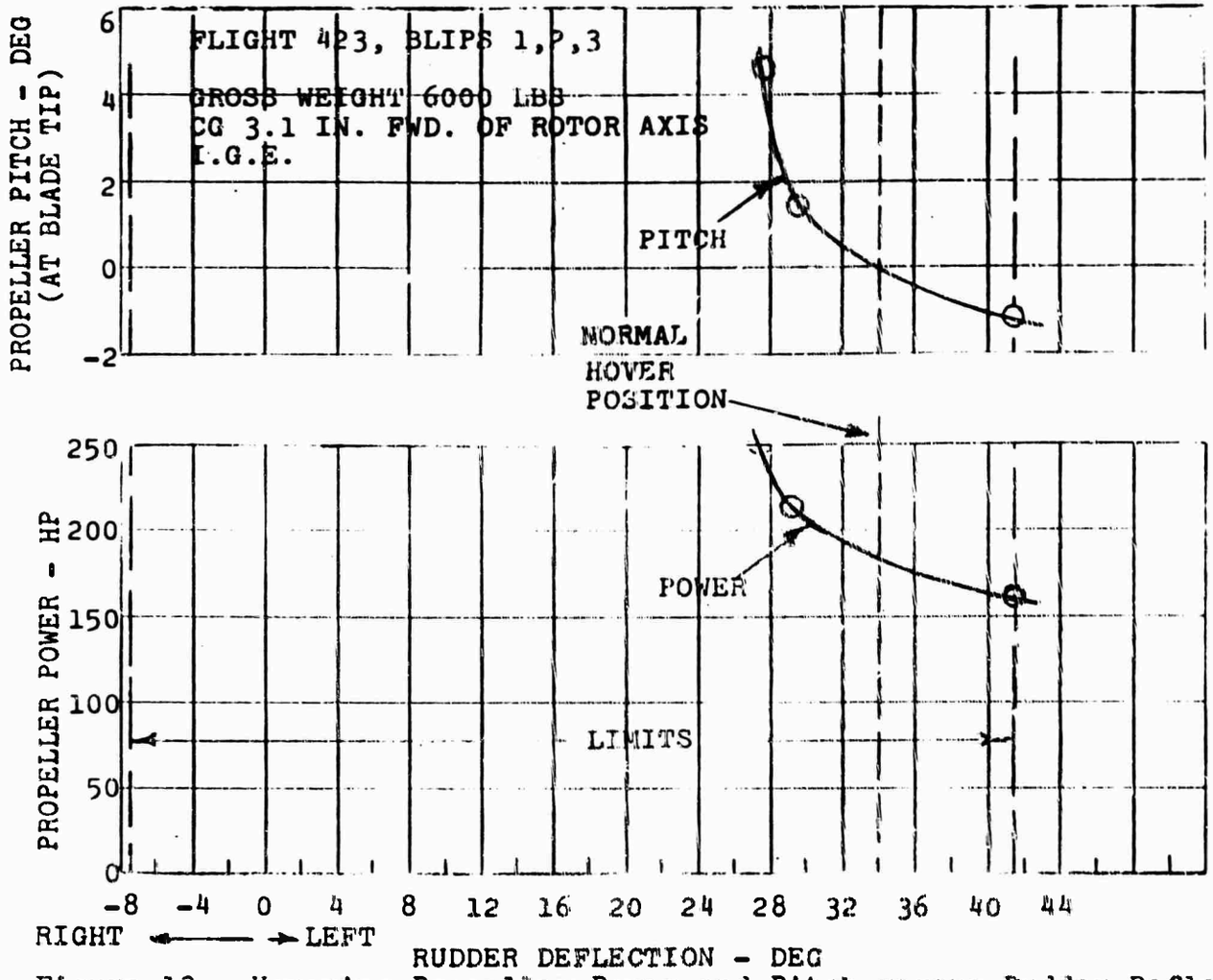


Figure 13. Hovering Propeller Power and Pitch versus Rudder Deflection.

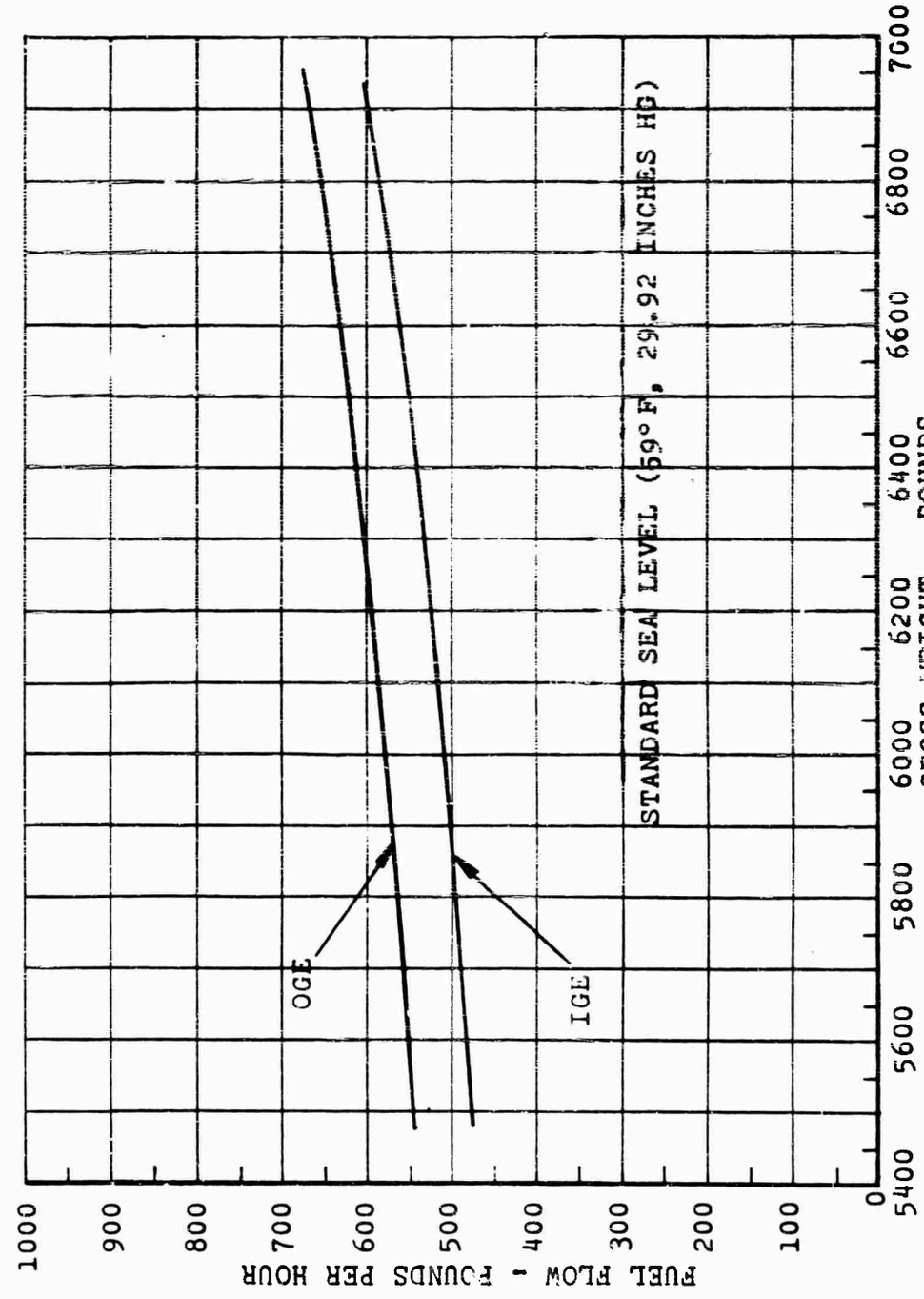


Figure 14. Fuel Flow vs Gross Weight in Hover, In Ground Effect and out of Ground Effect.

Turbine power in Figures 9 and 10 is derived from the combined faired curves of rotor and propeller power (shown as dotted lines in Figures 9 and 10), corrected for mechanical losses as explained under "Data Reduction Methods".

Throughout the range of gross weights tested, 5200 to 8800 pounds referred weight (referred to sea level, 59 degrees Fahrenheit, and standard rotor speed; actual weight range was 5700 to 7500 pounds), tail propeller power increased gradually from 12 percent to 25 percent of total power required. This is in good agreement with the results obtained in measurements of power and side force during the ground test phase of the program. The balanced power requirements of the 16H-1A configuration are such that the installed power as determined by high-speed requirements also provides ample power for hovering, including the power requirements of the ring-tail.

## SIDEWARD AND REARWARD FLIGHT

Several factors influenced the scatter of the points presented. As the program progressed, pilot technique and ability to manage the aircraft necessarily improved. In an effort to compensate for this built-in error, certain points were deleted after research showed that a different technique was used. For example, all points used in right sideward flight were taken while the pilot used the technique of applying full left rudder, then causing the aircraft to translate by applying cyclic and collective as required while keeping the aircraft directionally oriented by varying propeller pitch. Within limits, the same maneuver could have been carried out by hovering at a higher propeller pitch setting, and then, while translating sideward, by varying rudder and/or propeller pitch to keep the aircraft directionally oriented.

In performing these maneuvers in ground effect, the aircraft was generally flown with the wheels 7 to 12 feet off the ground. The rotor disc was thus almost 1/2 rotor diameter from the ground. In hovering, this would mean that approximately 10 percent less power would be needed to lift the aircraft; but as the aircraft begins to translate sideward, much of this ground effect is lost. The resulting difference between the points taken on flights in ground effect and out of ground effect was so slight that they fell within the scatter for the test series.

As can be seen from the photographs, even the in-ground-effect flights were conducted at an altitude at which ground effect was considerably diminished. For this reason, out-

of-ground effect data are difficult to differentiate from in-ground-effect data.

Maneuvering close to the ground is not a situation which lends itself to long blips of stabilized flight conditions, and it was thus a source of error. Some error also comes from the method used to determine the lateral speed of the aircraft. Although the best means available and the method specified in the contract were used, the data would have been improved if speeds could have been more accurately ascertained.

Power versus airspeed in sideward flight is shown in Figure 15. Although data points were considerably scattered, the data presented are believed to reflect the actual power condition (considering the number of variables implicit in the data). Rotor- and propeller-power curves are faired through the measured points. Turbine power is constructed from the combined rotor and propeller power, corrected for mechanical losses as explained under "Data Reduction Methods". The points for zero speed are taken from the hover curves, Figures 9 and 10. Less power is required for flying to the left than to the right, because of the increased tail propeller power needed to fly to the right while deflecting air to the left. The trend of the points indicates that the most power is required at about 18 knots to the right, with power required dropping as the speed changes from this value.

The rotor power required decreases with speed, at an increasing rate, up to 30 knots in each direction. The small difference in rotor power between flight to the left and to the right may be attributable to the fact that the plane of the rotor is at a greater angle in flight to the left, and/or that the aircraft is rolled more in flight to the left than in flight to the right. The reason for the greater rotor angle in flight to the left is that the rotor must overcome the side component of thrust from the tail propeller.

Tail propeller power required increases at an increasing rate from a minimum at about 20 knots to the left. It becomes linear passing through the hover point and increases at a constant rate to 30 knots to the right. As speed to the left increases, less tail propeller power is needed because it is augmented by the directional stability of the aircraft (see Figure 16, showing rudder vane deflection in sideward flight).

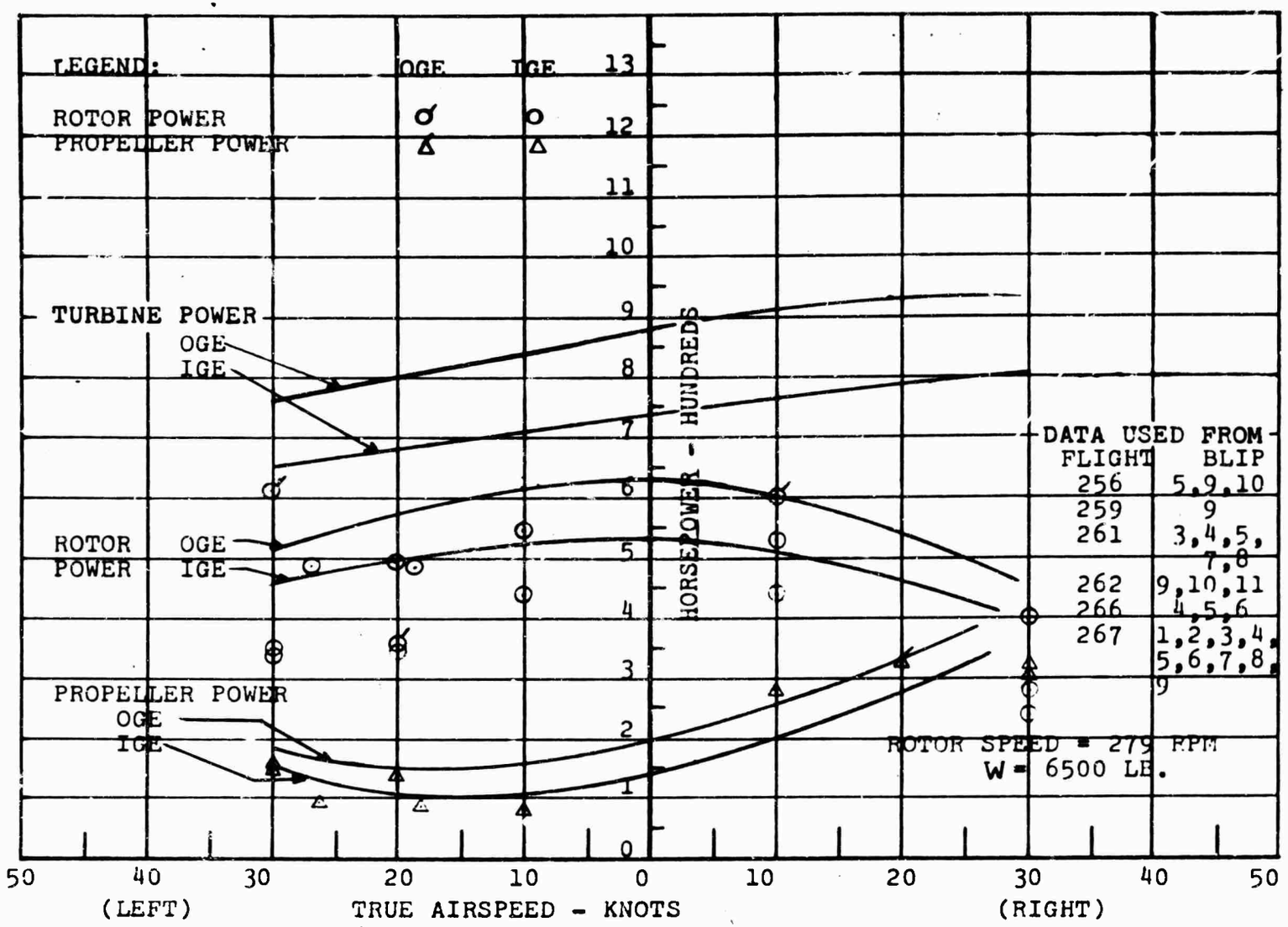


Figure 15. Power versus Airspeed, Sideward Flight.

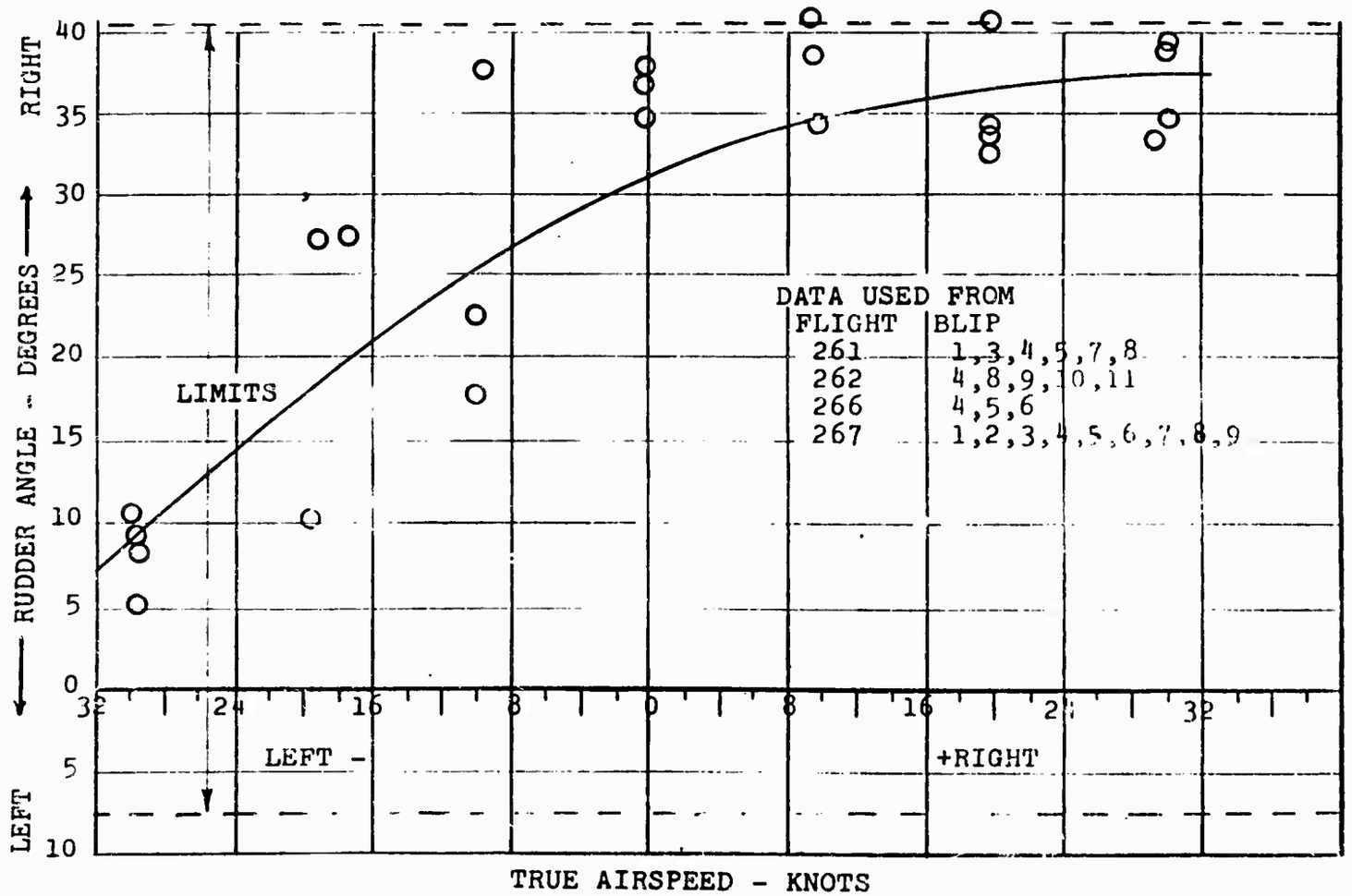


Figure 16. Rudder Position versus Speed, Sideward Flight.

Power versus airspeed in rearward flight is shown in Figure 17. Because of the inherent danger implicit in flying rapidly backward close to the ground, the in-ground-effect rearward flights were flown at an altitude of about 15 feet, rather than 5 to 7 feet as in the hover tests. Since some ground effect tends to be lost in translational flight, in any case, the resulting data are such that in ground effect cannot be effectively differentiated from out of ground effect, and only one set of curves is drawn. Rotor power decreases with increasing rearward flight speed within the range tested, as it does in forward or sideward flight. Propeller power increases, however, since the propeller efficiency itself is reduced by the reverse flow.

Figure 18 shows that, since the rudder vanes are less effective in rearward flight, more deflection is required. When full deflection was reached, further increase in rearward speed required increased propeller pitch.

## FORWARD-SPEED CLIMB

Rate of climb versus airspeed is shown in Figure 19. The curves were not extrapolated beyond the region of measured data, and where curves were faired through less than five points, they were drawn substantially parallel to curves faired through five or more points.

The data presented at constant altitude (sea level standard), power, gross weight, and rotor speed exhibit the usual trends with forward speed. That is, rate of climb increased to a maximum recorded value of 2300 feet per minute for the flaps-up configuration at 80 knots and then decreased with further increase in airspeed. Power used in these tests was 1050 horsepower, the normal rating of the turbine. No tests were made at military power (1250 horsepower).

Of primary importance is the effect of aircraft attitude at a given forward speed during the climb maneuver. By varying the rotor shaft attitude (relative to vertical) from approximately -4 to +10 degrees (flaps up), the fuselage angle of attack varied from approximately -5 to -15 degrees (relative to the flight path). The highly negative angle of attack is indicative of the helicopter flight technique (nose down).

Since the pilot had no presentation of angle of attack, this information became available only after the data were reduced. As a result, some of the angles of attack were obtained through only a limited speed range. There is,

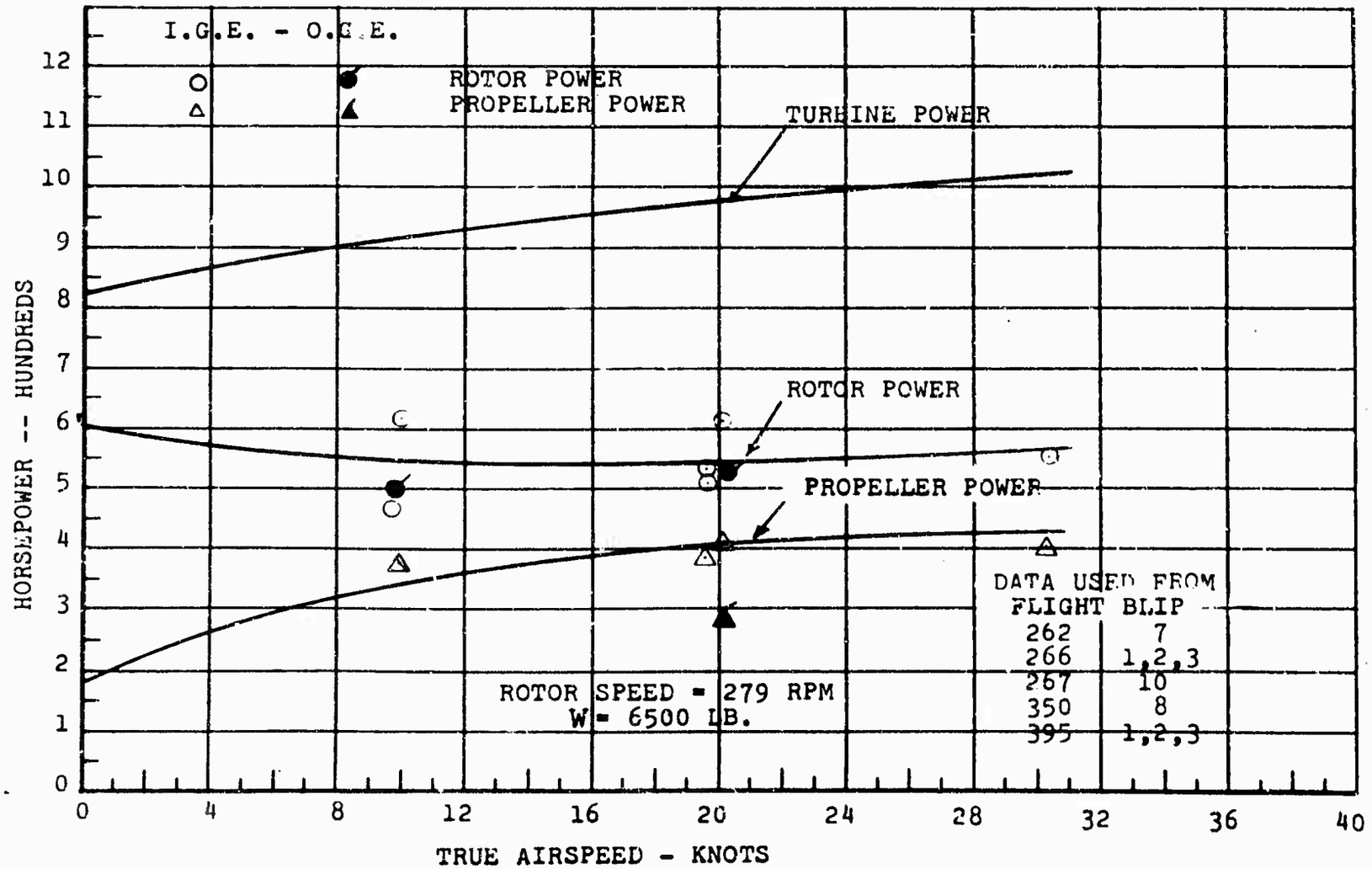


**Figure 17. Power versus Airspeed, Rearward Flight.**

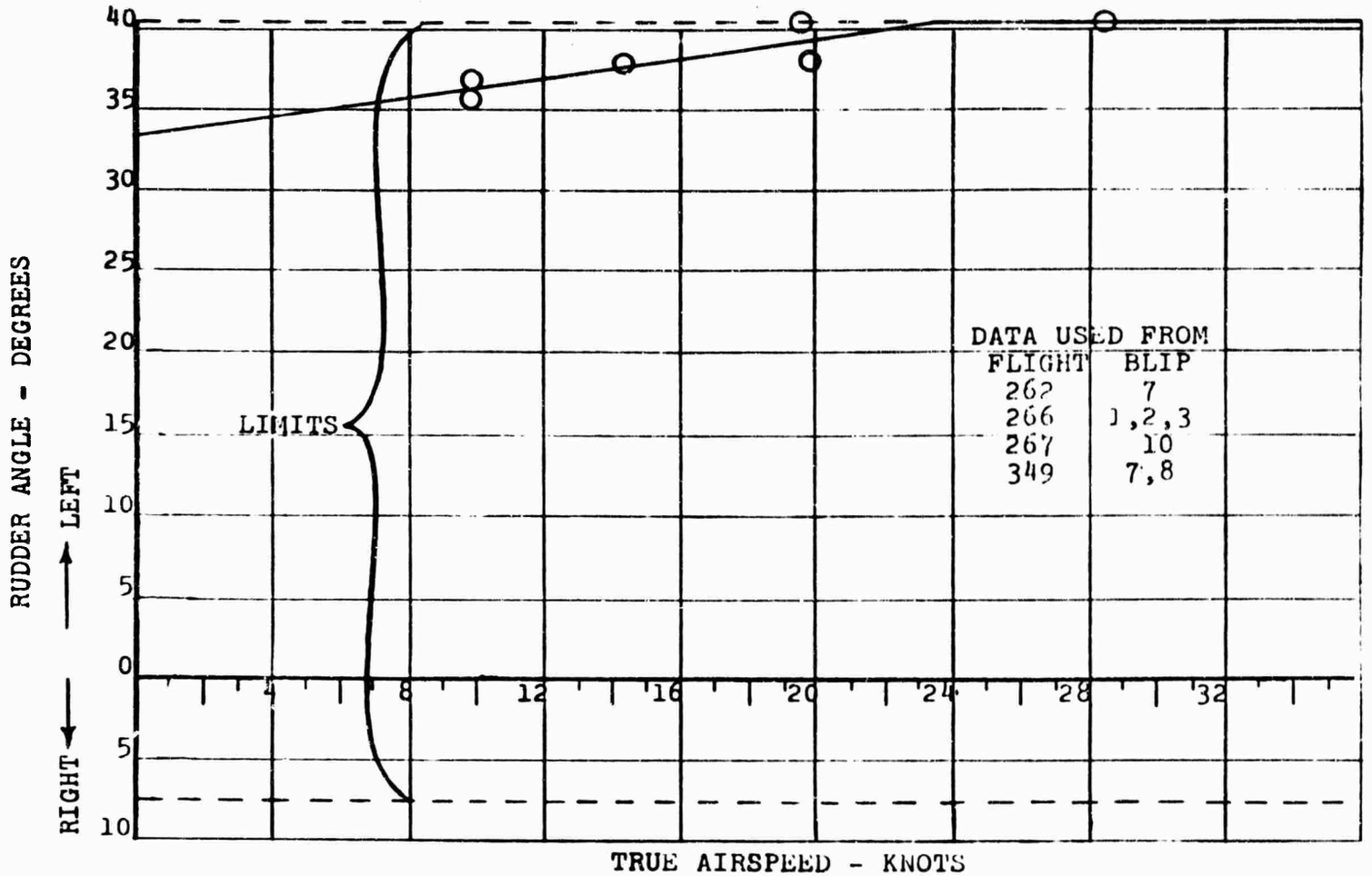


**Figure 18. Rudder Position versus Speed, Rearward Flight.**

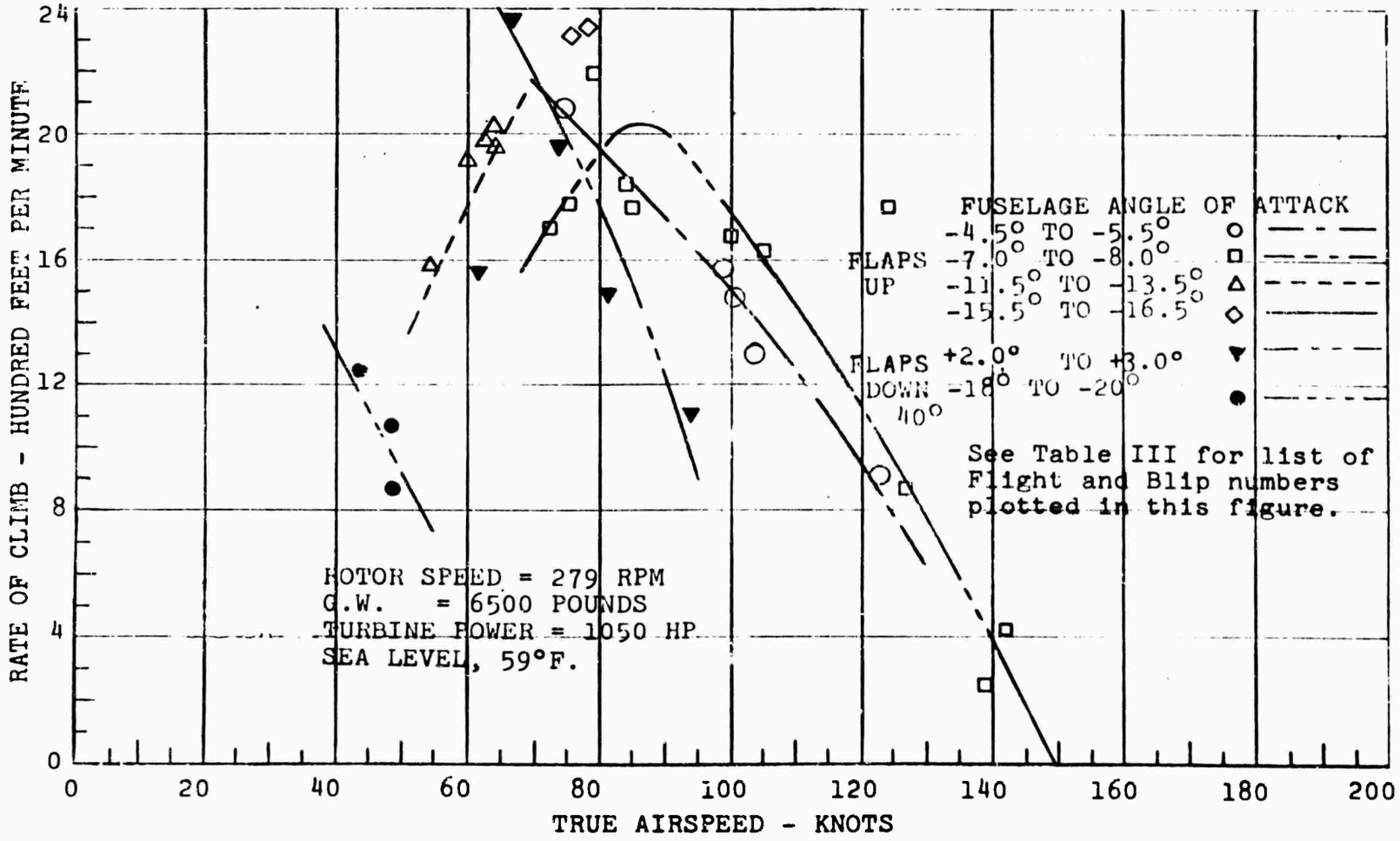


Figure 19. Rate of Climb versus Speed.

however, an indication that the helicopter technique of climb is superior at speeds below 80 knots. On the other hand, tests with flaps full down (40 degrees) and a fuselage angle of attack of about +3 degrees resulted in the highest rate of climb obtained (2380 feet per minute at 67 knots.)

Rotor and wing lift in climb are shown in Figure 20. As mentioned above, the climbs were performed primarily by the helicopter technique. As a result, the wing lift in climb is negative. Figure 20 shows that the effect of the flaps is to reduce the negative wing load, but that angle of attack has little effect (probably because the rotor downwash is the dominant influence).

AUTOROTATION

Data were obtained from steady autorotation descents from 49 to 104 knots with flaps up and from 47 to 102 knots with flaps down 40 degrees. Landing gear was extended in all cases. "Throttle chops" were conducted at speeds up to 139 knots, but the airspeed slowed so rapidly from the higher speeds that it was reduced below 110 knots by the time the needles split and steady autorotation had occurred. Figure 21 shows the results of the steady autorotation tests in the form of rate of descent versus airspeed at constant gross weight and rotor speed. Lowest rate of descent recorded was with flaps up, and was 1340 feet per minute at 58 knots. The rate of descent increased with speed until it was approximately 3200 feet per minute at 104 knots. The data do not yield a clear minimum point because the photo panel malfunctioned during several trials, but from pilot reports, the minimum appears to be between 50 and 60 knots. The flaps-down rate-of-descent curve is displaced from the flaps-up curve, indicating, as expected, that the aircraft lift/drag ratio is lower in the flaps-down configuration.

The rate-of-descent data were all obtained at minimum propeller pitch. An initial objective was to obtain additional data with propeller pitch increased 5 degrees. It was found, however, that the rotor speed could not be maintained at or near the test value with a 5-degree increase in pitch. The stabilized rotor speed at the higher propeller pitch setting could not be determined because of the engine governor limitations described in the next paragraph.

Time histories of sudden and complete loss of power could not be obtained because of the action of the turbine fuel control system, which is discussed under "Technical Problems". However, time histories within the operation limitations of the turbine governor were obtained. Figure 23

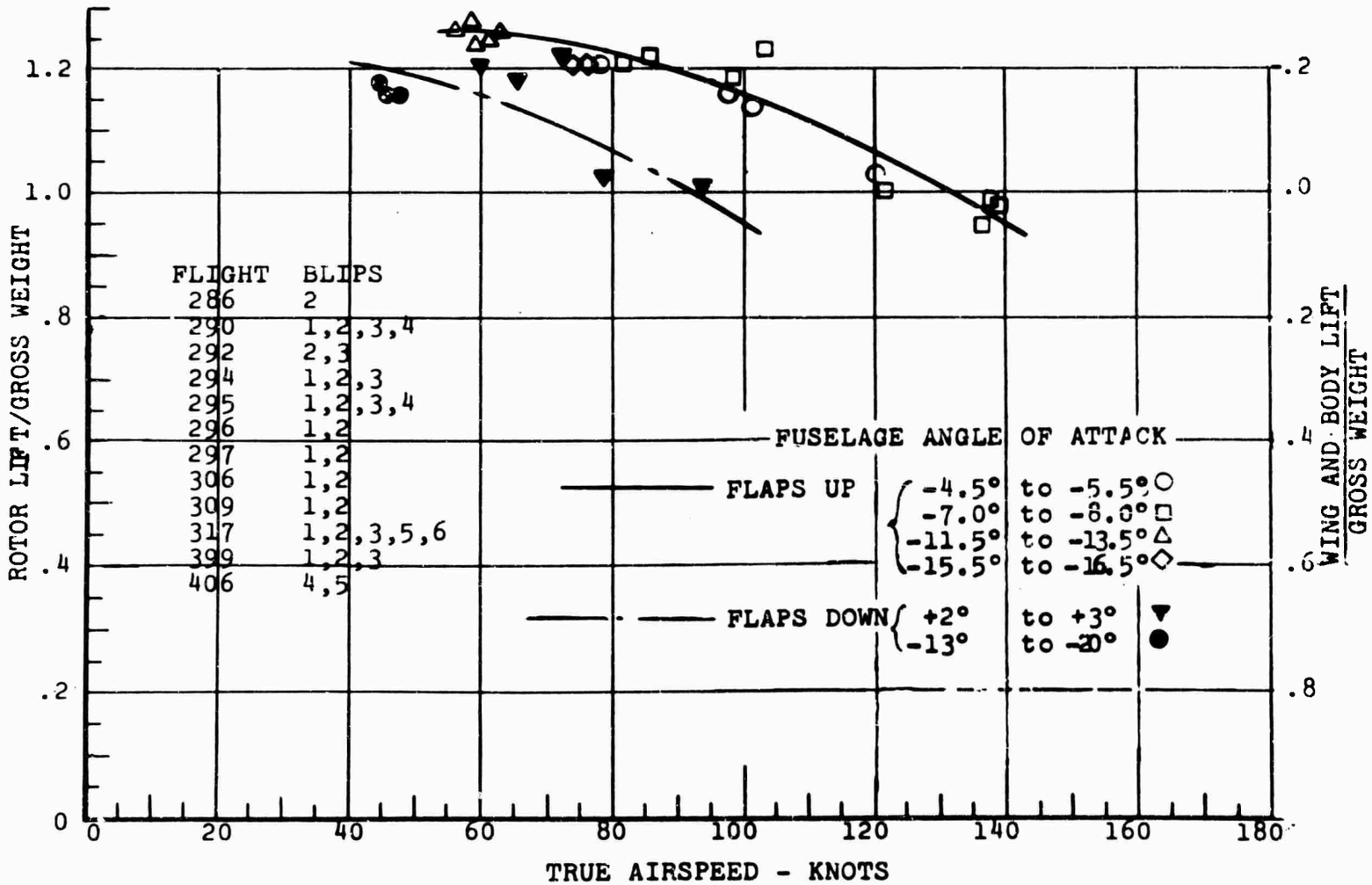


Figure 20. Rotor/Wing Lift Distribution in Climb.

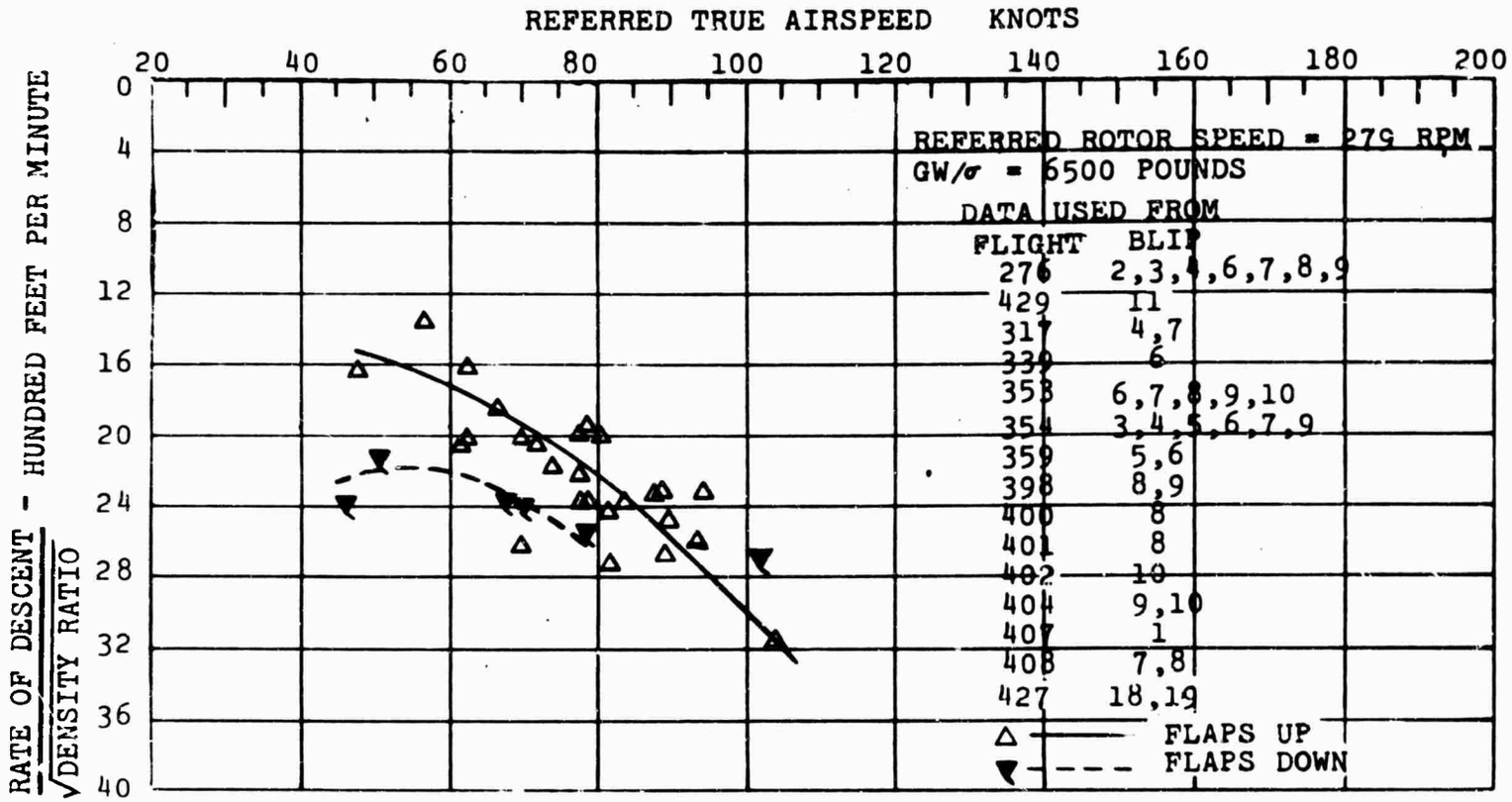


Figure 21. Autorotative Rate of Descent versus Speed.

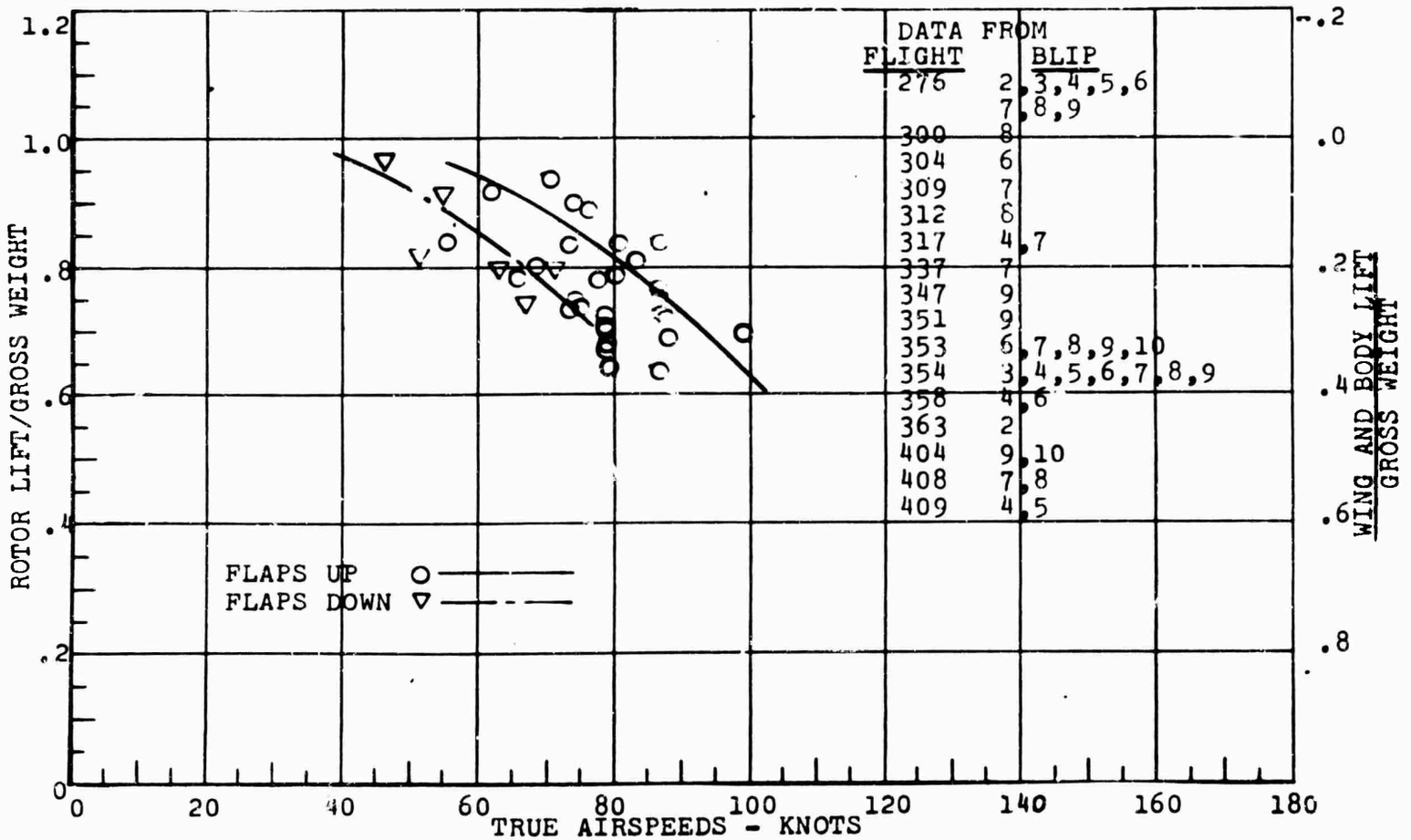


Figure 22. Rotor/Wing Lift Distribution in Autorotation.

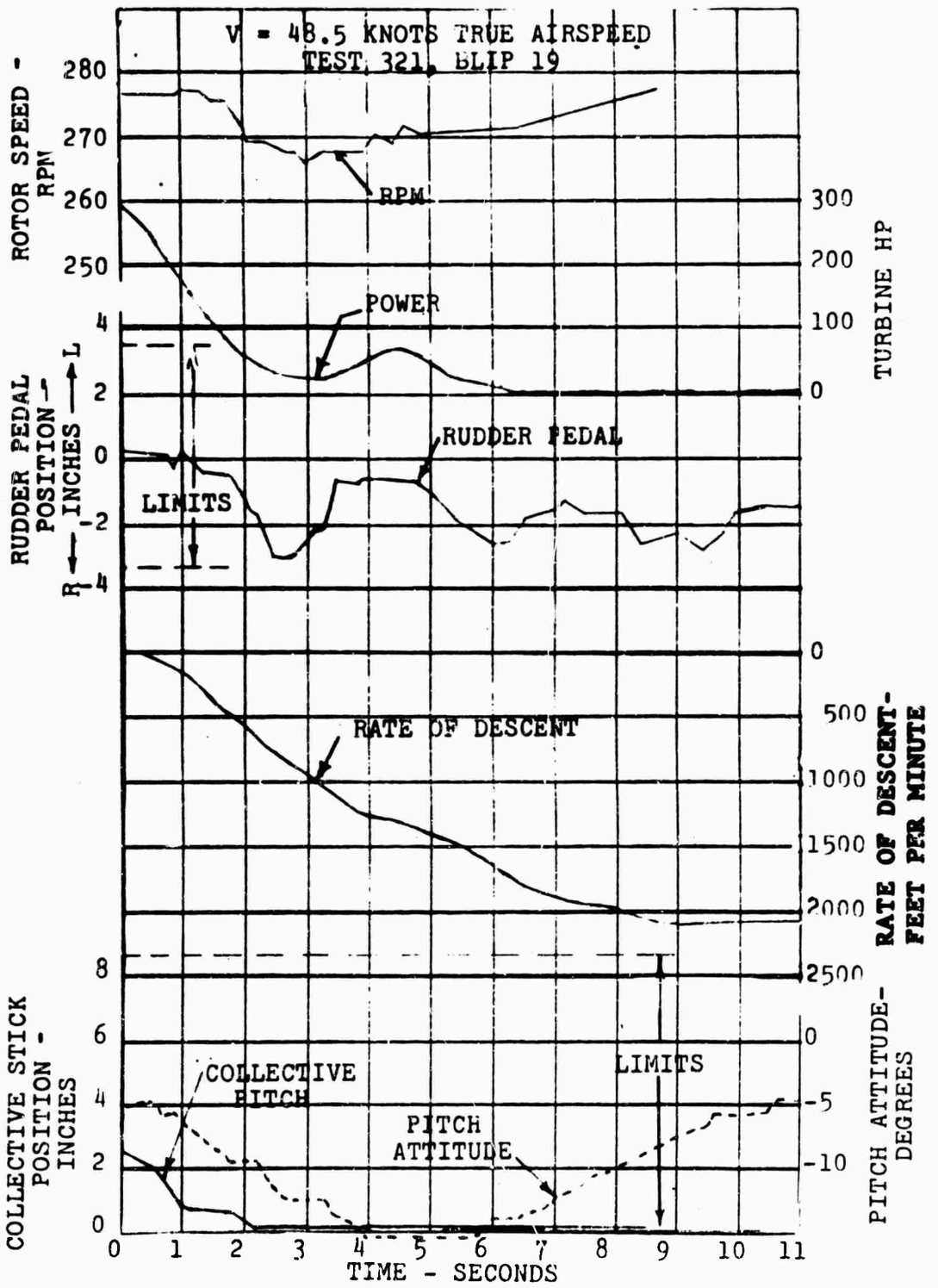


Figure 23. Autorotational Entry at 48.5 Knots.

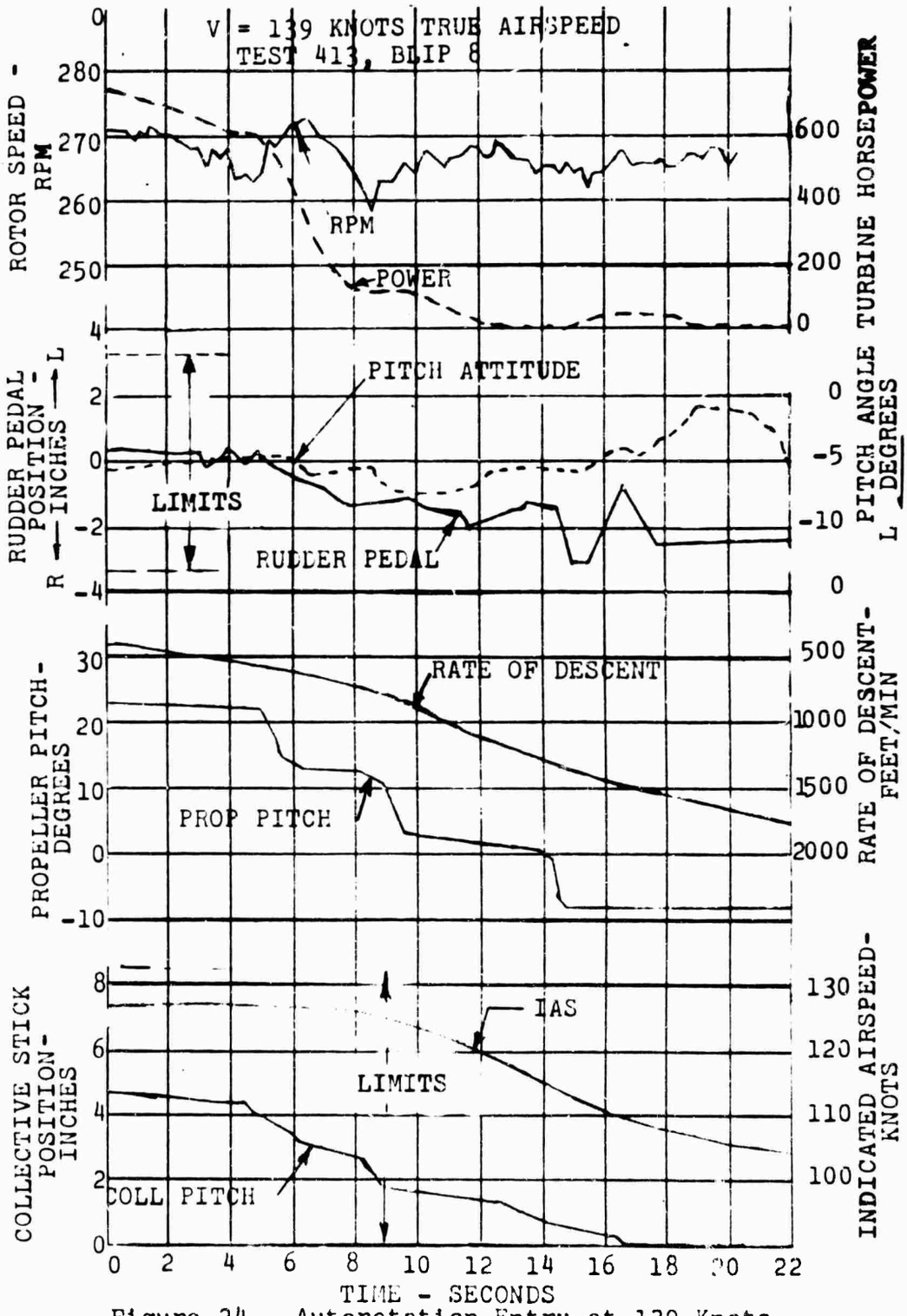


Figure 24. Autorotation Entry at 139 Knots.

shows one at an entry speed of 48.5 knots, and Figure 24 shows one at a true airspeed of 139 knots. From the behavior of the aircraft under the decreases in power typified by these time histories, the indications were that no significant differences would have occurred, except that the rotor speed would have initially drooped to a lower value than that sustained by the turbine governor. In the actual case, as soon as the turbine RPM dropped below the minimum governor setting, the governor would cause the turbine to supply enough power to maintain that RPM. In the 139-knot case (Figure 24) it is clearly seen that reduction of propeller pitch not only arrested the RPM decay but caused it to increase momentarily slightly above its initial value. The windmilling propeller supplies power to the rotor and also creates additional drag to decelerate the aircraft. In the 48-knot case (Figure 23), the propeller was already at essentially minimum pitch, and this effect does not appear. Airspeed is not plotted in Figure 23, but it was maintained at 48 to 50 knots.

Rotor and wing lift are shown in Figure 22. With flaps up, the rotor is 40 percent unloaded at about 100 knots. Within the speed range tested (45 to 100 knots), flap extension further unloads the rotor an additional 10 percent of gross weight at a given speed.

## VERTICAL CLIMB

Vertical rate of climb versus power is shown in Figure 26 for two different referred gross weights. Rotor and propeller power are derived from Figures 25 and 12, respectively. Turbine power is derived from the combined faired curves of rotor and propeller power, corrected for mechanical losses as explained under "Data Reduction Methods". Points from the out-of-ground-effect hover curves (Figure 10) are used for the zero rate-of-climb points.

## LEVEL FLIGHT

Level flight power data are presented for various ranges of fuselage attitude in terms of propeller and rotor power coefficients, as a function of rotor advance ratio. Results are given for two different test gross-weight-to-density ratios: $W/\sigma$ = 6200 pounds, and $W/\sigma$ = 6700 pounds. Procedures set forth prior to actual flight testing stipulated that data be obtained at 20-knot intervals, starting with 30 knots, for fuselage attitude increments of $\pm 5$ degrees to the maximum trimmable attitude for each steady-state speed. Since the pilot had no direct presentation of angle of attack, his procedure was to fly at various combinations of propeller

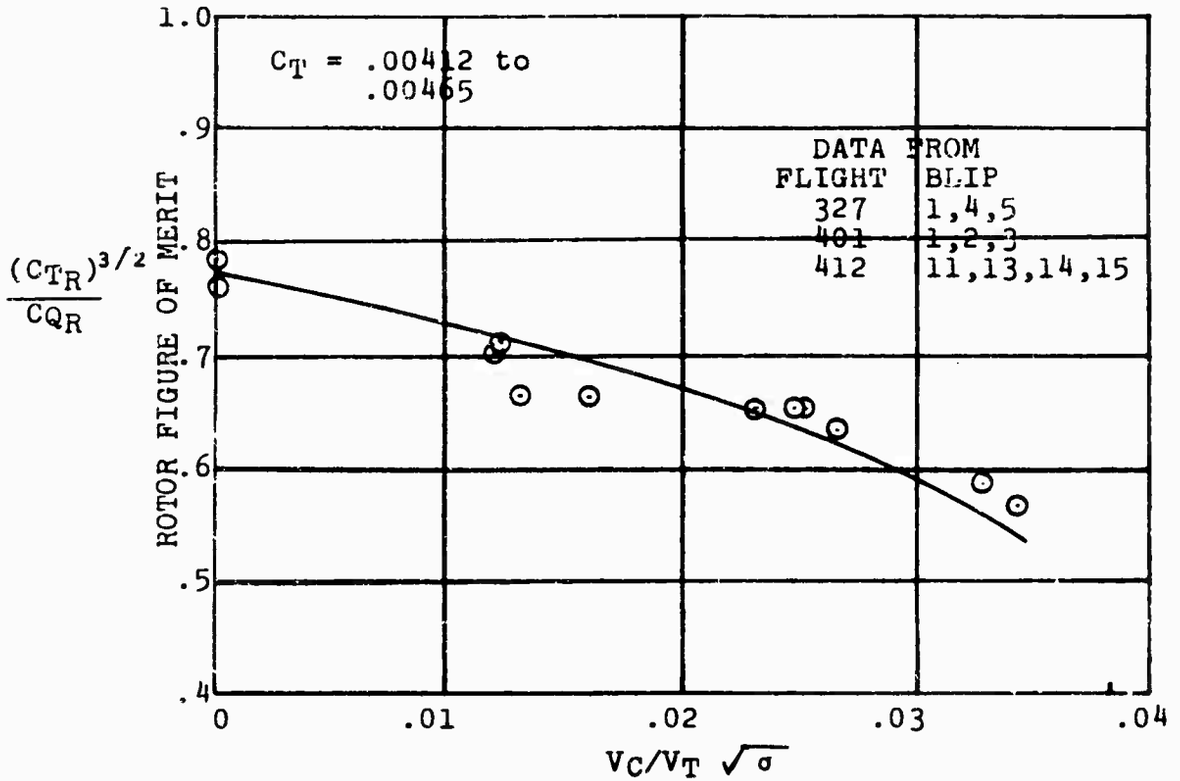


Figure 25. Vertical Climb; Rotor Figure of Merit versus Nondimensional Climb Velocity.

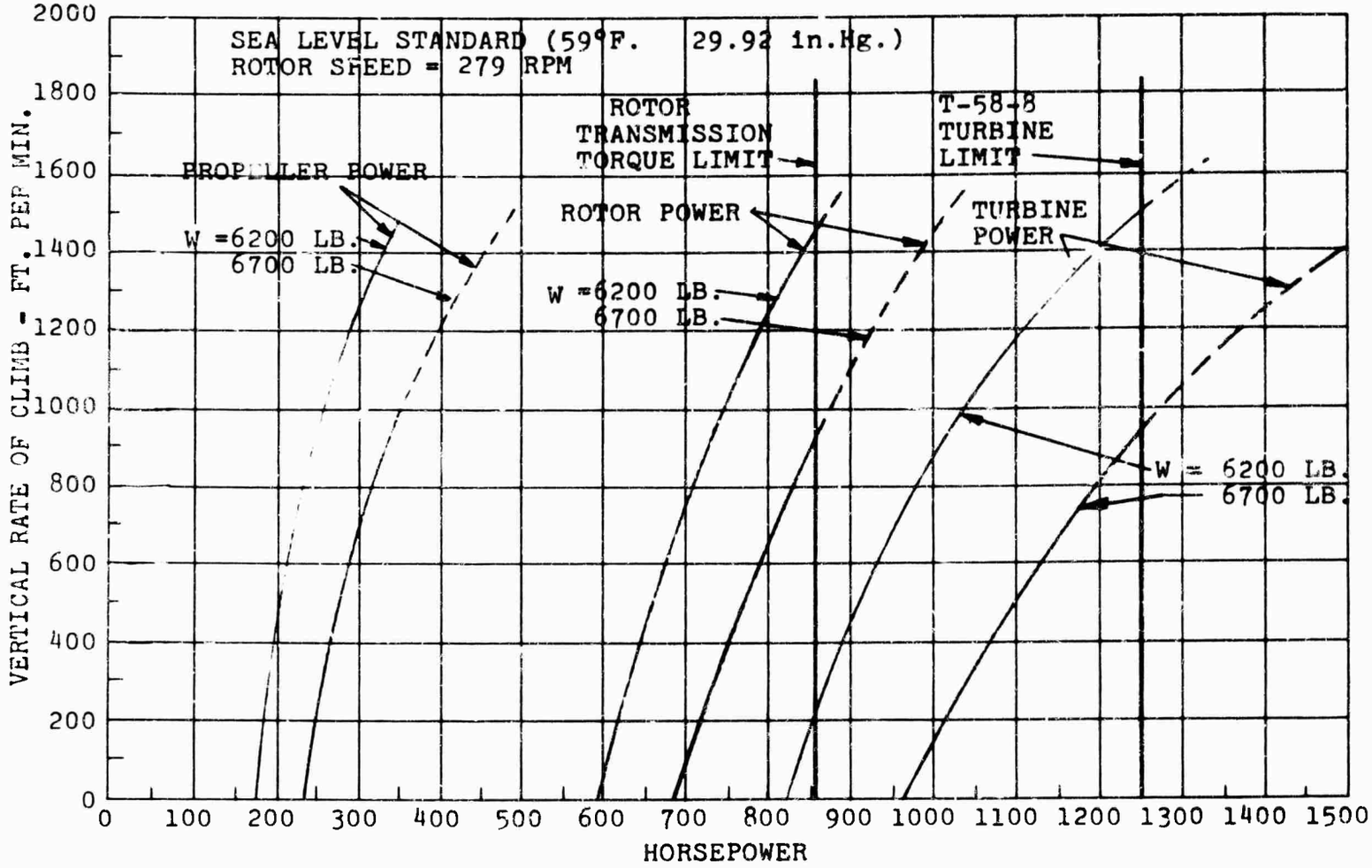


Figure 26. Vertical Rate of Climb versus Power.

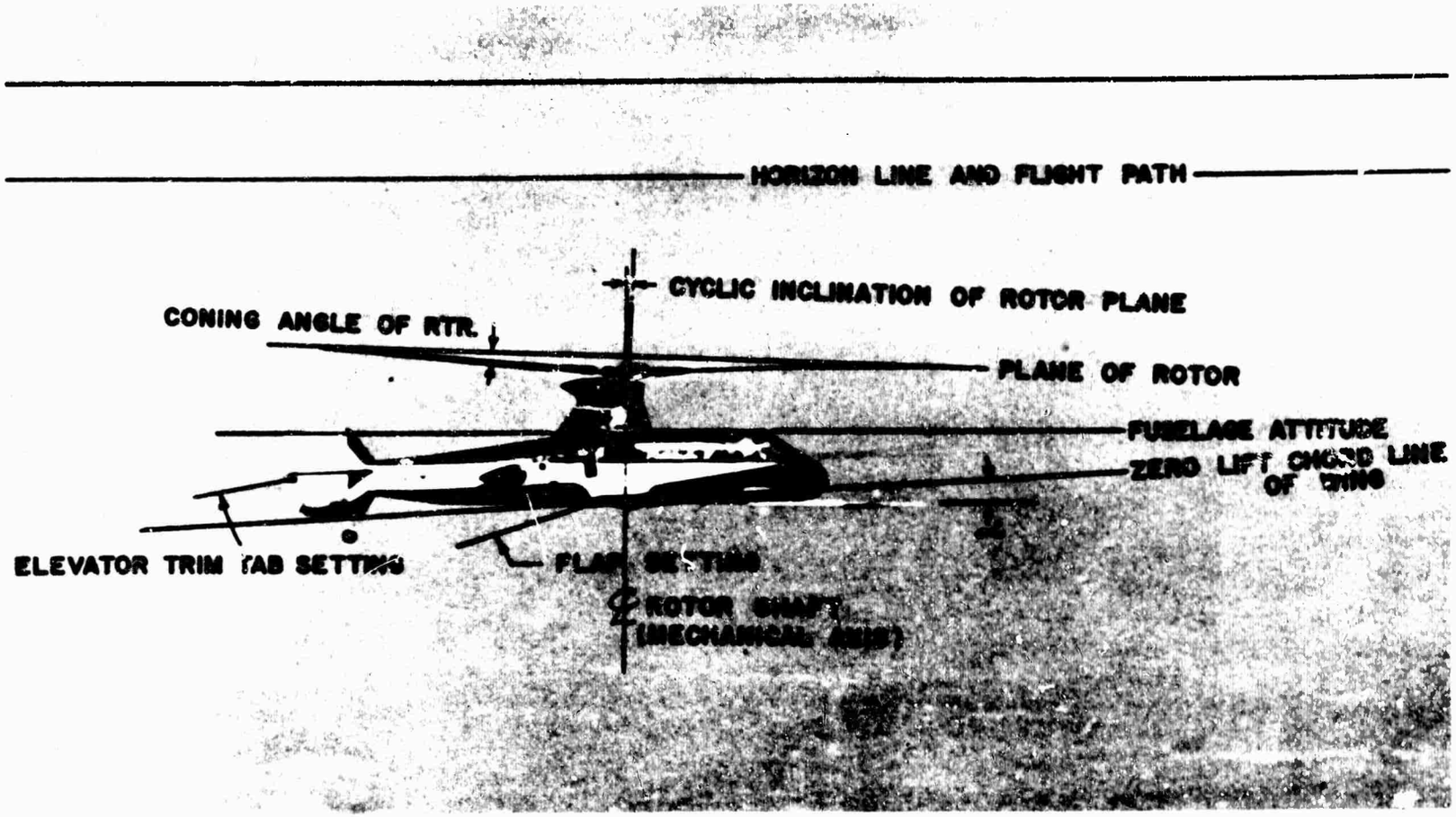


Figure 27. 16H-1A Flight Trim Parameters.

and collective pitch. The resulting flaps-up data are presented as a function of advance ratio in level flight for ranges of fuselage angle of attack of (1) -4 to -6 degrees, Figures 28a, 28c, 29a, and 29c; (2) -1 to +1 degree, Figures 28b, 28d, 29b, and 29d; (3) +4 to +6 degrees, Figures 28b and 29b. Data for tests with 40 degree flaps down are given in Figures 28e and 29e for an angle of attack of -0.5 to +2.5 degrees. The specific ranges of fuselage angle of attack were determined (1) on the basis of the abundance of data available within an interval and (2) because the midpoints of the intervals are separated by 5-degree increments. Significant additional data were also produced in the angle-of-attack range of -1.5 to -3.5 degrees (Figures 28a, 28c, 29a, and 29c).

The faired curves of flaps-up rotor and propeller power coefficient as a function of advance ratio are compared for the two gross weights and the angle-of-attack variations in the summary plots of Figures 28f and 29f. Two consistent families of curves result, exhibiting the effects of both attitude and weight on the component power coefficients. These curves have been utilized to establish the dimensional, component power for rotor and propeller based on standard atmosphere sea-level density and the referred rotor speed of 279 RPM shown on Figure 30. Included in Figure 30 are the flaps-down component power curves obtained from the data of Figures 28c and 29e.

The equivalent flat-plate area of the basic aircraft, as flown, is calculated to be 13.53 square feet, as shown in Table XX in Appendix II. The extra drag of test-equipment items and uninstalled fairings originally planned raised the flat-plate area for some flights up to 1.2 square feet more. The net effect of these items is that the tests were conducted at an average drag penalty of 4.20 square feet more than the configuration as designed. This extra drag amounts to 504 horsepower at 200 knots at sea level, and, combined with the lack of ram recovery in the engine-inlet duct (equivalent to 95 horsepower), was the limiting factor on the level flight speed reached.

**The highest true airspeed reached was 195 knots in a 10-degree dive at an altitude of 4200 feet. Highest true airspeeds reached in level flight were 160 knots at sea level (Flight 411), and 167 knots at 3670 feet (Flight 406).**

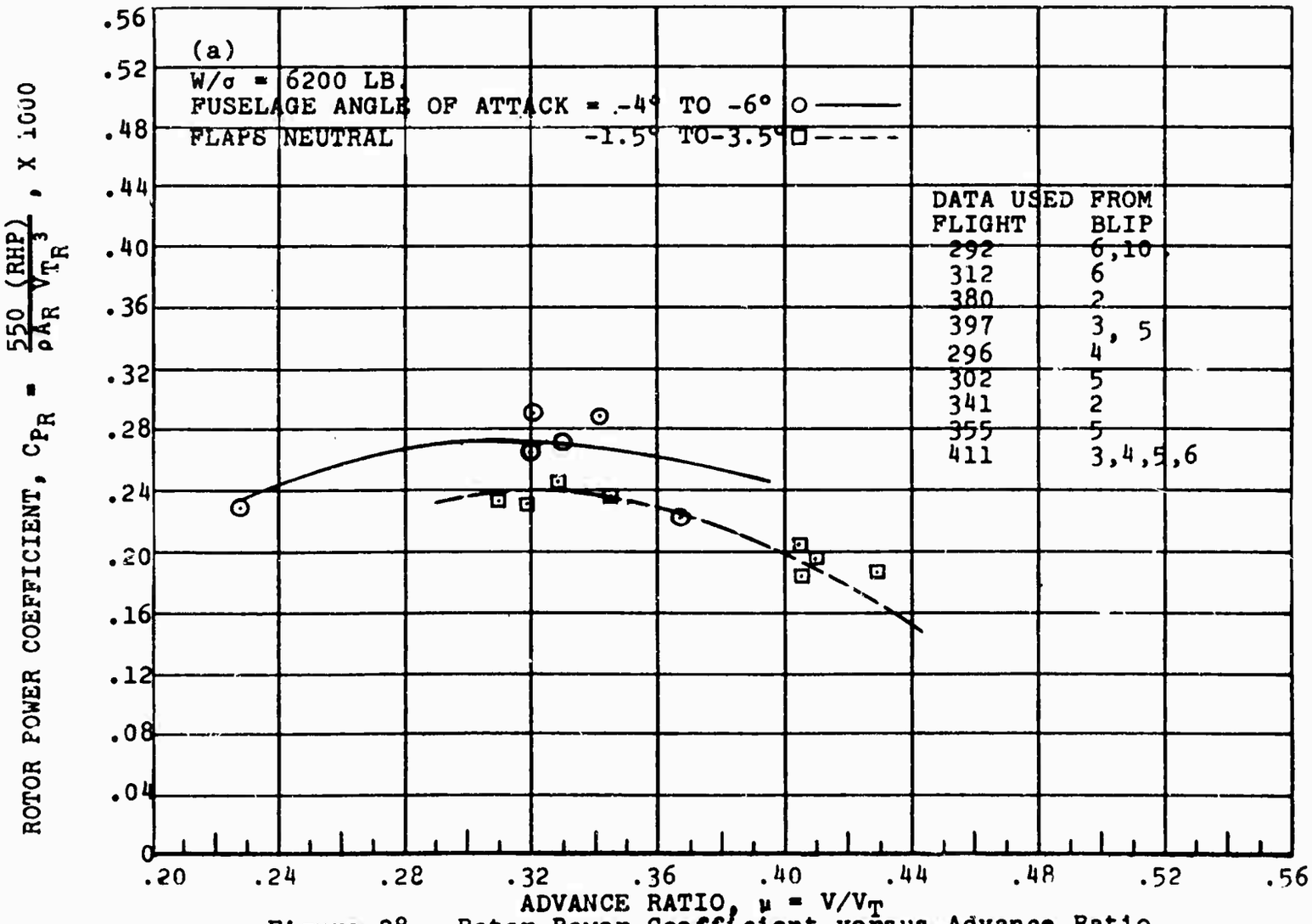


Figure 28. Rotor Power Coefficient versus Advance Ratio.

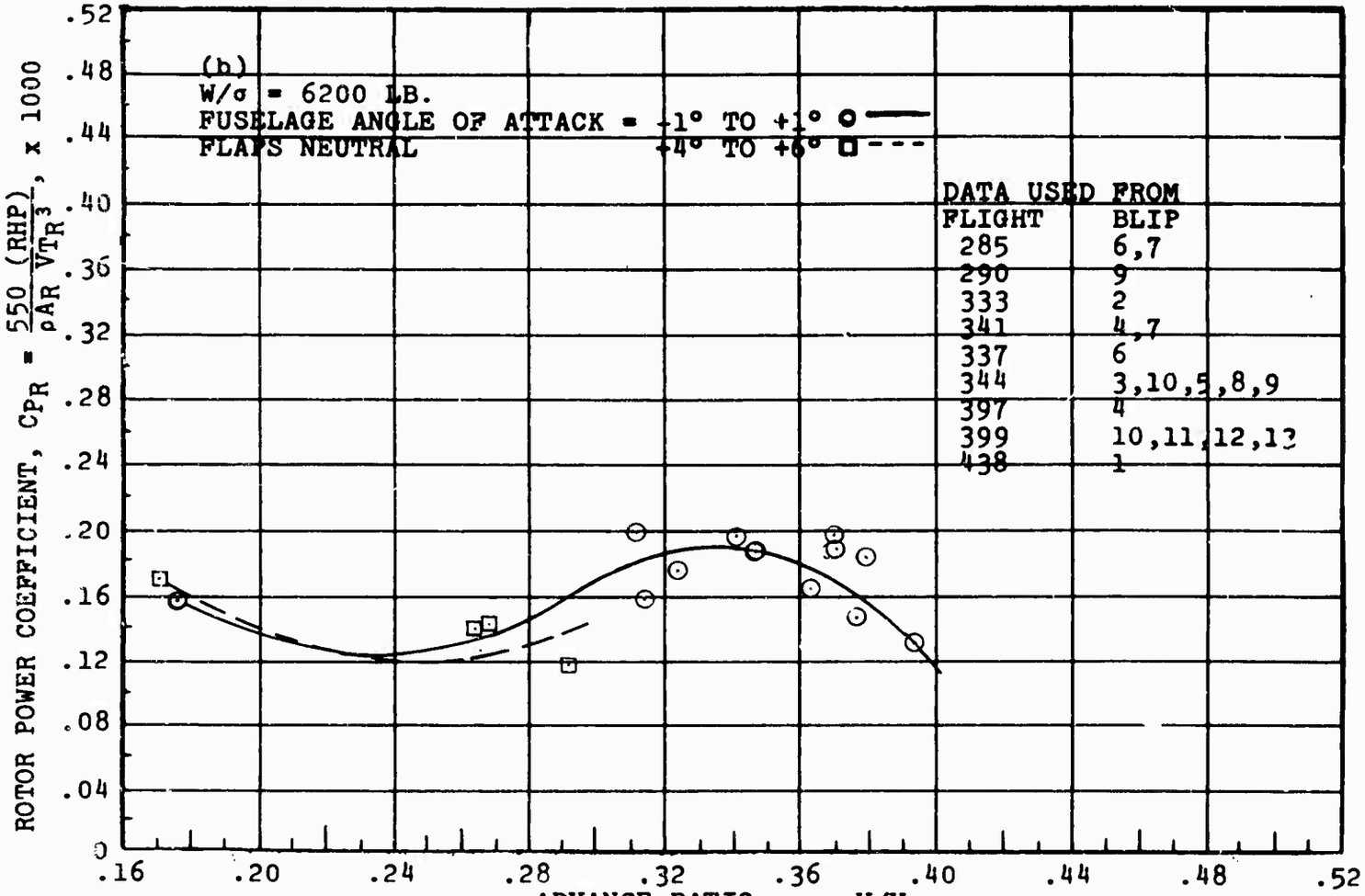


Figure 28. - Continued.

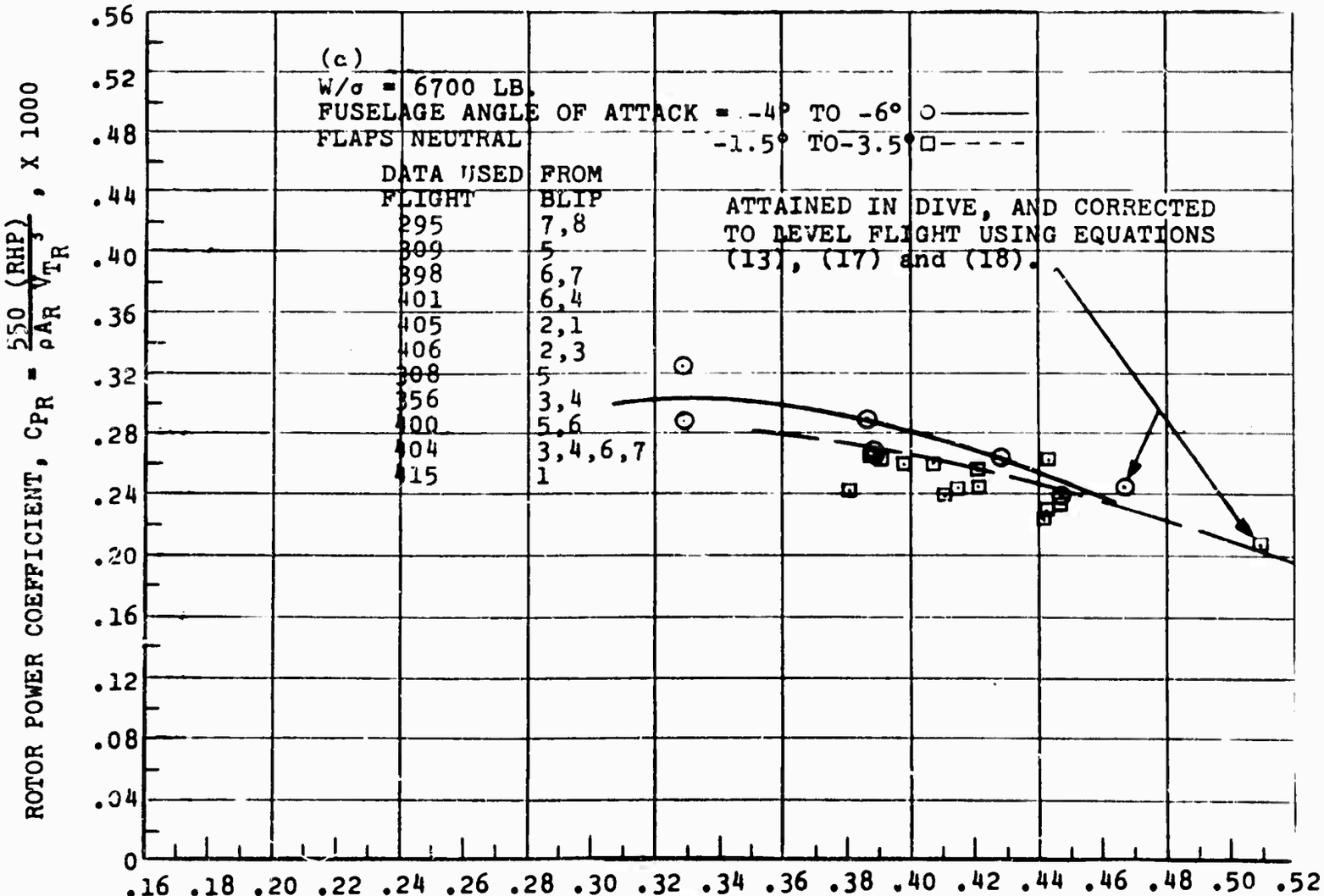


Figure 28. -- Continued.

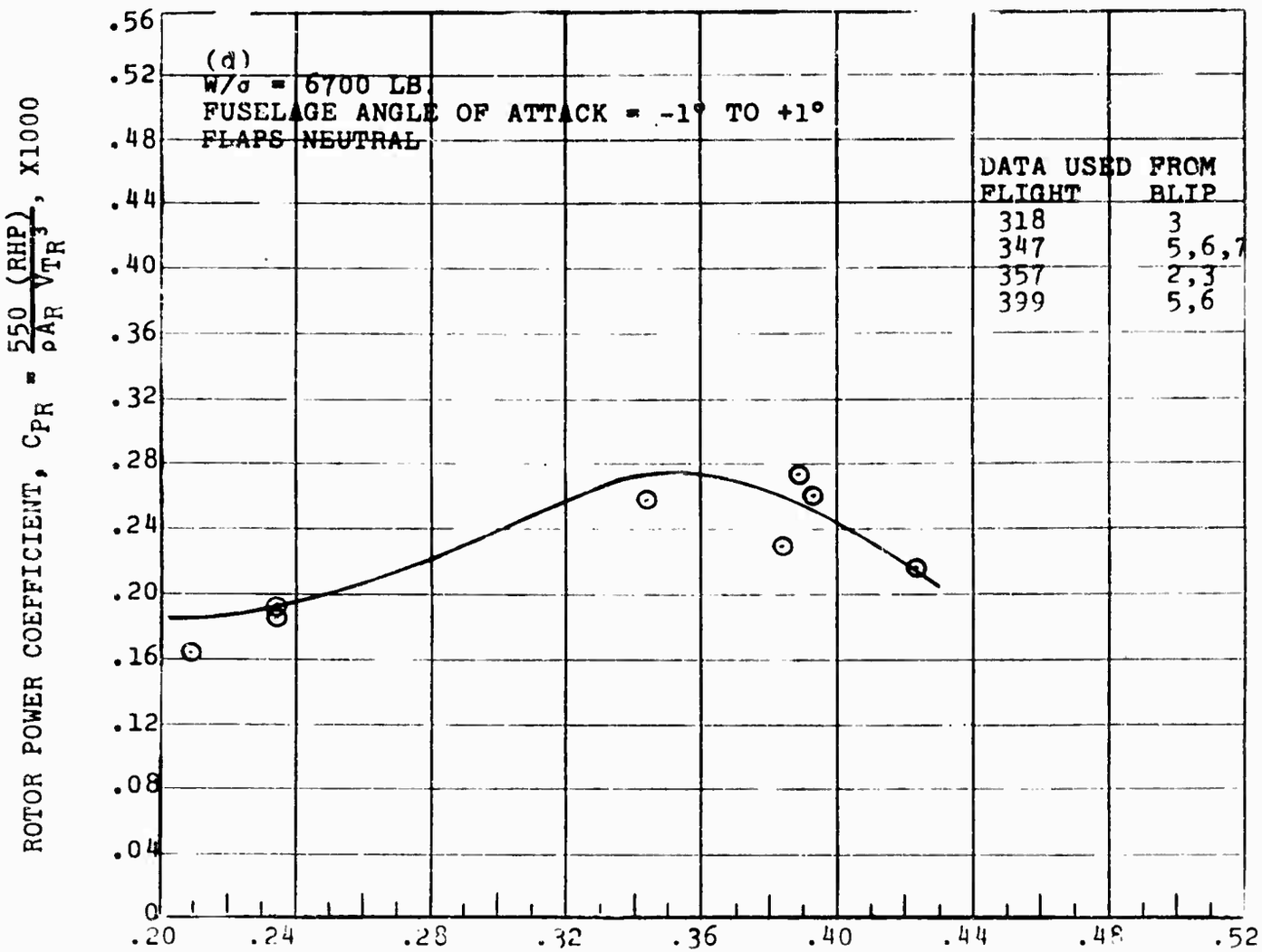


Figure 28. - Continued.

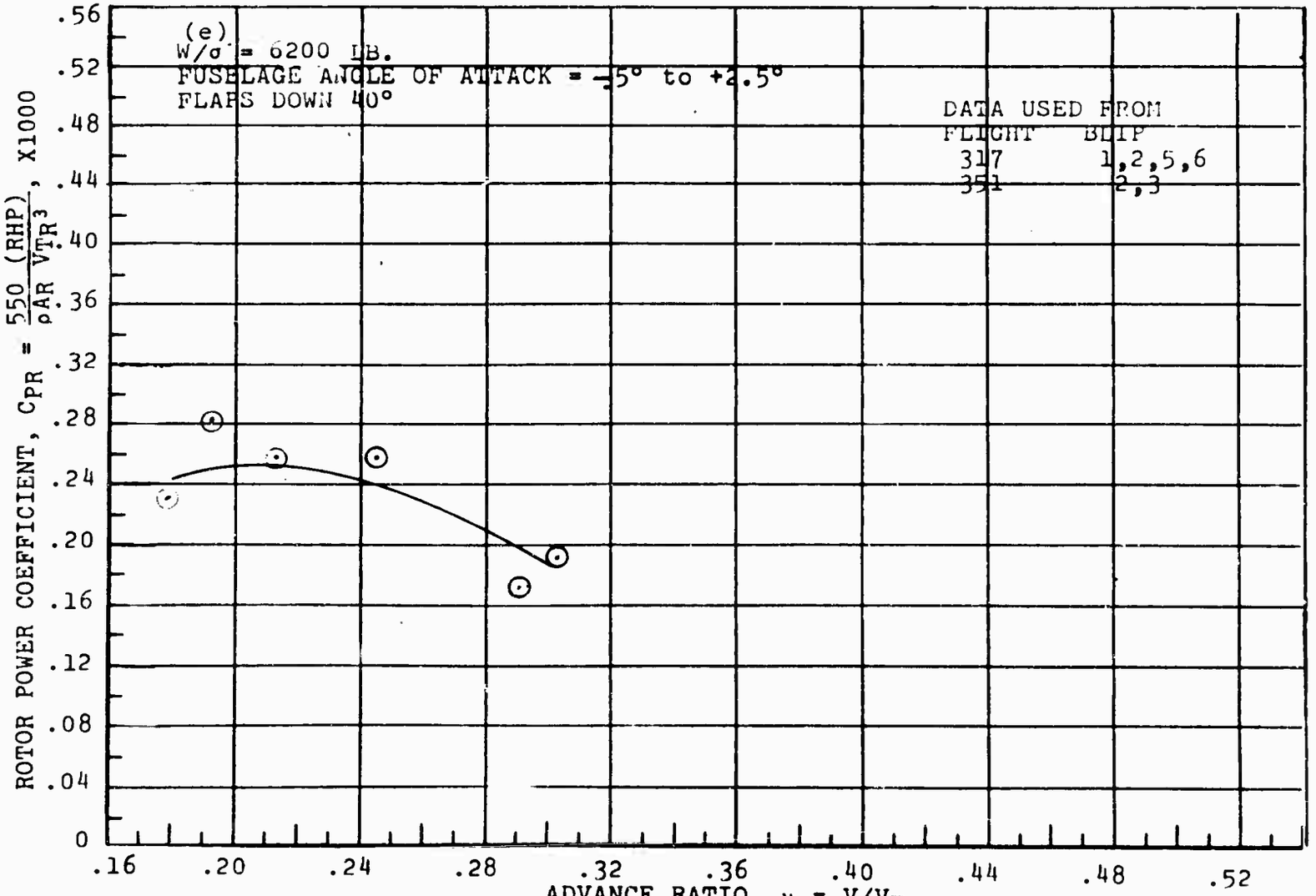


Figure 28.- Continued.

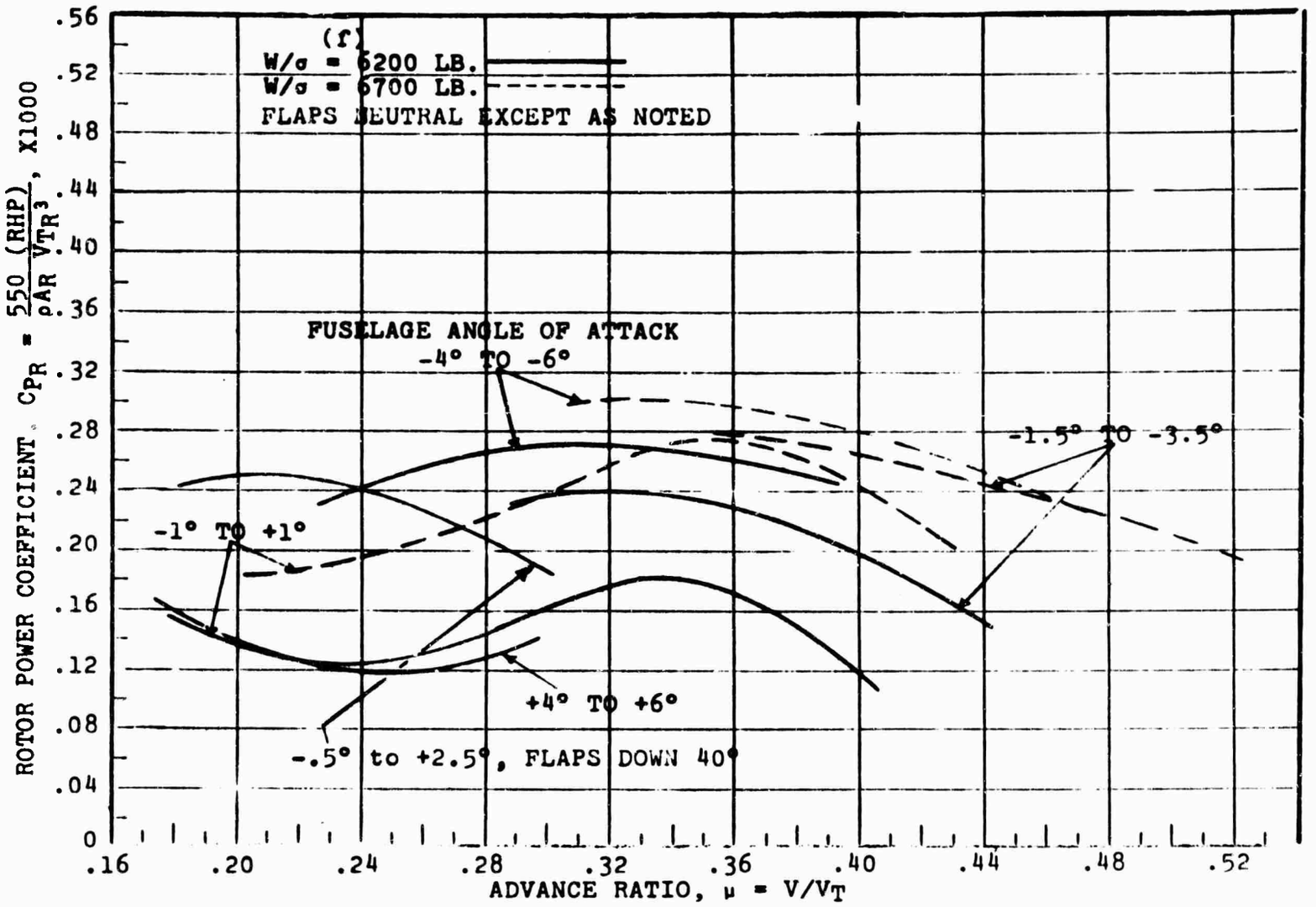


Figure 28.- Continued.

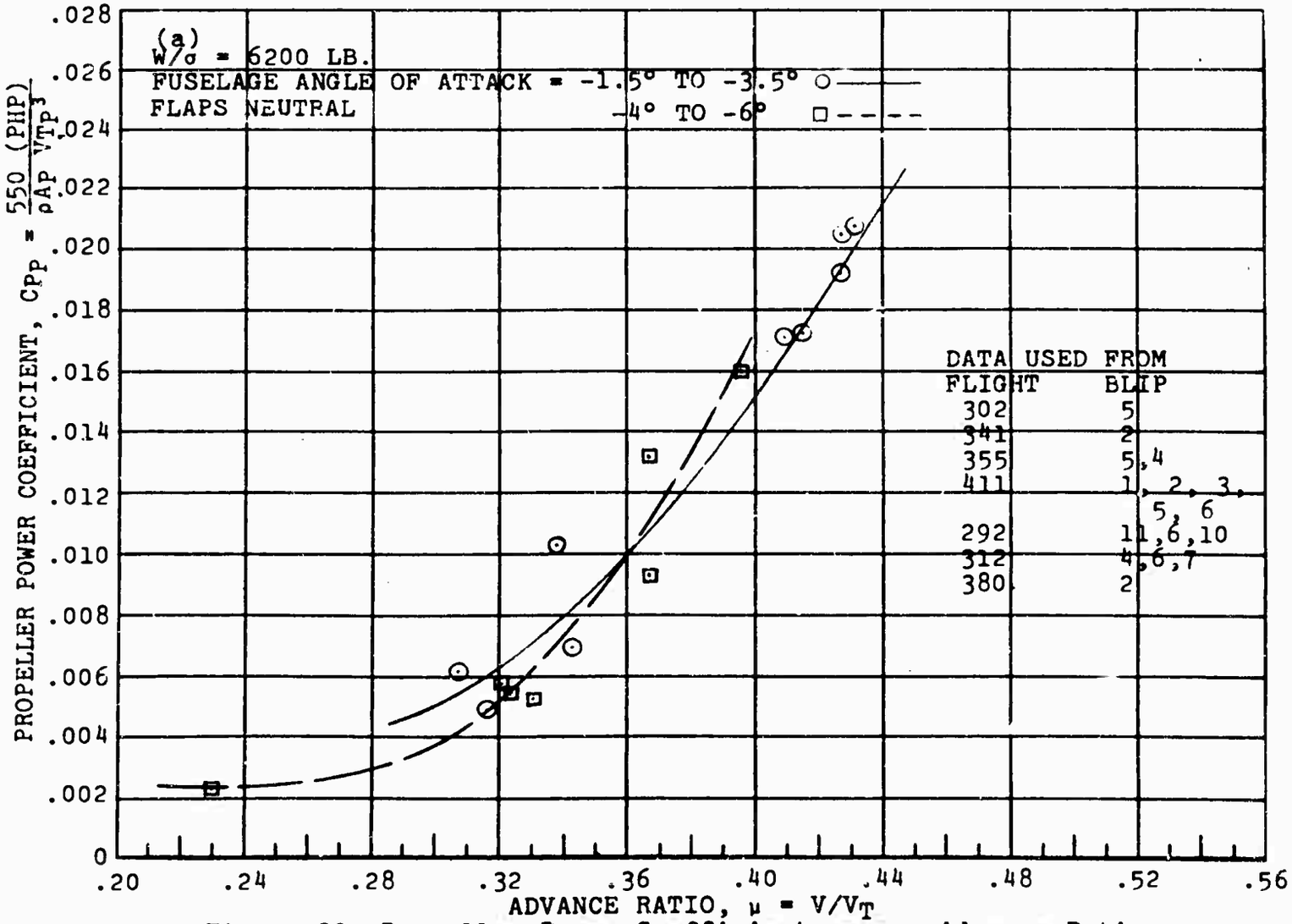


Figure 29. Propeller Power Coefficient versus Advance Ratio.

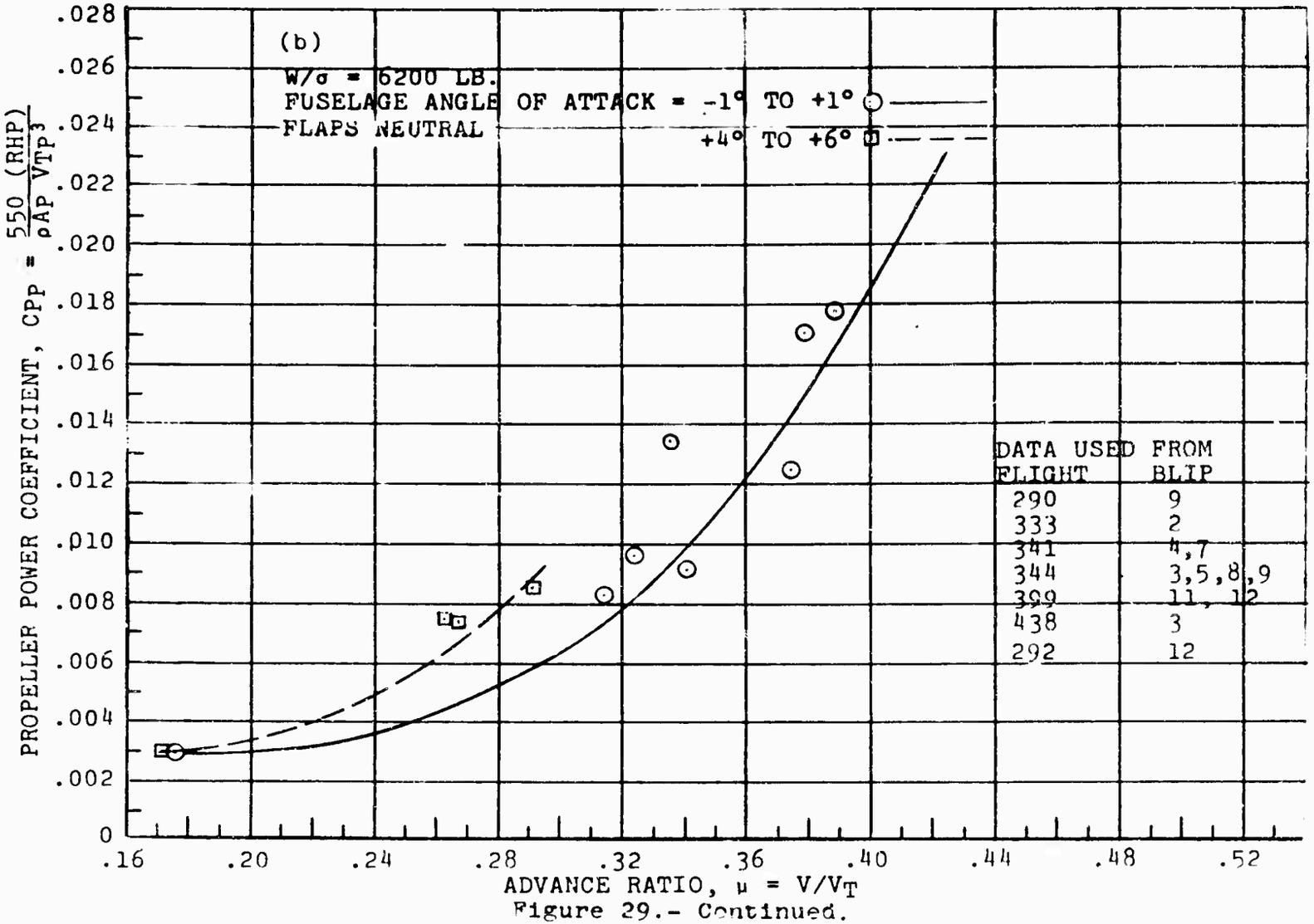


Figure 29.- Continued.

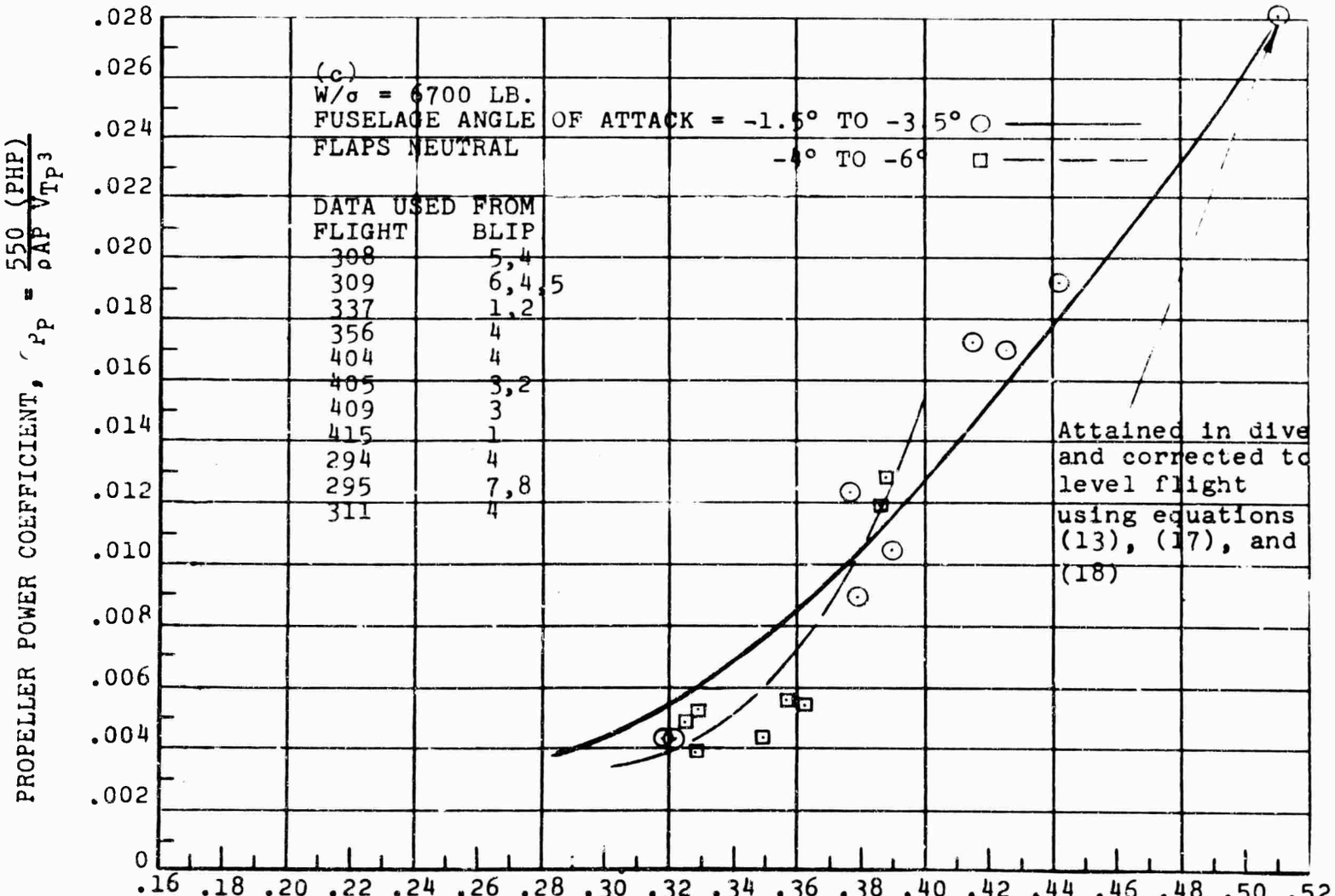


Figure 29. - Continued.

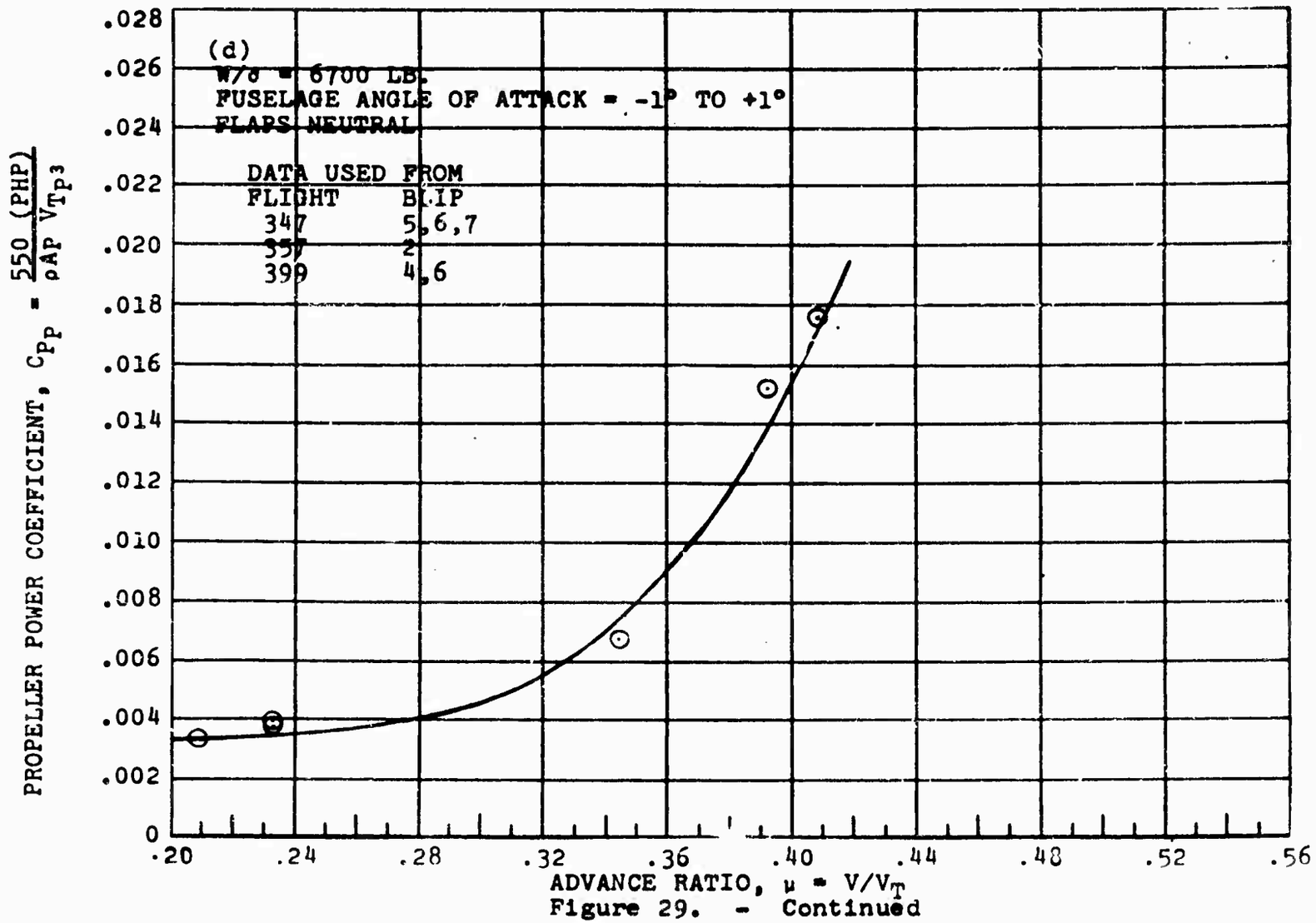


Figure 29. - Continued

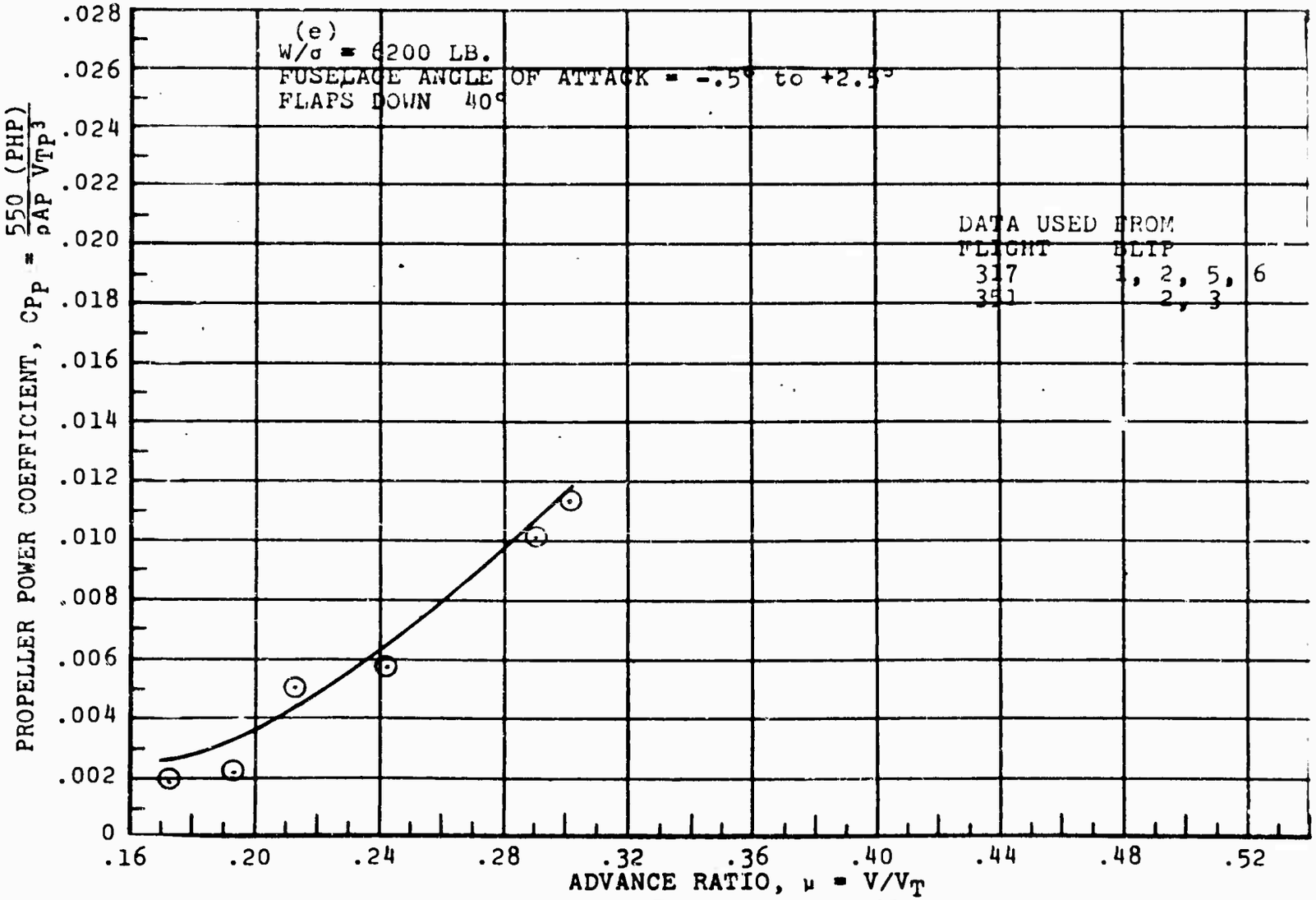


Figure 29. - Continued.

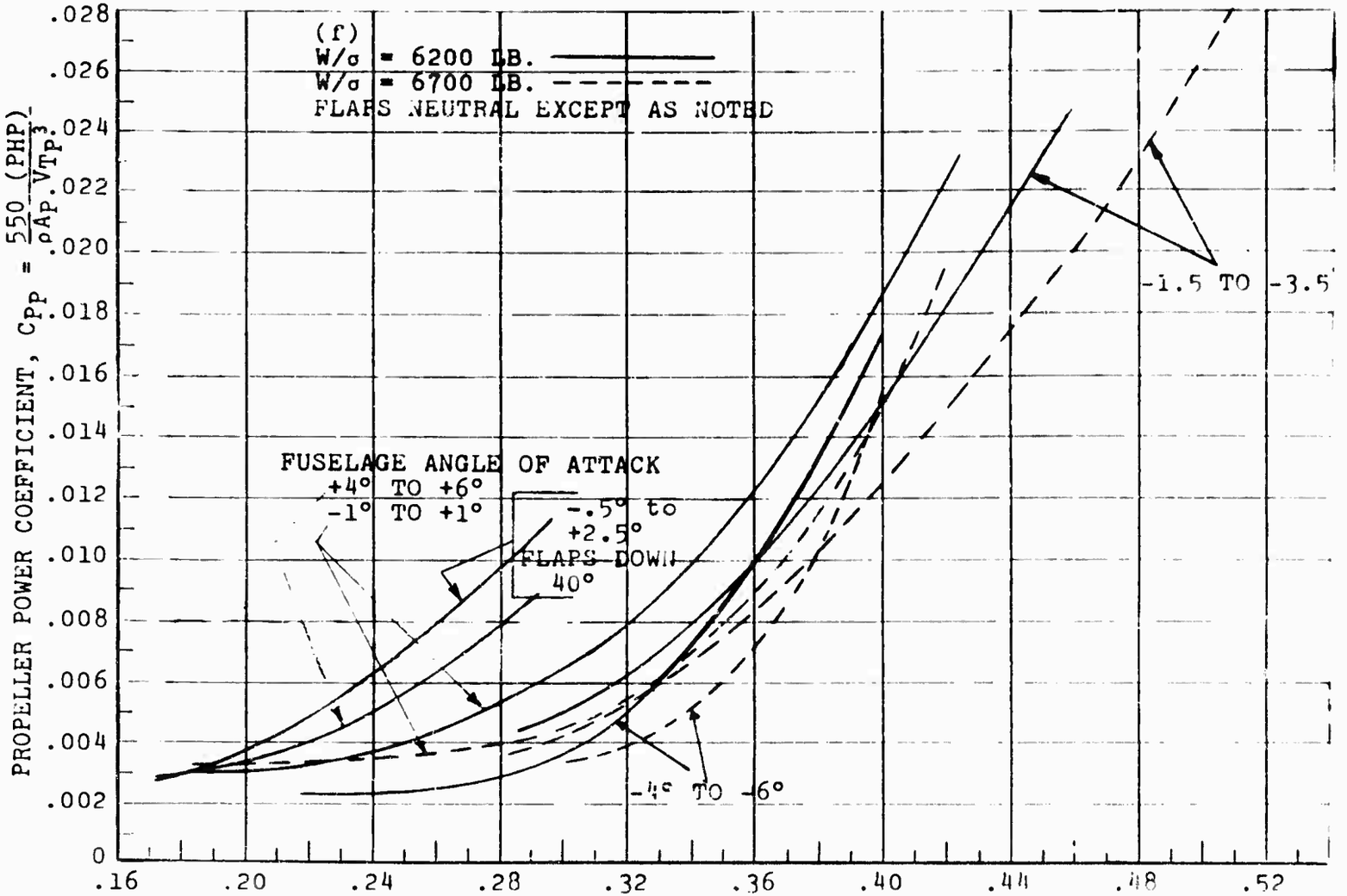


Figure 29. - Continued.

The rotor power coefficient curves in Figure 28 indicate the typical helicopter power trends in the range from $\mu = 0.16$ to $\mu = 0.32$ showing minimum rotor power and the subsequent rise. Above $\mu = 0.32$, the rotor power again decreases as the propulsive force is developed by the propeller for high speed flight, and the rotor becomes unloaded. The general effect of angle of attack, as shown, is as expected, in that algebraically increasing attitude angle at a given forward speed reduces the rotor propulsive force and hence total rotor power. The corresponding set of faired curves for propeller power coefficient given in Figure 29 exhibits a continuous increase in propeller power at advance ratios above $\mu = 0.20$. This is a natural result of the increased propeller thrust requirements as the speed increases and the rotor propulsive force decreases. The reduced propeller power at the heavier weight, at the same advance ratio and angle of attack, is the result of increased rotor propulsive force associated with increased rotor thrust.

The turbine power curves, in Figure 30, reconstructed from the faired power coefficients and mechanical efficiency data given in Figures 28, 29, and 8, indicate the dominance of the propeller contribution in the intermediate to high speed range. The effect of angle of attack on total power at 6700 pounds shows that the optimum angle varies from near zero at 80 knots to about -5 degrees at 130 knots and then increases in the positive direction gradually to -1.5 degrees at 190 knots. At 6200 pounds, the optimum angle-of-attack variation is seen to be similar but the maximum negative angle does not exceed -3.5 degrees.

Figure 31, which is transcribed from Figure 30, shows the effect of angle of attack and flap deflection on total brake horsepower (turbine power). From Figure 31 the flight-test-determined envelope of minimum power at the specified weight was obtained. In Figure 32, both envelope curves are shown for comparison. The effects of the gross weight difference which are significant at intermediate and low speeds are apparent. At speeds above 130 knots, the envelope curves are essentially coincident when considering the normal experimental error. Theoretical analysis of total power required above 130 knots indicates only about a 25-horsepower increase at the heavier weight.

In order to indicate more readily the percentage of total power attributed to the rotor and propeller, the ratio

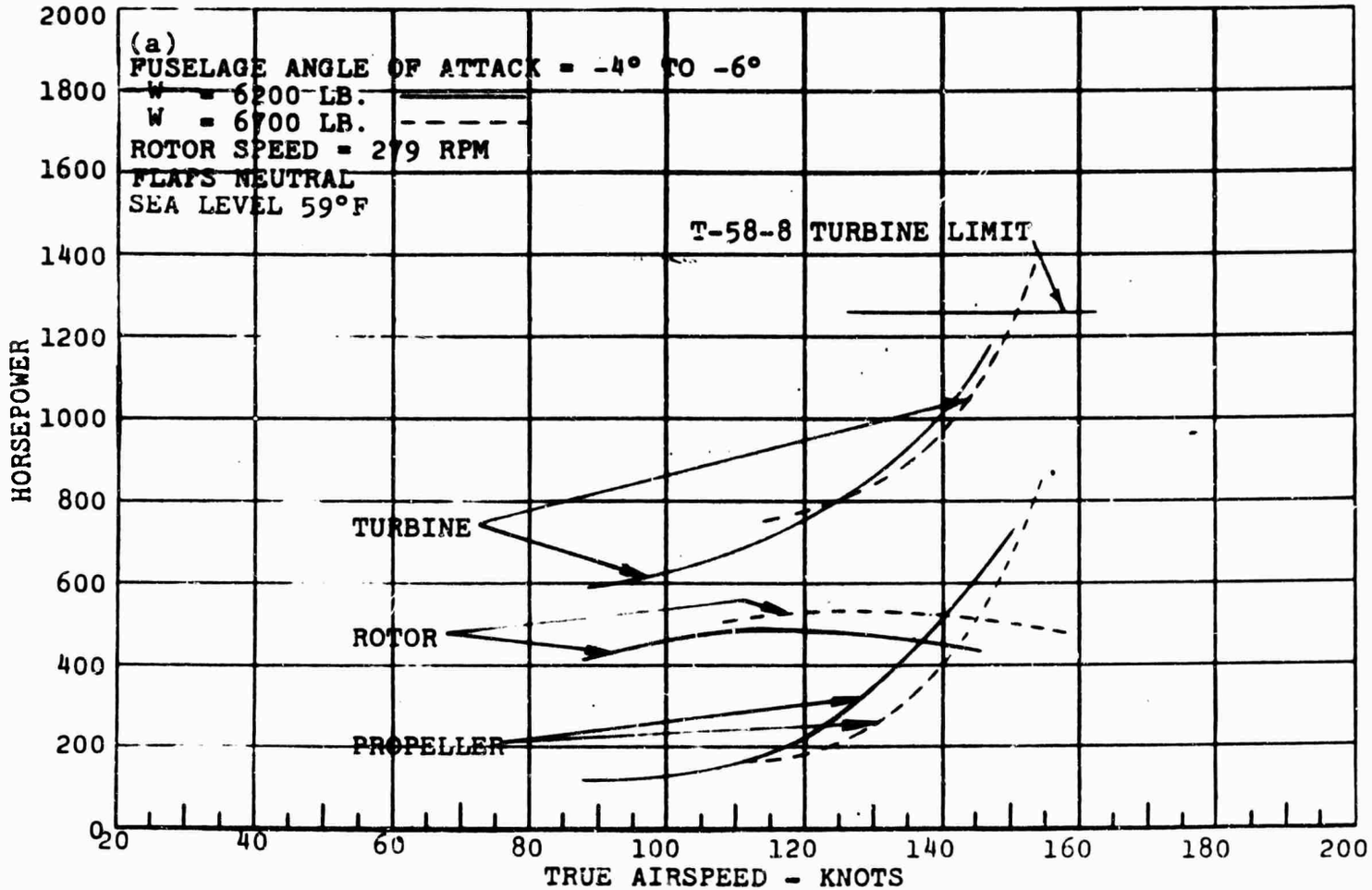


Figure 30. Power Versus Speed, Forward Flight.

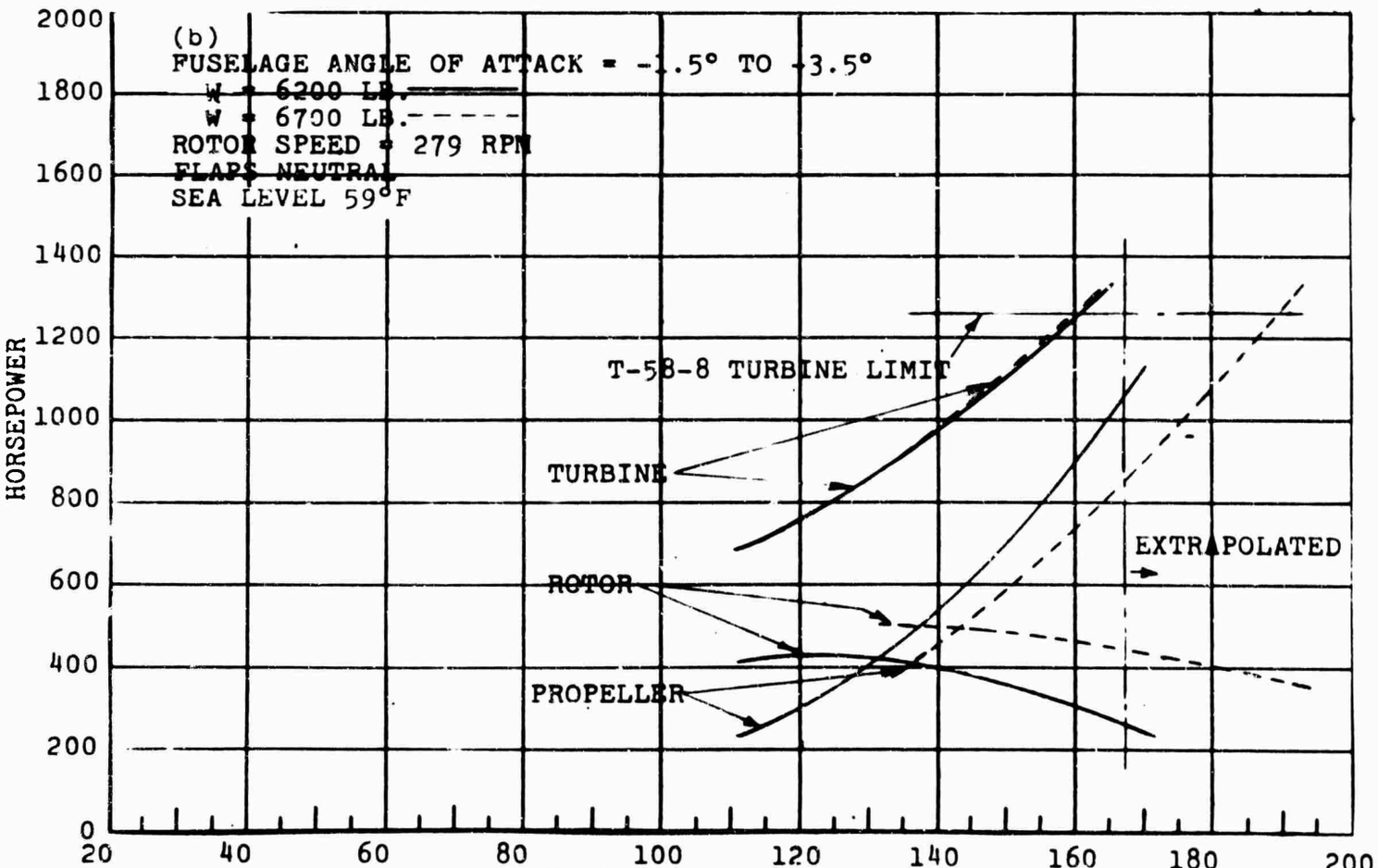


Figure 30.- Continued.

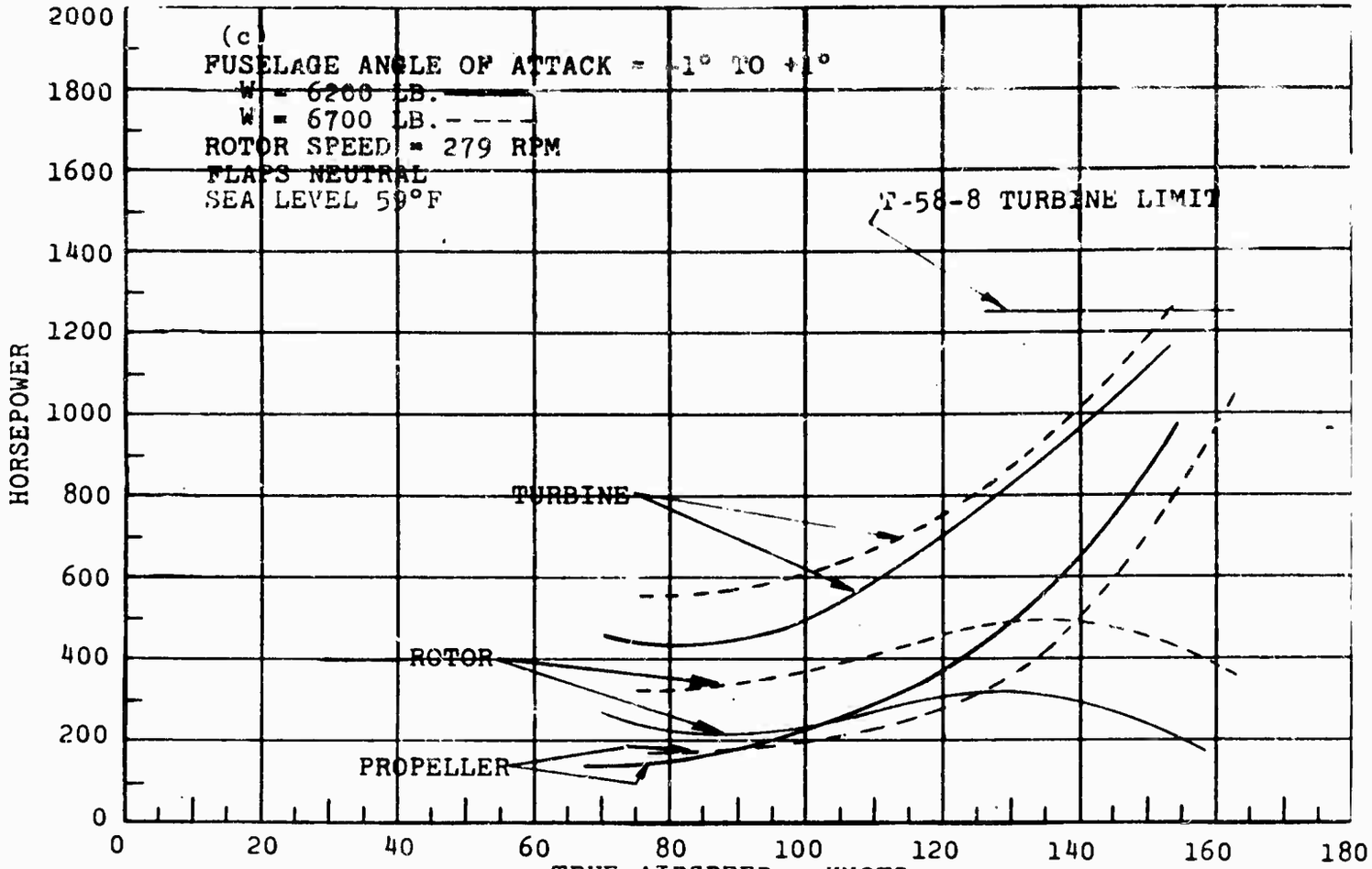


Figure 30. - Continued.

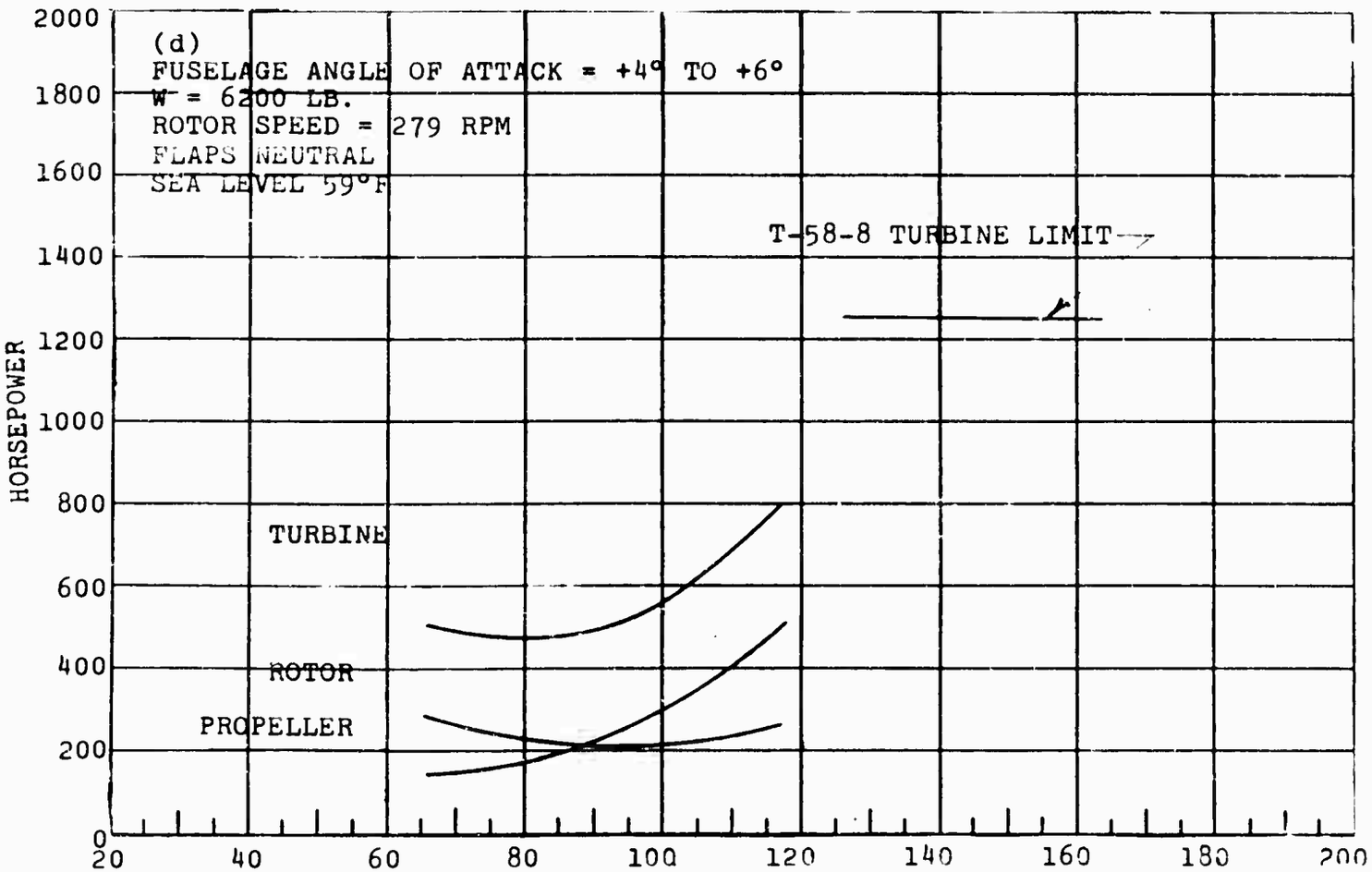


Figure 30. - Continued.

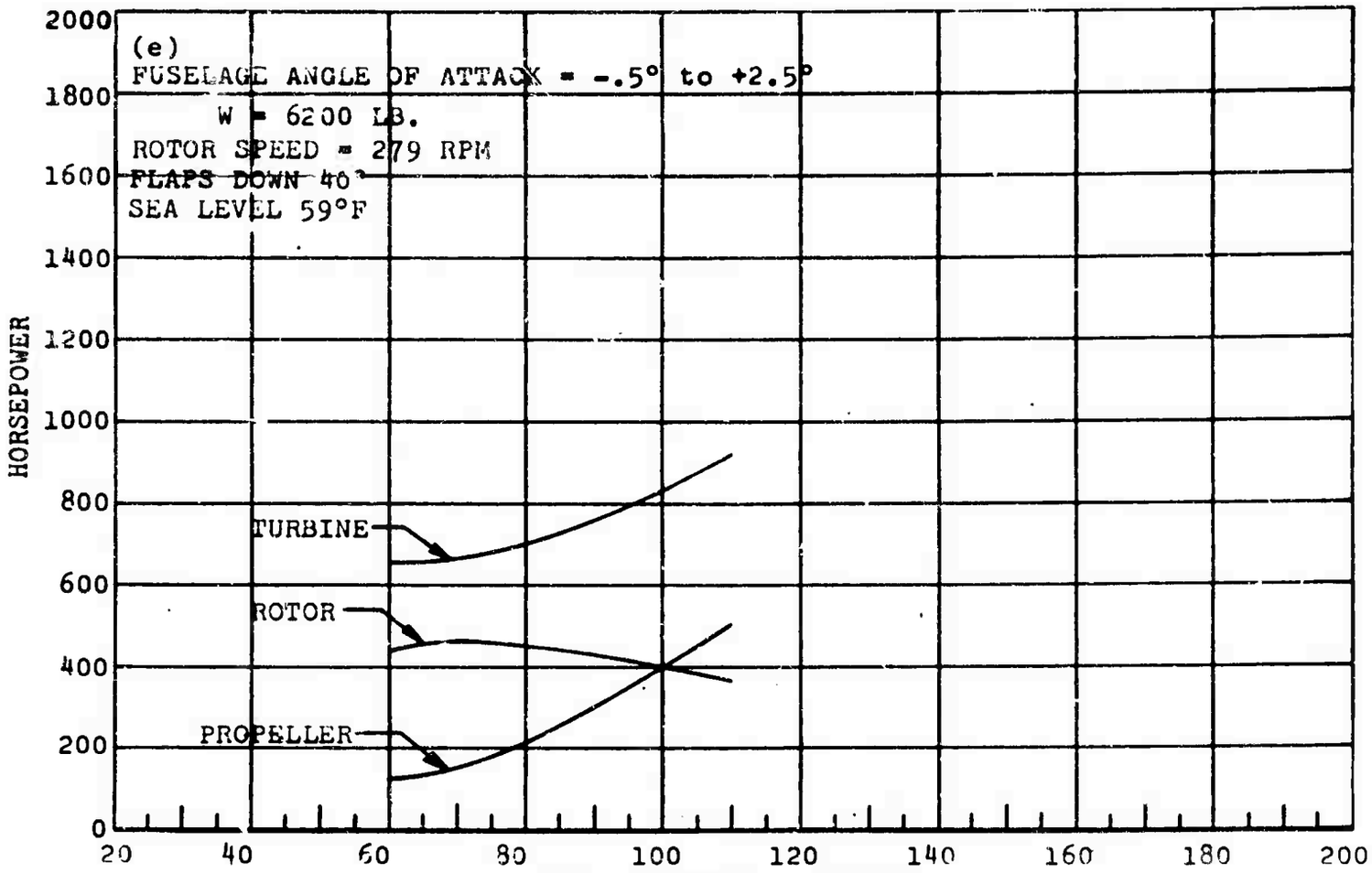


Figure 30. - Continued.

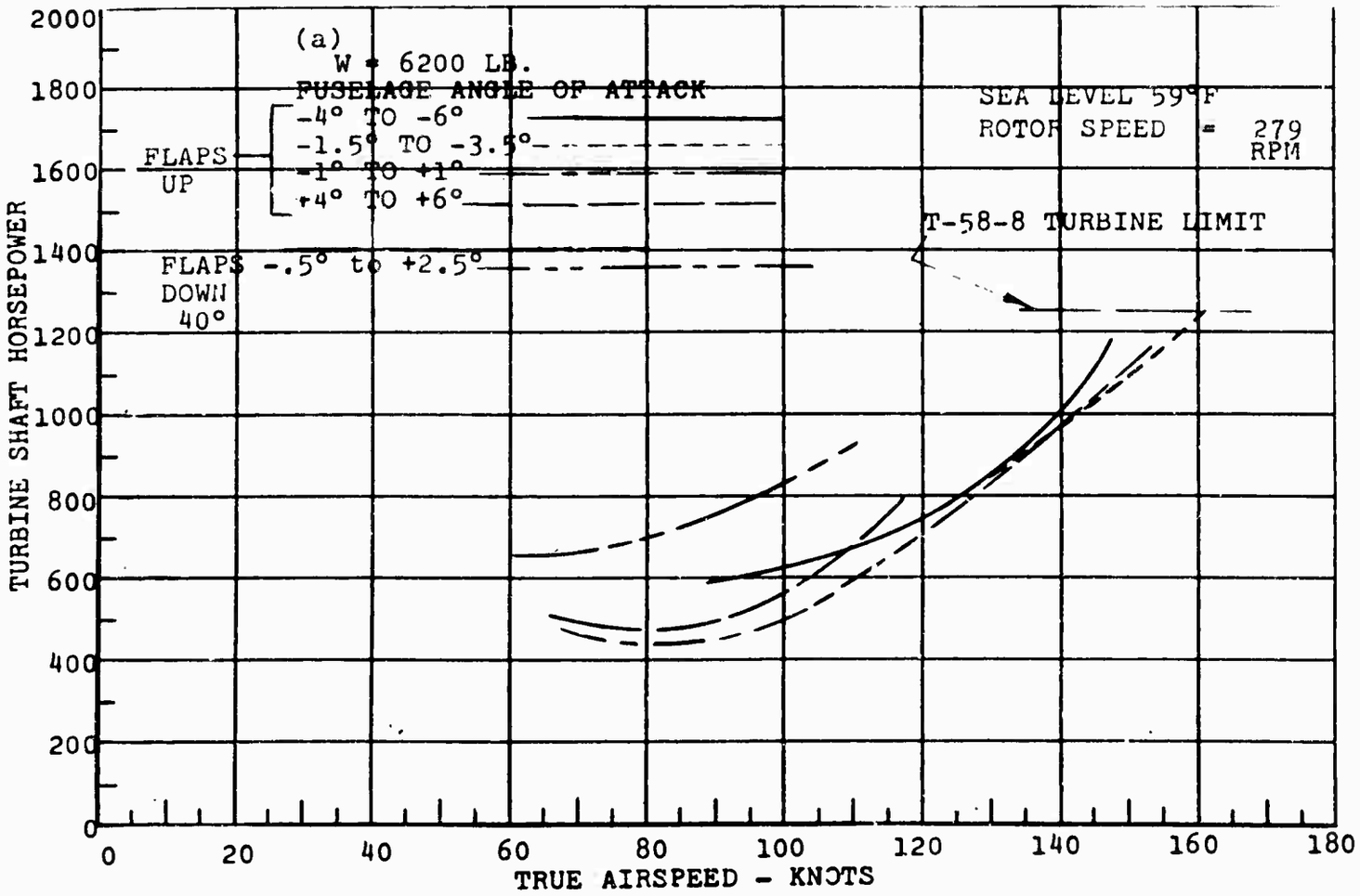


Figure 31. Turbine Power versus Speed, Forward Flight.

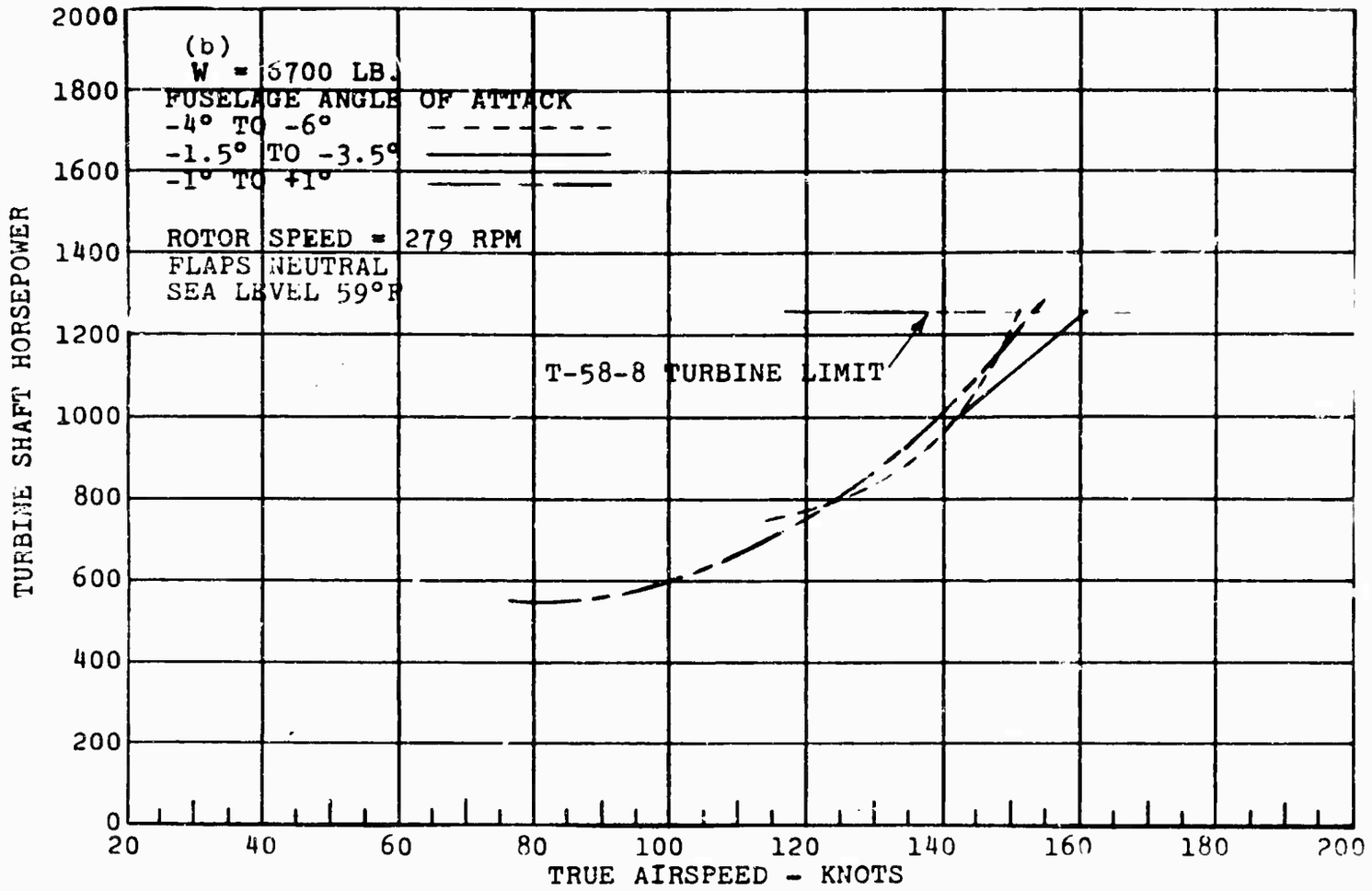


Figure 31. - Continued.

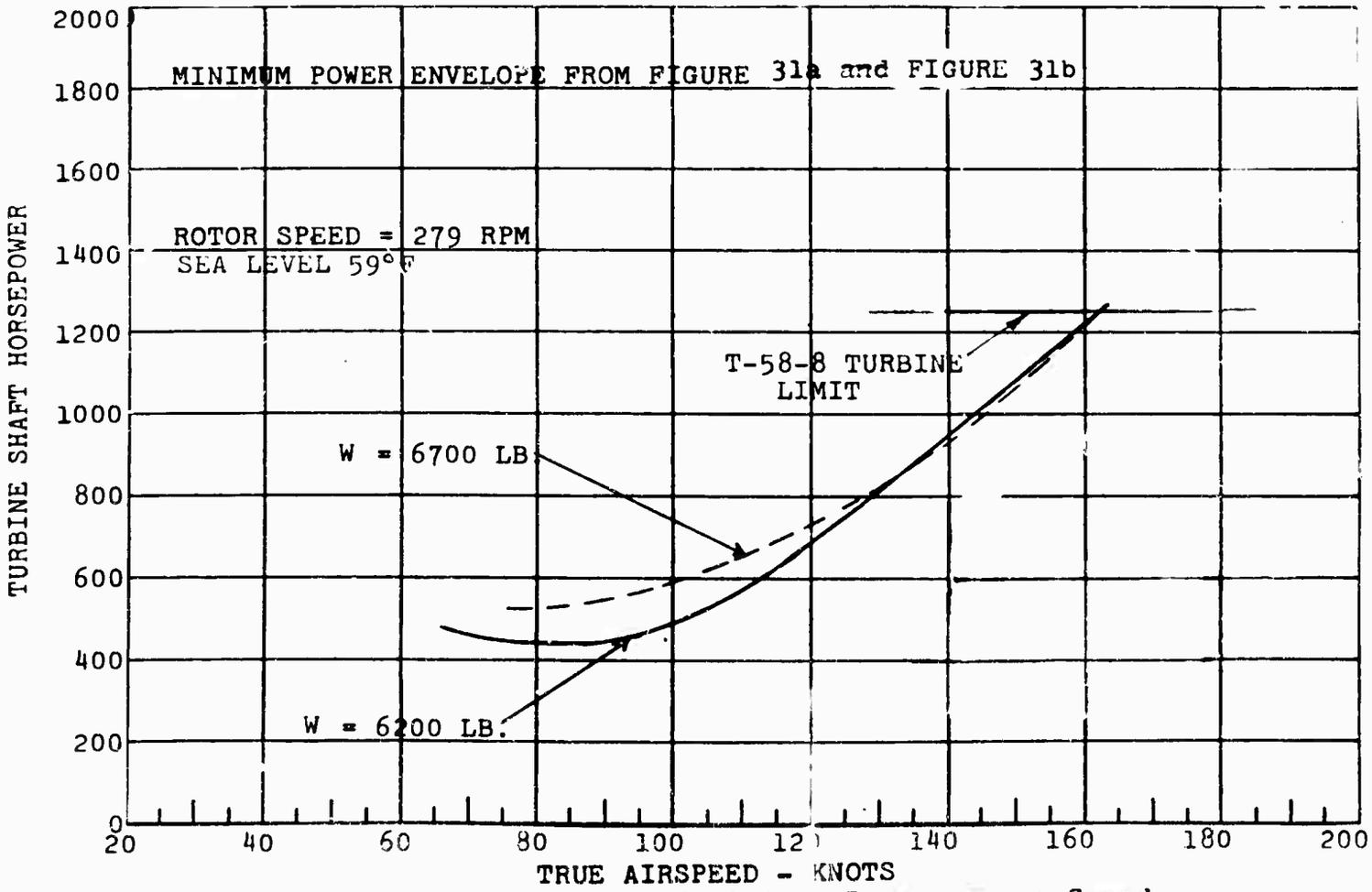


Figure 32. Envelope of Minimum Power versus Speed.

of rotor power to total power was plotted on Figure 33 as a function of airspeed for the various ranges of fuselage angle of attack with flaps neutral and extended.

Figure 34 shows the variation in rotor-lift-to-gross-weight ratio as a function of true airspeed with fuselage attitude considered as a parameter. The rotor lift-to-weight ratios are somewhat higher for the heavier gross weight, since the wing lift at a given angle of attack is constant and the added weight must be carried by the rotor. The variation in rotor loading with angle of attack shown in the plot reflects the increase in wing lift with increase in angle.

Rudder Position in Level Flight

Rudder position is presented as a function of true airspeed for various fuselage angles of attack. A separate curve is plotted for each fuselage angle of attack considered, and each plot shows the measured points from which it was constructed (Figure 36).

These curves show that rudder deflection changes in a direction that is to be expected as a function of airspeed and fuselage angle of attack. The individual plots for each fuselage angle of attack show that the left rudder decreases as forward speed increases. In the lower speed ranges of up to approximately 60 knots, with a fuselage angle of attack of +4 to +6 degrees, the reduction in left rudder angle is large. This is due to the rapid reduction in main rotor power as forward speed is increased from hover to approximately 60 knots. In addition, as airflow over the tail vanes is increasing with increasing forward speed, less left rudder deflection is required to counteract main rotor torque. This effect causes left rudder angle to continue to decrease with increasing forward speed even though main rotor power starts to increase as airspeed increases beyond the 60 knot range. The rate of decrease of left rudder angle starts to decrease as airspeed increases beyond the 60 knot range, due to the effect of increasing main rotor power and the rudder approaching neutral.

Comparison of the four curves for different angles of attack shows that left rudder decreases as fuselage angle of attack varies from negative to positive. This is as expected and results from the fact that, at a given speed, main rotor power decreases with increasing fuselage angle of attack.

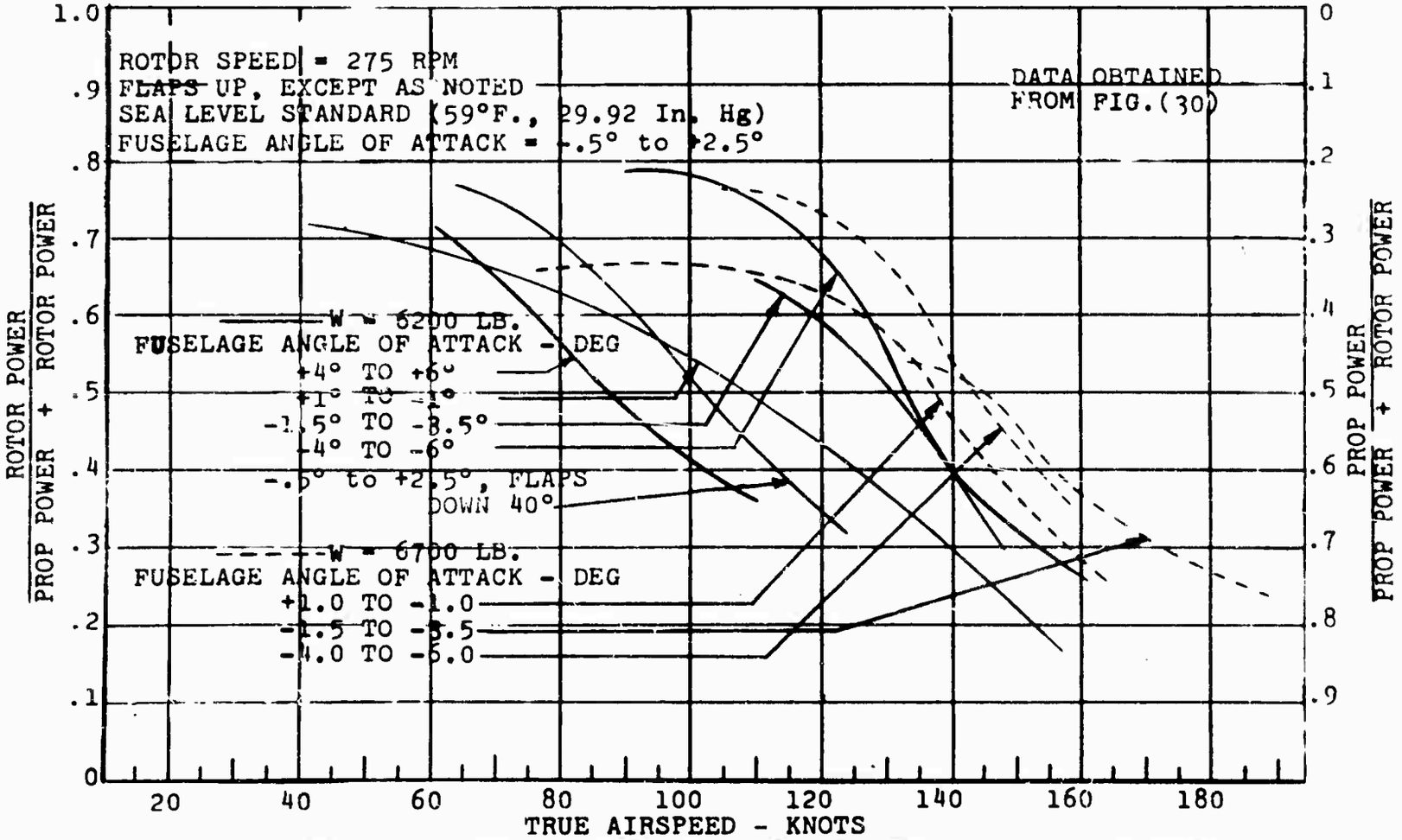


Figure 33. Division of Power Between Rotor and Propeller versus Airspeed.

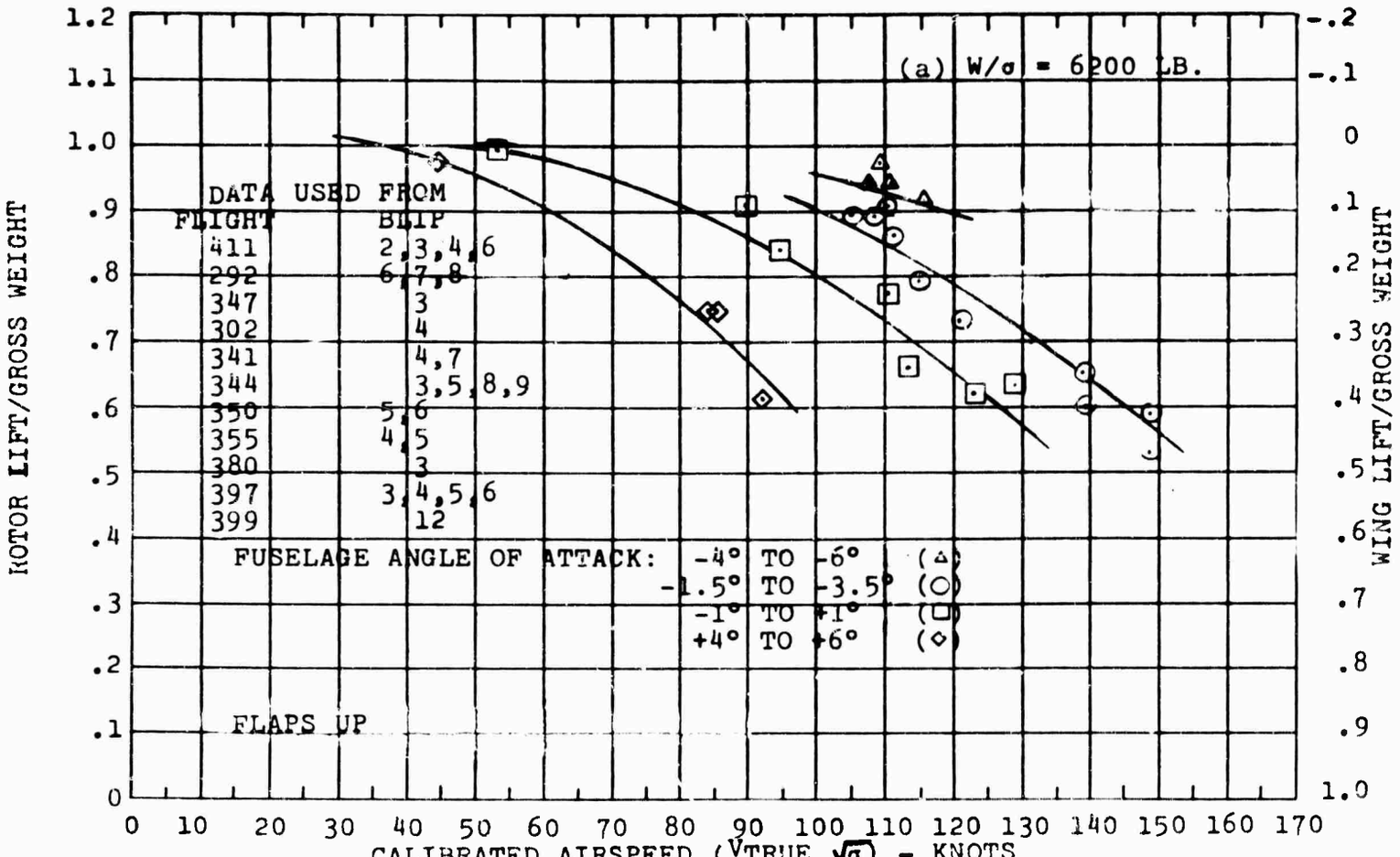


Figure 34. Rotor/Wing Lift Distribution versus Speed.

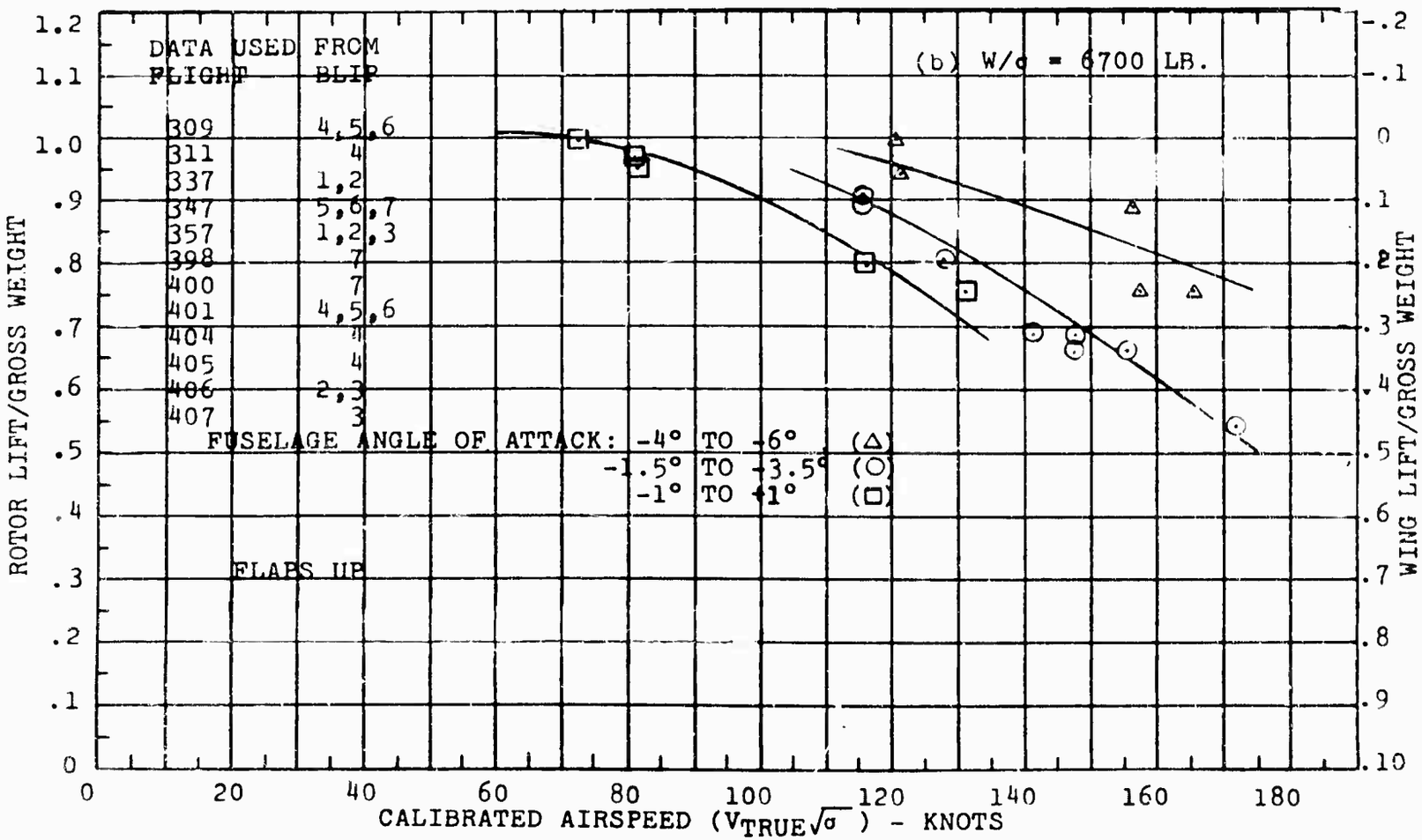


Figure 34.- Continued.

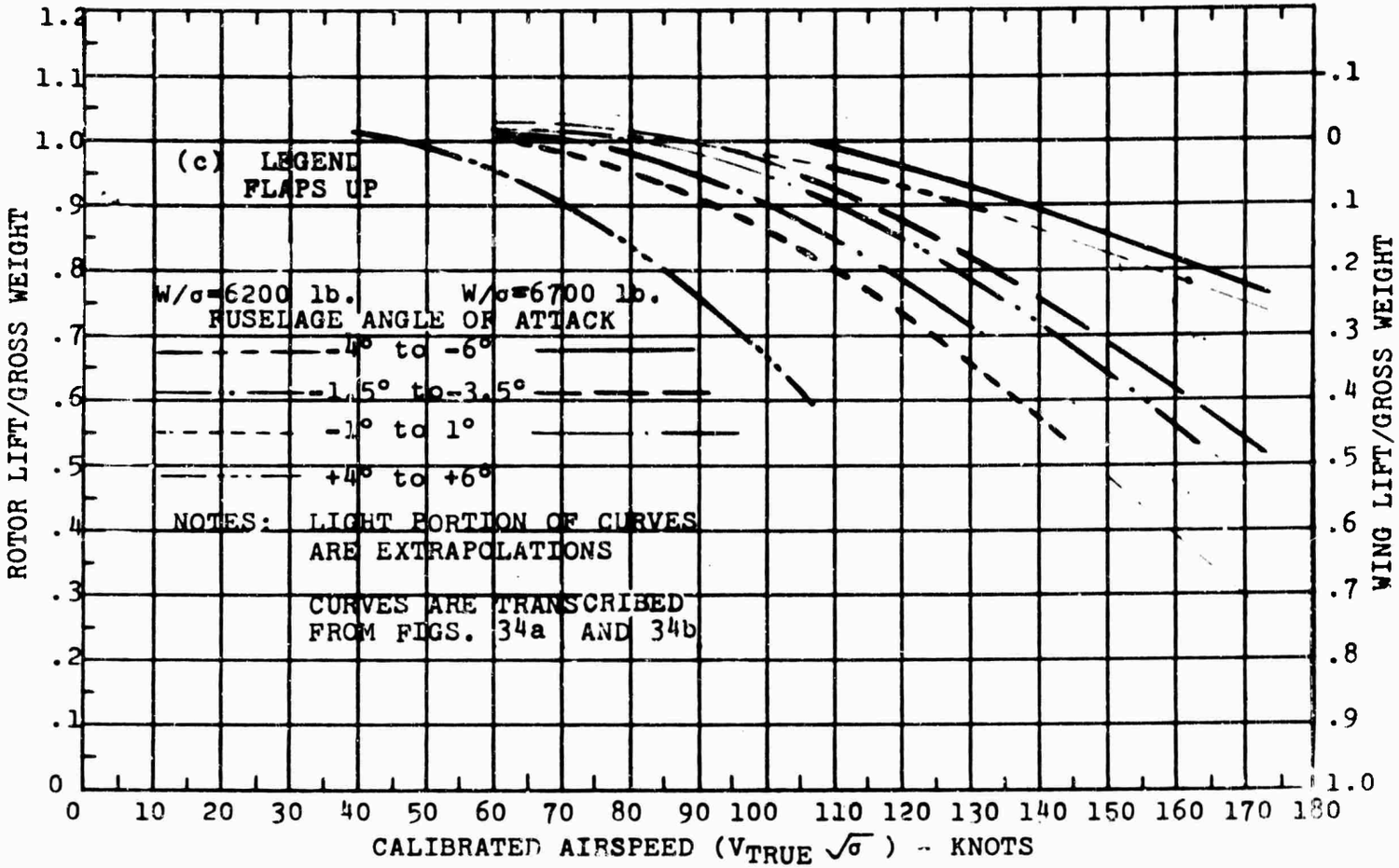


Figure 34.- Continued.

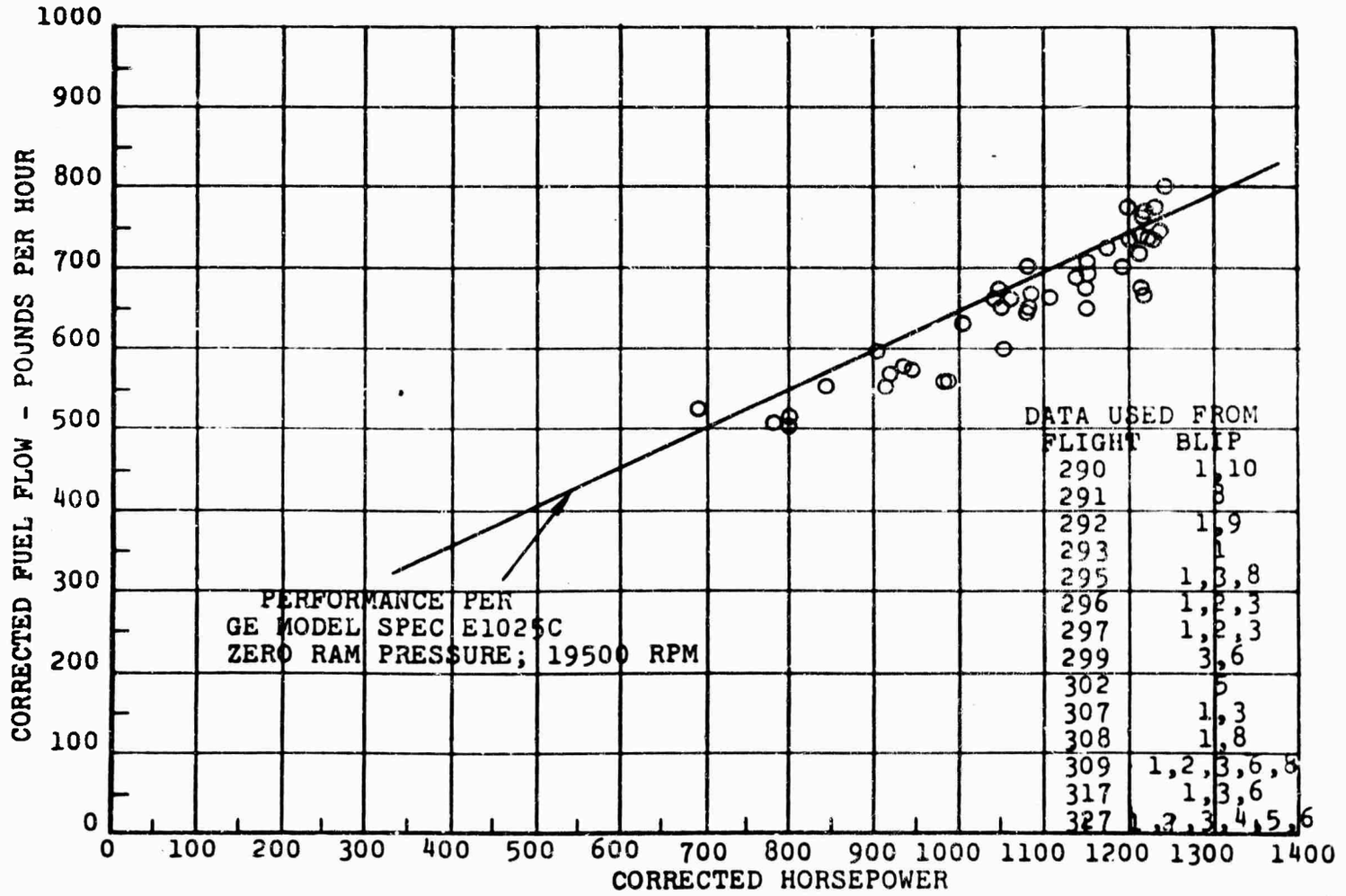


Figure 35. Fuel Flow versus Horsepower.

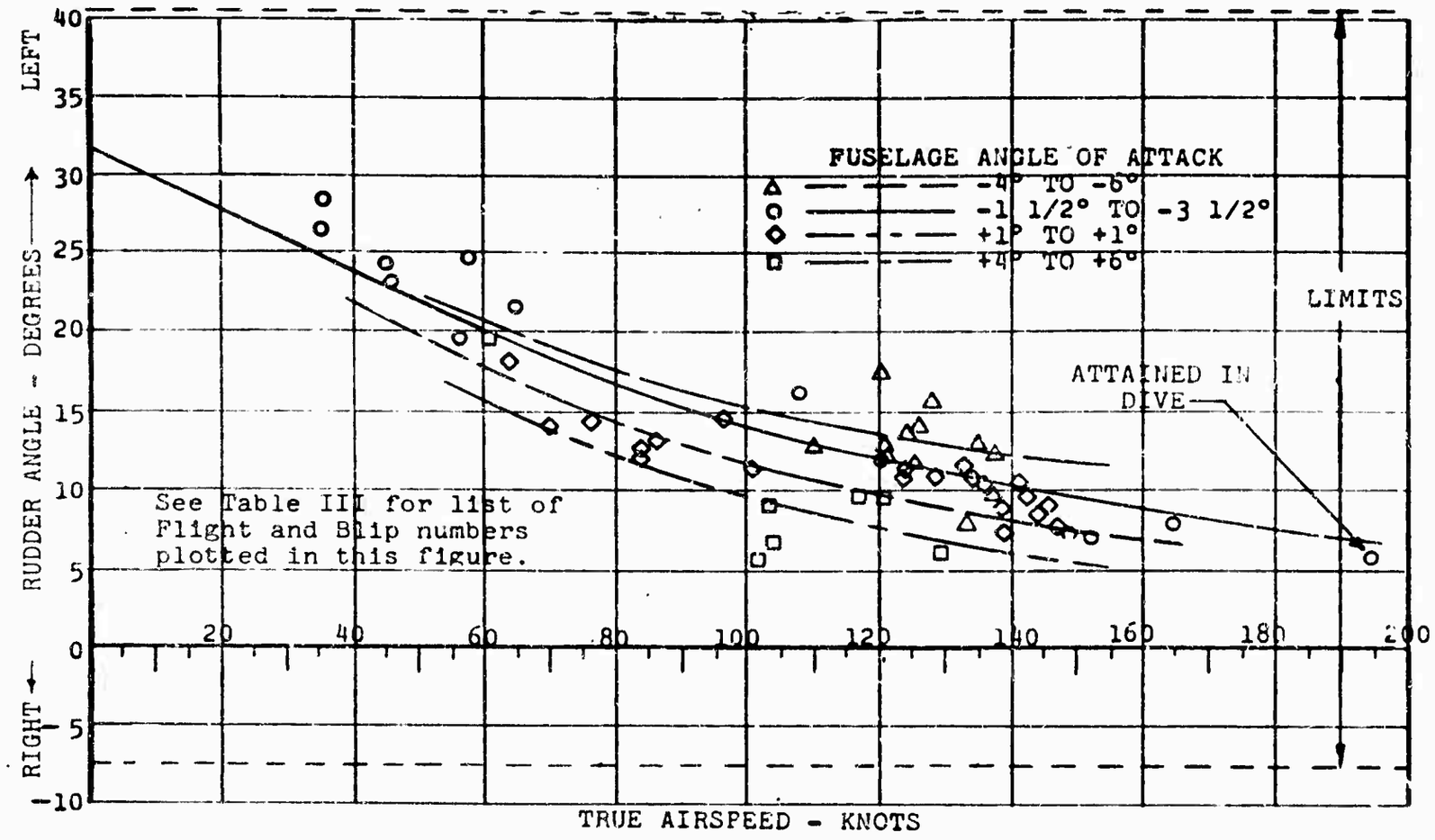


Figure 36. Rudder Position versus Speed, Level Flight.

TABLE III. FLIGHT AND BLIP NUMBERS FOR DATA USED IN PERFORMANCE CURVES

| FIG. NO. | FLIGHT | BLIPS | FLIGHT | BLIPS |
|---|---|---|---|---|
| 11 | 255 | 5 | 293 | 1 |
| | 257 | 1,2,3,4,5,6, 7,8,9,10,11, 12,14,15,16 | 412 | 1,2,3,4,5, 6.7,8,9 |
| | 262 | 1,8 | 420 | 1,2,3,4,5 |
| | 264 | 1,2,3,4,5,6, 7,8,9,11,13 14,17,18,19 | | 6,7,8,10,11 |
| | | | 422 | 1,2,3 |
| | 284 | 3,4,5 | | |
| | 285 | 1,8 | | |
| 12 | 262 | 1,8 | 412 | 1,2,3,4 |
| | 264 | 1,2,3,4,5,6 7,8,9,10,11, 12,13,14,15,16, 17,18,19,20 | | 6,7,8,9,10,12, 13,14,15 |
| | | | 401 | 1,2,3 |
| | | | 420 | 1,2,3,4,5,6, 7,8,9,10,11 |
| | 284 | 3,4,5 | 422 | 1,2,3 |
| | 285 | 1,8 | | |
| | 293 | 1,2 | | |
| | 327 | 1,2,4 | | |
| 19 | 286 | 2 | 297 | 2 |
| | 290 | 1,2,3,4 | 306 | 1,2 |
| | 292 | 2,3 | 309 | 1,2 |
| | 294 | 1,2,3 | 317 | 1,2,3,5,6 |
| | 295 | 1,2,3,4 | 399 | 1,2,3 |
| | 296 | 1,2 | 406 | 4,5 |
| 36 | 272 | 5,7 | | |
| | 274 | 5,7 | 337 | 1,2,4 |
| | 275 | 7,8,10 | 341 | 2,4,7 |
| | 285 | 4,6,7 | 344 | 5 |
| | 290 | 7 | 347 | 5,6,7 |
| | 292 | 4,5,6,7, 10,11 | 350 | 4,7 |
| | | | 353 | 3,4,5 |
| | 295 | 10 | 355 | 4,5,7 |
| | 296 | 4 | 356 | 2,3 |
| | 302 | 4 | 357 | 1,2,3 |
| | 306 | 4,5,7 | 375 | 4 |
| | 307 | 1,2,3 | 380 | 2,3 |
| | 309 | 5,6 | 397 | 6 |
| | 311 | 4,5,6 | 404 | 2,3,5,6 |
| | 312 | 7 | 405 | 1,3,4 |
| | 328 | 2,3 | 407 | 3,4 |

## STOL PERFORMANCE

The handling qualities of the Model 16H-1A compound helicopter during forward velocity takeoff and landing are of conventional tail-wheel airplane nature. From the pilot's standpoint, the aircraft is directionally stable and controllable at ground speeds up to 60 knots (the highest attained).

Takeoffs were conducted using a low collective pitch setting in an attempt to simulate a STOL gross weight. Constant collective pitch setting was held throughout the run from start to lift-off. There was no provision for maintaining a constant longitudinal cyclic control position except by pilot "feel". Thus, different cyclic control settings between takeoff runs are partly responsible for the variation in takeoff distances which appear in the test results shown in the Table IV. Another factor which contributed to this was the variation of tail propeller torque between takeoff runs due to variations in the rate of pilot application of tail propeller pitch after brake release. The propeller pitch actuator is controlled by the pilot through a beep-type switch and visual pitch angle indicator on the instrument panel.

The 16H-1A tests were performed at gross weights considerably lower than the normal STOL gross weight. As a consequence, rotor thrusts were arbitrarily reduced and the major propulsive force was developed by the propeller rather than by inclination of the thrust vector. For this reason the results do not represent STOL capability at the higher gross weights but they do confirm the adequacy of control and handling qualities in takeoff operation.

Since the STOL flights were all made at gross weights at which VTOL could have been performed, direct plots of takeoff or landing distance versus gross weight are not feasible. A new analytical method needs to be developed whereby the data can be applied to an equivalent higher STOL weight by using measured power and thrust in the rotor and propeller versus speed and distance and available power.

The ground distance data have been analyzed by establishing the rotor and propeller thrust forces and power from records. It was found that the distance could be predicted with reasonable accuracy by the relation

TABLE IV. FORWARD VELOCITY TAKEOFF DATA

| FLIGHT NUMBER | BLIP NUMBER | GROSS WEIGHT (LB) | C.G. FWD. (IN) | * COLL. PITCH (DEG) | * PROP PITCH (DEG) | FLAP POSITION (DEG) | * HORIZ. TRIM (DEG) | WIND DIR. (DEG) | WIND VEL. (KN) | LIFTOFF AIR SPEED (KN) | GROUND RUN TO TAKEOFF (FT) | TAKE-OFF DIR. (DEG) |
|---|---|---|---|---|---|---|---|---|---|---|---|---|
| 329 | 1 | 6422 | 8.7 | 5 | 25 | 0 | 0 | 220 | 7 | 45 | 440 | 300 |
| 329 | 3 | 6422 | 8.7 | 2 | 25 | 0 | 0 | 220 | 7 | 60 | 680 | 300 |
| 329 | 5 | 6422 | 8.7 | 4 | 25 | 0 | 0 | 220 | 7 | 55 | 750 | 300 |
| 367 | 1 | 6115 | 6.7 | 4 | 25 | 10 | 0 | 240 | 5 | 55 | 750 | 120 |
| 367 | 3 | 6115 | 6.7 | 4 | 25 | 20 | 0 | 240 | 5 | 45 | 500 | 120 |
| 367 | 5 | 6115 | 6.7 | 4 | 25 | 30 | 0 | 240 | 5 | 45 | 522 | 120 |
| 367 | 7 | 6115 | 6.7 | 4 | 25 | 40 | 0 | 240 | 5 | 45 | 575 | 120 |
| 366 | 1 | 6115 | 6.7 | 4 | 25 | 0 | 0 | 230 | 5 | 40 | 424 | 120 |
| 392 | 4 | 6113 | 9.3 | 3 | 25 | 0 | 0 | 160 | 5 | 39 | 440 | 120 |
| 392 | 5 | 6140 | 9.3 | 3 | 25 | 0 | 0 | 160 | 5 | 50 | 380 | 120 |
| 394 | 1 | 6140 | 9.6 | 5 | 25 | 40 | 0 | 110 | 3 | -- | 350 | 120 |
| 395** | 4 | 6140 | 9.6 | 3 | 25 | 0 | 0 | 180 | 2 | 35 | 400 | 300 |
| 395** | 5 | 6165 | 9.6 | 3 | 25 | 40 | 0 | 180 | 10 | 40 | 250 | 300 |
| 404 | 1 | 6166 | 9.5 | 2 | 25 | 40 | 0 | 210 | 10 | 50 | 580 | 300 |
| 419 | 8 | 7000 | 10.1 | | | 0 | 0 | 330 | 11 | 50 | 440 | 300 |
| 420 | 12 | 7000 | 10.1 | 5 | 28 | 0 | 0 | 350 | 7 | 50 | 350 | 300 |
| 420 | 13 | 7000 | 10.1 | 0-5 | 28 | 0 | 0 | 350 | 7 | 50 | 440 | 300 |

* Recorded in Cockpit

** 5600 RPM (All others at 6000 RPM)

TABLE V. FORWARD-VELOCITY/FIXED COLLECTIVE-PITCH RUN-ON LANDINGS

| FLIGHT NUMBER | BLIP NUMBER | GROSS WEIGHT (LB) | C.G. FWD. (IN) | * COLL. PITCH (DEG) | * PROP PITCH (DEG) | FLAP POSITION (DEG) | HORIZ. TRIM (DEG) | WIND DIR. (DEG) | WIND VELOCITY (KN) | LAND DIR. (DEG) | A/S AT TOUCH DOWN (KN) | GROUND RUN TO STOP (FT) |
|---|---|---|---|---|---|---|---|---|---|---|---|---|
| 329 | 2 | 6422 | 8.7 | 5 | -5 | 0 | 0 | 220 | 7 | 120 | 45 | 258 |
| 329 | 4 | 6422 | 8.7 | 2 | -5 | 0 | 0 | 220 | 7 | 120 | 47 | 327 |
| 329 | 6 | 6422 | 8.7 | 4 | -5 | 0 | 0 | 220 | 7 | 120 | 45 | 323 |
| 356 | 10 | 6030 | 8.9 | 3 | -5 | 0 | 0 | 260 | 3 | 120 | 46 | 325 |
| 366 | 2 | 6115 | 6.7 | 4 | -5 | 0 | 0 | 230 | 9 | 120 | 42 | --- |
| 367 | 2 | 6115 | 6.7 | 4 | -5 | 10 | 0 | 240 | 5 | 300 | 40 | --- |
| 367 | 4 | 6115 | 6.7 | 4 | -5 | 20 | 0 | 240 | 5 | 300 | 45 | 350 |
| 367 | 6 | 6115 | 6.7 | 4 | -5 | 30 | 0 | 240 | 5 | 300 | 45 | 325 |
| 367 | 8 | 6115 | 6.7 | 4 | -5 | 40 | 0 | 240 | 5 | 300 | 55 | 500 |
| 396 | 3 | 6140 | 9.6 | 2 | -12 | 0 | 0 | 230 | 6 | 300 | 40 | 400 |
| 402 | 11 | 6153 | 9.6 | 0 | -12 | 40 | 0 | 290 | 6 | 300 | 37.5 | 315 |
| 415 | 2 | 6170 | 9.7 | 4 | -12 | 0 | 0 | 300 | 6 | 300 | 40 | --- |

* Recorded in Cockpit

$$S_g = 1.1 \frac{W}{2g} \frac{V_{T.O.}^2}{F_{avr}} \qquad (37)$$

where $S_g$ = ground roll distance, feet

$W$ = gross weight, pounds
$g$ = 32.2 feet per second per second
$V_{T.O.}$ = takeoff speed, feet per second
$F_{avr}$ = the average propulsive force which is the sum of the rotor force horizontal component and the propeller thrust.

This relation is shown in Figure 37.

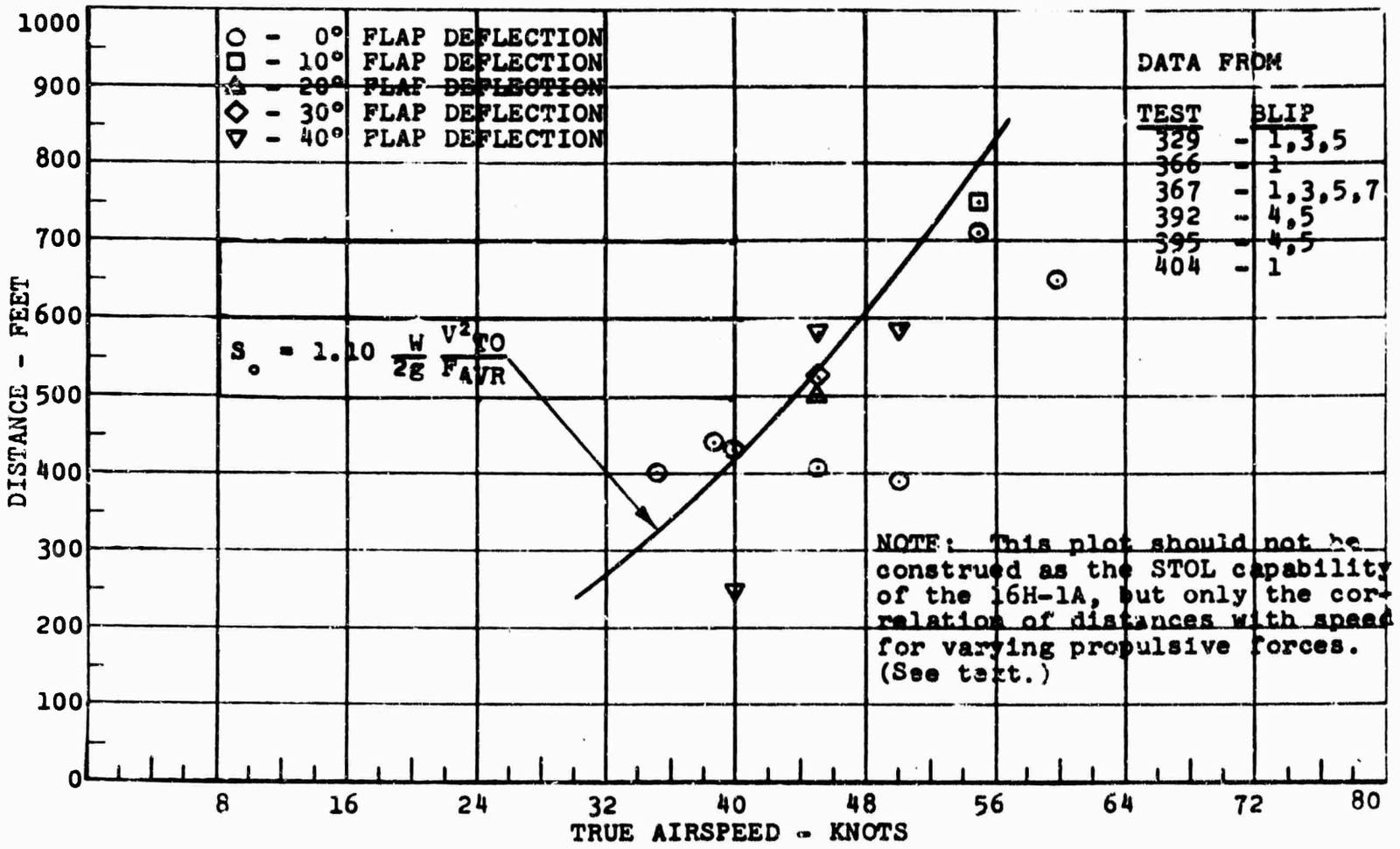


Figure 37. Ground Roll Distance versus Lift-Off Speed.

## VIBRATION

Vibration records were obtained at a number of fuselage locations throughout the test operational range. Suitable data for analysis and discussion of vibration amplitude and frequencies were confined to the data obtained at the pilot's station. (Actually, it was the copilot's station, which has structure identical to the pilot's). Effort was concentrated on this item because of its importance in establishing acceptable flying qualities.

Fourier analyses of the measured vertical accelerations at the pilot's station were performed in order to determine the amplitudes at discrete rotor harmonic frequencies. This was done because pilot perception and tolerance levels depend upon frequency. (MIL-H-8501A (Reference 4) gives upper limits of acceptable accelerations as a function of frequency.) The extracted first through the tenth rotor harmonic components of the vertical acceleration are plotted in Figures 38 through 47 as a function of forward speed. Included in each figure is the acceleration from the data obtained with the original control system; that is, before stiffening. This aspect is discussed in the "Technical Problems" section, and it is apparent that acceleration levels were markedly reduced by stiffening, particularly at the third rotor harmonic, which is the largest acceleration component.

In MIL-H-8501A it is stated that accelerations at airspeeds below cruise speed are to be less than 0.15g for frequencies up to 32 cycles per second (through the sixth rotor harmonic for the 16H-1A); at airspeeds above cruise, accelerations are to be less than 0.20g for frequencies up to 36 cycles per second (through the seventh rotor harmonic for the 16H-1A). At frequencies higher than these, the specification cites vibration limits in terms of displacement, so that the allowable acceleration is a function of frequency. These allowable acceleration limits are shown in Figures 38 through 47. Cruise speed is taken as speed for best range, which is 130 knots true airspeed for the test aircraft.

Figures 38 through 47 show that vibration amplitudes throughout the speed range are well below the limits allowed by MIL-H-8501A, with the exception of the third harmonic. The latter is within the specification limit at speeds between 50 and 120 knots. It is slightly in excess of this limit at speeds between 130 and 155 knots and in the transition range between 20 and 45 knots. One point obtained in a 195-knot, 10-degree dive shows a third-harmonic component of 0.55g.

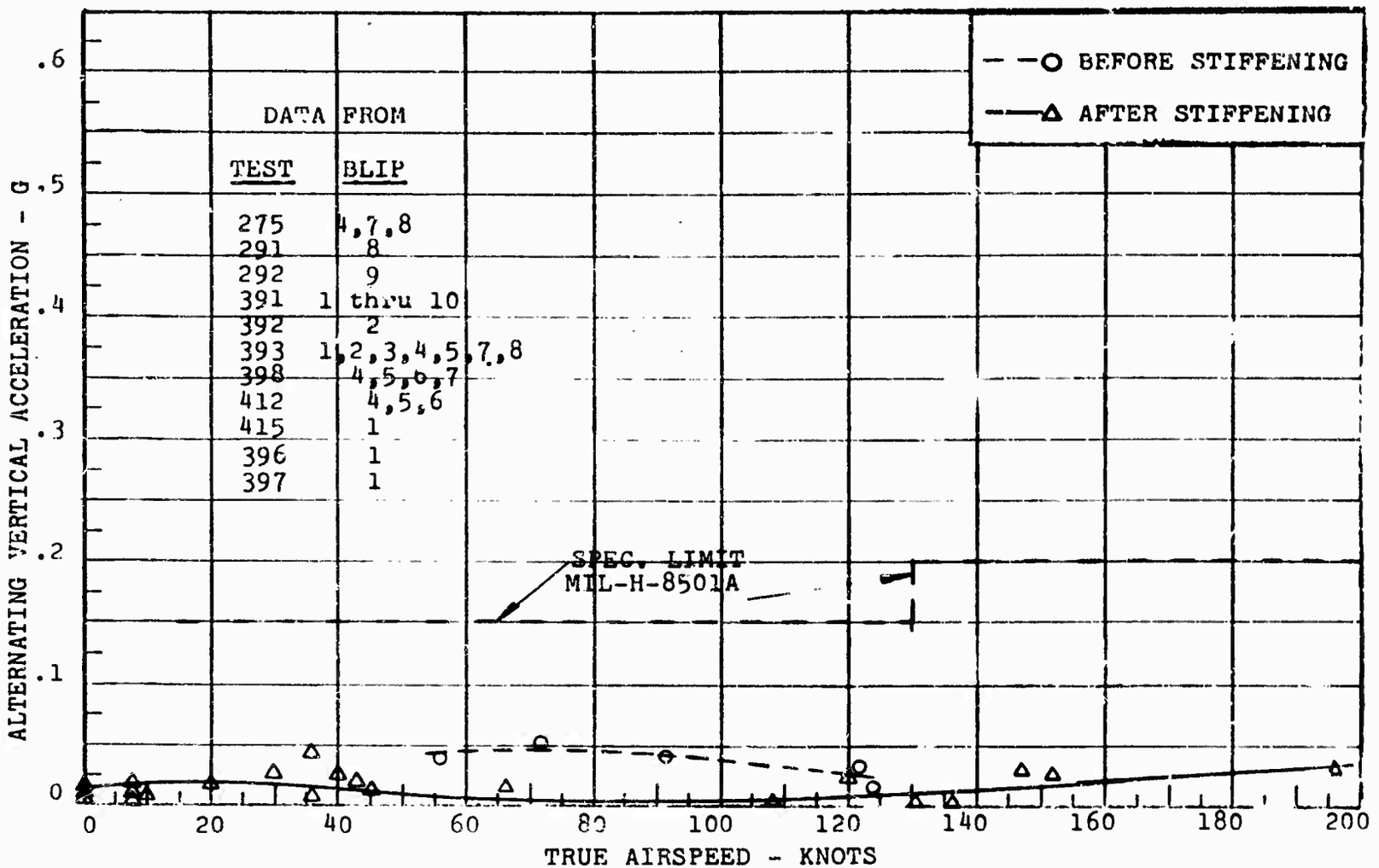


Figure 38. 1st Harmonic Vertical Acceleration at Pilot Station versus True Airspeed.

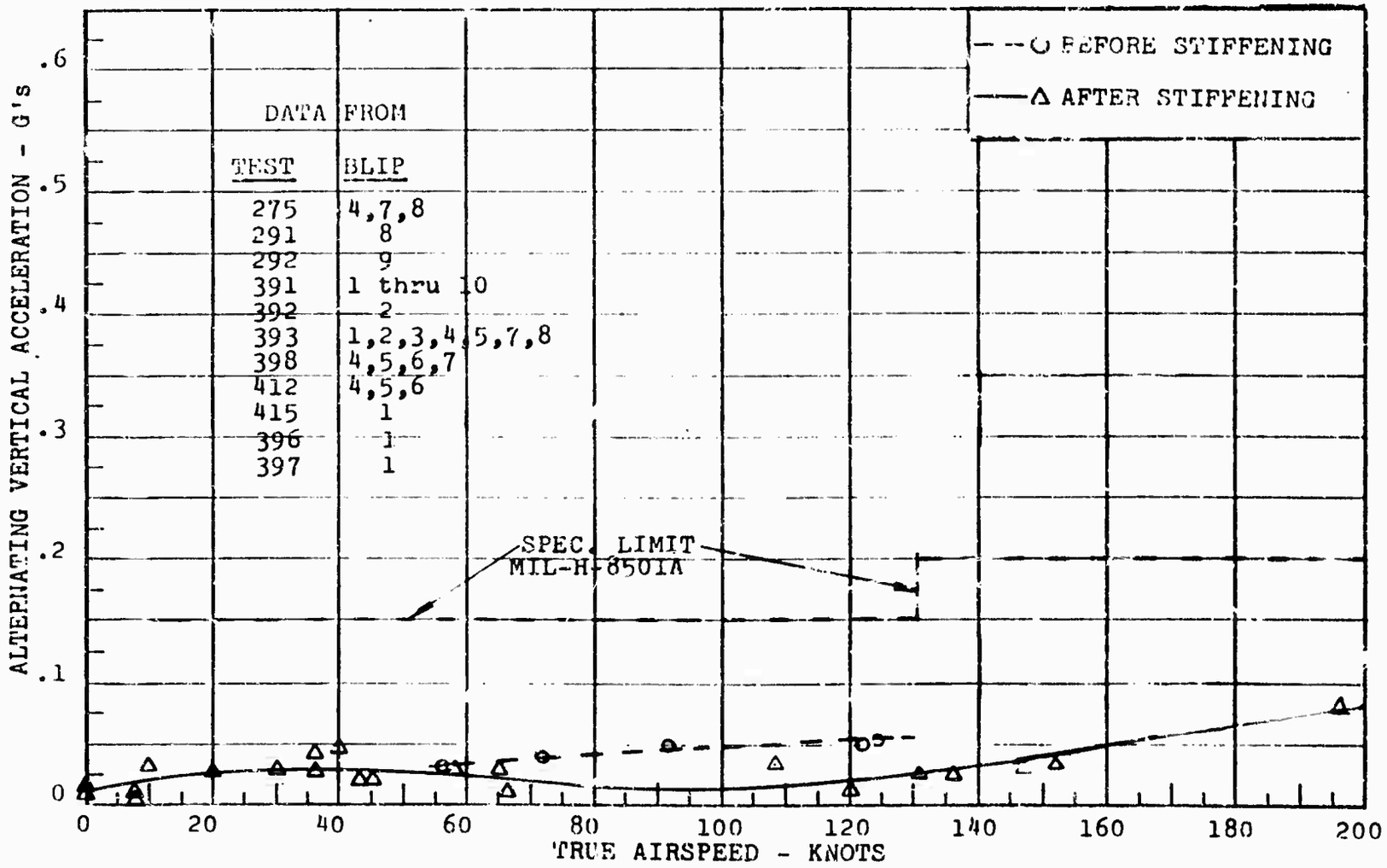


Figure 39. 2nd Harmonic Vertical Acceleration at Pilot Station versus True Airspeed.

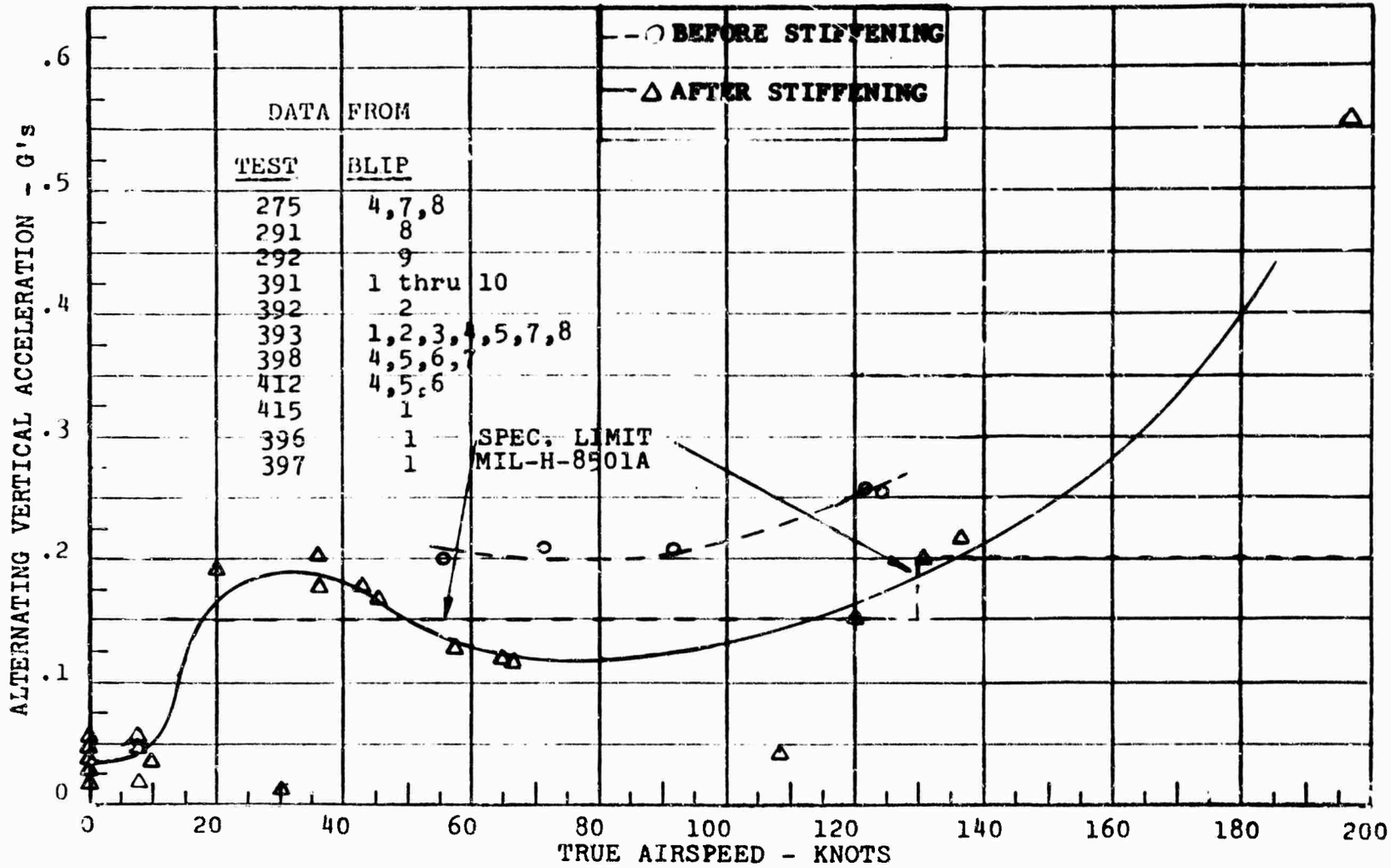


Figure 40. 3rd Harmonic Vertical Acceleration at Pilot Station versus True Airspeed.

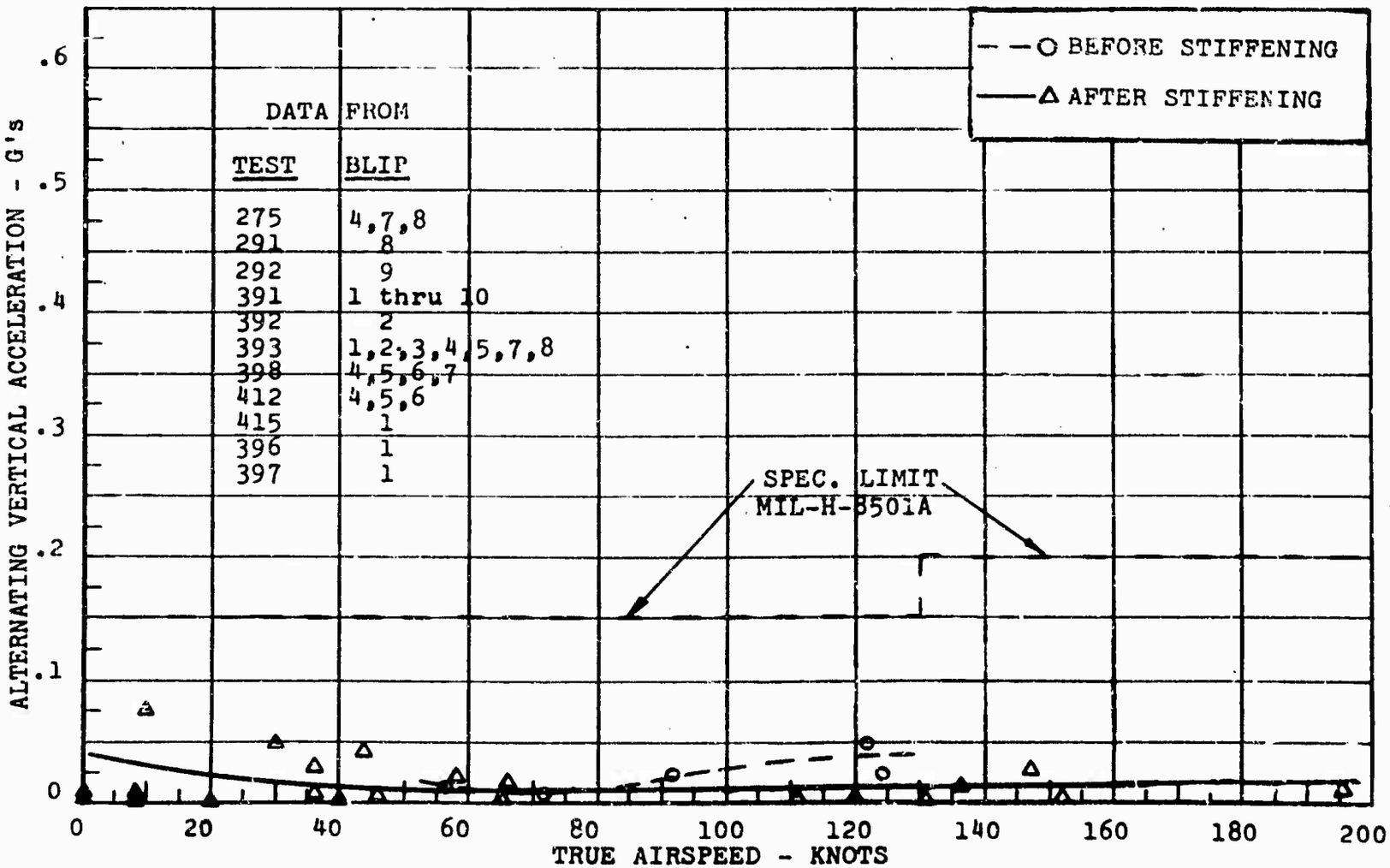


Figure 41. 4th Harmonic Vertical Acceleration at Pilot Station versus True Airspeed.

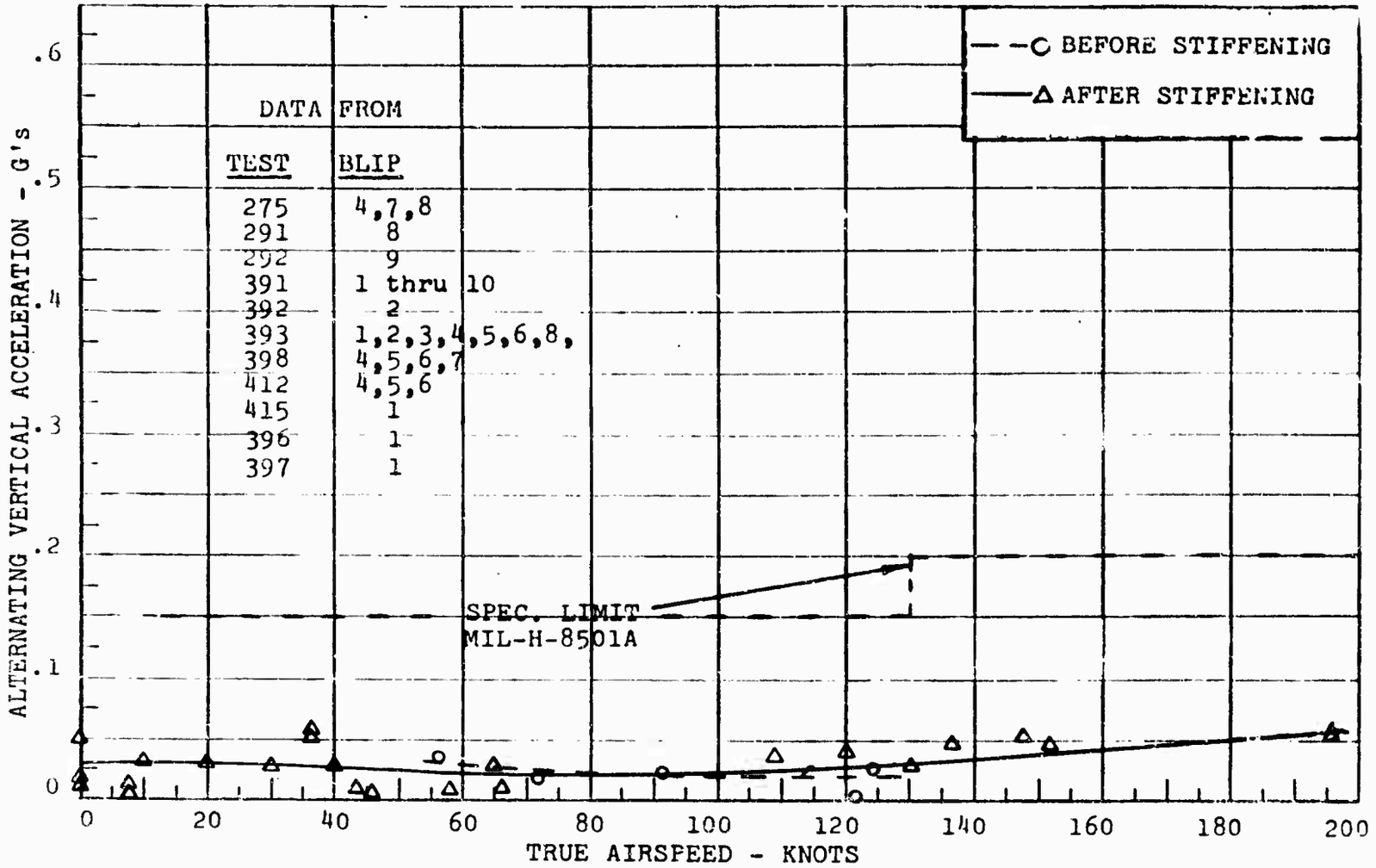


Figure 42. 5th Harmonic Vertical Acceleration at Pilot Station versus True Airspeed.

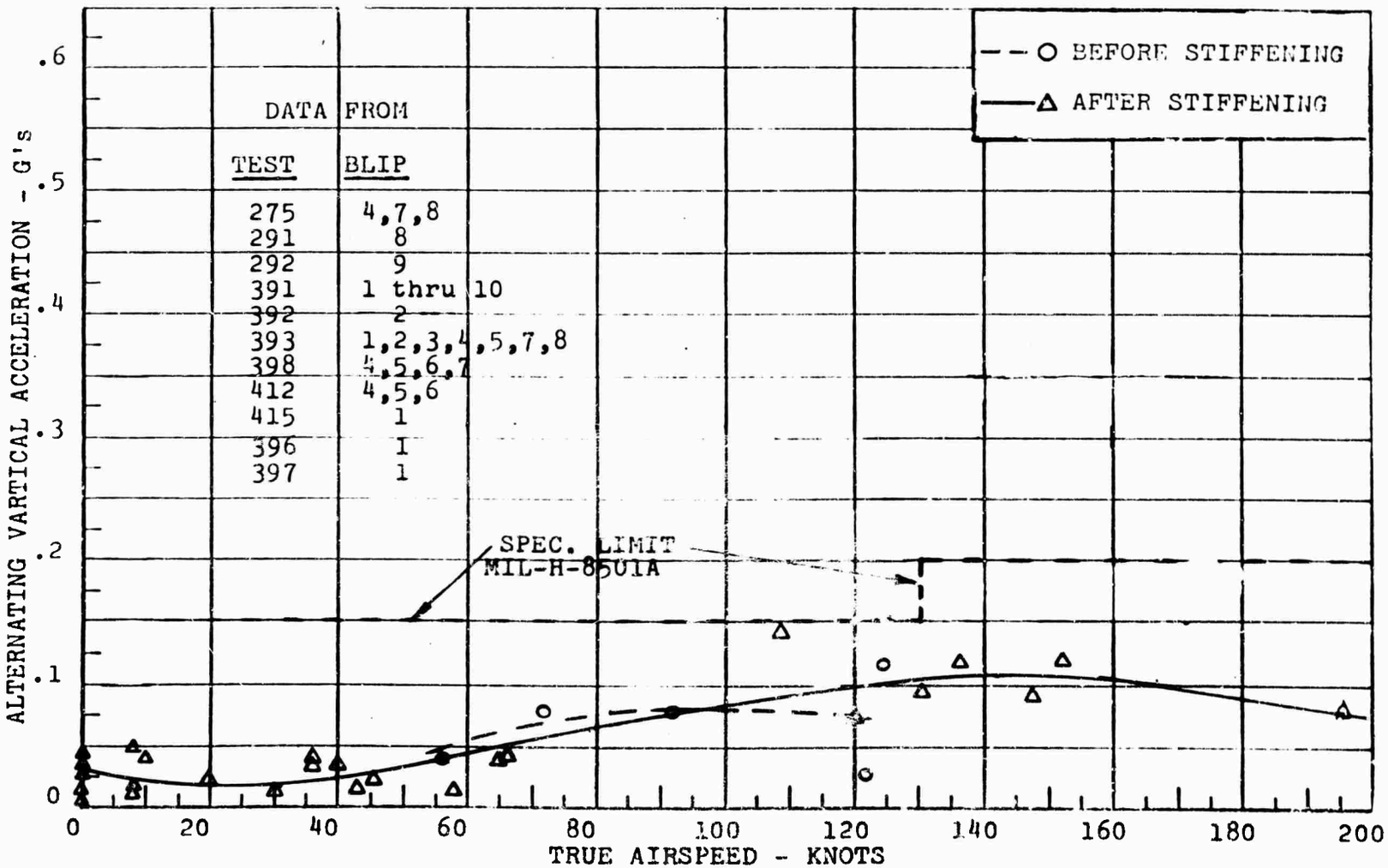


Figure 43. 6th Harmonic Vertical Acceleration at Pilot Station versus True Airspeed.

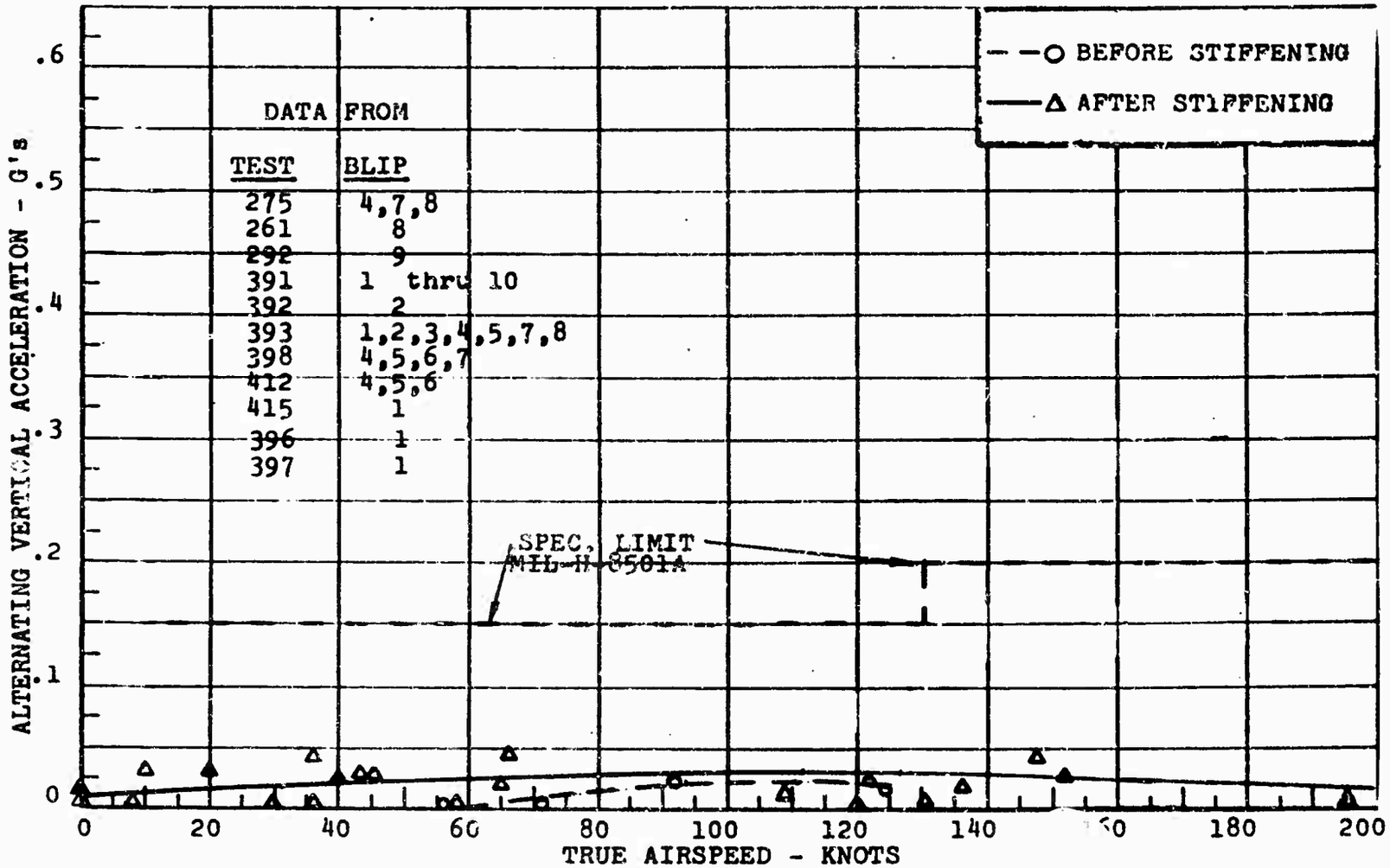


Figure 44. 7th Harmonic Vertical Acceleration at Pilot St
versus True Airspeed.

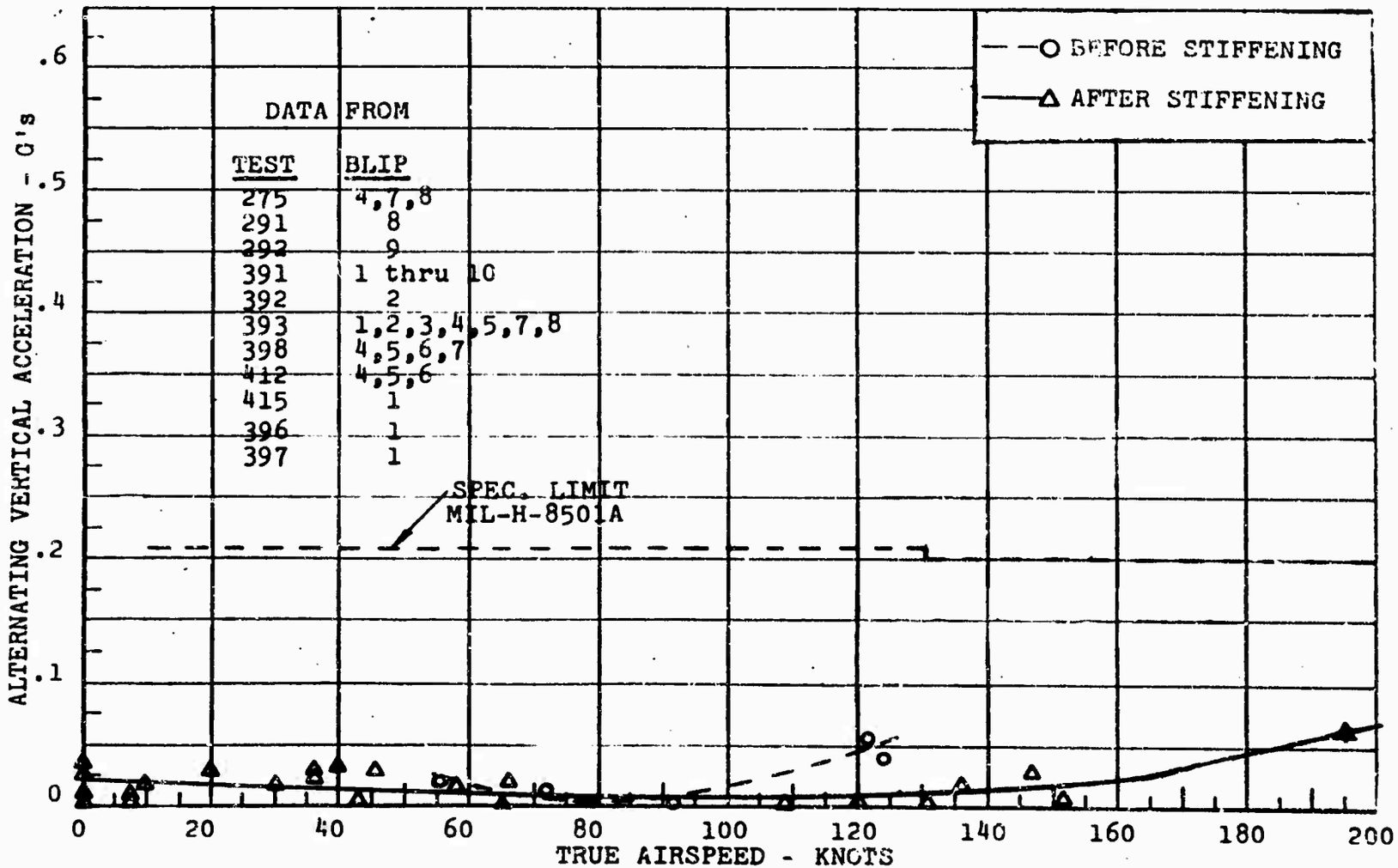


Figure 45. 8th Harmonic Vertical Acceleration at Pilot Station versus True Airspeed.

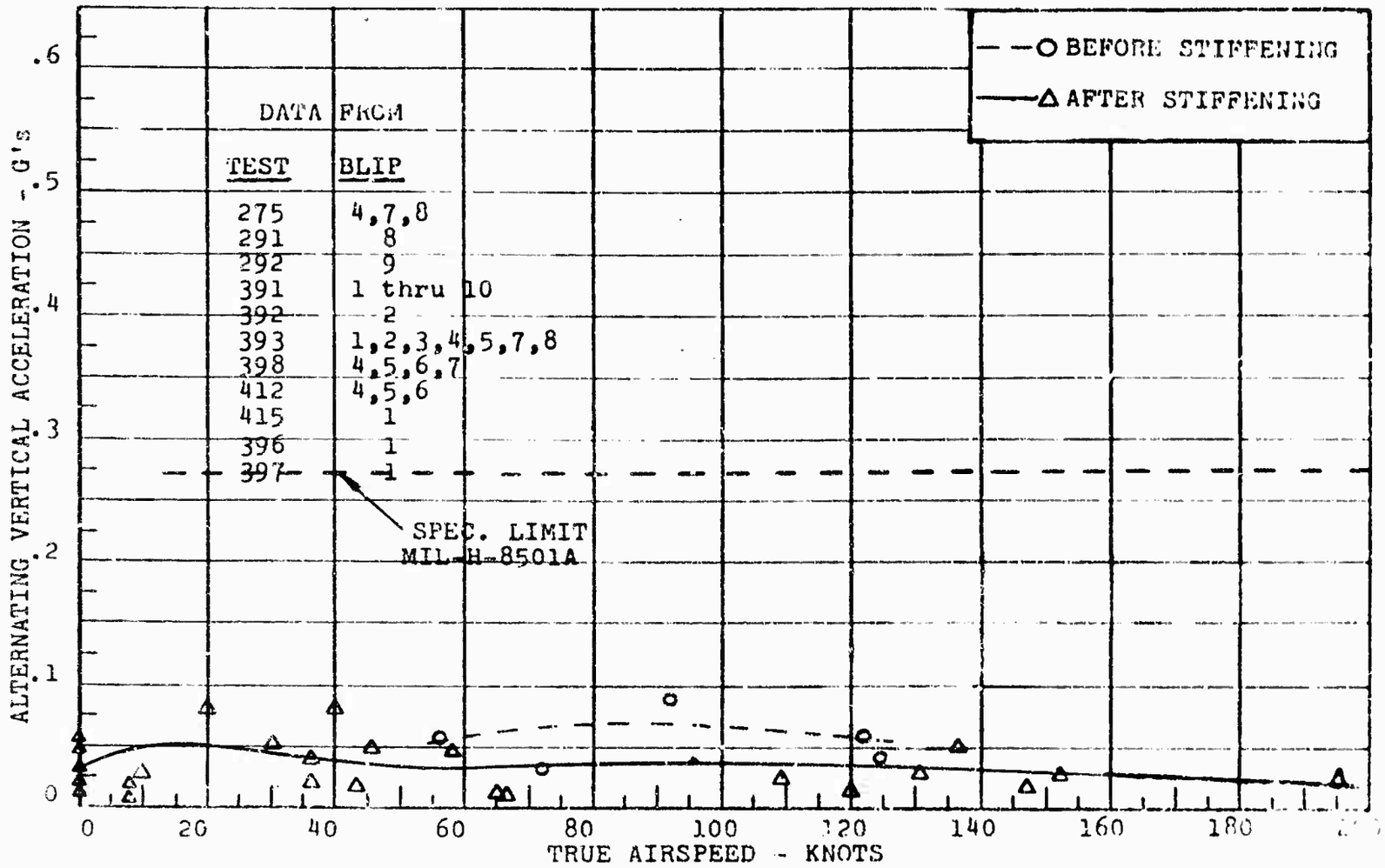


Figure 46. 9th Harmonic Vertical Acceleration at Pilot Station versus True Airspaed.

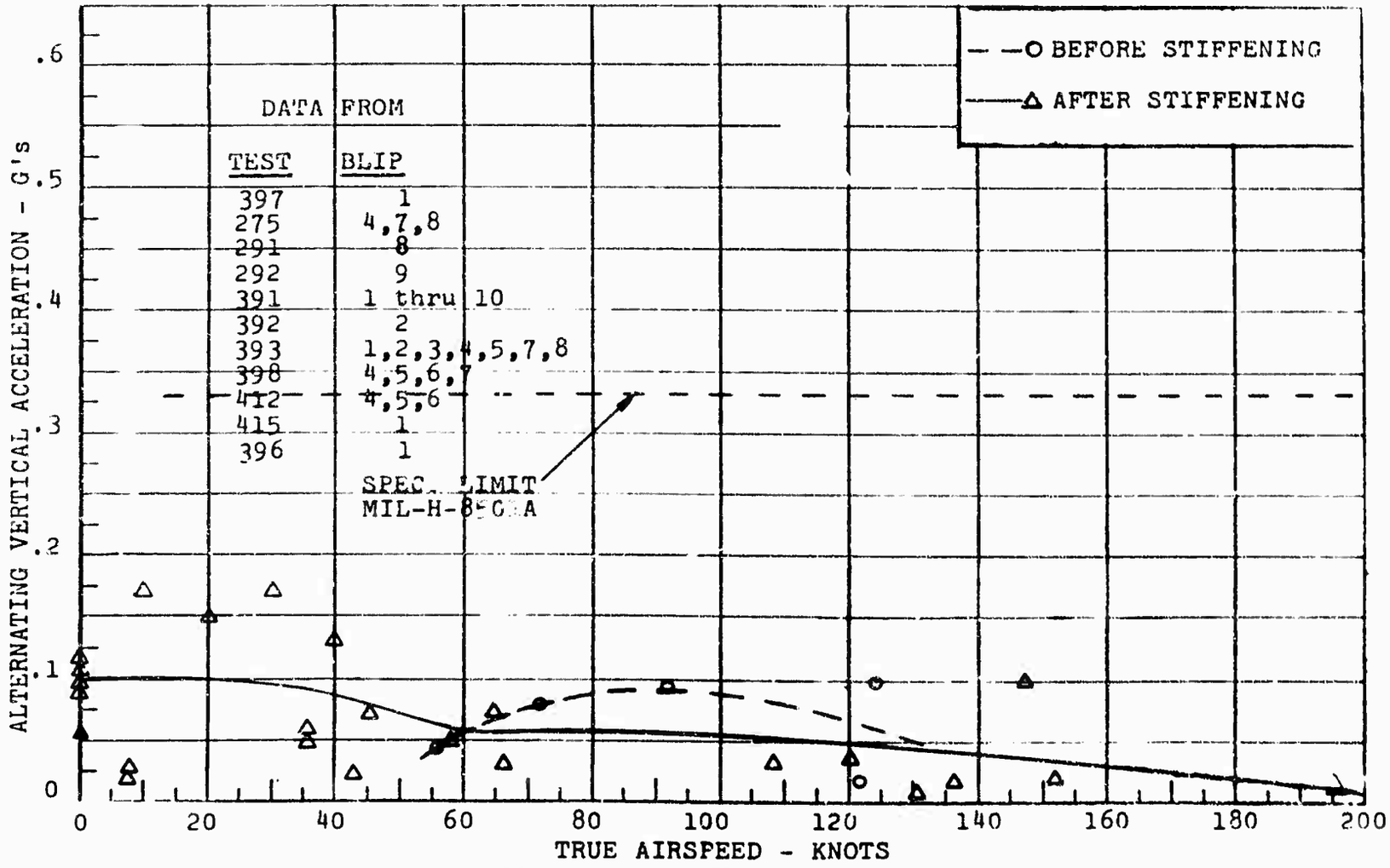


Figure 47. 10th Harmonic Vertical Acceleration at Pilot Station versus True Airspeed.

## Vibrational Frequencies

The vibrational frequencies of the dominant acceleration components have been measured at the rotor transmission main case (Figure 48), at the propeller drive shaft bearing support (Figure 49), at the propeller shaft (Figures 50, 51, and 52), and at fuselage station 9.5 (Figure 53). It is seen that the vibrational frequencies are about 36 cycles per second for the transmission and tail propeller drive shaft bearing support. The tail propeller shaft rotational speed is 45 revolutions per second. The measured propeller shaft frequencies are 40 cycles per second in the longitudinal, vertical, and lateral directions, and are thus closer to the propeller rotational speed. At fuselage station 9.5, the frequencies are approximately 12 cycles per second. Three-per-rotor revolution is 14 cycles per second.

In general, it may be seen that the higher-frequency vibrations present at the transmission, tail propeller shaft, and tail propeller bearing support are influenced mostly by the forced vibrations from the tail propeller, whereas the vibrations of the forward fuselage station 9.5 (nose of aircraft) are influenced mostly by the three-per-revolution forced vibrations of the rotor. There appeared to be no significant interaction between the high harmonics of the rotor and the corresponding tail propeller frequencies.

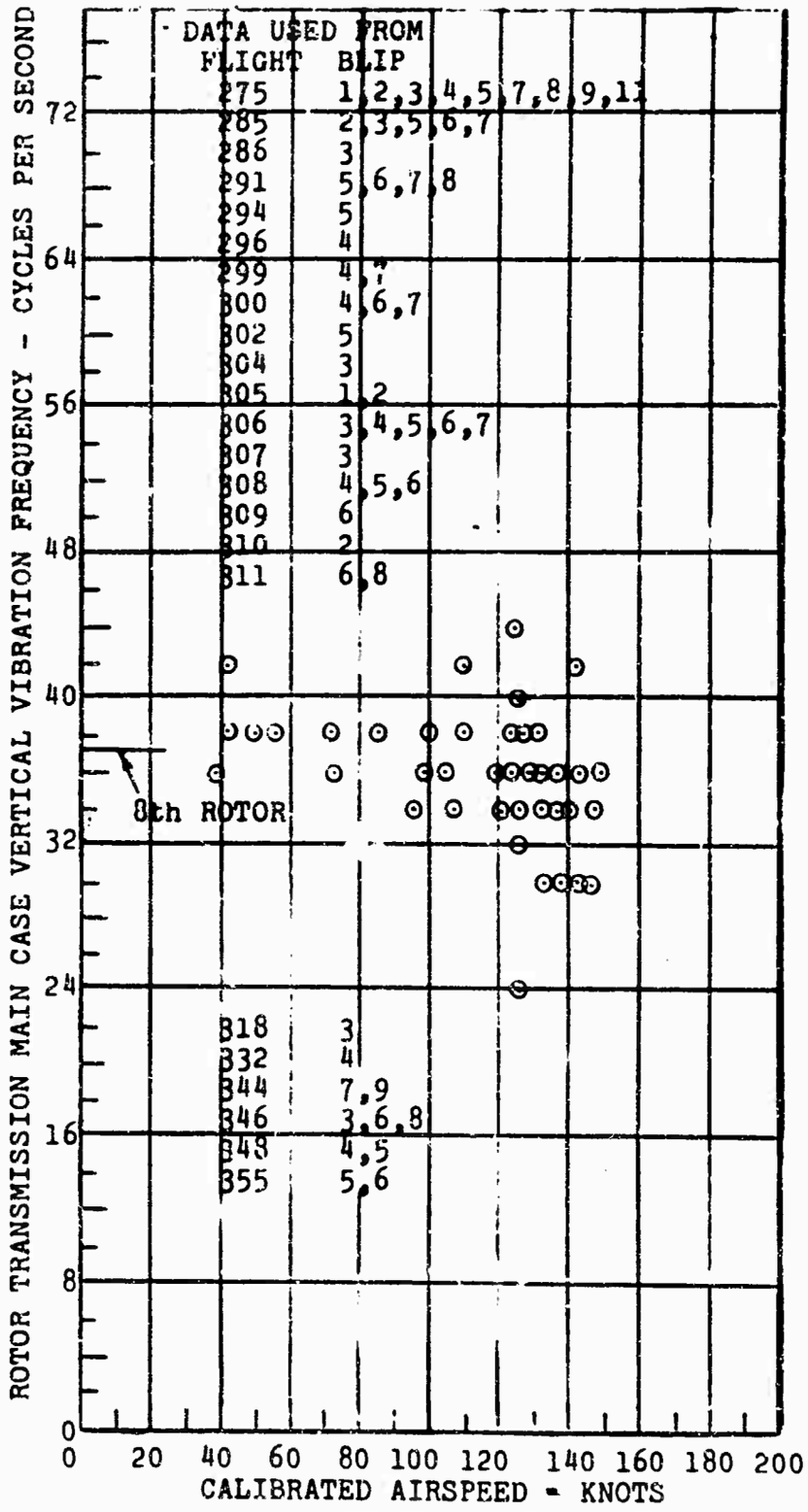


Figure 48. Rotor-Transmission Main Case Vibration.

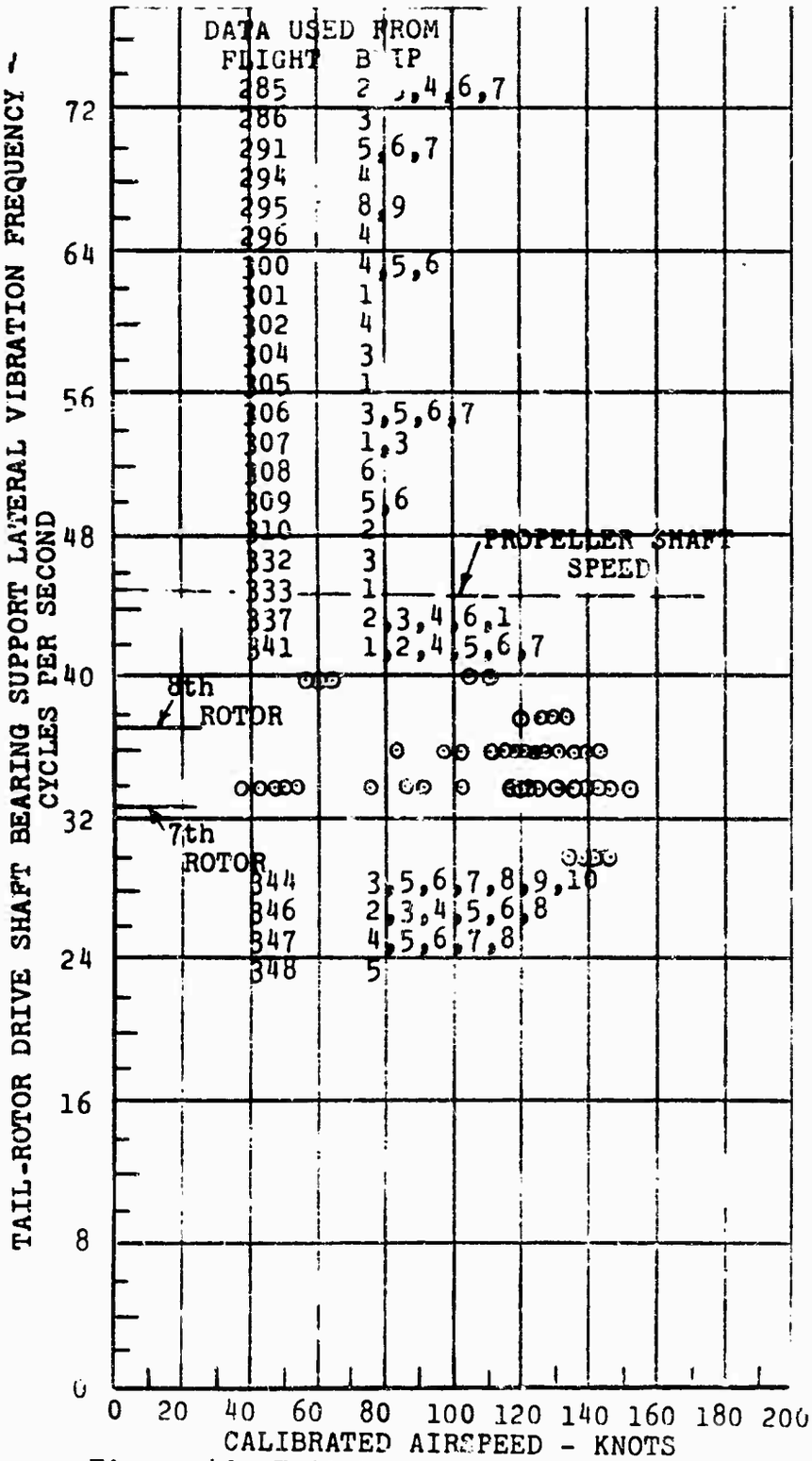


Figure 49. Tail-Rotor Drive Shaft Bearing-Support Vibration.

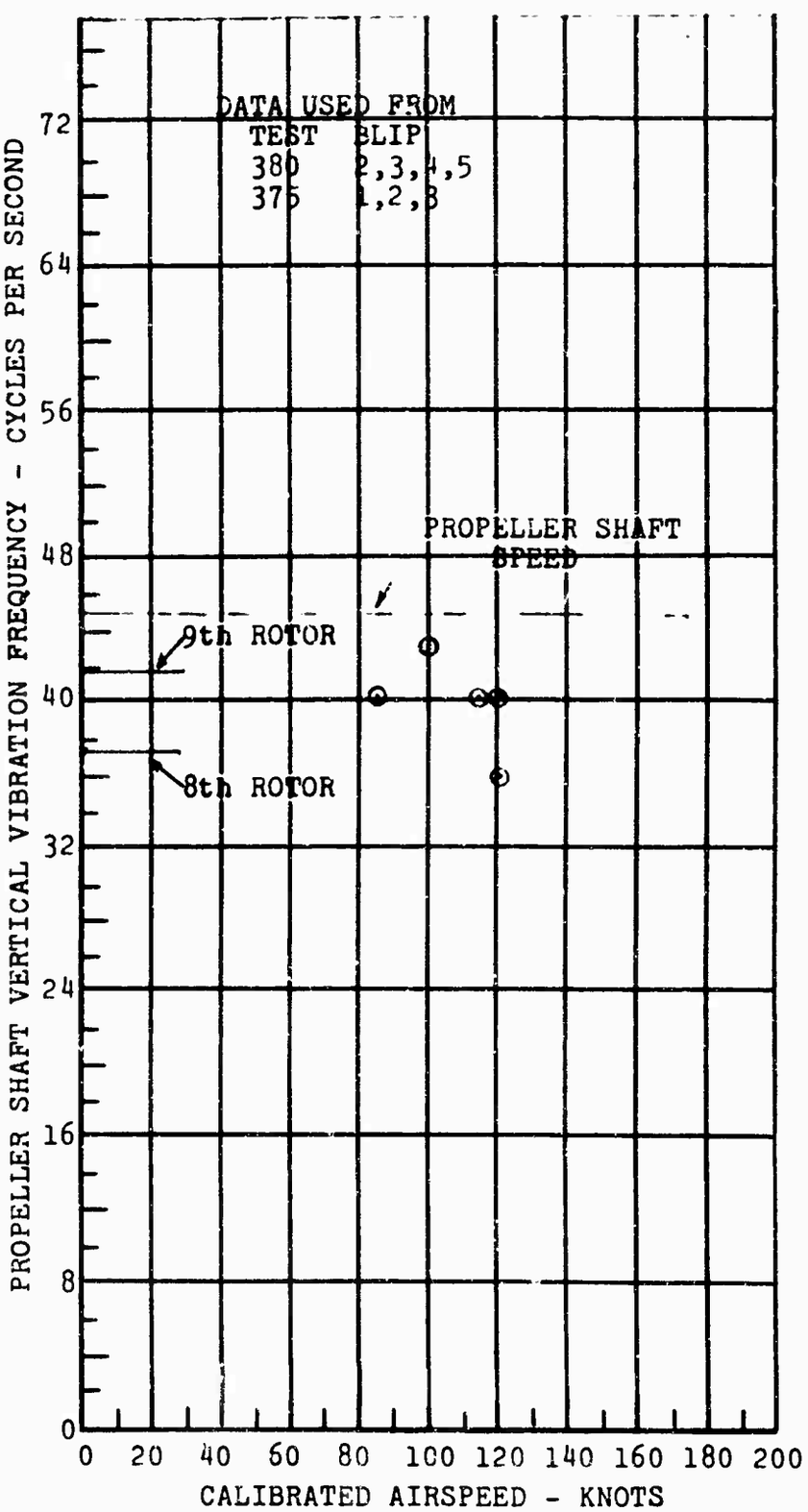


Figure 50. Vertical Vibration, Propeller Shaft.

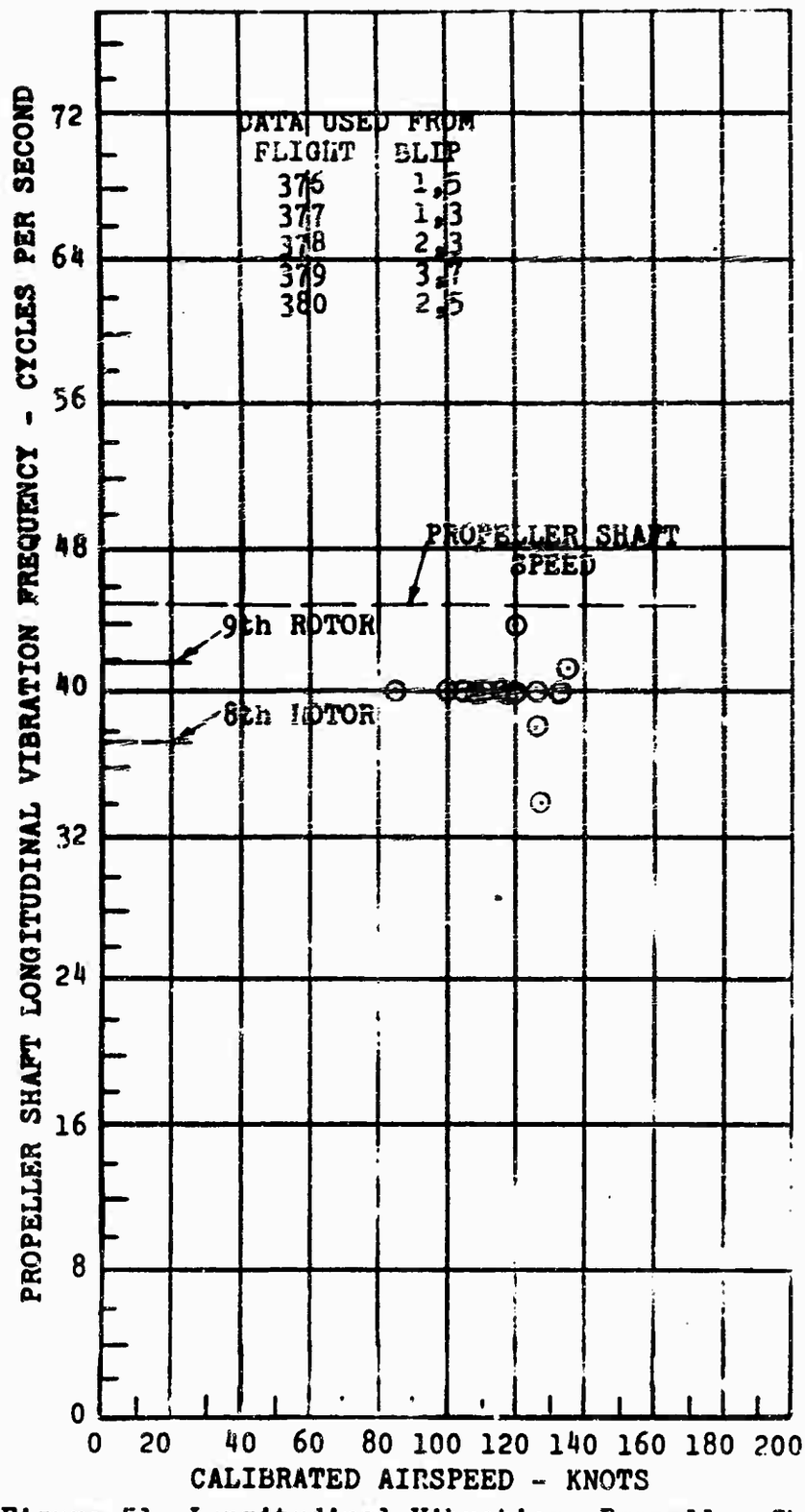


Figure 51. Longitudinal Vibration, Propeller Shaft.

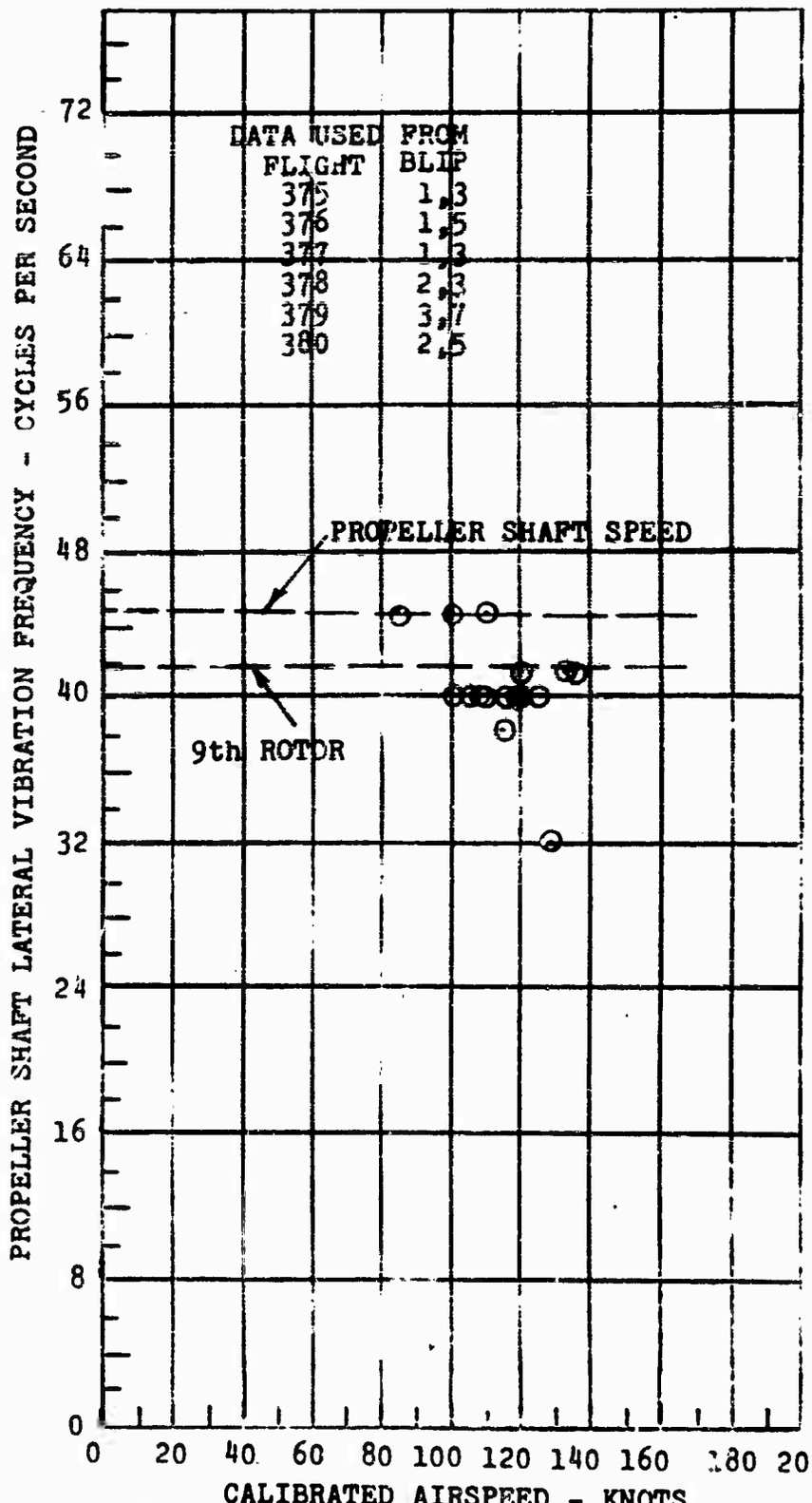


Figure 52. Lateral Vibration, Propeller Shaft.

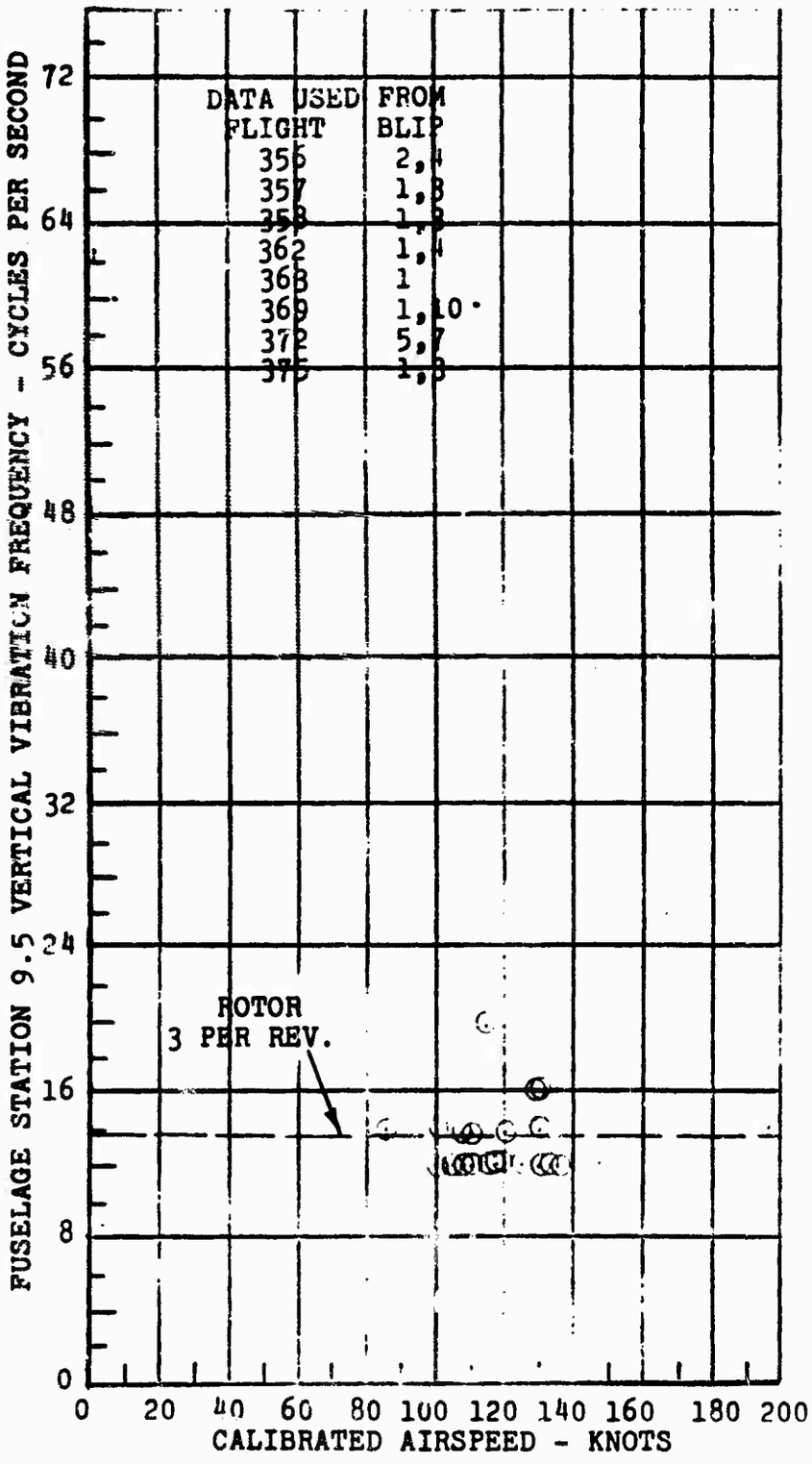


Figure 53. Vertical Vibration, Fuselage, Station 9.5 (Location of Instrument Panel).

## FLYING AND HANDLING QUALITIES AND MANEUVERABILITY

This section contains the test results and related analysis, theory, and discussion on the 16H-1A flying and handling qualities. Its major purpose is to compare the pertinent flight characteristics with the corresponding requirements as given in the Military Specification MIL-H-8501A (Reference 4). Throughout, the cited paragraphs refer to those of this reference.

In addition, Appendix III contains the basic dynamic and static stability and control test data and analyses required for this section.

### LONGITUDINAL CHARACTERISTICS

3.2.1 (Reference 4)

A sufficient margin of longitudinal control power is required so that 10 percent of the maximum attainable pitching moment in hover shall be available throughout the steady flight operating range.

From Figure 54 it is seen that the hover trim position is 1.9 inches forward, leaving 5.6 inches of forward displacement available. At 167 knots, (highest speed reached in level flight), the trim position is 5.0 inches forward with a 2.5 inch margin remaining, and the pitching moment per inch of stick is 77 percent of the hover value. Thus, to meet the requirement, stick displacement available at the high speed condition should be

$$\frac{0.10 \times 5.6}{0.77} = 0.7 \text{ inch}$$

Hence, sufficient margin is available for this center of gravity position (9.6 inches forward). At the critical test center of gravity of 3.1 inches forward, elevator trim alone can be made to compensate the center of gravity shift for the same stick position. From the data of Figure 55, which were obtained at 130 knots, it is estimated that the elevator deflection per inch of aft center of gravity movement is 1.9 degrees per inch at the high-speed condition. Thus, 10 degrees of down elevator, or 55 percent of full deflection, is required. Examination of all maneuvers performed, including autorotation, quick stops, rearward and sideward flight (see Figures 102, 60, 56, 57, 84, 88, and 94), shows that control margin for aft stick was always more than ample.

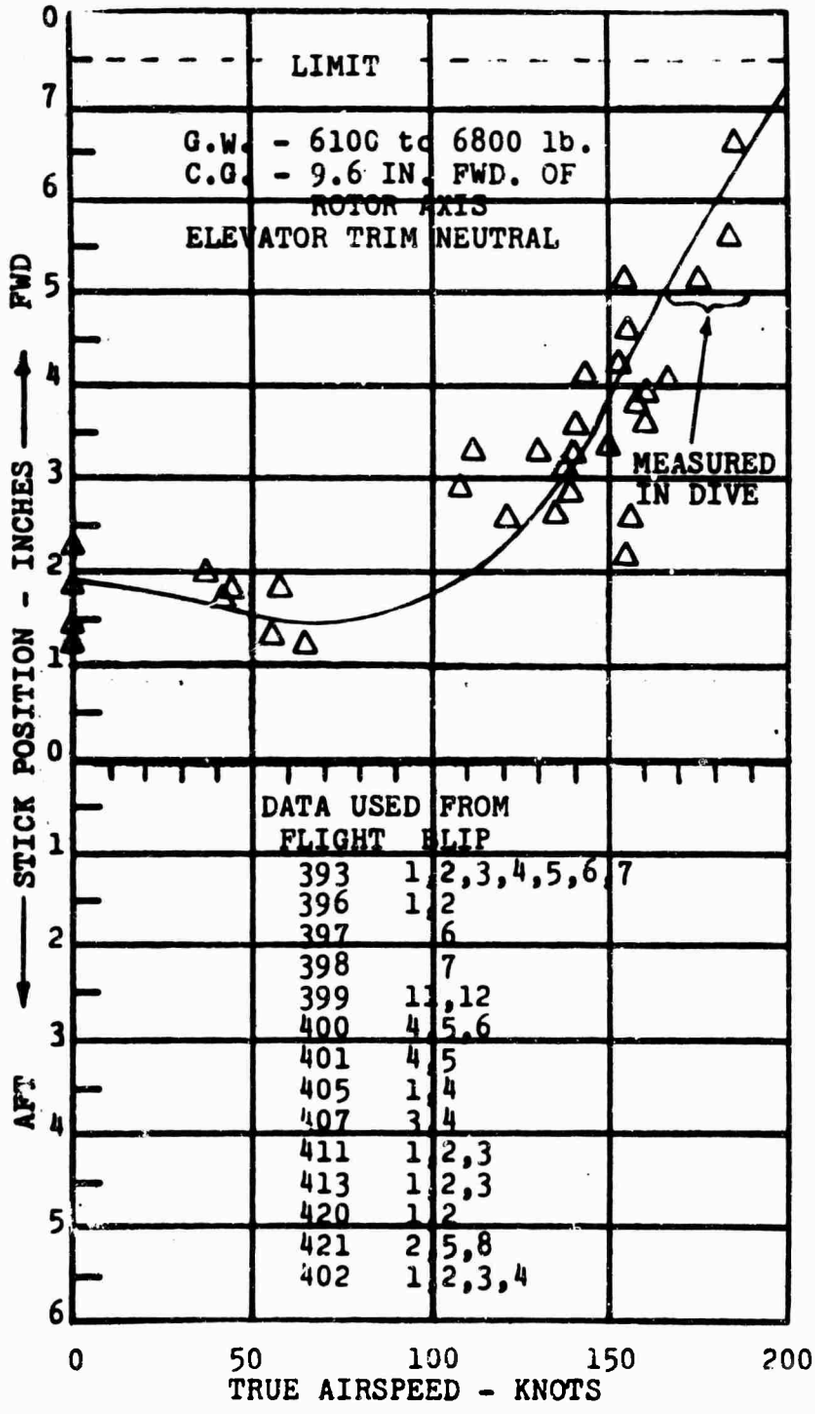


Figure 54. Longitudinal Stability - Level Flight, Stick Position versus Speed.

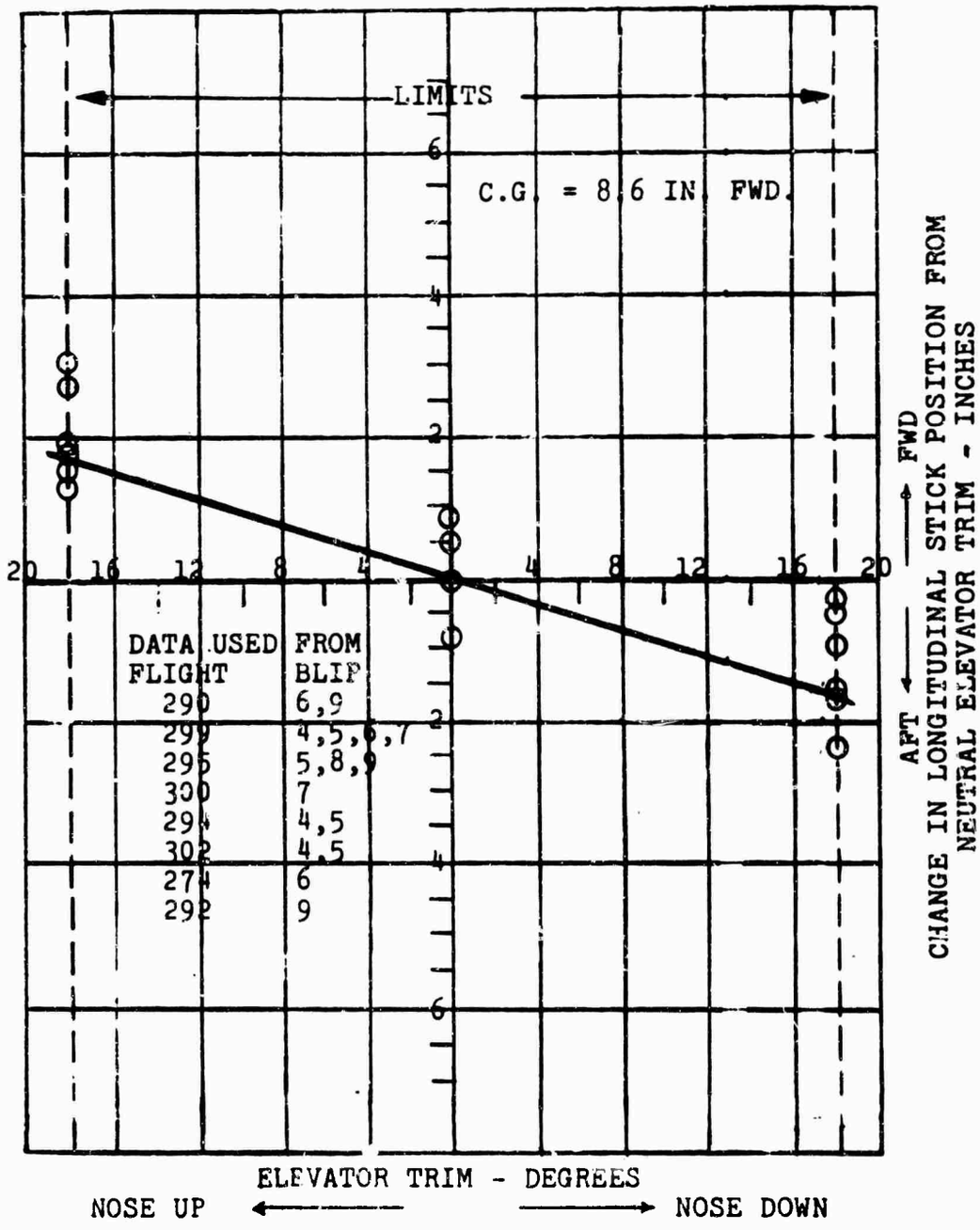


Figure 55. Longitudinal Stick Position Change versus Elevator Trim: 130 ± 5 Knots.

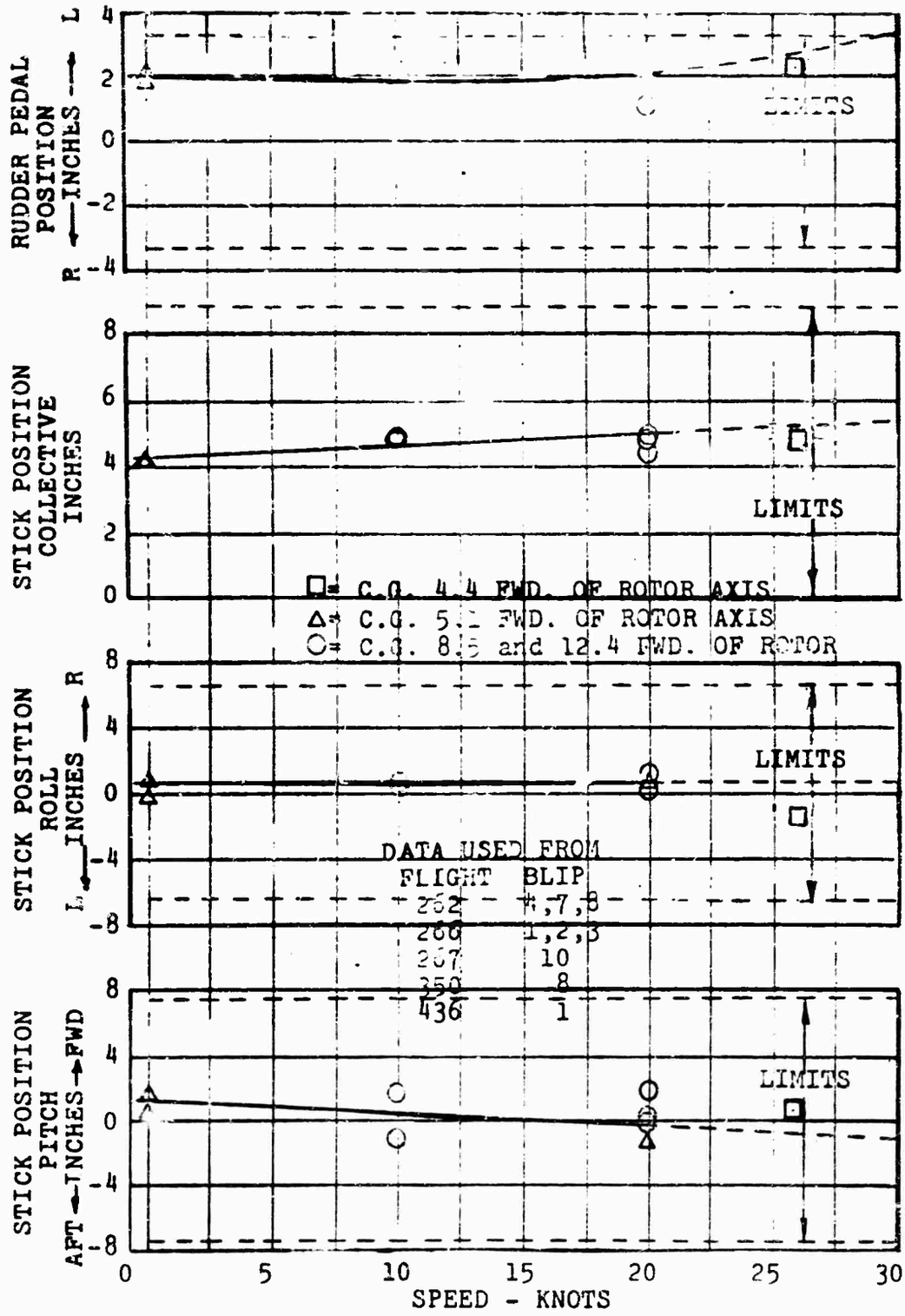


Figure 56. Control Position versus Airspeed, Rearward Flight.

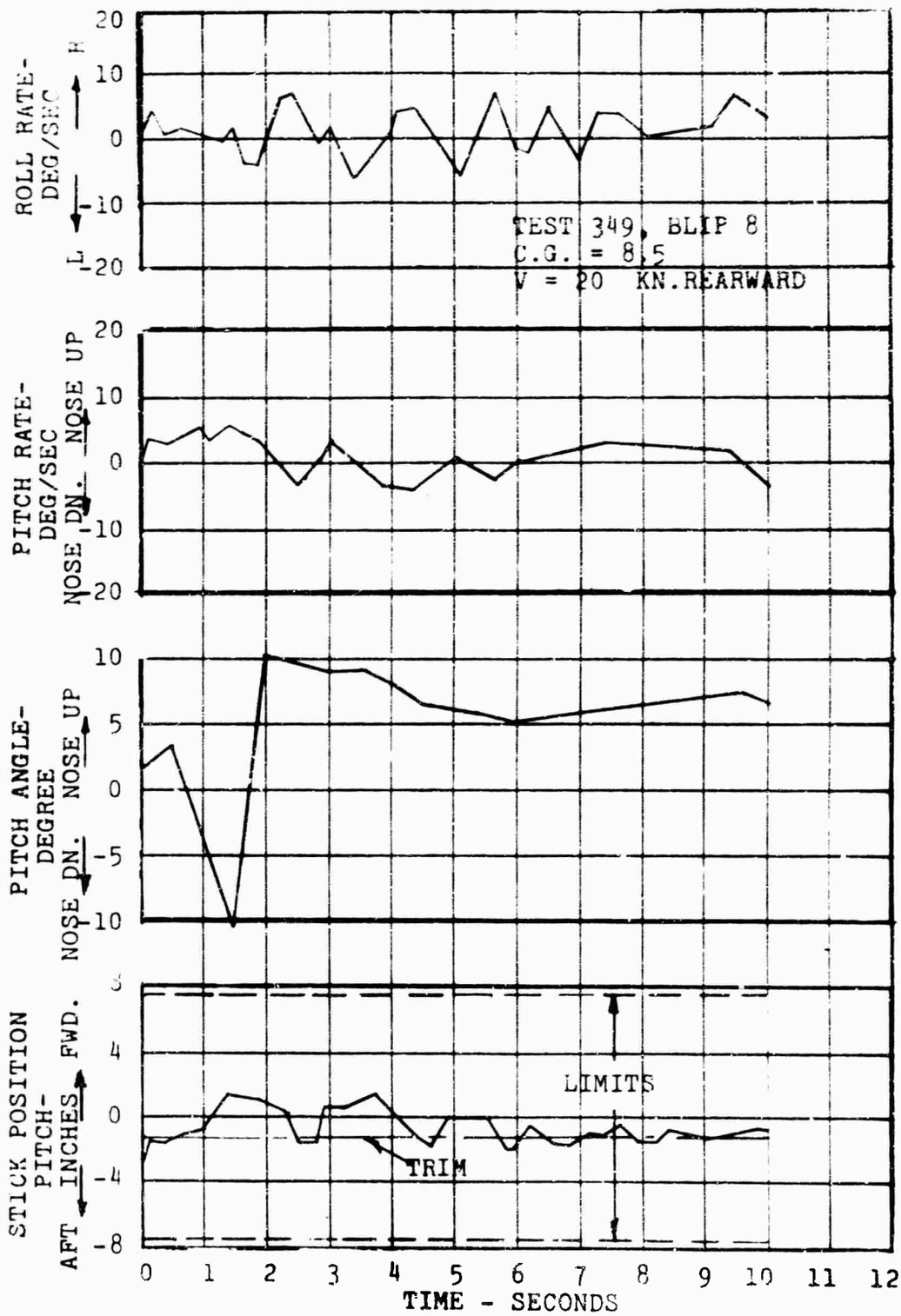


Figure 57. Pitch Response - Rearward Flight, Pitch Down.

3.2.2 (Reference 4)

This paragraph specifies a maximum longitudinal control motion of ±1 inch for still air precision hover in ground effect. This test was performed in Flight 264, Blip 10 in which the maximum motions recorded were less than ±1.0 inch over a recorded blip length of 17 seconds (see Figure 58). Therefore, the requirement is satisfied.

3.2.3, 3.2.4, 3.2.6, 3.2.7 and 3.2.8 (Reference 4)
Longitudinal Control Forces.

The aircraft, as tested, had fully powered controls with forces always reduced to zero (as verified by pilot's comments) but with no self-centering. An adjustable bungee system added to the fully powered controls would satisfy the requirement for positive self-centering characteristics and force gradient limitations.

3.2.5 (Reference 4)

Transitions from hover to an indicated airspeed of 70 knots in 18 seconds and decelerations from 70 knots to hover in 16 seconds were performed at constant altitude without excessive control motions and with greater variations of technique permissible than in conventional helicopter flight. Records of two methods of acceleration were obtained. The least change in attitude was by maintaining the ship level longitudinally and increasing the propeller pitch to accelerate the aircraft into forward speed. This would be the preferred method in IFR operations where the pilot would desire to keep his instruments and attitude of the aircraft to a minimum change. A time history of this method at a forward center of gravity is shown in Figure 59. The quick stop from the second part of this same blip is shown in Figure 60. Figures 61 and 62 show corresponding maneuvers at an aft center of gravity.

The conventional helicopter mode of pitching down and using the rotor thrust for acceleration is illustrated by the time history in Figure 63. Approximately the same acceleration was achieved (.26 g), as measured from the slope of the velocity-time curve. Figure 64 shows the quick stop which was performed immediately afterward.

The horizontal distance traveled during the transitions either way was about 1,000 feet. The accelerating portion of the maneuver of Figure 59 was accomplished almost entirely with the propeller. The attitude was never allowed to pitch nose down more than 5 degrees. On the other hand, as shown

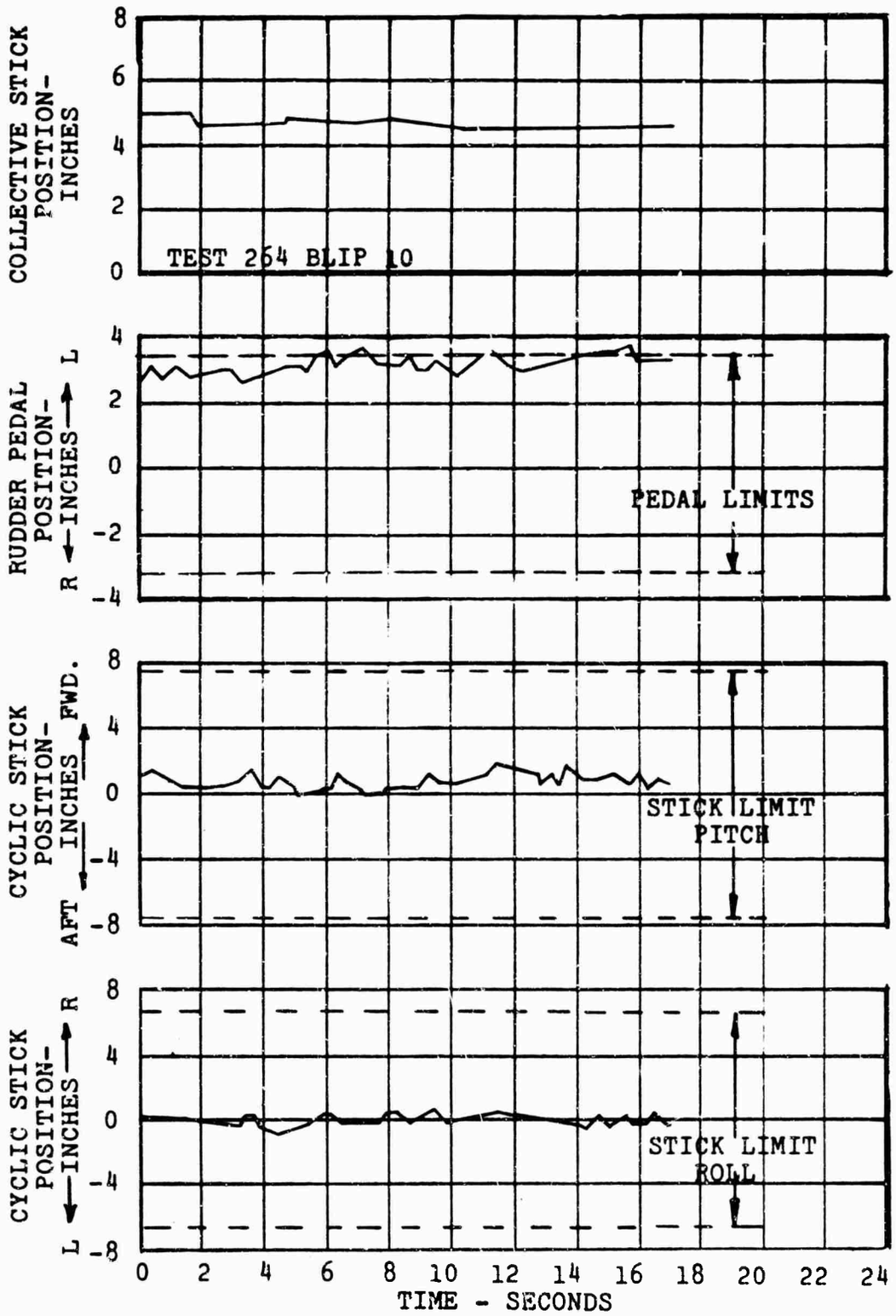


Figure 58. Time History of Control Motions During Steady Hover.

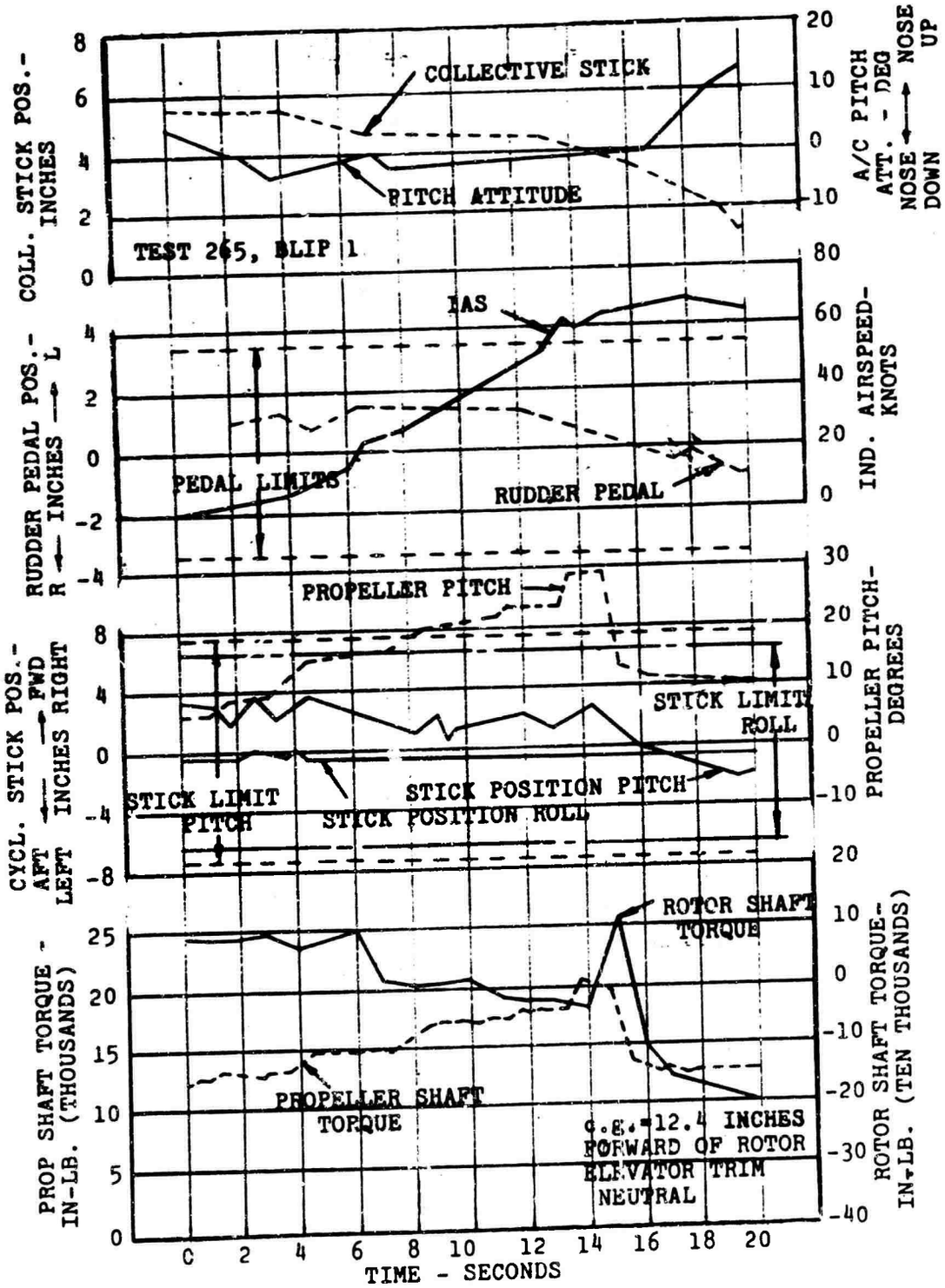


Figure 59. Airplane Mode Acceleration, Forward C.G.

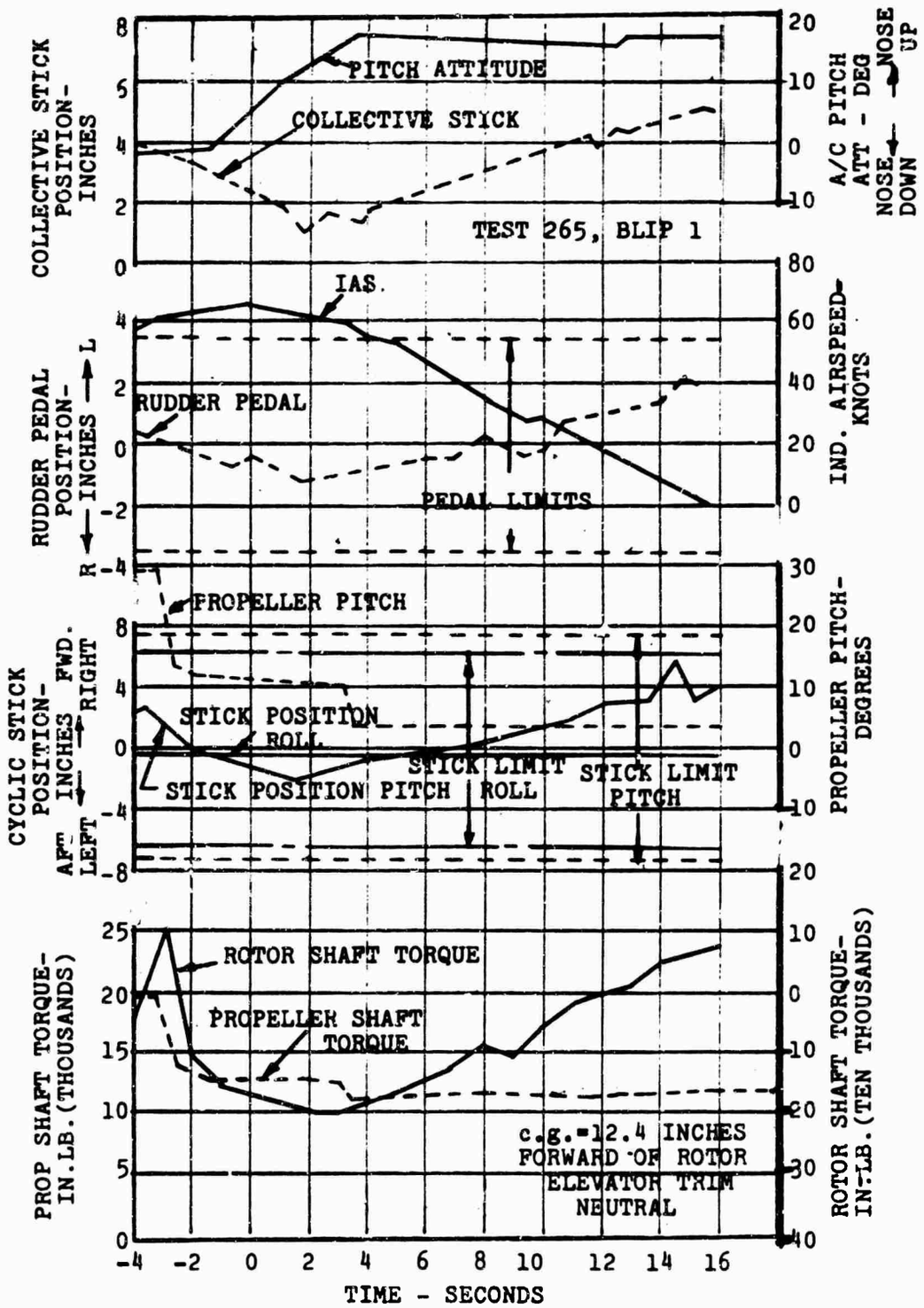


Figure 60. Quick Stop, Forward C.G.

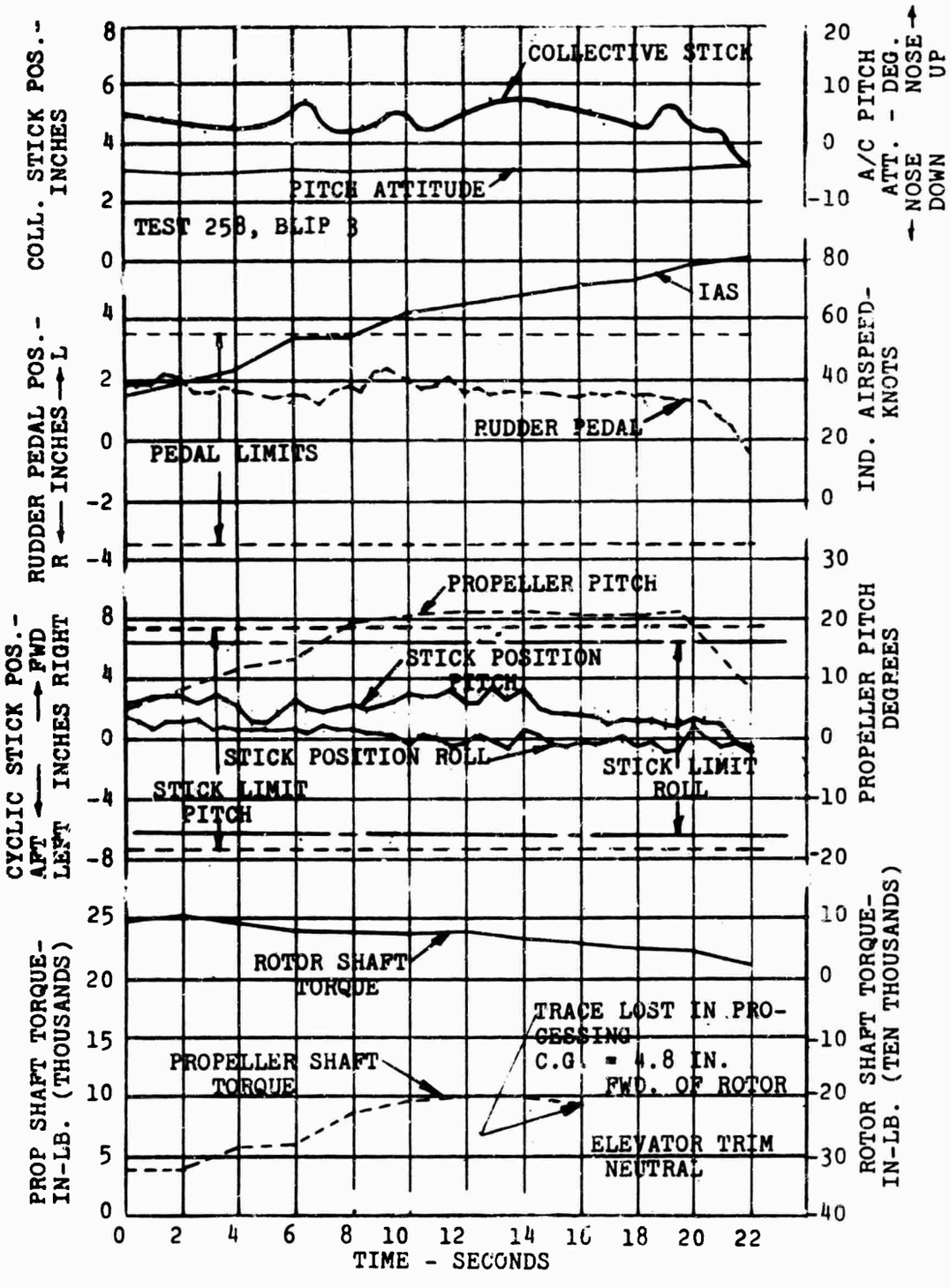


Figure 61. Airplane Mode Acceleration, Aft C.G.

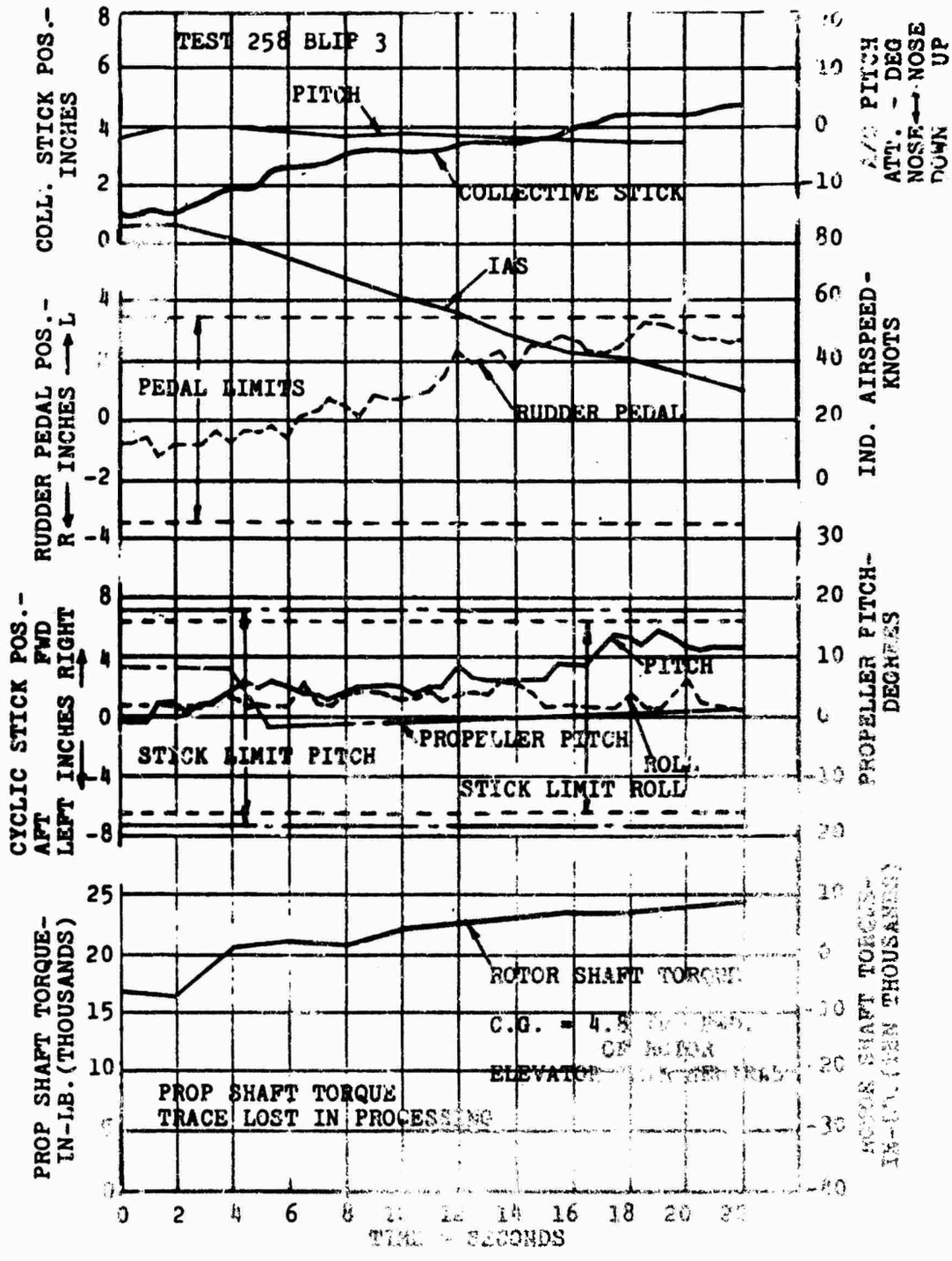


Figure 62. Quick Stop, Aft C.G.

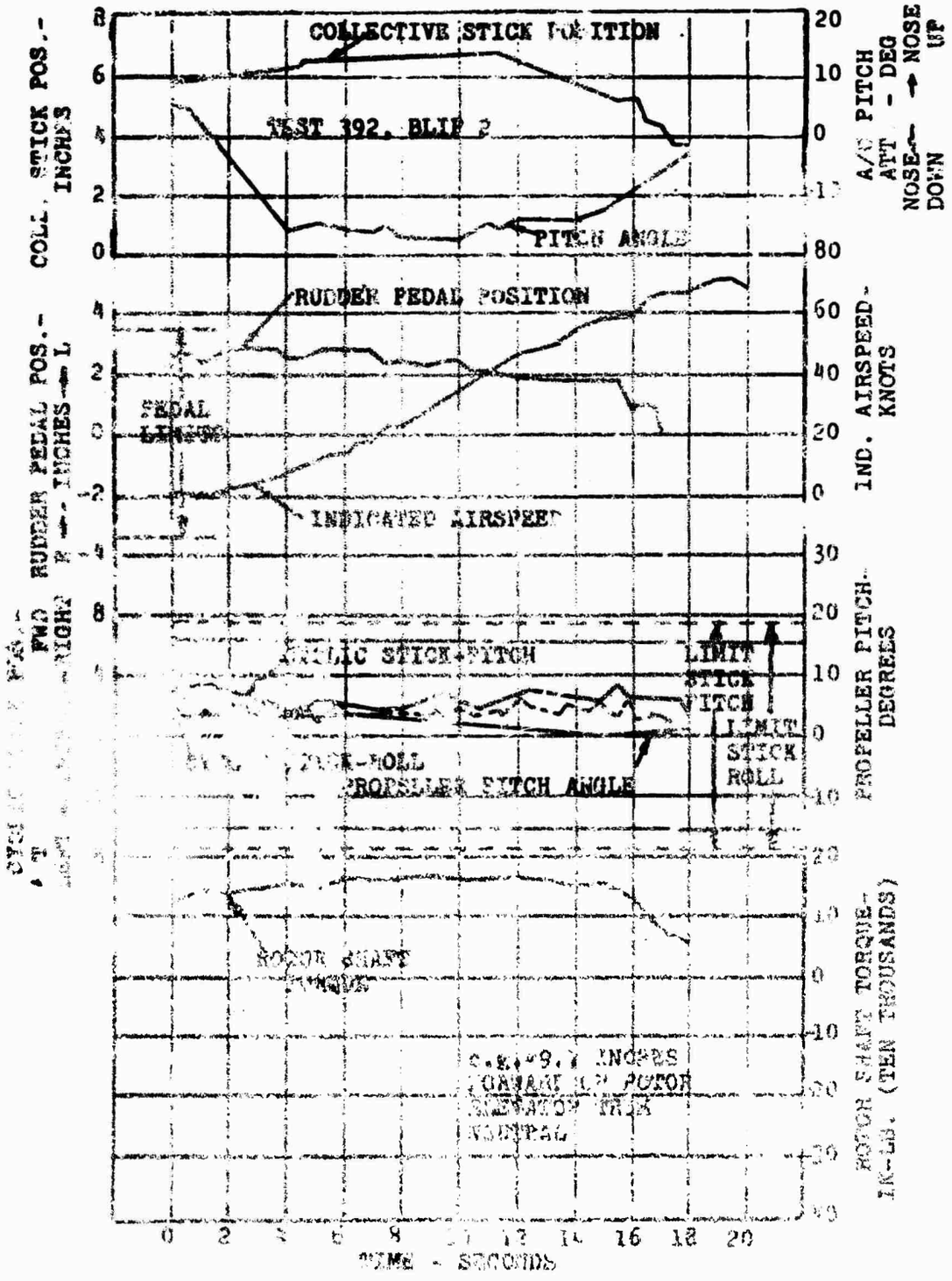


Figure 5. Helicopter Nose Acceleration.

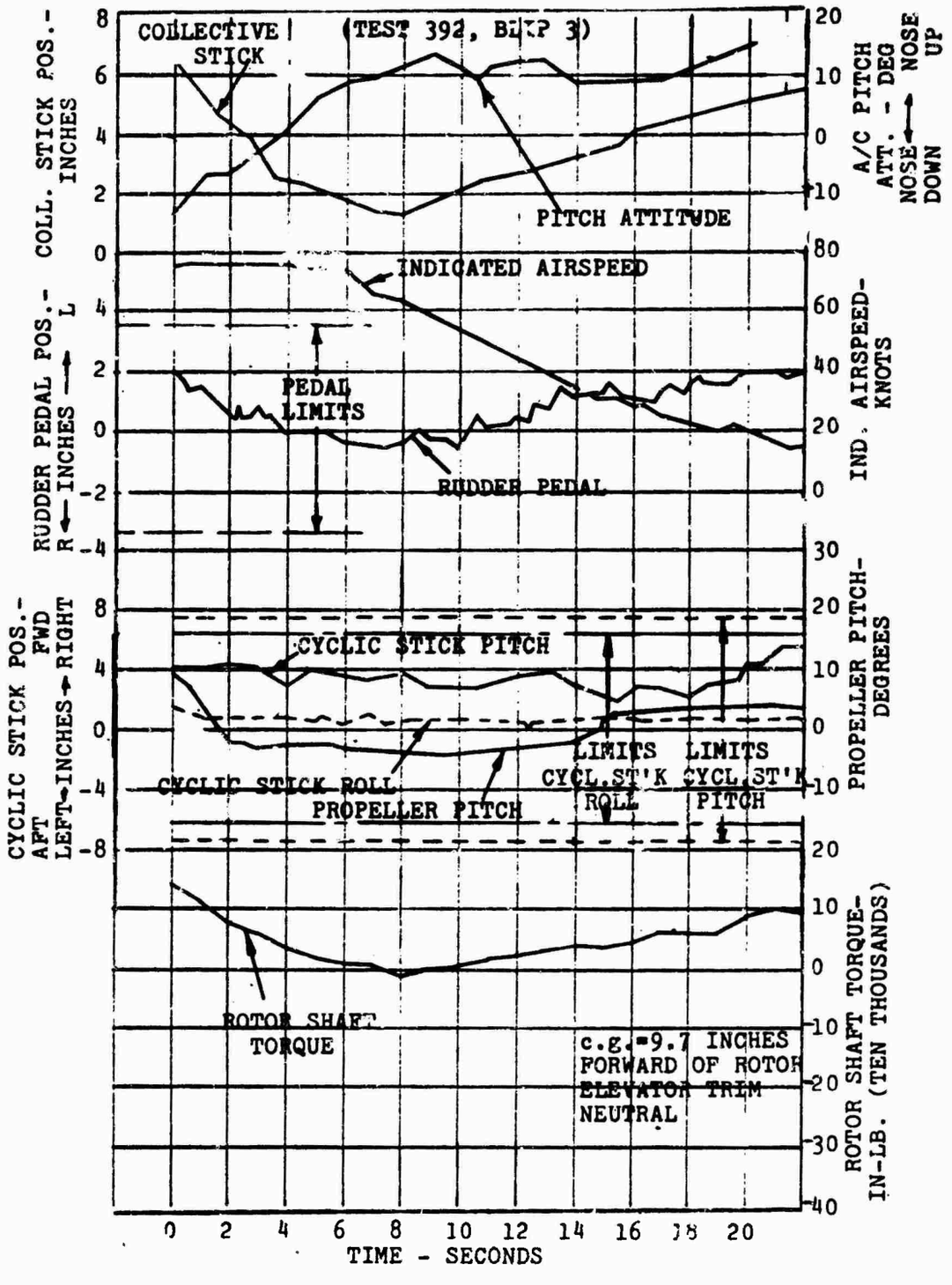


Figure 64. Quick Stop.

in Figure 63, the propeller pitch was reduced as speed increased, since the propeller was used only for antitorque and yaw control.

A third method would be the combination of the previous two, where some cyclic longitudinal stick motion forward is given to incline the rotor thrust, and simultaneously propeller pitch is increased to accelerate the aircraft. The time of initiation of the maneuvers can be observed from both the propeller pitch and the cyclic stick motion.

3.2.9 (Reference 4)

The requirement is that angular accelerations be developed, in the proper direction, within 0.2 second after application of longitudinal control for the speed range specified in paragraph 3.2.1. An examination of the following control responses indicates that the 16H-1A meets this requirement.

| Flight Speed | Test | Blip | Figure |
|---|---|---|---|
| Hover | 335 | 3 | 65 |
| Hover | 335 | 4 | 66 |
| Hover | 260 | 1 | 67 |
| Hover | 260 | 2 | 68 |
| 50 Knots | 315 | 5 | 69 |
| 150 Knots | 414 | 1 | 70 |
| 150 Knots | 414 | 2 | 71 |

3.2.10 (Reference 4)

This paragraph states the requirement for positive control force and position static stability as evidenced by a positive slope of the longitudinal stick position and force versus speed curves. A moderate instability is allowed at forward speeds of 15 to 50 knots and at rearward speeds of 10 to 30 knots. With a power-boost system, in conjunction with artificial feel, the force stability will be positive if the position stability is positive.

The 16H-1A possesses positive control position stability according to the requirement. This is seen in the level flight stick position versus speed plot of Figure 54, where the slope is positive from about 70 knots to the maximum speed, with a stick reversal of 0.4 inch between hover and 50 knots. Paragraph 3.2.10 allows a maximum reversal of 0.5 inch in this speed range. The data for this curve were obtained using the stiffened control system (see "Technical Problems") and are significantly different from the initial

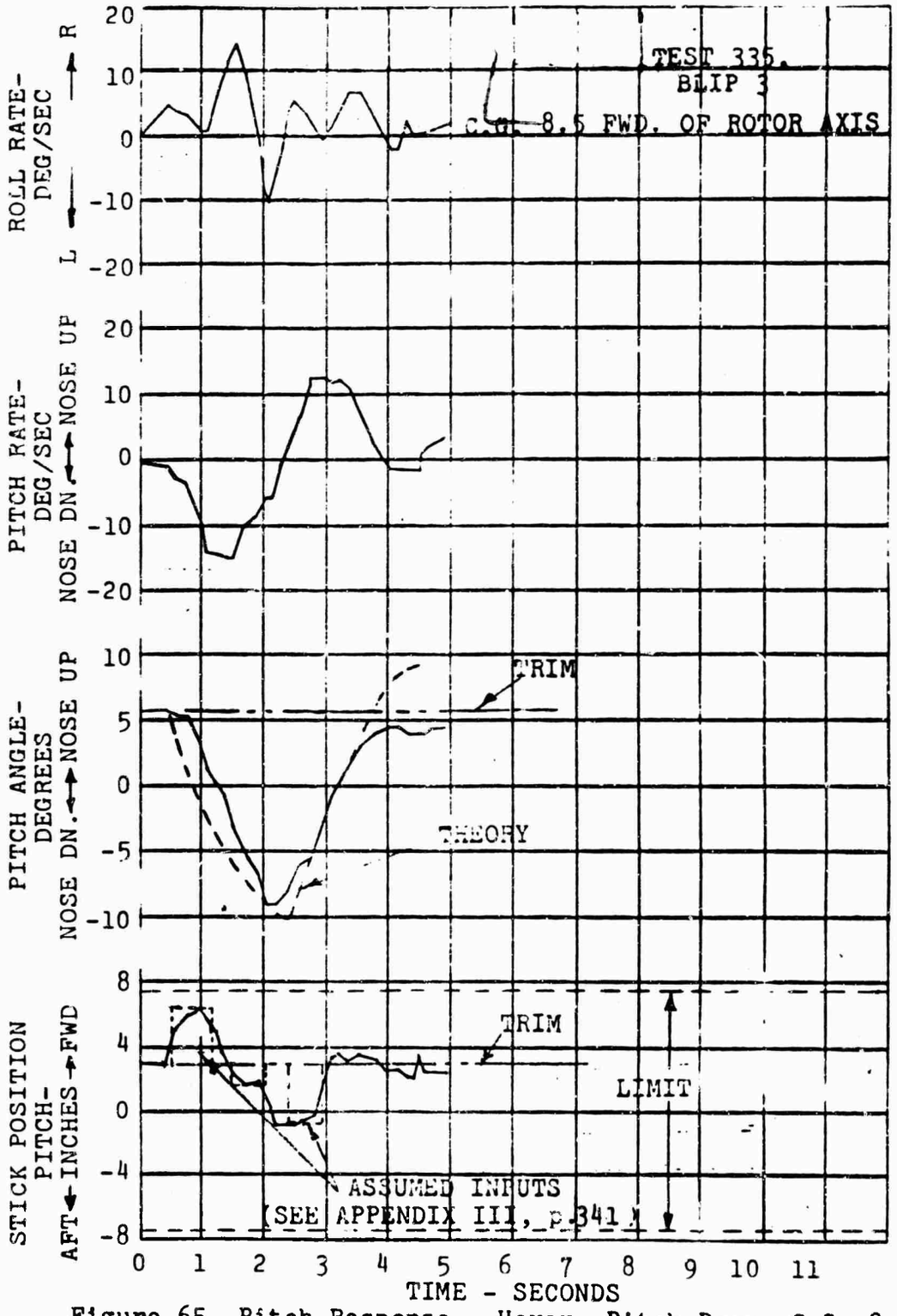


Figure 65. Pitch Response - Hover, Pitch Down, C.G. 8.5.

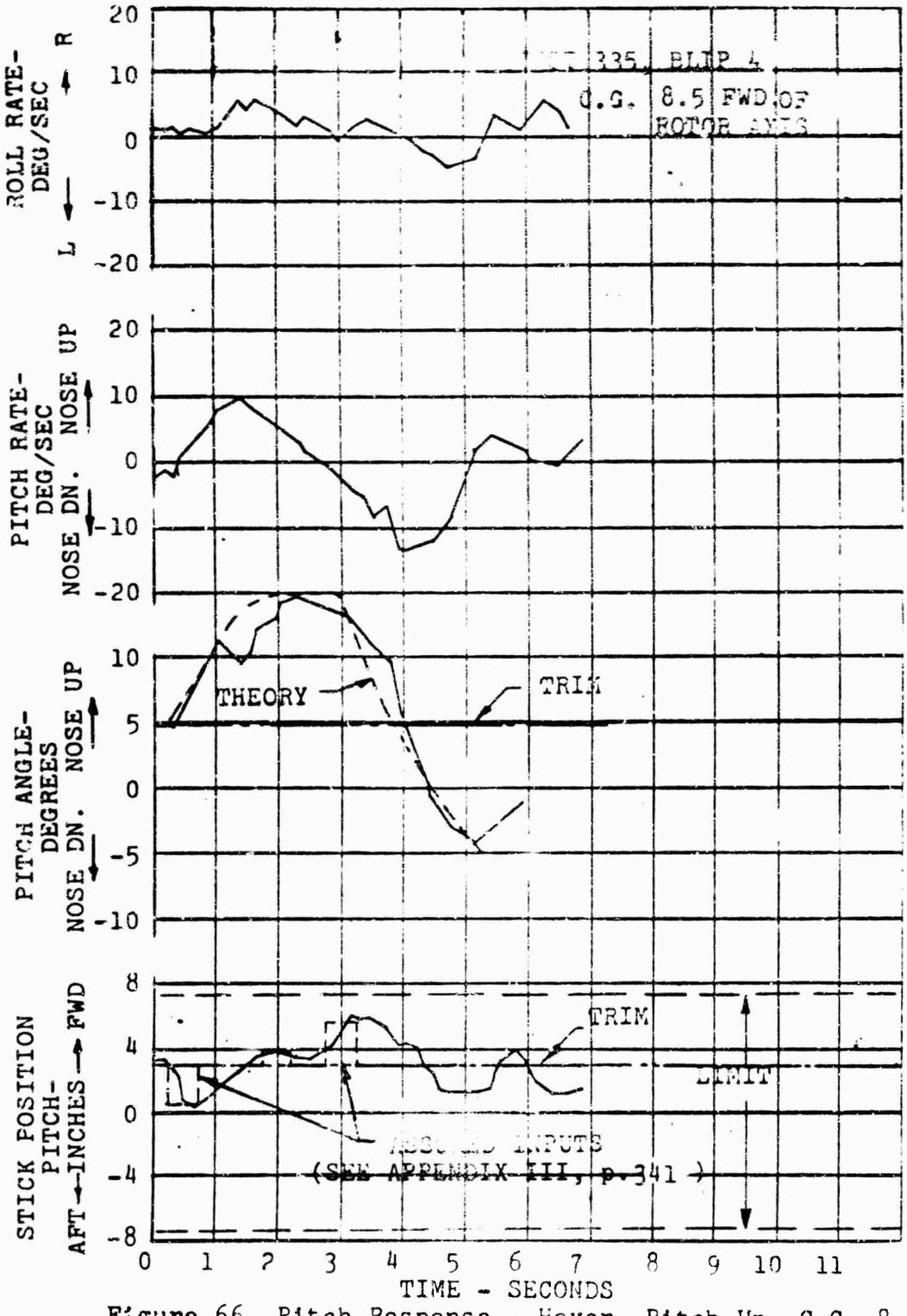


Figure 66. Pitch Response - Hover, Pitch Up, C.G. 8.5.

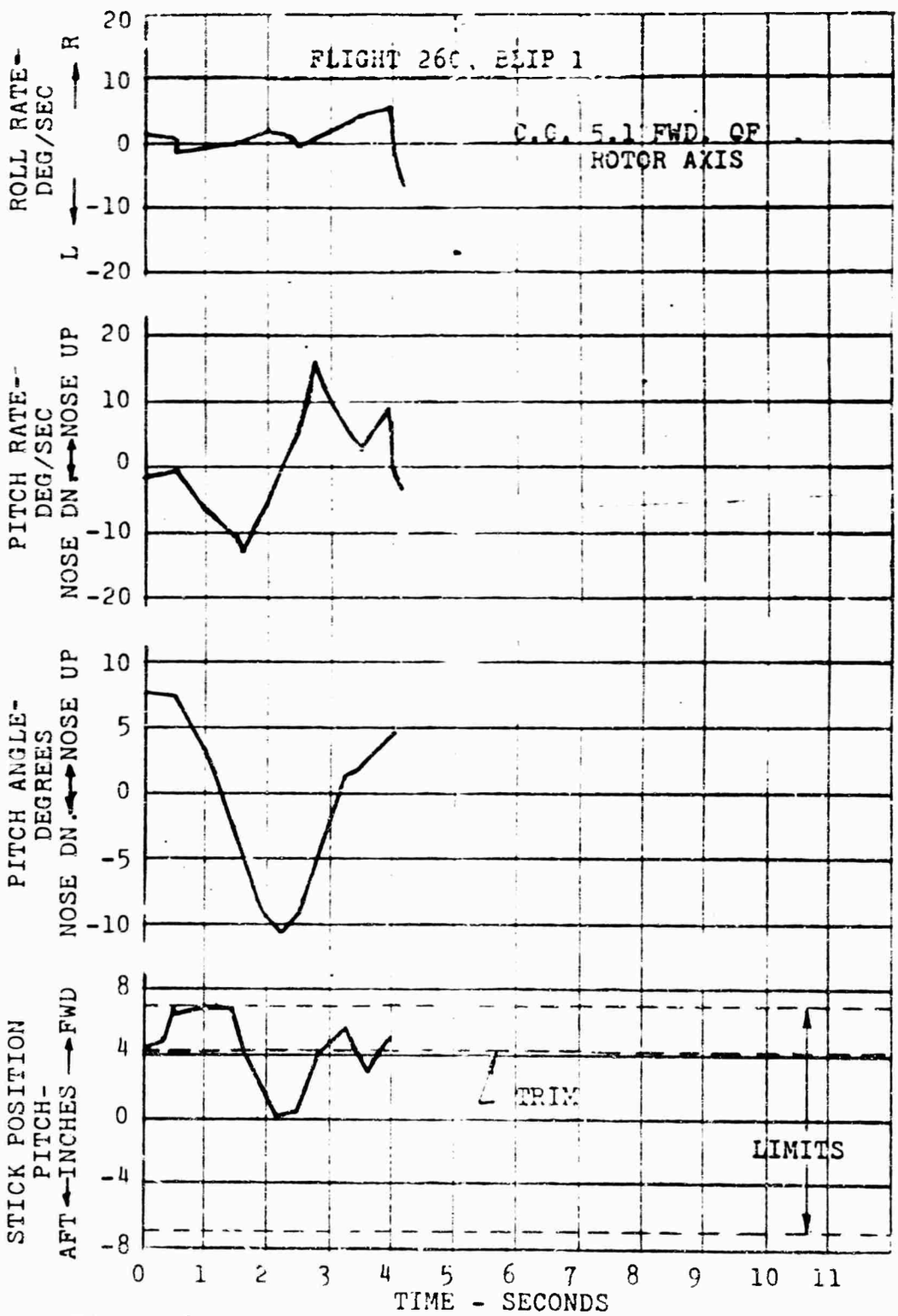


Figure 67. Pitch Response - Hover, Pitch Down, C.G. 5.1.

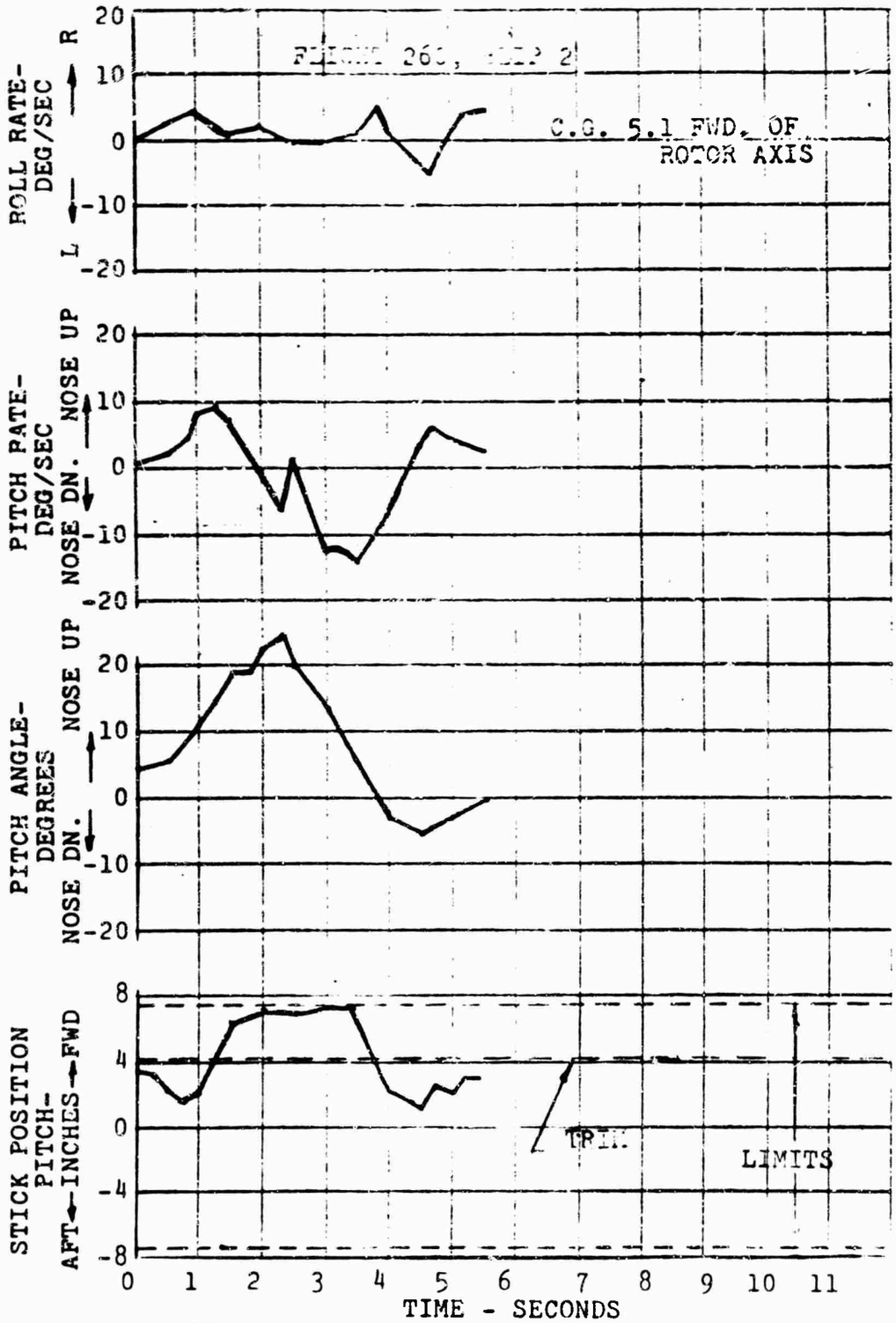


Figure 68. Pitch Response - Hover, Pitch Up, C.G. 5.1.

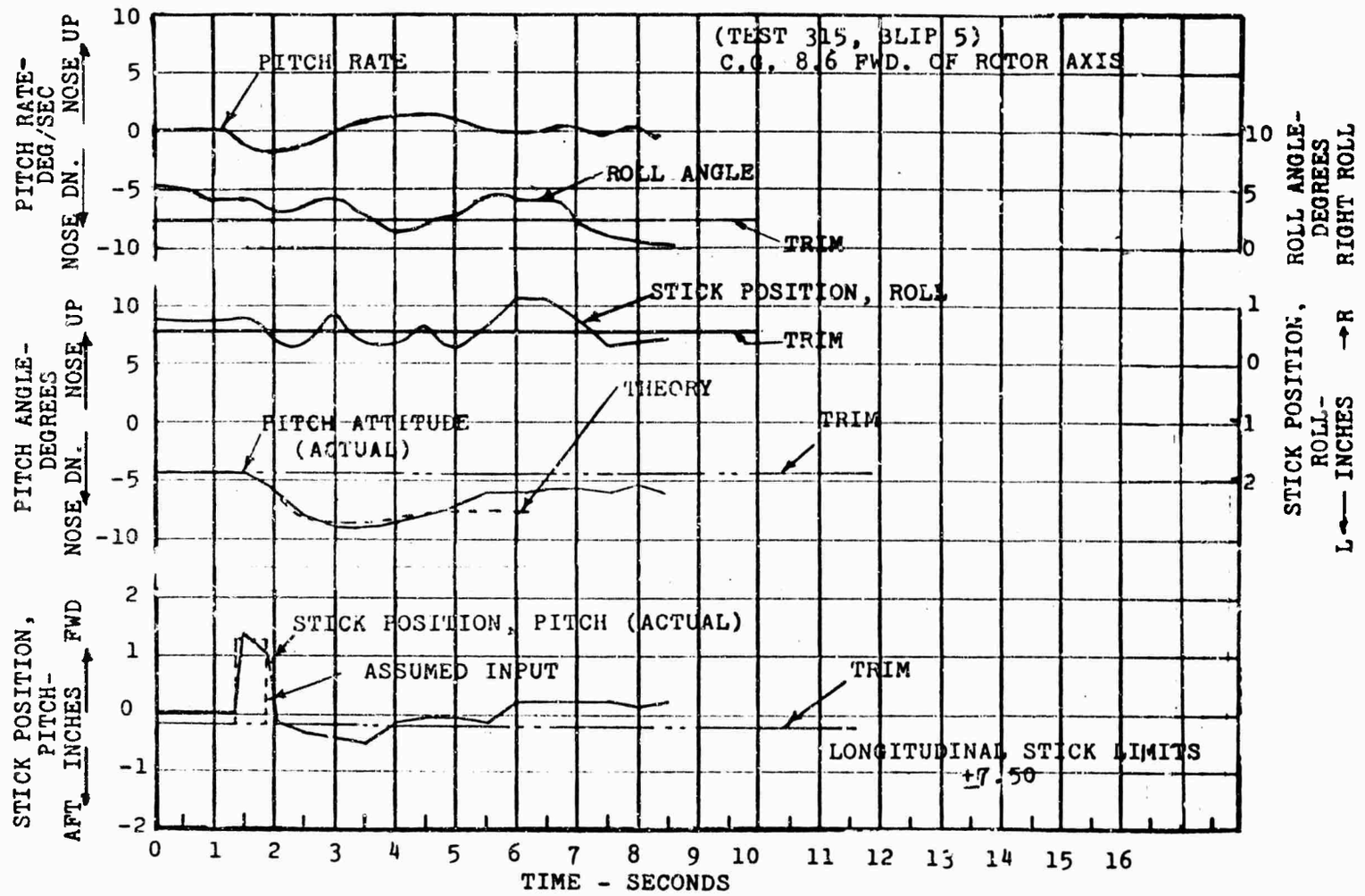


Figure 69. Dynamic Stability - Pitch Down, Speed 50 Knots, C.G. 8.6.

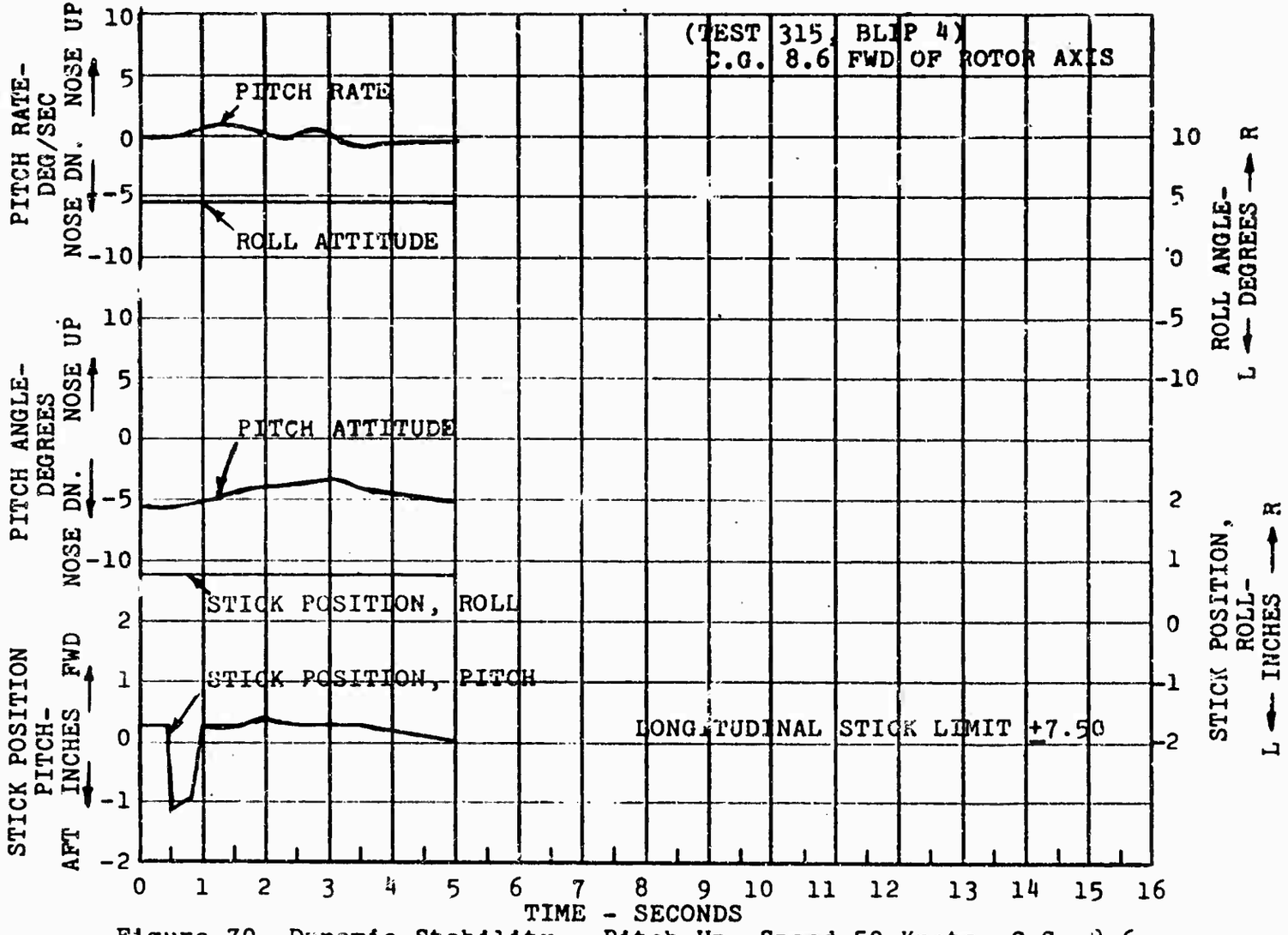


Figure 70. Dynamic Stability - Pitch Up, Speed 50 Knots, C.G. 8.6.

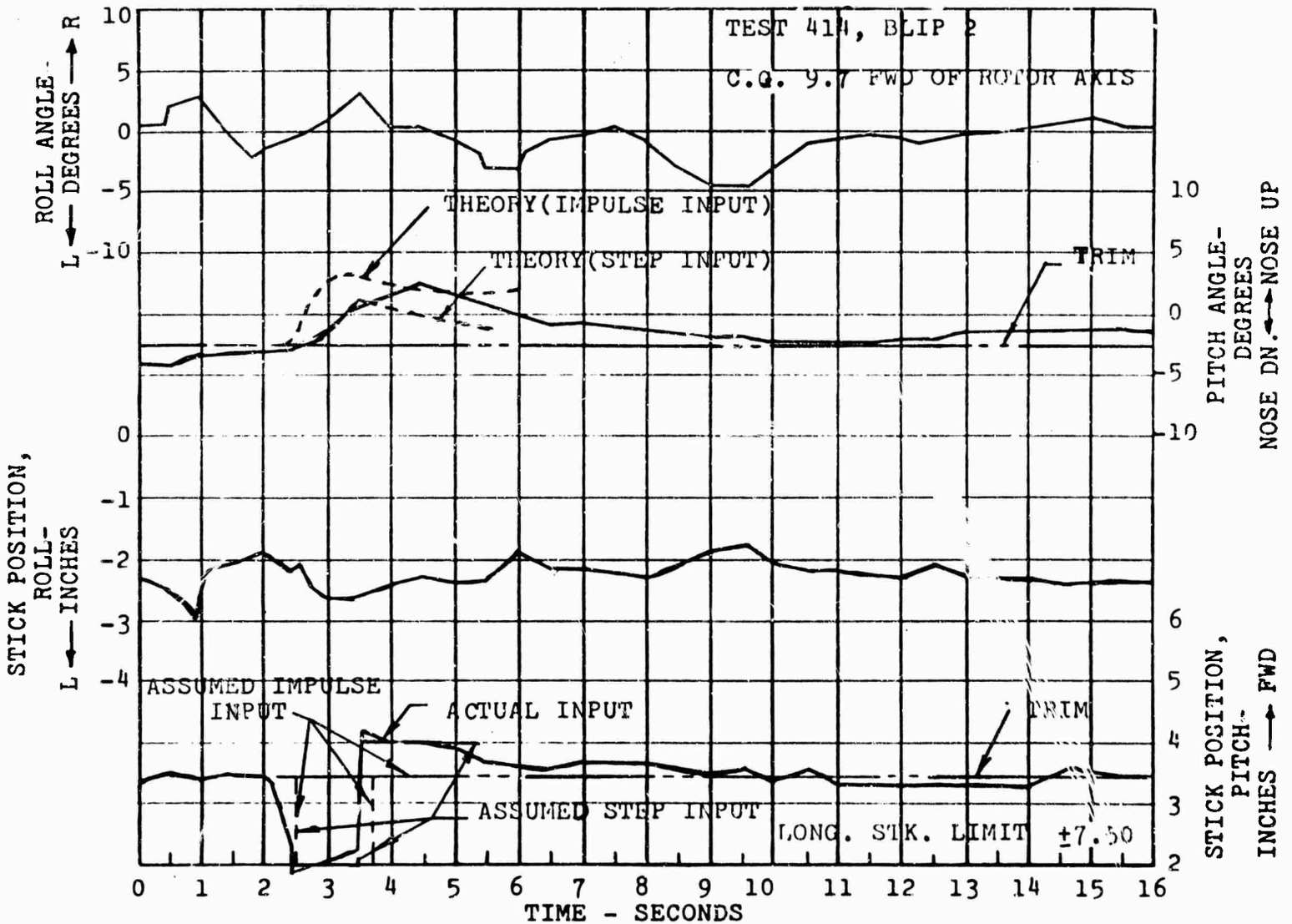


Figure 71. Dynamic Stability - Pitch Up, Speed 150 Knots, C.G. 9.7.

results obtained, which showed a curve of the same general shape but with slopes 20 to 30 percent greater. In general, absolute values of position are reduced as a result of the control modification.

The specified speed range for positive static stability in autorotation is from 60 to 100 percent of the maximum autorotative speed. This range is covered in the data of Figure 102 where a positive slope for both flaps-up and flaps-down conditions is shown. The climb condition for which the slope must be positive is the speed for maximum rate of climb ±15 knots. Since the normal rated power climb curve shown in Figure 72 has a positive slope at speeds above 65 knots, and since speed for maximum rate of climb is 75 to 80 knots, this requirement is satisfied.

The curves of Figures 54 and 72 are based on data from many different flights. In order to investigate the static longitudinal stability more closely, flights were performed in which the aircraft was trimmed to a particular speed in level flight, and a blip was taken. Then, holding all other controls fixed, the longitudinal stick was successively trimmed to new speeds (not necessarily level flight) ±10 knots and ±20 knots from the initial trimmed level-flight speed, and blips were taken at each trim point. The same procedure was used in climbs, where the initial trim point was in a climb at normal rated power rather than level flight. This procedure is in strict accordance with Reference 4.

Results of these tests are shown in Figure 73 for initial trim speeds of 60 knots in level flight and 50 knots in climb. Reference to Figures 74 and 72 shows that at these speeds the 16H-1A has least static stability in level flight and climb, respectively. Figure 74, in which the curves of Figure 73 are superimposed on those of Figures 54 and 72, shows somewhat greater static stability when the maneuvers are performed in the prescribed manner, even with a more aft center of gravity.

3.2.10.1 (Reference 4)

This paragraph refers to the operating conditions to be considered in 3.2.10. All steady flights for more than short time intervals are to be considered, as well as the most critical center-of-gravity position. The data referred to in the preceding paragraph cover all conditions specified in MIL-H-8501A except partial power descents, for which data were not required. Considering the overall stability characteristics of the 16H-1A there is no indication of instability for this operating condition. Tests at centers

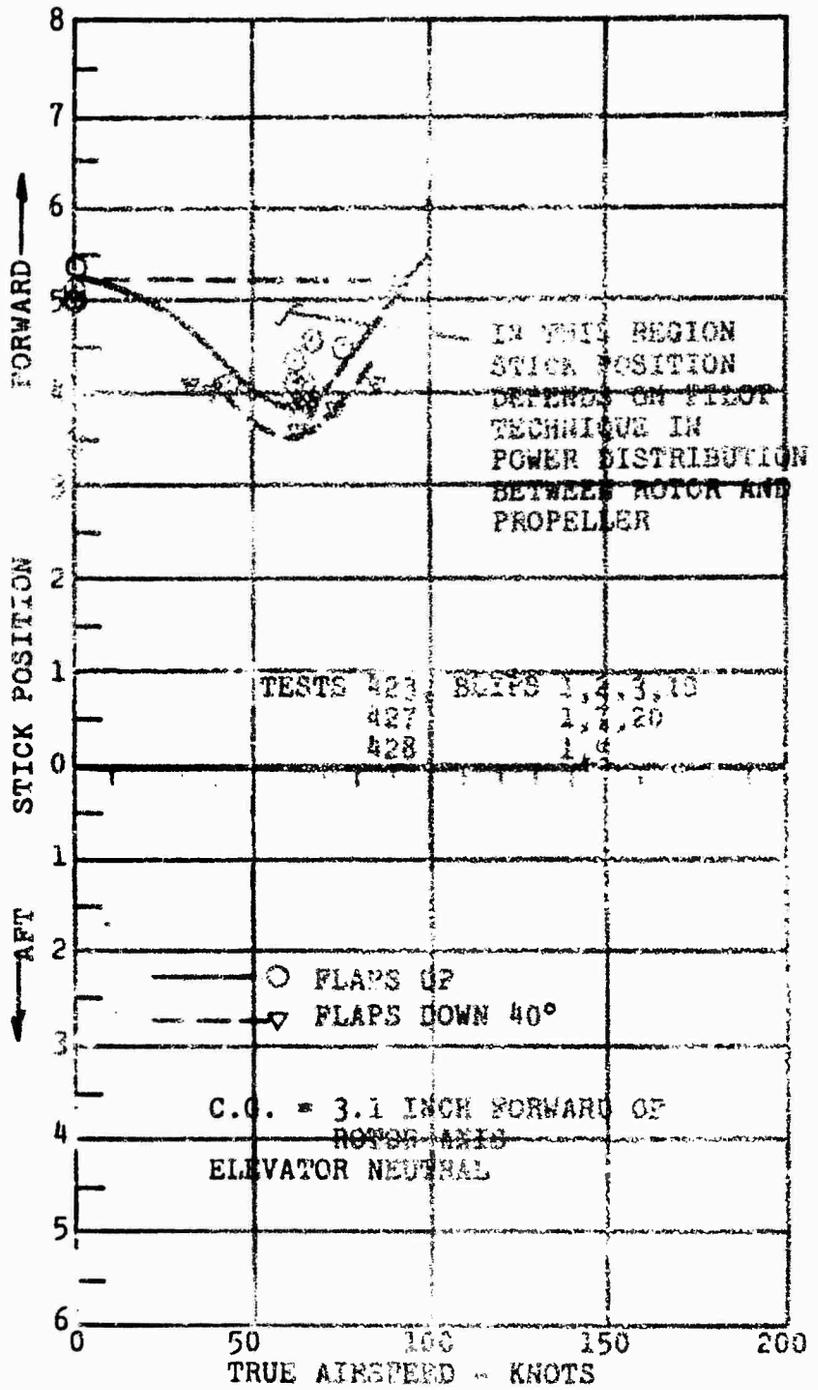


Figure 72. Longitudinal Stability - Climb, Stick Position Versus Speed, C.G. Fwd.

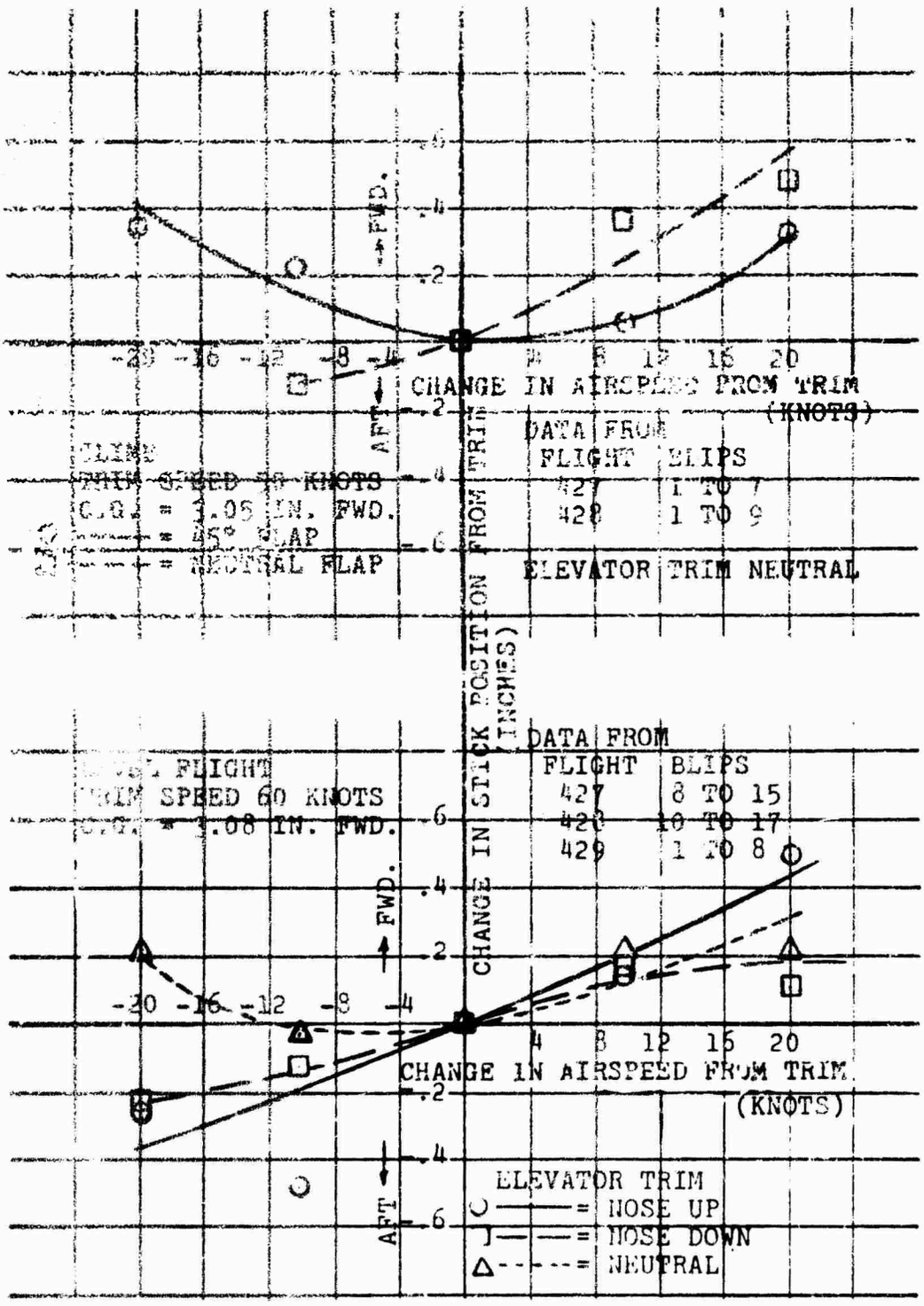


Figure 73. Change in Cyclic Stick Position from Trim versus Change in Airspeed from Trim.

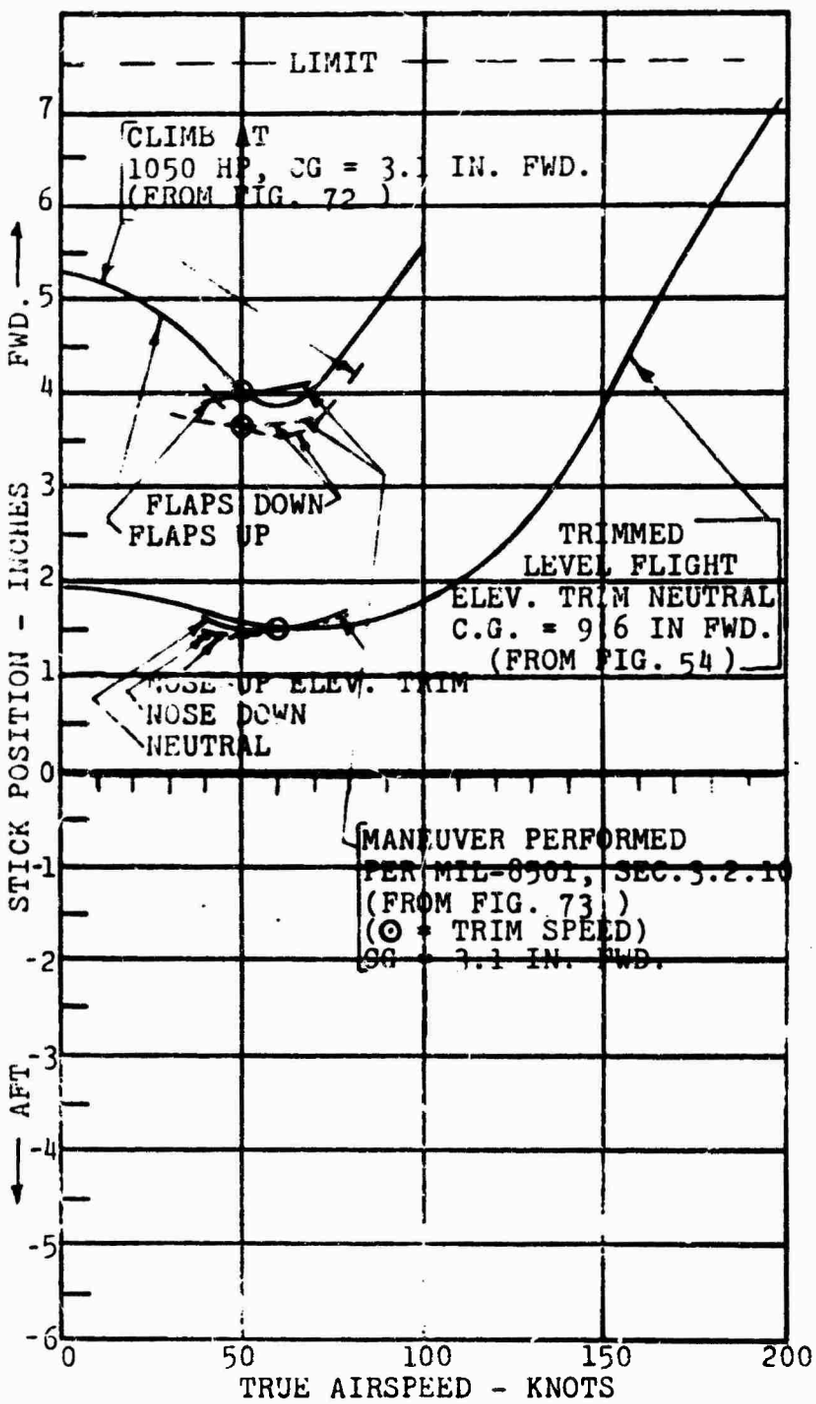


Figure 74. Longitudinal Static Stability - Climb and Level Flight.

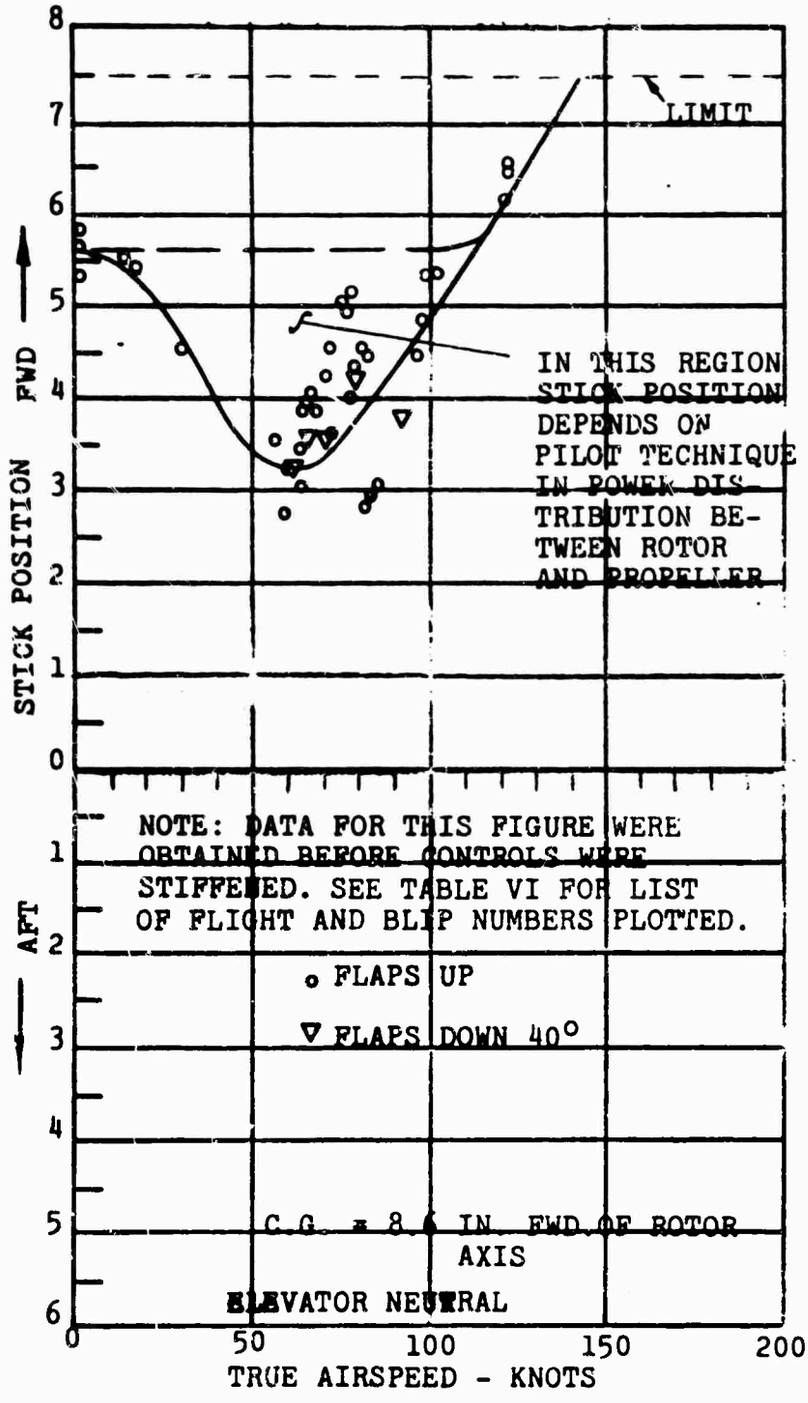


Figure 75. Longitudinal Stability - Climb Stick Position versus Speed, C.G. 8.6.

of gravity between 9.6 inches and 3.1 inches forward of the shaft do not indicate any significant alteration of the stability and control derivatives.

3.2.10.2 (Reference 4)

The longitudinal control variations for trim in climb, level flight, or partial power descent at a constant speed within the flight envelope are specified to be not more than +3 inches. The speeds mentioned as needing the most specific investigation are $V_{max}$ and speeds between zero and one-half the speed for minimum power (50 knots for the 16H-1A).

Referring to the curves of Figures 54 and 72 for level flight and climb, respectively, it is seen that at zero forward speed, the apparent stick position change is 3.4 inches, and it becomes less than 3 inches at speeds between 30 knots and 80 knots. At 100 knots, the indicated change between climb and level flight is 3.5 inches. It should be realized that the climb data were obtained for a center-of-gravity position of 3.1 inches forward, and the level flight results are for a center-of-gravity position of 9.6 inches forward. The center-of-gravity difference would tend to indicate smaller changes when considering the same center-of-gravity position.

Although partial power descents were made on many occasions, data thereon were not required under the contract, and were not obtained. However, comparison of data for full autorotative descents (from Figure 102) with climb data (from Figure 72) shows a maximum trim change of 5 inches at 70 knots between zero power descent and normal rated power climb. Again, part of this trim change can be attributed to a center-of-gravity difference of 6 inches.

3.2.11 (Reference 4)

This specification fixes the longitudinal dynamic stability requirements. It is stated that satisfactory dynamic stability characteristics shall be exhibited. Specifically, the short-period and phugoid mode minimum damping requirements are given as a function of the oscillation period. These stability limits in terms of the time to damp to half amplitude or the time to double amplitude, following longitudinal disturbances, are presented in Figure 76; the corresponding specification paragraph is noted. They appear as shaded limit lines denoting the minimum damping, and they have been made functions of inverse time in order to obtain a continuous boundary over the entire period range.

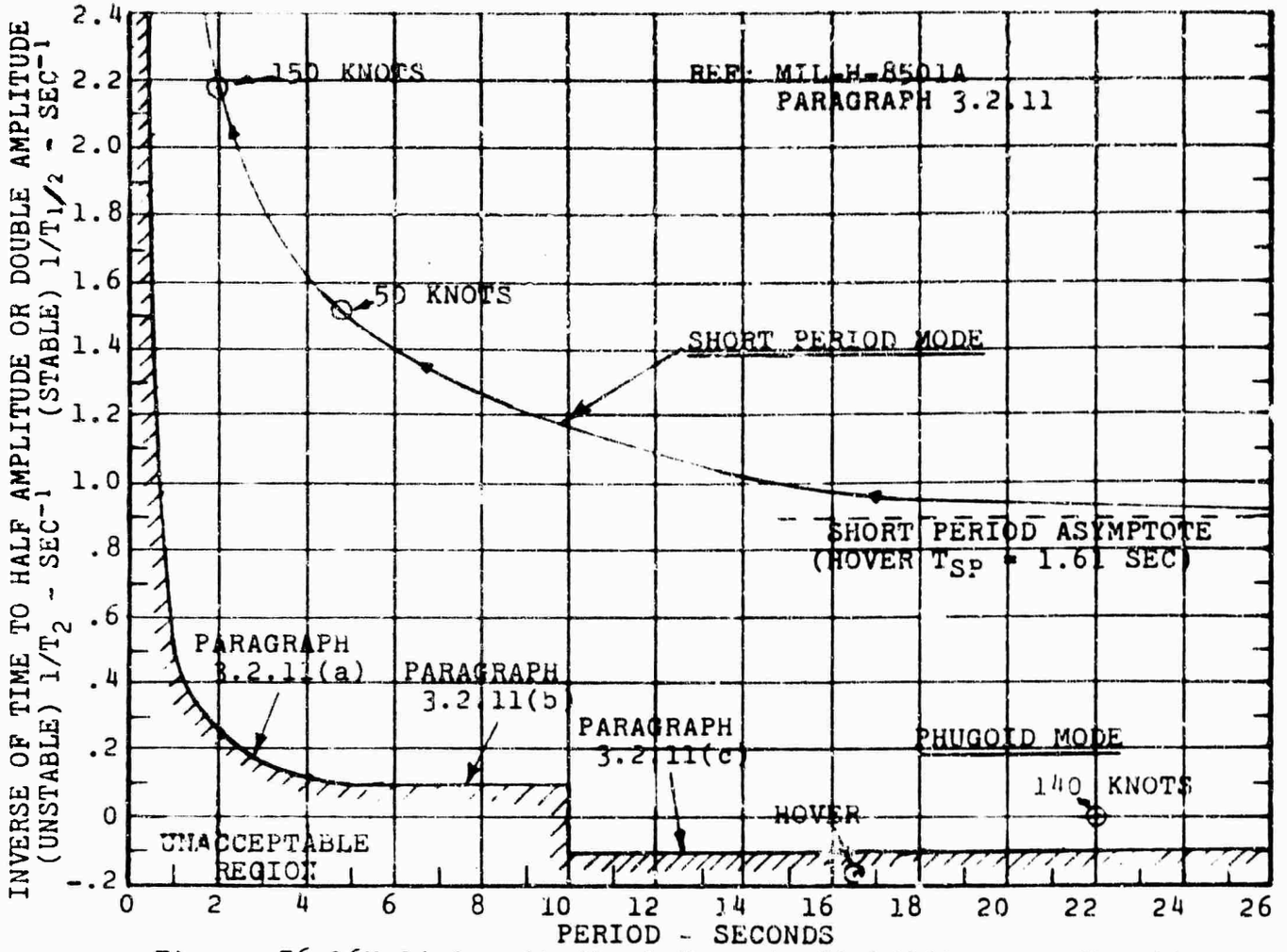


Figure 76.16H-1A Longitudinal Dynamic Stability as a Function of Level Flight Trim Speed.

TABLE VI. FLIGHT AND BLIP NUMBERS FOR DATA USED IN FLYING AND HANDLING QUALITIES (FIGURE 75)

| FLIGHT | BLIP | FLIGHT | BLIP |
|---|---|---|---|
| 286 | 2 | 297 | 1,2 |
| 290 | 1,2,3 | 299 | 1,2,3 |
| 291 | 1,2,3,4 | 304 | 1,2 |
| 292 | 1,2,3 | 308 | 1,2 |
| 294 | 1,2,3 | 309 | 1,3 |
| 295 | 1,2,3,4 | 317 | 1,2,3,5,6 |
| 296 | 1,2 | 327 | 1,2,3,4,5,6 |

The figure shows the locus curve representing the 16H-1A short-period damping and period as they vary with initial flight speed from hover to maximum velocity (there are negligible stability changes above 150 knots). Also shown is a point at 140 knots representing phugoid damping and period. The short-period curve is based on the recorded dynamic responses obtained at hover, 50 knots, and 140 knots. The analyses of these damping levels and periods are contained in Appendix III, (pages 339 to 341, 348 to 352, and 363 to 366) together with the theory-test correlations which substantiate the theoretical results.

The phugoid-mode point is based on the recorded high-speed responses of Test 410, Blips 1 and 2 (Figures 77 and 78). These directly discernible phugoid oscillations at high speed indicate an essentially neutrally stable mode with a period of approximately 22 seconds. In addition, a phugoid excited response at 80 knots (Figure 79) shows characteristics which are consistent with the data at 140 knots.

An examination of Figure 76 indicates that the short-period damping and the phugoid damping are in the acceptable region and far removed from the specification minimum. The hover aperiodic mode (with a time constant, $T_{SP}$ = 1.61 seconds) develops into a well damped short-period mode at forward speeds with a period between 2 and 5 seconds.

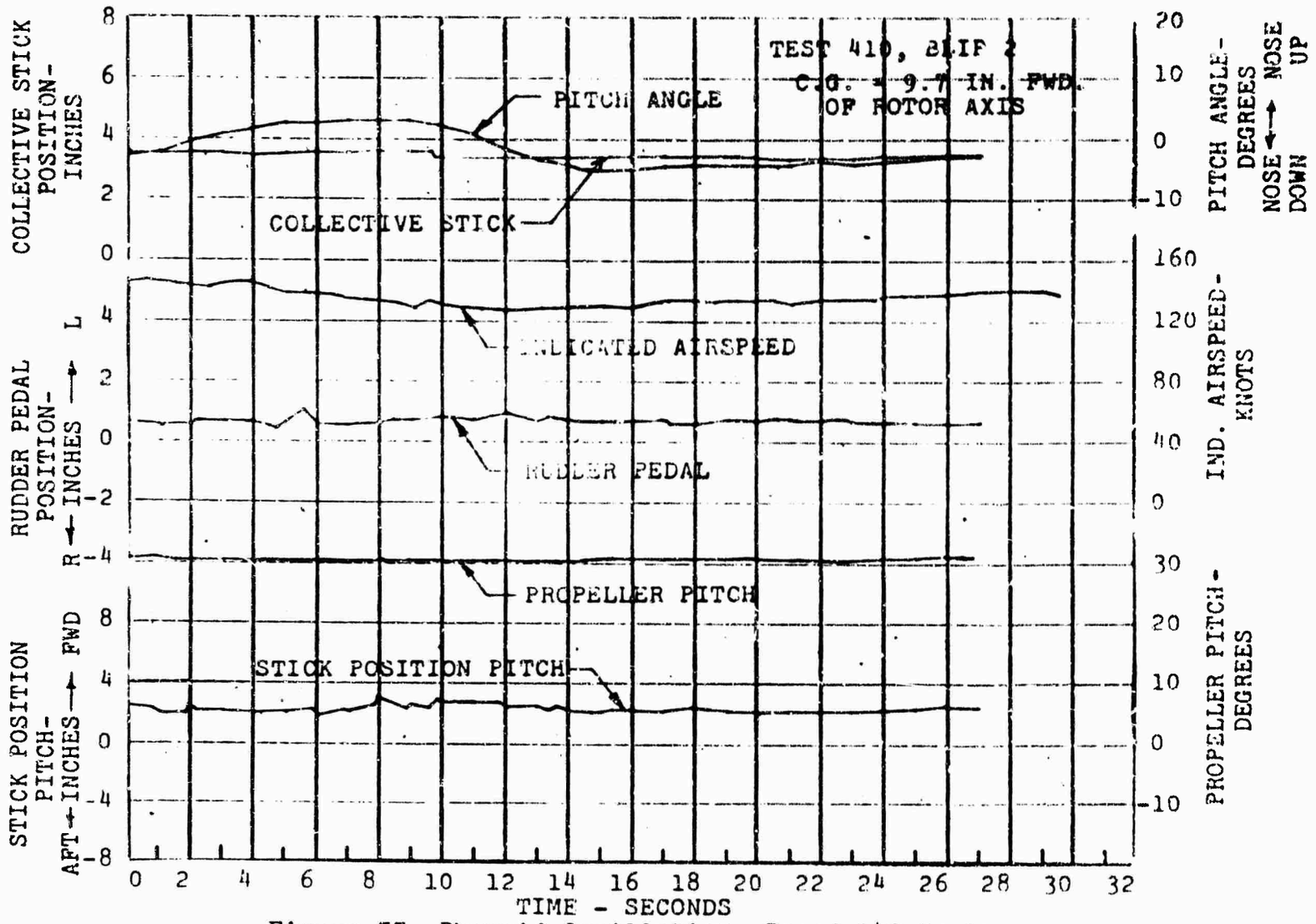


Figure 77. Phugoid Oscillation, Speed 140 Knots.

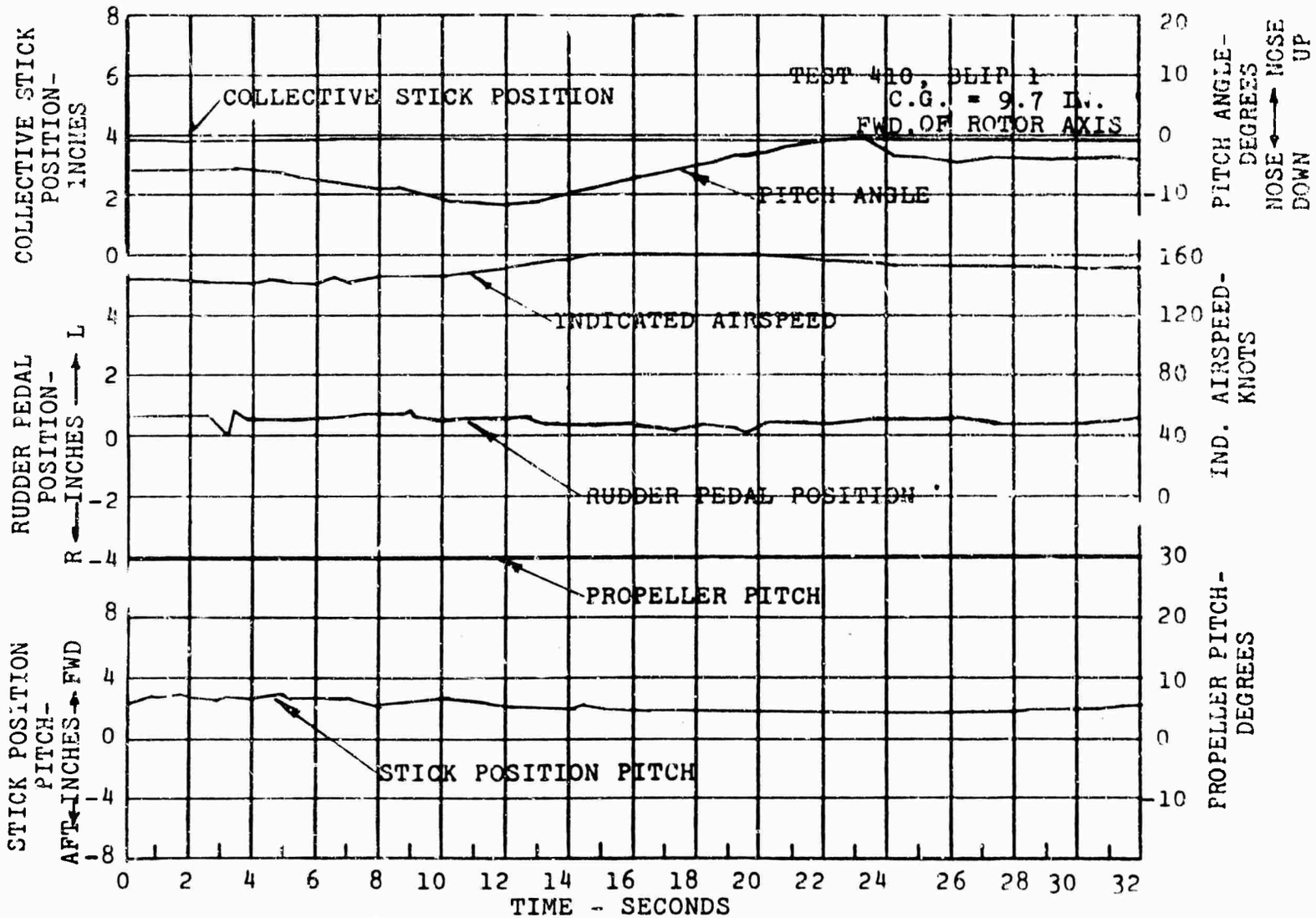


Figure 78. Phugoid Oscillation, Speed 140 Knots.

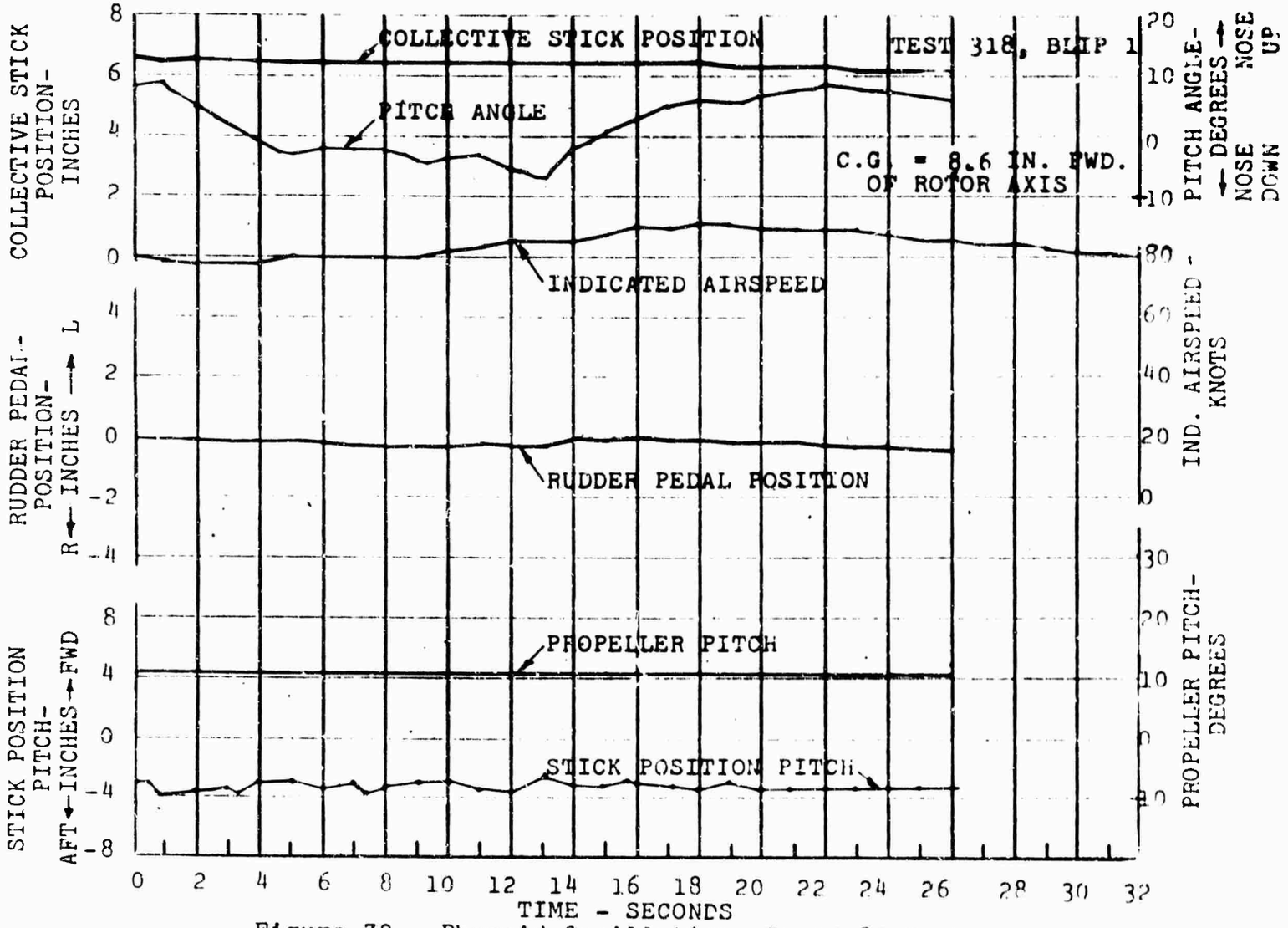


Figure 79. Phugoid Oscillation, Speed 80 Knots.

3.2.11.1 (a) (Reference 4)

This paragraph presents the well-known "concave-down" requirement for the normal acceleration time history following a longitudinal control step input. Specifically, the demonstration calls for an inflection point within 2 seconds following a control application and downward concavity to be maintained from that point to the development of maximum acceleration. This is to insure maneuver stability and is to be shown at all speeds above that for minimum power required.

Figure 80 sets forth the planned flight test maneuver envelope. Sufficient data defining the basic longitudinal dynamics, upon which the above characteristic depends, were obtained throughout the speed range. These parameters, principally the damping and period of the short-period mode, were obtained in the dynamic response tests and analyses discussed in paragraph 3.2.11. Consideration of control and response variable magnitudes is immaterial, since the usual linear analysis approach has been used.

The incremental normal acceleration load factor response (at constant speed) to longitudinal stick displacement is given by

$$\Delta n = \left[ \frac{K_\alpha \left( D + \frac{1}{T} \right)}{(D^2 + 2\zeta\omega_o D + \omega_o{}^2)} + K_\delta \right] \delta(t) \qquad (38)$$

where

$$K_\alpha = - \frac{L_\alpha}{W} \times \frac{L_\delta}{mV_o}$$

$$K_\delta = \frac{L_\delta}{W}$$

$$\frac{1}{T} = -\frac{M_q}{I_y} \quad \frac{M_\delta / I_y}{L_\delta / mV_o}$$

and $\zeta$, $\omega_o$ are the short-period-mode critical damping ratio and undamped frequency as given in the analysis contained in Appendix III. $\delta(t)$ is the stick input time function in inches. For a 1-inch aft (negative) displacement of control, and with the 150-knot derivative values applied, this equation

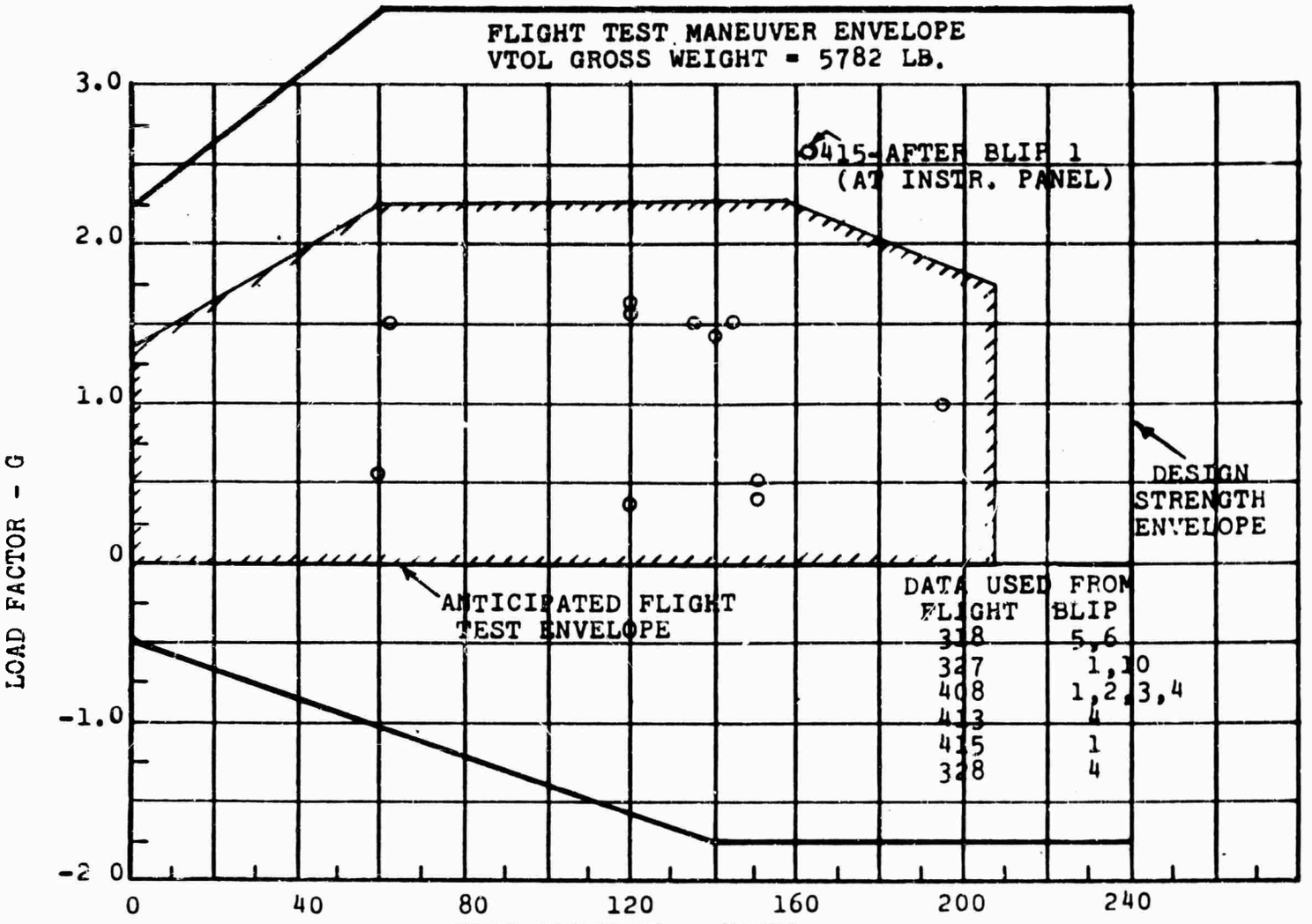


Figure 80. Flight Test Maneuver Envelope.

in terms of the Laplace variable becomes (from Appendix II)

$$\frac{1}{T} = \frac{15,600}{11,000} - \frac{1,300 \times 47,000}{11,000 \times 1,500} \quad (39)$$

$$= 1.42 - 3.70 = -2.28 \text{ sec}^{-1}$$

$$K_a = \frac{76,000}{6,000} \times \frac{1,500}{47,000} \quad (40)$$

$$= 0.405 \text{ g/inch-sec}$$

$$K_\delta = -\frac{1,500}{6,000} \quad (41)$$

$$= -0.25 \text{ g/inch}$$

$$\zeta = 0.430$$

$$\omega_o = 3.52 \text{ rad/sec}$$

$$\Delta n(s) = \frac{-0.405\ (s-2.28)}{s[s^2 + 2(0.430)(3.52)\ s + (3.52)^2]} + \frac{0.325}{s} \quad (42)$$

and the inverse transform or time response equation is

$$\Delta n = 0.325 + 0.179e^{-1.52t} \sin(3.18t + 3.57) \quad (43)$$

Equating the second derivative of $\Delta n$ to zero in order to determine the inflection-point time yields

$$\frac{d^2(\Delta n)}{dt^2} = [(1.52)^2 - (3.18)^2] \sin(3.18t + 3.57) -$$

$$(2 \times 1.52 \times 3.18) \cos(3.18t + 3.57) = 0 \quad (44)$$

$$\text{or} \quad \tan(3.18t + 3.57) = -1.24 \quad (45)$$

$$\text{and} \quad t = 0.57 \text{ sec}$$

[illegible] the normal acceleration response becomes concave [illegible] after the start of the maneuver, and since the response is a damped second-order oscillation, it must remain concave down from this time until the maximum is reached. At flight speeds between approximately 80 knots (minimum power required) and 150 knots, the inflection-point time will be somewhat longer but will be within the required limit of 2 seconds.

3.2.11.1 (b) (Refer to 4)

For the maneuver described in paragraph 3.2.11.1 (a), the pitch-rate response also becomes concave down within [illegible] after the start of the maneuver. Here all flight speeds, including hover, are to be considered. Because aerodynamic lifting considerations in hover are meaningless (except for the pure vertical response mode which has no coupling pitch response), the more severe operating condition of 50 knots is analyzed for this case.

The pitch-rate response equation to control motion is given by

$$D\theta = \frac{K\left(D + \frac{1}{T}\right)\delta(t)}{(D^2 + 2\zeta\omega_0 D + \omega_0^2)} \qquad (46)$$

where

$$K = \frac{M_\delta}{I_y}$$

$$\frac{1}{T} = \frac{L_\alpha}{mV_0} - \frac{M_\alpha}{M_\delta} \chi \frac{L_\delta}{mV_0}$$

and the remaining parameters are as previously defined. For a 1-inch aft step control displacement, and with the 50-knot derivatives (as given in Appendix III) applied, this equation in terms of the Laplace variable and in degree-per-second units is

$$\dot{\theta}(s) = \frac{7.89\ (s + 1.513)}{s[s^2 + 2(0.57)(1.59)\ s + (1.59)^2]} \qquad (47)$$

and the time solution, or inverse transform, is then

$$\dot{\theta} = 4.65 - 5.40e^{-0.91t} \sin(1.31t + 2.10) \qquad (48)$$

Equating the second derivative of $\dot{\theta}$ to zero in order to establish the inflection-point time yields

$$\frac{d^2(\dot{\theta})}{dt^2} = [(0.91)^2 - (1.31)^2] \sin (1.31t + 2.10) -$$

$$(2 \times 0.91 \times 1.31) \cos (1.31t + 2.10) = 0 \qquad (49)$$

or $$\tan (1.31t + 2.10) = -2.69$$

and $$t = 2.26 \text{ sec} \qquad (50)$$

Thus, under the most critical condition, the inflection-point time exceeds the specified maximum, but only by 13 percent. Since the response is a damped second-order oscillation, it must remain concave down from the inflection point to the maximum pitch rate.

3.2.11.2 (Reference 4)

This paragraph concerns the capability of inherent limiting of acceleration response due to short duration disturbances. Operating speeds are not specified, but the high-speed (150-knot) case is first analyzed. It is stated that when the stick motion is a 0.5-second aft square pulse (to simulate a disturbance) the change in normal acceleration magnitude shall not exceed 0.25 g after the control has been returned to trim. The control input magnitude is to be the least of: 1 inch, the step size required to produce a 0.2 radian per second pitch rate within 2 seconds, or the step size required to develop a normal acceleration (total) of 1.5 g within 3 seconds. Considering steady-state values, it is found from the response equations given in the preceding paragraphs that the stick deflection for the pitch-rate criterion is

$$\delta_1 = -\frac{0.2 \times 57.3}{4.65} \qquad (51)$$

$$= -2.46 \text{ inches}$$

For the normal acceleration criterion, the stick deflection is

$$\delta_2 = -\frac{(1.5 - 1.0)}{0.325} \qquad (52)$$

$$= -1.54 \text{ inches}$$

with response times less than the maximum times cited. Thus, a 1-inch aft square pulse is adopted, and for the purposes of analysis, this response can be closely approximated by an impulse input of -0.5 inch-second.

Since only accelerations after control is returned to trim need be considered, the direct control contribution to acceleration is omitted and only that due to angle of attack is computed. It can be seen from the response equation of paragraph 3.2.11.1 (a) that, for a -0.5 inch-second impulse input, the response equation in the Laplace variable is

$$(\Delta n)_\alpha(s) = \frac{-0.5 \times 0.405\ (s - 2.28)}{[s^2 + 2(0.430)(3.52)\ s + (3.52)^2]} \qquad (53)$$

and the time solution is then

$$(\Delta n)_\alpha = -0.315\ e^{-1.52t} \sin\ (3.18t + 5.60) \qquad (54)$$

Examination of this response indicates that a negative peak of -0.120 g is reached at 0.568 second. Succeeding peaks are smaller in magnitude as the response is damped.

At a 50-knot forward speed, the acceleration response due to $\alpha$ is larger than at 150 knots, whereas that produced by direct control contribution is smaller (-0.07 g/inch compared to -0.25 g/inch), so that this peak acceleration change should be increased accordingly. If a correction proportional to the ratio of steady state $(\Delta n)_\alpha$ from a step input at the two speeds is applied,

$$\text{peak } (\Delta n) = \frac{0.134}{0.075}\ (-0.12) \qquad (55)$$

$$= -0.215 \text{ g}$$

This is less than the maximum allowable of 0.25 g and hence the specification requirement is satisfied.

3.2.12 (Reference 4)

The requirement is that, for the maneuver of paragraph 3.2.11.1, the normal acceleration always increases with time until the maximum is attained. As the basic acceleration response established in the preceding analyses is damped second-order response and takes place only in the short-

period mode, it is apparent that acceleration reversal as described in this paragraph does not occur.

3.2.13 (Reference 4)

Longitudinal control power in hover at maximum overload weight or rated power shall be such that a 1-inch step input from trim will produce, within 1 second, a minimum pitch change of

$$\theta = \frac{45}{\sqrt[3]{W + 1000}} \text{ degrees} \tag{56}$$

The test weight of 6000 pounds is applied. Hence,

$$\theta = \frac{45}{\sqrt[3]{6000 + 1000}} \tag{57}$$

$$= 2.35 \text{ degrees}$$

Referring to the hover pitch-angle response equation presented in Appendix III, the pitch angle response to a 1-inch aft step is given by

$$\theta(s) = \frac{7.80\,(s + 0.0064)}{s(s + 0.622)[s^2 + 2(-0.305)(0.403)s + (0.403)^2]} \tag{58}$$

and the corresponding inverse transform or time solution is

$$\theta = 0.50 + 11.0e^{-0.622t} + 24.4e^{0.123t}\sin(0.385t + 5.80)$$

From this equation, at t = 1 second, $\theta$ = 3.36 degrees. Therefore the requirement is satisfied for the test weight. At higher gross weights, the requirement would be satisfied by an increasing margin, since control power in hover is essentially proportional to weight, while the required response becomes less as weight increases.

The paragraph also stipulates that when maximum available displacement from trim of the longitudinal control is applied, the pitch angle shall be at least 4 times as great as the pitch change for a 1-inch displacement. The control position curve for the 16H-1A reveals that trim is at 1.9 inches forward in hover. Since 5.6 inches of travel remains, and a linear analysis approach is applicable, this requirement is also satisfied.

3.2.14 (Reference 4)

The minimum pitch damping in hover is specified to be at least

$$M_q = -8\ (I_y)^{0.7}\ \text{ft-lb-sec/rad} \qquad (59)$$

For the 16H-1A the required damping is then

$$M_q = -8(11,000)^{0.7} \qquad (60)$$

$$= -5,400\ \text{ft-lb-sec/rad}$$

The 16H-1A estimated value is -3,840 foot-pound-seconds per radian, as shown in Appendix III. The stated purpose of this specification is to insure satisfactory initial response characteristics following a control input and to minimize the effects of external disturbances. These handling qualities in hover are essentially functions of longitudinal control power, inertia, and damping. The acceptable handling qualities boundaries for helicopters have been established as a function of these same parameters and are a fairly standard basis for stability evaluation (Reference 8). They are presented in Figure 81, together with the characteristics for the 16H-1A in hover, at 50 knots, and at 150 knots. It is seen that the combination of available damping and control power is such as to locate all points in the acceptable region. The MIL-H-8501A damping requirement is more than fulfilled by the 16H-1A at all forward speeds above approximately 30 knots.

LATERAL-DIRECTIONAL CHARACTERISTICS

3.3.1 (Reference 4)

Directional control in taxiing operation should be sufficient to permit turns and straight path motion in winds of 35 knots.

Taxi tests were conducted on the concrete mat adjacent to the Piasecki facilities at the Philadelphia International Airport, with winds up to 25 knots and gusting to 30 knots. Higher winds were not available during the test period.

1. Upwind, crosswind, and downwind without the use of brakes at ground speeds of up to 10 knots. When taxiing downwind at ground speeds of 20 knots, brakes and/or increased collective pitch

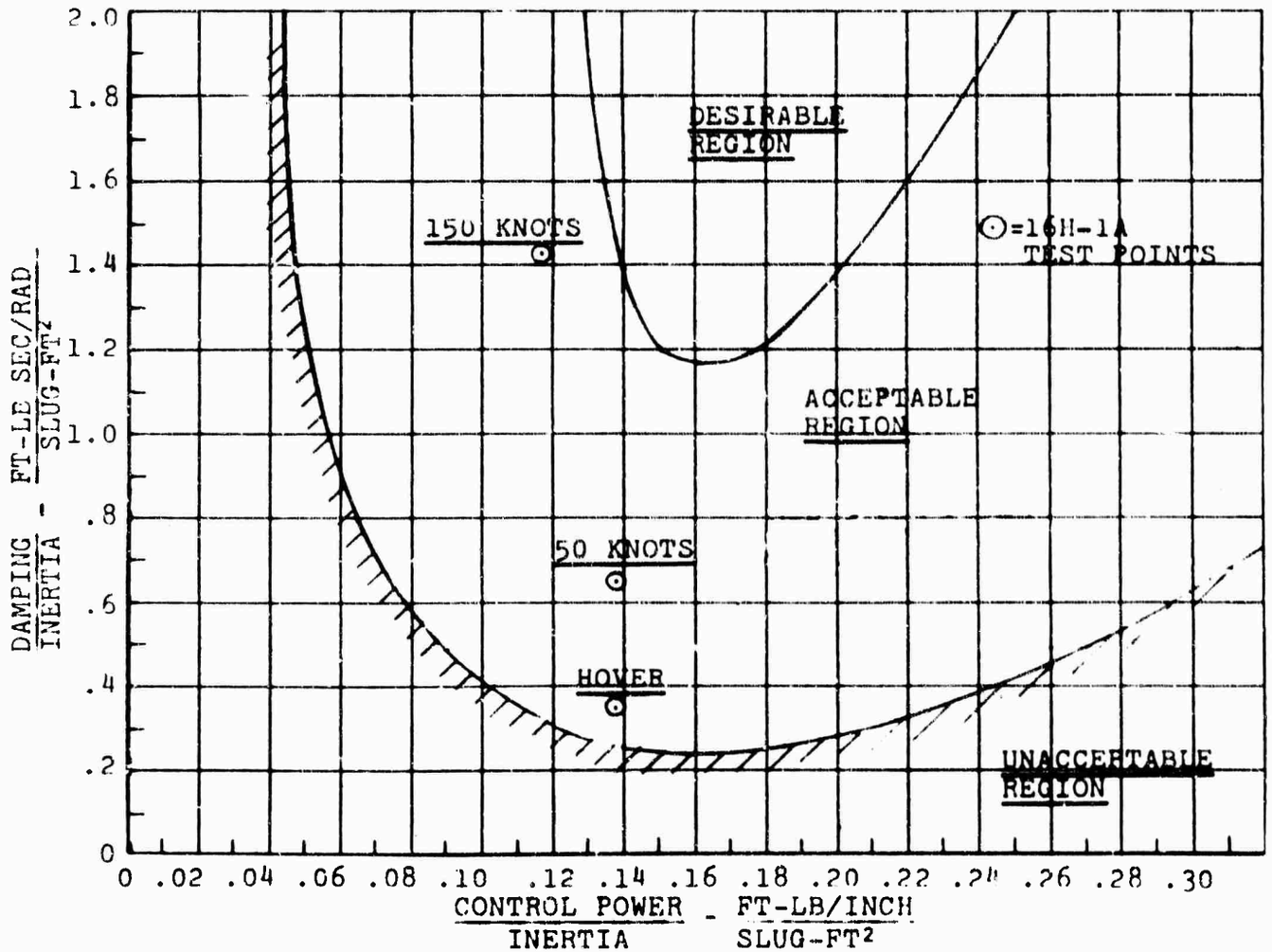


Figure 81. Helicopter Handling Qualities Criteria in Pitch (From Ref. 8).

with aft cyclic control were required to stop the aircraft.

2. Figure eights and box patterns were accomplished at ground speeds of up to 10 knots without the use of brakes. Above 10 knots in the above wind condition, brakes and/or increased collective pitch were required.

3. Main rotor blade clearances were ample at all times with 100 percent rotor RPM and minimum collective pitch. Rotor engagements were accomplished without difficulty in the above winds.

4. The aircraft could be stopped at any time while performing these maneuvers by the application of brakes or cyclic control and the addition of collective pitch.

The control positions (collective pitch, tail propeller pitch, tail vane settings and rotor cyclic pitch) were monitored by the pilot and copilot-engineer during most of these tests. Oscillograph records were obtained for two figure-eight maneuvers in 10-knot winds. Engine RPM was held constant by the engine governor.

A camera was used to record the clearance between the rotor tip path plane and the tail duct, which never was less than 41 inches.

The following techniques were developed:

1. When taxiing upwind or crosswind, the tail propeller pitch was used for acceleration and deceleration and the rudders were used for directional control. The cyclic stick was held neutral for acceleration, back for deceleration, and into the wind at all times during crosswind taxiing.

2. When taxiing downwind, collective pitch was increased and cyclic control was used for acceleration and deceleration.

All of the above taxiing was repeated at 93 percent main-rotor RPM (5600 engine RPM) without difficulty. Deceleration was more easily performed under these power conditions. Figures 82 and 83 illustrate this capability in the recorded data for figure-eight maneuvers in 10-knot winds.

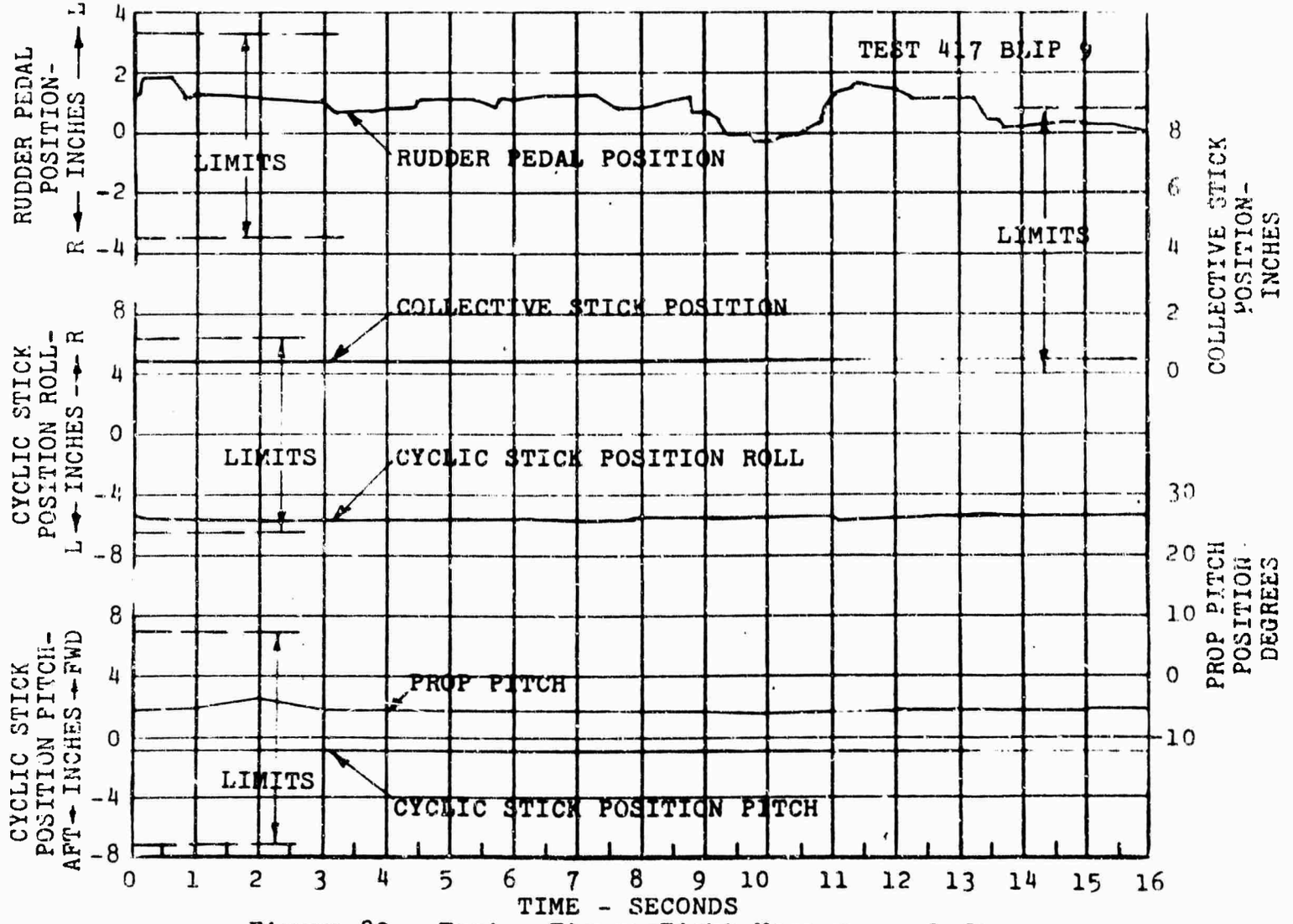


Figure 82. Taxi - Figure-Eight Maneuvers, Left.

Figure 83. Taxi - Figure Eight Maneuvers, Right.

3.3.2 (Reference 4)

Figure 84 presents the required control positions for sideward flight in both directions up to speeds of 30 knots, the contract requirement.

Margin of Control Power

30-Knot Left Sideward Flight

An examination of Figure 84 reveals that the maximum control positions are 4 inches aft stick, 2 inches lateral stick, and 1 inch right pedal. Thus, control displacement margins for longitudinal stick, lateral stick, and pedal respectively are 47 percent, 69 percent, and 69 percent of travel from neutral.

30-Knot Right Sideward Flight

Figure 84 also indicates maximums for this flight condition of 3.5 inches forward stick, 2 inches right stick, and 2.5 inches left pedal. The resulting control margins are then 53 percent longitudinal stick, 69 percent lateral stick, and 23 percent pedal.

Consideration should also be given to the data contained in Figures 85 through 96 in connection with sideward flight control margins. It is evident in these time histories that roll, pitch, and yaw maneuvers during sideward flight in each direction were successfully performed.

3.3.3 (Reference 4)

Hover over a given spot should be possible with no more than ±1 inch of lateral and directional control motions. Hover data for Flight 264, Blip 10 (Figure 58), indicate that lateral stick motions were less than ±0.75 inch and pedal motions were less than ±0.60 inch, for the 17-second duration of the blip.

3.3.4 (Reference 4)

In all steady operating conditions, sufficient lateral control margin amounting to at least 10 percent of the maximum hover control moment shall be available.

The hover lateral trim position is 1 inch left (Figure 97), leaving a maximum left control displacement from trim of 5.3 inches. The control power, based on the ratio of

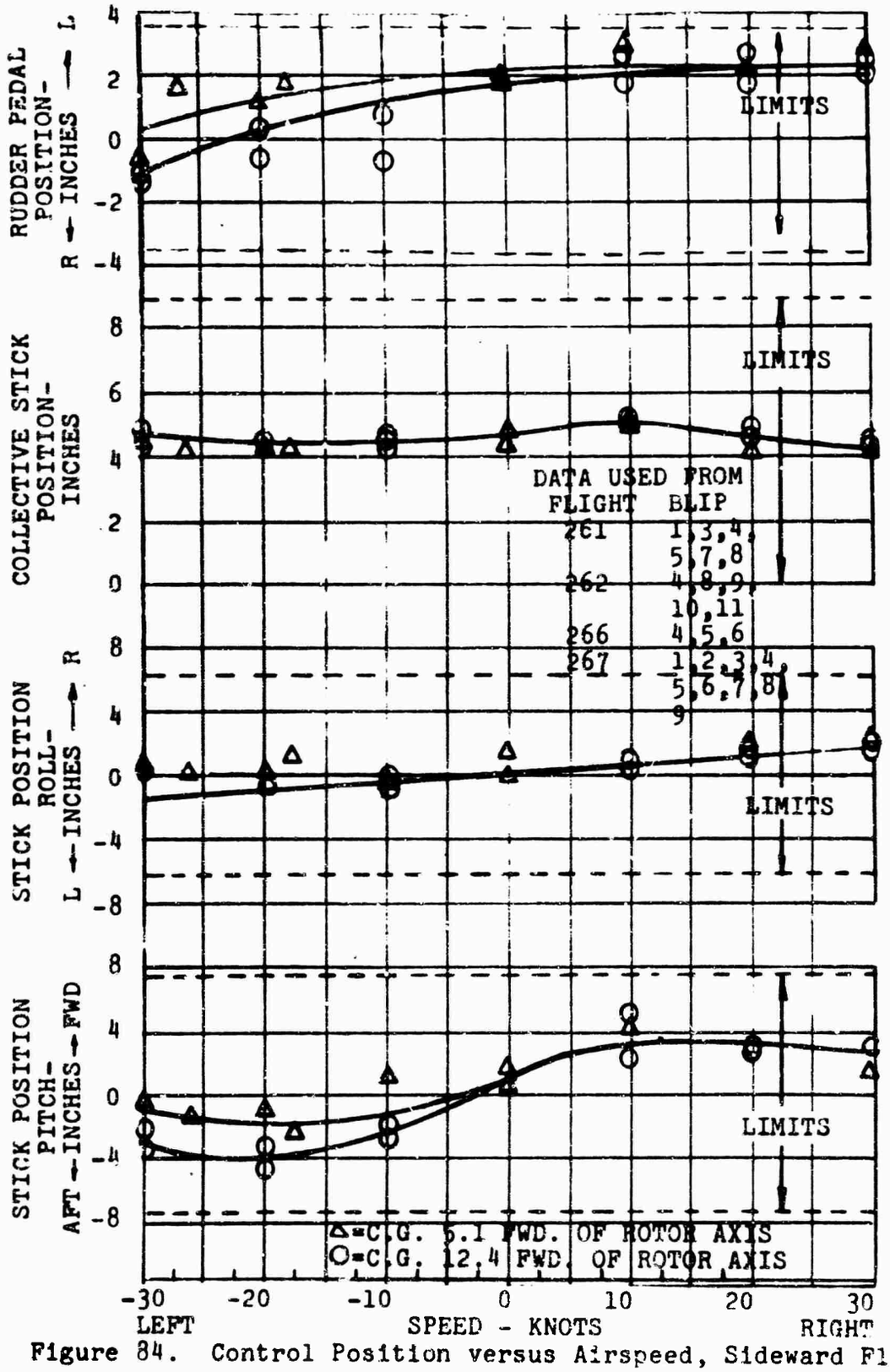


Figure 84. Control Position versus Airspeed, Sideward Flight.

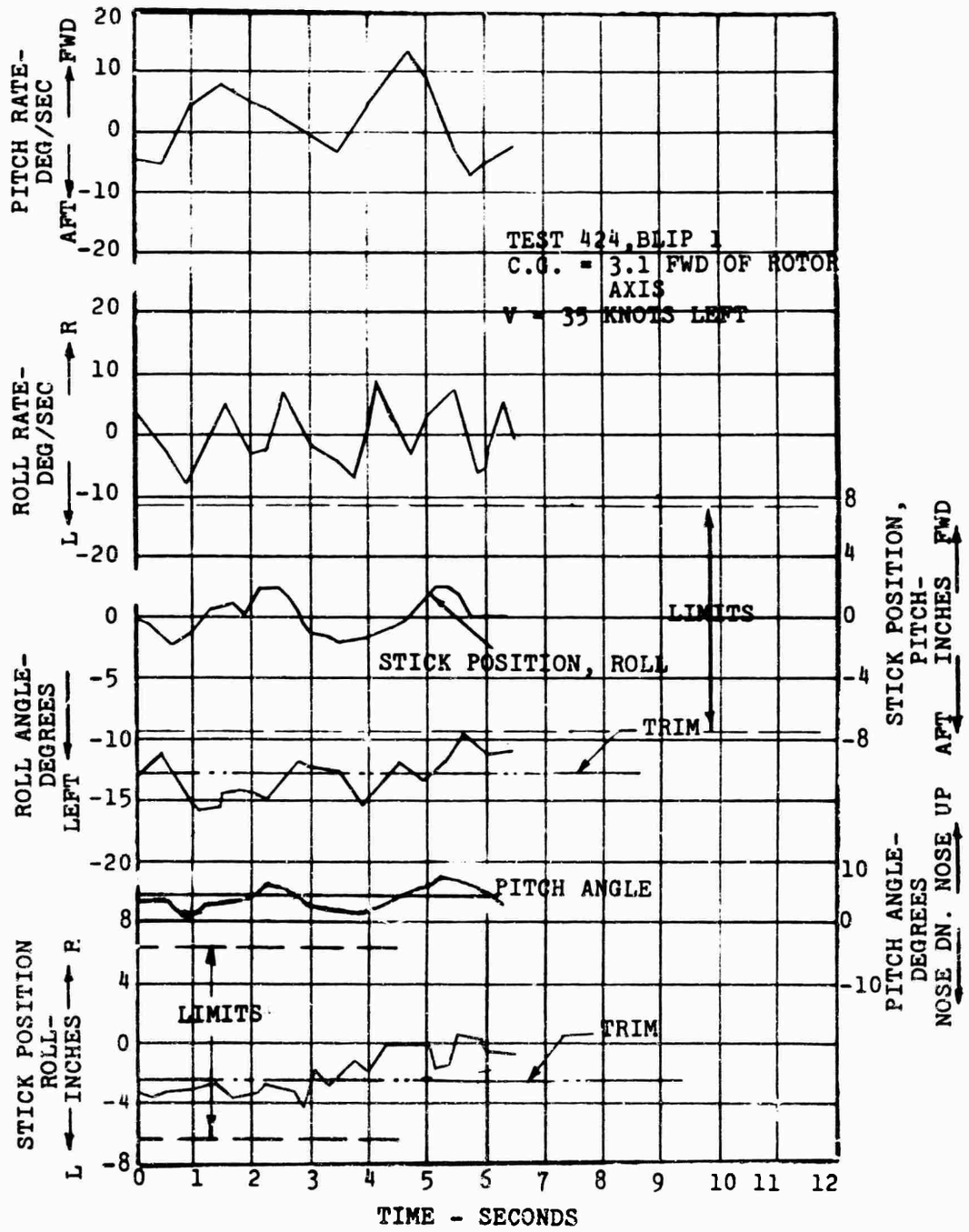


Figure 85. Roll Response - Left Sideward Flight, Roll Left.

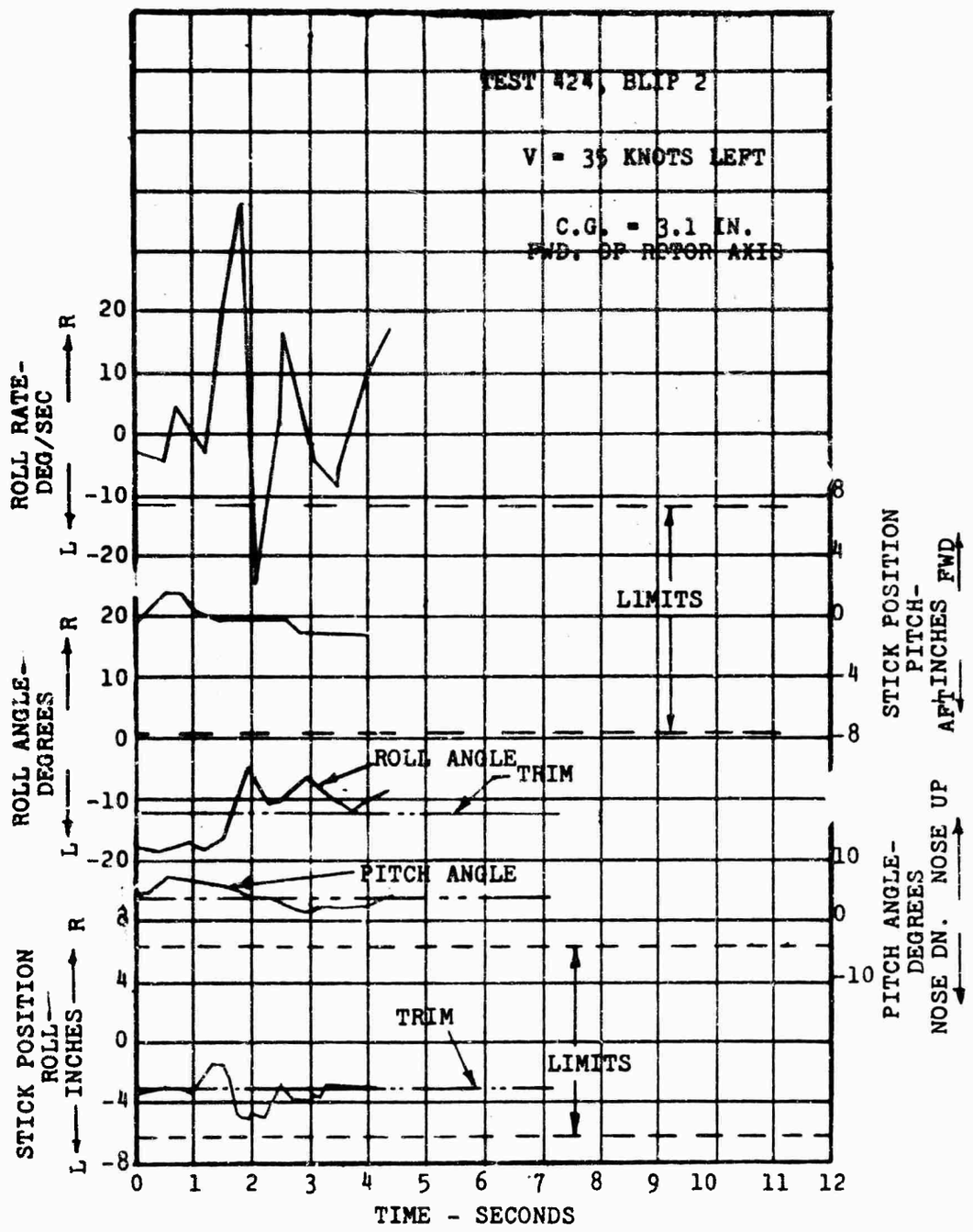


Figure 86. Roll Response - Left Sideward Flight, Roll Right.

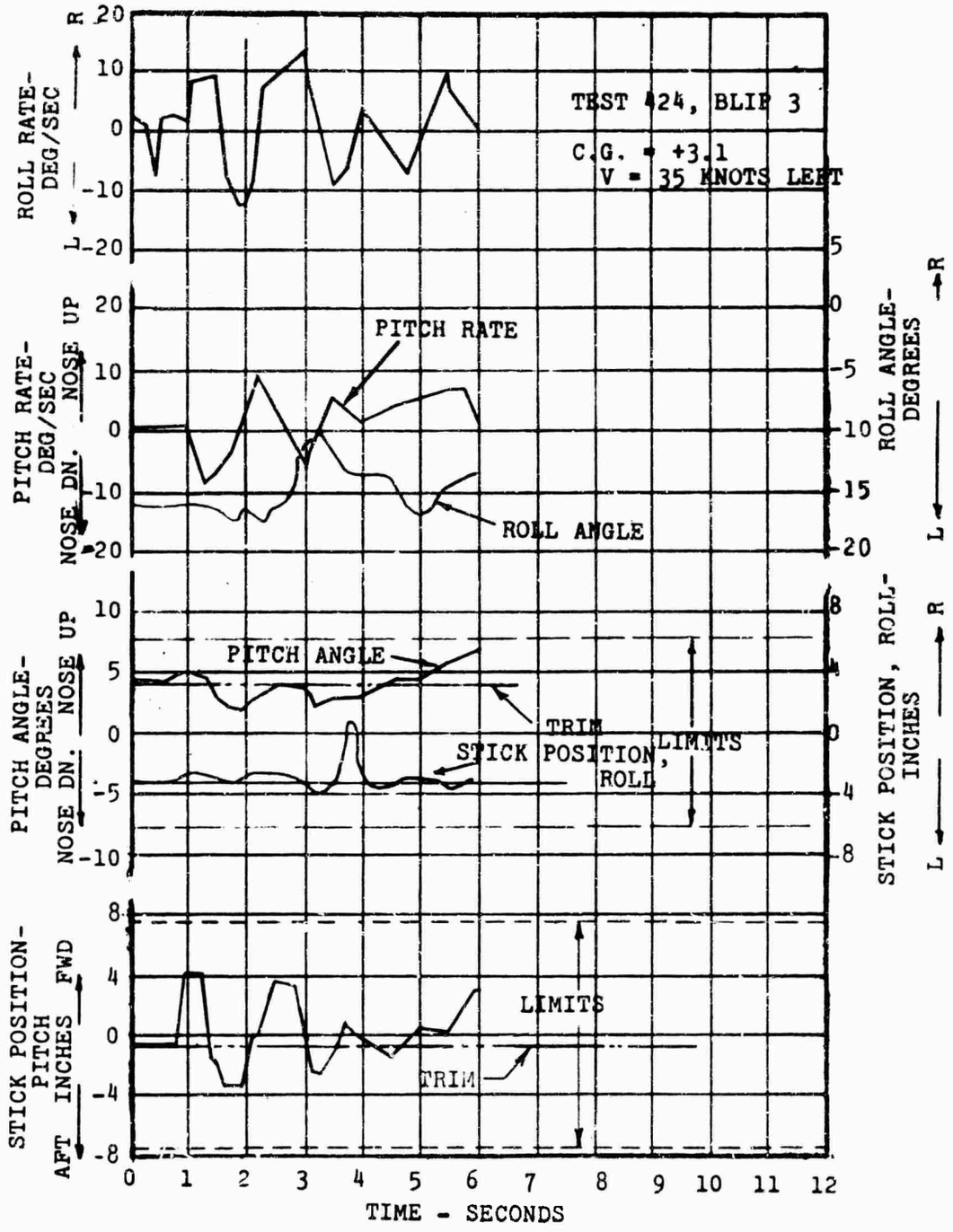


Figure 87. Pitch Response - Left Sideward Flight, Pitch Down.

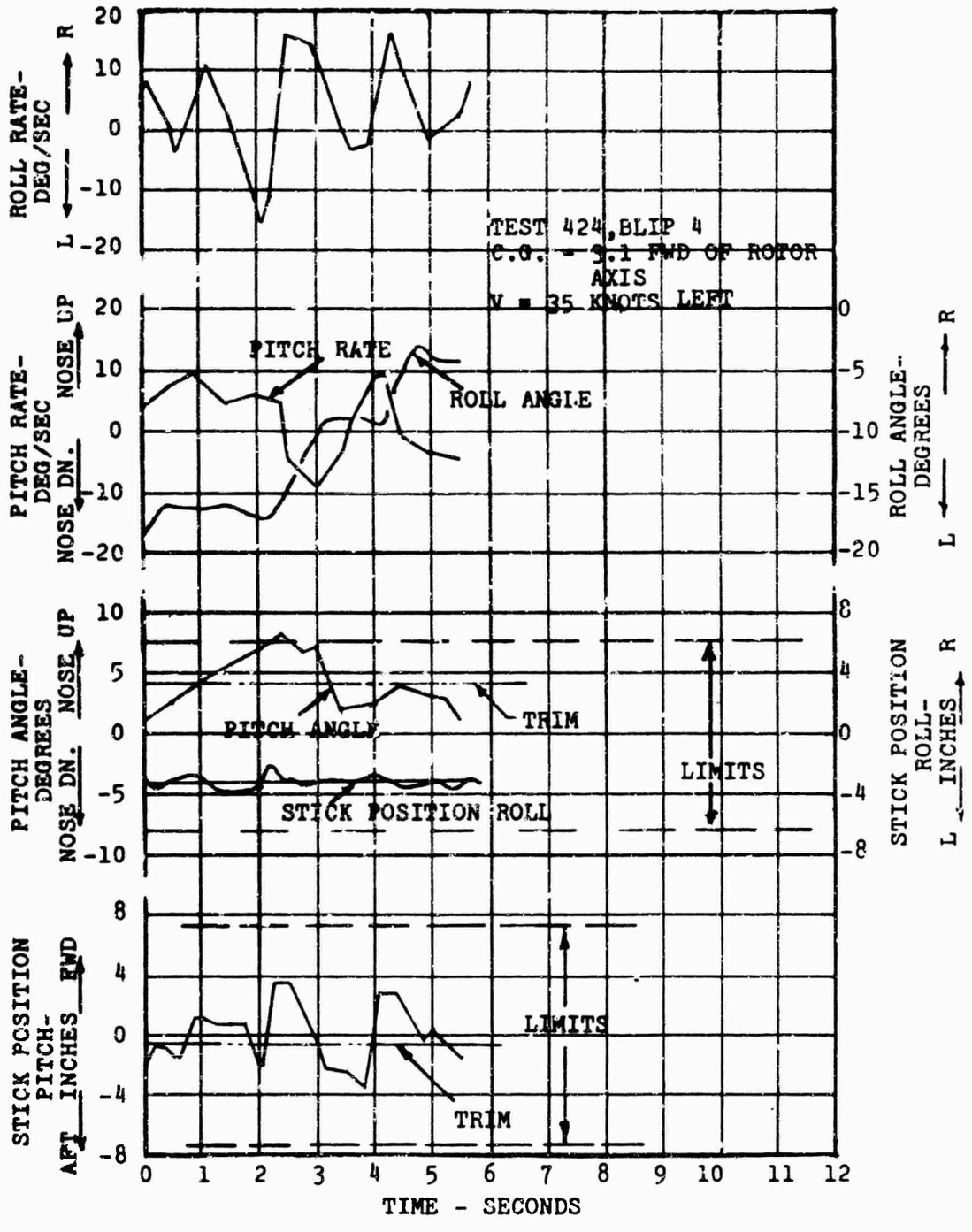


Figure 88. Pitch Response - Left Sideward Flight, Pitch Up.

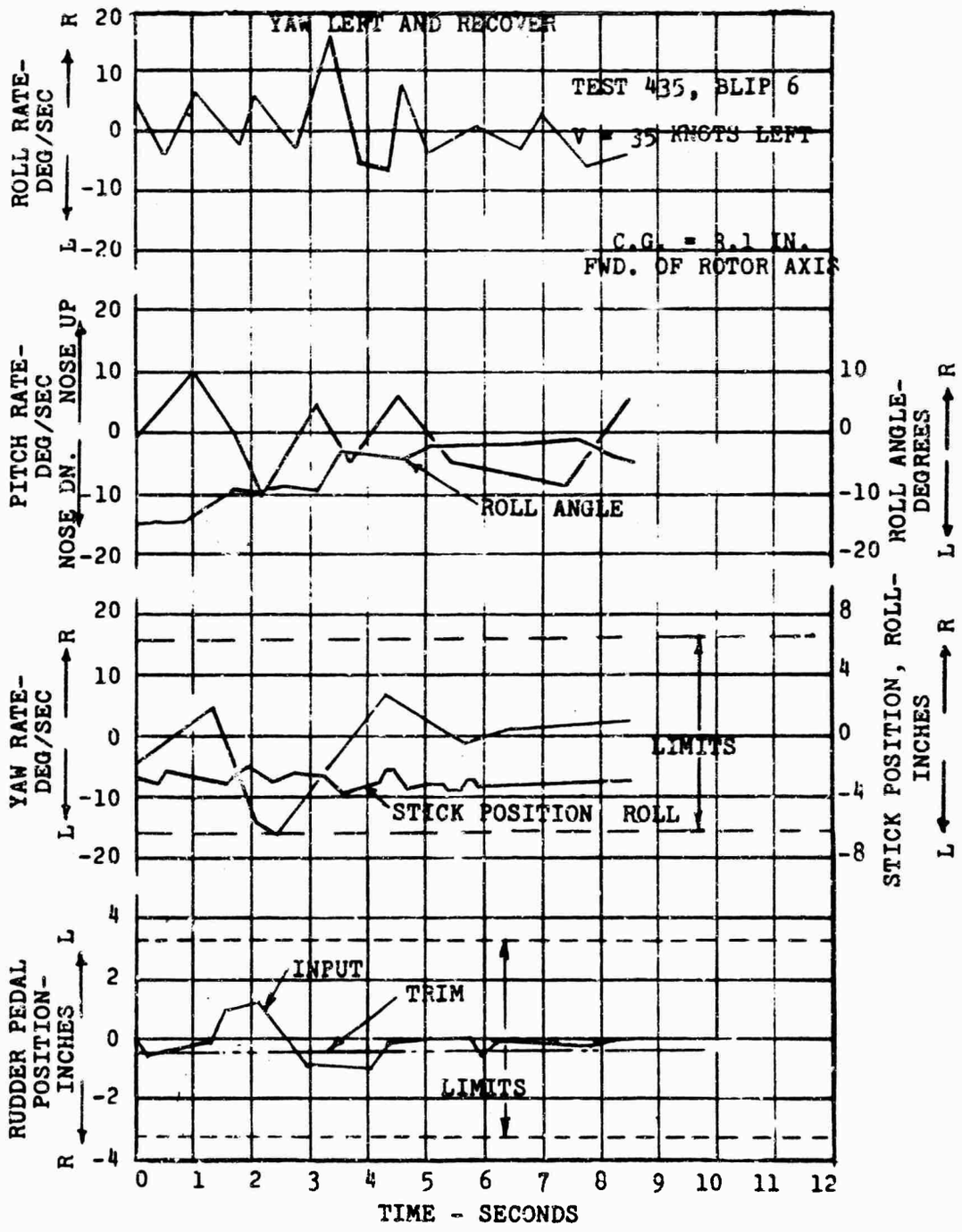


Figure 89. Yaw Response - Left Sideward Flight, Yaw Left.

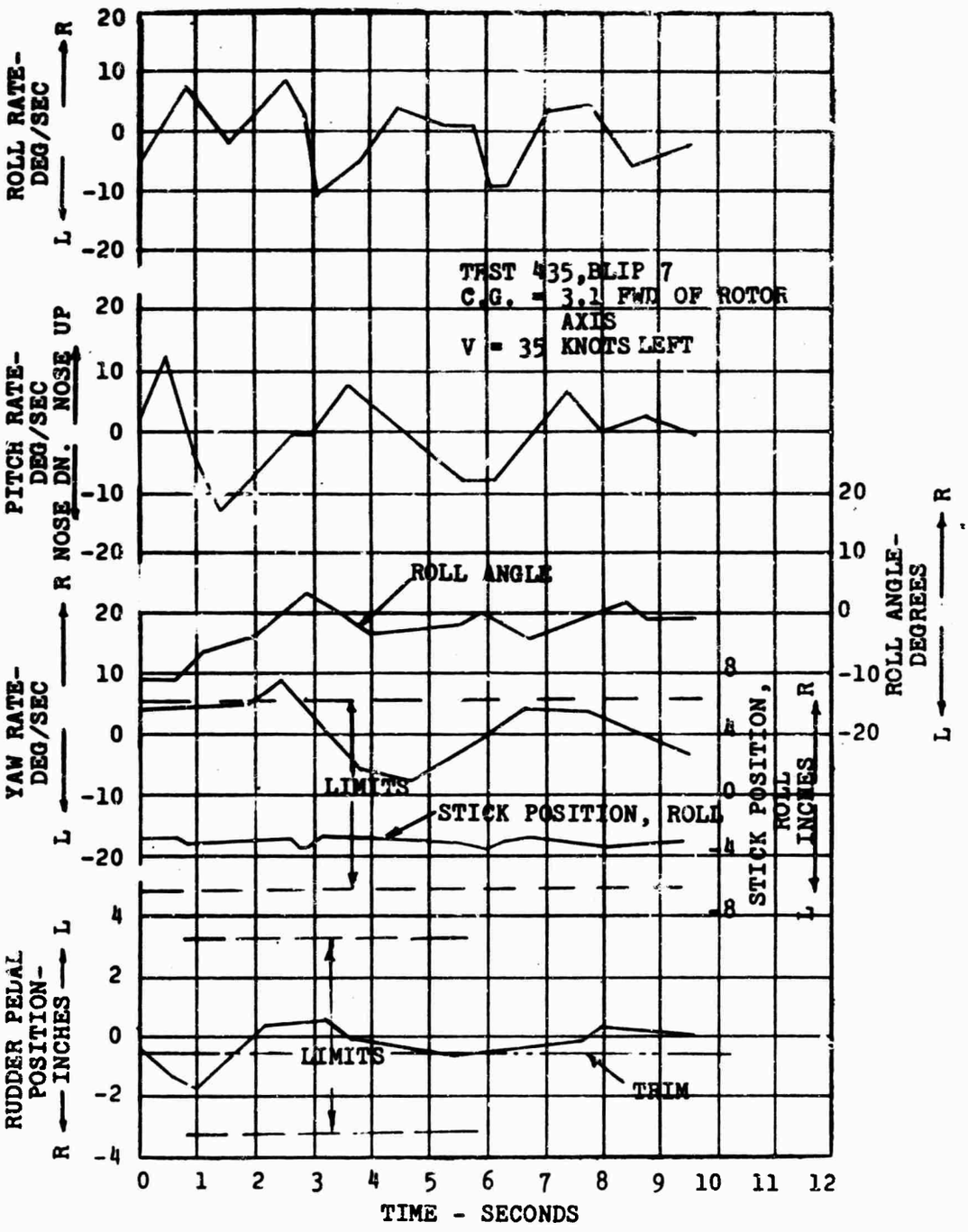


Figure 90. Yaw Response - Left Sideward Flight, Yaw Right.

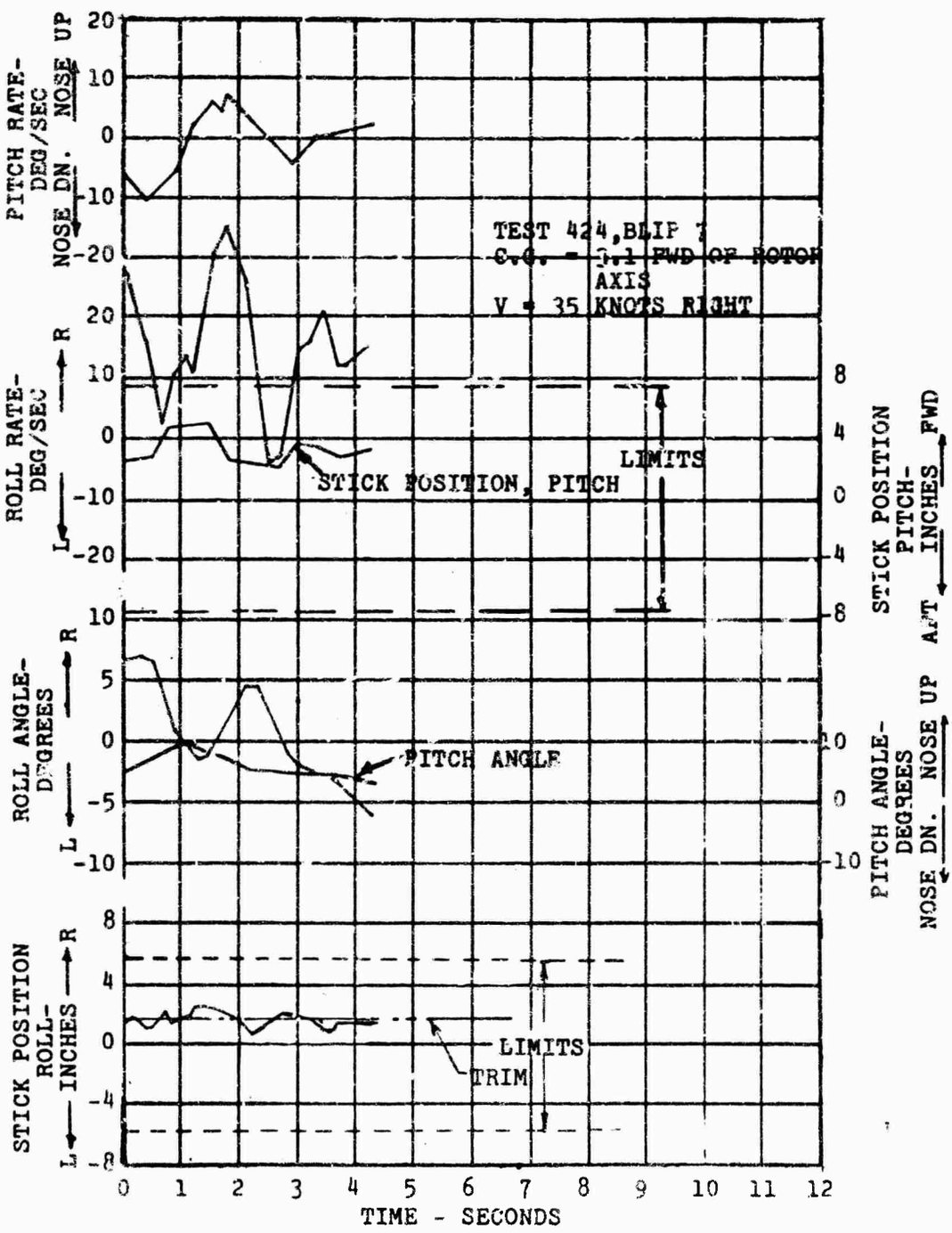


Figure 91. Roll Response - Right Sideward Flight, Roll Left.

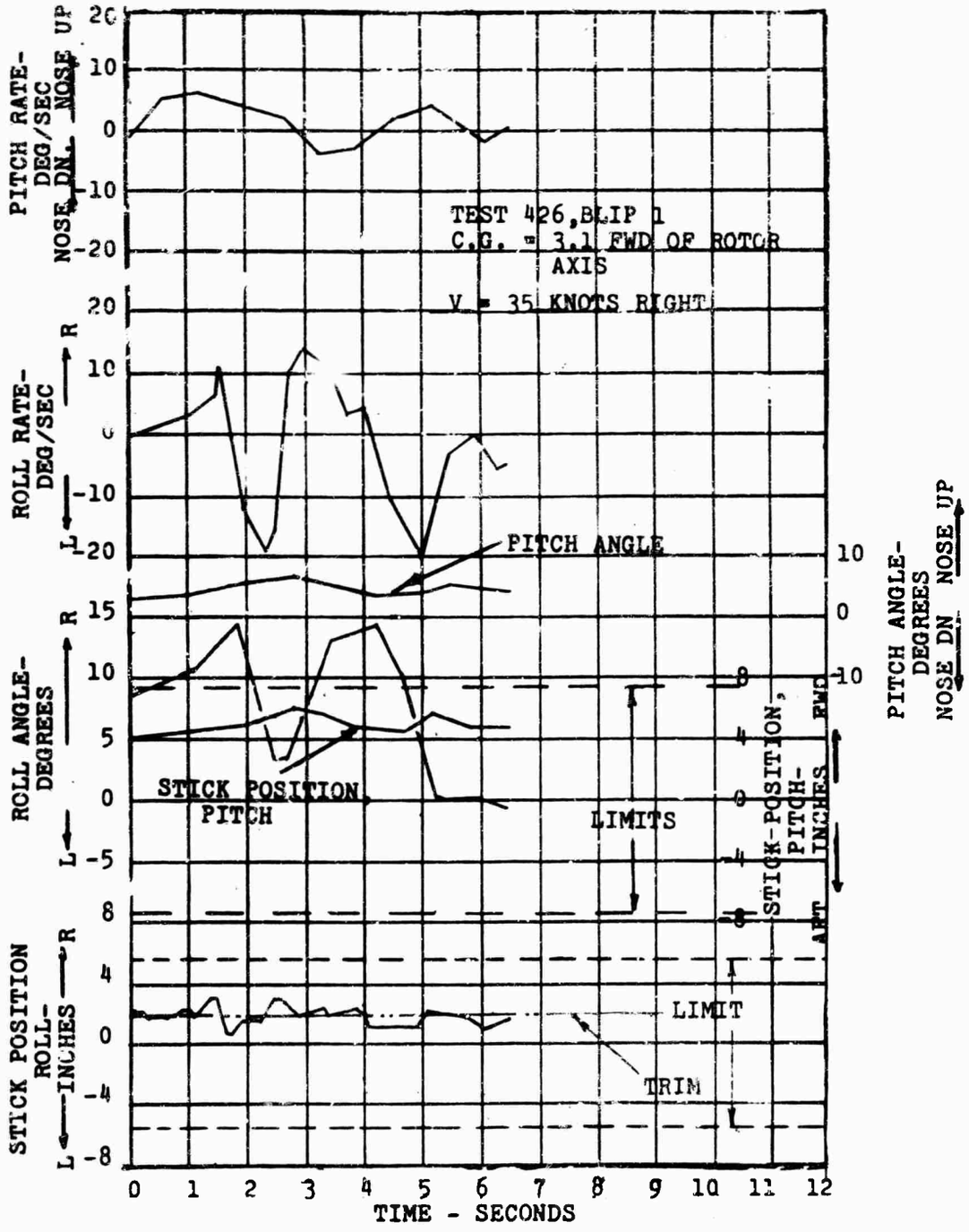


Figure 92. Roll Response - Right Sideward Flight, Roll Right.

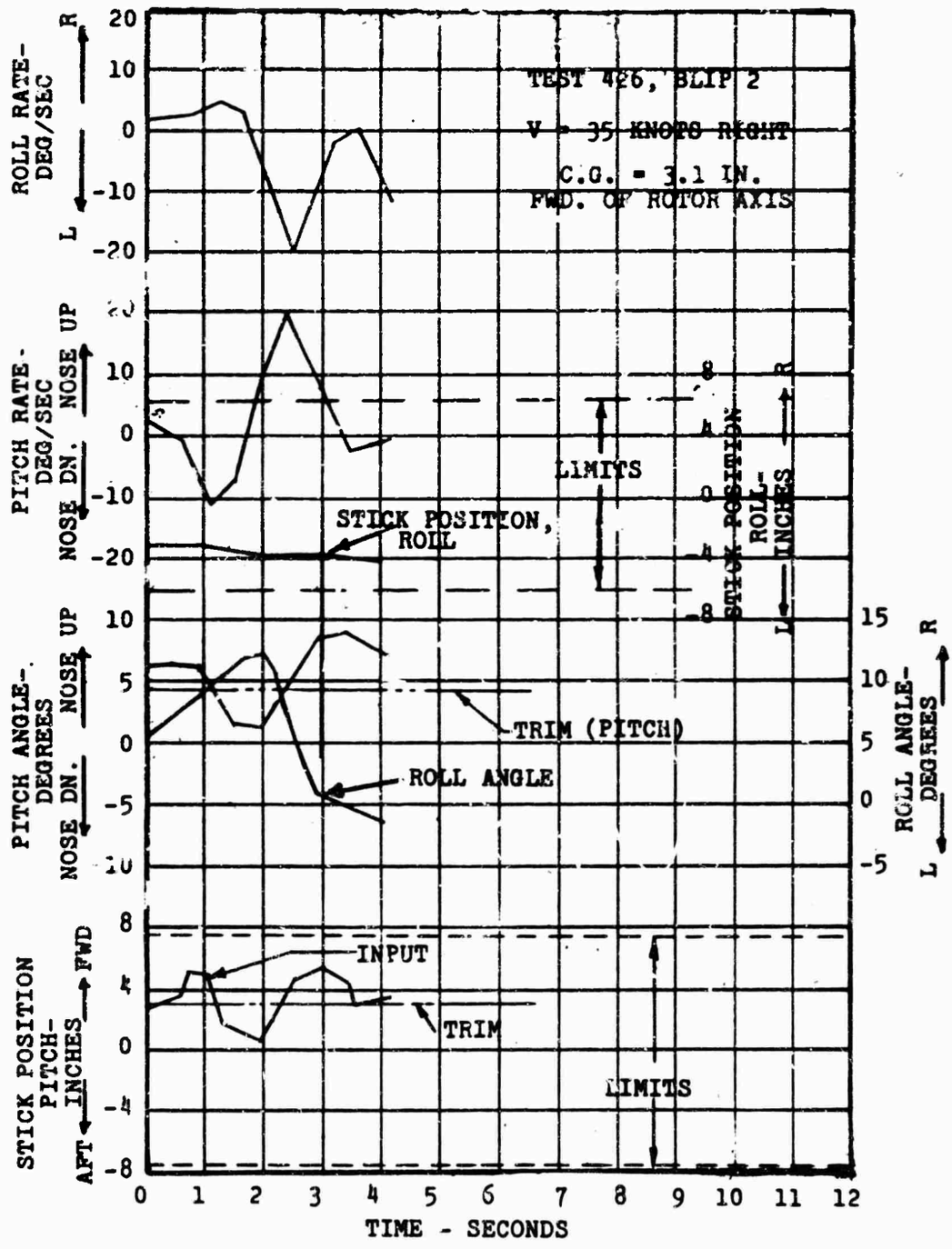


Figure 93. Pitch Response - Right Sideward Flight, Pitch Down.

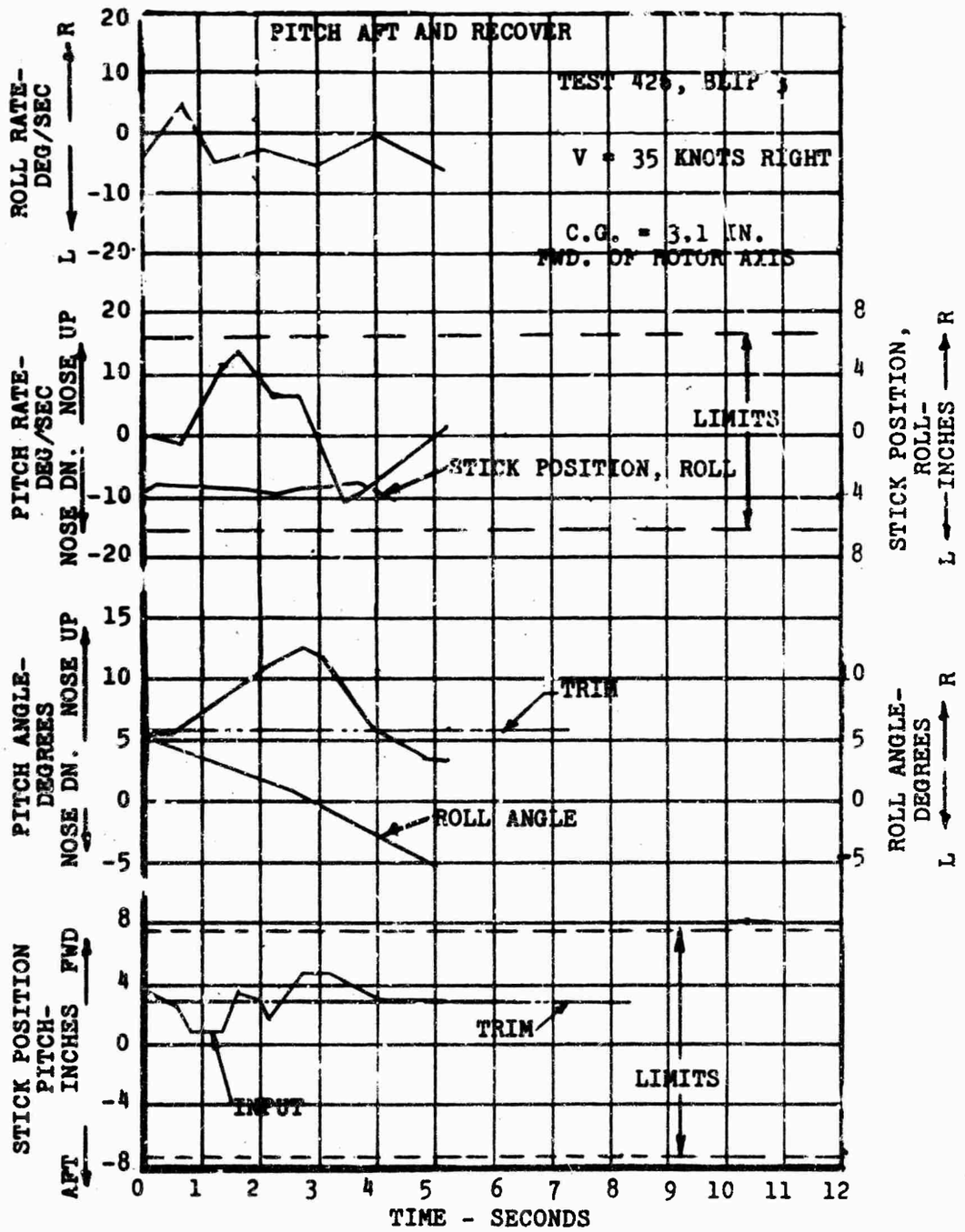


Figure 94. Pitch Response - Right Sideward Flight, Pitch Up.

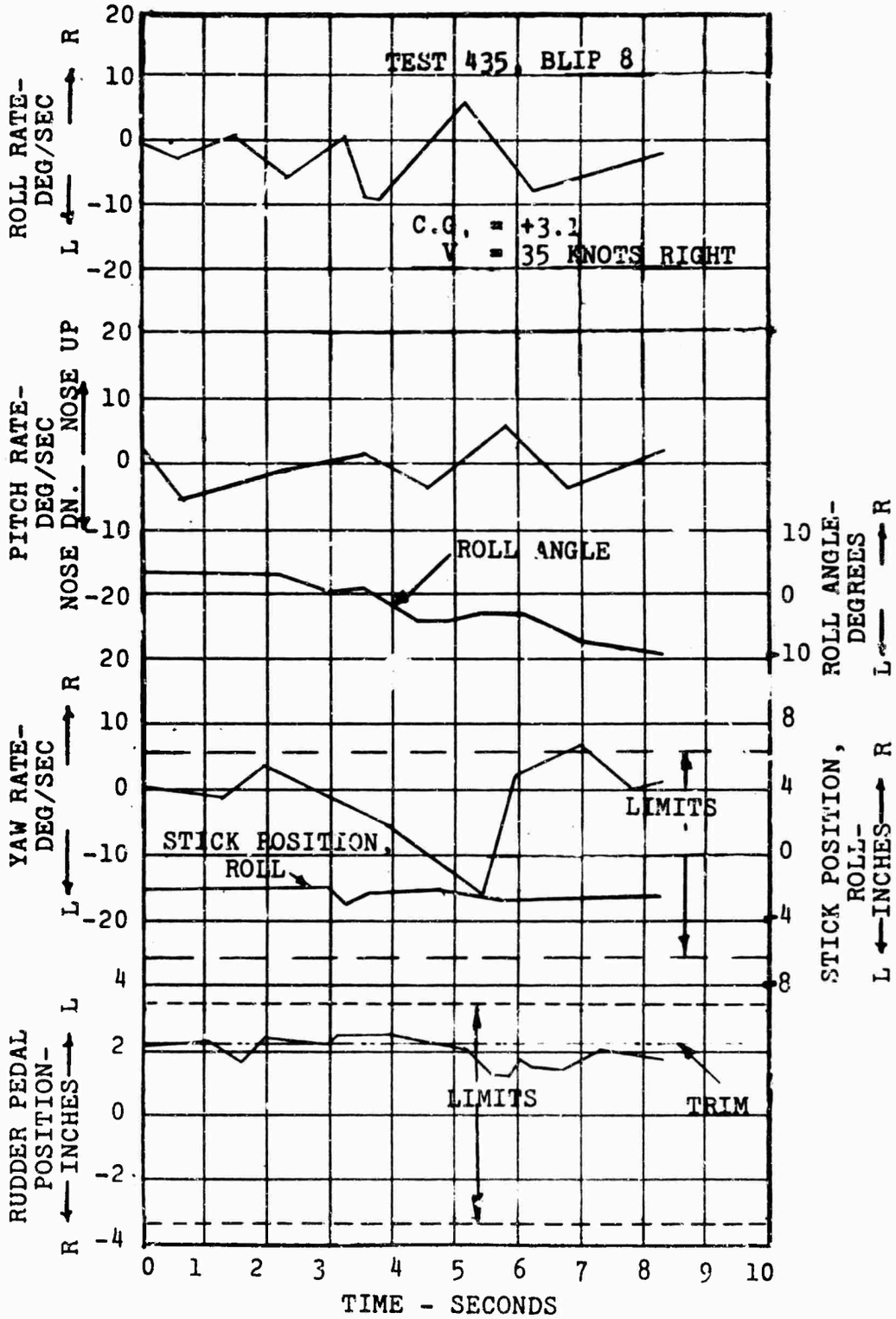


Figure 95. Yaw Response - Right Sideward Flight, Yaw Left.

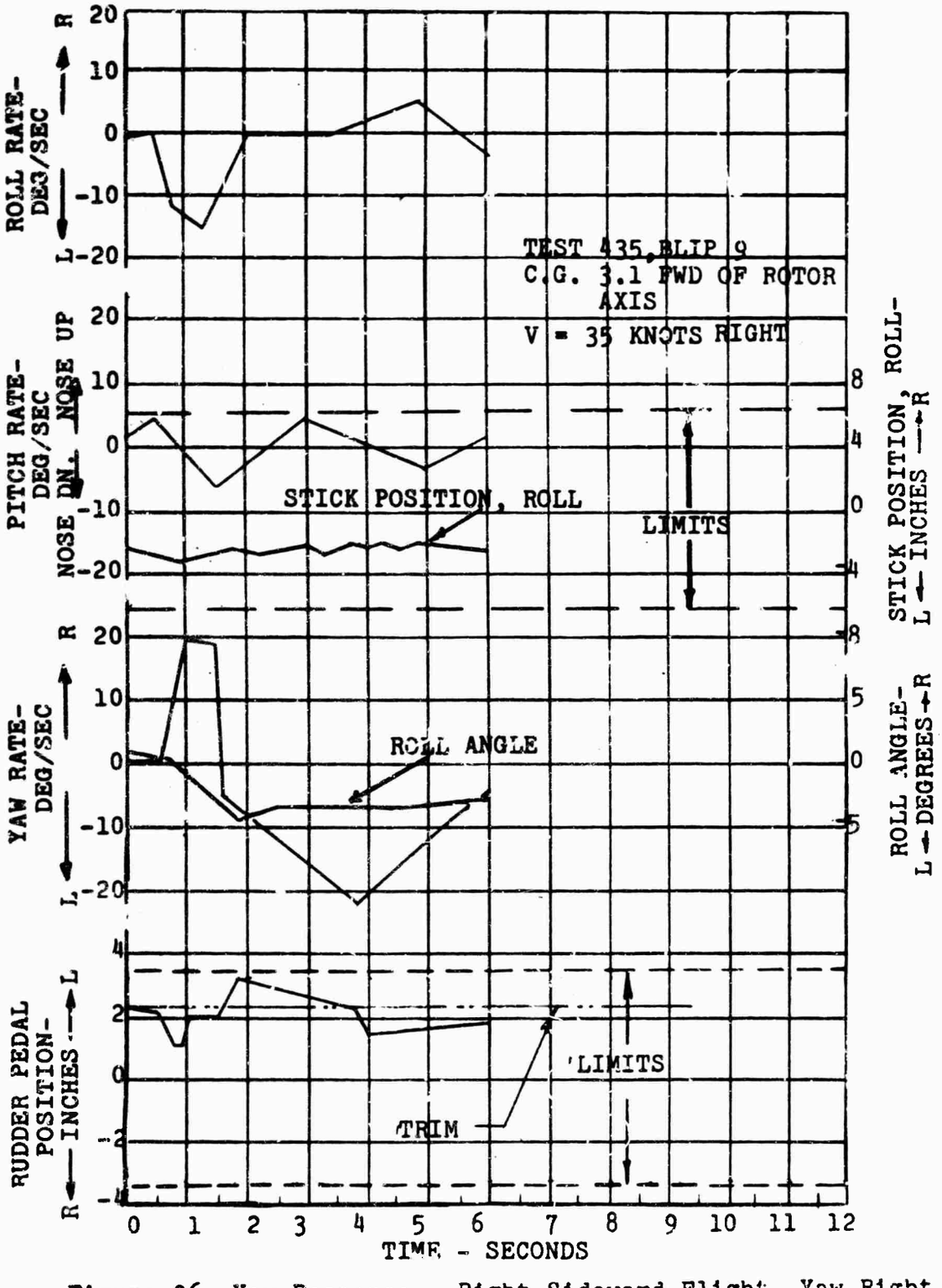


Figure 96. Yaw Response - Right Sideward Flight, Yaw Right.

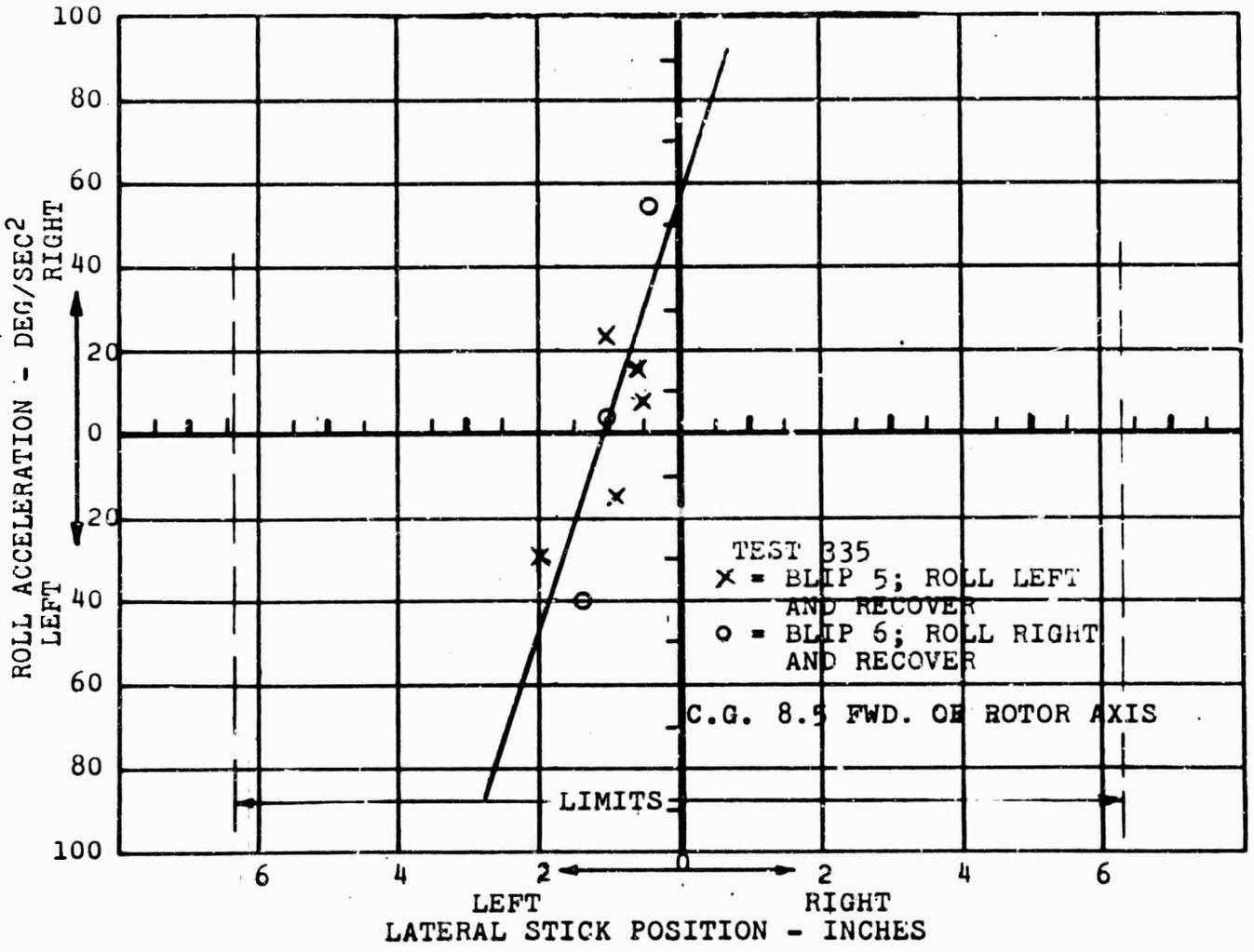


Figure 97. Roll Response in Hover - Acceleration versus Lateral Stick Position.

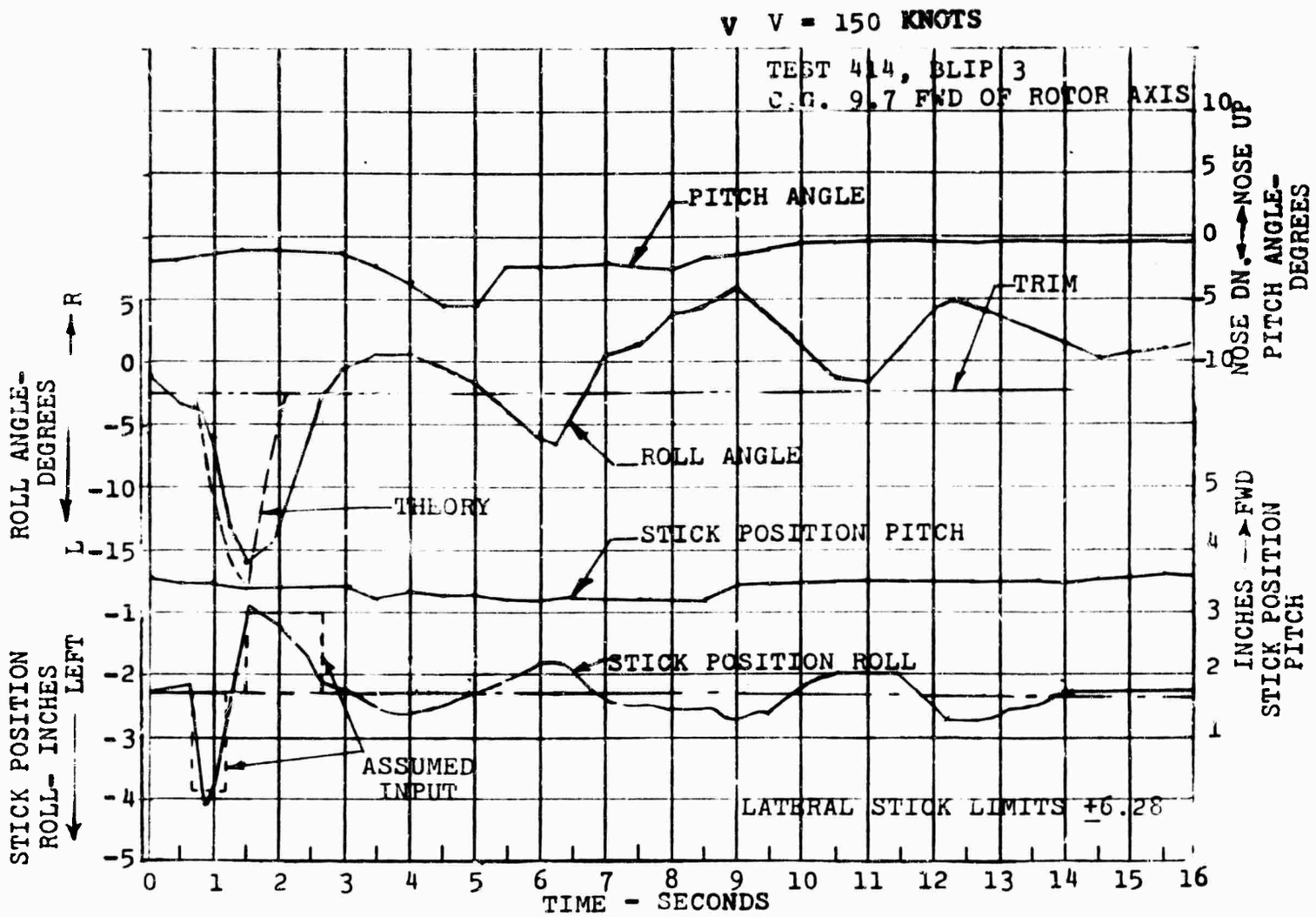


Figure 98. Dynamic Stability - Roll Left, Speed 150 Knots, C.G. 9.7.

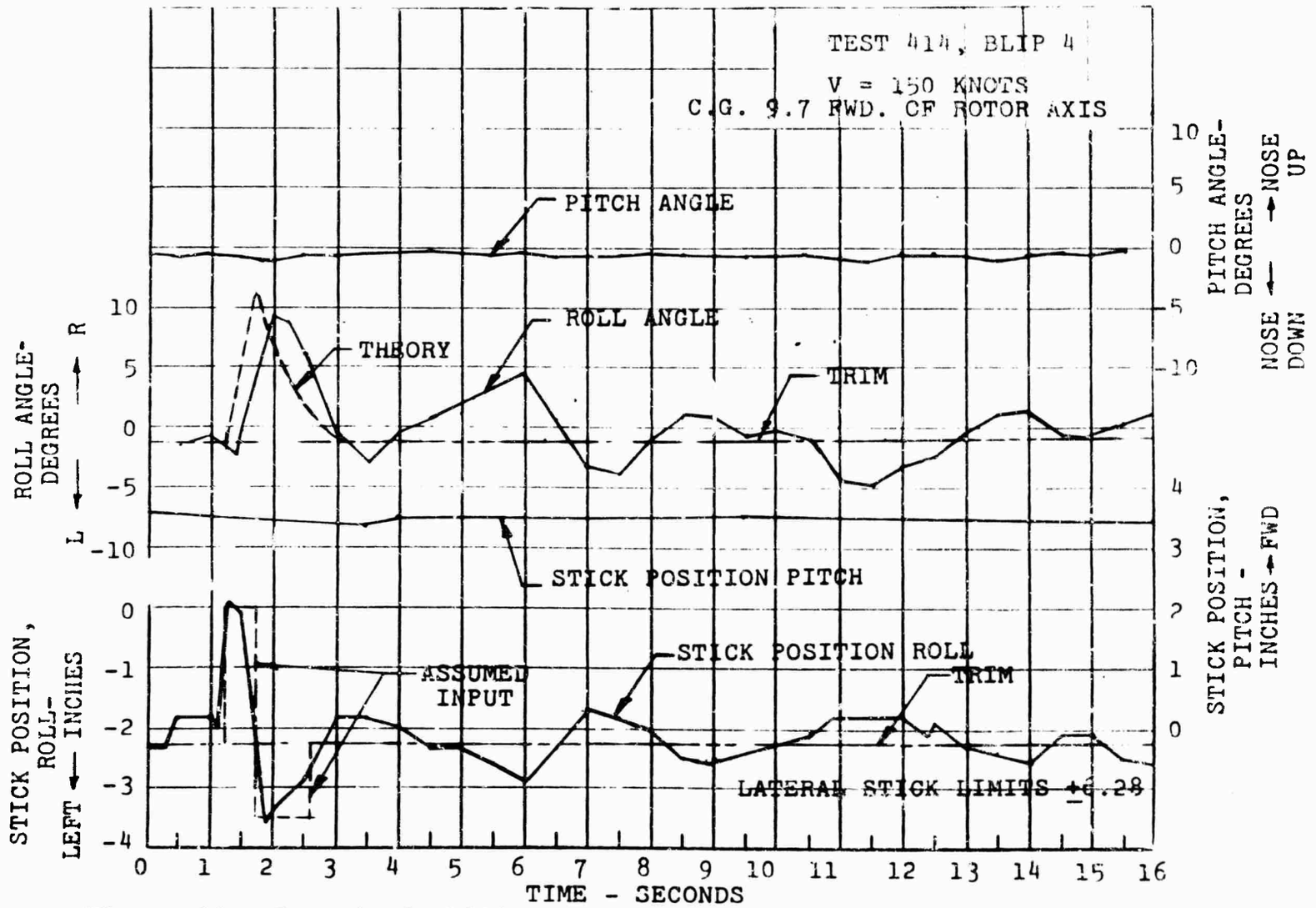


Figure 99. Dynamic Stability - Roll Right, Speed 150 Knots, C.G. 9.7.

control moment per inch to inertia, is 51.0 degrees/second$^2$ per inch in hover (Appendix III, page 325). This gives a required margin of at least

$$0.10 \times 5.3 \times 51.0 = 27 \text{ degrees per second}^2$$

The critical operating condition is at high speed (150 knots) where the trim position is 2.3 inches left (Figures 98 and 99). At this speed, lateral control power is 35.8 degrees per second per second per inch (Appendix III, page 367). Thus the minimum available control is

$$4.0 \times 35.8 = 143 \text{ degrees per second}^2$$

or 5.3 times the required value.

3.3.5 (Reference 4)

Directional control power should be such that in the hover condition a 1-inch step pedal input will produce a yaw angle displacement at the end of 1 second of at least

$$\psi = \frac{110}{\sqrt[3]{W + 1000}} \text{ degrees} \qquad (61)$$

or, for the 16H-1A test gross weight

$$\psi = \frac{110}{\sqrt[3]{6000 + 1000}} \qquad (62)$$

$$= 5.74 \text{ degrees}$$

In hover, the yaw response to a 1-inch pedal step displacement is computed for the 16H-1A from the directional response equation given in Appendix III, page 345, equation (84). This solution has been verified by dynamic response correlations as described in the appendix. In the Laplace variable, the equation for a unit step is

$$\psi = \frac{K}{s^2 \left(s + \frac{1}{T}\right)} \qquad (63)$$

where $K = -14.4$ degrees per second per second for left pedal

$\frac{1}{T} = 0.159 \text{ sec}^{-1}$

With these parameters, the response solution for a 1-inch left-pedal step displacement is

$$\psi = -570\ (e^{-0.159t} + 0.159t - 1) \qquad (64)$$

This response indicates a yaw motion at the end of 1 second of -6.83 degrees, which is approximately 20 percent better than the minimum requirement. For a right-pedal displacement, the yaw angle at the end of 1 second is 150 percent better than the specified value, since in this case K = -30.0 degrees per second per second, as given in Appendix III.

When maximum available pedal motion from trim is applied, the yaw angle at the end of 1 second should be 3 times the 1-inch requirement. The 16H-1A was tested in accordance with contract requirements, with the "most critical tail-propeller-pitch/vane combination", so that only 1-inch left-pedal travel from trim remains, which is not the normal pilot technique. With the combination of propeller pitch and vane deflection used in normal technique, this requirement can be met.

3.3.6 (Reference 4)

It should be possible to execute complete turns in hover in a 35-knot wind. In a steady hover at the most critical azimuth angle relative to the wind, full pedal displacement in the critical direction should produce a yaw displacement (for the 16H-1A) of at least 5.74 degrees at the end of 1 second.

Complete hovering turn data in both directions are shown in Figures 100 and 101 for a 15-knot wind velocity. The stick position shown is well within limits; however, in the left turn, full left pedal was required. However, again it is noted that the maneuver was performed with the "most critical tail- propeller-pitch/vane combination", which is not the normal configuration of pitch and vane deflection. Using a more favorable combination, the requirement can easily be met in a 15-knot wind, and probably in the required 35-knot wind as well, although such winds did not occur during the test period.

3.3.7 (Reference 4)

This paragraph specifies a maximum directional control power value in hover as that which produces a 50-degree yaw displacement at the end of 1 second following a sudden 1-inch pedal displacement.

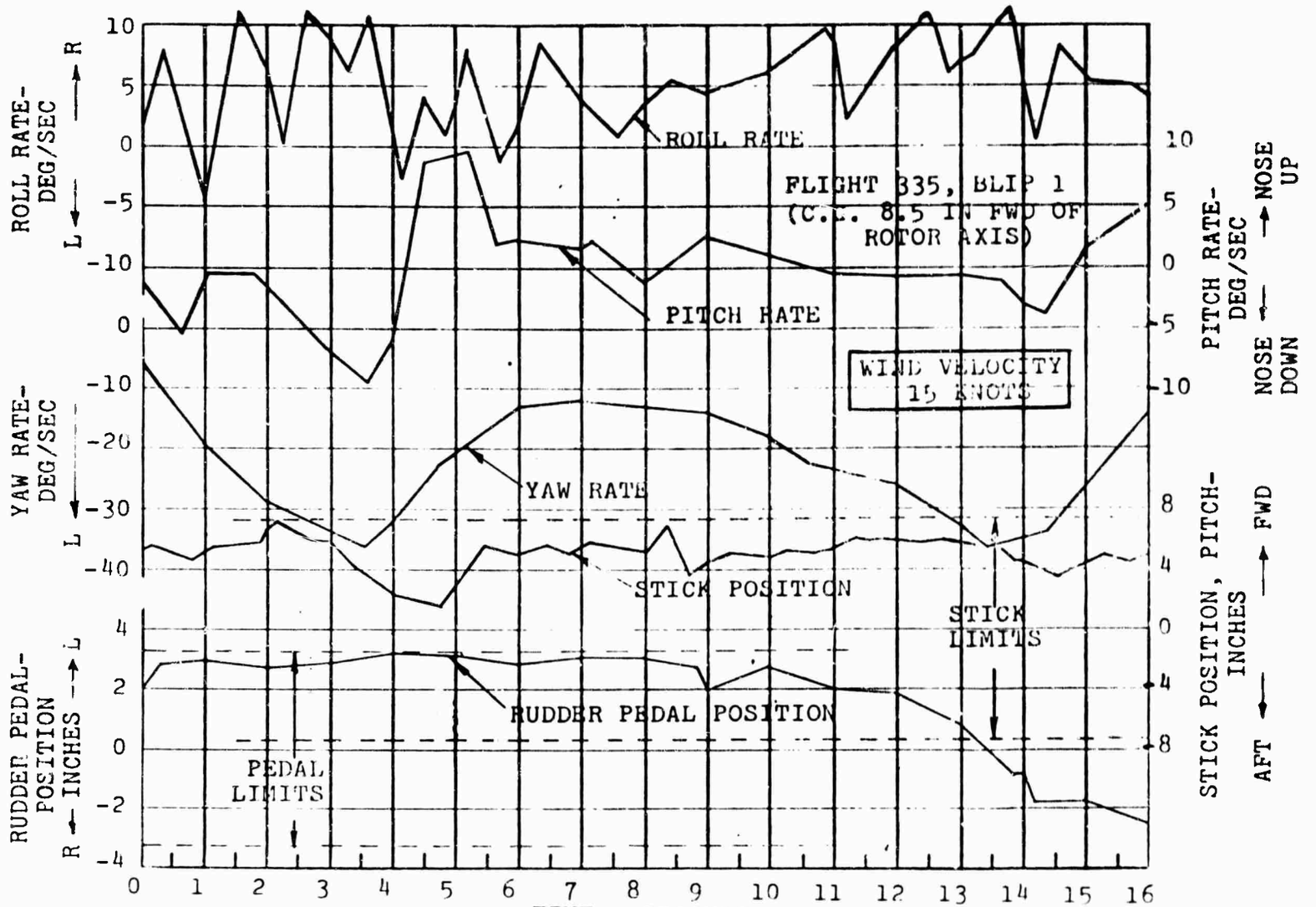


Figure 100. Hovering Turn - Left.

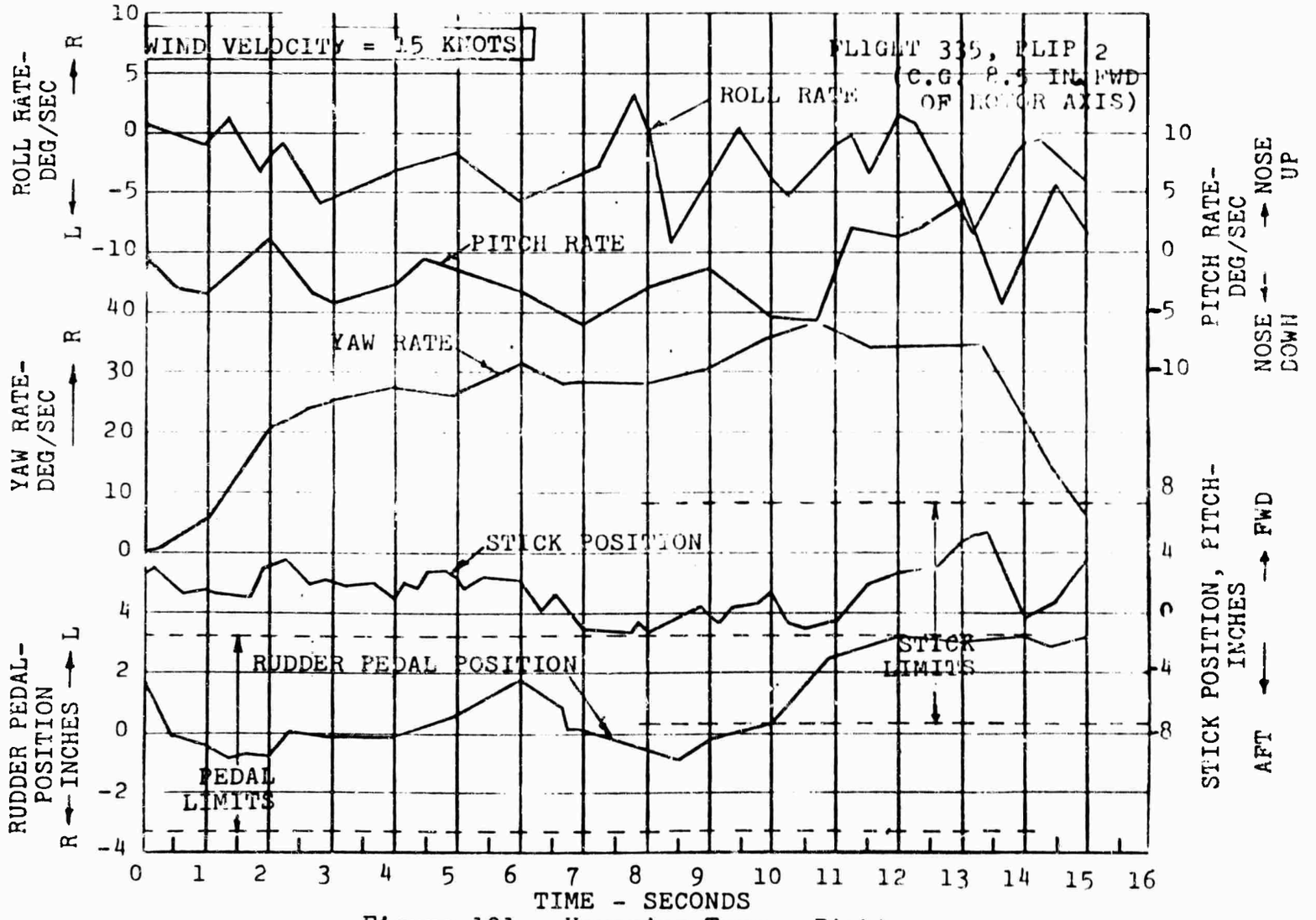


Figure 101. Hovering Turn - Right.

At the lightest normal service loading (as included in the specification), the estimated ratio of control moment to inertia is 30.0 degrees per second per second per inch for right-pedal inputs. Based on the results contained in the paragraph 3.3.5 analysis, this value will produce a yaw change of 16 degrees at the end of 1 second for a 1-inch pedal step input. Thus, maximum directional control is well within the limit.

3.3.8 (Reference 4)

Although coordinated turn tests were made in autorotation, data thereon were not required under the contract and were not obtained. However, based on the near-neutral stick positions and vane deflections shown in the control position versus autorotative speed curves of Figure 102, this requirement posed no difficulty.

3.3.9 (Reference 4)

This paragraph covers the general requirement for positive static directional stability and positive effective dihedral, as indicated by a positive slope of the pedal-displacement and lateral-stick position versus sideslip curves. The 16H-1A static directional characteristics are analyzed in Appendix III with the test data as shown in Figure 103. Here, positive static stability is indicated from a minimum forward speed of 50 knots (the lower requirement limit) to high speed. At low speed, a sideslip angle range of ±25 degrees was covered.

Essentially zero dihedral effect was indicated at 50 knots by a constant lateral-stick position over the ±25-degree sideslip range. At 100 knots, the limited sideslip angle range did not permit conclusive evaluation of the high speed dihedral effect. The 16H-1A wing contribution is near zero (geometric dihedral plus the wing-fuselage juncture effects); however, the rotor contribution is always stabilizing. Hence, at and above 100 knots, it is estimated that the 16H-1A possesses a positive level of effective dihedral.

3.3.10, 3.3.11, 3.3.12, 3.3.13, 3.3.14 (Reference 4)

Lateral and Directional Control Forces

As discussed under longitudinal characteristics, the aircraft, as tested, had fully powered controls with forces

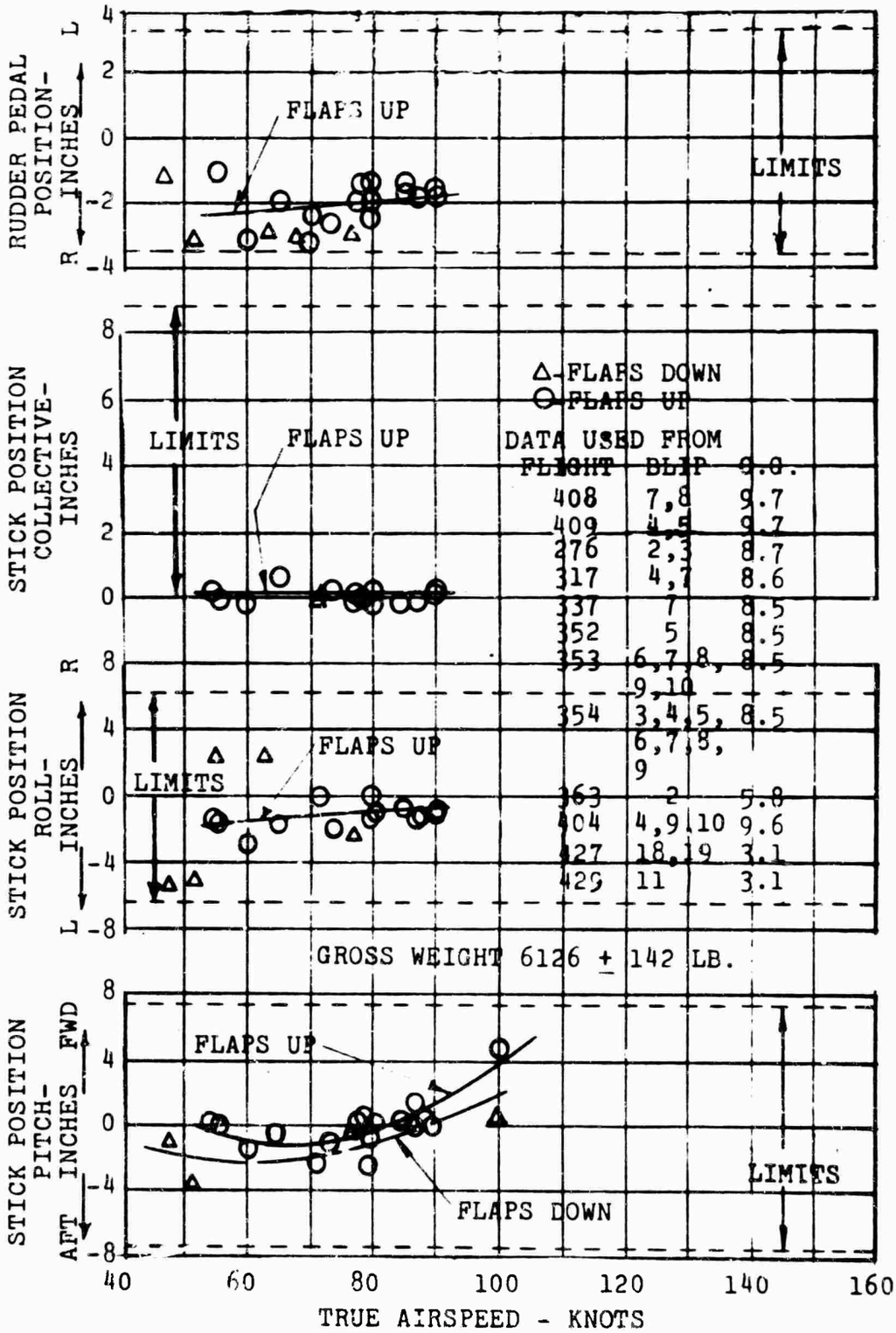


Figure 102. Control Position versus Airspeed, Autorotation.

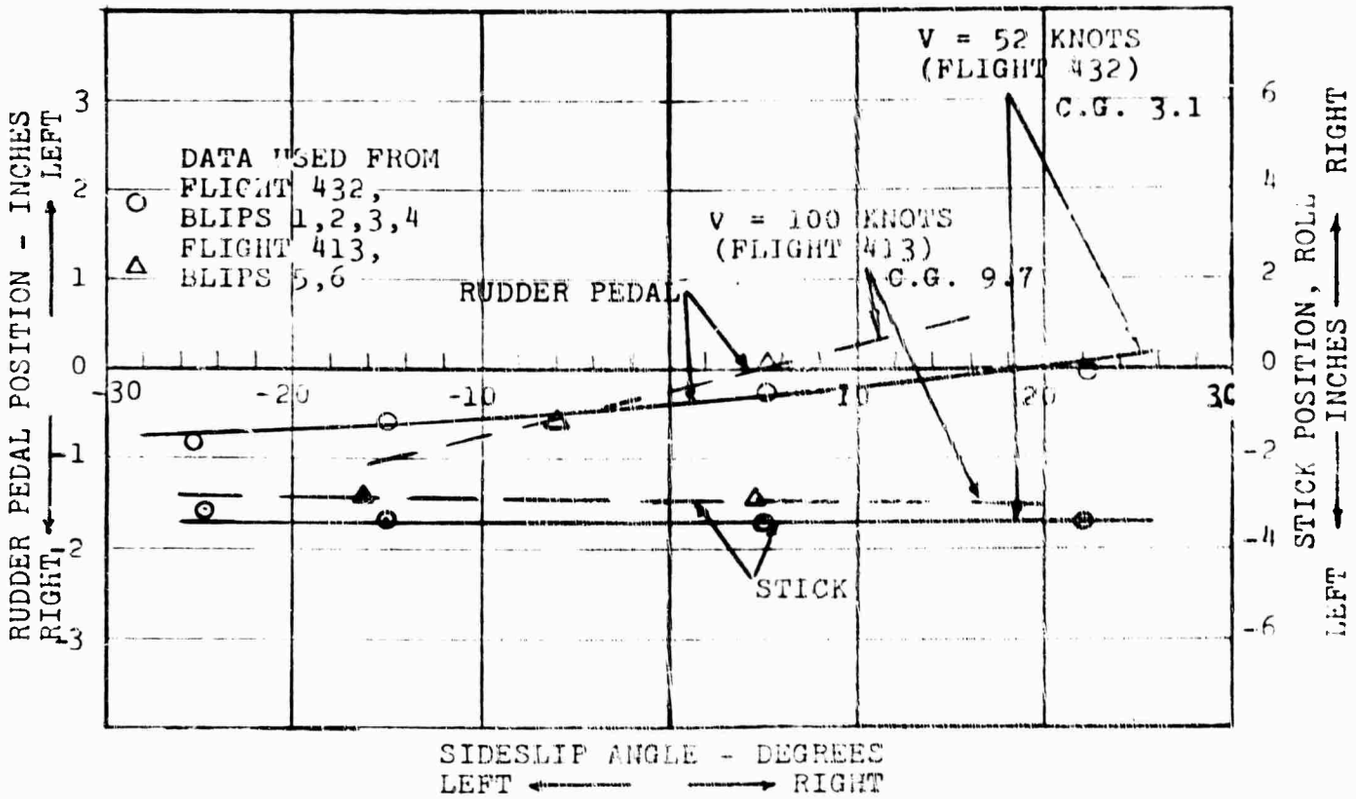


Figure 103. Directional Stability, Lateral Stick and Rudder Pedal Position versus Sideslip Angle.

always reduced to zero, but with no self-centering. An adjustable bungee system added to the fully powered controls would satisfy the requirement for positive self-centering characteristics and force gradient limitations.

3.3.15 (Reference 4)

This paragraph specifies an upper limit on response to lateral control deflection at all speeds. The maximum rate of roll per inch of lateral stick displacement is not to exceed 20 degrees per second.

As shown by the lateral stability and control analysis in Appendix III, page 341, and in the flight data plots (Figures 198 through 201), the 16H-1A research vehicle has a steady-state or maximum roll rate per inch of stick of 39.0 degrees per second at hover, 34.0 degrees per second at 50 knots, and 15.4 degrees per second at 150 knots.

Using only lateral cyclic control as provided in the research aircraft, it was necessary to have a high degree of control power in hover in order to have adequate control at $V_{max}$. Control modification involving reduced lateral-stick-cyclic gearing in conjunction with ailerons (differential flaperon deflection) operated by the stick would yield maximum roll rates of less than 20 degrees per second and yet of sufficient magnitude at all operating speeds.

3.3.16 (Reference 4)

This paragraph limits the delay in the development of angular velocity to lateral or directional control to 0.2 second.

An examination of the lateral and directional control responses contained in Appendix III (Figures 194, 195, and 198 through 203) indicates that this requirement is satisfied.

3.3.17 (Reference 4)

The helicopter shall not exhibit lateral trim changes in excess of 2 inches with changes in power and/or collective pitch.

An examination of control positions in steady vertical climb at various collective and power settings (Figure 104) shows that the lateral trim position is essentially constant over the test range. In Figure 105 lateral stick position

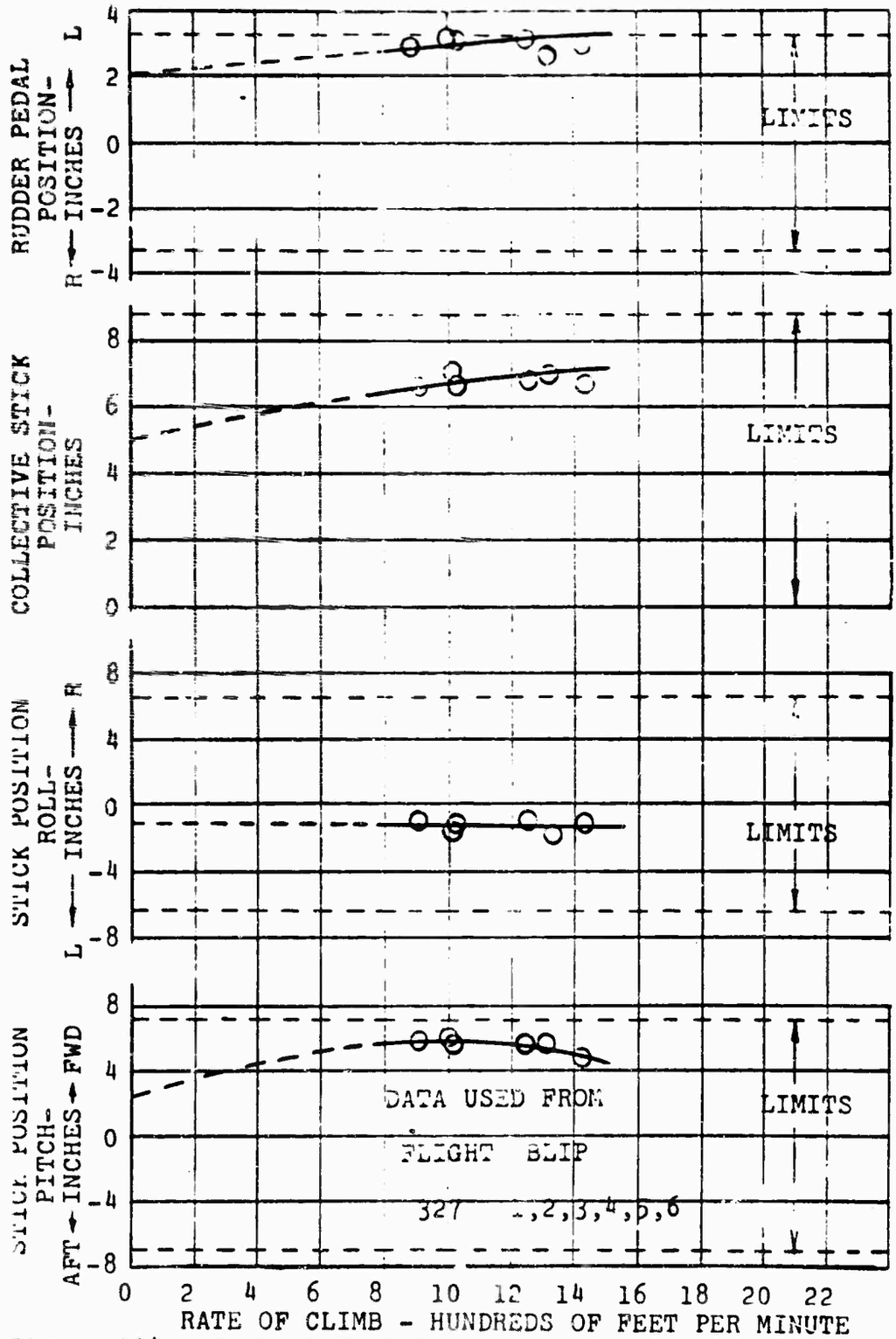


Figure 104. Control Position versus Rate of Climb (Vertical).

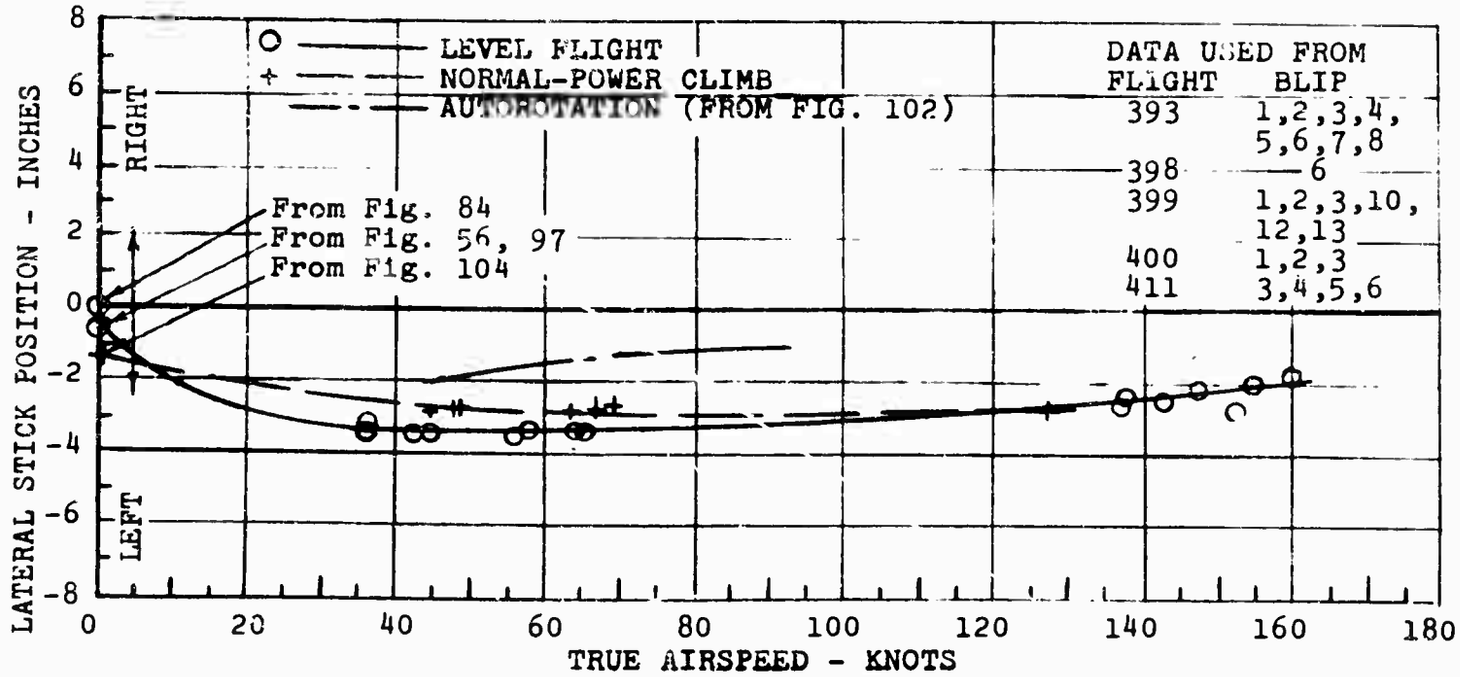


Fig. 105. Lateral Control Position versus Airspeed.

is plotted against speed for level flight, climb and autorotation. This figure shows that throughout the range tested lateral trim does not vary more than the allowed 2 inches.

3.3.18 (Reference 4)

Lateral control power in hover shall be such that a rapid 1-inch lateral control step displacement shall produce an angular change at the end of 0.5 second of at least

$$\phi = \frac{27}{\sqrt[3]{W + 1000}} \qquad (65)$$

$$= \frac{27}{\sqrt[3]{6000 + 1000}}$$

$$= 1.41 \text{ degrees}$$

The 16H-1A response is determined from the test-verified characteristics given in Appendix III (page 353). The unit step response is given by

$$\phi(s) = \frac{K}{s^2\left(s + \frac{1}{T}\right)} \qquad (66)$$

where, based on the 50-knot dynamic response correlation,

$$K = 53.8 \text{ deg/sec}^2 \text{ per inch}$$

$$\frac{1}{T} = 1.38 \text{ sec}^{-1}$$

With these values, the response solution is

$$\phi = 28.2\ (e^{-1.38t} + 1.38t - 1)$$

Setting $t = 0.5$ second in this expression yields a roll angle of $\phi = 5.40$ degrees. Thus the 16H-1A more than fulfills the specification requirement by a factor of 3.8. Referring back to paragraph 3.3.15, it was shown that the roll sensitivity in hover exceeded the maximum permitted in that paragraph by a factor of 1.9. Hence, cutting the lateral-stick swash-plate gear ratio in half would result in meeting that requirement while still satisfying this one.

3.3.19 (Reference 4)

This paragraph cites the minimum roll angular damping values required in the hover condition. The roll damping specification is given as

$$L_p = -18\ (I_x)^{0.7} \qquad (67)$$

which for the 16H-1A is

$$L_p = -18\ (1{,}600)^{0.7}$$

$$= -3{,}150 \text{ ft-lb-sec/rad}$$

The 16H-1A estimated value is -2,200 foot-pound-seconds per radian (consistent with the values given in Appendix III). The stated purpose of this requirement is to insure satisfactory initial response characteristics following either control inputs or external disturbance inputs. These hover handling qualities are principally functions of the lateral control power, inertia, and damping. Acceptable quality boundaries have been established and are a fairly standard basis for stability evaluation (Reference 8). They are presented in Figure 106, together with the 16H-1A characteristics in hover, at 50 knots, and at 150 knots.

In this summary plot of handling qualities (Figure 106), it is evident that with a 50-percent reduction in the lateral hover control power, the 16H-1A characteristics would be completely within the acceptable region. Since it is rigged to this high value only for the high-speed flight condition, the lateral-cyclic ratio can be reduced, in conjunction with ailerons (differential flaperon deflection) that would be operated by the stick. The damping levels are already sufficient to meet the boundary requirements. The MIL-H-8501A damping requirement is satisfied at speeds above about 100 knots.

TECHNIQUE FOR ENTRY INTO AUTOROTATION FROM MAXIMUM SPEED

When the engine RPM drops off at high speed from a simulated engine failure, the aircraft decelerates rapidly, and at the same time the noise level reduces in pitch very suddenly. The tail propeller pitch is reduced and the RPM of both rotor and propeller will stabilize or even increase as the aircraft decelerates extremely rapidly. Since the rotor is geared in a fixed ratio to the propeller, it will absorb energy from the propeller in forward flight as the aircraft speed is retarded. Since the longitudinal attitude

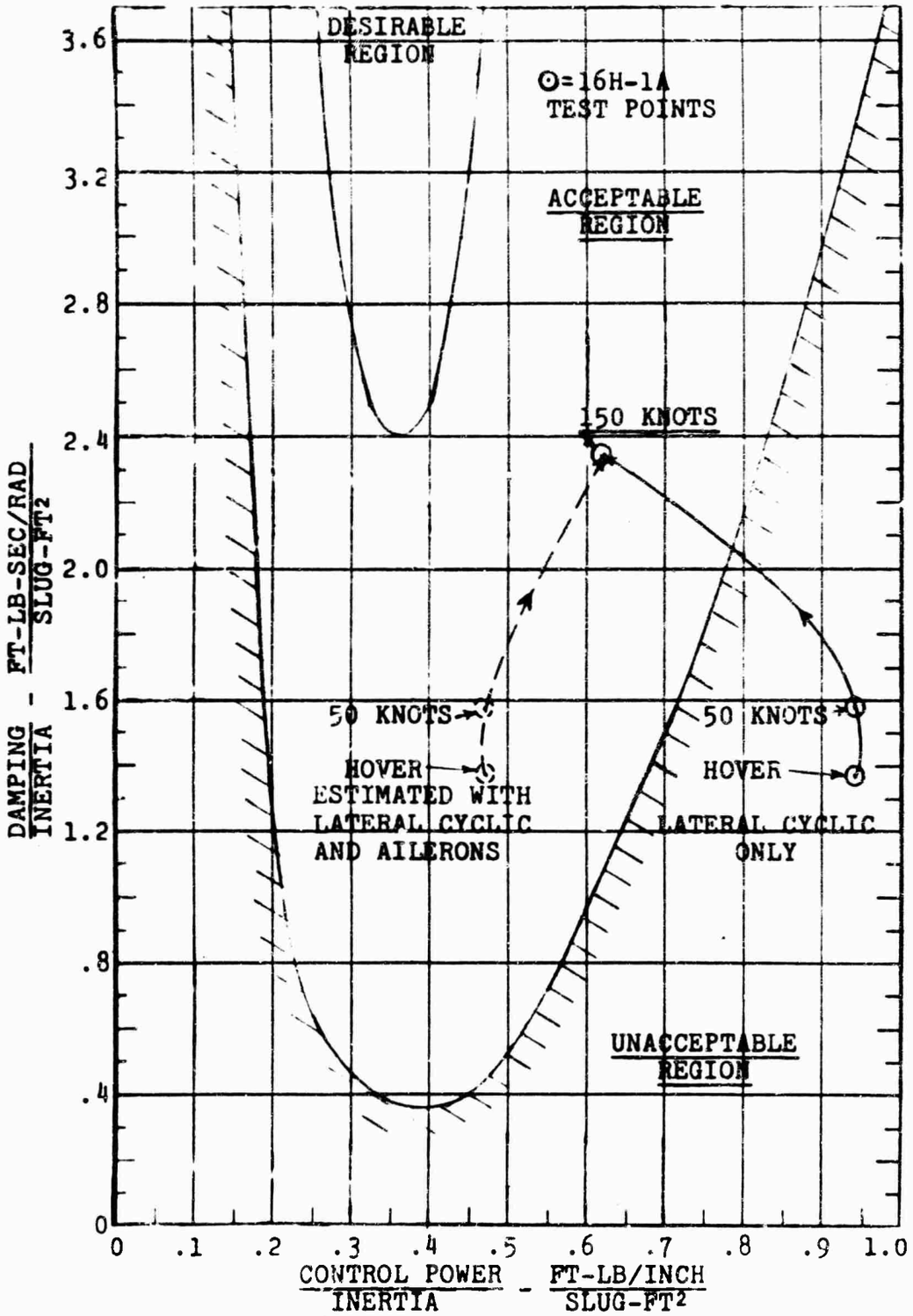


Figure 106. Helicopter Handling Qualities - Criteria in Roll (From Reference 8).

of the aircraft is approximately level at $V_{max}$, the cyclic stick may be held in the same longitudinal position, although some aft longitudinal cyclic will aid in reducing the airspeed and maintaining or increasing the rotor RPM. The collective pitch is of secondary importance in entry into autorotation from $V_{max}$ because it is already at a low setting. Therefore, it may be reduced after the initial deceleration or after the airspeed is reduced to 100 to 120 knots.

For least rate of descent, a 60-knot glide with minimum tail propeller pitch and minimum collective pitch should be established.

A step-by-step procedure follows:

1. Reduce tail propeller pitch.

2. Decelerate, holding slight aft longitudinal cyclic stick.

3. Reduce collective pitch to minimum at 100 to 125 knots.

4. Establish 60-knot glide.

## STRESSES AND LOADS

### OBJECTIVES

The primary reason for measurement of loads and stresses was to assure safety of flight in the conduct of the test program. For this reason, the objective was to gather data during all regimes of flight on rotor and propeller bending moments, both flapwise and chordwise, shaft torsion, rotor shaft bending and tension, and rotor and propeller blade control moments.

### DESCRIPTION OF TESTS

One rotor blade was instrumented to read flapwise bending at stations 46, 59.5, 79.2, 105.6, 124, 132, 158.4, 184.8, 211.2, and 237.6. The choice of these stations for measurement of flapwise bending was based on several factors as follows:

1. To have gages spaced close enough together (every 10% of blade radius) to give a reasonably clear picture of blade flapwise moments and stresses along the entire length of the blade.

2. To determine the flapwise moments and stresses at locations on the blade spar where there are transitions from one size and/or shape cross section to another. Instances of this are station 46, which is a round section; station 59.5, which is in a transition area just inboard of the first trailing edge box; and stations 124 and 132, which are at each end a transition section on the D spar.

3. To use locations for gages previously used on tests of the H-21 metal blade for purposes of comparison.

Strain gages were installed on the rotor shaft to measure rotor life (tension), bending moment in two perpendicular planes, and torsion.

On the tail propeller, strain gages were installed to measure hub bending; flapwise bending stresses on one blade at 40, 50, 70, and 90 percent blade span; and propeller pitch link load.

## ANALYSIS OF RESULTS

In general, the results of the flight test strain gage survey have shown that all of the major parts of the aircraft are good for infinite fatigue life except the universal joint bearings in the main rotor pitch links and the vertical rotor shaft, which have an expected life of more than 420 hours at the highest test speeds flown.

## ROTOR BLADE

Rotor blade flapwise and chordwise moments and stresses at each instrumented blade station are plotted against aircraft forward speed. The graphs are presented so that bending moments may be read on the left ordinate and stress on the right. Both steady and alternating moments and stresses are given for each station. See figures 107 through 126 and 129 through 132 for level flight and forward speed climb, and Figures 133 through 154 for autorotation.

In determining the steady stresses, the stress from centrifugal force at normal rated RPM is included. The value of the centrifugal force stress may be read opposite the zero moment for each station. In determining the total steady stress, which is the stress from centrifugal force plus the stress from bending, the stress from centrifugal force is calculated assuming the normal RPM of the rotor. This is slightly conservative for those flight tests in which the rotor is operated at reduced RPM.

In order to see the variation of blade bending moments along the whole blade, steady and alternating moments are plotted against blade station (see Figures 127 and 128).

Chordwise bending gages are located at one inboard station, 46, and at 50-percent blade radius at the outboard end of the spar transition area (see Figures 129 through 132 and 151 through 154 for plots of chordwise bending moments versus airspeed).

Strain gages for measuring blade trailing edge stresses are located at stations 92 and 210. These stresses are not plotted, since they were of lesser magnitude than the trailing edge stresses at blade station 131.5.

In calculating steady stresses in the steel spar, it is conservatively assumed that the continuous trailing edge takes no centrifugal force.

Referring to Figures 107 through 126, the plots of steady and alternating flapwise moments and stresses versus airspeed show, in general, that the steady stresses in the rotor blade inboard of station 132 decrease slightly and outborad of station 132 increase slightly, with an increase in forward speed. The alternating flapwise moments and stresses increase gradually with an increase in forward speed.

Variation of rotor-blade flapwise moments and stresses along the blade span for typical flights at airspeeds of 60, 120, 150, and 195 knots show that inboard, the steady flapwise moments are those which put tension in the bottom surface of the rotor blade, and outboard, the steady flapwise moments are those which put tension in the top surface of the rotor blade. The point of inflection, or zero steady moment, moves inboard as the speed of the aircraft increases (see Figures 127 and 128). The rotor-blade flapwise alternating bending moments peak at 40 percent radius at all airspeeds plotted, from 60 knots to 195 knots.

Chordwise moments and stresses also show a definite pattern. The steady chordwise moments and stresses decrease with an increase in airspeed at station 46 and at station 131.5, whereas the alternating chordwise moments and stresses increase with an increase in airspeed.

Examination of the alternating stresses in the rotor-blade steel spar at each blade station shows that they are all below the allowable alternating stress for infinite fatigue lift of $\pm$25,000 pounds per square inch.

TABLE VII. ROTOR BLADE SECTION PROPERTIES AND CENTRIFUGAL FORCE (H-21 METAL BLADE, DWG. 42R1003)

| BLADE STATION | $\frac{r}{R}$ | AREA OF SPAR | FLAPWISE $\frac{1}{Z}$ | CHORDWISE $\frac{1}{Y}$ | LIMIT C.F. STRESS NORMAL RPM |
|---|---|---|---|---|---|
| | | $IN.^2$ | $IN.^{-3}$ | $IN.^{-3}$ | PSI |
| 237.6 | .90 | .635 | 2.545 | -- | 11,300 |
| 211.2 | .80 | .635 | 2.545 | -- | 17,550 |
| 184.8 | .70 | .635 | 2.545 | -- | 23,000 |
| 158.4 | .60 | .635 | 2.545 | -- | 27,800 |
| 132.0 | .50 | .635 | 2.545 | *{ .358 L.E.<br>.157 A.E.<br>1.335 T.E. | 31,800 |
| 124.0 | .47 | .879 | 1.783 | -- | 23,900 |
| 105.6 | .40 | .879 | 1.783 | -- | 25,600 |
| 79.2 | .30 | .879 | 1.783 | -- | 28,000 |
| 59.5 | .2255 | .879 | 1.030 | -- | 29,200 |
| 46.0 | .174 | 1.51 | 0.699 | 0.699 | 17,900 |

Z = Flapwise Section Modulus
Y = Chordwise Section Modulus
*These values of $\frac{1}{Y}$ assume T.E. Strip Effective
L.E. = Leading Edge
A.E. = Aft Edge of Spar
T.E. = Trailing Edge

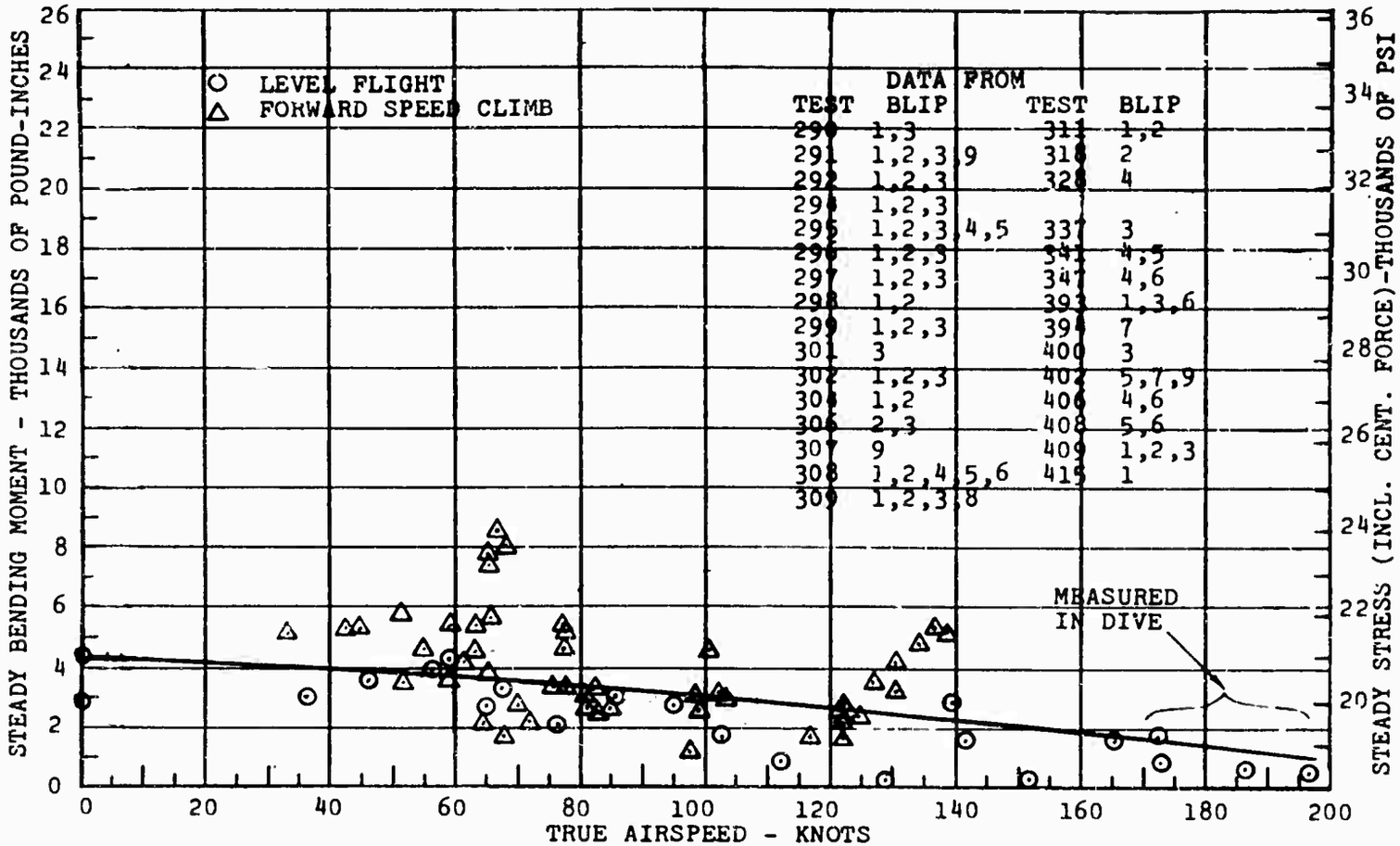


Figure 107. Rotor Blade Flapwise Bending versus Airspeed, Level and Climb, Steady Component, Station 46.

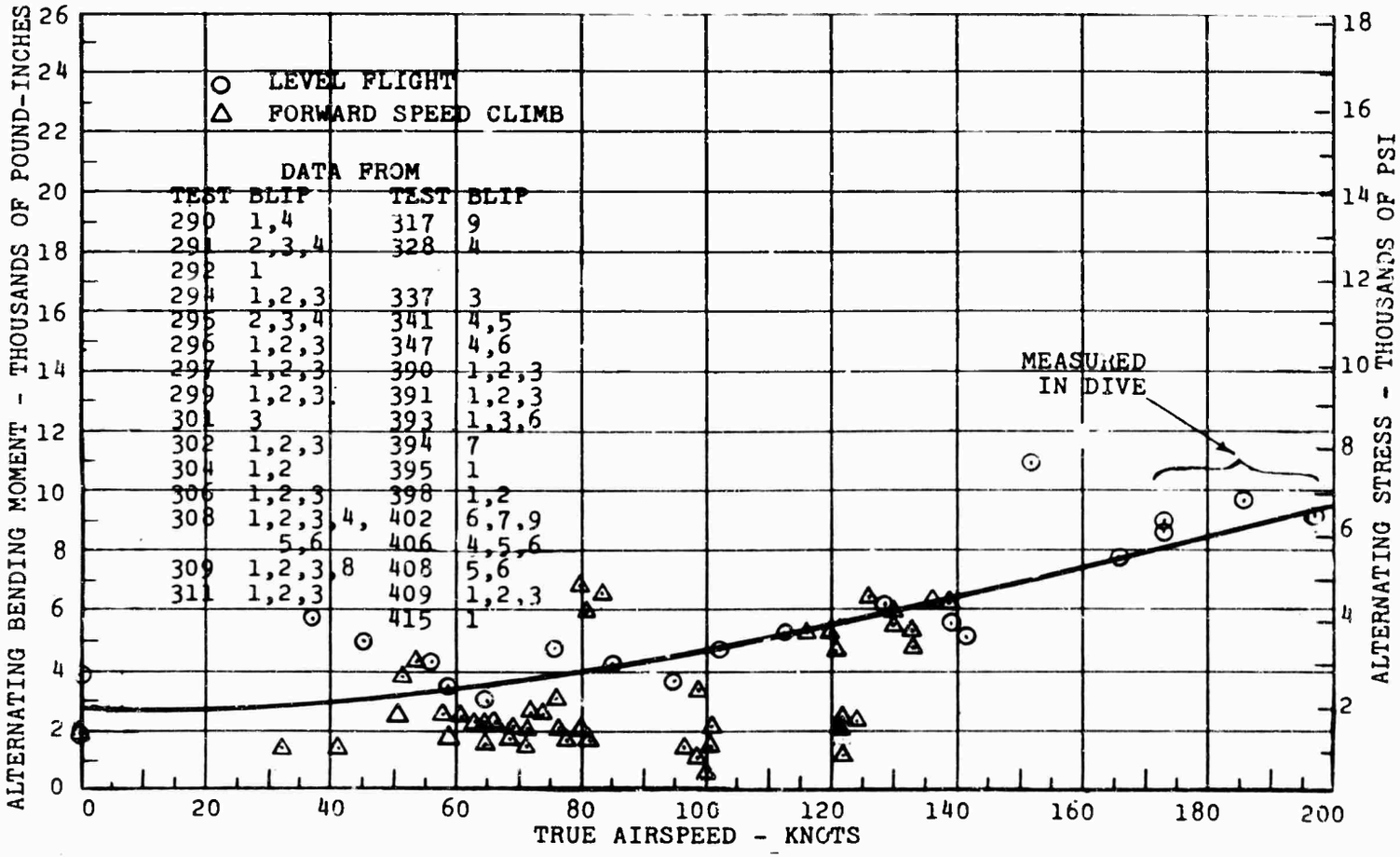


Figure 108. Rotor Blade Flapwise Bending versus Airspeed, Level and Climb, Alternating Component, Station 46.

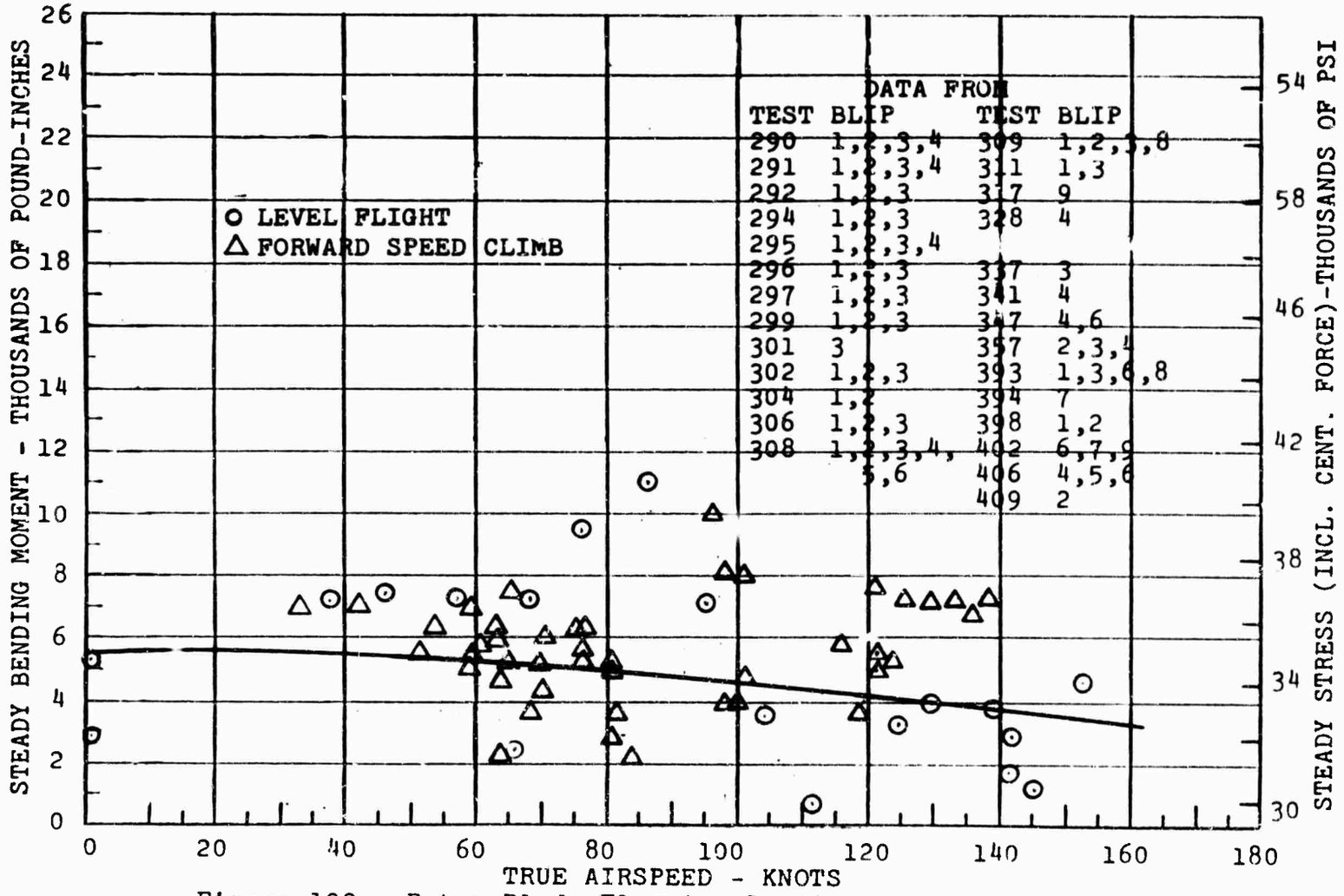


Figure 109. Rotor Blade Flapwise Bending versus Airspeed, Level and Climb, Steady Component, Station 59.5.

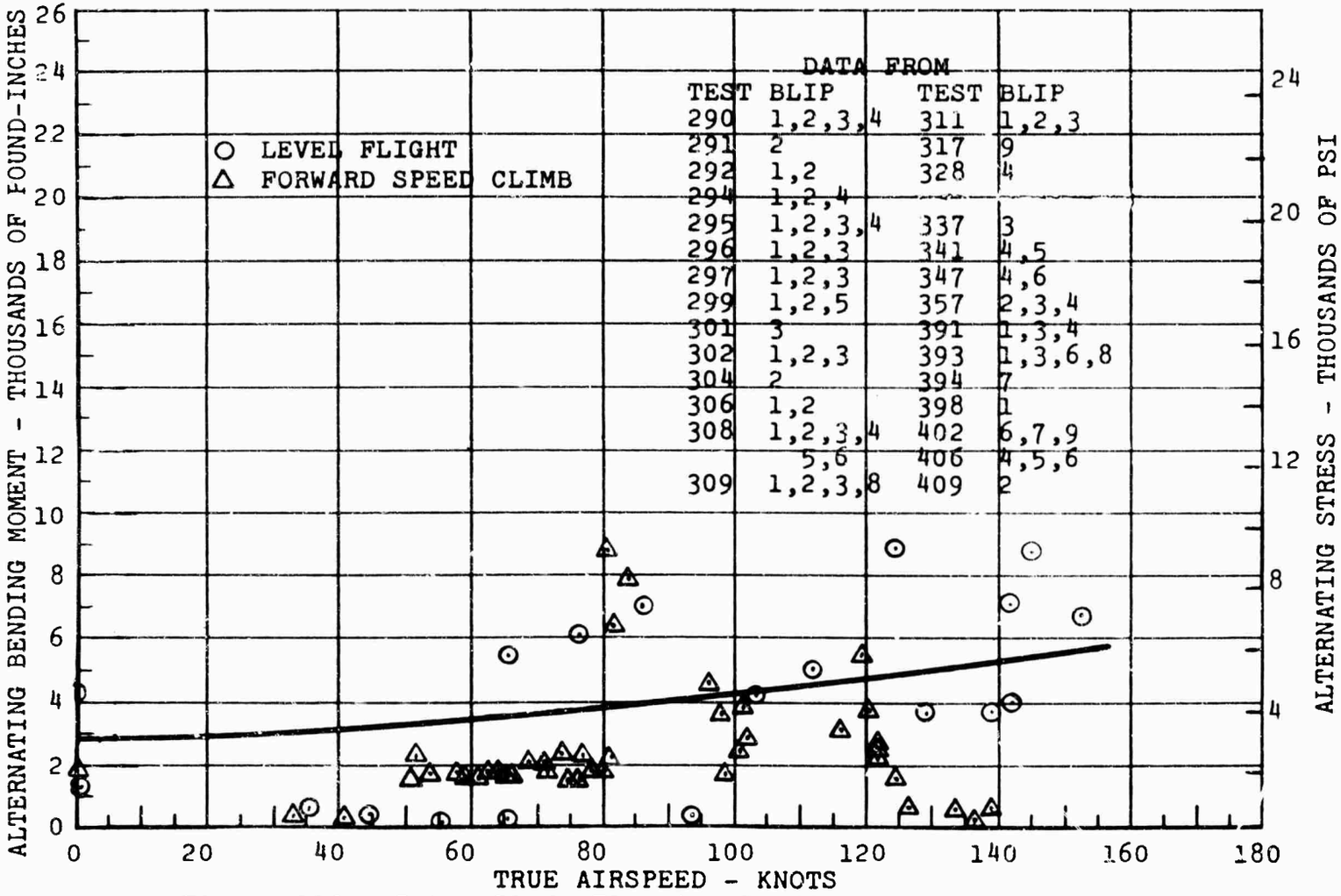


Figure 110. Rotor Blade Flapwise Bending versus Airspeed, Level and Climb, Alternating Component, Station 59.5.

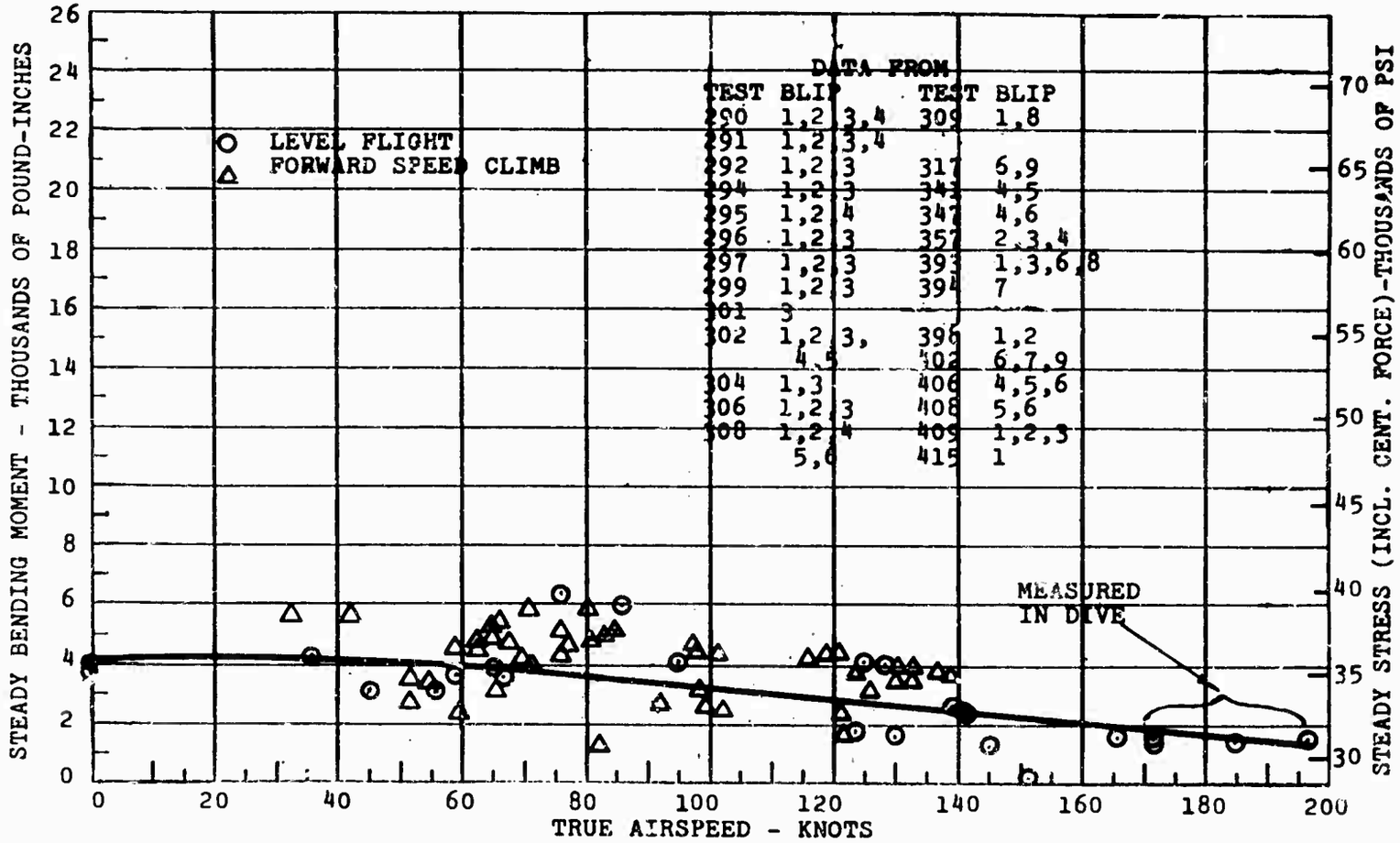


Figure 111. Rotor Blade Flapwise Bending versus Airspeed, Level and Climb, Steady Component, Station 79.2.

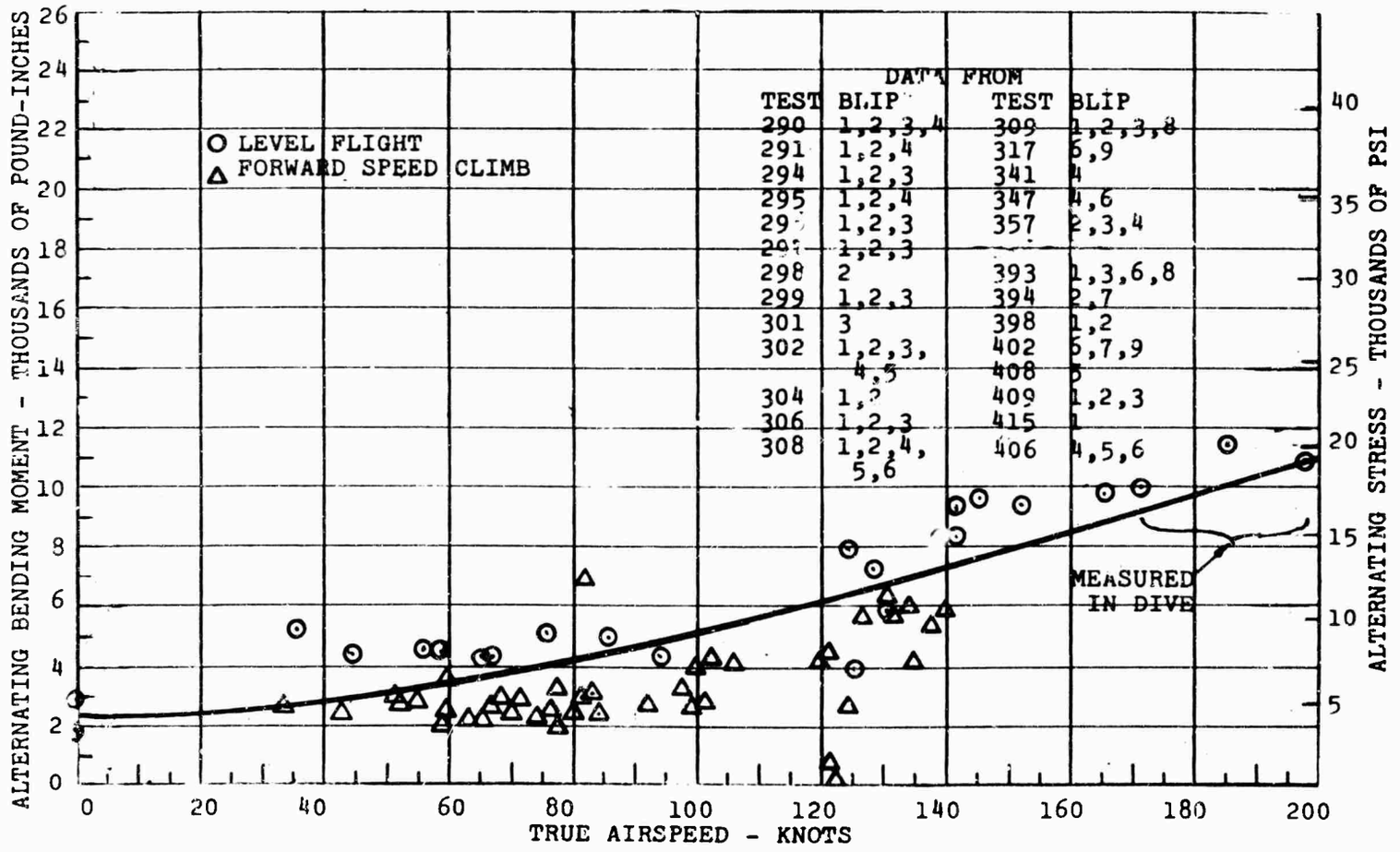


Figure 112. Rotor Blade Flapwise Bending versus Airspeed, Level and Climb, Alternating Component, Station 79.2.

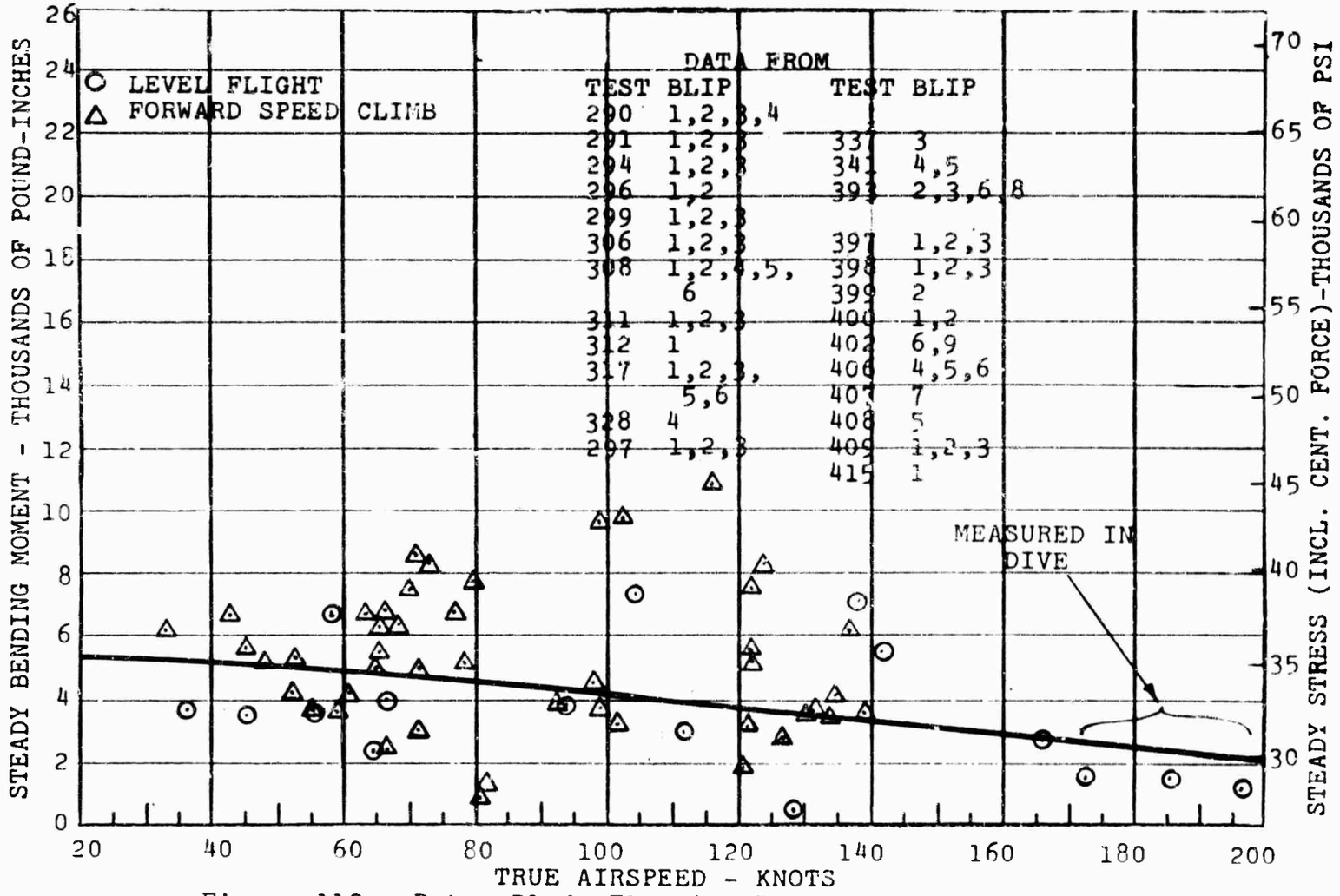


Figure 113. Rotor Blade Flapwise Bending versus Airspeed, Level and Climb, Steady Component, Station 105.6.

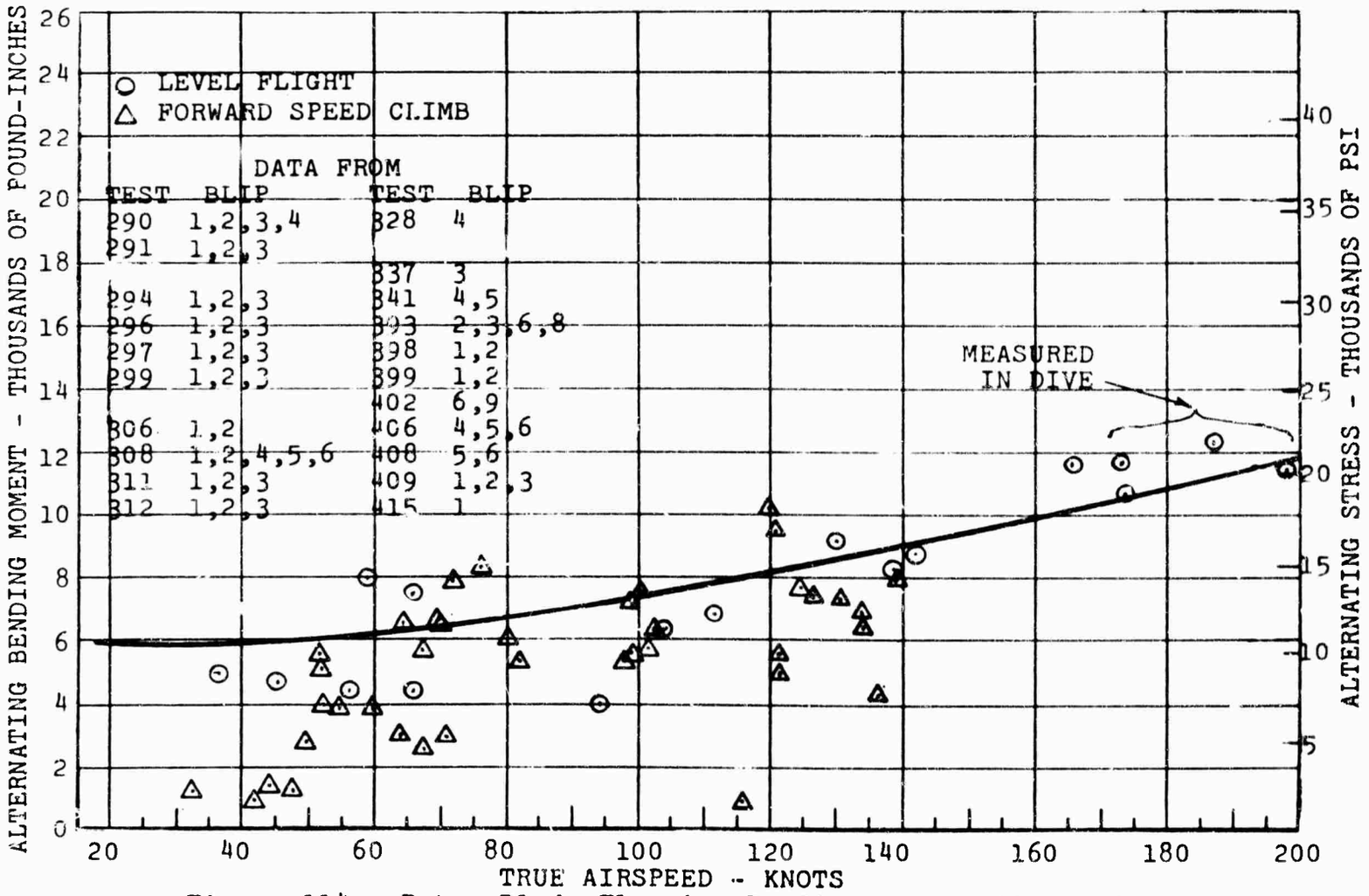


Figure 114. Rotor Blade Flapwise Bending versus Airspeed, Level and Climb, Alternating Component, Station 105.6.

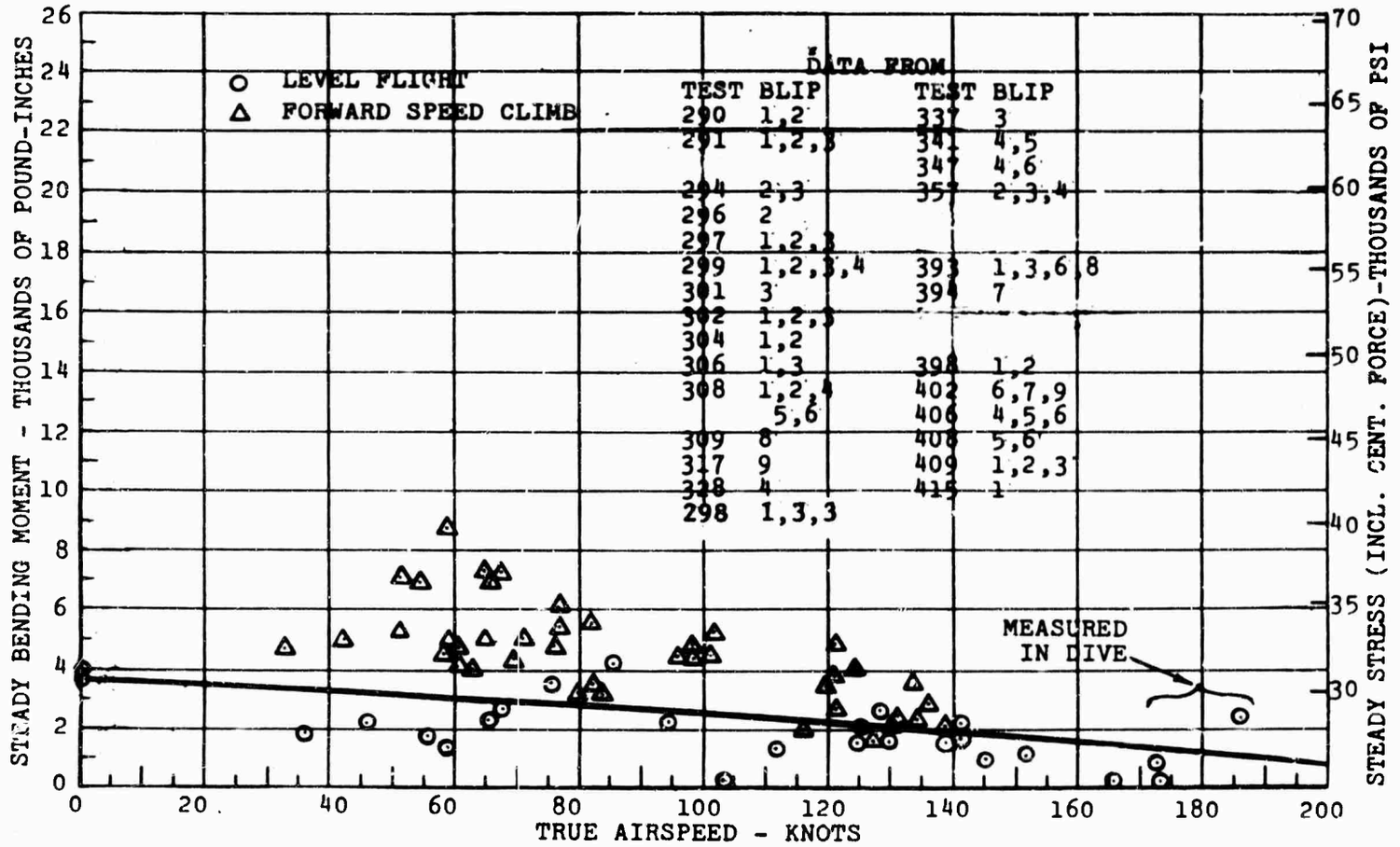


Figure 115. Rotor Blade Flapwise Bending versus Airspeed, Level and Climb, Steady Component, Station 124.

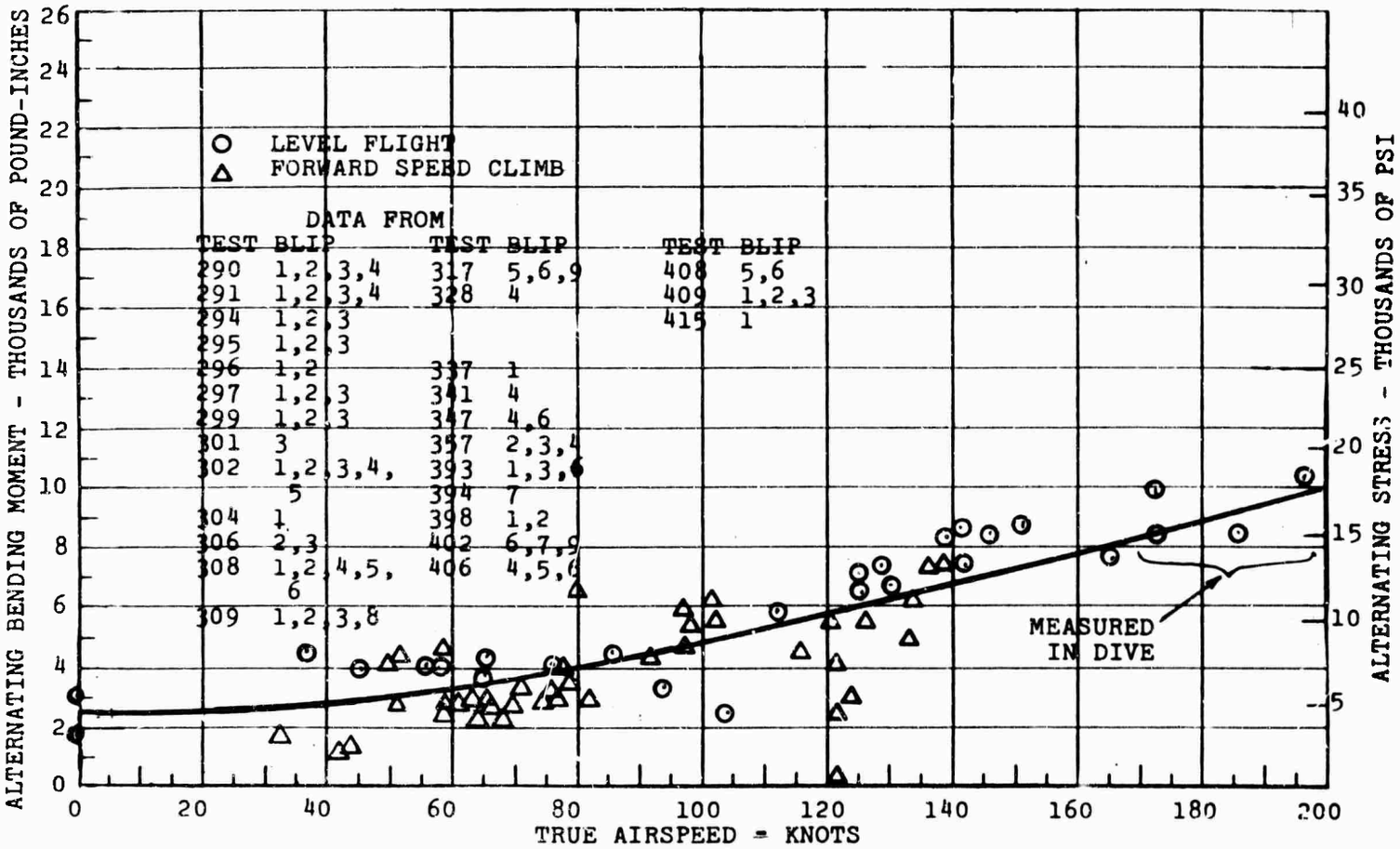


Figure 116. Rotor Blade Flapwise Bending versus Airspeed, Level and Climb, Alternating Component, Station 124.

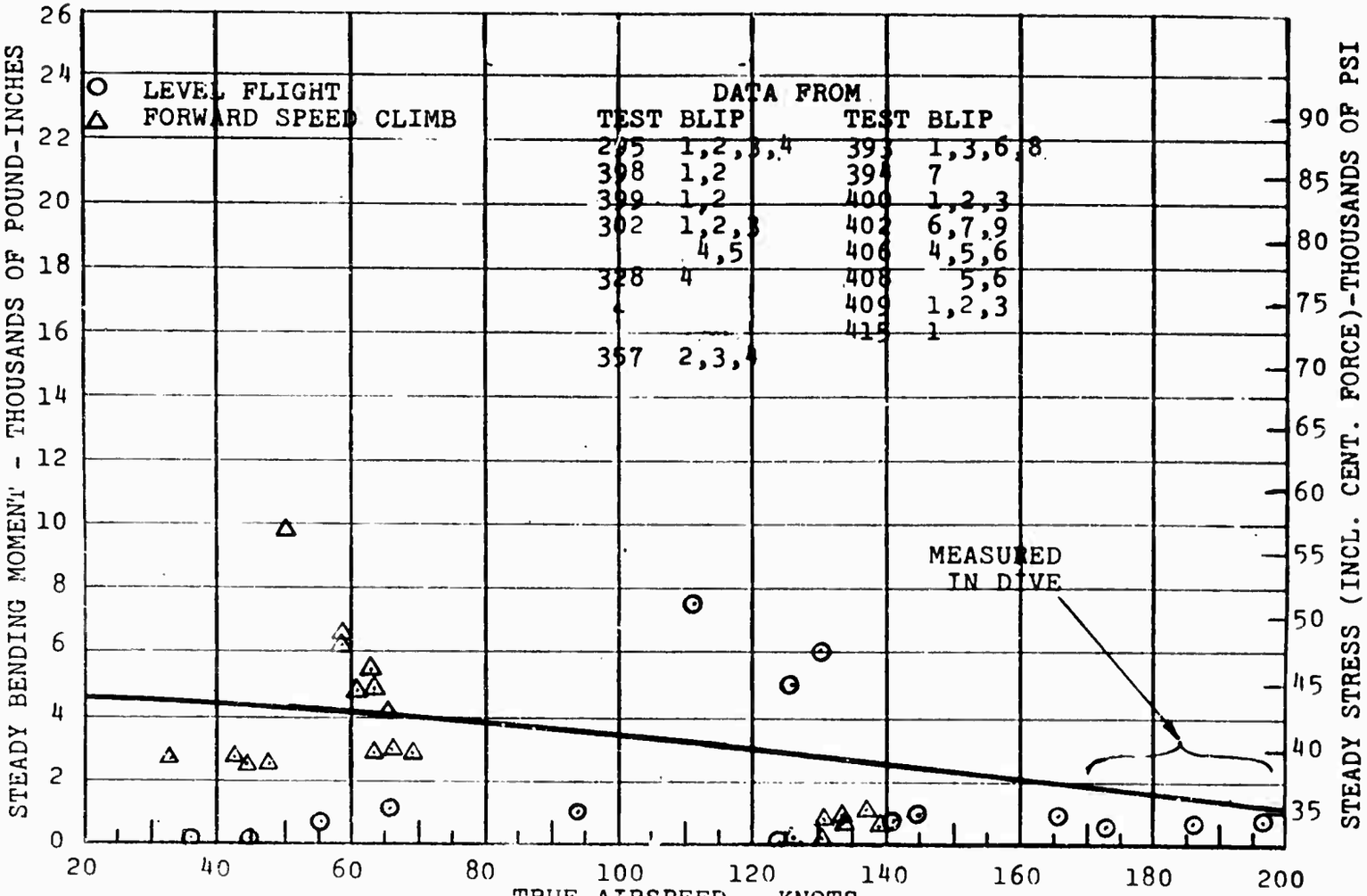


Figure 117. Rotor Blade Flapwise Bending versus Airspeed, Level and Climb, Steady Component, Station 132.

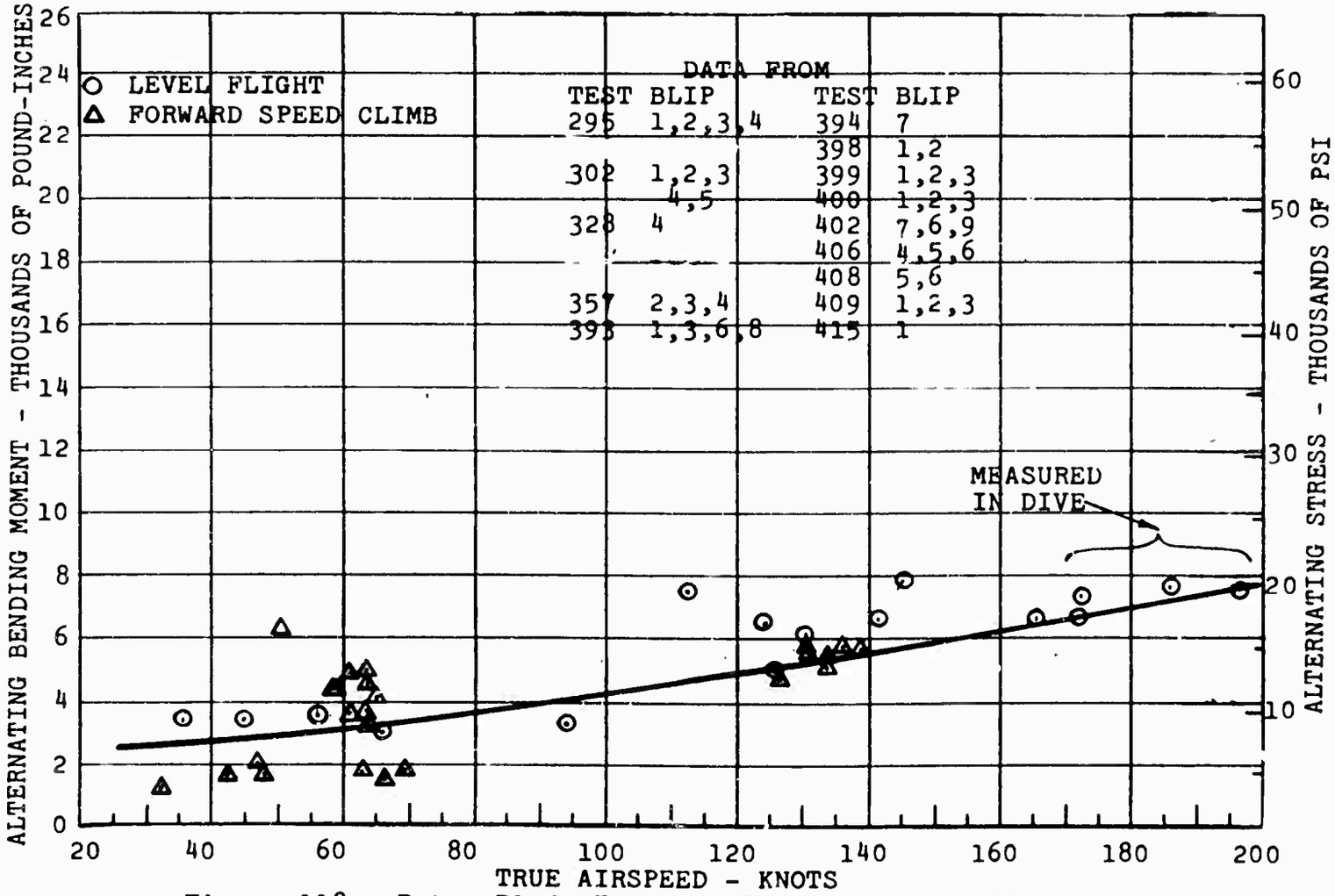


Figure 118. Rotor Blade Flapwise Bending versus Airspeed, Level and Climb, Alternating Component, Station 132.

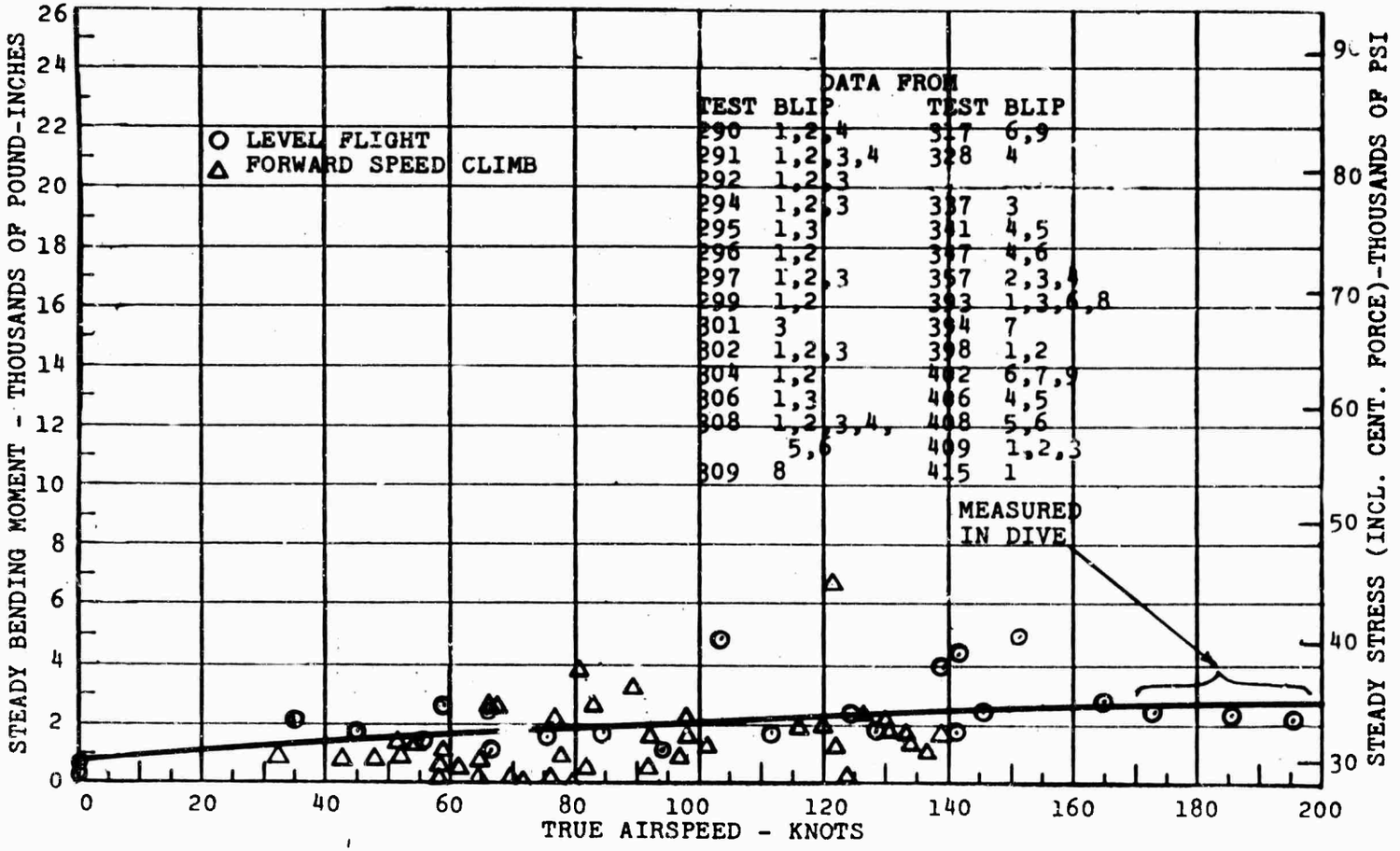


Figure 119. Rotor Blade Flapwise Bending versus Airspeed, Level and Climb, Steady Component, Station 158.4.

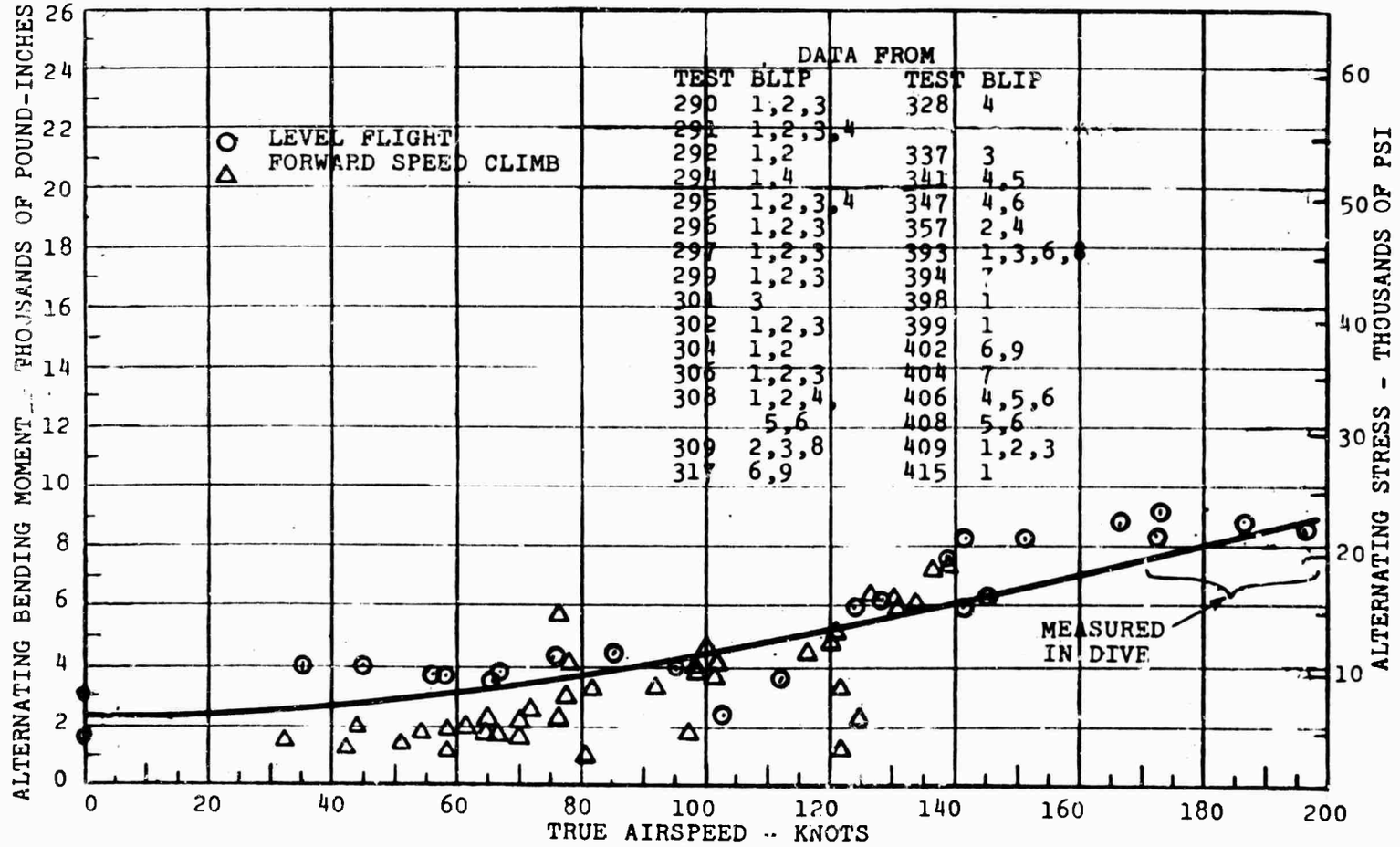


Figure 120. Rotor Blade Flapwise Bending versus Airspeed, Level and Climb, Alternating Component, Station 158.4.

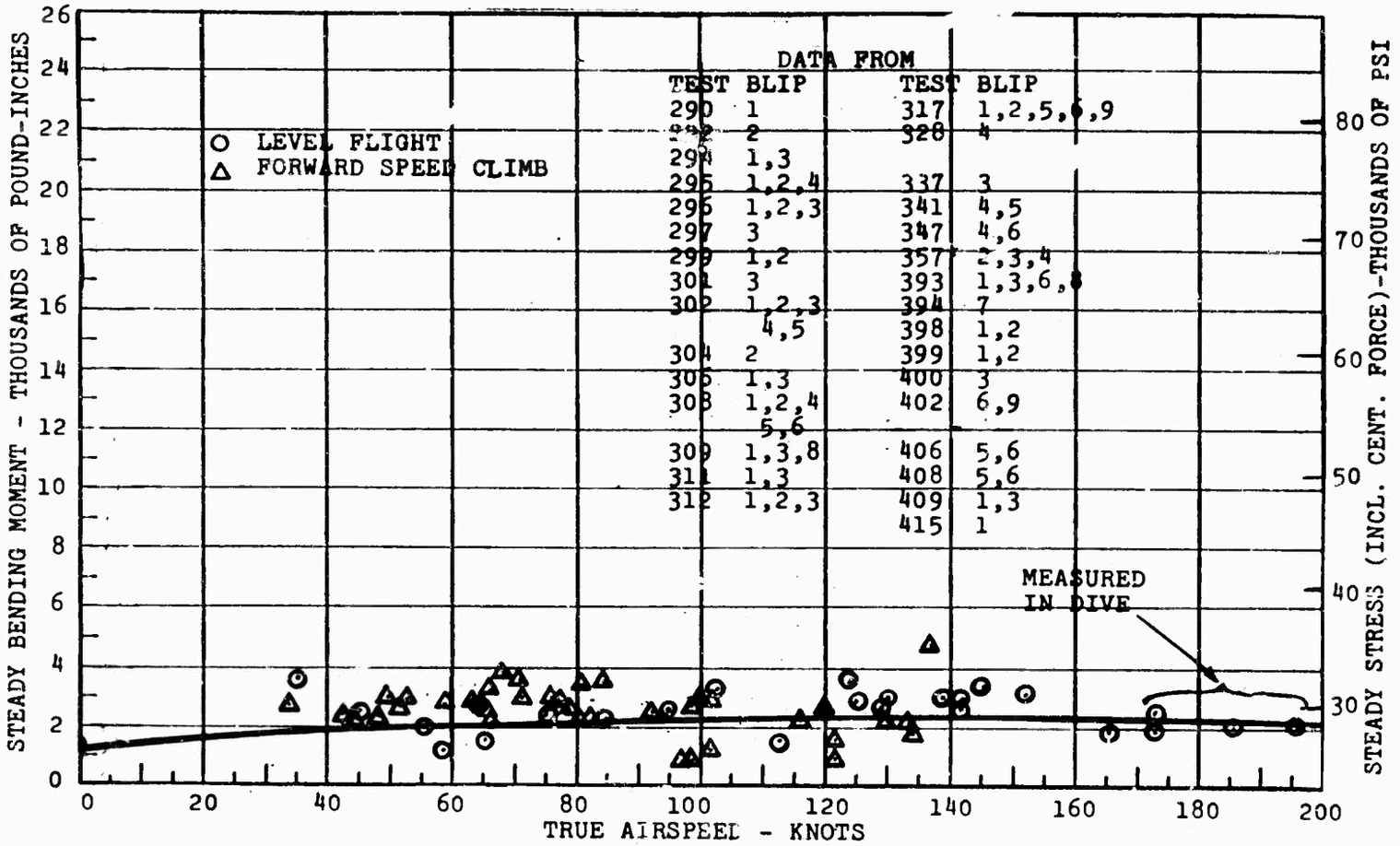


Figure 121. Rotor Blade Flapwise Bending versus Airspeed, Level and Climb, Steady Component, Station 184.8.

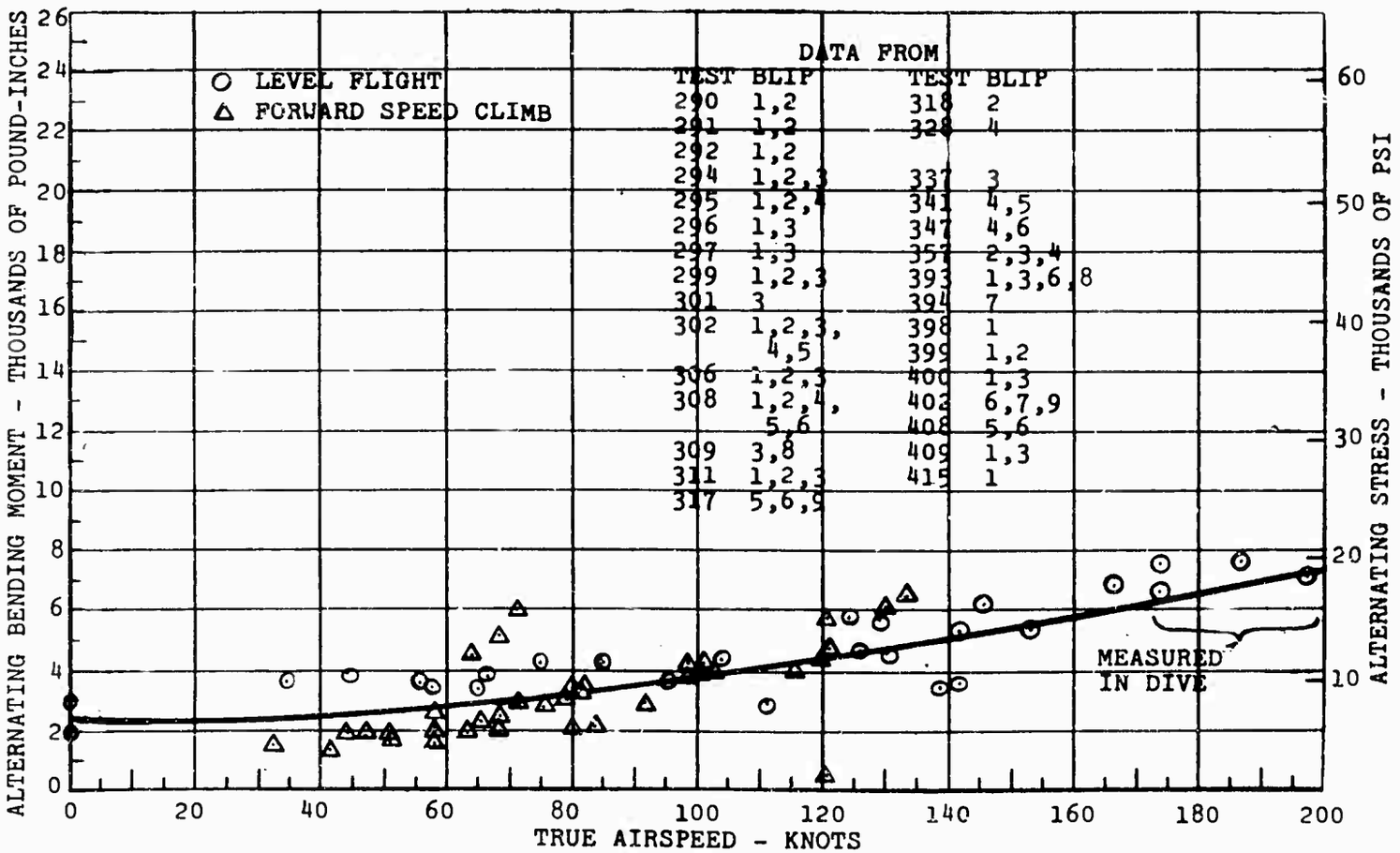


Figure 122. Rotor Blade Flapwise Bending versus Airspeed, Level and Climb, Alternating Component, Station 184.8.

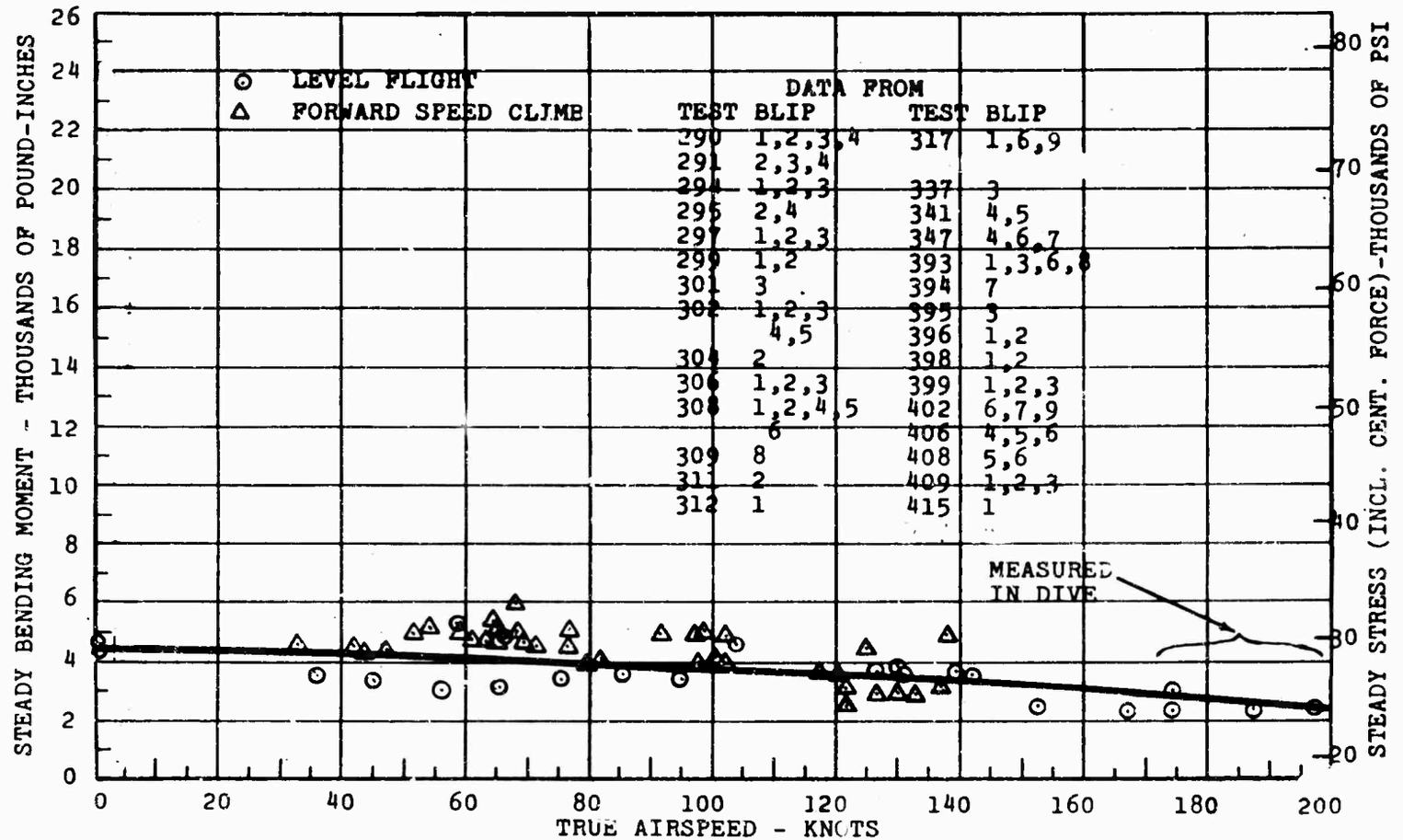


Figure 123. Rotor Blade Flapwise Bending versus Airspeed, Level and Climb, Steady Component, Station 211.2.

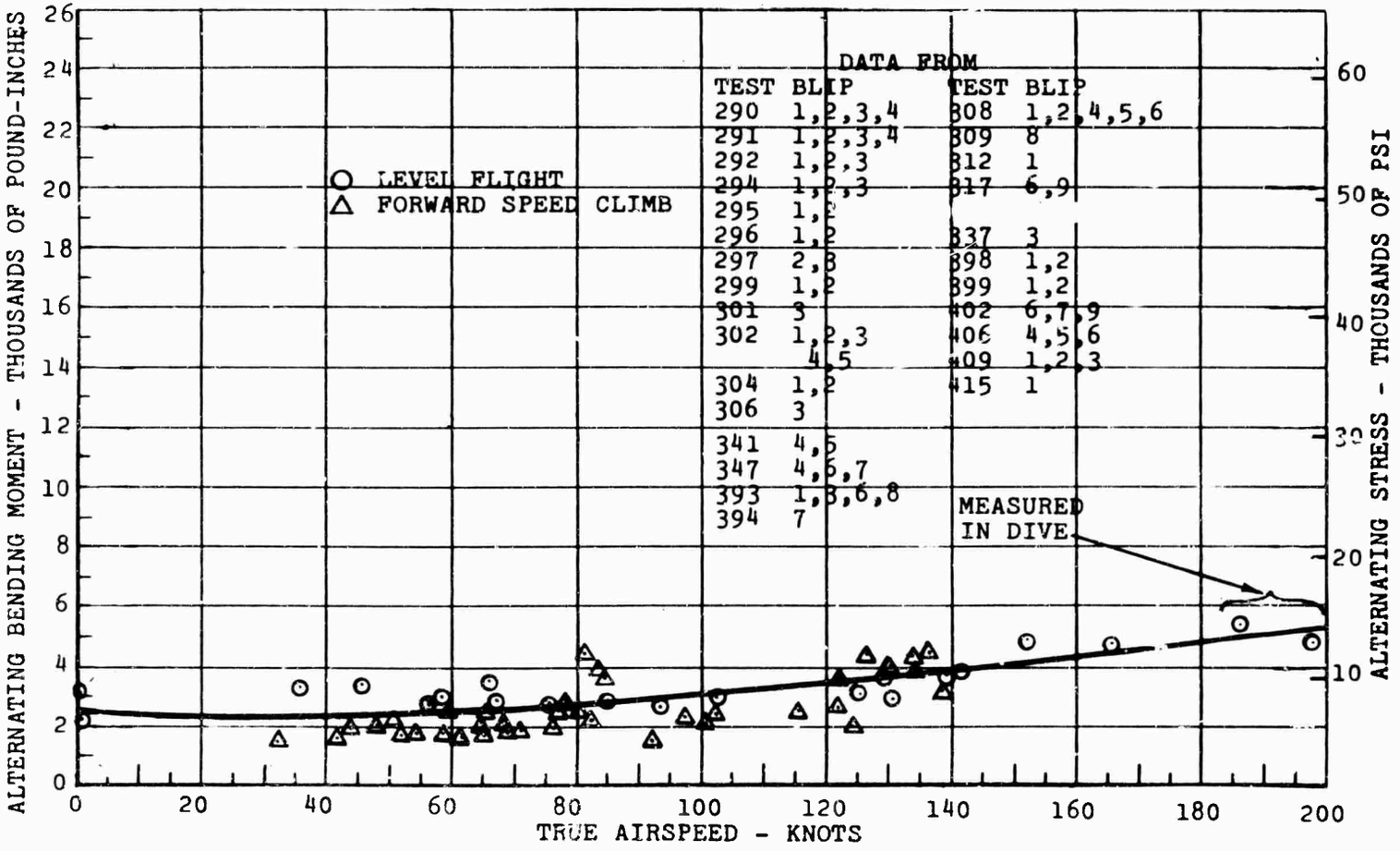


Figure 124. Rotor Blade Flapwise Bending versus Airspeed, Level and Climb, Alternating Component, Station 211.2.

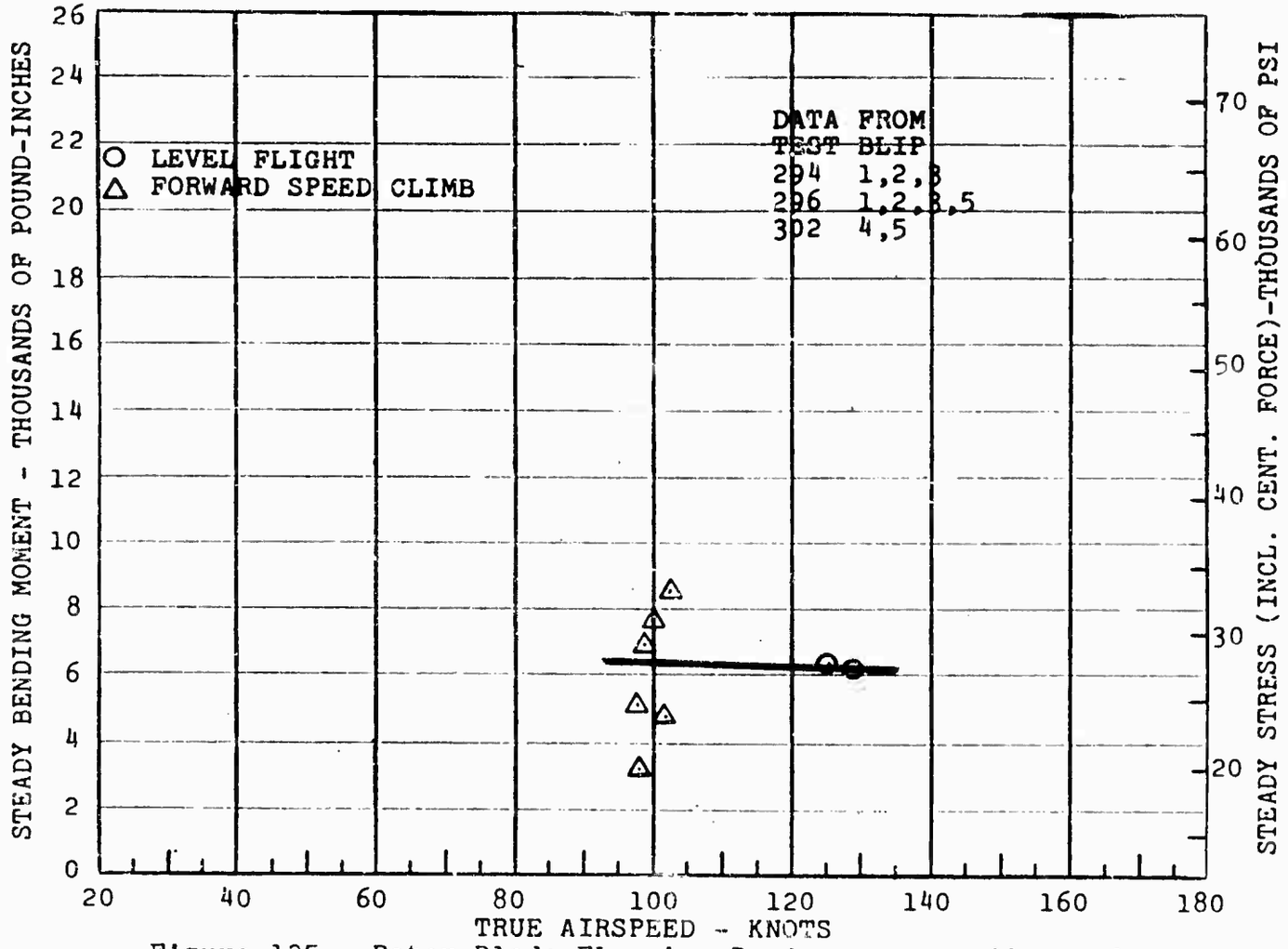


Figure 125. Rotor Blade Flapwise Bending versus Airspeed, Level and Climb, Steady Component, Station 237.6.

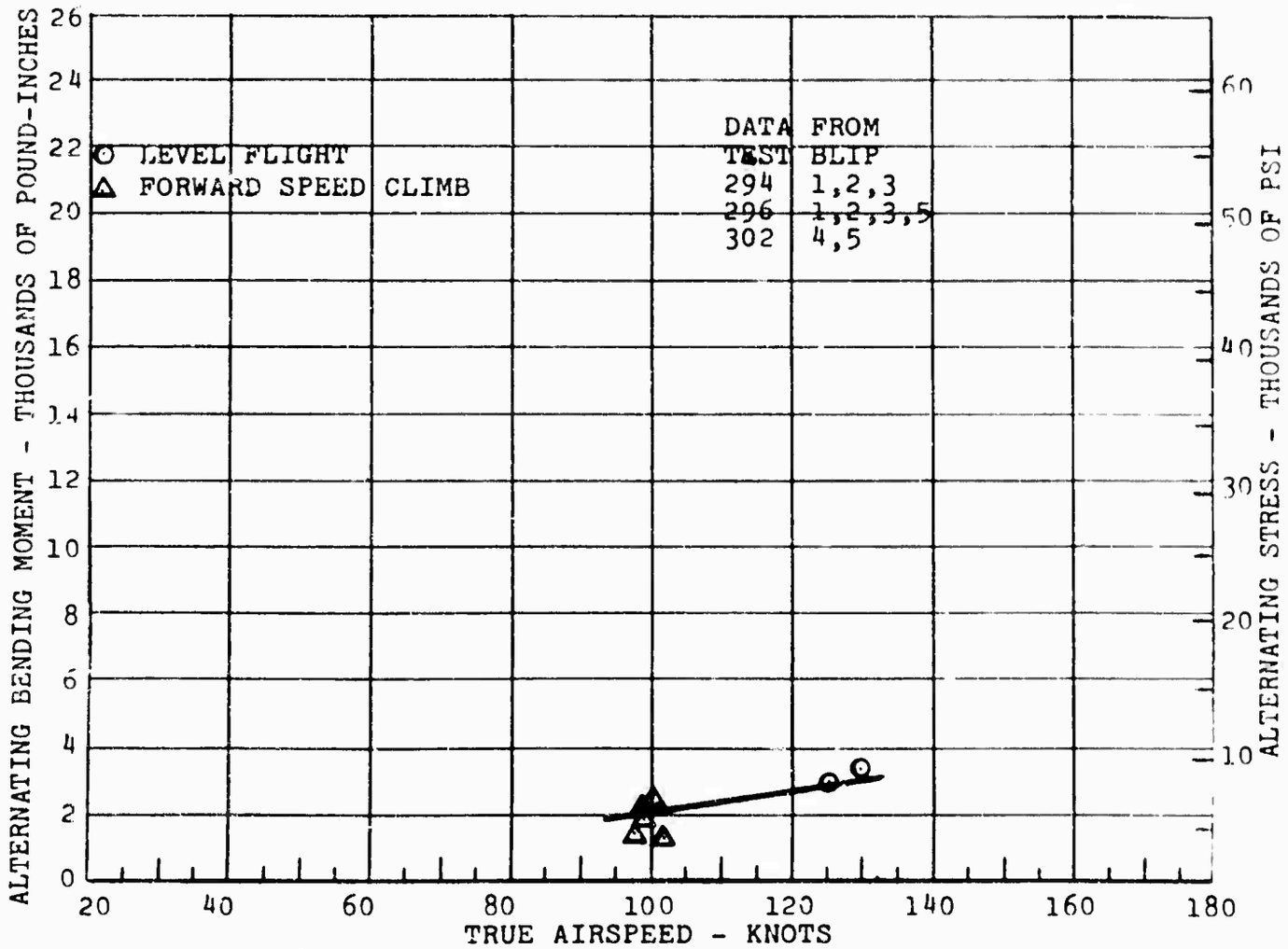


Figure 126. Rotor Blade Flapwise Bending versus Airspeed, Level and Climb, Alternating Component, Station 237.6.

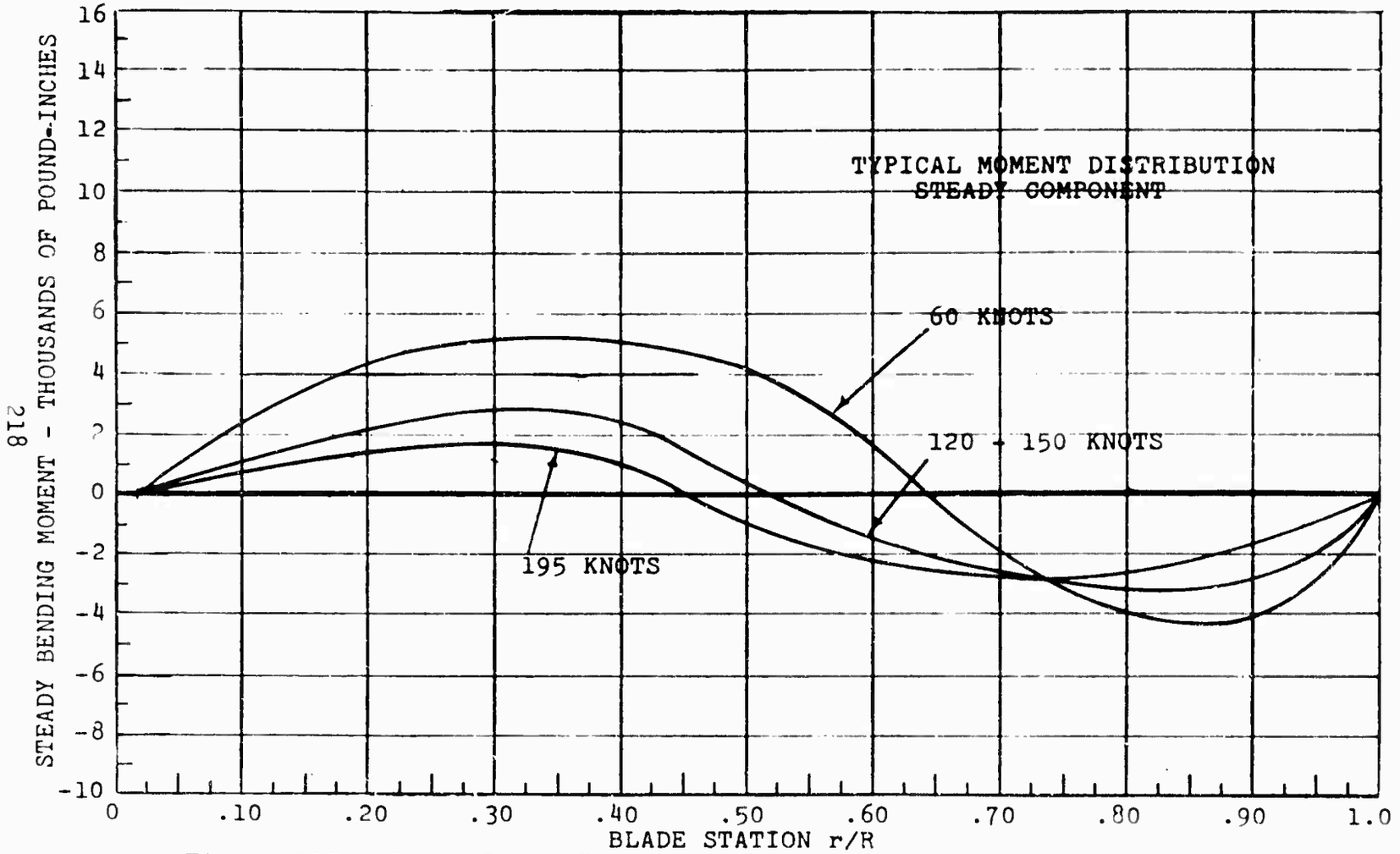


Figure 127. Rotor Blade Flapwise Bending Moment versus Blade Station.

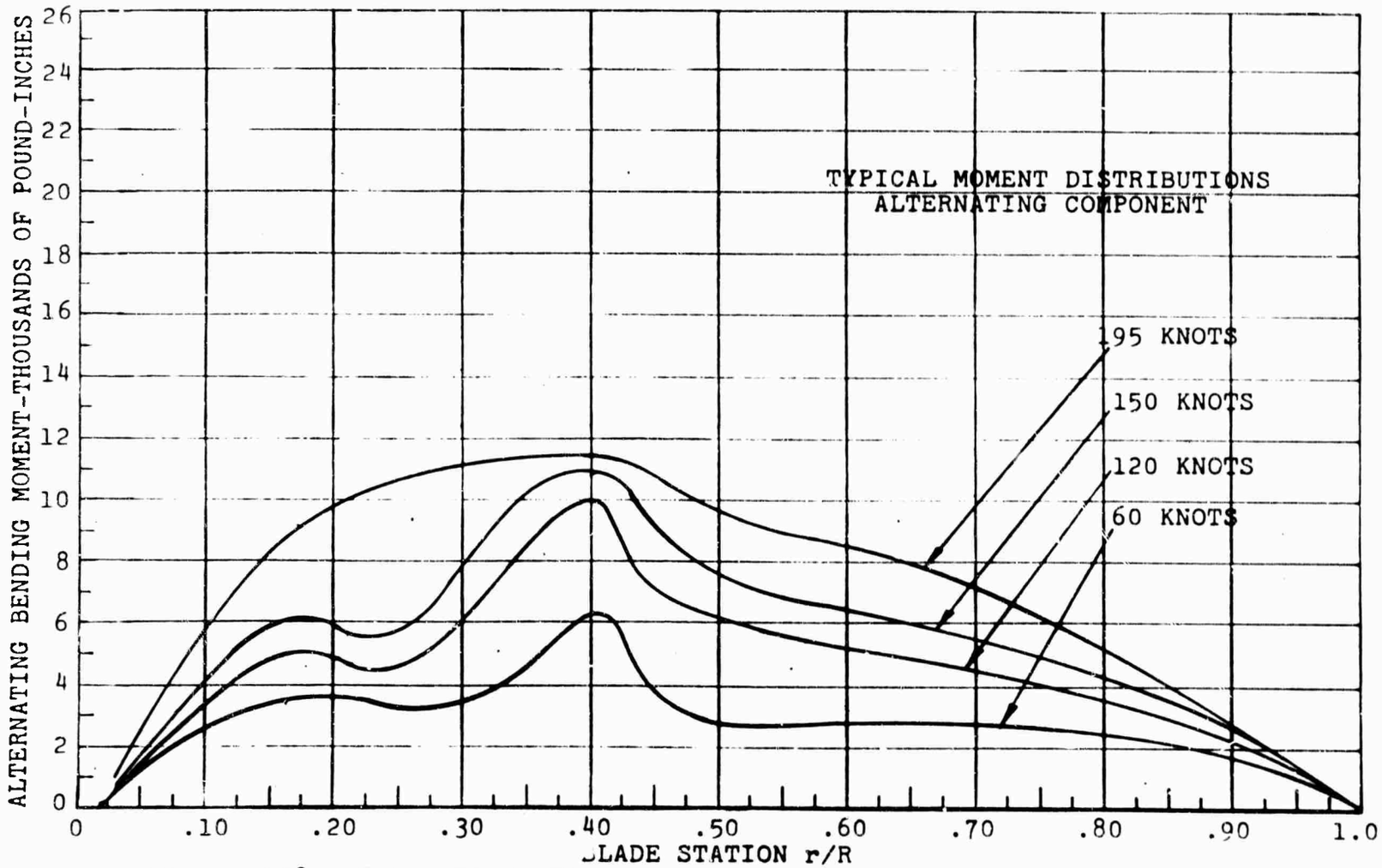


Figure 128. Rotor Blade Flapwise Bending Moment versus Blade Station.

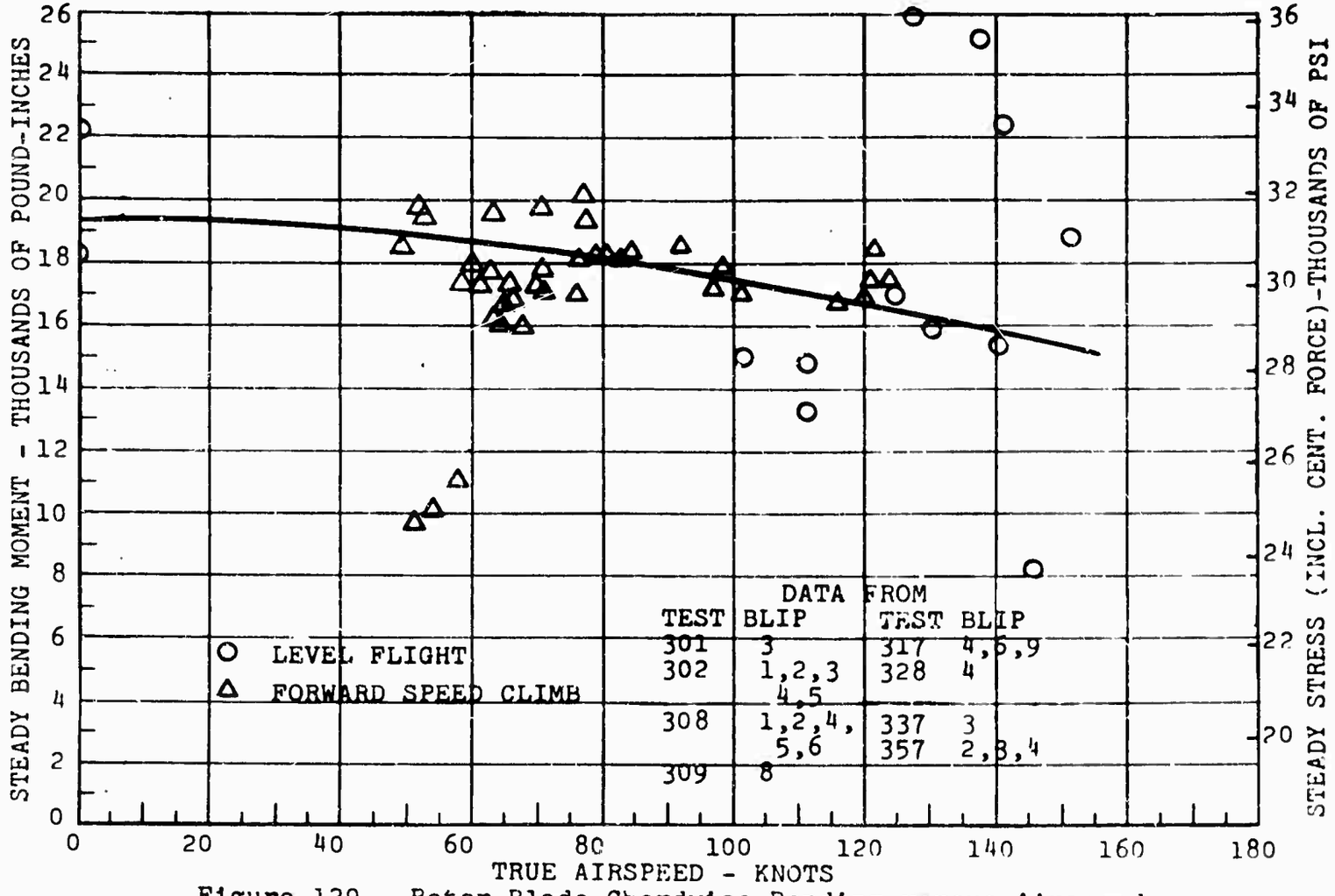


Figure 129. Rotor Blade Chordwise Bending versus Airspeed, Level and Climb, Steady Component, Station 46.

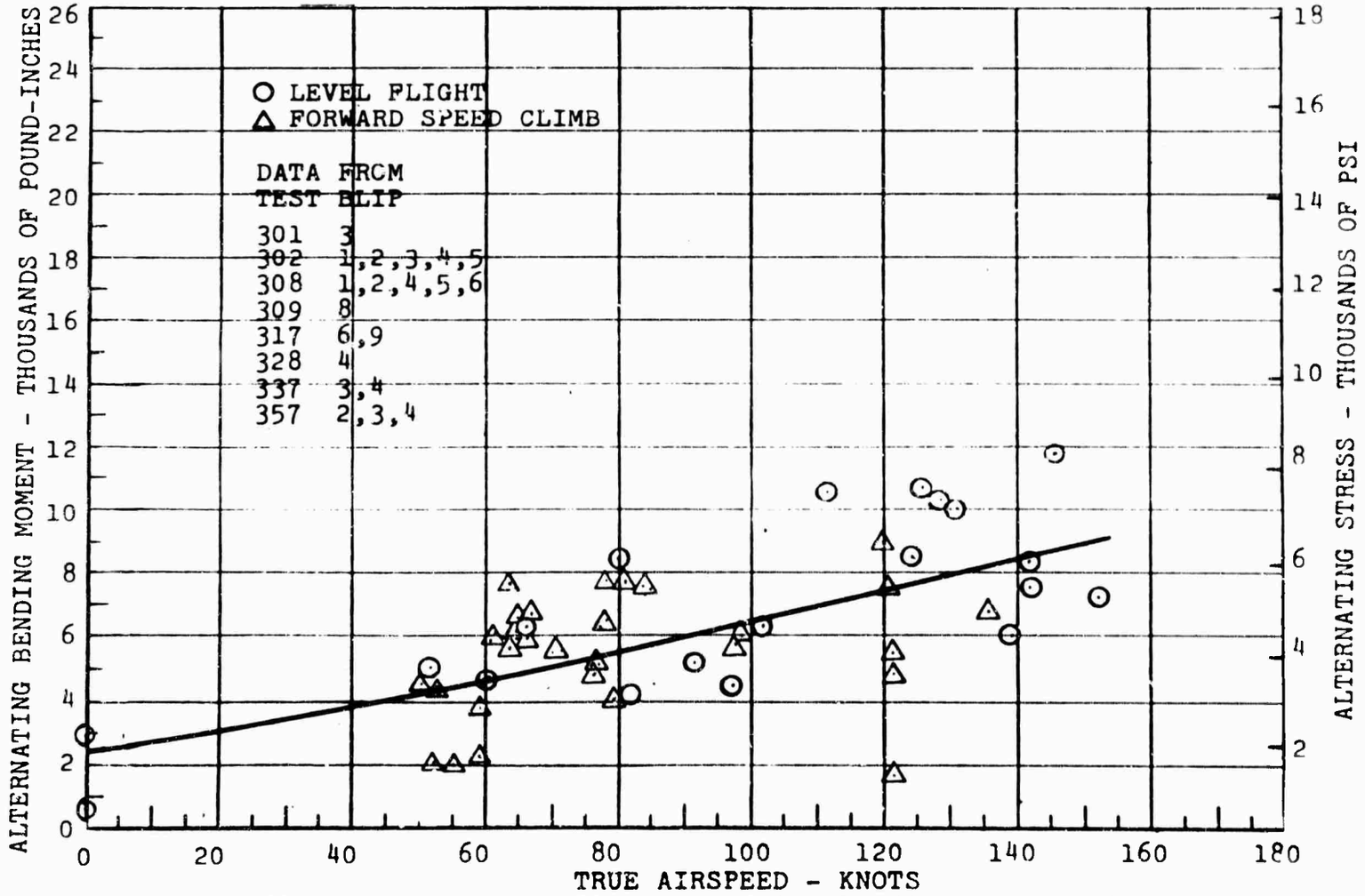


Figure 130. Rotor Blade Chordwise Bending versus Airspeed, Level and Climb, Alternating Component, Station 46.

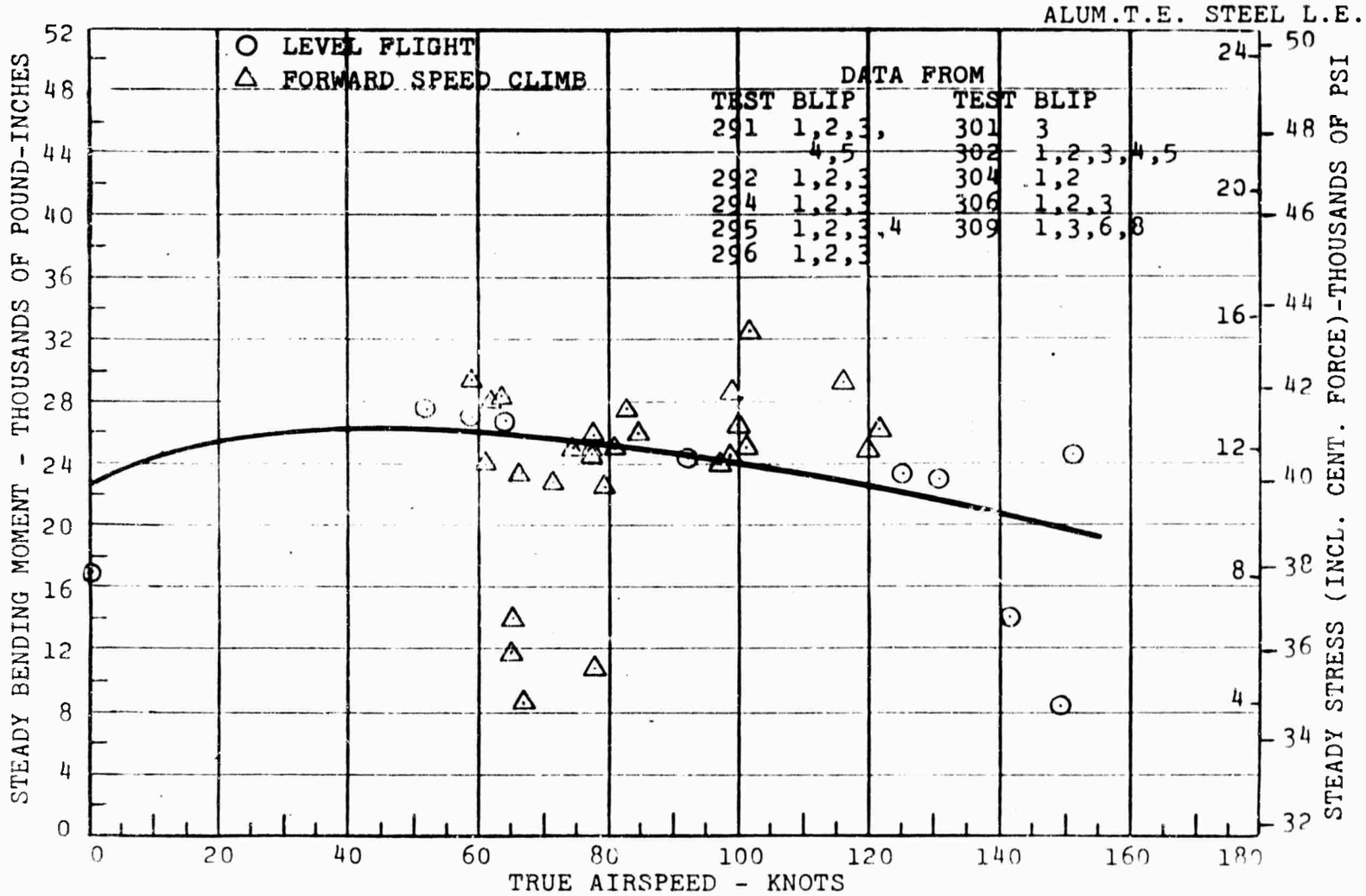


Figure 131. Rotor Blade Chordwise Bending versus Airspeed, Level and Climb, Steady Component, Station 131.5.

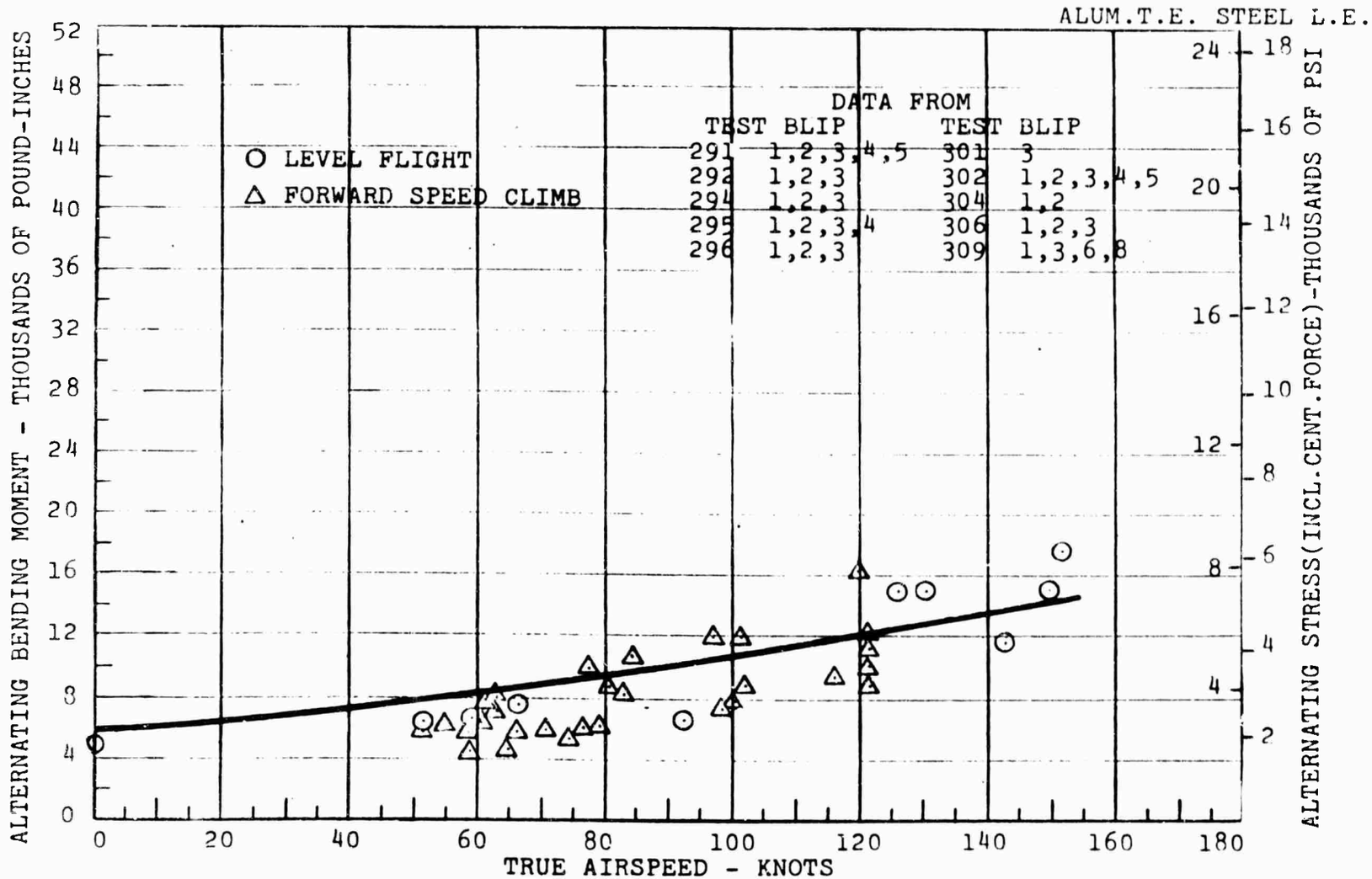


Figure 132. Rotor Blade Chordwise Bending versus Airspeed, Level and Climb, Alternating Components, Station 131.5.

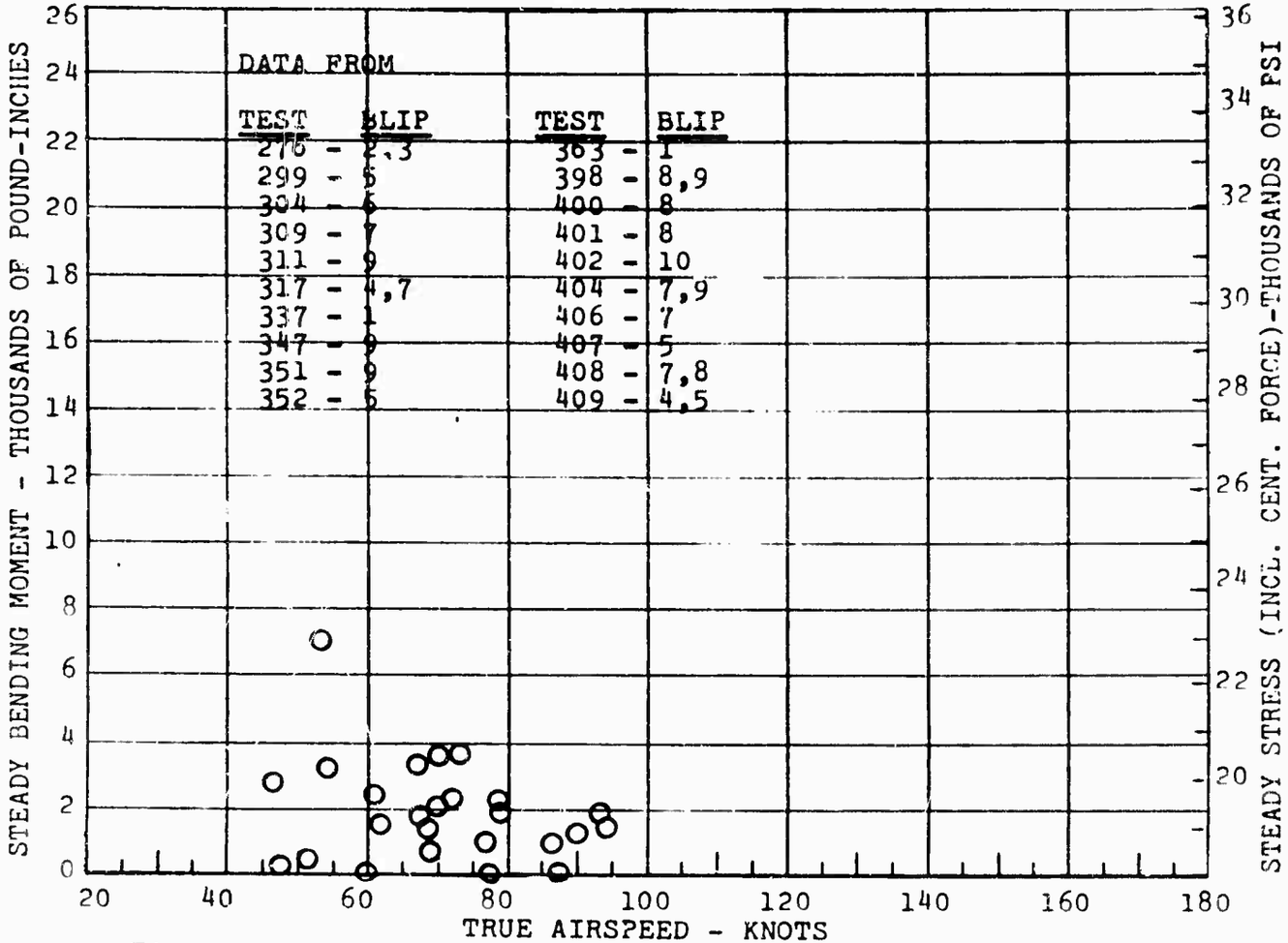


Figure 133. Rotor Blade Flapwise Bending versus Airspeed, Autorotation, Steady Component, Station 46.

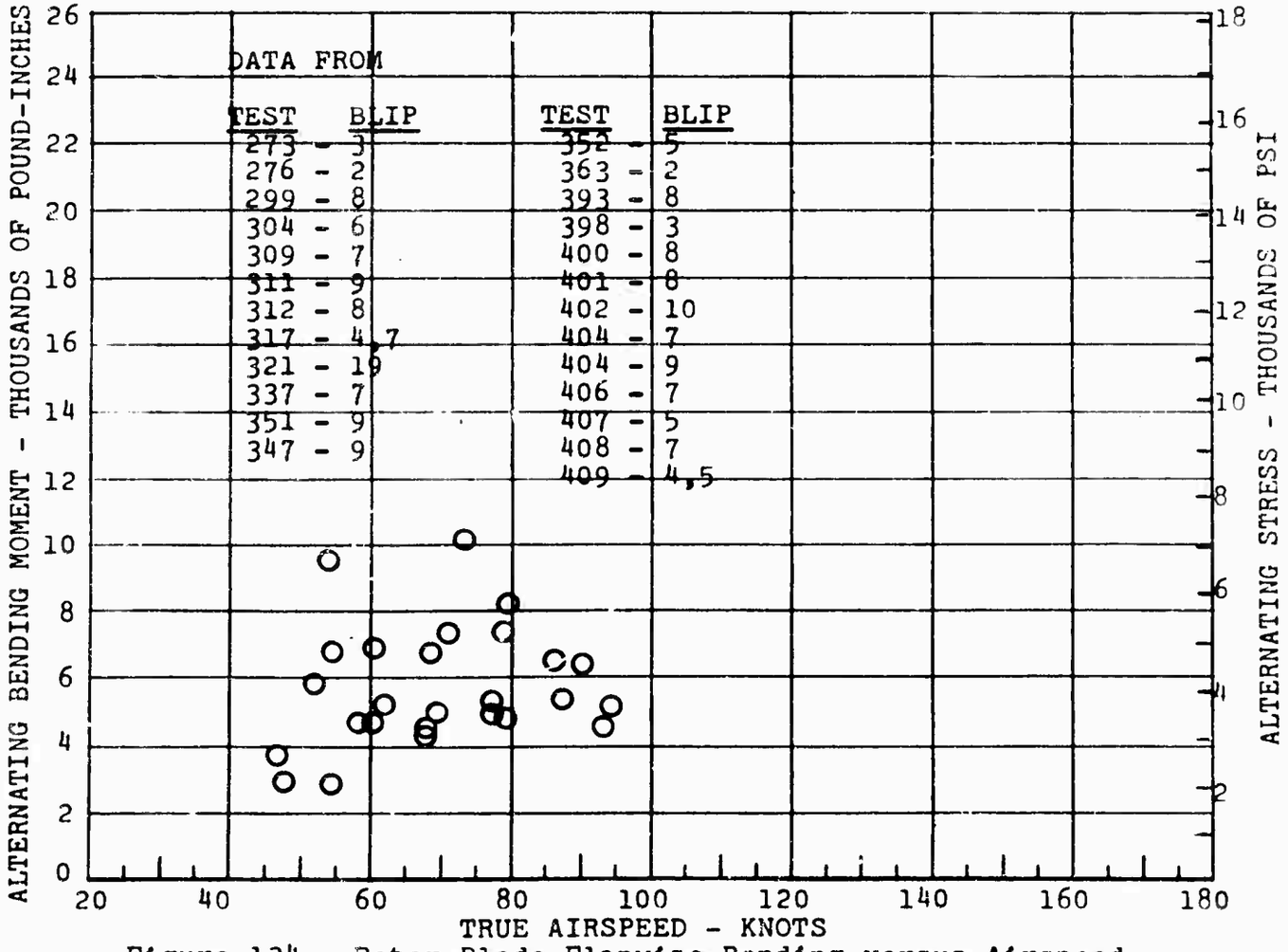


Figure 134. Rotor Blade Flapwise Bending versus Airspeed, Autorotation, Alternating Component, Station 46.

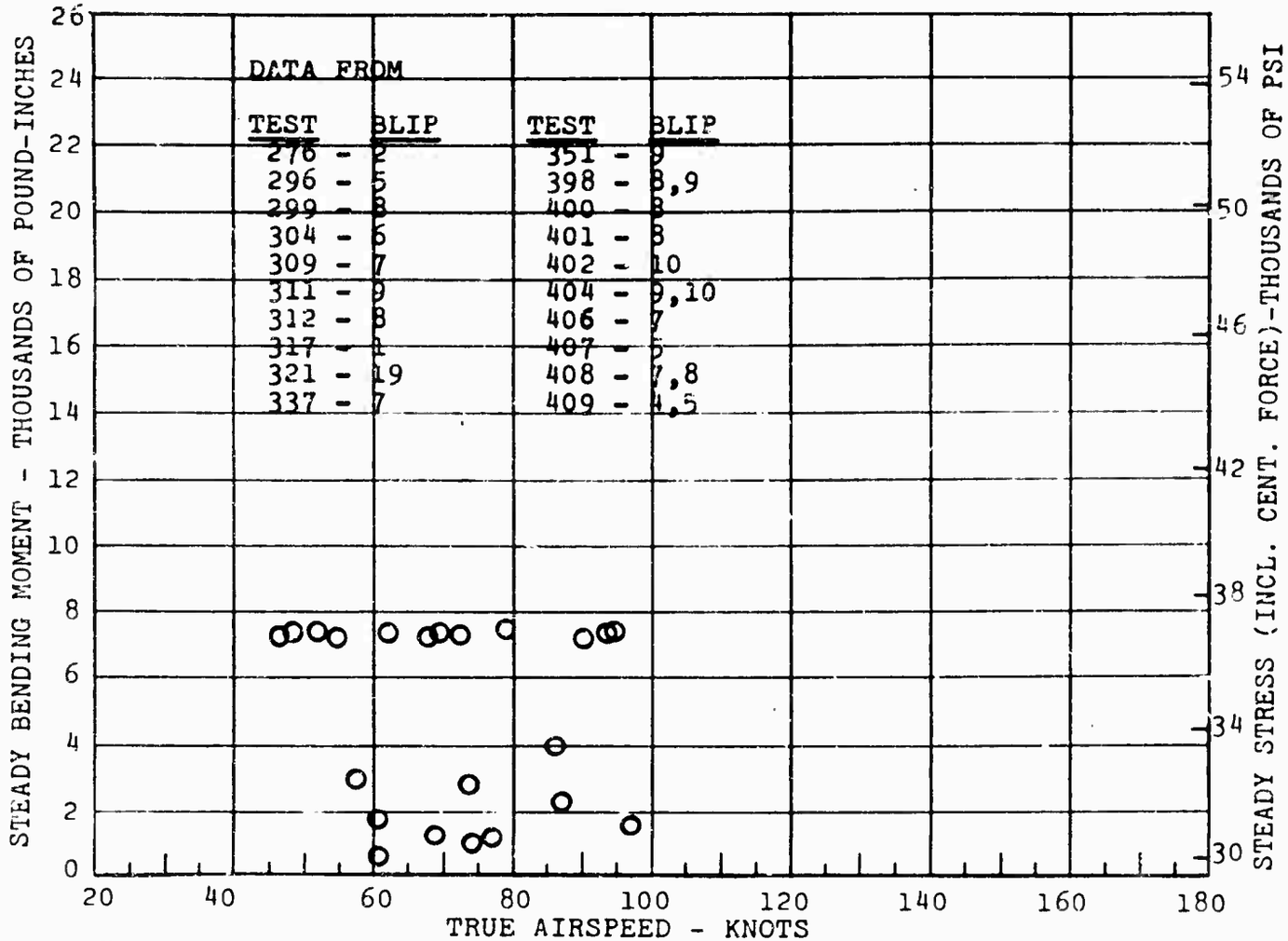


Figure 135. Rotor Blade Flapwise Bending versus Airspeed, Autorotation, Steady Component, Station 59.5.

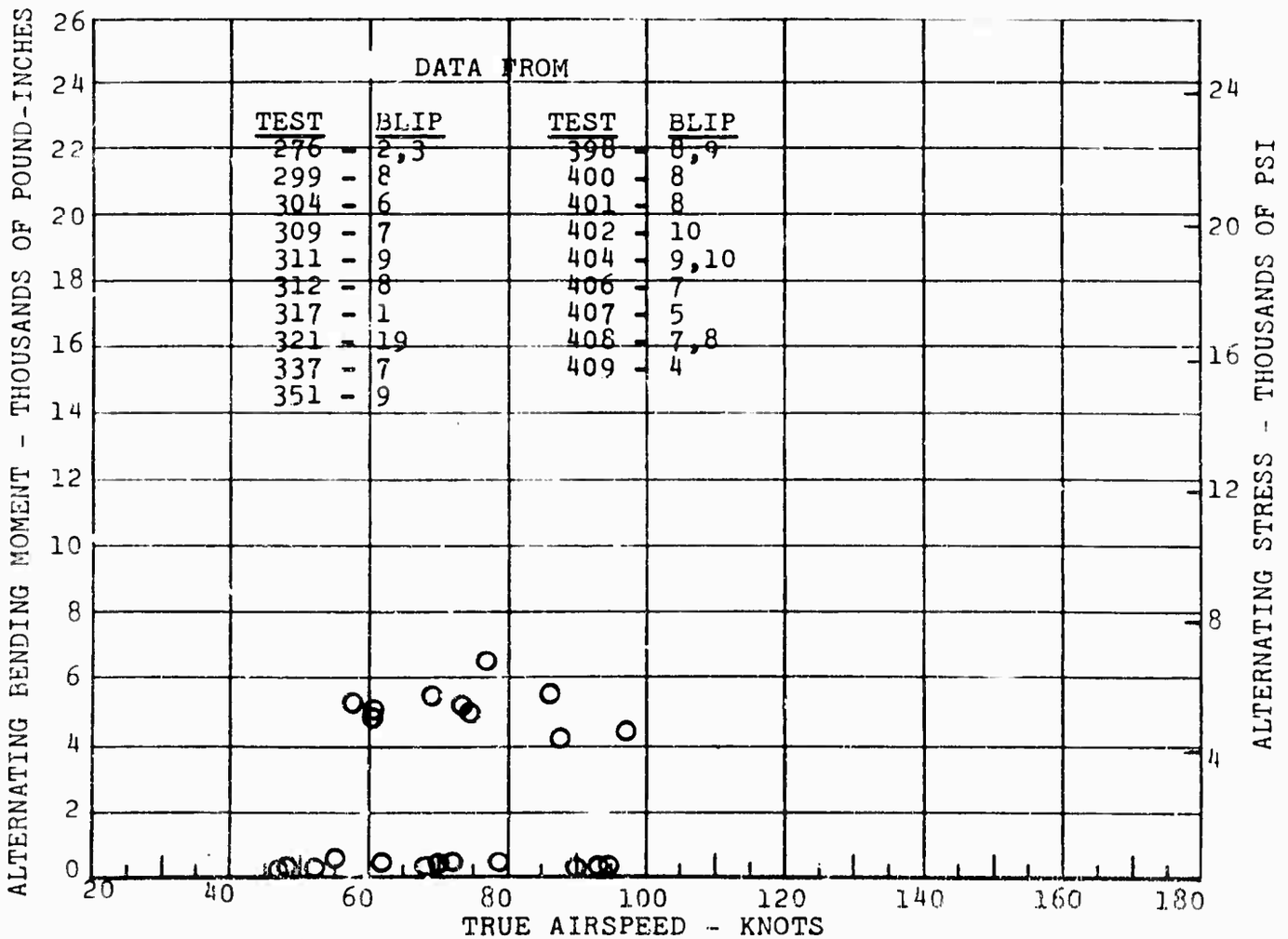


Figure 136. Rotor Blade Flapwise Bending versus Airspeed, Autorotation, Alternating Component, Station 59.5.

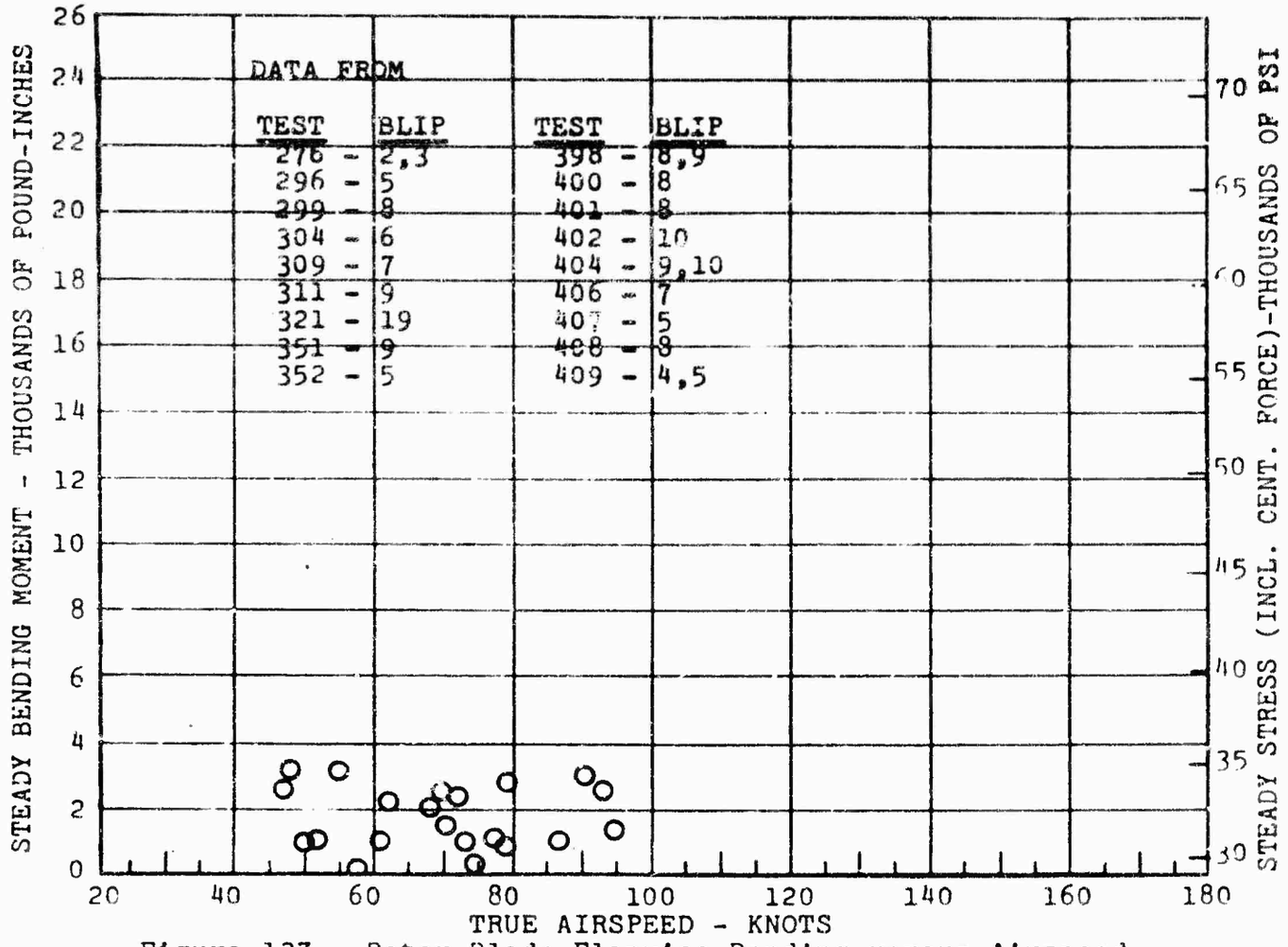


Figure 137. Rotor Blade Flapwise Bending versus Airspeed, Autorotation, Steady Component, Station 79.2.

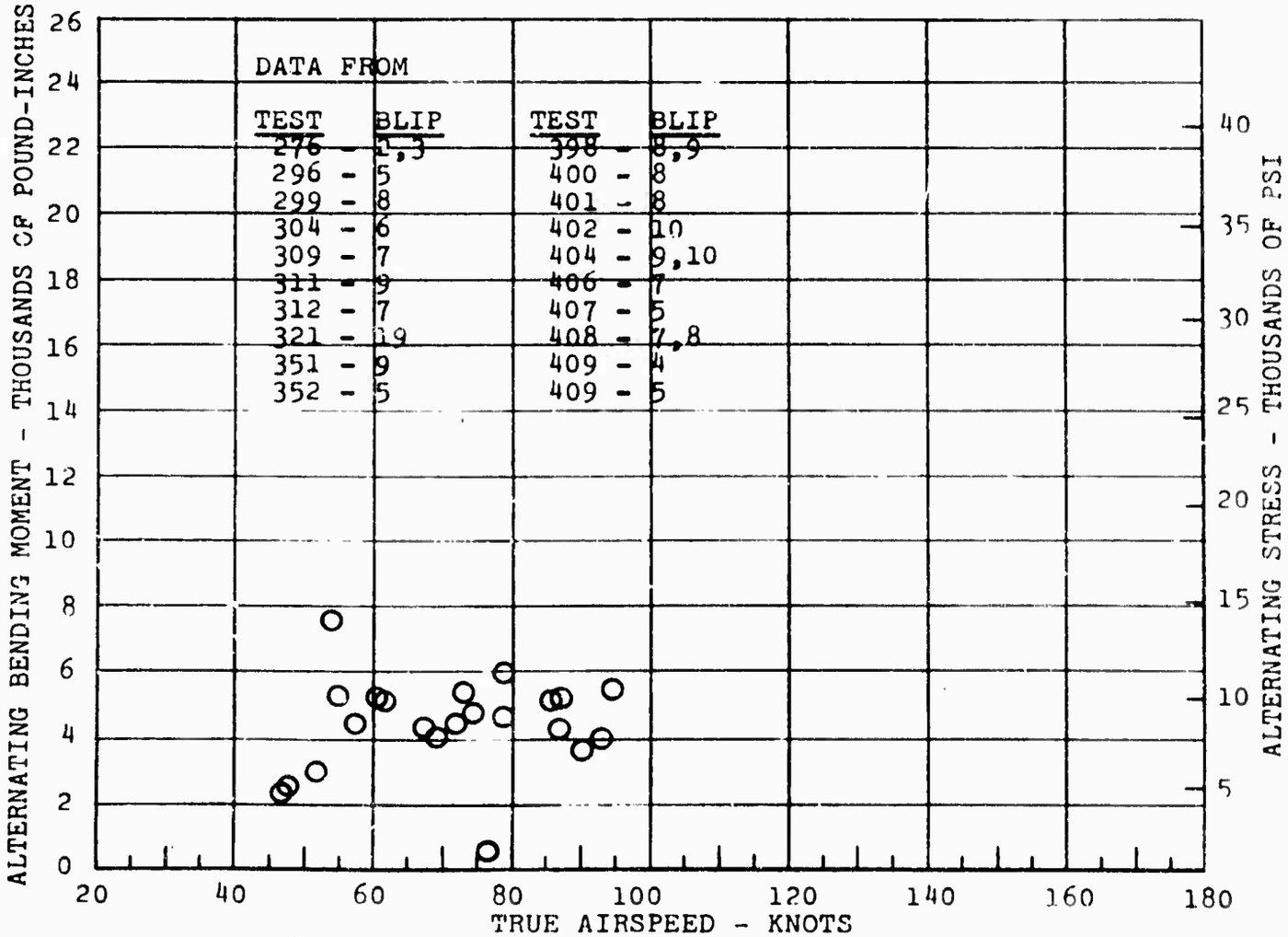


Figure 138. Rotor Blade Flapwise Bending versus Airspeed, Autorotation, Alternating Component, Station 79.2.

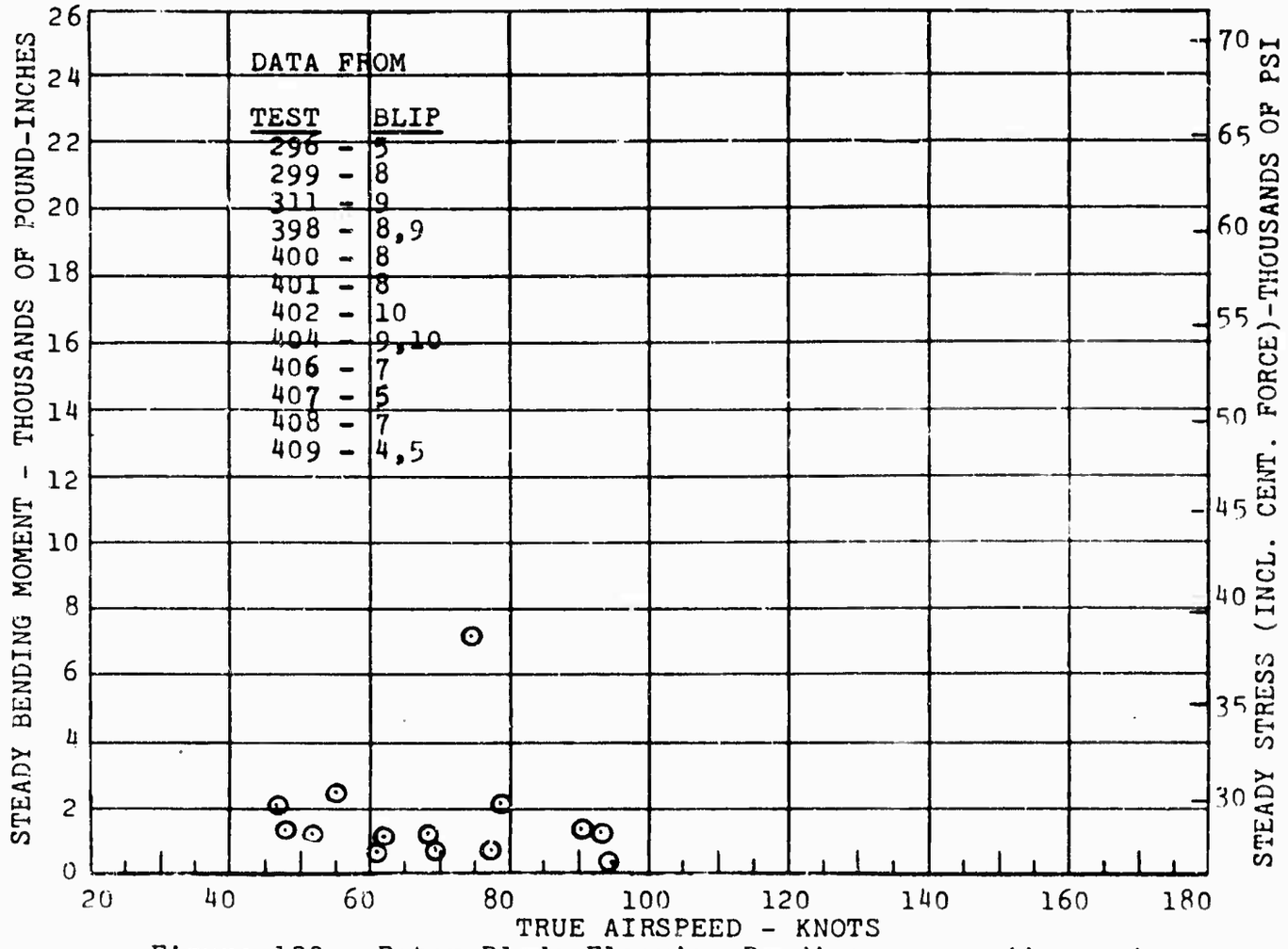


Figure 139. Rotor Blade Flapwise Bending versus Airspeed, Autorotation, Steady Component, Station 105.6.

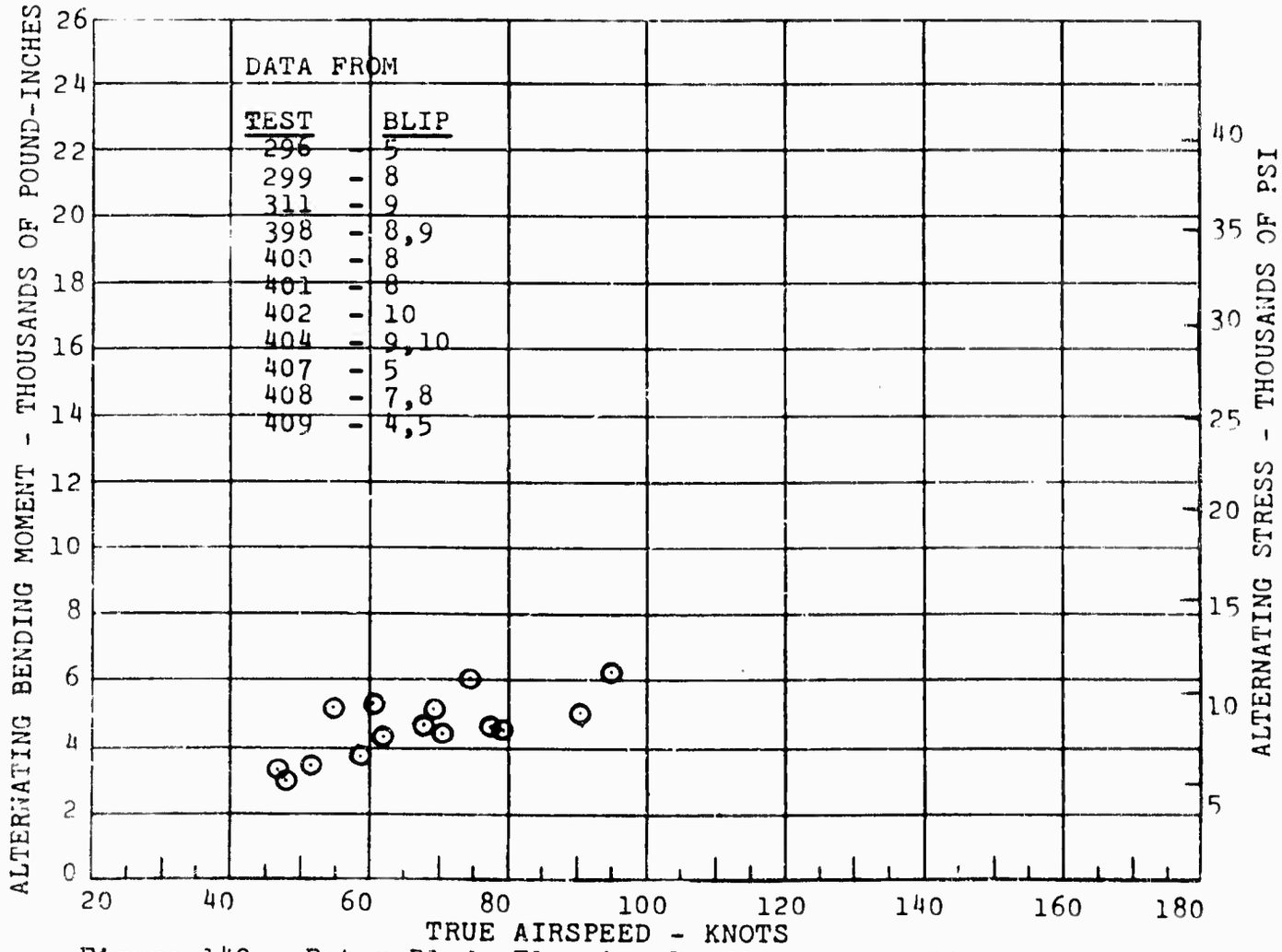


Figure 140. Rotor Blade Flapwise Bending versus Airspeed, Autorotation, Alternating Component, Station 105.6.

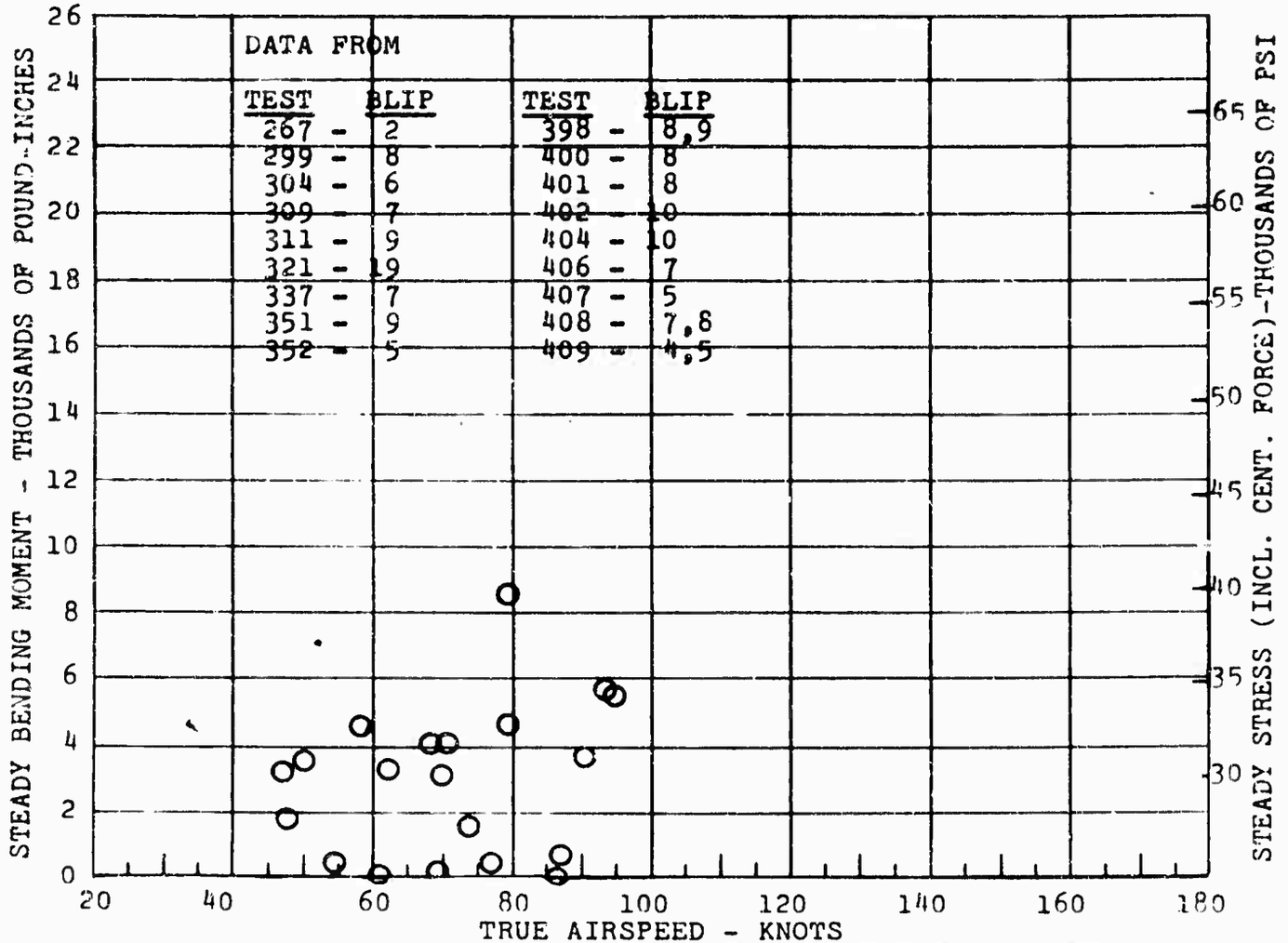


Figure 141. Rotor Blade Flapwise Bending versus Airspeed, Autorotation, Steady Component, Station 124.

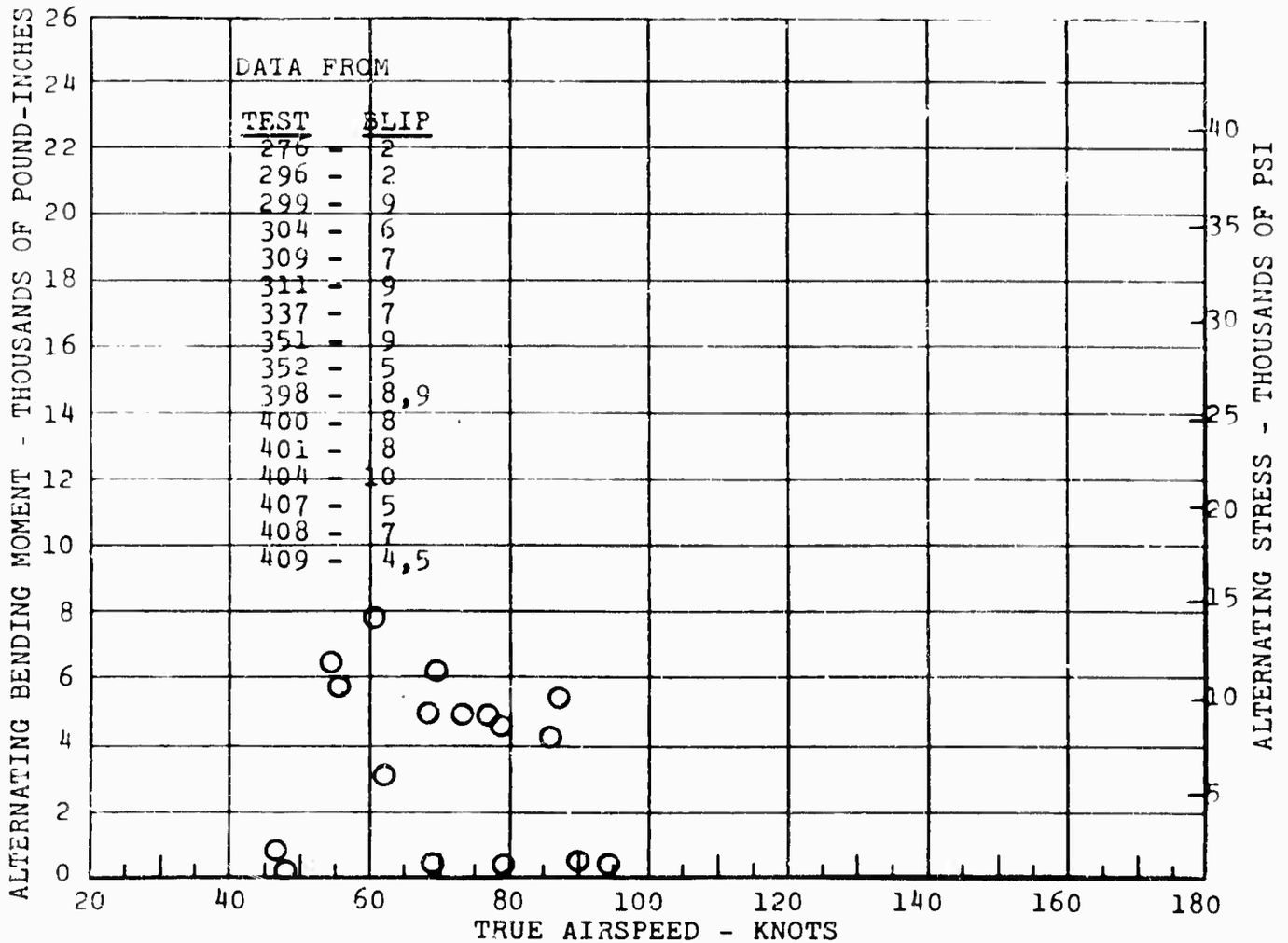


Figure 142. Rotor Blade Flapwise Bending versus Airspeed, Autorotation, Alternating Component, Station 124.

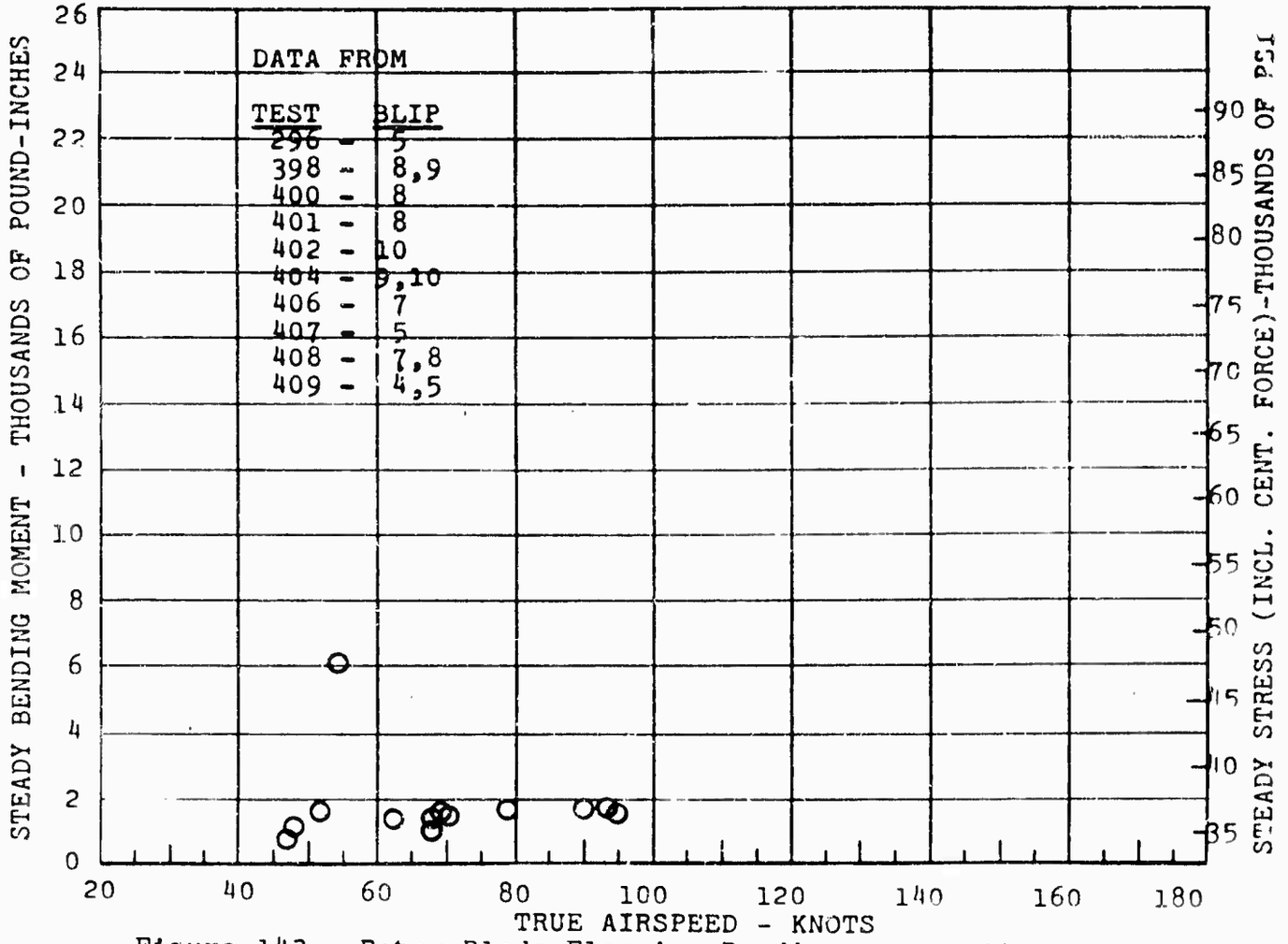


Figure 143. Rotor Blade Flapwise Bending versus Airspeed, Autorotation, Steady Component, Station 132.

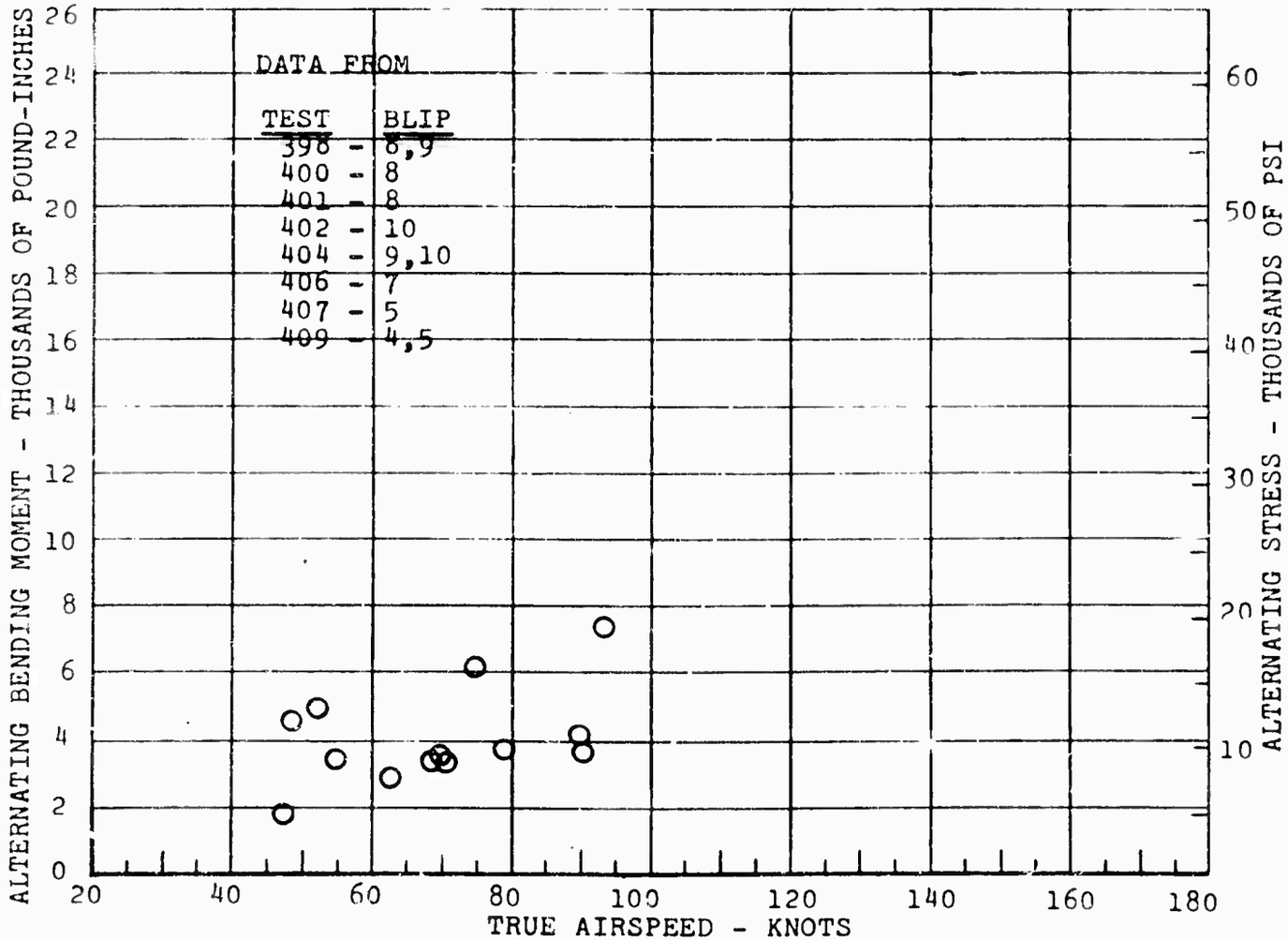


Figure 144. Rotor Blade Flapwise Bending versus Airspeed, Autorotation, Alternating Component, Station 132.

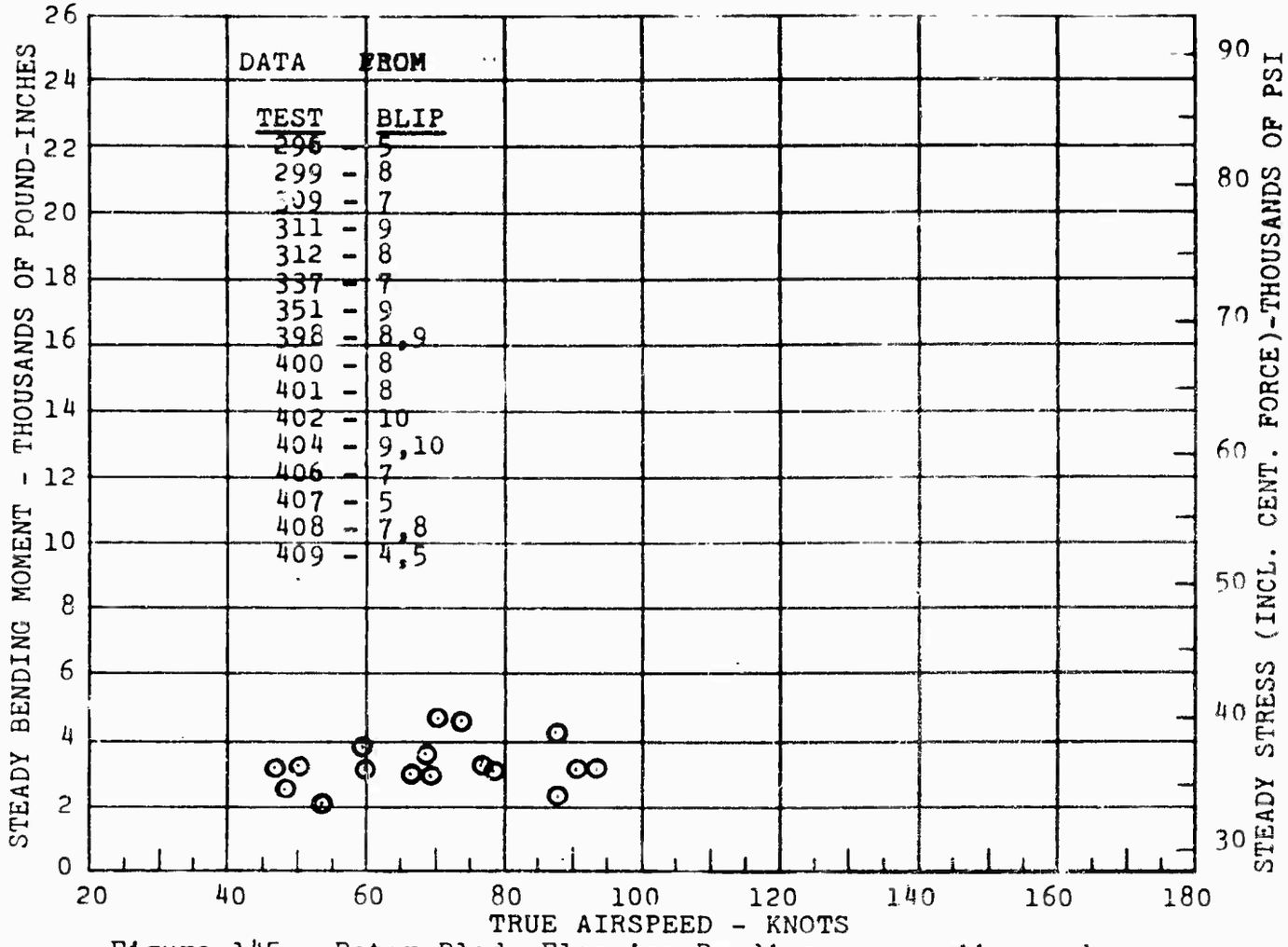


Figure 145. Rotor Blade Flapwise Bending versus Airspeed, Autorotation, Steady Component, Station 158.4.

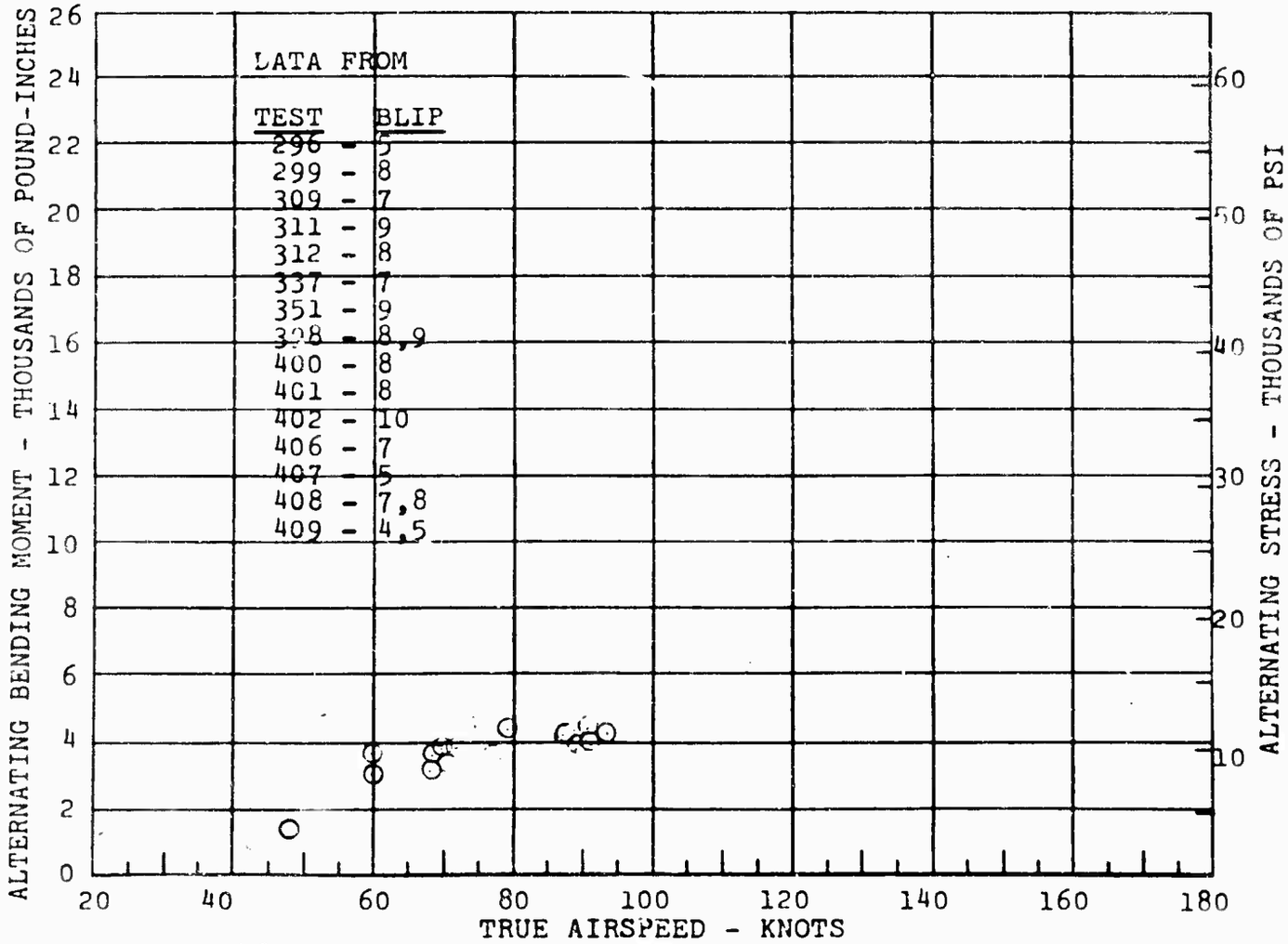


Figure 146. Rotor Blade Flapwise Bending versus Airspeed, Autorotation, Alternating Component, Station 158.4.

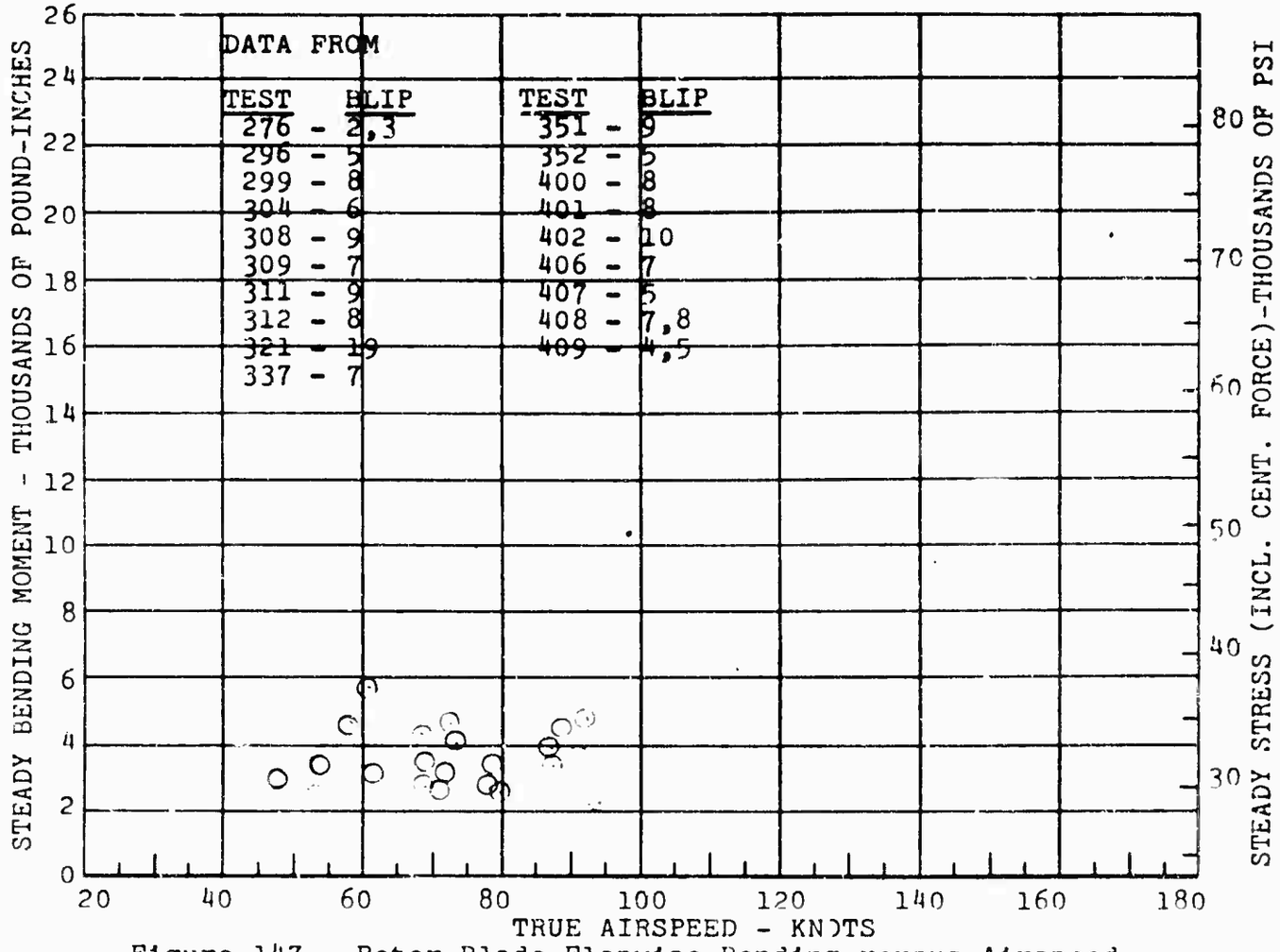


Figure 147. Rotor Blade Flapwise Bending versus Airspeed, Autorotation, Steady Component, Station 184.8.

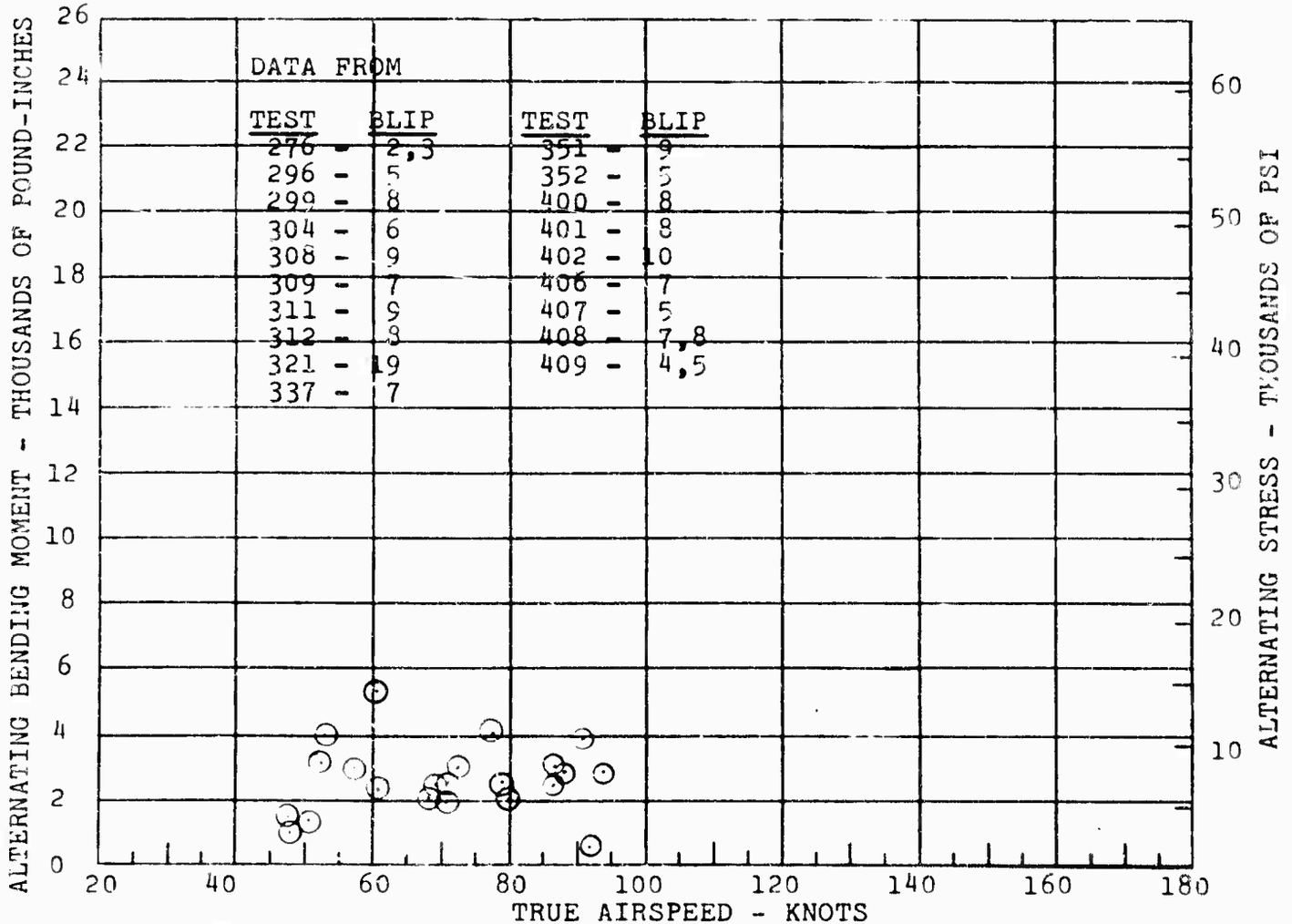


Figure 148. Rotor Blade Flapwise Bending versus Airspeed, Autorotation, Alternating Component, Station 184.8.

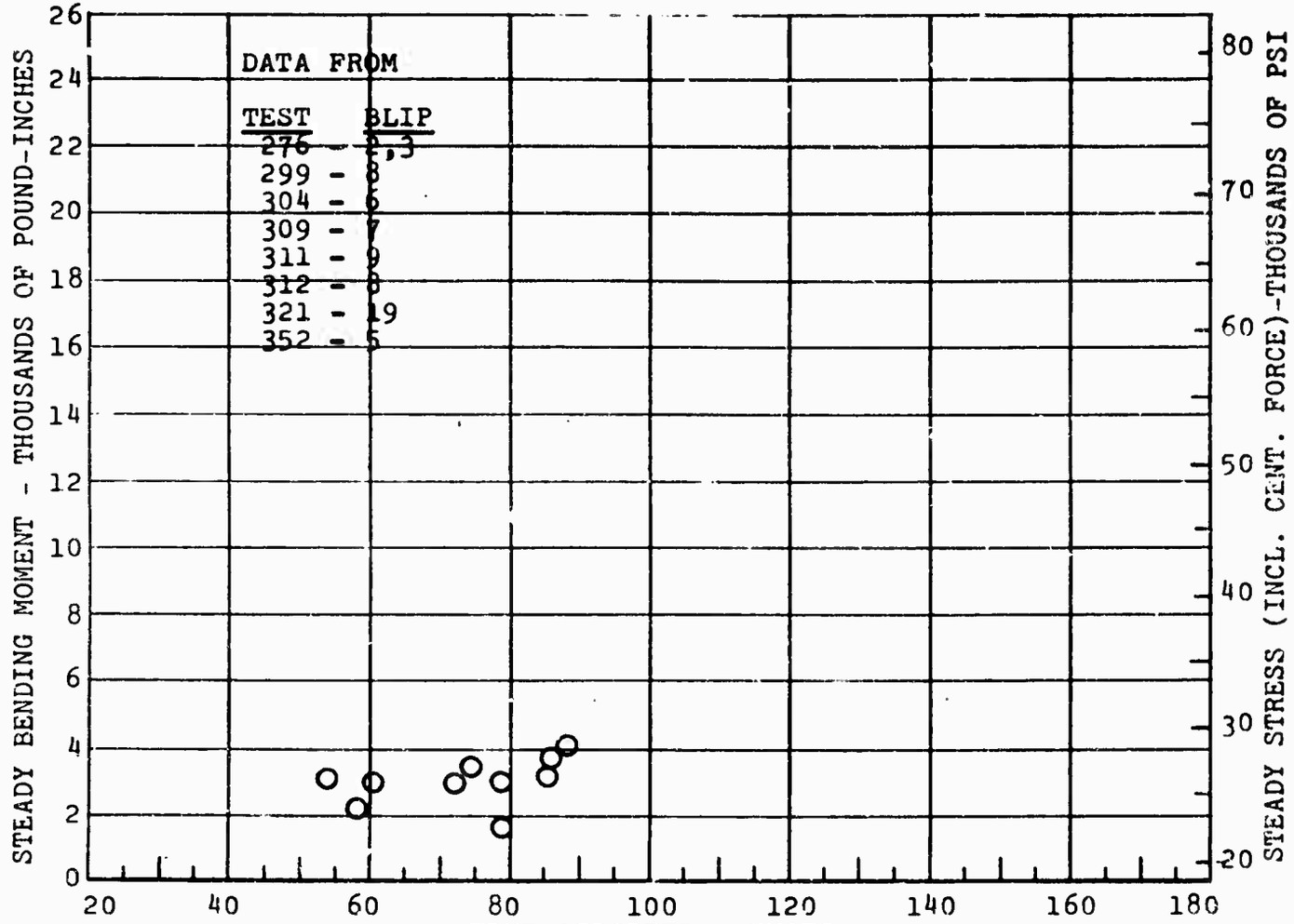


Figure 149. Rotor Blade Flapwise Bending versus Airspeed, Autorotation, Steady Component, Station 211.2.

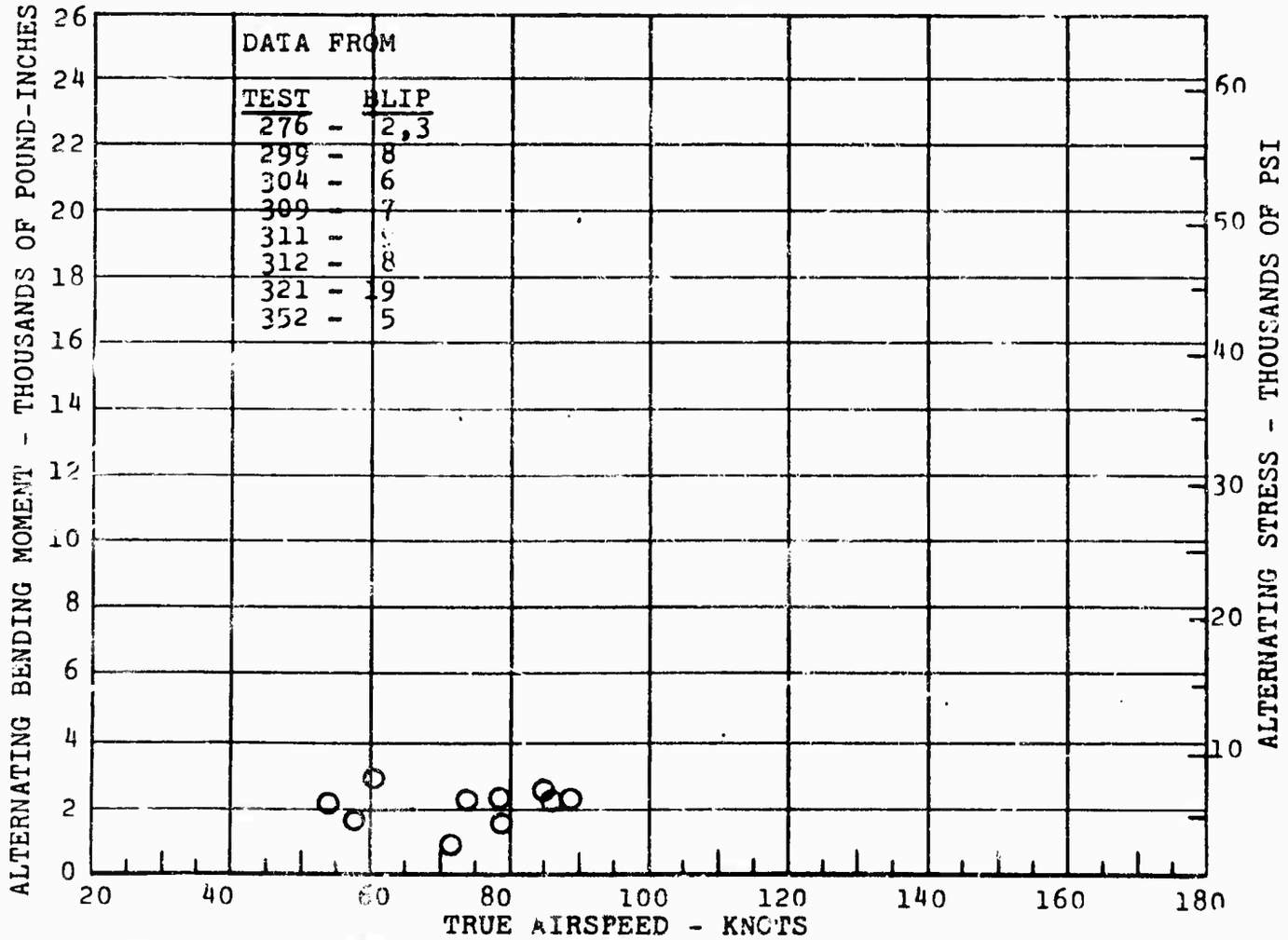


Figure 150. Rotor Blade Flapwise Bending versus Airspeed, Autorotation, Alternating Component, Station 211.2.

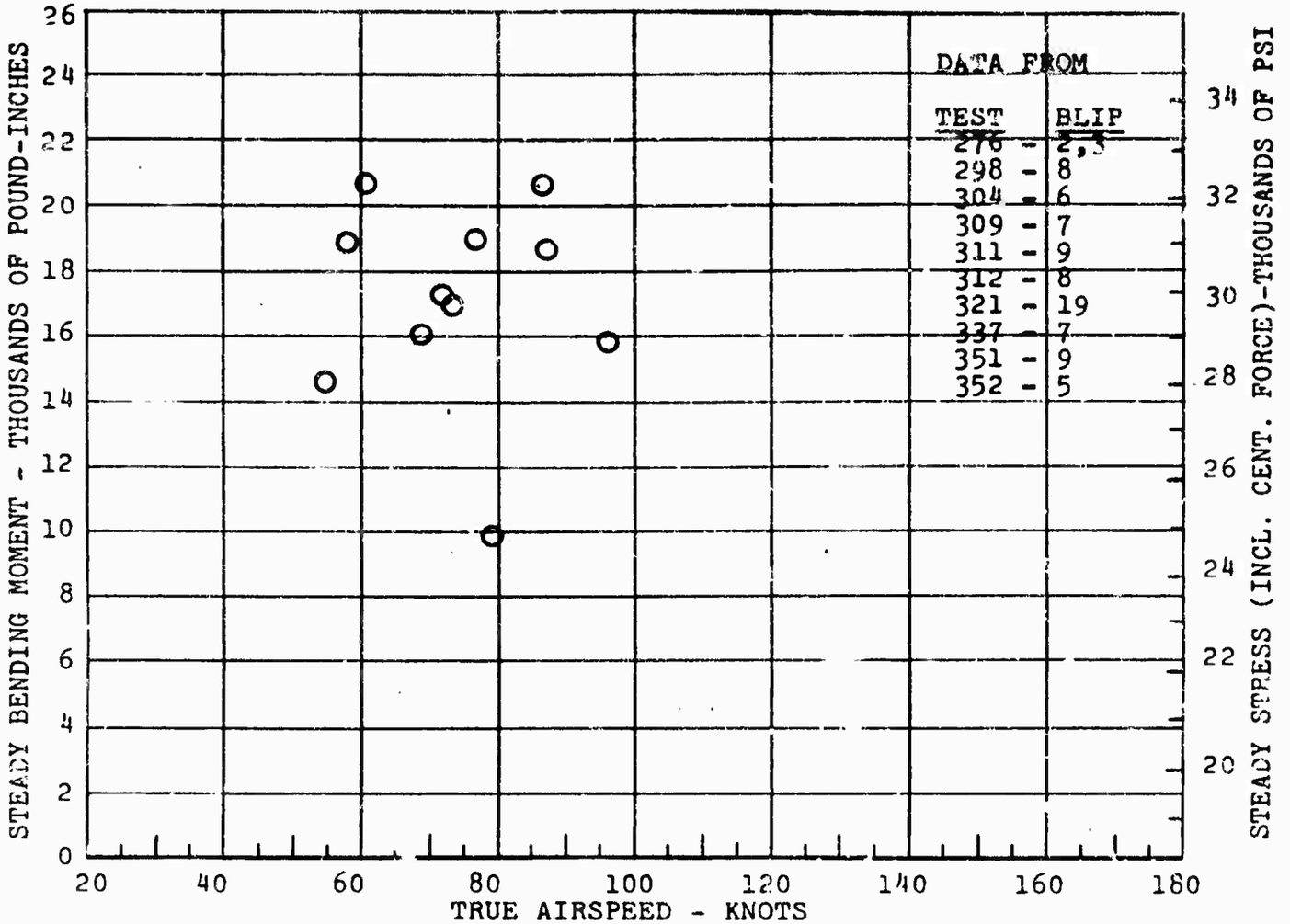


Figure 151. Rotor Blade Chordwise Bending versus Airspeed, Autorotation, Steady Component, Station 46.

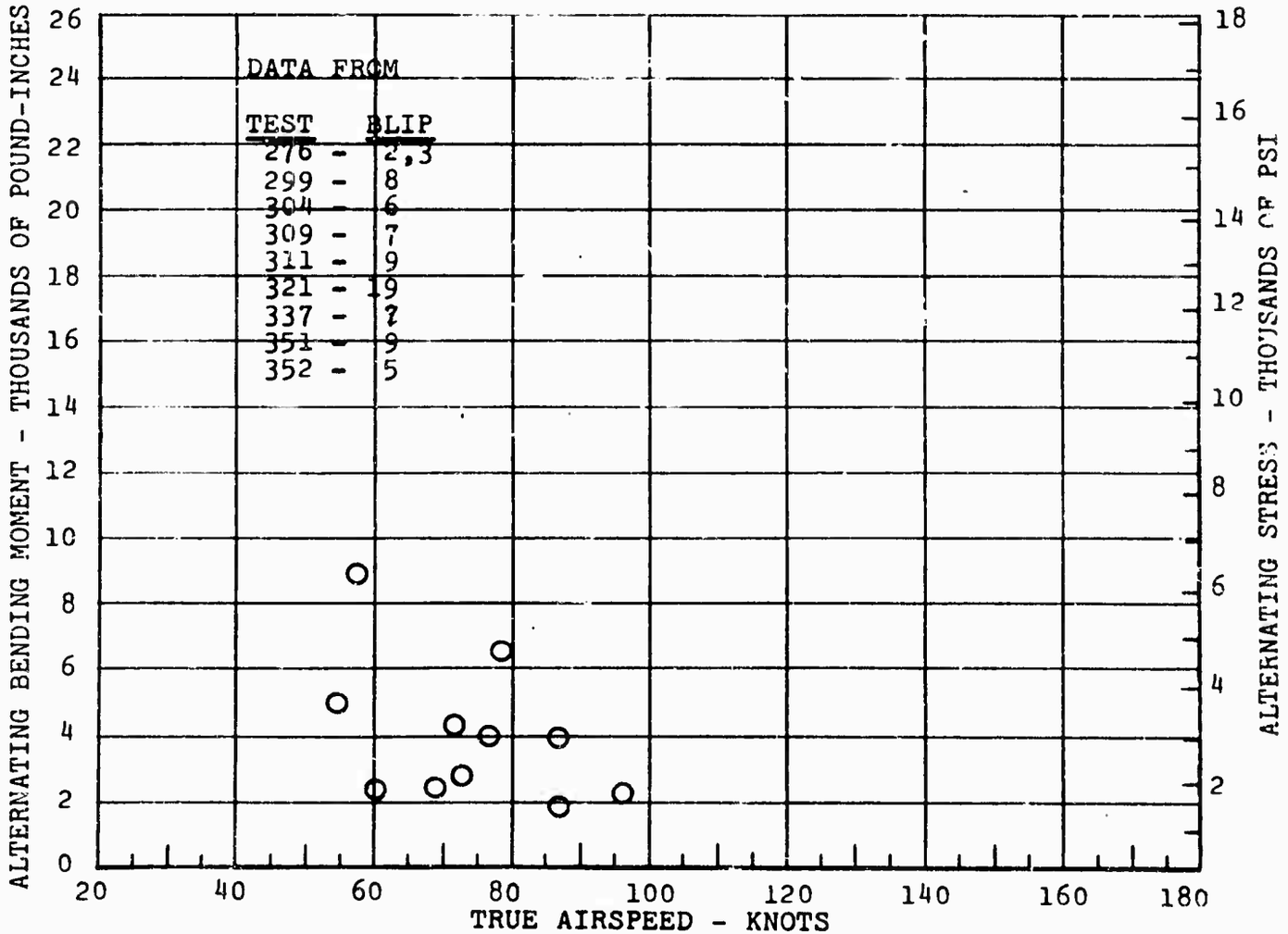


Figure 152. Rotor Blade Chordwise Bending versus Airspeed, Autorotation, Alternating Component, Station 46.

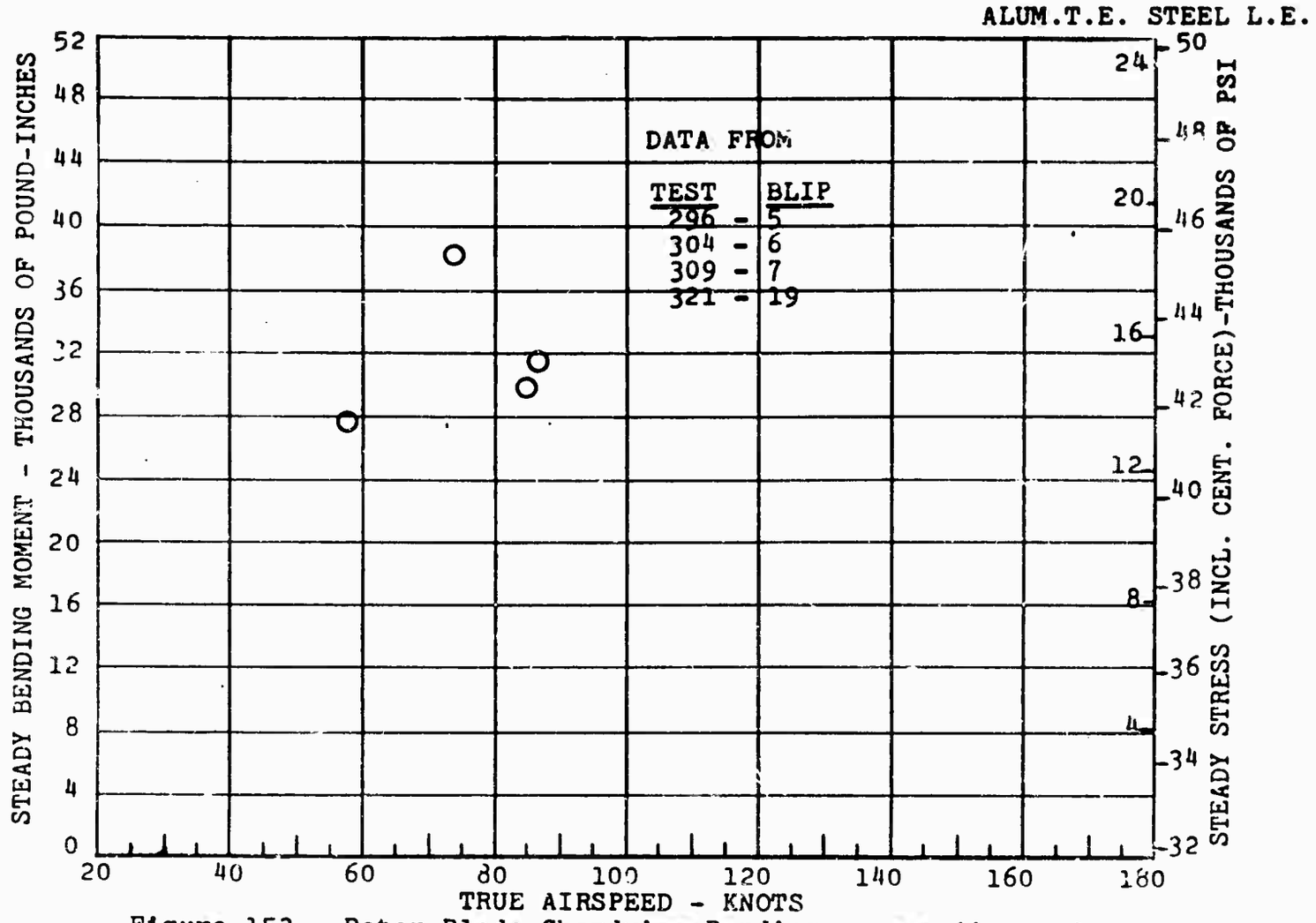


Figure 153. Rotor Blade Chordwise Bending versus Airspeed, Autorotation, Steady Component, Station 131.5.

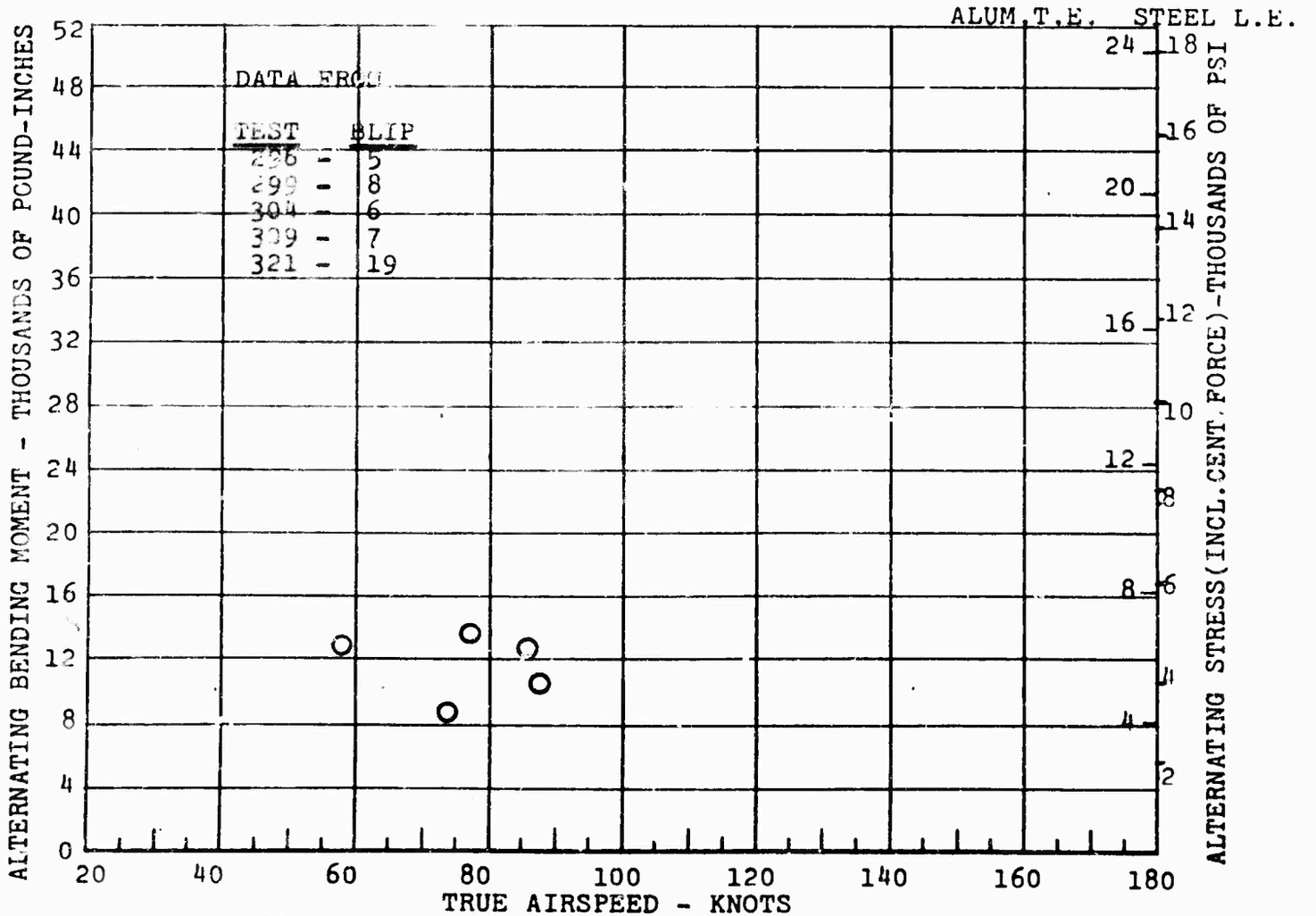


Figure 154. Rotor Blade Chordwise Bending versus Airspeed, Autorotation, Alternating Component, Station 131.5.

## BLADE FLAPPING MOTIONS

Blade flapping data are given in terms of the steady first harmonic longitudinal and lateral flapping components with respect to the shaft. These results for all steady flight conditions over the operating speed range are presented in Figure 155. The vertical spread in the test points at a given speed is predominately due to cyclic stick trim position variations in fuselage angle of attack. It is evident that even with the changes in operating conditions, the flapping angles are restricted to relatively limited amplitudes not exceeding 6 degrees longitudinally or 4 degrees laterally.

## ROTOR PITCH LINK

The steady rotor pitch link loads were mainly compressive and low in magnitude.

The alternating pitch link loads were small at low airspeed and increased gradually and steadily with speed.

In general, they were of lesser magnitude than originally predicted and summarized in PiAC Report 16-S-27, where the maximum alternating pitch link load derived was ±562 pounds at 220 knots. All parts have been analyzed for this fatigue load, and minimum fatigue life of parts under this load is 420 hours (see Figure 156).

## ROTOR SHAFT TORQUE

The rotor shaft torque is well below the allowable limit torque of 241,703 pound-inches (ultimate torque - 362,555 pound-inches) for which it was designed. The plot of rotor shaft torque versus airspeed (Figure 157) shows the measured steady torque for both level flight and forward speed climb.

The alternating torque is very small and increases slightly with an increase in airspeed. It is well below the allowable design alternating torque of ±19,523 pound-inches for infinite fatigue life.

## ROTOR SHAFT LIFT

The rotor shaft lift curve (Figure 158) shows, as expected, that the steady lift on the rotor decreases with airspeed because of unloading by the wing.

The alternating lift is approximately constant with forward speed. Except for a few isolated points it is less than

the ±1073-pound allowable alternating load for infinite design fatigue life.

TABLE VIII. FLIGHT AND BLIP NUMBERS FOR DATA USED IN ROTOR BLADE FLAPPING ANGLE CURVE (FIGURE 155)

| FLIGHT | BLIP | FLIGHT | BLIP |
|---|---|---|---|
| 219 | 5 | 357 | 1,2,3,4,5,6 |
| 274 | 1,2,3,5,6,7 | 392 | 9 |
| 285 | 2,3,4,5,6,7 | 394 | 2,3,4,5,6,7,8,9 |
| 290 | 5,6,7,9,10 | 396 | 1,2 |
| 292 | 10,11,12 | 397 | 1,2,3,4,6 |
| 300 | 4,5 | 398 | 4,5,6,7 |
| 308 | 4,5,6 | 399 | 4,5,6,7,8,9,10 |
| 310 | 1,2 | | 11,12,13 |
| 312 | 4 | 400 | 4,5,6,7 |
| 318 | 3 | 404 | 2,3,4,5,6,7 |
| 332 | 1,2,3,4 | 405 | 1,3,4 |
| 333 | 1,8 | 406 | 1,2,3 |
| 350 | 1,2,3,4,5,6,7 | 407 | 2,3,4 |
| 355 | 4,5,6,7 | 409 | 1,3 |
| 356 | 2,3,4,5,6,7,8,9 | 411 | 1,2 |

ROTOR-HEAD HORIZONTAL FORCE AND MOMENT AND REACTIONS AT UPPER AND LOWER ROTOR SHAFT SUPPORT BEARINGS (See Figure 159)

The vertical rotor shaft has loads applied to it at the rotor head: the lift, a local moment caused by offset of the rotor blade horizontal pin from the axis of rotation, and a horizontal force caused by drag on the rotor and inclination of the rotor thrust vector. From strain gage measurements on the rotor shaft taken in flight tests, the bending-moment diagram, shear diagram, reactions of the upper and lower bearings, and horizontal force at the rotor hub may be obtained as follows.

Assuming that no fixity in bending is afforded by either the upper or lower bearing, as in the stress analysis, the horizontal reaction $R_L$ on the lower bearing can be obtained directly from the moment at the lower bending gage:

$$R_L = M_{LG}/21.87 \qquad (68)$$

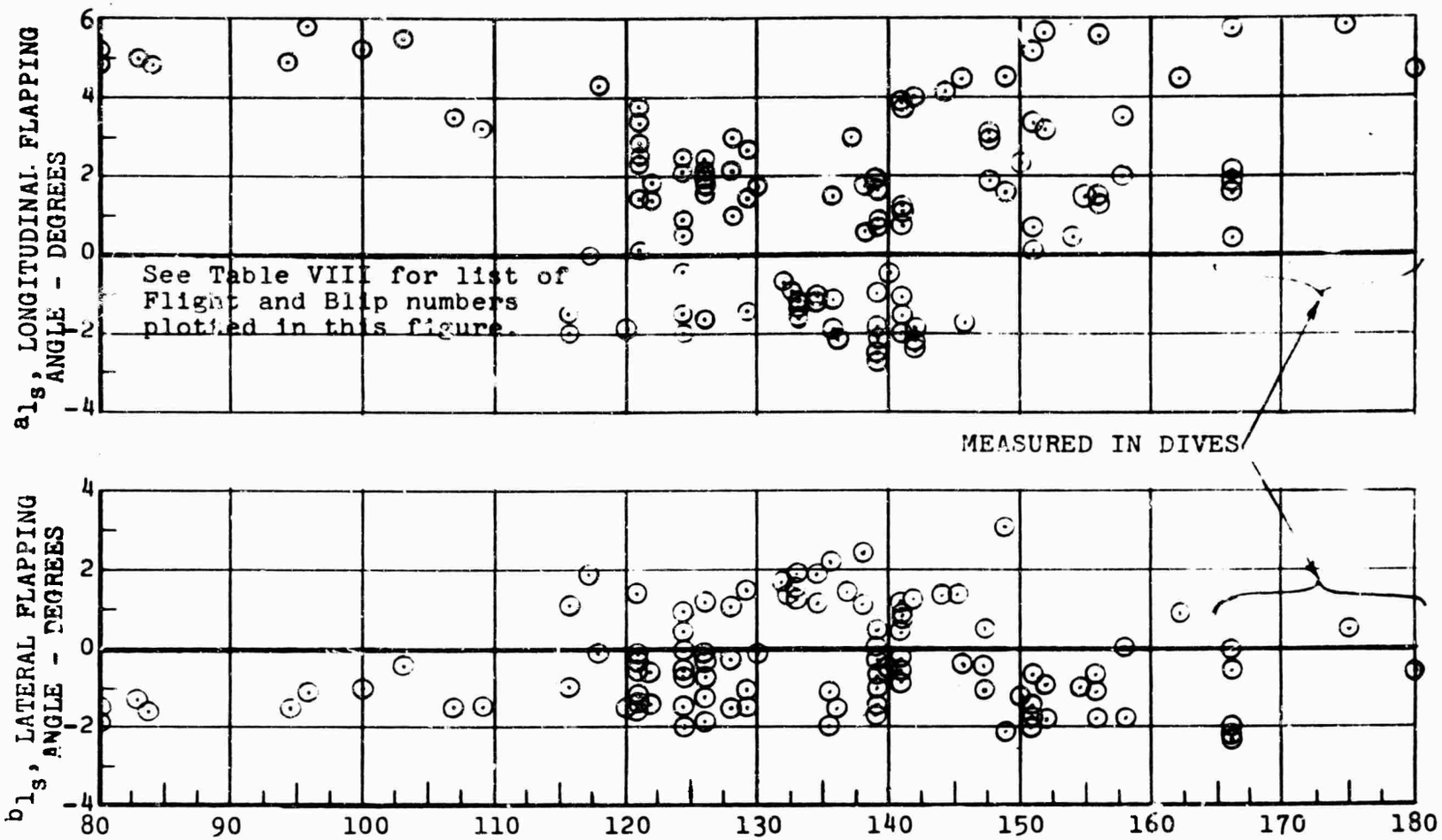


Figure 155. Rotor Blade Flapping Angle versus Airspeed.

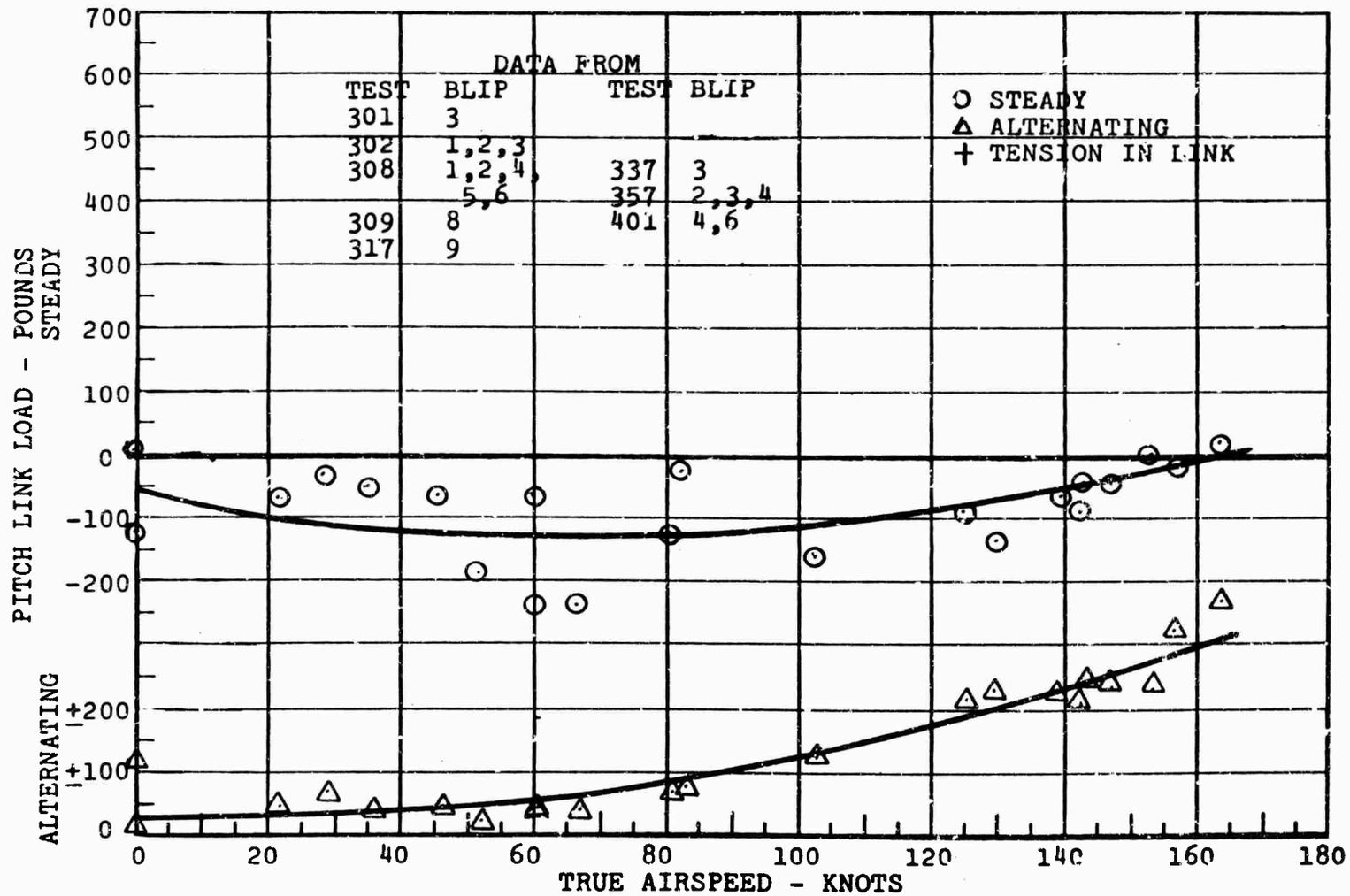


Figure 156. Rotor Pitch Link Load versus Airspeed.

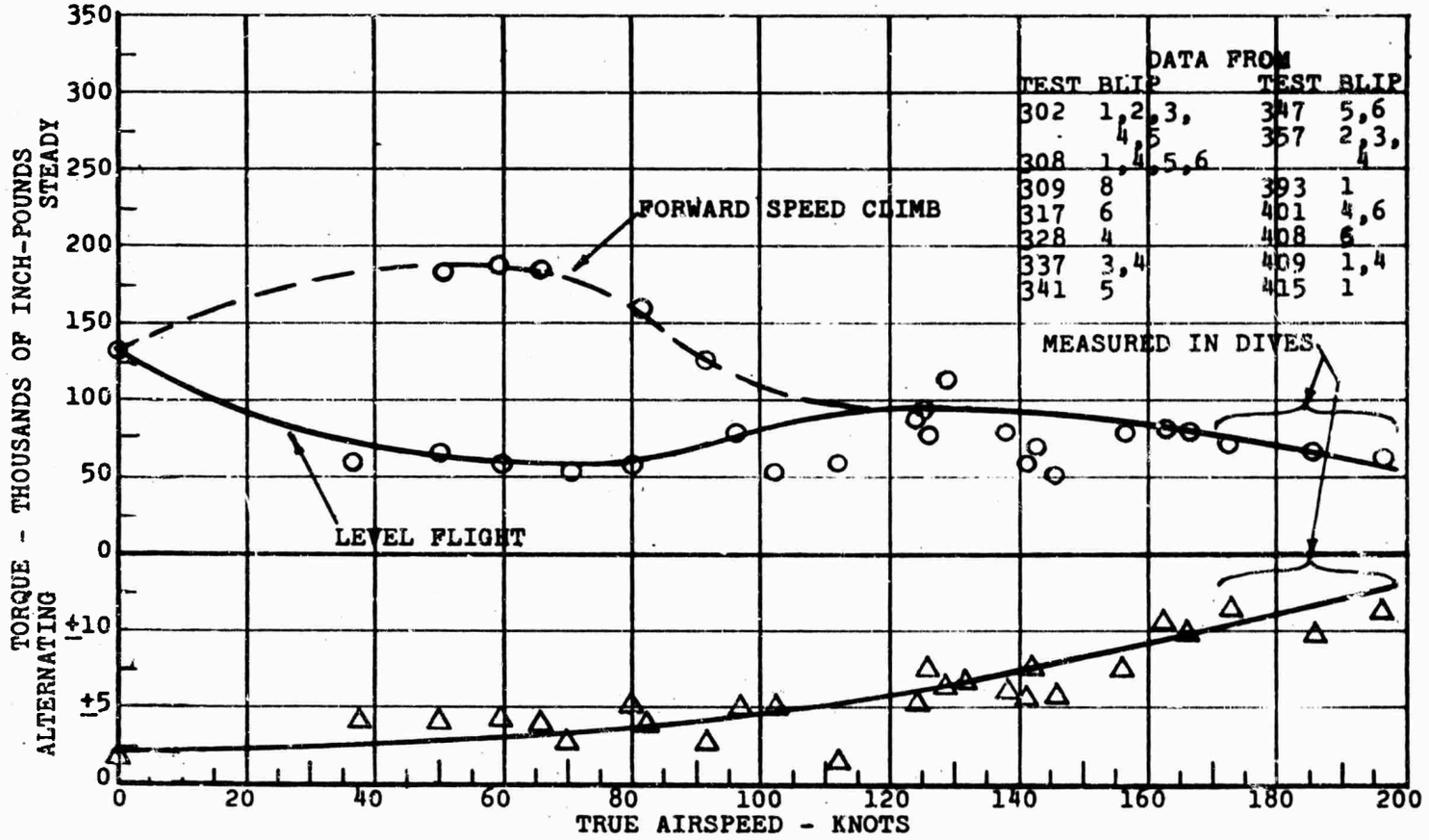


Figure 157. Rotor Shaft Torque versus Airspeed.

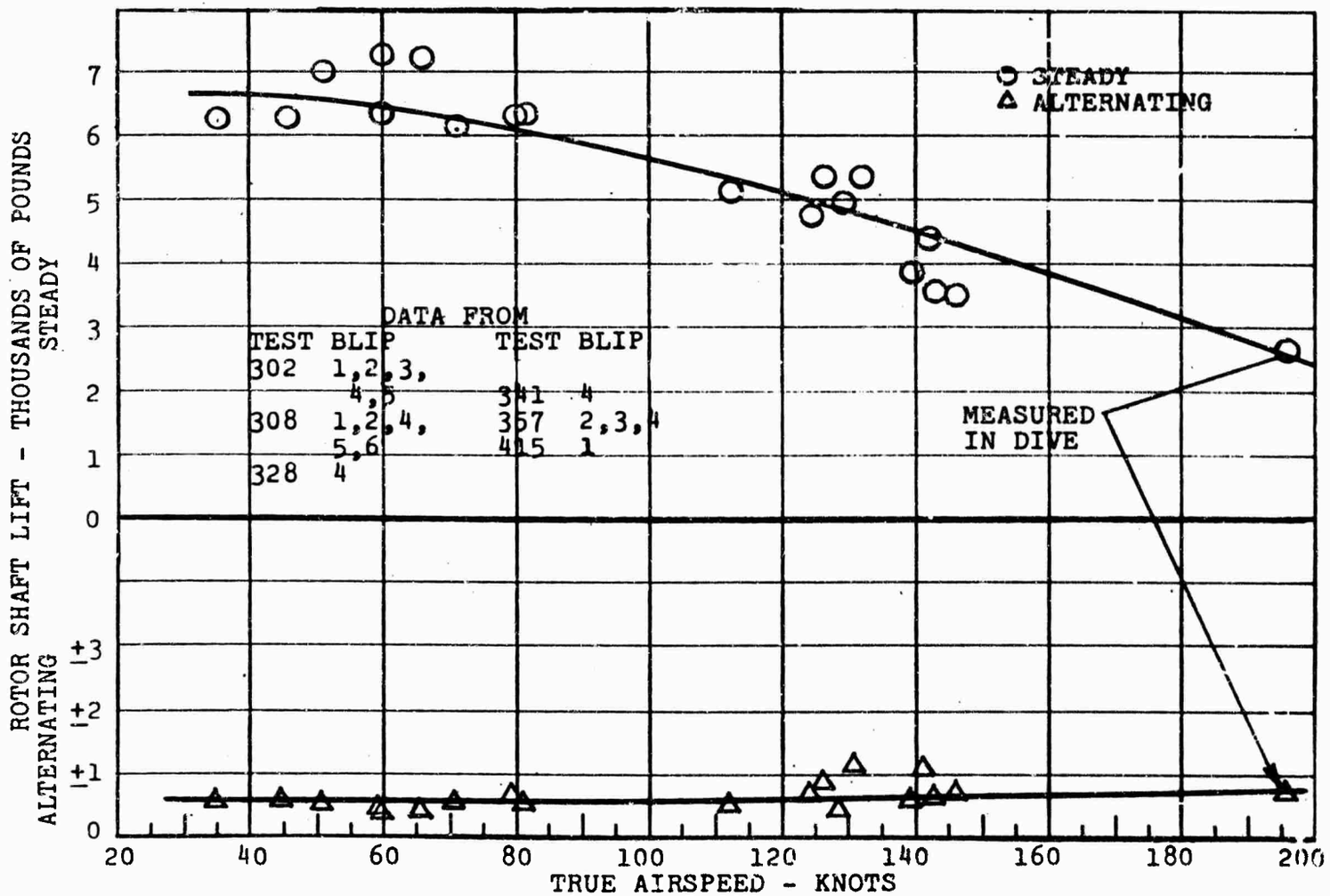


Figure 158. Rotor Shaft Lift versus Airspeed.

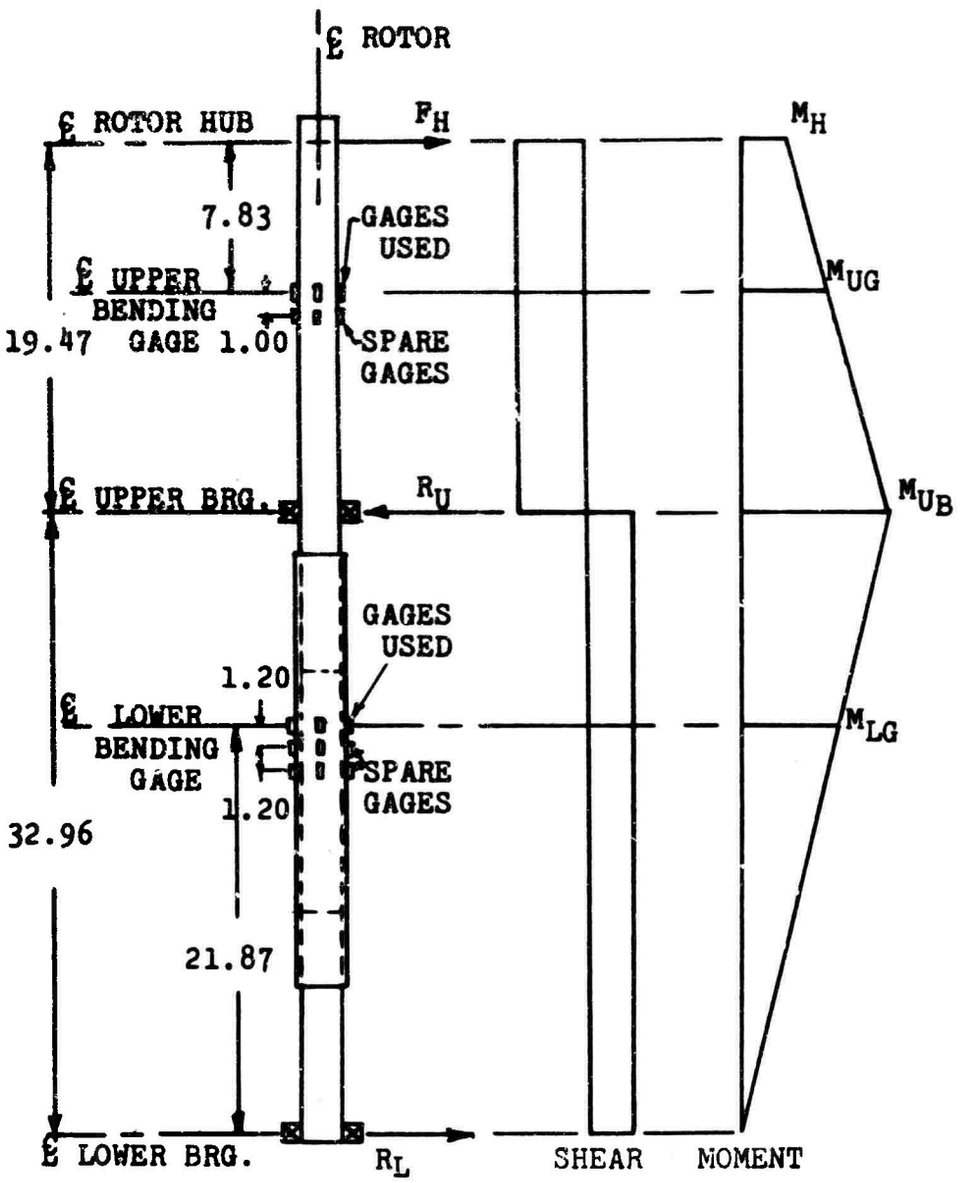


Figure 159. Geometry of Rotor Shaft
(Showing Bearing Supports, Strain Gages for Bending and Typical Shear and Moment Diagrams with Symbols.)

The slope of the bending-moment curve is constant until it reaches the upper bearing support, and the value of the bending moment at the upper bearing is

$$M_{UB} = 1.5071\ M_{LG} \tag{69}$$

Above the upper bearing, the moment curve is also a straight line of constant slope. Knowing the bending moment at the upper bearing and also at the upper bending gage, the moment at the rotor hub can be determined. The rotor hub moment $M_H$ is

$$\begin{aligned} M_H &= M_{UG} - \left[(M_{UB} - M_{UG}) \times \frac{7.83}{11.64}\right] \\ &= M_{UG} - \left[(M_{UB} - M_{UG})\ (0.6727)\right] \end{aligned} \tag{70}$$

The local moment at the rotor head is caused by the effective offset of the rotor blade lift. All other moments are caused by drag or longitudinal or lateral forces on the rotor.

The rotor lift is known from flight test measurements.

The horizontal force of the rotor hub $F_H$ may be obtained from knowing the moment at the upper bearing:

$$F_H = (M_{UB} - M_H)/\ 19.47 \tag{71}$$

The horizontal reaction at the upper bearing $R_U$ can be obtained by taking moments about the upper gage location:

$$R_U = (44.60R_L - M_{UG})/\ 11.64 \tag{72}$$

For a check,

$$\Sigma\ (F_H + R_U + R_L) = 0$$

Tabulations of these loads and moments on the rotor shaft follow for various flight conditons.

TABLE IX.
ROTOR SHAFT ALTERNATING LOADS AND MOMENTS,
HOVER

| FLIGHT TEST & BLIP NO. | TRUE AIRSPEED (Kn.) | $M_{LG}$ (lb-in.) | $M_{UG}$ (lb-in.) | $M_{UB}$ (lb-in.) | $M_H$ (lb-in.) | $R_L$ (lb.) | $F_H$ (lb) | $R_U$ (lb) |
|---|---|---|---|---|---|---|---|---|
| 309-8 | 0 | 17,828 | 13,982 | 26,868 | 5,314 | 815 | 1,107 | 1,922 |
| 317-9 | 0 | 16,938 | 18,063 | 25,527 | 13,042 | 774 | 641 | 1,414 |
| 355-1 | 0 | 32,515 | 28,472 | 49,003 | 14,661 | 1,487 | 1,764 | 3,252 |
| 286-1 | 0 | 13,654 | 7,884 | 20,578 | -655 | 624 | 1,090 | 1,714 |

TABLE X.
ROTOR SHAFT ALTERNATING LOADS AND MOMENTS,
RIGHT SIDEWARD FLIGHT

| FLIGHT TEST & BLIP NO. | TRUE AIRSPEED (Kn.) | $M_{LG}$ (lb-in.) | $M_{UG}$ (lb-in.) | $M_{UB}$ (lb-in.) | $M_H$ (lb-in.) | $R_L$ (lb) | $F_H$ (lb) | $R_U$ (lb) |
|---|---|---|---|---|---|---|---|---|
| 416-1 | 10.5 | 15,341 | 12,887 | 23,120 | 5,987 | 701 | 880 | 1,580 |
| 416-2 | 21.0 | 15,609 | 12,701 | 23,542 | 5,420 | 714 | 930 | 1,645 |
| 416-3 | 31.5 | 31,467 | 37,007 | 47,424 | 30,117 | 1,439 | 890 | 2,328 |
| 417-4 | 0 | 35,992 | 42,691 | 54,244 | 34,919 | 1,646 | 992 | 2,639 |

TABLE XI.
ROTOR SHAFT ALTERNATING LOADS AND MOMENTS,
LEFT SIDEWARD FLIGHT

| FLIGHT TEST & BLIP NO. | TRUE AIRSPEED (Kn.) | $M_{LG}$ (lb-in.) | $M_{UG}$ (lb-in.) | $M_{UB}$ (lb-in.) | $M_H$ (lb-in.) | $R_L$ (lb) | $F_H$ (lb) | $R_U$ (lb) |
|---|---|---|---|---|---|---|---|---|
| 416-5 | -10.4 | 14,726 | 14,678 | 22,194 | 9,622 | 673 | 646 | 1,318 |
| 416-6 | -21.0 | 18,695 | 13,976 | 28,175 | 4,424 | 855 | 1,220 | 2,075 |
| 416-7 | -31.5 | 14,892 | 14,500 | 22,444 | 9,156 | 681 | 682 | 1,364 |
| 417-5 | 0 | 23,536 | 29,315 | 35,471 | 25,174 | 1,076 | 529 | 1,604 |

TABLE XII.
ROTOR SHAFT ALTERNATING LOADS AND MOMENTS,
REARWARD FLIGHT

| FLIGHT TEST & BLIP NO. | TRUE AIRSPEED (Kn.) | $M_{LG}$ (lb-in.) | $M_{UG}$ (lb-in.) | $M_{UB}$ (lb-in.) | $M_H$ (lb-in.) | $R_L$ (lb) | $F_H$ (lb) | $R_U$ (lb) |
|---|---|---|---|---|---|---|---|---|
| 395-1 | 10.2 | 12,888 | 15,033 | 19,424 | 12,079 | 589 | 377 | 965 |
| 395-2 | 20.6 | 15,949 | 21,343 | 24,037 | 19,531 | 729 | 231 | 960 |
| 395-3 | 30.8 | 23,900 | 25,958 | 36,020 | 19,189 | 1,093 | 864 | 1,958 |
| 417-7 | 0 | 21,230 | 26,934 | 31,996 | 23,529 | 971 | 435 | 1,407 |

TABLE XIII.

ROTOR SHAFT ALTERNATING LOADS AND MOMENTS,
VERTICAL CLIMB

| FLIGHT TEST & BLIP NO. | TRUE AIRSPEED (Kn.) | $M_{LG}$ (lb-in) | $M_{UG}$ (lb-in) | $M_{UB}$ (lb-in) | $M_H$ (lb-in) | $R_L$ (lb) | $F_H$ (lb) | $R_U$ (lb) |
|---|---|---|---|---|---|---|---|---|
| 327-1 | 0 | 16,624 | 21,116 | 25,054 | 18,467 | 760 | 338 | 1,098 |
| 327-4 | 0 | 22,204 | 21,116 | 33,464 | 12,810 | 1,015 | 1,061 | 2,075 |
| 327-5 | 0 | 17,764 | 22,071 | 26,772 | 18,909 | 812 | 404 | 1,215 |
| 327-3 | 0 | 24,251 | 19,084 | 36,549 | 7,335 | 1,109 | 1,500 | 2,610 |
| 327-2 | 0 | 18,320 | 22,954 | 27,610 | 19,822 | 838 | 400 | 1,239 |

TABLE XIV.
ROTOR SHAFT ALTERNATING LOADS AND MOMENTS,
FORWARD SPEED CLIMB

| FLIGHT TEST & BLIP NO. | TRUE AIRSPEED (Kn.) | $M_{LG}$ (lb-in) | $M_{UG}$ (lb-in) | $M_{UB}$ (lb-in) | $M_H$ (lb-in) | $R_L$ (lb) | $F_H$ (lb) | $R_U$ (lb) |
|---|---|---|---|---|---|---|---|---|
| 296-1 | 98.5 | 10,309 | 5,982 | 15,537 | -446 | 471 | 821 | 1,292 |
| 296-2 | 102 | 13,104 | 7,138 | 19,749 | -1,345 | 599 | 1,083 | 1,683 |
| 297-1 | 40 | 12,347 | 9,146 | 18,608 | 2,781 | 564 | 813 | 1,375 |
| 297-2 | 54.7 | 13,249 | 10,142 | 19,968 | 3,536 | 606 | 844 | 1,450 |
| 312-2 | 53.2 | 14,392 | 15,176 | 21,690 | 10,794 | 658 | 560 | 1,218 |
| 308-1 | 81.8 | 10,002 | 5,939 | 15,073 | -205 | 457 | 785 | 1,241 |
| 308-2 | 80.1 | 11,618 | 12,304 | 17,508 | 8,803 | 531 | 447 | 978 |

TABLE XV.
ROTOR SHAFT ALTERNATING LOADS AND MOMENTS,
LEVEL FLIGHT

| FLIGHT TEST & BLIP NO. | TRUE AIRSPEED (Kn.) | $M_{LG}$ (lb-in) | $M_{UG}$ (lb-in) | $M_{UB}$ (lb-in) | $M_H$ (lb-in) | $R_L$ (lb) | $F_H$ (lb) | $R_U$ (lb) |
|---|---|---|---|---|---|---|---|---|
| 285-2 | 120.3 | 22,556 | 18,557 | 33,994 | 8,173 | 1,031 | 1,326 | 2,358 |
| 285-3 | 124.2 | 23,975 | 8,587 | 36,133 | -9,943 | 1,096 | 2,367 | 3,463 |
| 285-6 | 128.6 | 17,521 | 7,018 | 26,406 | -6,024 | 801 | 1,666 | 2,467 |
| 286-3 | 110.6 | 13,684 | 13,625 | 20,623 | 8,917 | 626 | 601 | 1,227 |
| 296-4 | 124.3 | 23,531 | 12,366 | 35,464 | -3,172 | 1,076 | 1,984 | 3,060 |
| 312-5 | 139.7 | 20,559 | 26,097 | 30,984 | 22,810 | 940 | 420 | 1,359 |
| 321-10 | 47.6 | 21,206 | 6,380 | 31,960 | -10,828 | 970 | 2,198 | 3,165 |
| 321-13 | 62.4 | 20,188 | 5,601 | 30,425 | -11,098 | 923 | 2,133 | 3,055 |
| 308-4 | 128.3 | 12,647 | 5,376 | 19,059 | -3,829 | 578 | 1,179 | 1,753 |
| 308-5 | 138.5 | 11,765 | 12,418 | 17,730 | 8,845 | 538 | 456 | 994 |
| 308-6 | 141.1 | 15,288 | 7,747 | 23,039 | -2,540 | 699 | 1,314 | 2,013 |
| 408-5 | 171.5 | 40,674 | 36,552 | 61,300 | 19,904 | 1,860 | 2,126 | 3,986 |
| 408-6 | 172.2 | 45,709 | 42,021 | 68,888 | 23,948 | 2,090 | 2,308 | 4,398 |
| 415-1 | 195. | 44,989 | 39,102 | 67,803 | 19,795 | 2,057 | 2,466 | 4,522 |

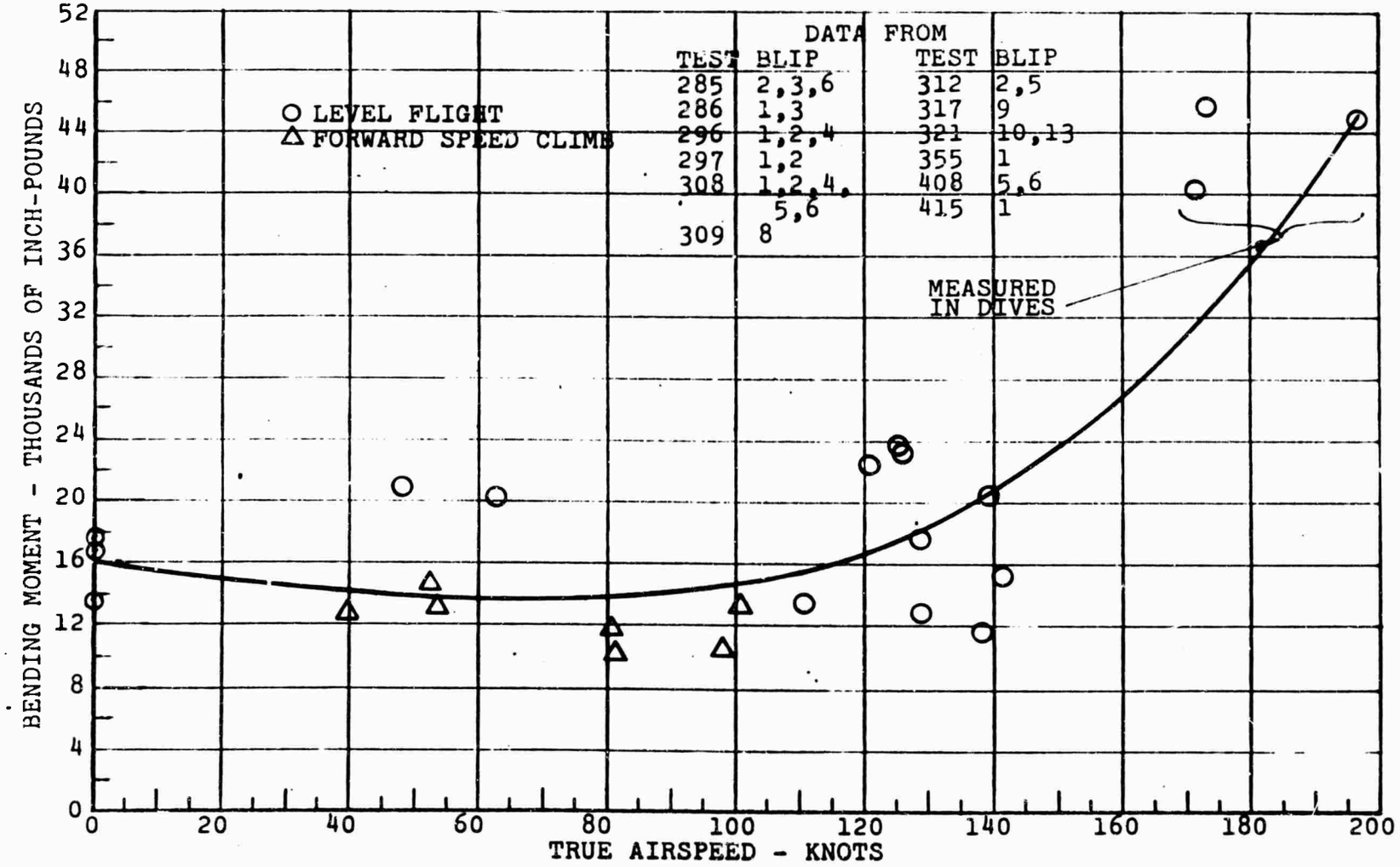


Figure 160. Alternating Bending Moment versus Airspeed - Rotor Shaft, Lower Gage.

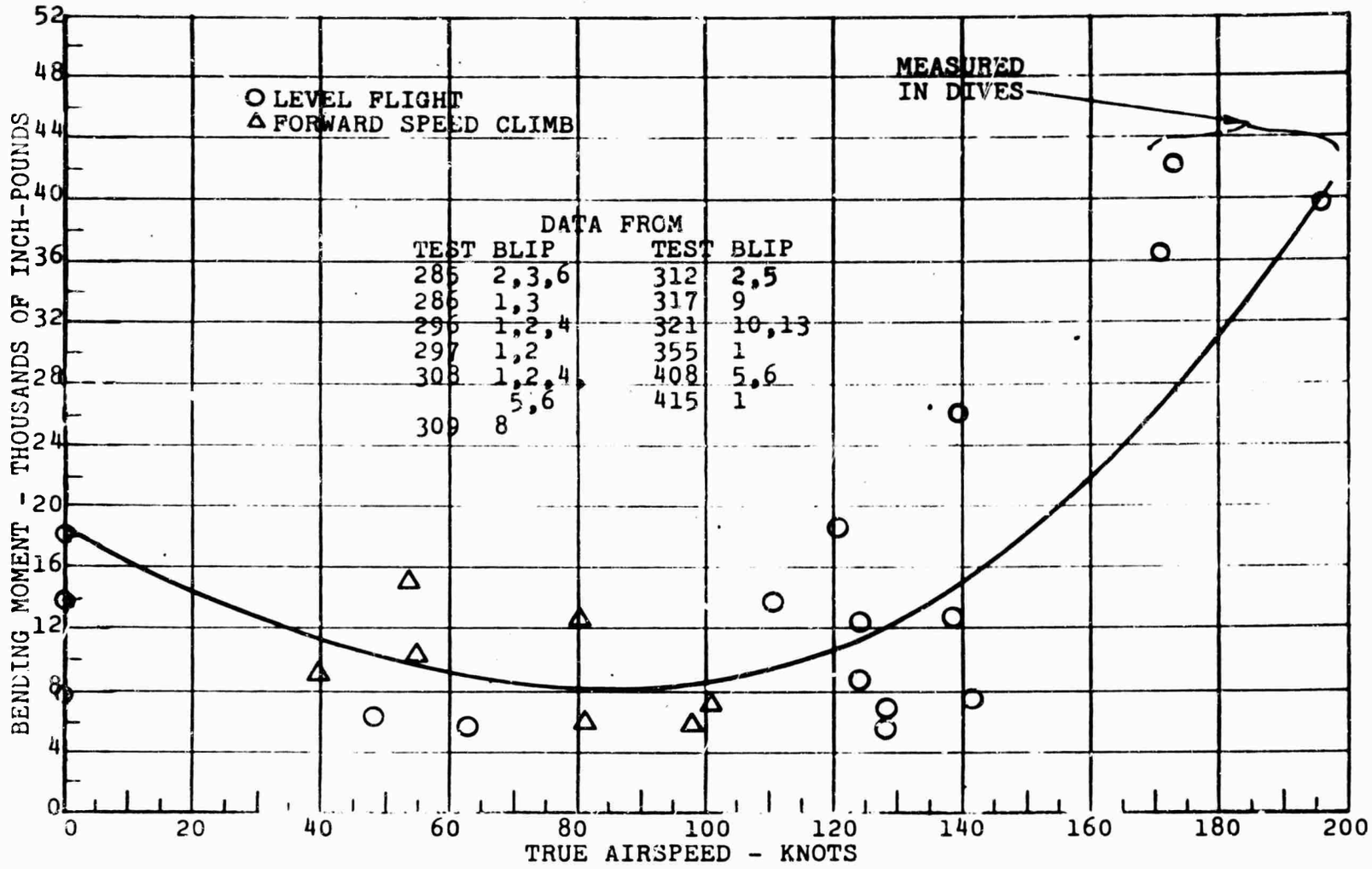


Figure 161. Alternating Bending Moment versus Airspeed - Rotor Shaft, Upper Gage.

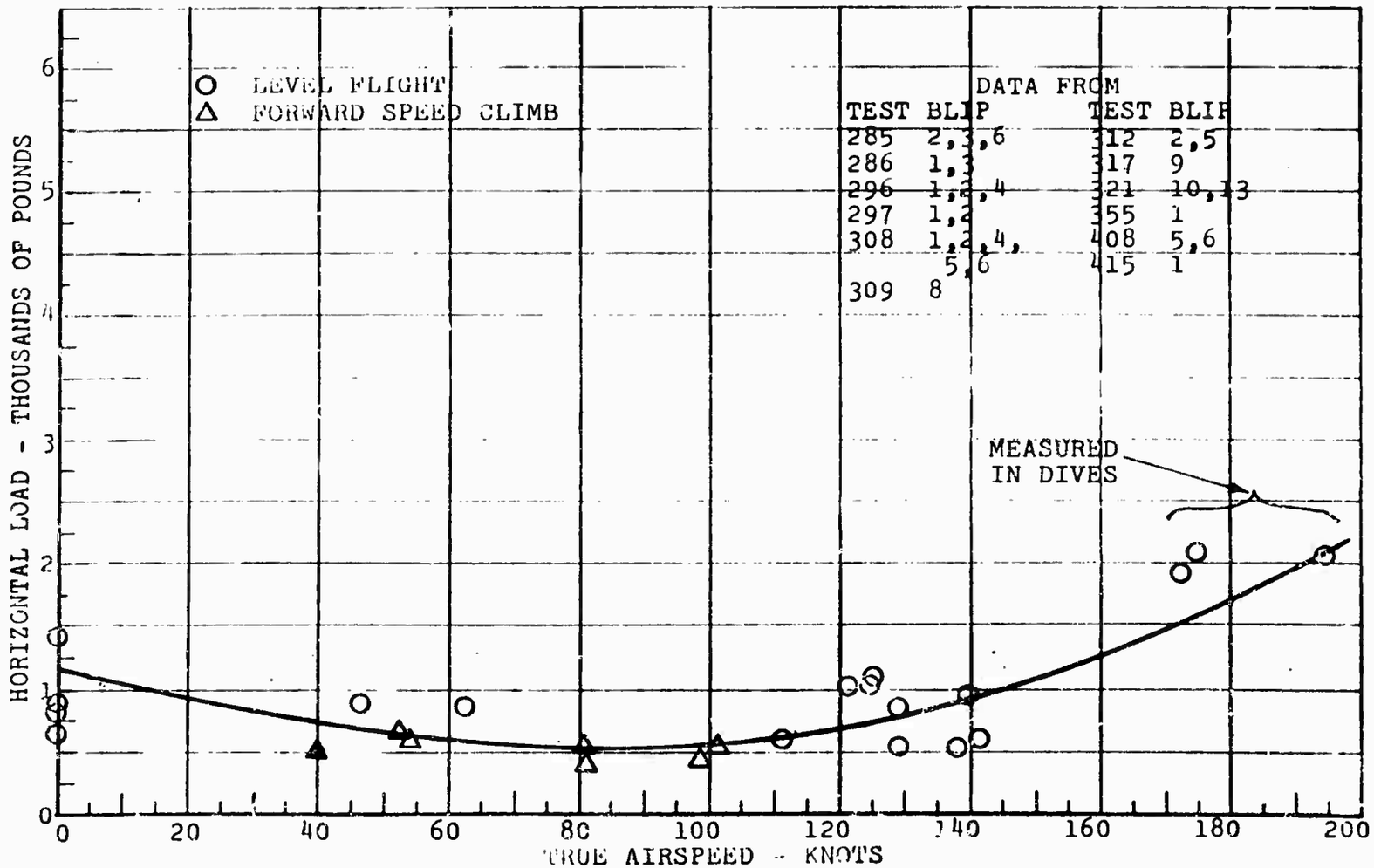


Figure 162. Rotor Shaft Horizontal Reaction at Lower Bearing versus Airspeed.

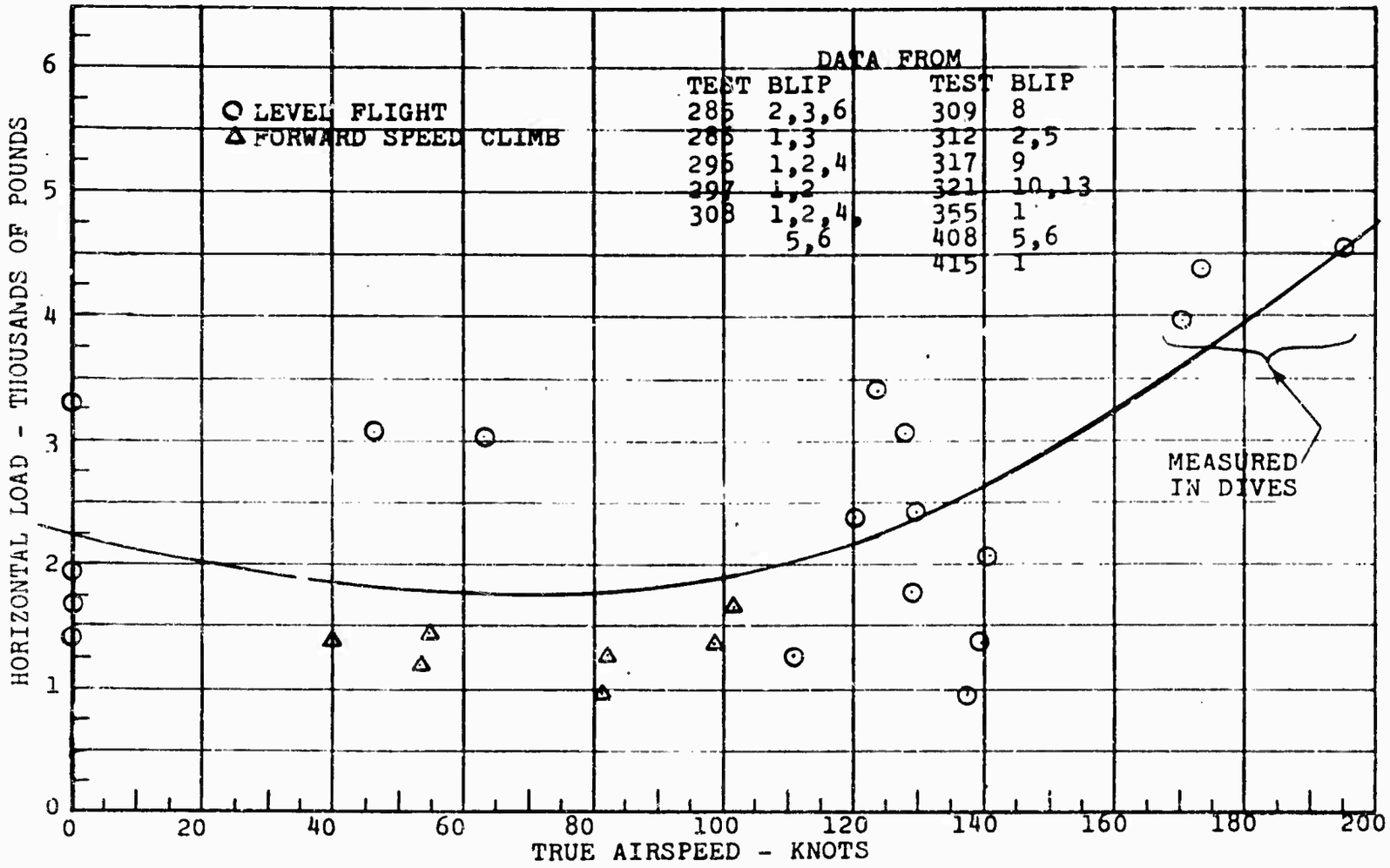


**Figure 163.** Rotor Shaft, Horizontal Reaction at Upper Bearing versus Airspeed.

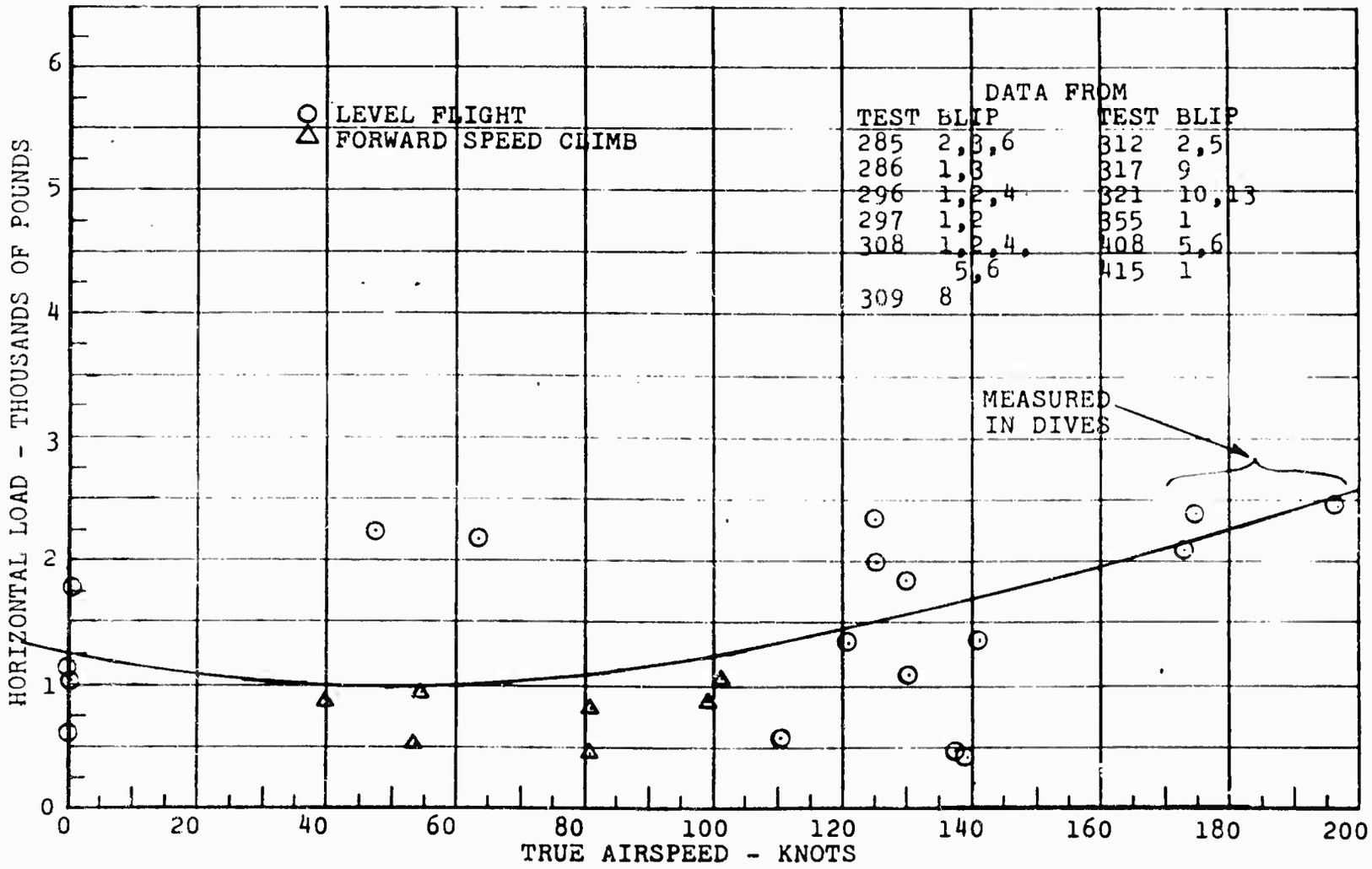


Figure 164. Rotor Shaft, Horizontal Reaction at Rotor Head versus Airspeed.

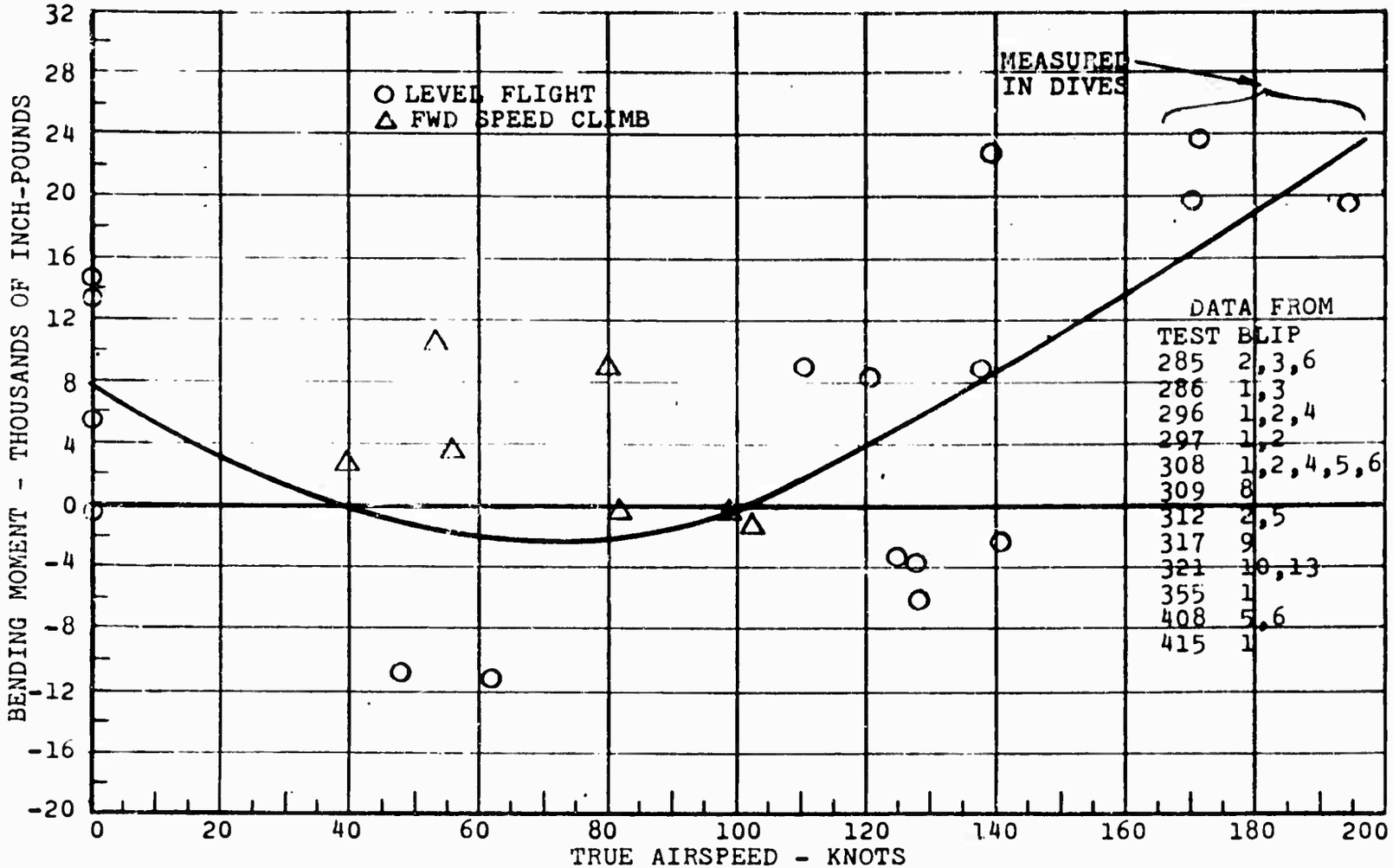


Figure 165. Rotor Shaft, Bending Moment at Rotor Head versus Airspeed.

## ROTOR SHAFT BENDING

The rotor shaft alternating bending moments at the lower and upper strain gage locations, the horizontal load at the rotor head, the horizontal reactions at the lower and upper bearings, and the moment at the rotor head are plotted versus airspeed of the aircraft in level flight and forward-speed climb (Figures 160 through 165).

They all exhibit similar characteristics beginning with a value at hover, then decreasing slightly with an increase in airspeed to about 80 knots, and finally increasing with a further increase in speed.

For airspeed up to approximately 160 knots, the rotor-shaft moments are within the fatigue limits for infinite life. Moments at speed above approximately 160 knots could limit the life of the rotor shaft, depending on the results of bench fatigue tests, which were not made under this program.

## TAIL PROPELLER SHAFT

A plot of propeller-shaft torsion versus forward speed is shown in Figure 166. It shows that the steady torsion in the propeller shaft increases with an increase in airspeed. The alternating torsion remains constant with airspeed at a value of approximately $\pm$1000 inch-pounds. This is well below the fatigue design allowable of 31000 $\pm$4650 inch-pounds for infinite fatigue life.

## TAIL PROPELLER

Propeller hub bending moments are rather small. The steady moments decrease slightly with an increase in airspeed, while the alternating bending moments remain nearly constant with forward speed (see Figure 167).

The tail propeller stresses are calculated using the bending moments measured in flight. Centrifugal-force stress is added directly to the steady bending stress to obtain total steady stress. The calculated bending stresses are slightly conservative, since the minimum section modulus is used. Actually, the airfoil section is unsymmetrical, so that although the moment of inertia is one value for any particular blade station, the distance from the neutral axis to the extreme fiber differs between surfaces.

Propeller flapwise stresses at blade stations 13.2 (40 percent) and 16.5 (50 percent) show a minimum of scatter (Figures 168 and 169), but for those at blade stations 23.1

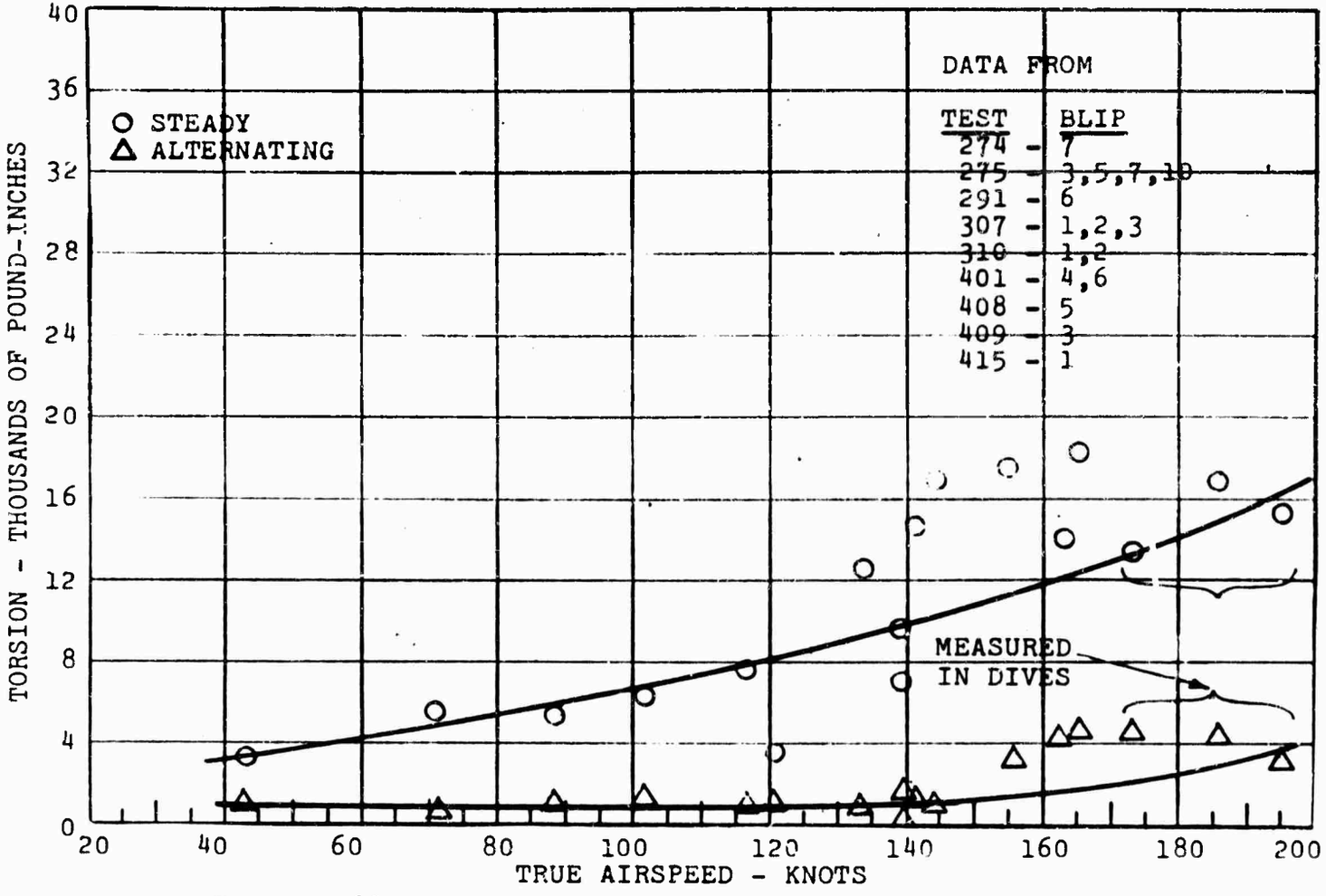


Figure 166. Tail Propeller Shaft Torsion versus Airspeed.

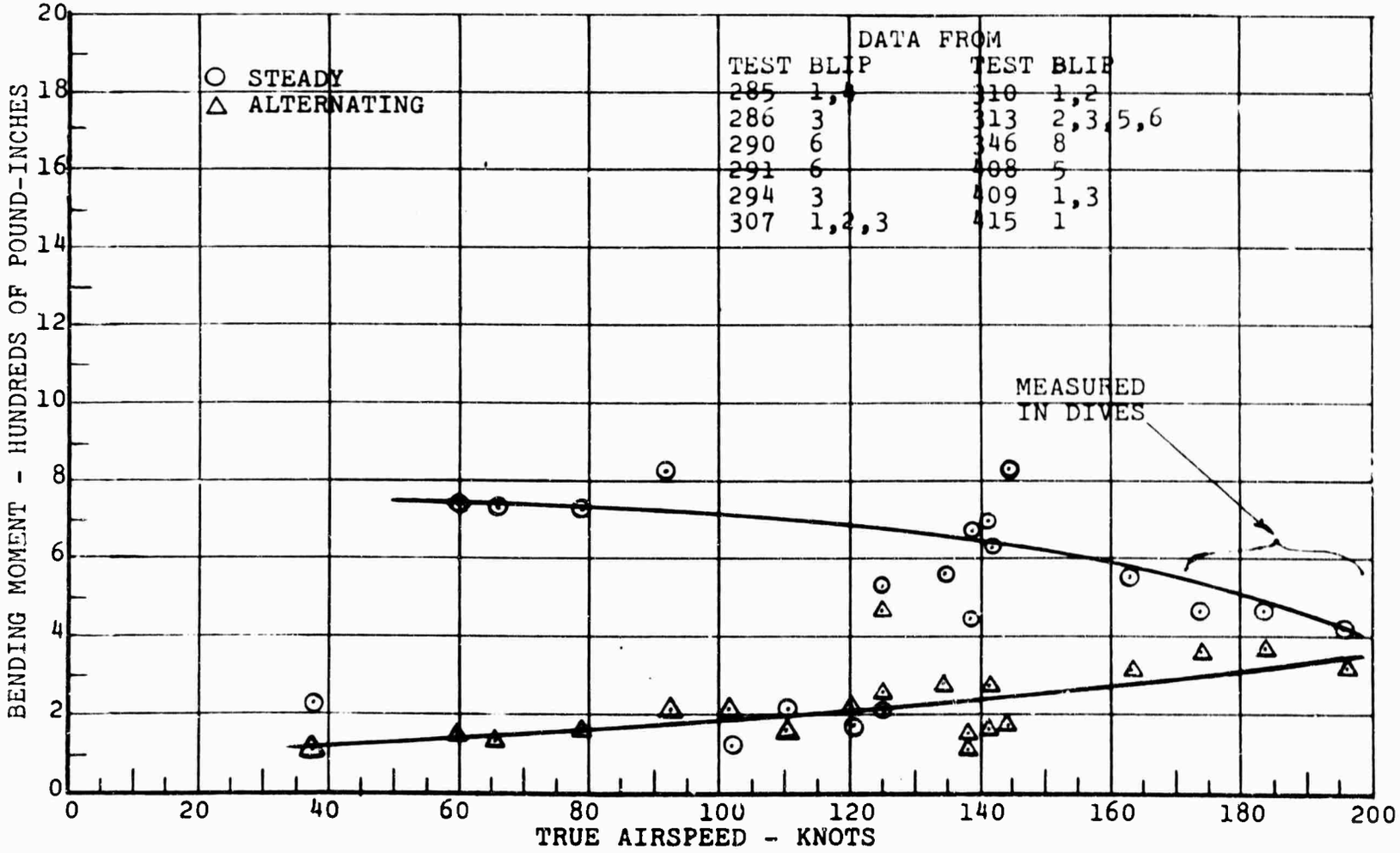


Figure 167. Tail Propeller Hub Bending versus Airspeed.

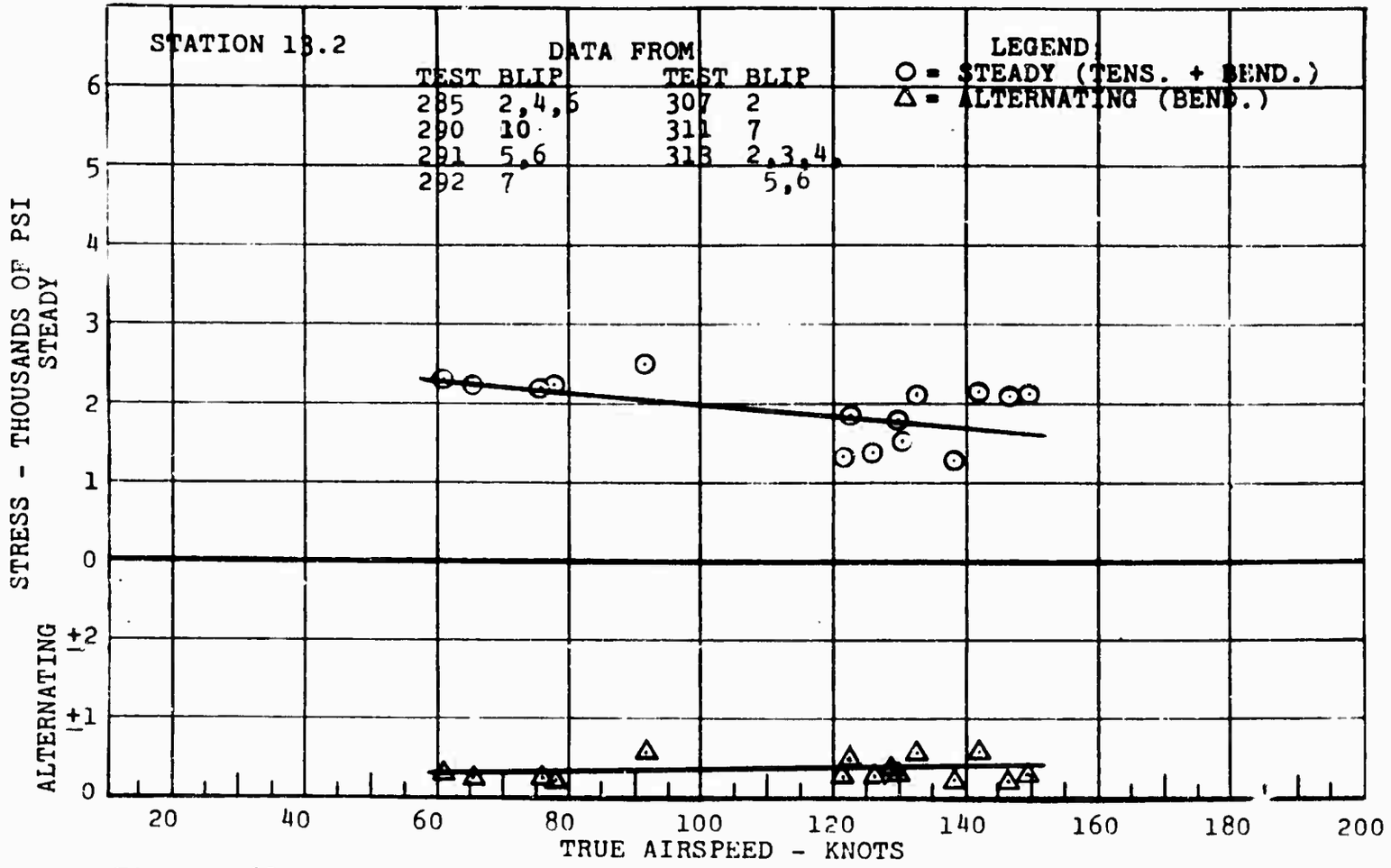


Figure 168. Propeller Blade Flapwise Stress versus Airspeed, Station 13.2.

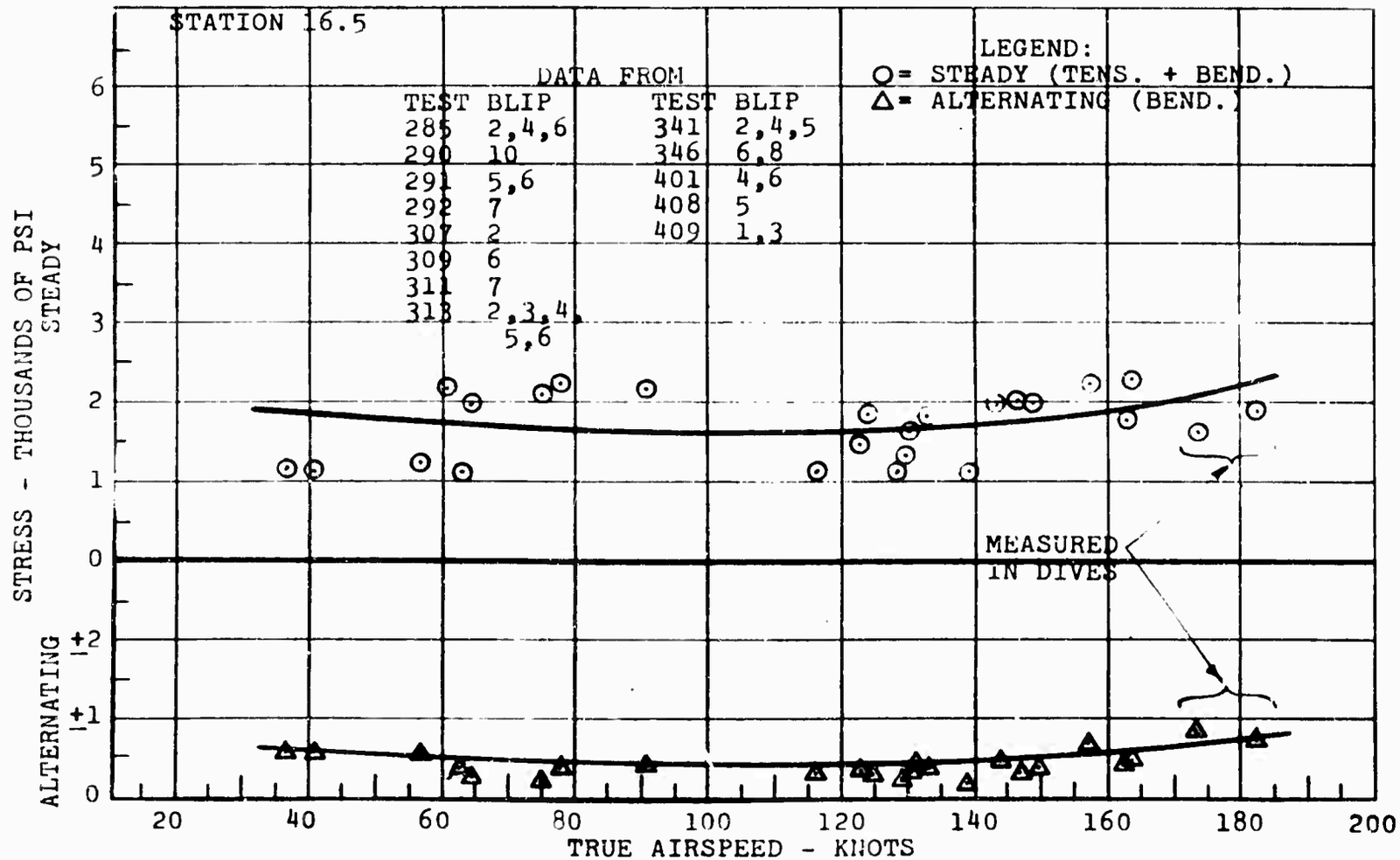


Figure 169. Propeller Blade Flapwise Stress versus Airspeed, Station 16.5.

(70 percent) and 29.7 (90 percent), the scatter is quite large (Figures 170 and 171). At blade stations 13.2 and 16.5, the stress averages about 2000 ±500 pounds per square inch and remains about constant with airspeed. At blade station 23.1, the steady stress averages about 3000 pounds per square inch and the alternating stress averages about ±1500 pounds per square inch, whereas at blade station 29.7 the steady stress averages about 2000 pounds per square inch and the alternating stress averages about ±1700 pounds per square inch. These are all well below the ultimate allowable bending stresses of 15,000 pounds per square inch and the allowable alternating stress of ±4500 pounds per square inch for the laminated birch propeller for infinite fatigue life. (Reference 10).

Flapwise steady bending moment versus span is plotted in Figure 172 for various flight conditions, including hover, level flight, and autorotation. This is significant in that it shows a negative bending moment on the propeller blade for some conditions and a positive bending moment for other conditions. At low blade angle of attack the spanwise bending due to the airload is overcome by the coning of the blade. At higher angles of attack, such as in forward flight, the airloads increase and the spanwise bending moment changes sign.

## TAIL PROPELLER PITCH LINK

The steady propeller pitch link loads average zero for low speed and increase in compressive force as the forward speed increases (Figure 173).

The alternating pitch link load is small in magnitude, averaging about ±25 pounds, and remains nearly constant with an increase in airspeed.

This is well below the alternating allowable load of ±200 pounds for infinite fatigue life for which this part was designed.

## TAIL PROPELLER PITCH CONTROL LEVER LOAD

The propeller pitch control lever load was monitored in the cockpit on all flights, using a microammeter to measure the output of a strain gage bridge on the lever. Loads were never greater than 60 percent of the 1250-pound design limit load for the system.

## LONGERONS

Alternating stresses in the upper-left and lower-right longerons at fuselage station 175 are plotted versus true

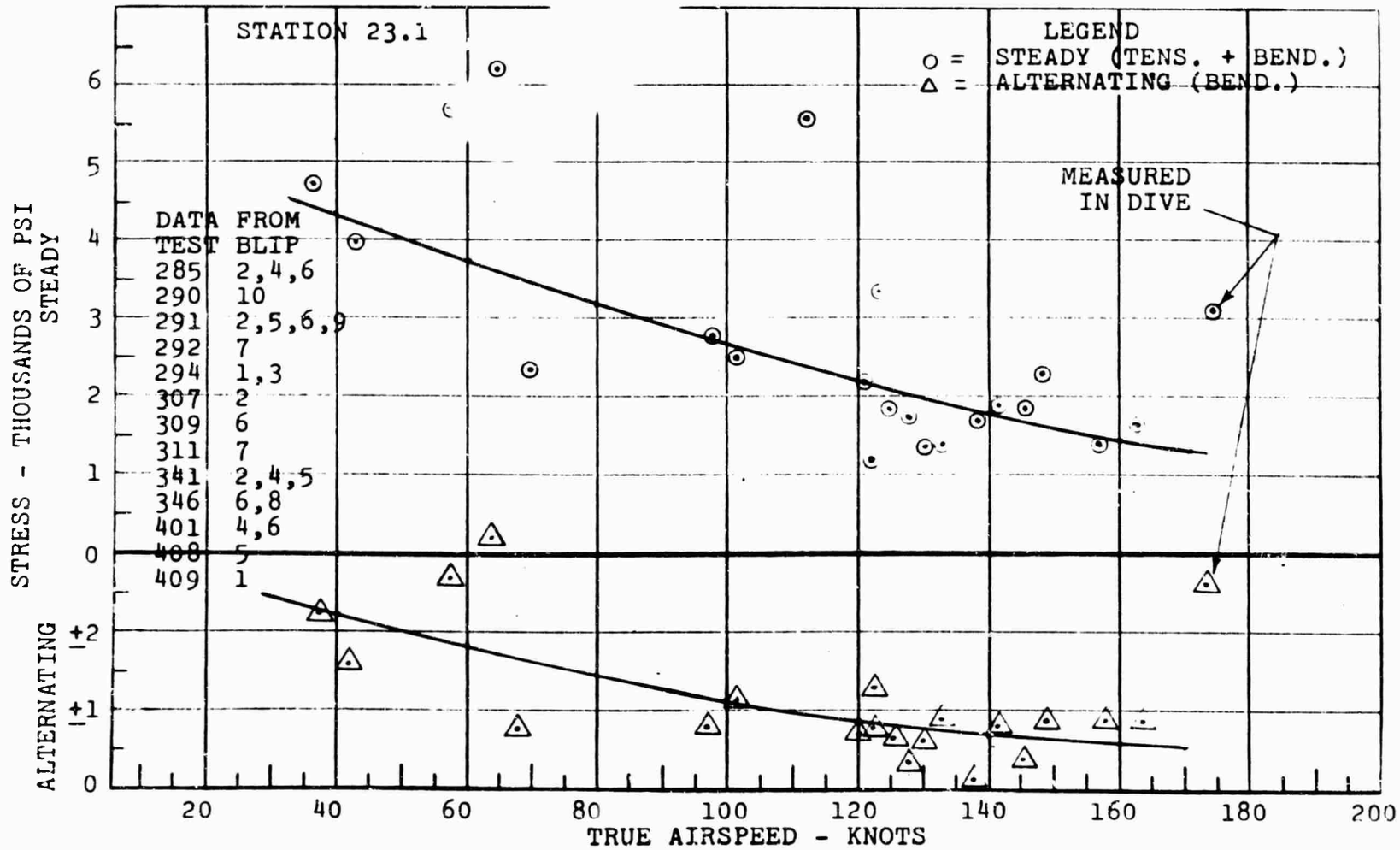


Figure 170. Propeller Blade Flapwise Stress versus Airspeed.

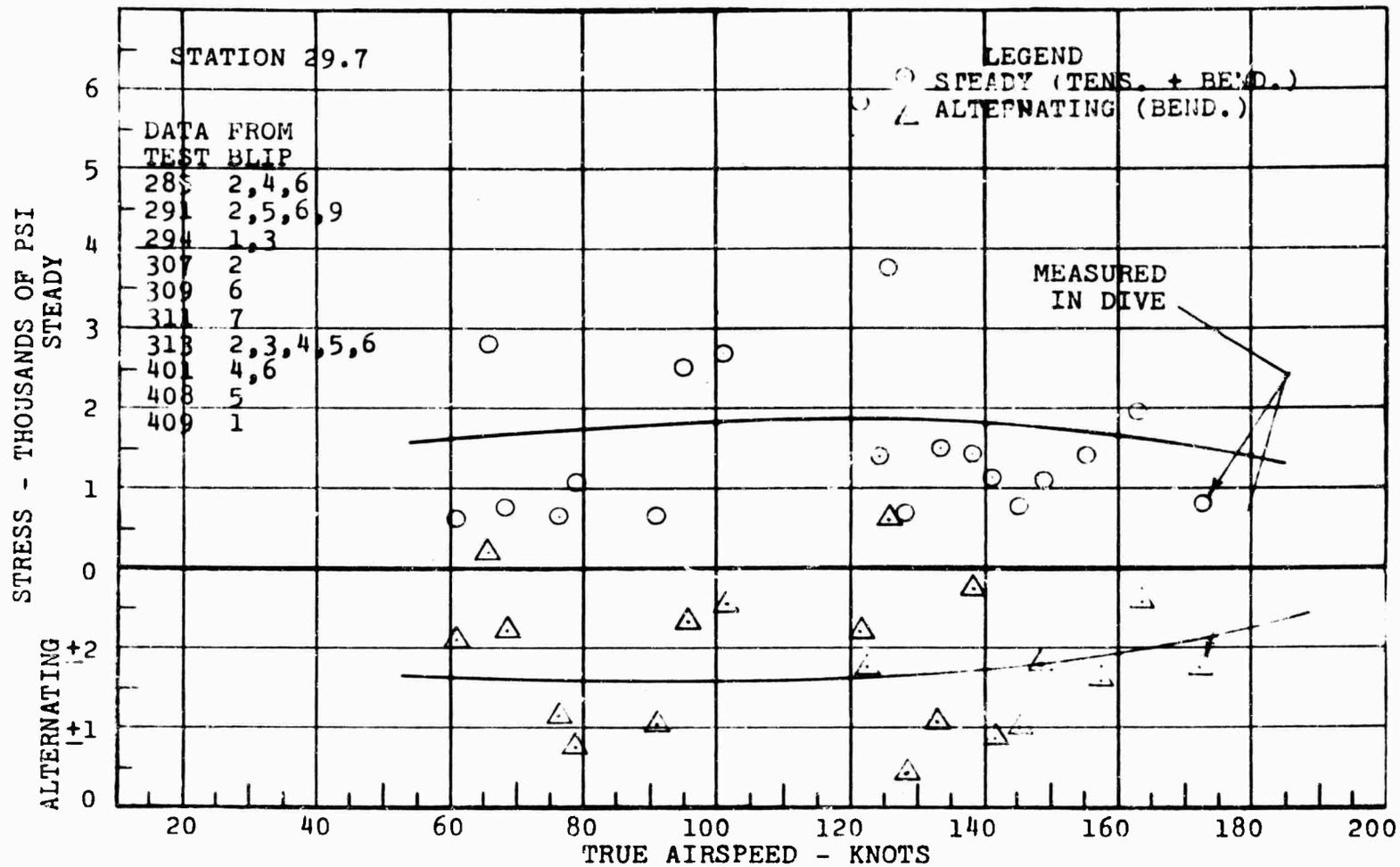


Figure 171. Propeller Blade Flapwise Stress versus Airspeed.

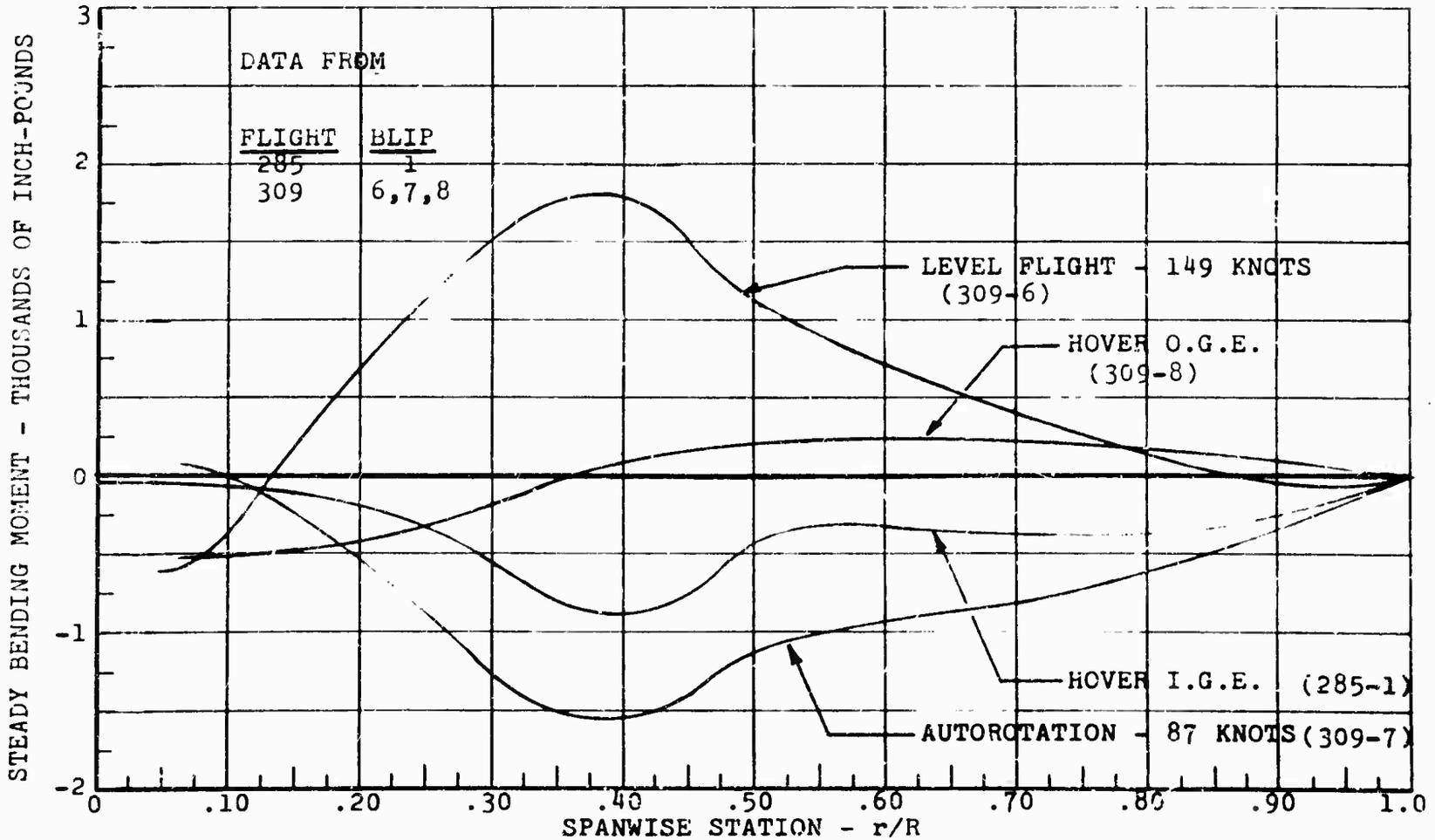


Figure 172. Propeller Blade - Flapwise, Steady Bending Moment versus Span.

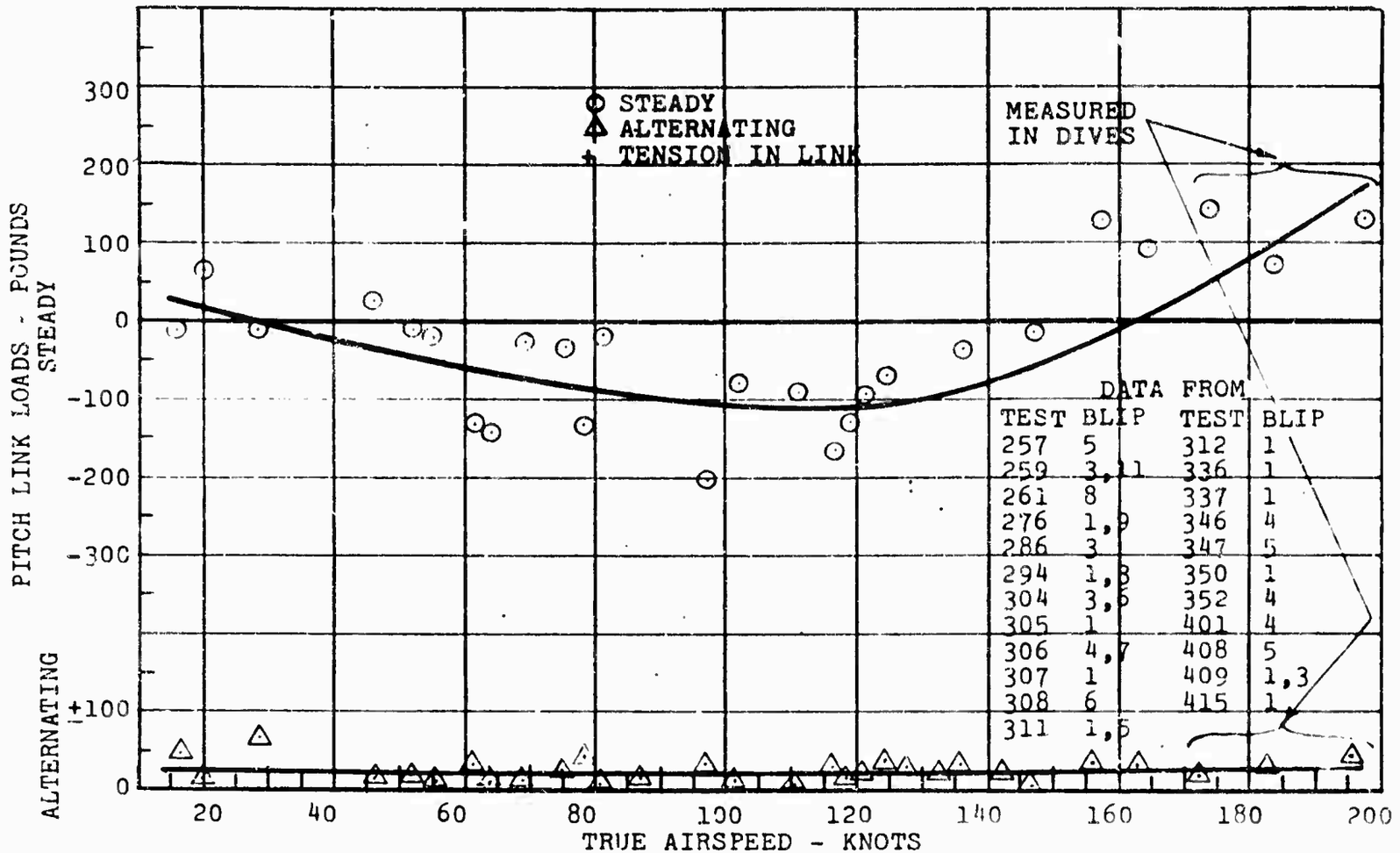


Figure 173. Propeller Pitch Link Load versus Airspeed.

airspeed (Figure 174). There is approximately the same magnitude of alternating stress in each longeron, so only one curve was drawn to represent both.

The alternating stress was small and increased slightly with an increase in airspeed.

MAIN LANDING GEAR

Axial load felt by the shock strut and axial load and bending in the main member were measured in run-on landing. A plot of these loads versus time for a typical run-on landing is shown in Figure 176.

All loads are well within the limit design loads for the gear. Maximum load in the shock strut in this typical run-on landing is 1900 pounds, compared to limit load for the shock strut of 3560 pounds compression.

Maximum load in the main member is 920 pounds compression plus 16,500 inch-pounds bending, whereas limit design load is 3830 pounds compression plus 66,700 inch-pounds moment. Other recorded loads in landing were less than these.

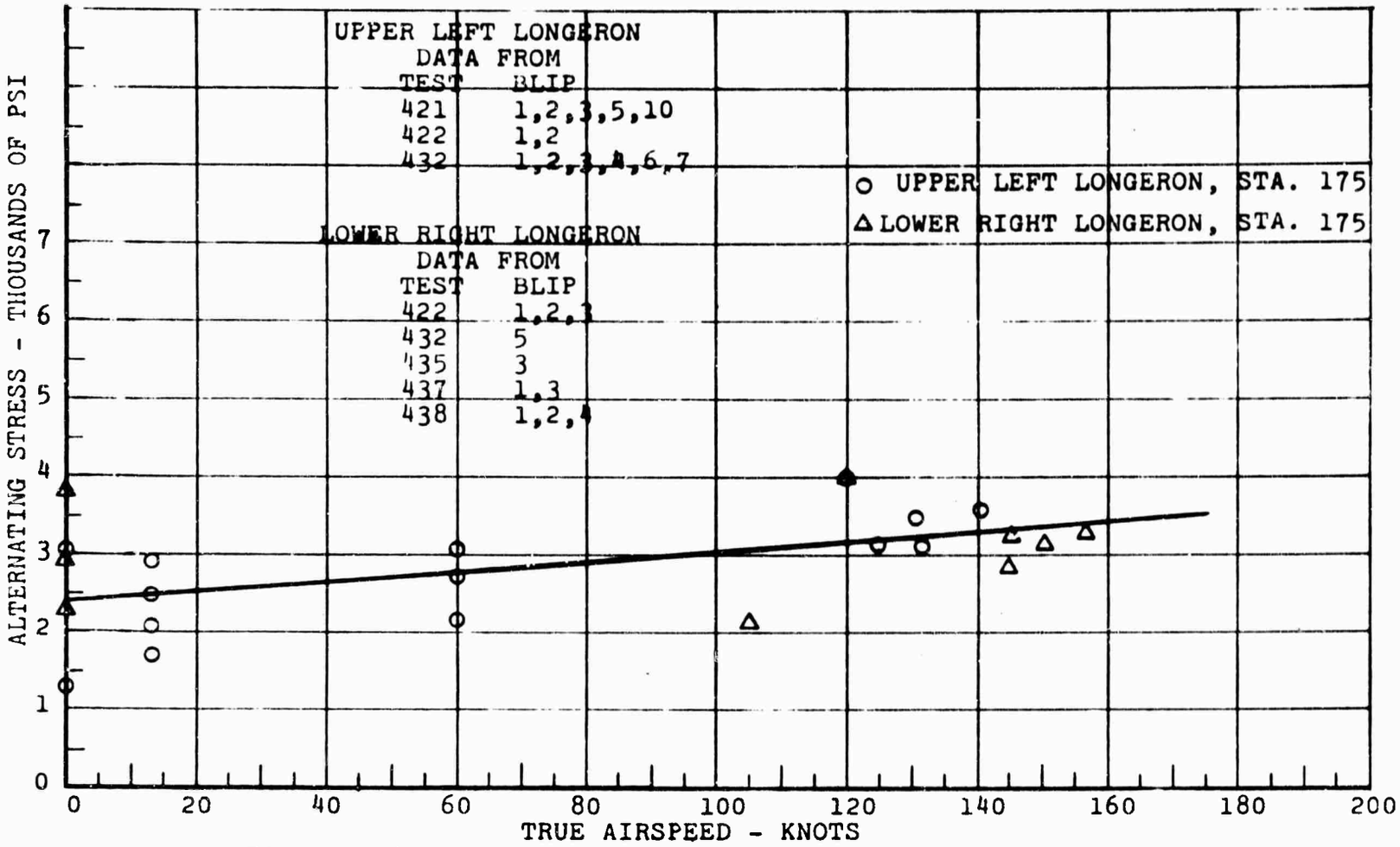


Figure 174. Longeron Alternating Stress versus Airspeed.

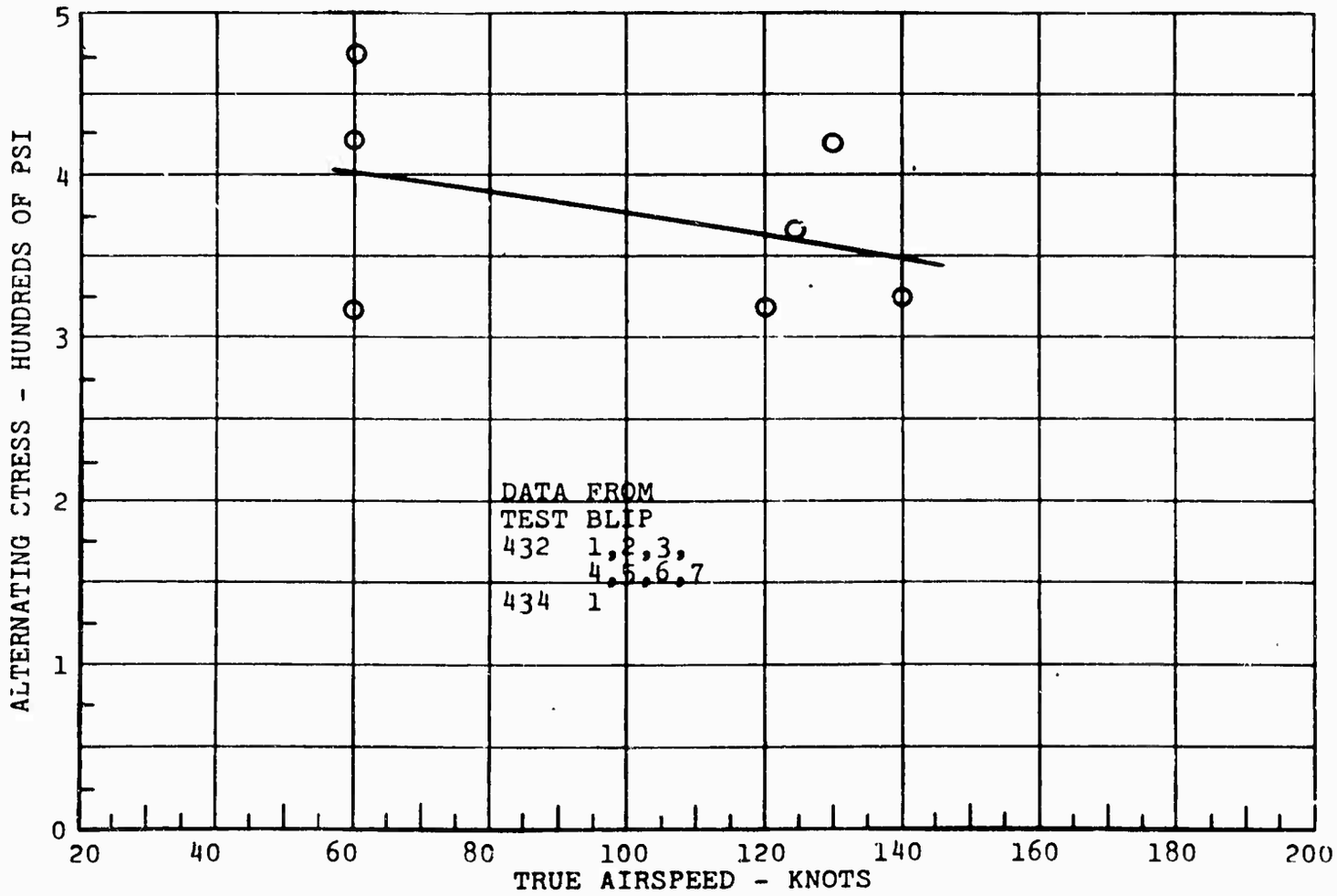


Figure 175. Alternating Stress versus True Airspeed - Forward Structure, Lower Beam, Left Side, Station 65.

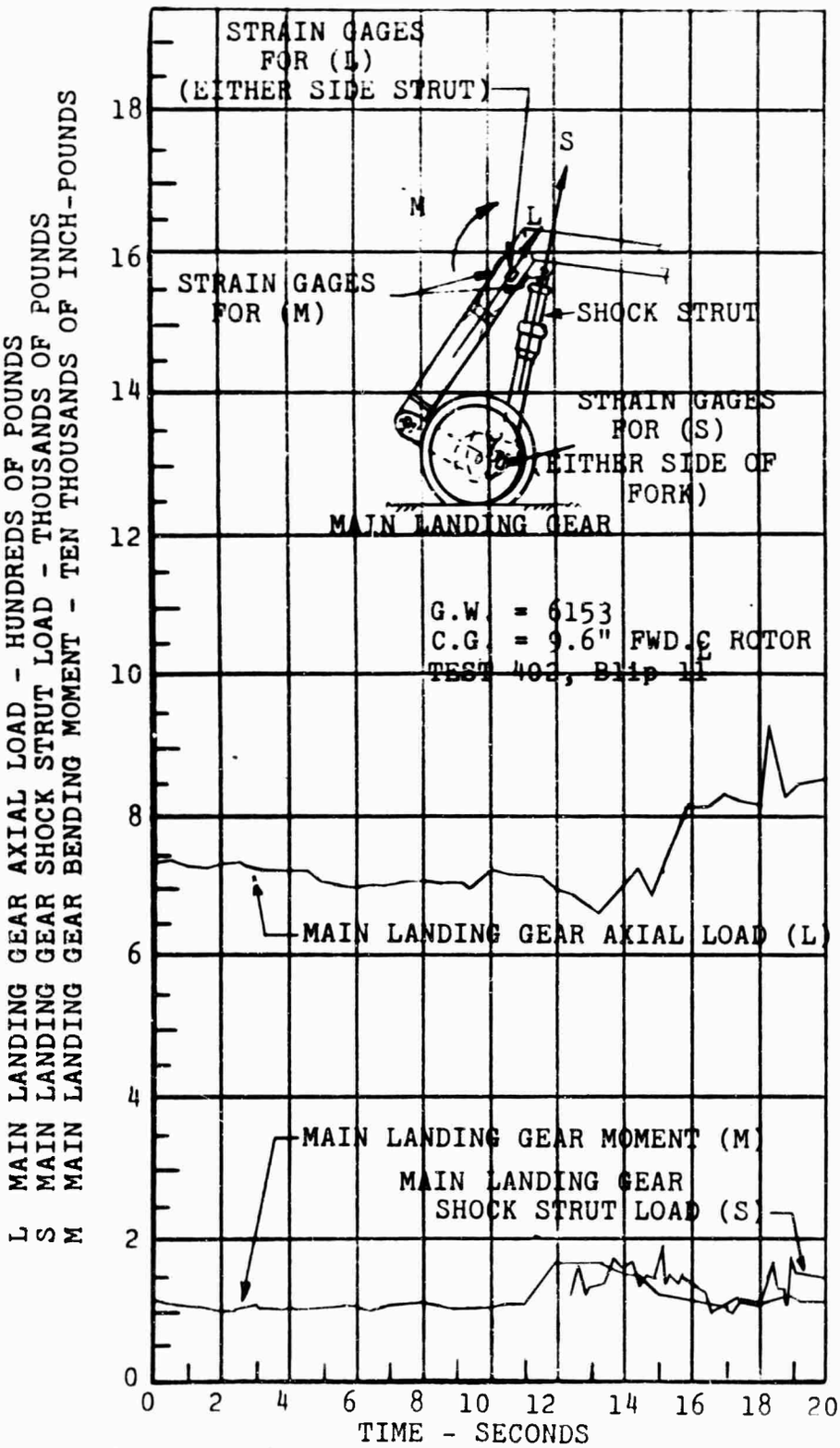

Figure 176. Typical Main Landing Gear Loads.

## TECHNICAL PROBLEMS

During the performance of the ground- and flight-test program with the 16H-1A, a number of problems developed, most of which had the effect of causing delays until they were solved but did not prevent continuation of the flight-test program. For the most part, the problems encountered were the mechanical structural type common in the development of new equipment rather than "state-of-the-art" knowledge.

### PROBLEMS ENCOUNTERED DURING GROUND TESTING

These were primarily structural in nature and were typical of the testing of almost any new dynamic components.

1. Oil pump drive - On two occasions, a draw-bolt which holds a lube-oil-pump drive adapter in driving engagement with a gear shaft in the transfer gearbox failed at the base of the threads. One of the failures occurred on the pressure-pump drive of the lube system; the other occurred on the scavenge-pump drive in almost the identical manner. The failures were attributed to lateral vibration of the bolt, which, if tightened to the standard torque, would be nearly in resonance with the gear-tooth-mesh frequency and could be brought exactly to resonance by overtorquing. The design was modified to incorporate a phenolic plug inside the hollow gear shaft which surrounded the draw bolt and prevented it from vibrating laterally.

   On two other occasions, the lube-pressure-pump drive shaft failed at a keyway. On both occasions, the pump continued to run, and the failure was only found after disassembly for other reasons. The first failure was attributed to fatigue caused by inadequate chamfers on the key and inadequate fillets in the keyway. After the second failure, however, the key drive was replaced with a splined connection many times stronger. After only 30 minutes of operation with the new splined shaft, the shaft suddenly seized in its journal bearings, shearing the splined section and causing stoppage and seizure of the oil pump. Analysis of this failure gave positive evidence of the basic trouble. Deflections of the shaft connection relative to the pump were causing a rotating bending moment between the pump shaft and the gear shaft to which it was splined. The stiff spline connection permitted the bending moment to be carried into the pump, causing local heating of its bronze journal bearing. Expansion of the pump-housing face eventually caused a seizure which sheared the

spline in pure torsion. (The same action had apparently previously broken out the former keyway, but then the rigidity was reduced enough so that the drive continued to function with the broken piece trapped in place.) At this point, the pump drive was redesigned to incorporate a floating quill shaft, splined at both ends, which could not transmit moment resulting from gear deflections. The pump drive then gave no further trouble.

2. Cracks in the fuselage skin - Part of the ground tests involved running at high power levels in the rotor and propeller, with the aircraft tied down to the concrete apron. As a result of local load concentrations at the tie-down points, cracks which required repair developed in the fuselage skin under these points. These loads were caused by the method of restraint during the tie-down tests, and were not representative of flight conditions. Local fatigue cracks became evident on the fairings and on trailing-edge structure. Sandwich panels were substituted for the riveted fairing skins which were being "oil canned" and showing signs of cracks. After such modifications, no further cracks appeared for the remainder of the ground testing or throughout the flight program.

3. Propeller pitch-control bearing - After 38 hours of running, excessive play developed in the propeller pitch-control mechanism. Disassembly revealed that the bronze retainer-cage had broken on a ball bearing inside the propeller support box. This was replaced with a stainless-steel cage of heavier cross section, which had to be supplied by the bearing manufacturer. The bearing caused no further trouble after this repair.

4. Propeller spinner - Near the conclusion of the 50-hour ground running, the propeller spinner suffered a fatigue failure at an attachment point which resulted in its tearing loose. It was struck by the propeller, disintegrated, and caused some damage to the propeller blades and the ring-tail duct. The damage to the blades and the duct was repaired promptly, but the spinner required redesign. Some of the early flight testing, involving hover and low-speed flights, was performed without a spinner.

PROBLEMS ENCOUNTERED DURING FLIGHT TESTING

1. Turbine speed control - The T-58 turbine is equipped with a fuel control system which includes a speed-selector lever, the position of which causes a governor to supply fuel in response to changes in output speed. The range of the governor setting, at no load, is from about 6500 to 5800 RPM (at the output of the speed-decreaser gearbox). Because of built-in droop characteristics of the governor, this range, at full load, is from 6000 to about 5200 RPM. If the lever is moved beyond the lowest governor setting, it passes through a transition region where the governor will not control the speed, thence to ground idle, and finally, to cut-off. Friction and other forces acting on the lever are such that pilot-effort loads on the conventional twist-grip control were too high for a direct mechanical linkage. Hence, a production electric servo system was installed wherein the position of the twist-grip positioned a potentiometer (dualized for safety of flight), the signal from which, in turn, positioned an electric actuator connected to the turbine speed selector lever.

   During the first autorotative descent in the 16H-1A the turbine speed-control system malfunctioned and the flight ended with an actual emergency power-off landing. When the pilot attempted his planned power recovery by twisting his grip to the full-speed position, the turbine did not respond, but remained at ground idle. As a result of landing in a rough field adjacent to the airport, damage was sustained by the tail landing gear, propeller, duct, and rudder vanes, all of which were repaired in due course. The speed-control failure was found to be an electrical open circuit which developed inside the actuator.

   To insure that such an event could not reoccur, a limit-switch in the actuator was adjusted so that the actuator could not run beyond the lower limit of the governed range unless a separate switch were operated from the cockpit. This switch was used only to shut down the turbine, and was always kept in the safety

position in flight. Thus, no electrical failure of any sort could place the speed setting lower than the minimum governed setting, where near-full power would be immediately available. This solution permitted trouble-free operation for the remainder of the test program. However, it did place a restraint on simulating abrupt power failures. The RPM of the autorotating rotor could not drop below that maintained by the governor at its minimum setting, which, at no load, was only 3 percent below the normal powered RPM. As soon as the decaying RPM reached that value, the governor would demand fuel and the turbine would supply torque to sustain that RPM.

2. Measurement of wing lift - One of the objectives of the flight test program was to evaluate the effect of variations in lift distribution between wing and rotor on performance. It was planned to measure the rotor thrust by measuring tension in the rotor shaft, and to measure wing lift independently with strain gages on the fuselage frames to which the wing spars are attached. Calibration of both systems was performed by hanging the aircraft at the rotor, through a dynamometer. Readings were taken of the rotor-shaft tension strain gage bridge and of the two bridges on each side of the fuselage frame which, when combined, measured the wing lift. The weight of the aircraft was then incrementally supported on the wings and unloaded from the rotor while the changes in readings were recorded. This procedure was repeated with two different spanwise points of support for the wings, to permit a solution independent of the spanwise center of lift, which was not known precisely. A series of multiplying constants for the four wing bridges was worked out which checked the calibration for both sets of loadings. However, the in-flight readings for these four bridges were so variable and inconsistent that no useful data could be derived from them, either individually or in combination. The data from the rotor-shaft tension, in conjunction with the known gross weights, on the other hand, were sufficiently consistent to supply the required information. Consequently, they were used in this report to the exclusion of the wing lift measurements.

3. Turbine air intake - In order to make use of existing gearing and other power-transmission components, the T-58 turbine was mounted in a buried installation inside the fuselage, behind the rotor transmission. The air-intake was designed to be of the side-inlet type, with a forward-facing scoop. The air entered a

plenum chamber after making a 90-degree turn and then entered the turbine through a bellmouth inlet from another existing helicopter installation. Early in the flight test program it became evident that the inlet losses in hover were so severe that the aircraft performance was limited by turbine inlet temperature at power levels well below the turbine rating. The losses were mainly caused by too small a radius in the 90-degree turn. The external portion of the inlet was therefore removed, so that the air simply entered a rectangular flush opening in the side of the fuselage, the area of which was over twice as large as the throat of the original external inlet. Although this expediency did not permit any ram-pressure recovery, it reduced the inlet losses sufficiently that most of the flight test program was conducted with this configuration. For flights at speeds above about 160 knots, however, the problem of limiting turbine inlet temperature again arose. Beginning with test 403, the external inlet was reinstalled in conjunction with an improved bellmouth from the plenum chamber into the turbine. An improvement in turbine performance at high speed was noted, but limit turbine inlet temperature was always reached before rated power could be obtained. An improved inlet was designed and fabrication was started, but it was not completed in time for use in the test program. Its use would have increased the power attainable at high speed by an estimated 160 horsepower, which would have increased the true airspeed to 174 knots.

4. Rotor control system stiffness - The 16H-1A, as modified from the 16H-1 and as ground tested, used an H-21 rotor, including blades, hub, and swash plate. The remainder of the rotor control system was the same as that flown in the 16H-1, with only those changes necessary to adapt to the H-21 swash plate. The system incorporated three irreversible hydraulic servo actuators, one each for longitudinal cyclic, lateral cyclic, and collective pitch. The system was stress-checked for the anticipated higher loads of the larger rotor and higher flight speeds and was found to be adequate.

   In the course of exploring progressively higher flight speeds, a vibration appeared at about 120 knots which increased rapidly with speed and became severe enough to limit the flight testing to about 140 knots. Investigation of the frequencies of vibration showed the largest contributors to be the second, third, and tenth harmonics of rotor speed. The tenth harmonic was

attributed to the tail propeller, which has a speed of 9.7 times rotor speed. Inspection uncovered a maladjustment which resulted in one propeller blade having a pitch of nearly 2 degrees more than the other two. Correction of this condition eliminated most of the ten-per-revolution vibration. Attempts were made to reduce the third harmonic component with a tuned dynamic vibration absorber which was placed at various locations in the aircraft ranging from the center of gravity to a position just ahead of the cockpit nose. Figure 177 shows the effect of the absorber mounted in this last position, an equivalent dead weight mounted there, and also with nothing mounted. Although the third harmonic component was significantly reduced, the other vibrations not absorbed resulted in a composite vibration spectrum still unsatisfactory to the pilot.

At this point, a motion picture camera was installed on the pylon to take in-flight pictures of swash-plate motion. The resulting pictures clearly showed swash-plate motions allowing the rotor blades' two- and three-per-revolution pitch changes of the order of $\pm$.5 degree, although the controls in the cockpit showed practically zero motion. The stiffness of the control system cables, pulley brackets, push-pull rods, and bellcranks between the swash plate and the irreversible actuators under the floor was insufficient, and the rotor blades were changing pitch in response to harmonic air load components.

To correct the situation, the rotor control system was changed to incorporate a set of dual irreversible hydraulic servo actuators, mounted in the pylon immediately under the swash plate, in the place of those under the floor. Thus, motion of the swash plate was arrested stiffly at its source. This change, which lowered the vibration level markedly, permitted test flying to continue and to proceed to the maximum speed reached in the program (195 knots). Figures 38 through 47 show the improvement throughout the speed range brought about by the control stiffening.

5. Propeller blade design - Measurements of tail propeller power at speeds up to 140 knots (the temporary vibration limit, see "Rotor control system stiffness" discussed above) indicated that the propeller-blade angle of attack at high speed would be above optimum, with attendant low propeller efficiency. During the period in which the control system was being modified, new blades

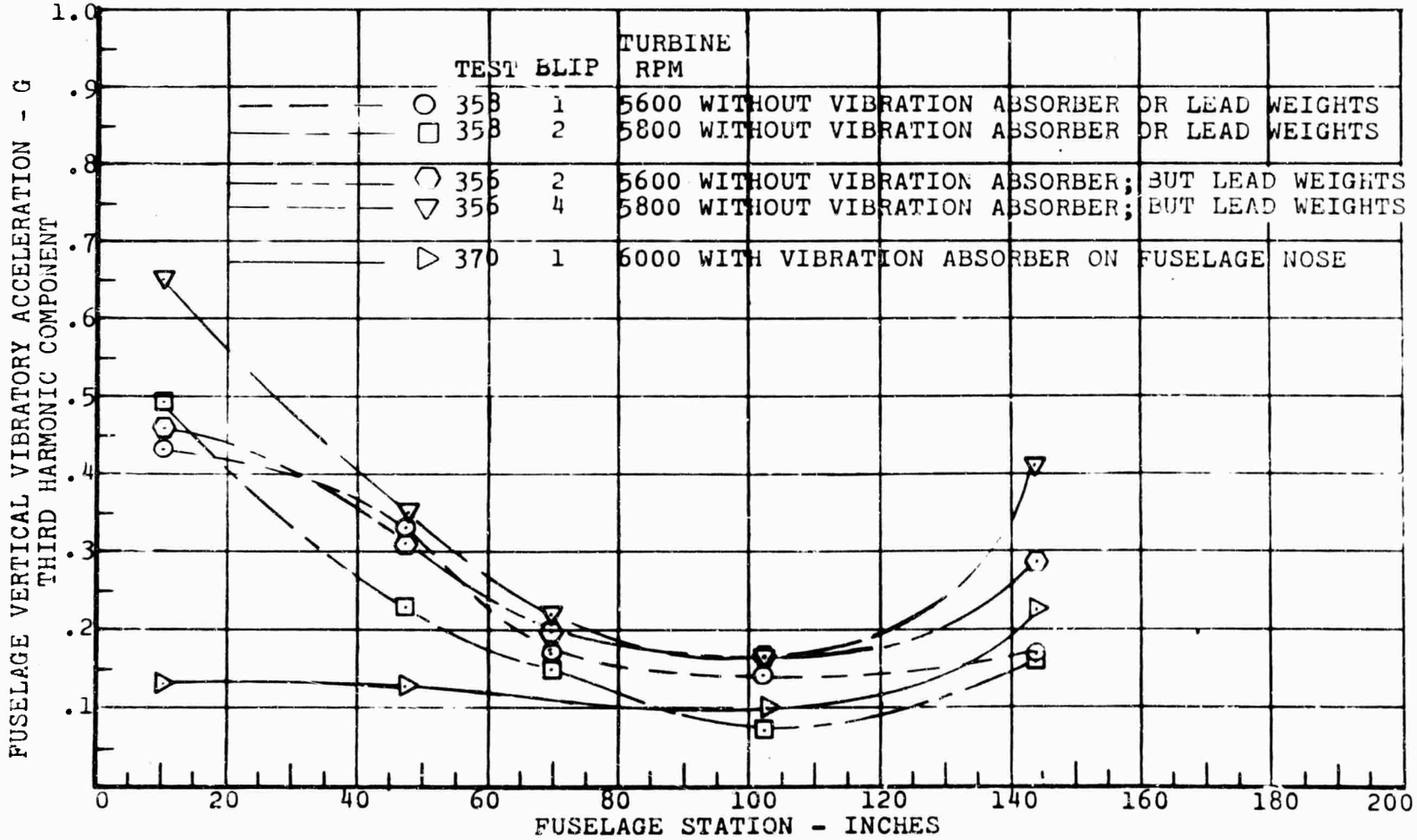


Figure 177. Forward Fuselage Vertical Vibration.

were fabricated for the propeller. All of the data presented for speeds above 140 knots was obtained with the new propeller blades. Data obtained in hover and at the lower forward speeds with the new propeller were not significantly different from those obtained with the original one.

6. Rod-end in rotor control system - During the period of vibration investigation, prior to control stiffening, one of the rod-ends in the longitudinal cyclic control system failed at the bearing-retaining lug. Upon rolling out of a climbing turn, there was a loud noise and the aircraft pitched to a nose-high attitude. Control was recovered, and a cautious check revealed at least partial control about all axes. The pilot decided to make a roll-on landing using propeller pitch control to control rate of descent. During the approach and landing, the cyclic stick was used only for lateral control. Longitudinal trim was maintained with the elevator trim, and collective pitch was not used. A normal roll-on landing was performed, with touchdown between 50 and 60 knots.

   All longitudinal, lateral, and collective push-pull rods, bellcranks, levers, and quadrants subject to rotor control loads were inspected, with no other evidence of damage. However, the failed rod-end and others similar to it, if subject to loads of the same order, were replaced with new, stronger parts.

   The ability of the elevator trim to serve as a backup for longitudinal cyclic pitch in an emergency was a feature not appreciated in the original design concept. Its emergency usefulness proved to be a significant asset, and in this instance it probably saved the aircraft.

7. Landing-gear emergency extension - The landing gear is extended manually on the 16H-1A in the event of failure of the normal electrically operated retraction system. The emergency system consists of a hand-crank in the cockpit, on which is mounted a sprocket connected by roller-chain to another sprocket on the retraction actuating shaft. The hand-crank drives through a spring-loaded clutch, so that it remains stationary during electrical actuation of the gear, but the chain and sprockets are in motion. On one occasion, while the aircraft was in the shop for maintenance, the roller-chain broke during a trial gear-retraction cycle and became jammed, preventing

both electrical and manual operation.

The failure was traced to the faulty installation of the removable side-link at the spot where the two ends of chain are joined to make the chain "endless". A failure of this type occurring in flight would have prevented a normal landing. Hence, to preclude such an event, the sprocket on the main actuating shaft was remounted to drive through a shear-pin, designed to shear at a load well above the hand-crank extension load but well below the torque of the electric actuator. This would permit electrical operation, even with a jammed chain. No further difficulty was encountered with the retraction system.

## CONCLUSIONS

1. The use of a variable pitch pusher propeller mounted inside a duct, in conjunction with movable directional and longitudinal control surfaces, provides a convenient and efficient method of effecting the desired power distribution between that utilized for forward propulsion and that required for rotor lift over the entire speed range. Power management can be accomplished easily by control of both rotor and propeller pitch by one pilot, with one hand.

2. The use of a ducted pusher propeller for forward propulsion of a compound helicopter is an effective method of extending the speed capability by relieving the main rotor of its propulsive function. At speeds above 150 knots, the rotor required as little as 15 percent of the total power used.

3. The stators and the propeller duct render a high degree of longitudinal and directional static stability and produce aerodynamic damping for dynamic stability. The longitudinal control surface acts as an effective trim control even in a hover, where it produces an appreciable moment equivalent to a center-of-gravity shift of 4.4 inches in the 16H-1A.

4. The employment of a ducted pusher propeller and of deflector vanes in a compound helicopter is a feasible and adequate means of main-rotor torque compensation and directional control. Control was found to be sufficient for hovering and maneuvering sideward 0 to 30 knots and rearward 0 to 30 knots.

5. The employment of a ducted pusher propeller with rudder control surfaces provides favorable directional control for making running (STOL) takeoffs. Takeoffs at ground speed as high as 55 knots were conducted during this test program.

6. In the configuration tested, the 16H-1A was power limited. Level-flight true airspeeds approaching 200 knots would be possible with an engine air-intake and with the incorporation of drag-reduction items.

7. The maximum true airspeed of 195 knots was attained in a 10-degree dive. The limiting vibration levels, experienced in the early part of the test program in the speed range from 110 to 140 knots, were alleviated by the incorporation of a stiffer rotor control system.

8. The steady component of the rotor-blade bending moments and pitch link loads, and the alternating component of propeller-blade bending moments and pitch link loads, tend to remain nearly independent of airspeed. On the other hand, the alternating component of rotor-blade bending moments and pitch link loads, and the steady component of propeller-blade bending moments and pitch link loads, tend to increase gradually with airspeed. However, the net fatigue effect of the combined loadings remained within ample structural margins and showed only a gradual increase with speed.

9. Since the wing supports an ever greater proportion of the aircraft weight as speed increases, and the rotor supports a correspondingly smaller proportion, the rotor at some point begins to lose its effectiveness for controlling the aircraft in roll. For compound aircraft designed to unload the rotor much beyond 50 percent, incorporation of conventional ailerons should be beneficial in two respects.

   a. Roll control at high speed should be improved.

   b. Since the rotor now need not supply all of the roll control at high speed, its lateral cyclic control can be reduced with resulting improved hovering roll response.

## RECOMMENDATIONS

1. Flight tests of the ring-tail shaft-driven compound helicopter should be continued with a flight test article having additional power and an improved air induction system to permit exploration of the flight characteristics at higher speeds.

2. The aircraft for these extended tests should incorporate ailerons with an adjustable linkage ratio in the lateral cyclic control. The flight program should investigate various proportions of these two lateral control inputs to obtain the optimum controls for both low-speed, helicopter type flight and high-speed unloaded rotor flight.

## REFERENCES


1. Goldberg, J. H., Automatic Control: Principles of Systems Dynamics, Allyn and Bacon Incorporated, Boston, Massachusetts, 1964.

2. Seckel, E., Stability and Control of Airplanes and Helicopters, Academic Press, New York, 1964.

3. H-21C Phase IV - Performance Evaluation, Edwards Air Force Flight Test Center, California, Report AFFTC-TR-55-26, December 1955.

4. Helicopter Flying and Ground Handling Qualities; Ground Requirements for, Military Specification MIL-H-8501A, September 1961.

5. Helicopter Performance Testing Manual, Naval Air Test Center Test Pilot School, Patuxent Naval Air Station, Maryland, January 1965.

6. Phase IV Performance and Stability Tests of the H-21B, Edwards Air Force Flight Test Center, California, Report AFFTC-TR-57-4, March 1957.

7. Stapleford, R. L., et al, Systems Technology, Incorporated, An Analytical Study of V/STOL Handling Qualities in Hover and Transition, Report AFFDL-TR-65-73, Air Force Flight Dynamics Laboratory, Wright-Patterson Air Force Base, Ohio, October 1965.

8. Tapscott, R. J., Criteria for Control and Response Characteristics of Helicopters and VTOL Aircraft in Hovering and Low-Speed Flight, Aerospace Engineering, Volume 19, June 1960.

9. Test Requirements, Ground, Helicopter, Military Specification MIL-H-8679, 5 March 1954.

10. Bulletin ANC-18, Design of Wood Aircraft Structures, Aircraft Committee, Munitions Board, June 1951. Superintendent of Documents, U.S. Government Printing Office, Washington, D.C.

## APPENDIX I

## DESCRIPTION AND RESULTS OF GROUND TESTS

### 16H-1A WING PROOF LOAD TEST

The purpose of the test was to prove that the 16H-1A wing could safely withstand 120 percent of the limit loads expected in flight testing of the model 16H-1A aircraft. The test was performed with the wing installed on the aircraft.

The wing was loaded downward instead of upward to facilitate the testing, although the greatest airload acts upward. This was possible, since physically the outboard wing panel is symmetrical about the horizontal chordline, and the center section is nearly symmetrical. Two loading conditions were executed. In Condition I, the wing was uniformly loaded spanwise and chordwise with the center of pressure at the 25-percent chordline, representing a maximum spanwise bending condition. In Condition II, the wing was uniformly loaded spanwise and chordwise with the center of pressure at the 35-percent chordline. The loading was 71 percent of the loading of Condition I, and represented a maximum wing torsion condition.

In each of the above loading conditions, the port wing was loaded to 120 percent of the expected flight test load, while the starboard wing was loaded to approximately 70 percent of this load. This dissymmetry of loading represents the unsymmetrical flight condition and is critical for the wing spar webs in the wing center section.

After the completion of the test, the wing was inspected and was found to be free of any evidence of damage.

### CONTROL SYSTEM PROOF TESTS

The purpose of these tests was to proof load the 16H-1A control system (longitudinal and lateral cyclic, collective, and rudder) in order to insure its structural integrity and to determine whether any excessive deflections existed throughout the system.

For tests beyond the stops (tests 1 and 3), the rotor was locked out at the main rotor pitch locks on the rotor hub, thereby preventing any movement of the swash plate in cyclic and collective pitch. In all tests, loads were applied with a tension scale to the handgrip of the particular stick being tested. Boost pressure of 1700 pounds per square inch was

applied with hand-operated hydraulic equipment. For the test up to the stops (test 3), the fore and aft loads on the cyclic stick were applied with the aid of a turnbuckle in series with a spring balance. The system was observed throughout, and deflections of pilot stick were measured.

The rudder was blocked out at the tail with a wood frame. Boost pressure was applied with hand-operated hydraulic equipment. Proof loads were applied to the foot pedal by the test operator sitting in the pilot's seat. Loads were measured with a compression scale.

Results

The cyclic and collective pitch system withstood all loads satisfactorily, and no apparent excessive deflections were noted in the pulleys or brackets in tests 1 and 2. In test 3, deflections and permanent set occurred in the stop of the copilot's stick and were corrected by structural modification.

The rudder system withstood all loads satisfactorily. The only apparent deflection noticeable was the "walking beam" which, under right pedal load, deflected a slight amount.

AIRFRAME SHAKE TEST

The purpose of this test was to determine the magnitude of vibration throughout the aircraft while it was suspended from the boom and tied down in the ground testing in order that any condition considered undesirable, intolerable, or unsafe could be corrected before flight tests. It was not intended to supply absolute vibration levels, as the environmental conditions of these tests would not permit the simulation of the same vibration levels that will occur in flight. Vibration levels varied greatly with the tension on the tie-down cables, the number of tie-down cables that were installed, the dead load placed in the aircraft, and the degree of cyclic stick used. Also, ground wind conditions affected the vibration levels.

The most severe vibrations were obtained with the aircraft tied down and occurred in the rudders, horizontal stabilizer, and stators. Some vibration also occurred in the side skin of the fuselage. Vibration in the cockpit was minor. Some of the vibration that the aircraft experienced while tied down was induced or aggravated by the tie-down cables. The aircraft, when undergoing tests suspended by its rotor head, was observed to run with less vibration than

when tied down to the ground.

Excessive vibration in the rudder control cable in the bottom hatch area was observed. Also, slight vertical movements of the rotor longitudinal control rods at the swash plate were noted. In order to improve maintenance in the areas outlined above, the following was accomplished:

The rudders and fittings were stiffened and the tolerances in the rudder controls were reduced to a minimum to reduce dynamic loads on the system. The horizontal stabilizer was reinforced by addition of doublers and skin stiffeners, making use of bonding to increase fatigue life further. The thin aluminum skin of the stators was changed to sandwich construction .25 inch thick with aluminum honeycomb cores and aluminum faces bonded together. The sides of the fuselage, wherever the thin aluminum skin was buckling, were reinforced with a .62-by-.62-by-.032-inch 2024T3 angle stiffener installed circumferentially to break the 7-inch skin panels into two 3.5-inch-wide panels wherever needed. An aluminum bracket with a phenolic guide was installed to divide the rudder cable length in two parts where it was vibrating excessively.

The rotor longitudinal control rods and fittings were strengthened, as well as the attachment of the fittings to the rods.

Changes that were made to the tie-down arrangement were as follows:

1. The vertical restraints, from the pylon to the ground, were moved to a more nearly vertical position in order to react the vertical thrust loads as close to the origin as possible.

2. Additional vertical cables were added from the wing-root to the ground in order to take out the horizontal thrust load produced by the rotor.

3. Horizontal restraints were added, from the underside of the fuselage, near the center of gravity aft approximately 8 feet, in order to take out the horizontal thrust load produced by the propeller.

After the incorporation of the changes described, the vibration level was considered to be acceptable by the pilot even at the extreme propeller and/or collective pitch settings. The degree of vibration varied from practically negligible with controls neutral to moderate when the cyclic

was fully displaced (nearly to the stops).

At no time during the testing was any vibration felt, as feedback, in the cyclic or collective pitch levers. Although high frequency vibrations were initially noted in the rudder pedals, no further vibrations were noted after the changes were incorporated. Because of the significant reduction of vibration caused by the changes in the tie-down arrangement and the practically vibration-free tail tests with the aircraft suspended, it was concluded that no correlation between vibration during ground tests and those that might become apparent during flight test could be made.

TIE-DOWN TESTS

The purpose of these tests was to subject the airframe systems, transmission system, and other dynamic components to a series of tests to check their structural integrity and functional operation prior to flight. The ground tests commenced 8 April 1965 and 45 hours were completed 8 July 1965. They were conducted utilizing the entire airframe and dynamic components, including the rotor and tail propeller. Consequently, the aircraft had to be restrained to resist all loads induced by the main rotor, tail propeller, and rudder vanes.

The first 15 hours of testing were conducted primarily to prove the main rotor and the transfer transmission and to discover any discrepancies so that they might be corrected before flight.

The main rotor loads (rotor lift and side loads) were taken out by four cables extending down at 45 degrees from the rotor pylon to anchor points ir the ground. These cables were tensioned to 800 pounds, giving a total of 1600 pounds downward load. To decrease the load in the cables during high collective setting, approximatley 1000 pounds of ballast was positioned in the aircraft directly beneath the transmission. Cables were also attached to the wing fittings and extended to anchor points in the ground to act as backup to the cables attached to the rotor pylon. The thrust loads from the propeller were taken out by cables attached to the lower longerons at station 169 and extending aft at 25 degrees to the horizontal to anchor points on the ground. The side loads at the tail were taken out by cables wrapped around station 345 and extending laterally and downward to the ground. The aircraft, itself, was resting on wooden blocks with the main and tail gear oleos completely depressed to obviate any possibility of ground resonance and to make the tie-down configuration more rigid. The power

distribution schedule shown in Table XVI was repeated ten times to complete the 15 hours.

TABLE XVI. TIE-DOWN TEST POWER DISTRIBUTION SCHEDULE

| TRANSMISSION TEST NUMBER | HP TO MAIN ROTOR | HP TO TAIL ROTOR | TIME (MINUTES) |
|---|---|---|---|
| 1 | 50 | 200 | 5 |
| 2 | 50 | 400 | 5 |
| 3 | 50 | 600 | 5 |
| 4 | 50 | 800 | 5 |
| 5 | 50 | 1000 | 20 |
| 6 | 50 | 1100 | 5 |
| 7 | 400 | 200 | 5 |
| 8 | 400 | 400 | 5 |
| 9 | 400 | 600 | 5 |
| 10 | 400 | 800 | 5 |
| 11 | 600 | 200 | 5 |
| 12 | 600 | 400 | 5 |
| 13 | 600 | 600 | 5 |
| 14 | 800 | 200 | 5 |
| 15 | 800 | 400 | 5 |

The test revealed a deficiency in the transmission oil pump bolt (16D5251), the design of which was subsequently changed.

The next 30 hours of testing was performed according to a schedule derived from paragraph 3.6.3.3 of MIL-H-8679 (Reference 9), except that the times for each test were reduced. During the tests, data were recorded on rotor and propeller stresses; rotor, propeller, and turbine power and RPM; engine mount vibrations; rotor and propeller pitch settings; and powerplant and transmission oil temperatures and pressures.

## RESULTS

### 1. Transmission System

With the exception of several oil-pump-drive failures which are discussed under "Technical Problems", the transmission functioned satisfactorily. The pump drives were redesigned before flight testing began, were retested, and gave no further trouble.

### 2. Rotor System

The rotor system, itself, performed without showing any problems. However, shortcomings in the instrumentation came

to light during these tests. The rotor-shaft-torque strain gage bridges had two active arms on the shaft and two dummy arms in the external circuit. The bridges picked up spurious signals from rotor-shaft bending which were superimposed on the torque signals and resulted in a loss of accuracy. The bridges were replaced with four-active-arm bridges for the flight test program; these bridges proved much more satisfactory.

3. Tail Propeller

The propeller blade, hub, and pitch link stresses were well within safe levels throughout the ground tests. Instrumentation operated satisfactorily except for blade flapping moment at station 29.7. Several attempts were made to repair the gages at this station, but none was successful. (They were finally repaired prior to the flight test phase).

At the conclusion of the 45 hours of tie-down testing, the propeller-ring-tail combination was tested for an additional 5.8 hours. During these series of tests, the rotor blades and hub were removed and the aircraft was suspended by cable from a boom to the rotor pylon. Supporting structure at the ring-tail was instrumented with strain gages to provide longitudinal, lateral, and vertical force data. Propeller torque, RPM, and pitch, as well as rudder deflections were measured in the normal manner by using the 16H-1A instrumentation.

## APPENDIX II

### PERTINENT DATA ON INSTRUMENTATION, AIRCRAFT DRAG, WEIGHT, AND CENTER OF GRAVITY

Instrumentation used in the flight test program is shown in Table XVII.

TABLE XVII. 16H-1A INSTRUMENTATION

| PARAMETER | READOUT | TRANSDUCER | SENSITIVITY CHECK |
|---|---|---|---|
| Airspeed | Photo Panel | Not Reqd. | Not Reqd. |
| Altitude | Photo Panel | Not Reqd. | Not Reqd. |
| Clock | Photo Panel | Not Reqd. | Not Reqd. |
| Gas Generator | Photo Panel | A.C. Generator | Not Reqd. |
| Engine RPM | Photo Panel | A.C. Generator | Not Reqd. |
| Engine Torque | Photo Panel | Autosyn | Not Reqd. |
| Air Temperature | Photo Panel | Resistance | Not Reqd. |
| Fuel Flow | Photo Panel | Autosyn | Not Reqd. |
| Flight Counter | Photo Panel | Not Reqd. | Not Reqd. |
| Vertical Rate | Photo Panel | Not Reqd. | Not Reqd. |
| Rudder Position | Oscillograph | Potentiometer | Full Throw |
| Propeller Pitch | Oscillograph | Potentiometer | Full Throw |
| Cyclic Force Pitch | Oscillograph | Strain Gage | Rcal* |
| Cyclic Force Roll | Oscillograph | Strain Gage | Rcal* |
| Rudder Force | Oscillograph | Strain Gage | Rcal* |

* See Note at End of Table.

TABLE XVII. - Continued

| PARAMETER | READOUT | TRANSDUCER | SENSITIVITY CHECK |
|---|---|---|---|
| Collective Force | Oscillograph | Strain Gage | Rcal* |
| Cyclic Pitch Position | Oscillograph | Potentiometer | Full Throw |
| Cyclic Roll Position | Oscillograph | Potentiometer | Full Throw |
| Collective Stick Position | Oscillograph | Potentiometer | Full Throw |
| Rudder Pedal Position | Oscillograph | Potentiometer | Full Throw |
| Pitch Rate | Oscillograph | Potentiometer | Rcal* |
| Roll Rate | Oscillograph | Potentiometer | Rcal* |
| Yaw Rate | Oscillograph | Potentiometer | Rcal* |
| Angle of Attack | Oscillograph | Autosyn | Regulated Power Supply |
| Sideslip | Photo Panel | D.C. Autosyn | Not Reqd. |
| Roll Angle | Oscillograph | Potentiometer | Rcal* |
| Pitch Angle | Oscillograph | Potentiometer | Rcal* |
| Rotor Azimuth Indicator | Oscillograph | Magnetic Pickup | Not Reqd. |
| Blade Flap Angle | Oscillograph | Autosyn | Regulated Power Supply |
| Blade Lead-Lag Angle | Oscillograph | Autosyn | Regulated Power Supply |
| Blade Pitch Angle | Oscillograph | Autosyn | Regulated Power Supply |

* See Note at End of Table.

TABLE XVII. - Continued

| PARAMETER | READOUT | TRANSDUCER | SENSITIVITY CHECK |
|---|---|---|---|
| Pitch Link Load | Oscillograph | Strain Gage | Rcal* |
| Blade Flap Bending Station 46 | Oscillograph | Strain Gage | Rcal* |
| Blade Flap Bending Station 9.5 | Oscillograph | Strain Gage | Rcal* |
| Blade Flap Bending Station 79.2 | Oscillograph | Strain Gage | Rcal* |
| Blade Flap Bending Station 105.6 | Oscillograph | Strain Gage | Rcal* |
| Blade Flap Bending Station 124 | Oscillograph | Strain Gage | Rcal* |
| Blade Flap Bending Station 132 | Oscillograph | Strain Gage | Rcal* |
| Blade Flap Bending Station 158.4 | Oscillograph | Strain Gage | Rcal* |
| Blade Flap Bending Station 184.8 | Oscillograph | Strain Gage | Rcal* |
| Blade Flap Bending Station 211.2 | Oscillograph | Strain Gage | Rcal* |
| Blade Flap Bending Station 237.2 | Oscillograph | Strain Gage | Rcal* |

* See Note at End of Table.

TABLE XVII. - Continued

| PARAMETER | READOUT | TRANSDUCER | SENSITIVITY CHECK |
|---|---|---|---|
| Blade Chord Bending Station 46 | Oscillograph | Strain Gage | Rcal* |
| Blade Chord Bending Station 131.5 | Oscillograph | Strain Gage | Rcal* |
| Blade Trailing Edge Station 92 | Oscillograph | Strain Gage | Rcal* |
| Blade Trailing Edge Station 131.5 | Oscillograph | Strain Gage | Rcal* |
| Blade Trailing Edge Station 210 | Oscillograph | Strain Gage | Rcal* |
| Rotor Shaft Bending Upper 90° | Oscillograph | Strain Gage | Rcal* |
| Rotor Shaft Bending Upper 0° | Oscillograph | Strain Gage | Rcal* |
| Rotor Shaft Torsion | Oscillograph | Strain Gage | Rcal* |
| Rotor Shaft Bending Lower 90° | Oscillograph | Strain Gage | Rcal* |
| Rotor Shaft Bending Lower 0° | Oscillograph | Strain Gage | Rcal* |
| Rotor Shaft Lift | Oscillograph | Strain Gage | Rcal* |

* See Note at End of Table.

TABLE XVII. - Continued

| PARAMETER | READOUT | TRANSDUCER | SENSITIVITY CHECK |
|---|---|---|---|
| Prop Hub Flap Bending | Oscillograph | Strain Gage | Rcal* |
| Prop Blade Flap Bending Station 13.2 | Oscillograph | Strain Gage | Rcal* |
| Prop Blade Flap Bending Station 16.5 | Oscillograph | Strain Gage | Rcal* |
| Prop Blade Flap Bending Station 23.1 | Oscillograph | Strain Gage | Rcal* |
| Prop Blade Flap Bending Station 29.7 | Oscillograph | Strain Gage | Rcal* |
| Prop Blade Chord Bending Station 13.2 | Oscillograph | Strain Gage | Rcal* |
| Prop Shaft Torsion | Oscillograph | Strain Gage | Rcal* |
| Prop Pitch Control Lever Load | Cockpit | Strain Gage | Rcal* |
| Prop Pitch Link Load | Oscillograph | Strain Gage | Rcal* |
| Left Wing Lift Forward | Oscillograph | Strain Gage | Rcal* |
| Left Wing Lift Aft | Oscillograph | Strain Gage | Rcal* |
| Right Wing Lift Forward | Oscillograph | Strain Gage | Rcal* |

* See Note at End of Table.

TABLE XVII. - Continued

| PARAMETER | READOUT | TRANSDUCER | SENSITIVITY CHECK |
|---|---|---|---|
| Right Wing Lift Aft | Oscillograph | Strain Gage | Rcal* |
| Upper Left Longeron Station 175 | Oscillograph | Strain Gage | Rcal* |
| Lower Left Longeron Station 175 | Oscillograph | Strain Gage | Rcal* |
| Left Main Gear Bending (Fore & Aft) | Oscillograph | Strain Gage | Rcal* |
| Fuselage Structure Lower Longeron Station 65 | Oscillograph | Strain Gage | Rcal* |
| Left Main Gear Axial | Oscillograph | Strain Gage | Rcal* |
| Left Main Gear Shock Strut | Oscillograph | Strain Gage | Rcal* |
| Engine Mount Lower Aft | Oscillograph | Strain Gage | Rcal* |
| Engine Mount Upper Aft | Oscillograph | Strain Gage | Rcal* |
| Engine Mount Lower Forward | Oscillograph | Strain Gage | Rcal* |
| Engine Mount Upper Forward | Oscillograph | Strain Gage | Rcal* |

* See Note at End of Table.

TABLE XVII. - Continued

| PARAMETER | READOUT | TRANSDUCER | SENSITIVITY CHECK |
|---|---|---|---|
| C.G. Vertical Acceleration | Oscillograph | Strain Gage Accelerometer | Rcal* |
| Pilot's Compartment Vertical Acceleration | Oscillograph | Strain Gage Accelerometer | Rcal* |
| Fuselage Lateral Acceleration Station 286 | Oscillograph | Strain Gage Accelerometer | Rcal* |
| Fuselage Vertical Acceleration Station 180 | Oscillograph | Strain Gage Accelerometer | Rcal* |
| Rotor Transmission Vertical Acceleration | Oscillograph | Strain Gage Accelerometer | Rcal* |
| Rotor Shaft Vertical Acceleration | Oscillograph | Strain Gage Accelerometer | Rcal* |
| Propeller Shaft Lateral Acceleration | Oscillograph | Strain Gage Accelerometer | Rcal* |
| Pylon Lateral Acceleration | Oscillograph | Strain Gage Accelerometer | Rcal* |
| Pylon Longitudinal Acceleration | Oscillograph | Strain Gage Accelerometer | Rcal* |
| Vertical Acceleration Station 87 | Oscillograph | Strain Gage Accelerometer | Rcal* |

* See Note at End of Table.

TABLE XVII. - Continued

| PARAMETER | READOUT | TRANSDUCER | SENSITIVITY CHECK |
|---|---|---|---|
| Vertical Acceleration Station 9.5 | Oscillograph | Strain Gage Accelerometer | Rcal* |
| Vertical Acceleration Station 114 | Oscillograph | Strain Gage Accelerometer | Rcal* |
| Propeller Box Vertical Acceleration | Oscillograph | Strain Gage Accelerometer | Rcal* |
| Propeller Box Lateral Acceleration | Oscillograph | Strain Gage Accelerometer | Rcal* |
| Flap Deflection | Photo Panel | Potentiometer | Full Throw |

*Rcal: Calibration by biasing measurement circuit with known electrical resistance.

## ERROR ANALYSIS

All instrumentation utilized during flight testing of the 16H-1A was analyzed for probable error. Where applicable, manufacturer's specifications were employed as standards, and random errors were statistically analyzed. It was considered that there are four main types of errors:

1. Errors inherent in the parameter calibration
2. Errors resulting from the $R_{cal}$ method of relating calibrated sensitivity to the pre- and postflight system
3. In-flight errors
4. Inaccuracies of readout and data reduction

The gages were calibrated by applying known loads or configurations as required by the particular parameter. Error is unavoidable in every measurement because instruments are used, but the precision of commercial instruments is well defined. Manufacturer's specifications or recent calibration records were consulted for accuracy.

The input versus output for the system was plotted graphically and a linear relationship was determined. The possible error here was investigated by the method of least squares curve-fitting or the similar method of averages.

A resistor in parallel with one leg of the Wheatstone bridge is used as an indicator of the transducer circuit sensitivity. The apparent strain caused by the resistor in the calibration test is used as a standard for data reduction. This standard removes the effects of any inconsistencies between the calibration and the pre- and postflight measurements. If the same resistor is used for calibrations and flights, there is no error in correlation. If the resistor is changed, there is a possible error of 1 percent due to resistor tolerances.

The in-flight errors arise from differences between the pre- and postflight and airborne conditions. Typical sources of error are temperature gradients in the ship and atmosphere. These errors are removed when a temperature compensating bridge is used. For parameters not compensated, the worst case was investigated. Other effects present were considered indeterminate.

There are two sources of error in readout and data reduction. The oscillograph tapes were read with a probable precision of $\pm$.02 inch for dynamic traces and $\pm$.01 inch for static traces. These errors were expressed in parameter

TABLE XVIII. SUMMARY OF MEASUREMENT ACCURACY

| ITEM | | OVERALL ACCURACY (Including Readout) | | |
|---|---|---|---|---|
| | | Maximum Absolute Error | Units | Relative Error % of Maximum Value Recorded |
| Forces, Moments, Stresses | Rotor Blade Pitch Link Force | 43.5 | Lb. | 12.6 |
| | Rotor Blade Flapwise Moment | | | |
| | Station 46 | 646 | In.-Lb. | 3.8 |
| | 59.5 | 590 | In.-Lb. | 4.8 |
| | 79.2 | 639 | In.-Lb. | 5.2 |
| | 105.6 | 412 | In.-Lb. | 2.9 |
| | 124 | 559 | In.-Lb. | 5.1 |
| | 132 | 393 | In.-Lb. | 4.2 |
| | 158.4 | 360 | In.-Lb. | 3.1 |
| | 184.8 | 175 | In.-Lb. | 1.6 |
| | 211.2 | 231 | In.-Lb. | 3.1 |
| | 237.2 | 446 | In.-Lb. | 1.9 |
| | Rotor Blade Chordwise Moment | | | |
| | Station 46 | 1530 | In.-Lb. | 7.1 |
| | 131.5 | 1900 | In.-Lb. | 5.6 |
| | Rotor Shaft Bending | | | |
| | Upper 90° Azimuth | 2850 | PSI | 6.8 |
| | Upper 0° Azimuth | 2170 | PSI | 5.2 |
| | Lower 90° Azimuth | 2030 | PSI | 4.4 |
| | Lower 0° Azimuth | 3620 | PSI | 7.9 |
| | Rotor Shaft Torque | 9070 | In.-Lb. | 5.1 |
| | Rotor Shaft Lift | 298 | Lb. | 3.8 |
| | Propeller Hub Moment | 218.5 | In.-Lb. | 2.4 |
| | Propeller Blade Flap Flapwise Moment | | | |
| | Station 13.2 | 92.0 | In.-Lb. | 1.6 |
| | 16.5 | 181.0 | In.-Lb. | 4.9 |
| | 23.1 | 164.5 | In.-Lb. | 3.8 |
| | 29.7 | 27.9 | In.-Lb. | 4.2 |
| | Propeller Shaft Torque | 480 | In.-Lb. | 2.5 |
| | Turbine Torquemeter Pressure | 367 | In.-Lb. | 3.9 |
| | Propeller Blade Pitch Link Force | 6.53 | Lb. | 4.4 |

TABLE XVIII. - Continued

| ITEM | | OVERALL ACCURACY (Including Readout) | | |
|---|---|---|---|---|
| | | Maximum Absolute Error | | Relative Error % of Maximum Value Recorded |
| | | | Units | |
| Stresses (Cont'd) | Upper Left Longeron Stress Station 175 | * | PSI | |
| | Lower Left Longeron Stress Station 175 | * | PSI | |
| | Forward Structure, Lower Beam, Left Station 65 | * | PSI | |
| | Main Landing Gear Knee | 676 | in.-Lb. | 3.5 |
| | Main Landing Gear Axial | 124 | Lb. | 13.2 |
| | Main Landing Gear Shock | 288 | Lb. | 15.2 |
| Control Motions | Longitudinal Stick | .665 | Deg. | **1.9 |
| | Lateral Stick | .413 | Deg. | **1.3 |
| | Rudder Pedal | .122 | Deg. | **2.0 |
| | Collective Stick | .274 | Deg. | **3.0 |
| | Propeller Pitch | 1.427 | Deg. | **3.5 |
| | Rudder Vane Angle | 1.058 | Deg. | **2.2 |
| | Rotor Blade Pitch Angle | .519 | Deg. | **2.4 |
| | Elevator Trim Deflection | .72 | Deg. | **2.0 |
| | Flap Deflection | 1.0 | Deg. | **2.0 |
| | Rotor Blade Flap Angle | .238 | Deg. | **3.6 |
| | Rotor Blade Lag Angle | 1.42 | Deg. | |
| Aircraft Motions | Pitch Attitude | .683 | Deg. | **1.8 |
| | Roll Attitude | 2.35 | Deg. | **4.7 |
| | Sideslip Angle | .56 | Deg. | **1.2 |
| | Pitch Rate | 2.32 | Deg./Sec | **5.2 |
| | Roll Rate | .997 | Deg./Sec | **2.2 |
| | Yaw Rate | 2.55 | Deg./Sec | 5.6 |
| | Angle of Attack | 2.32 | Deg. | 6.6 |

* Calibrating theoretical, accuracy indeterminate

** Relative Error for items marked ** is in % of full travel

TABLE XVIII. - Continued

| | ITEM | OVERALL ACCURACY (Including Readout) | | |
|---|---|---|---|---|
| | | Maximum Absolute Error | | Relative Error % of Maximum Value Recorded |
| | | | Units | |
| Vibrations and Accelerations | C.G. Vertical Acceleration | .085 | G | 4.0 |
| | Pilot Compartment Vertical Acceleration | .085 | G | 4.0 |
| | Transmission Case Vertical Acceleration | Negligible | Cyc/Sec | Negligible |
| | Propeller Shaft Bearing Support Vibration | Negligible | Cyc/Sec | Negligible |
| | Propeller Shaft Vibration - Vertical | Negligible | Cyc/Sec | Negligible |
| | Propeller Shaft Vibration - Longitudinal | Negligible | Cyc/Sec | Negligible |
| | Propeller Shaft Vibration - Lateral | Negligible | Cyc/Sec | Negligible |
| Miscellaneous | Airspeed (Indicated) | 2.24 | Kn. | 1.2 |
| | Pressure Altitude | 11.2 | Ft. | 0.5 |
| | Clock | .5 | Sec. | Negligible |
| | Turbine RPM | 50 | RPM | 0.8 |
| | Outside Air Temperature | 2.24 | Deg.(C) | 0.8 |
| | Fuel Flow | 12.2 | Lb./Hr. | 2.0 |
| | Rate of Climb | 173 | Ft./Min. | 5.7 |
| | Gas Generator RPM | 156 | RPM | 0.5 |
| Combined Quantities | Turbine Power (Torque X RPM) | 55.8 | HP | 3.96 |
| | Rotor Power (Torque X RPM) | 44.1 | HP | 5.16 |
| | Propeller Power (Torque X RPM) | 34.8 | HP | 2.62 |
| | True Airspeed (I.A.S., Pressure Altitude, OAT) | 2.52 | Kn. | 1.33 |
| | Density Ratio | .008 | | 0.8 |

units by using the circuit sensitivity.

The difference between the initial and final static readings of a parameter leads to an uncertainty as to the zero reading for any blip. When a difference occurred, the drift was distributed linearly throughout each flight blip in the data reduction computer program. Data from any circuits having a drift of 10 percent or greater were disregarded. It was considered that the most probable drift distribution was one-half of the worst case. The drift error does not apply to alternating readings.

The only probable error originating from the oscillographs is the input frequency effects on the galvanometer. This effect was corrected in the computer program.

Pythagorean addition of errors was used where the parameter is a determinate function of the quantity measured. Where there is not a direct relation, the more conservative algebraic addition was used.

The tabulated errors are total errors for each parameter; the percentage figures relate to the maximum measurements (see Table XVIII).

All performance parameters (torque of rotor, tail propeller, and engine, all tachometers, airspeed, altitude and outside air temperature together with the combined values of turbine, rotor and propeller powers, true airspeed, and density altitude) have errors of 5 percent or less. In addition, 85 percent of the remaining data submitted have probable instrumentation errors less than 5 percent.

## SAMPLE CALCULATION

Rotor shaft torque measurement errors from calibration of 2 August 1966.

$$R_{cal}^{*} = 121 \text{ K ohms}$$

$$I_{cal}^{*} = 20.53°$$

Lever Arm = 258 in. $\pm$ 1/16 in. = 258 in. $\pm$.03%

Scale - Chatillian S/N 207 Accuracy $\pm$1.3% at 148 lb.

* $R_{cal}$ is the value in thousands of ohms of the shunt resistor used in calibration and sensitivity checks.
$I_{cal}$ is the signal change caused by the shunt resistor expressed in degrees of galvanometer deflection.

| READING NUMBER | APPLIED WEIGHT (LB) | NET MOMENT (IN-LB) | AVERAGE MOMENT | GALVO DEFLECTION | AVERAGE GALVO DEFLECTION |
|---|---|---|---|---|---|
| 1 | 43 | 11094 | 10836 | 1.794 | 1.945 |
| 2 | 64 | 16512 | 17286 | 2.975 | 3.450 |
| 3 | 84 | 21672 | 22962 | 4.358 | 4.893 |
| 4 | 105 | 27090 | 28251 | 5.702 | 6.197 |
| 5 | 119 | 30702 | 31476 | 6.705 | 7.036 |
| 6 | 135 | 34830 | 35604 | 7.563 | 7.978 |
| 7 | 148 | 38184 | 38184 | 8.437 | 8.437 |
| 8 | 141 | 36378 | | 8.292 | |
| 9 | 125 | 32250 | | 7.367 | |
| 10 | 114 | 29412 | | 6.692 | |
| 11 | 94 | 24252 | | 5.427 | |
| 12 | 70 | 18060 | | 3.925 | |
| 13 | 41 | 10578 | | 2.095 | |

These readings are averages of increasing and decreasing readings.

Curve fitting by method of averages.

Total of first four average moments

10836
17286
22962
28251
79335

Total of first four average deflections

1.945
3.450
4.893
6.197
16.485

Using equation of straight line

Moment = na X deflection + b

Where n is the number of readings 4

79,335 = 4a X 16.485 + b

Total of second four average moments (using number 4 twice because of odd number of readings)

28251
31476
35604
38184
133515

Total of second four average deflections

6.197
7.036
7.978
8.437
29.648

$$133.515 = 4a \times 29.648 + b$$

Solution of the two simultaneous equations yields

$$\text{Moment} = 4116 \text{ Deflection} + 2870$$

In the $I_{cal}$ value 20.53°, the moment = 84,501 in.-lb.

Value of moment used = 81,900 in.-lb.

$$\text{Error in slope} = \frac{84,501 - 81,900}{84,501} = 3.08\%$$

Assume 3-inch trace, for two readings within .01 inch

$$\text{Readout error} = \frac{2 \times .01}{3.00} = .66\%$$

Overall accuracy for calibration

.03 lever arm length error
1.30 scale error
3.08 slope error
.66 readout error
5.07 percent

No resistor change between calibration and flights, therefore no error from this source.

Error in static reading ±.01 in.
Error in trace reading ±.02 in.
Error in $I_{cal}$ reading ±.01 in.

$$\text{Probable error in reading} = \sqrt{(.01)^2 + (.02)^2 + (.01)^2} = .0245 \text{ in.}$$

Drift = .0085 in. (from random samples)
Sensitivity = 43.323 in.-lb/in. deflection
Maximum torque = 192,000 in.-lb. (reference Figure 149)

$$\text{Reading error} = \frac{.0245 \times 43,323}{192,000} = .553$$

$$\text{Drift error} = \frac{.0085 \times 43,320}{192,000} = .192\%$$

$$\text{Overall error} = \sqrt{(5.07)^2 + (.553)^2 + (.192)^2} = 5.11\%$$

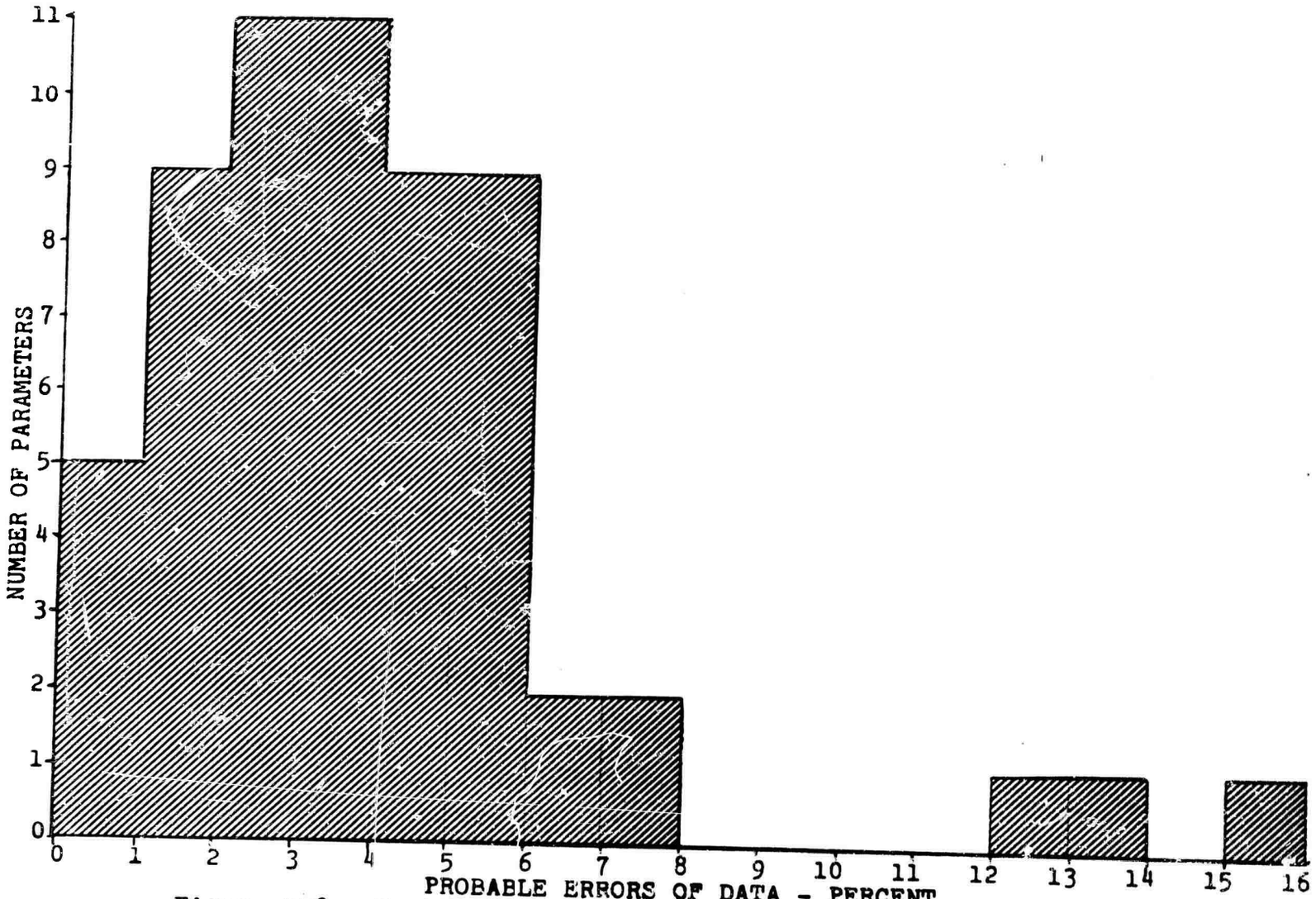


Figure 178. Probable Errors of Data versus Number of Parameters.

## TABLE XIX. 16H-1A WEIGHT AND CENTER-OF-GRAVITY LOG

| FLT. NO. | DATE (1966) | G.W. (lb.) | C.G.* (in.) | BALLAST* 1 lb. | 1 in. | 2 lb. | 2 in. | 3 lb. | 3 in. | 4 lb. | 4 in. | 5 lb. | 5 in. |
|---|---|---|---|---|---|---|---|---|---|---|---|---|---|
| 255 | 24 Nov | 5789 | + 5.5 | 215 | 150 | | | | | | | | |
| 256 | 24 Nov | 5689 | + 2.9 | 115 | 150 | 50 | 106 | | | | | | |
| 257 | 24 Nov | 5759 | + 5.0 | 215 | 150 | | | | | | | | |
| 258 | 27 Nov | 6350 | + 4.8 | 15 | 150 | 50 | 106 | 349 | 52 | 349 | 10 | | |
| 259 | 29 Nov | 6350 | + 4.8 | 15 | 150 | 50 | 106 | 349 | 52 | 349 | 10 | | |
| 260 | 29 Nov | 6372 | + 5.1 | 15 | 150 | 50 | 106 | 349 | 52 | 349 | 10 | | |
| 261 | 1 Dec | 6382 | + 5.1 | 15 | 150 | 50 | 106 | 349 | 52 | 349 | 10 | | |
| 262 | 1 Dec | 6382 | + 5.1 | 15 | 150 | 50 | 106 | 349 | 52 | 349 | 10 | | |
| 263 | 2 Dec | 6330 | +11.6 | 215 | 150 | 100 | 106 | 399 | 66 | | | | |
| 264 | 3 Dec | 6305 | +12.2 | 43 | 190 | 215 | 150 | 100 | 106 | 349 | 66 | | |
| 265 | 3 Dec | 6316 | +12.4 | 43 | 190 | 215 | 150 | 100 | 106 | 349 | 66 | | |
| 266 | 3 Dec | 6316 | +12.4 | 43 | 190 | 215 | 150 | 100 | 106 | 349 | 66 | | |
| 267 | 3 Dec | 6316 | +12.4 | 43 | 190 | 215 | 150 | 100 | 106 | 349 | 66 | | |
| 268 | 16 Dec | 5928 | + 7.4 | 43 | 190 | 215 | 150 | | | | | | |
| 269 | 16 Dec | 5917 | + 7.5 | 43 | 190 | 215 | 150 | | | | | | |
| 270 | 16 Dec | 5909 | + 7.5 | 43 | 190 | 215 | 150 | | | | | | |
| 271 | 17 Dec | 5917 | + 7.5 | 43 | 190 | 215 | 150 | | | | | | |
| 272 | 18 Dec | 5972 | + 8.4 | 43 | 190 | 215 | 150 | 50 | 106 | | | | |
| 273 | 18 Dec | 5972 | + 8.4 | 43 | 190 | 215 | 150 | 50 | 106 | | | | |
| 274 | 21 Dec | 5934 | + 7.8 | 43 | 190 | 215 | 150 | | | | | | |
| 275 | 22 Dec | 5934 | + 7.8 | 43 | 190 | 215 | 150 | | | | | | |
| 276 | 22 Dec | 5984 | + 8.7 | 43 | 190 | 215 | 150 | | | | | | |
| 277 | 23 Dec | GROUND RUN | | | | | | | | | | | |
| 278 | 27 Dec 1966 | GROUND RUN | | | | | | | | | | | |
| 279 | 13 Jan | GROUND RUN | | | | | | | | | | | |
| 280 | 13 Jan | GROUND RUN | | | | | | | | | | | |

* Ballast and C.G. location measured in inches forward of the rotor axis

TABLE XIX. - Continued

| FLT. NO. | DATE (1966) | G.W. (lb.) | C.G.* (in.) | BALLAST* 1 lb. | 1 in. | 2 lb. | 2 in. | 3 lb. | 3 in. | 4 lb. | 4 in. | 5 lb. | 5 in. |
|---|---|---|---|---|---|---|---|---|---|---|---|---|---|
| 281 | 14 Jan | 5938 | + 7.7 | 43 | 190 | 215 | 150 | | | | | | |
| 282 | 14 Jan | 5938 | + 7.7 | 43 | 190 | 215 | 150 | | | | | | |
| 283 | 15 Jan | 5938 | + 7.7 | 43 | 190 | 215 | 150 | | | | | | |
| 284 | 17 Jan | 5988 | + 8.5 | 43 | 190 | 215 | 150 | | | | | | |
| 285 | 18 Jan | 5988 | + 8.5 | 43 | 190 | 215 | 150 | | | | | | |
| 286 | 18 Jan | 5988 | + 8.5 | 43 | 190 | 215 | 150 | | | | | | |
| 287 | 18 Jan | GROUND RUN | | | | | | | | | | | |
| 288 | 18 Jan | GROUND RUN | | | | | | | | | | | |
| 289 | 18 Jan | 5988 | + 8.5 | 43 | 190 | 215 | 150 | | | | | | |
| 290 | 20 Jan | 5988 | + 8.5 | 43 | 190 | 215 | 150 | | | | | | |
| 291 | 20 Jan | 5988 | + 8.5 | 43 | 190 | 215 | 150 | | | | | | |
| 292 | 20 Jan | 5988 | + 8.5 | 43 | 190 | 215 | 150 | | | | | | |
| 293 | 21 Jan | 5423 | + 7.8 | 43 | 190 | 215 | 150 | | | | | | |
| 294 | 22 Jan | 5988 | + 8.5 | 43 | 190 | 215 | 150 | | | | | | |
| 295 | 22 Jan | 5988 | + 8.5 | 43 | 190 | 215 | 150 | | | | | | |
| 296 | 22 Jan | 5988 | + 8.5 | 43 | 190 | 215 | 150 | | | | | | |
| 297 | 22 Jan | 5988 | + 8.5 | 43 | 190 | 215 | 150 | | | | | | |
| 298 | 22 Jan | 5988 | + 8.5 | 43 | 190 | 215 | 150 | | | | | | |
| 299 | 26 Jan | 6021 | + 8.6 | 43 | 190 | 215 | 150 | | | | | | |
| 300 | 26 Jan | 6021 | + 8.6 | 43 | 190 | 215 | 150 | | | | | | |
| 301 | 26 Jan | 6021 | + 8.6 | 43 | 190 | 215 | 150 | | | | | | |
| 302 | 27 Jan | 6021 | + 8.6 | 43 | 190 | 215 | 150 | | | | | | |
| 303 | 27 Jan | 6021 | + 8.6 | 43 | 190 | 215 | 150 | | | | | | |
| 304 | 28 Jan | 6021 | + 8.6 | 43 | 190 | 215 | 150 | | | | | | |
| 305 | 28 Jan | 5988 | + 8.6 | 43 | 190 | 215 | 150 | | | | | | |
| 306 | 28 Jan | 5988 | + 8.6 | 43 | 190 | 215 | 150 | | | | | | |
| 307 | 28 Jan | 5988 | + 8.6 | 43 | 190 | 215 | 150 | | | | | | |
| 308 | 29 Jan | 5988 | + 8.6 | 43 | 190 | 215 | 150 | | | | | | |

* Ballast and C.G. location measured in inches forward of the rotor axis

TABLE XIX. - Continued

| FLT. NO. | DATE (1966) | G.W. (lb.) | C.G.* (in.) | BALLAST* 1 lb. | 1 in. | 2 lb. | 2 in. | 3 lb. | 3 in. | 4 lb. | 4 in. | 5 lb. | 5 in. |
|---|---|---|---|---|---|---|---|---|---|---|---|---|---|
| 309 | 29 Jan | 5988 | + 8.6 | 43 | 190 | 215 | 150 | | | | | | |
| 310 | 29 Jan | 5988 | + 8.6 | 43 | 190 | 215 | 150 | | | | | | |
| 311 | 1 Feb | 6023 | + 8.6 | 43 | 190 | 215 | 150 | | | | | | |
| 312 | 1 Feb | 6023 | + 8.6 | 43 | 190 | 215 | 150 | | | | | | |
| 313 | 1 Feb | 6023 | + 8.6 | 43 | 190 | 215 | 150 | | | | | | |
| 314 | 4 Feb | 6023 | + 8.6 | 43 | 190 | 215 | 150 | | | | | | |
| 315 | 4 Feb | 6023 | + 8.6 | 43 | 190 | 215 | 150 | | | | | | |
| 316 | 4 Feb | 6023 | + 8.6 | 43 | 190 | 215 | 150 | | | | | | |
| 317 | 5 Feb | 6023 | + 8.6 | 43 | 190 | 215 | 150 | | | | | | |
| 318 | 5 Feb | 6023 | + 8.6 | 43 | 190 | 215 | 150 | | | | | | |
| 319 | 5 Feb | 6023 | + 8.6 | 43 | 190 | 215 | 150 | | | | | | |
| 320 | 5 Feb | 6023 | + 8.6 | 43 | 190 | 215 | 150 | | | | | | |
| 321 | 7 Feb | 6023 | + 8.6 | 43 | 190 | 215 | 150 | | | | | | |
| 322 | 7 Feb | 6023 | + 8.6 | 43 | 190 | 215 | 150 | | | | | | |
| 323 | 9 Feb | GROUND RUN | | | | | | | | | | | |
| 324 | 9 Feb | GROUND RUN | | | | | | | | | | | |
| 325 | 9 Feb | 6023 | + 8.6 | 43 | 190 | 215 | 150 | | | | | | |
| 326 | 9 Feb | 6023 | + 8.6 | 43 | 190 | 215 | 150 | | | | | | |
| 327 | 10 Feb | 6023 | + 8.6 | 43 | 190 | 215 | 150 | | | | | | |
| 328 | 10 Feb | 5990 | + 8.6 | 43 | 190 | 215 | 150 | | | | | | |
| 329 | 10 Feb | 6422 | + 8.7 | 43 | 190 | 215 | 150 | 399 | 10 | | | | |
| 330 | 11 Feb | BLADE TRACKING | | | | | | | | | | | |
| 331 | 12 Feb | BLADE TRACKING | | | | | | | | | | | |
| 332 | 12 Feb | 5929 | + 8.8 | 43 | 190 | 215 | 150 | | | | | | |
| 333 | 12 Feb | 5929 | + 8.8 | 43 | 190 | 215 | 150 | | | | | | |
| 334 | 6 Mar | 6268 | + 8.5 | 43 | 190 | 100 | 106 | 399 | 66 | | | | |
| 335 | 7 Mar | 6268 | + 8.5 | 43 | 190 | 100 | 106 | 399 | 66 | | | | |
| 336 | 7 Mar | 6268 | + 8.5 | 43 | 190 | 100 | 106 | 399 | 66 | | | | |

* Ballast and C.G. location measured in inches forward of the rotor axis

TABLE XIX. - Continued

| FLT. NO. | DATE (1966) | G.W. (lb.) | C.G.* (in.) | BALLAST* 1 lb. | 1 in. | 2 lb. | 2 in. | 3 lb. | 3 in. | 4 lb. | 4 in. | 5 lb. | 5 in. |
|---|---|---|---|---|---|---|---|---|---|---|---|---|---|
| 337 | 7 Mar | 6268 | + 8.5 | 43 | 190 | 100 | 106 | 399 | 66 | | | | |
| 338 | 7 Mar | 6268 | + 8.5 | 43 | 190 | 100 | 106 | 399 | 66 | | | | |
| 339 | 7 Mar | 6268 | + 8.5 | 43 | 190 | 100 | 106 | 399 | 66 | | | | |
| 340 | 8 Mar | 6268 | + 8.5 | 43 | 190 | 100 | 106 | 399 | 66 | | | | |
| 341 | 8 Mar | 6268 | + 8.5 | 43 | 190 | 100 | 106 | 399 | 66 | | | | |
| 342 | 8 Mar | 6268 | + 8.5 | 43 | 190 | 100 | 106 | 399 | 66 | | | | |
| 343 | 9 Mar | 6268 | + 8.5 | 43 | 190 | 100 | 106 | 399 | 66 | | | | |
| 344 | 9 Mar | 6268 | + 8.5 | 43 | 190 | 100 | 106 | 399 | 66 | | | | |
| 345 | 9 Mar | BLADE TRACKING | | | | | | | | | | | |
| 346 | 9 Mar | 6268 | + 8.5 | 43 | 190 | 100 | 106 | 399 | 66 | | | | |
| 347 | 10 Mar | 6268 | + 8.5 | 43 | 190 | 100 | 106 | 399 | 66 | | | | |
| 348 | 10 Mar | 6268 | + 8.5 | 43 | 190 | 100 | 106 | 399 | 66 | | | | |
| 349 | 14 Mar | 6006 | + 8.5 | 43 | 190 | 215 | 150 | | | | | | |
| 350 | 14 Mar | 6006 | + 8.5 | 43 | 190 | 215 | 150 | | | | | | |
| 351 | 14 Mar | 6006 | + 8.5 | 43 | 190 | 215 | 150 | | | | | | |
| 352 | 14 Mar | 6006 | + 8.5 | 43 | 190 | 215 | 150 | | | | | | |
| 353 | 15 Mar | 6006 | + 8.5 | 43 | 190 | 215 | 150 | | | | | | |
| 354 | 15 Mar | 6006 | + 8.5 | 43 | 190 | 215 | 150 | | | | | | |
| 355 | 16 Mar | 6114 | + 8.8 | 43 | 190 | 215 | 150 | | | | | | |
| 356 | 17 Mar | 6030 | + 8.9 | 43 | 190 | 215 | 150 | | | | | | |
| 357 | 17 Mar | 5986 | + 7.6 | 215 | 150 | | | | | | | | |
| 358 | 17 Mar | 5915 | + 5.4 | 43 | 190 | 100 | 106 | | | | | | |
| 359 | 18 Mar | 5960 | + 8.0 | 43 | 190 | 215 | 150 | 50 | 106 | | | | |
| 360 | 18 Mar | SERVICE TEST | | | | | | | | | | | |
| 361 | 19 Mar | 5960 | + 8.0 | 43 | 190 | 215 | 150 | 50 | 106 | | | | |
| 362 | 21 Mar | 6045 | + 5.8 | 43 | 190 | 50 | 106 | 300 | 66 | | | | |
| 363 | 21 Mar | 6045 | + 5.8 | 43 | 190 | 215 | 150 | 50 | 106 | | | | |
| 364 | 21 Mar | 6030 | + 8.9 | 43 | 190 | 215 | 150 | | | | | | |

* Ballast and C.G. location measured in inches forward of rotor axis

## TABLE XIX. - Continued

| FLT. NO. | DATE (1966) | G.W. (lb.) | C.G.* (in.) | BALLAST* 1 lb. | 1 in. | 2 lb. | 2 in. | 3 lb. | 3 in. | 4 lb. | 4 in. | 5 lb. | 5 in. |
|---|---|---|---|---|---|---|---|---|---|---|---|---|---|
| 365 | 22 Mar | 6045 | + 5.8 | 43 | 190 | 50 | 106 | 300 | 66 | | | | |
| 366 | 22 Mar | 6115 | + 6.7 | 43 | 190 | 300 | 66 | | | | | | |
| 367 | 22 Mar | 6115 | + 6.7 | 43 | 190 | 300 | 66 | | | | | | |
| 368 | 23 Mar | 6001 | + 8.0 | 43 | 190 | 38 | 66 | | | | | | |
| 369 | 24 Mar | 6001 | + 8.0 | 43 | 190 | 38 | 66 | | | | | | |
| 370 | 24 Mar | 6001 | + 8.0 | 43 | 190 | 38 | 66 | | | | | | |
| 371 | 25 Mar | 5998 | + 8.0 | 43 | 190 | 38 | 66 | | | | | | |
| 372 | 26 Mar | 6071 | + 9.8 | 43 | 190 | 200 | 150 | | | | | | |
| 373 | 26 Mar | 6278 | +11.2 | 43 | 190 | 200 | 150 | | | | | | |
| 374 | 28 Mar | 6071 | + 9.2 | 43 | 190 | 200 | 150 | | | | | | |
| 375 | 29 Mar | 6071 | + 9.8 | 43 | 190 | 200 | 150 | | | | | | |
| 376 | 29 Mar | 6071 | + 9.8 | 43 | 190 | 200 | 150 | | | | | | |
| 377 | 29 Mar | 6071 | + 9.8 | 43 | 190 | 200 | 150 | | | | | | |
| 378 | 30 Mar | 6071 | + 9.8 | 43 | 190 | 200 | 150 | | | | | | |
| 379 | 30 Mar | 6071 | + 9.8 | 43 | 190 | 200 | 150 | | | | | | |
| 380 | 1 Apr | 6071 | + 9.8 | 43 | 190 | 200 | 150 | | | | | | |
| 381 | 11 May | SERVICE TEST | | | | | | | | | | | |
| 382 | 19 May | SERVICE TEST | | | | | | | | | | | |
| 383 | 20 May | 6113 | + 9.3 | 43 | 190 | 200 | 150 | | | | | | |
| 384 | 20 May | SERVICE TEST | | | | | | | | | | | |
| 385 | 20 May | SERVICE TEST | | | | | | | | | | | |
| 386 | 20 May | SERVICE TEST | | | | | | | | | | | |
| 387 | 21 May | SERVICE TEST | | | | | | | | | | | |
| 388 | 21 May | SERVICE TEST | | | | | | | | | | | |
| 389 | 23 May | 6135 | + 9.7 | 43 | 190 | 200 | 150 | | | | | | |
| 390 | 25 May | 6135 | + 9.7 | 43 | 190 | 200 | 150 | | | | | | |
| 391 | 25 May | 6135 | + 9.7 | 43 | 190 | 200 | 150 | | | | | | |
| 392 | 25 May | 6135 | + 9.7 | 43 | 190 | 200 | 150 | | | | | | |
| 393 | 25 May | 6140 | + 9.6 | 43 | 190 | 200 | 150 | | | | | | |

* Ballast and C.G. location measured in inches forward of rotor axis

TABLE XIX. - Continued

| FLT. NO. | DATE (1966) | G.W. (lb.) | C.G.* (in.) | BALLAST* 1 lb. | 1 in. | 2 lb. | 2 in. | 3 lb. | 3 in. | 4 lb. | 4 in. | 5 lb. | 5 in. |
|---|---|---|---|---|---|---|---|---|---|---|---|---|---|
| 394 | 25 May | 6140 | + 9.6 | 43 | 190 | 200 | 150 | | | | | | |
| 395 | 26 May | 6140 | + 9.6 | 43 | 190 | 200 | 150 | | | | | | |
| 396 | 26 May | 6140 | + 9.6 | 43 | 190 | 200 | 150 | | | | | | |
| 397 | 28 May | 6140 | + 9.6 | 43 | 190 | 200 | 150 | | | | | | |
| 398 | 29 May | 6140 | + 9.6 | 43 | 190 | 200 | 150 | | | | | | |
| 399 | 29 May | 6140 | + 9.6 | 43 | 190 | 200 | 150 | | | | | | |
| 400 | 29 May | 6140 | + 9.6 | 43 | 190 | 200 | 150 | | | | | | |
| 401 | 31 May | 6140 | + 9.6 | 43 | 190 | 200 | 150 | | | | | | |
| 402 | 31 May | 6153 | + 9.6 | 43 | 190 | 200 | 150 | | | | | | |
| 403 | 31 May | 6153 | + 9.6 | 43 | 190 | 200 | 150 | | | | | | |
| 404 | 1 Jun | 6166 | + 9.6 | 43 | 190 | 200 | 150 | 40 | 106 | | | | |
| 405 | 1 Jun | 6166 | + 9.6 | 43 | 190 | 200 | 150 | 40 | 106 | | | | |
| 406 | 1 Jun | 6166 | + 9.7 | 43 | 190 | 200 | 150 | 40 | 106 | | | | |
| 407 | 2 Jun | 6171 | + 9.7 | 43 | 190 | 200 | 150 | 40 | 106 | | | | |
| 408 | 3 Jun | 6171 | + 9.7 | 43 | 190 | 200 | 150 | 40 | 106 | | | | |
| 409 | 3 Jun | 6171 | + 9.7 | 43 | 190 | 200 | 150 | 40 | 106 | | | | |
| 410 | 3 Jun | 6171 | + 9.7 | 43 | 190 | 200 | 150 | 40 | 106 | | | | |
| 411 | 4 Jun | 6171 | + 9.7 | 43 | 190 | 200 | 150 | 40 | 106 | | | | |
| 412 | 4 Jun | 6171 | + 9.7 | 43 | 190 | 200 | 150 | 40 | 106 | | | | |
| 413 | 4 Jun | 6171 | + 9.7 | 43 | 190 | 200 | 150 | 40 | 106 | | | | |
| 414 | 4 Jun | 6171 | + 9.7 | 43 | 190 | 200 | 150 | 40 | 106 | | | | |
| 415 | 6 Jun | 6171 | + 9.7 | 43 | 190 | 200 | 150 | 40 | 106 | | | | |
| 416 | 6 Jun | 6138 | + 9.2 | 43 | 190 | 200 | 150 | 40 | 106 | | | | |
| 417 | 6 Jun | 6002 | + 9.8 | 43 | 190 | 200 | 150 | 40 | 106 | | | | |
| 418 | 23 Jun | 7000 | +10.1 | 43 | 190 | 100 | 150 | 40 | 106 | 399 | 52 | 541 | 10 |
| 419 | 23 Jun | 7000 | +10.1 | 43 | 190 | 100 | 150 | 40 | 106 | 399 | 52 | 541 | 10 |
| 420 | 23 Jun | 7000 | +10.1 | 43 | 190 | 100 | 150 | 40 | 106 | 399 | 52 | 541 | 10 |
| 421 | 24 Jun | 6833 | +10.4 | 43 | 190 | 100 | 150 | 40 | 106 | 399 | 52 | 541 | 10 |
| 422 | 24 Jun | 7500 | + 9.8 | 43 | 190 | 100 | 150 | 40 | 106 | 399 | 52 | 541 | 10 |

* Ballast and C.G. location measured in inches forward of rotor axis

TABLE XIX. - Continued

| FLT. NO. | DATE (1966) | G.W. (lb.) | C.G.* (in.) | BALLAST* 1 lb. | 1 in. | 2 lb. | 2 in. | 3 lb. | 3 in. | 4 lb. | 4 in. | 5 lb. | 5 in. |
|---|---|---|---|---|---|---|---|---|---|---|---|---|---|
| 423 | 3 Jul | 6000 | + 3.1 | 129 | 10 | | | | | | | | |
| 424 | 3 Jul | 6000 | + 3.1 | 129 | 10 | | | | | | | | |
| 425 | 3 Jul | 6000 | + 3.1 | 129 | 10 | | | | | | | | |
| 426 | 3 Jul | 6000 | + 3.1 | 129 | 10 | | | | | | | | |
| 427 | 3 Jul | 6005 | + 3.1 | 129 | 10 | | | | | | | | |
| 428 | 4 Jul | 6005 | + 3.1 | 129 | 10 | | | | | | | | |
| 429 | 4 Jul | 6005 | + 3.1 | 129 | 10 | | | | | | | | |
| 430 | 4 Jul | 6005 | + 3.1 | 129 | 10 | | | | | | | | |
| 431 | 5 Jul | 6005 | + 3.1 | 129 | 10 | | | | | | | | |
| 432 | 5 Jul | 6005 | + 3.1 | 129 | 10 | | | | | | | | |
| 433 | 5 Jul | 6005 | + 3.1 | 129 | 10 | | | | | | | | |
| 434 | 5 Jul | 6005 | + 3.1 | 129 | 10 | | | | | | | | |
| 435 | 6 Jul | 6005 | + 3.1 | 129 | 10 | | | | | | | | |
| 436 | 6 Jul | 6048 | + 4.4 | 43 | 190 | 129 | 10 | | | | | | |
| 437 | 6 Jul | 6005 | + 3.1 | 129 | 10 | | | | | | | | |
| 438 | 6 Jul | 6005 | + 3.1 | 129 | 10 | | | | | | | | |

* Ballast and C.G. location measured in inches forward of rotor axis

TABLE XX. ESTIMATED DRAG BREAKDOWN, 16H-1A

| ITEM | EQUIVALENT PARASITE Area ($FT^2$) | | APPLICABLE NET WETTED Area ($FT^2$) |
|---|---|---|---|
| Fuselage | | 6.27 | |
| A. Drag | | | |
| Basic Fuselage | 2.50 | | 408 |
| Surface Imperfections | .10 | | |
| Blisters, Gaps | .06 | | |
| Nose Boom | .21 | | |
| Nose Weights | .29 | | |
| Antenna | .04 | | |
| Pylon | .66 | | 42 |
| Engine Inlet | .28 | | |
| Engine Exhaust | .60 | | |
| B. Momentum Losses | | | |
| Oil Cooling Fan | .40 | | |
| Engine Net Drag | .35 | | |
| Fuselage Ventilation | .78 | | |
| Landing Gear | | .95 | |
| Main Gear (Open Wells) | .61 | | |
| Tail Gear | .34 | | |
| Rotor | | 3.15 | |
| Hinge Assembly | 2.85 | | |
| Blade Shanks | .30 | | |
| Wing | | 1.20 | 140 |
| Ring Tail | | 1.96 | |
| Duct (Including Surface Imperfection) | .95 | | 96 |
| Rudders (Fittings, Bolts, etc.) | .60 | | 49 |
| Elevators and Horizontal Stabilizer | .17 | | 18 |
| Stators | .24 | | 33 |
| TOTALS | | 13.53 | 786 |

NOTE: Wheels and Flaps Up.

## APPENDIX III

## STABILITY AND CONTROL ANALYSES

### LONGITUDINAL CONTROL POWER AND ELEVATOR TRIM POWER IN HOVER

Stick position required for trim has been measured in the hover condition for various center-of-gravity locations and elevator deflections. These results are shown in Figures 179 and 180.

The faired curves of stick position versus center-of-gravity locations and versus elevator setting are consistent with the final level flight stick position versus speed curve which illustrates the 16H-1A longitudinal static stability (Figure 54).

The rate of change of stick displacement with center-of-gravity shift shown in the plot is substantiated by the experimentally confirmed estimate of longitudinal control power discussed in the hover response analysis. This parameter, essentially independent of gross weight, is computed as follows:

$M_\delta$ = -1,500 ft-lb/inch, based on W = 6000 lb.

$$\frac{d\delta}{dx} = \frac{1}{12}\,\frac{W}{M_\delta} \qquad (73)$$

$$= \frac{-6,000}{12 \times 1,500}$$

= -0.333 inch stick per inch center-of-gravity displacement

With this parameter, the elevator trim effectiveness in hover can be determined in terms of both center-of-gravity displacement and pitching moment. These parameters are found as follows:

$$\frac{dx}{d\delta_e} = \frac{d\delta/d\delta_e}{d\delta/dx} \qquad (74)$$

where

$\frac{d\delta}{d\delta_e}$ = -0.0375 in/deg. from Figure 180

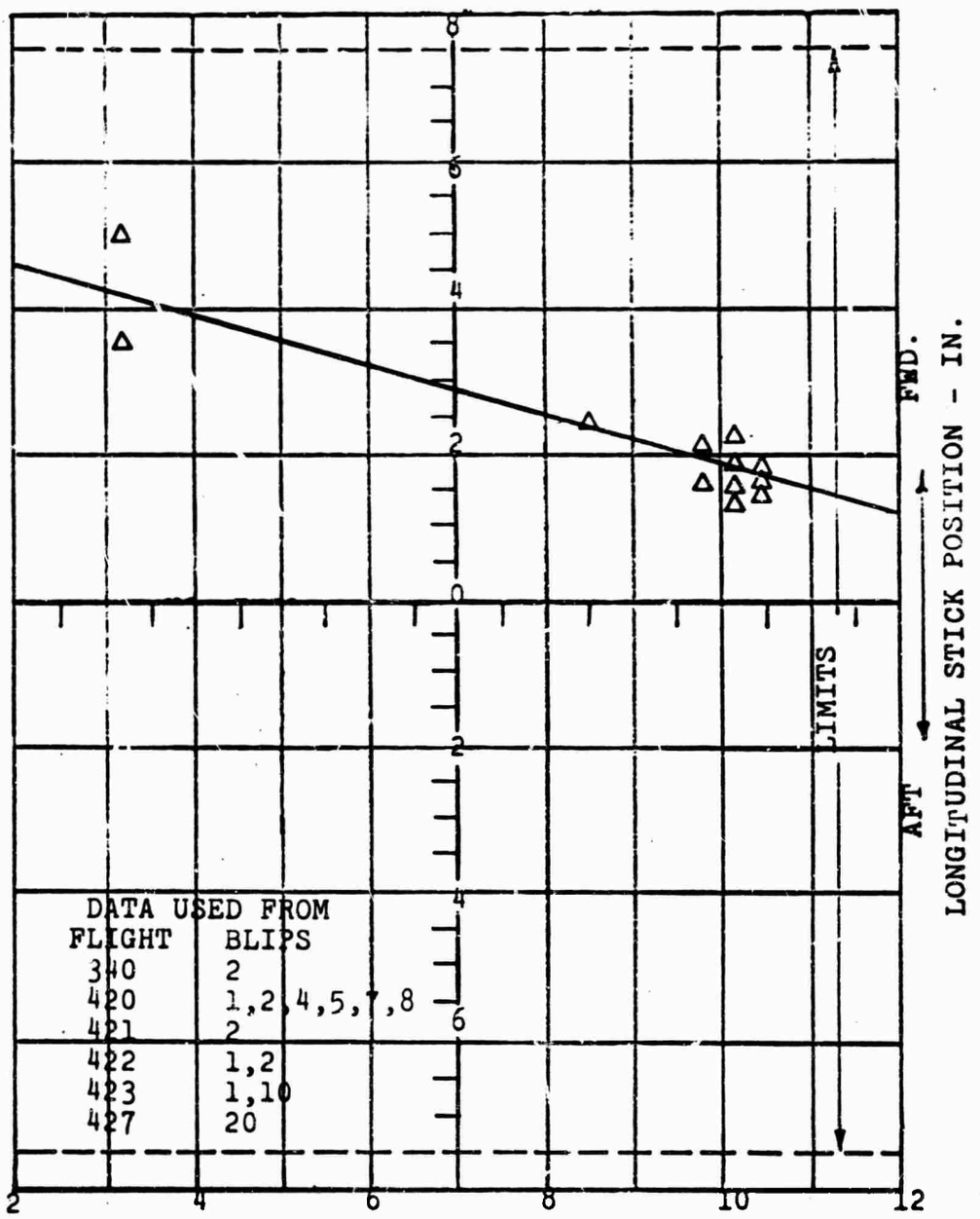


Figure 179. Longitudinal Stick Position versus C.G. Position - Hovering, Neutral Elevator.

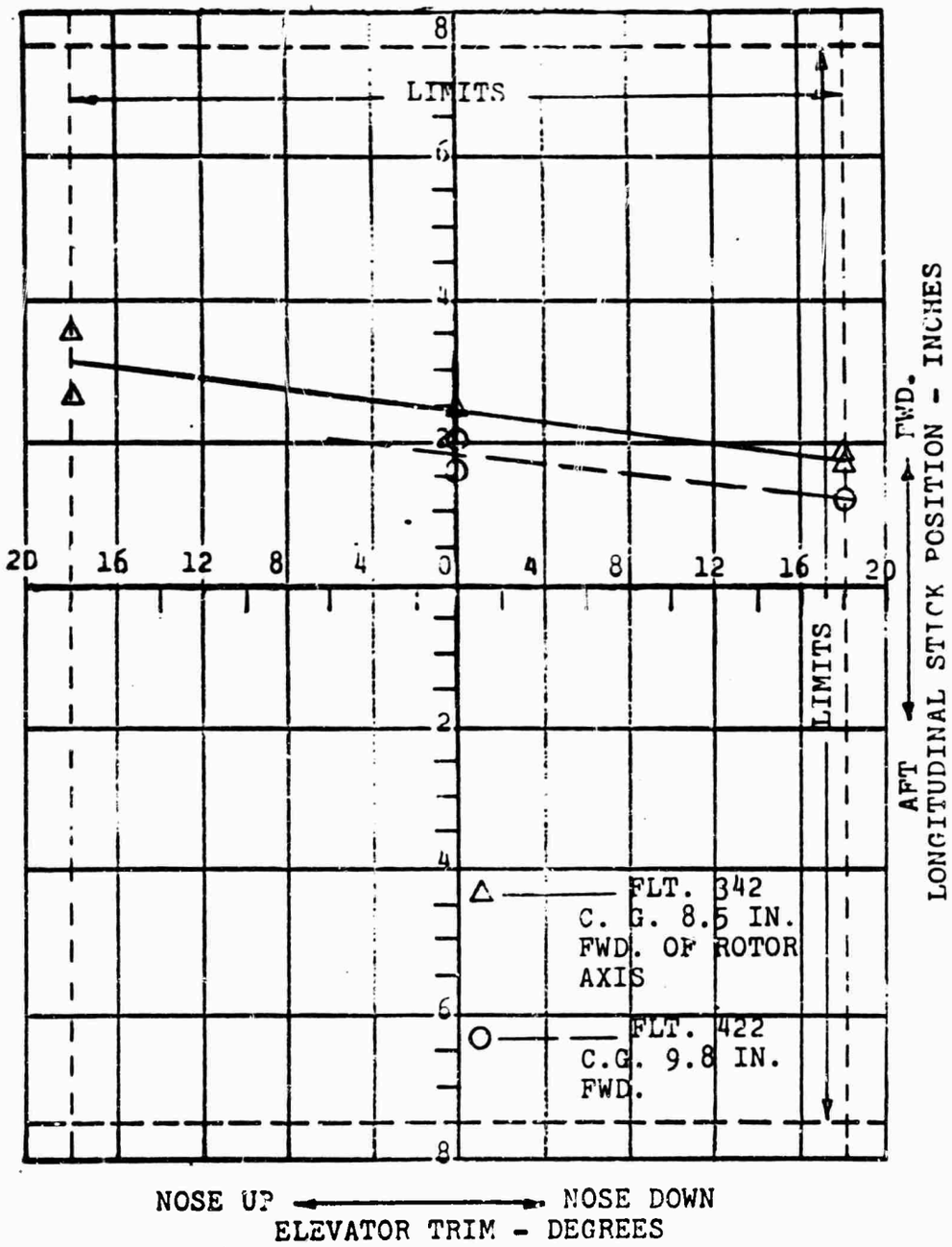


Figure 180. Longitudinal Stick Position versus Elevator Trim - Hovering Flight.

$$\frac{dx}{d\delta_e} = \frac{-0.0375}{-0.333}$$

= 0.113 inch center-of-gravity displacement per degree of elevator.

Thus the elevator is capable of balancing a 4.4-inch center-of-gravity shift in hover at a fixed stick position. The corresponding pitching-moment effectiveness is

$$M_{\delta_e} = -M_\delta \times \frac{d\delta}{d\delta_e} \qquad (75)$$

$$= -(-1,500)(-0.0375)$$

$$= -56.3 \text{ ft-lb/deg}$$

ANGULAR ACCELERATION IN HOVER

Control power, expressed in terms of initial angular acceleration per inch of control motion, has been evaluated from hover control response tests. Angular rate traces were used to obtain control power considered as the ratio of control moment per inch to the inertia about the corresponding motion axis.

The resultant control power is given by the slopes of the plotted angular velocity data (Figures 97, 181 and 184). The experimental values for these tests are compared with the experimental results from the 50-knot dynamic tests in the following table, together with the minimum requirements based on MIL-H-8501A hover specification (assuming a pure inertia system), and is summarized below.

CONTROL POWER (DEG/SEC$^2$ PER IN.)

| | HOVER | 50-KNOT DYNAMIC TESTS | MINIMUM HOVER REQUIREMENT, MIL-H-8501A |
|---|---|---|---|
| Pitch | -9.2 | -7.8 | -4.7 |
| Roll | 51.0 | 53.8 | 11.2 |
| Yaw (Right Pedal) | -30.0 | -33.4 | -11.5 |
| Yaw (Left Pedal) | -14.4 | -23.9 | -11.5 |

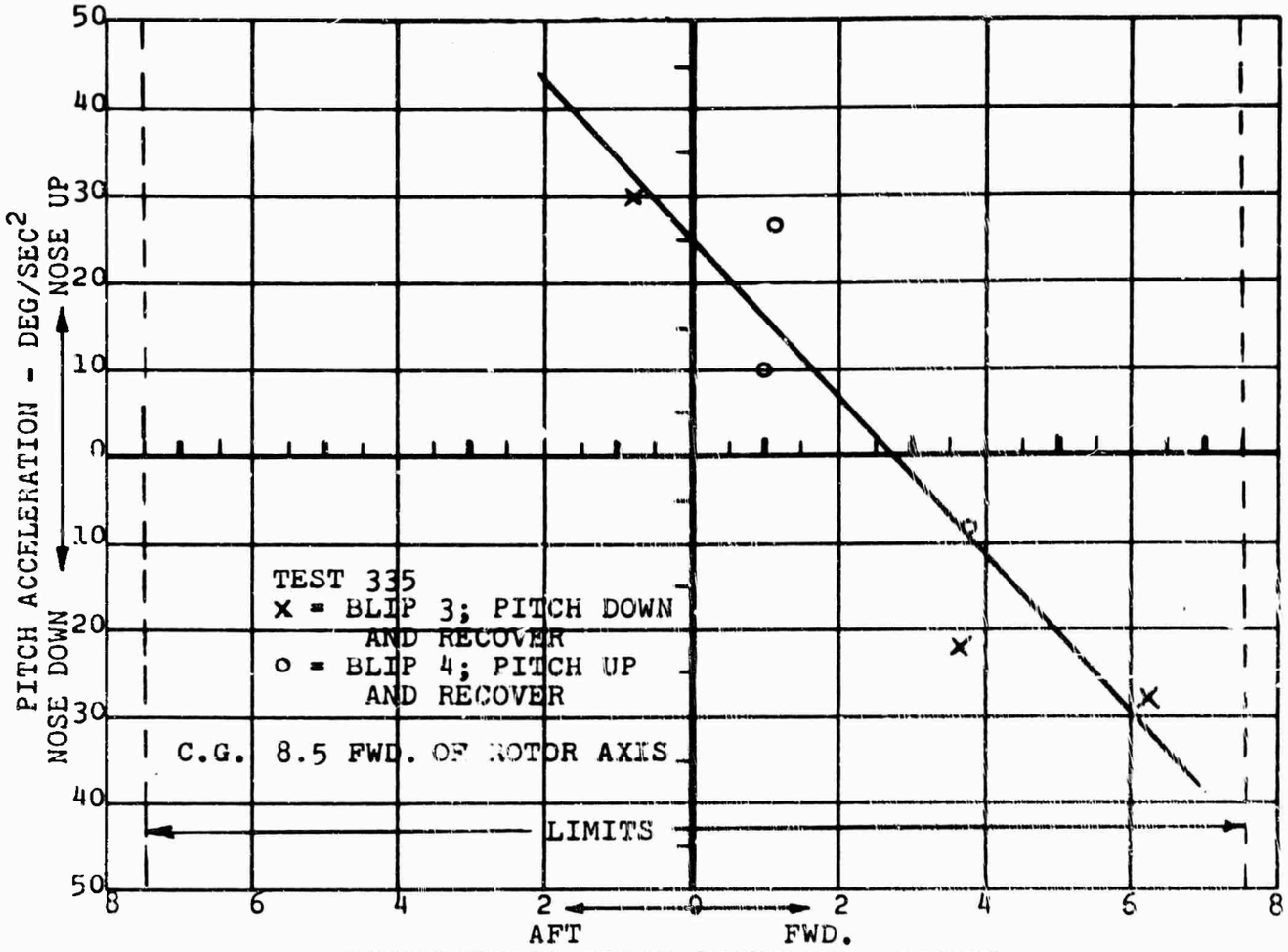


Figure 181. Pitch Response in Hover - Acceleration versus Longitudinal Stick Position.

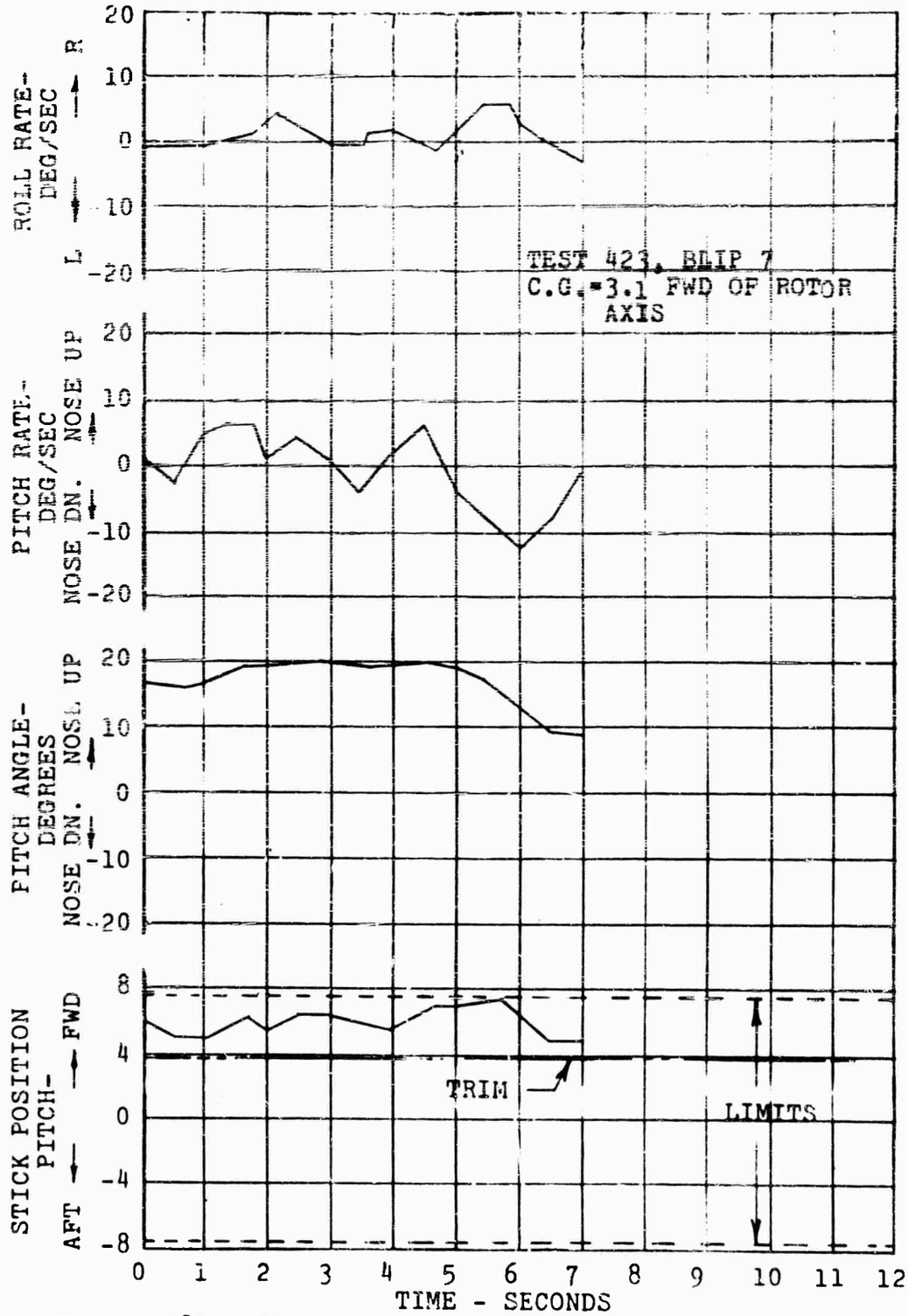


Figure 182. Pitch Response in Hover - Pitch Up, C.G. 3.1.

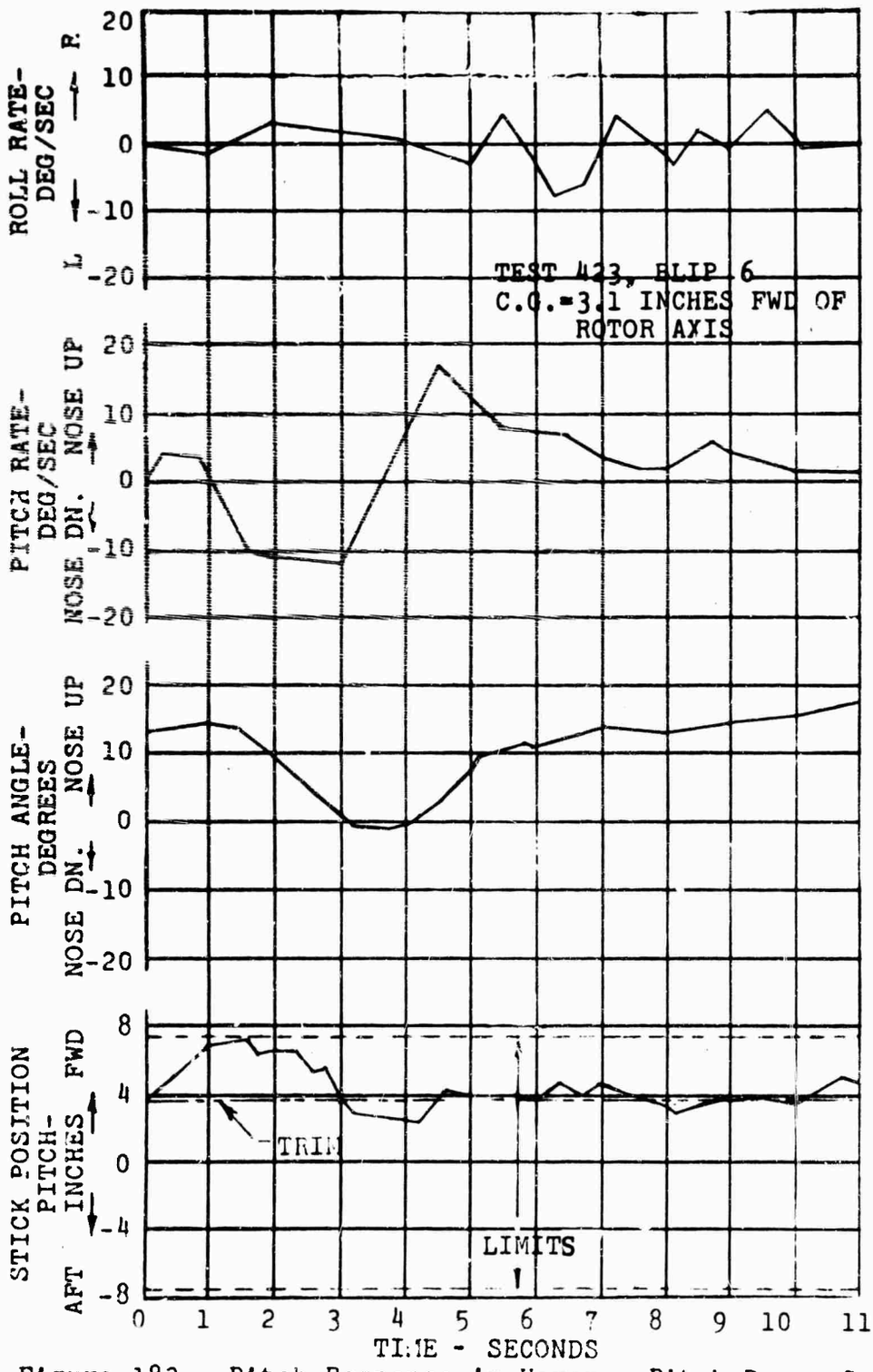


Figure 183. Pitch Response in Hover - Pitch Down, C.G. 3.1.

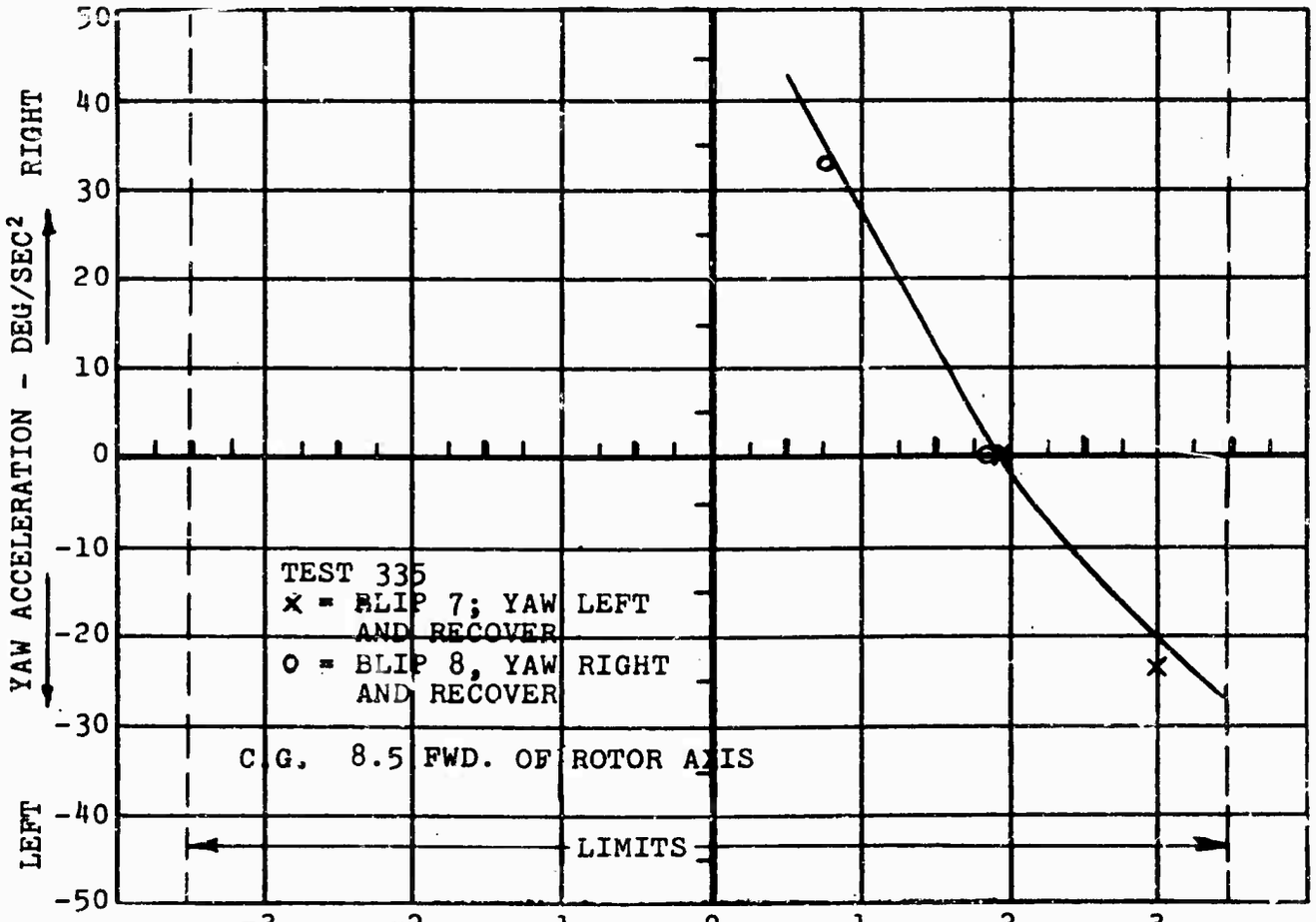


Figure 184. Yaw Response in Hover - Acceleration versus Rudder Pedal Position, C.G. 8.5.

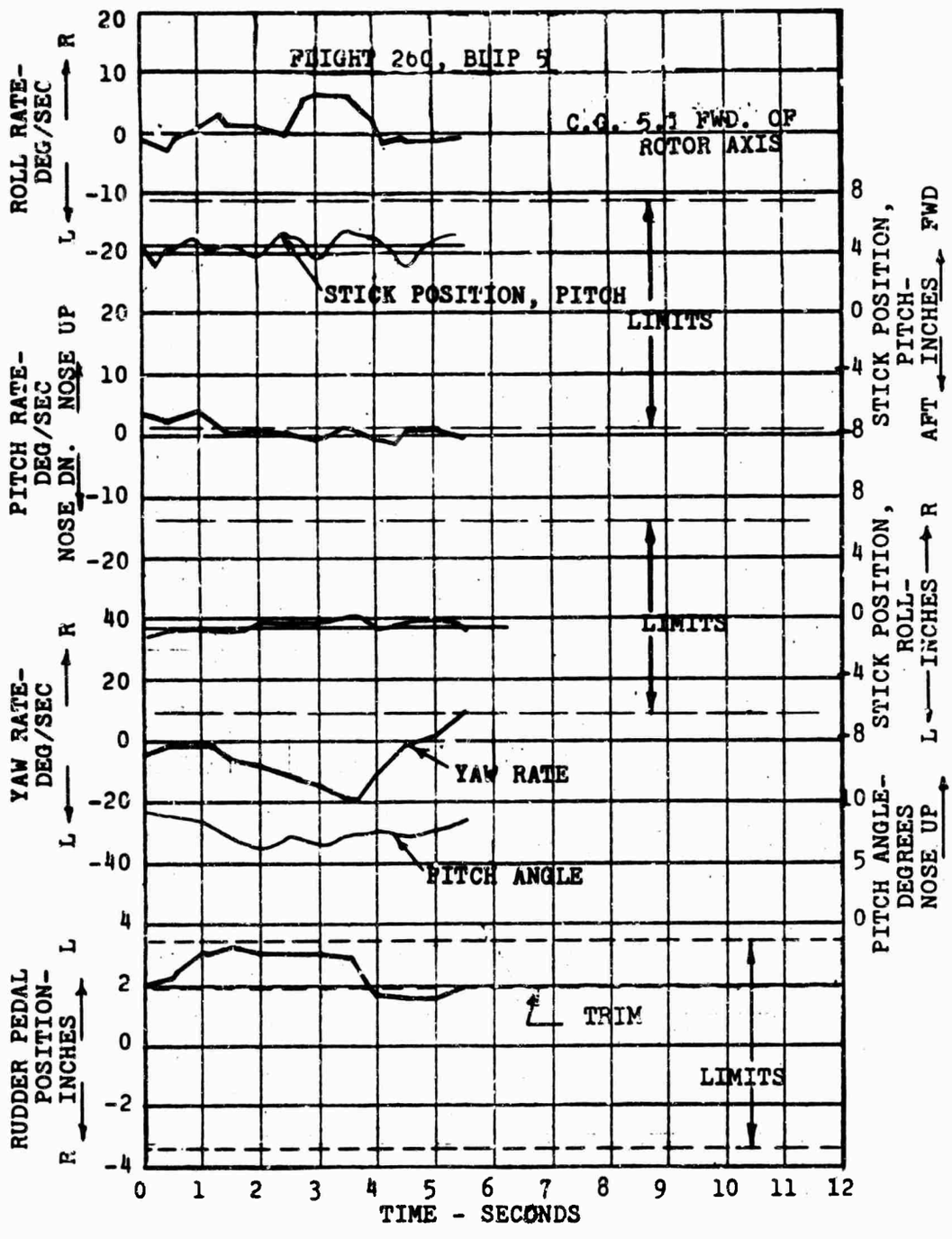


Figure 185. Yaw Response in Hover - Yaw Left, C.G. 5.1.

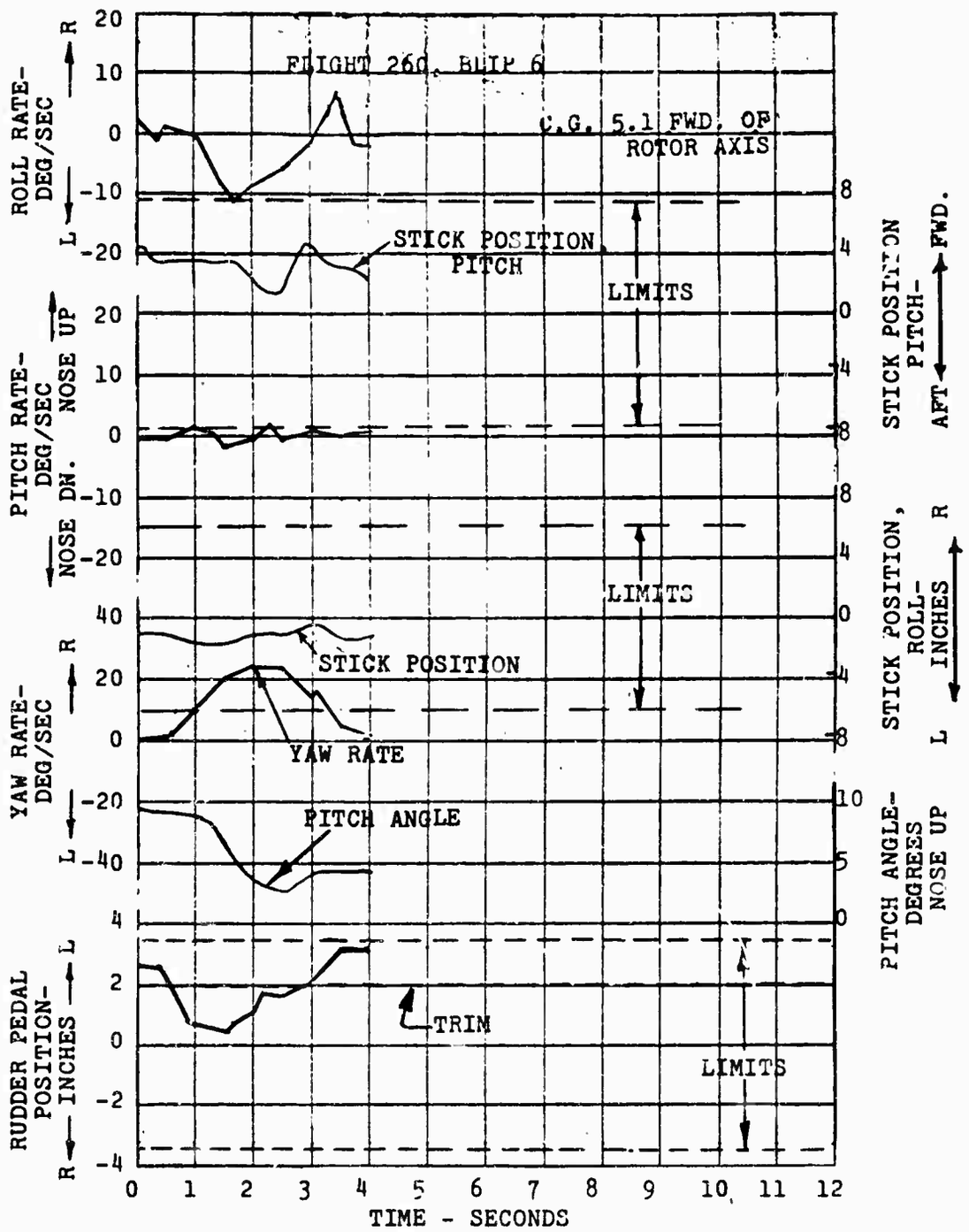


Figure 186. Yaw Response in Hover - Yaw Right, C.G. 5.1.

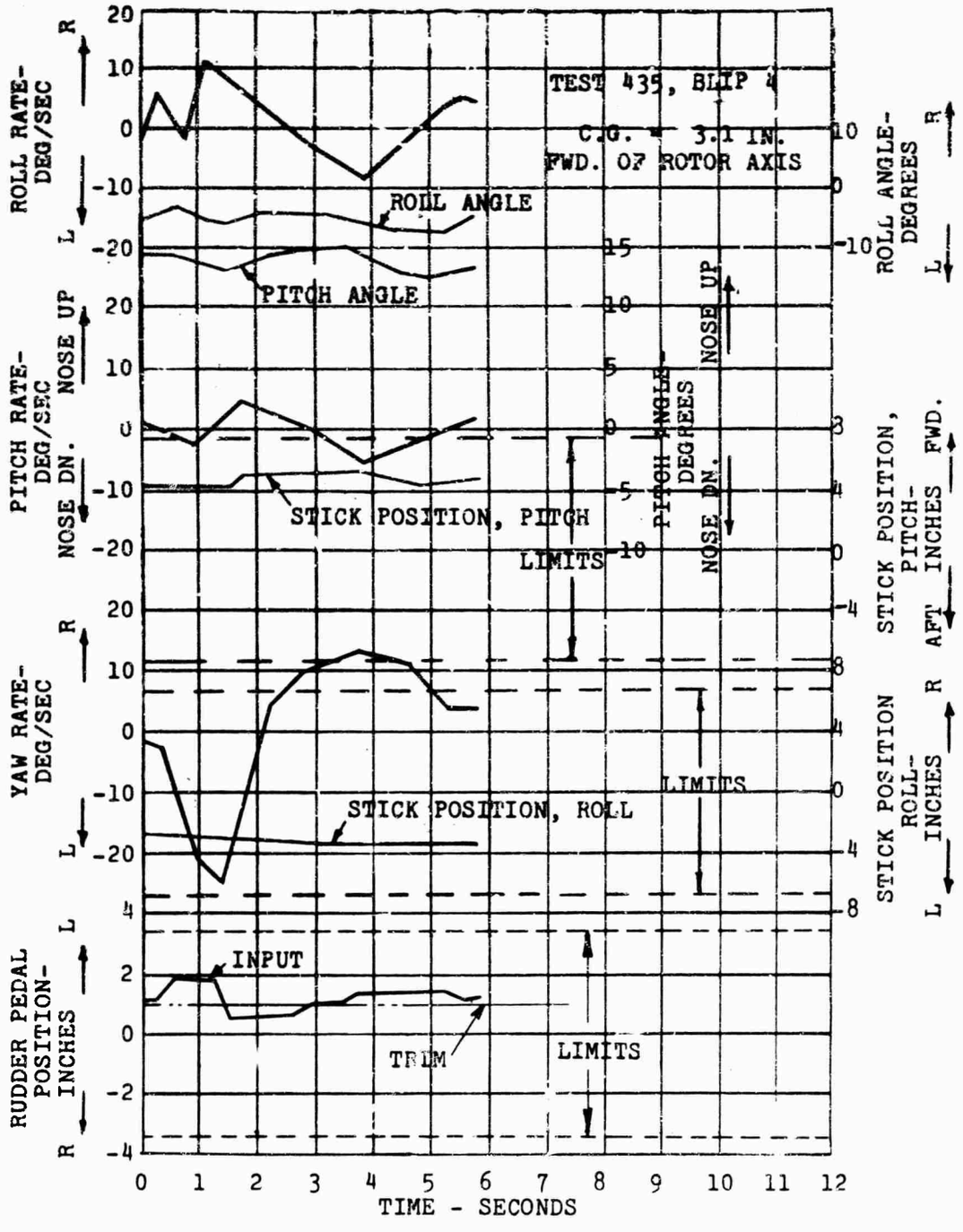


Figure 187. Yaw Response in Hover - Yaw Left, C.G. 3.1.

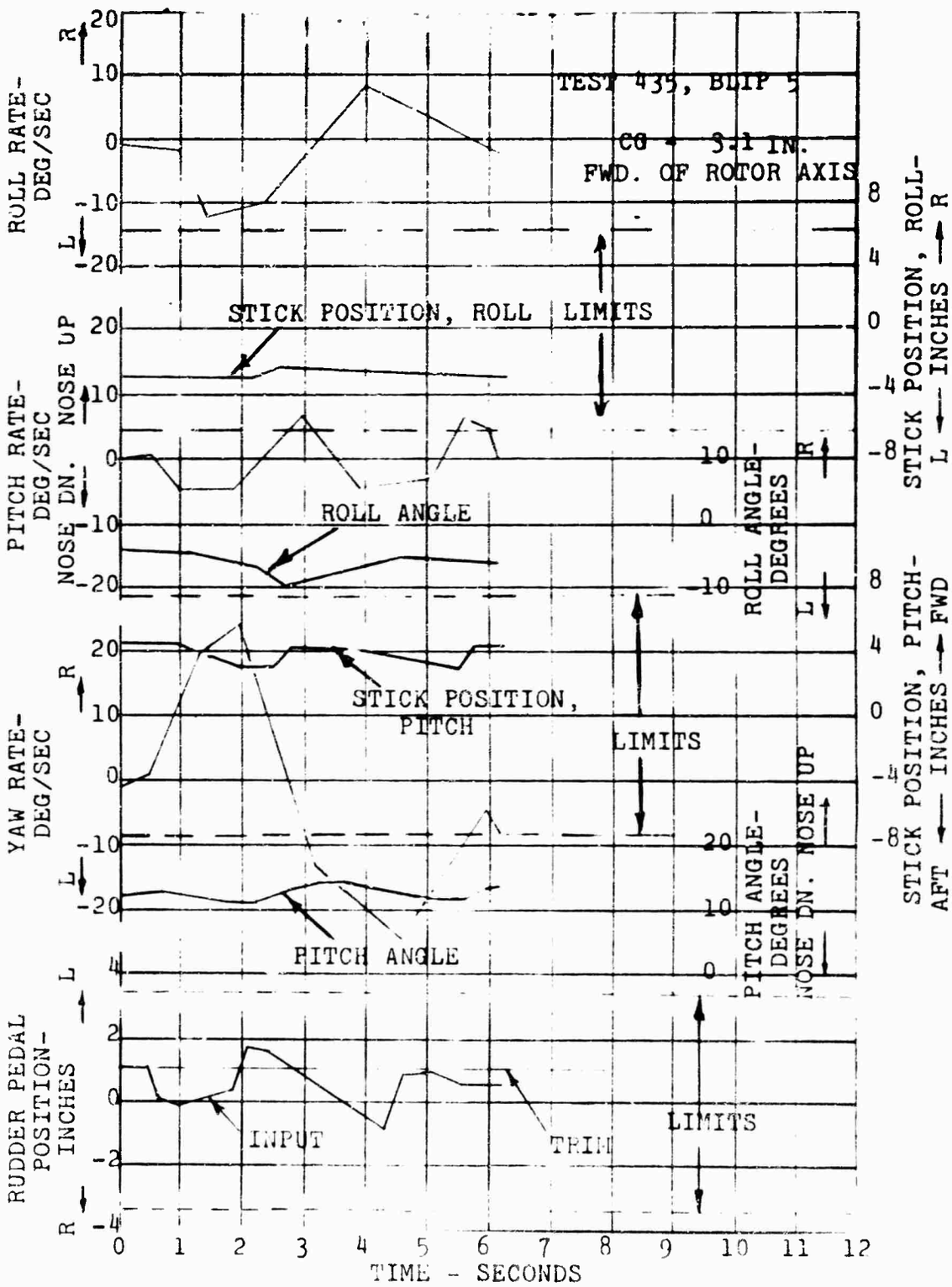


Figure 188. Yaw Response in Hover- Yaw Right, C.G. 3.1.

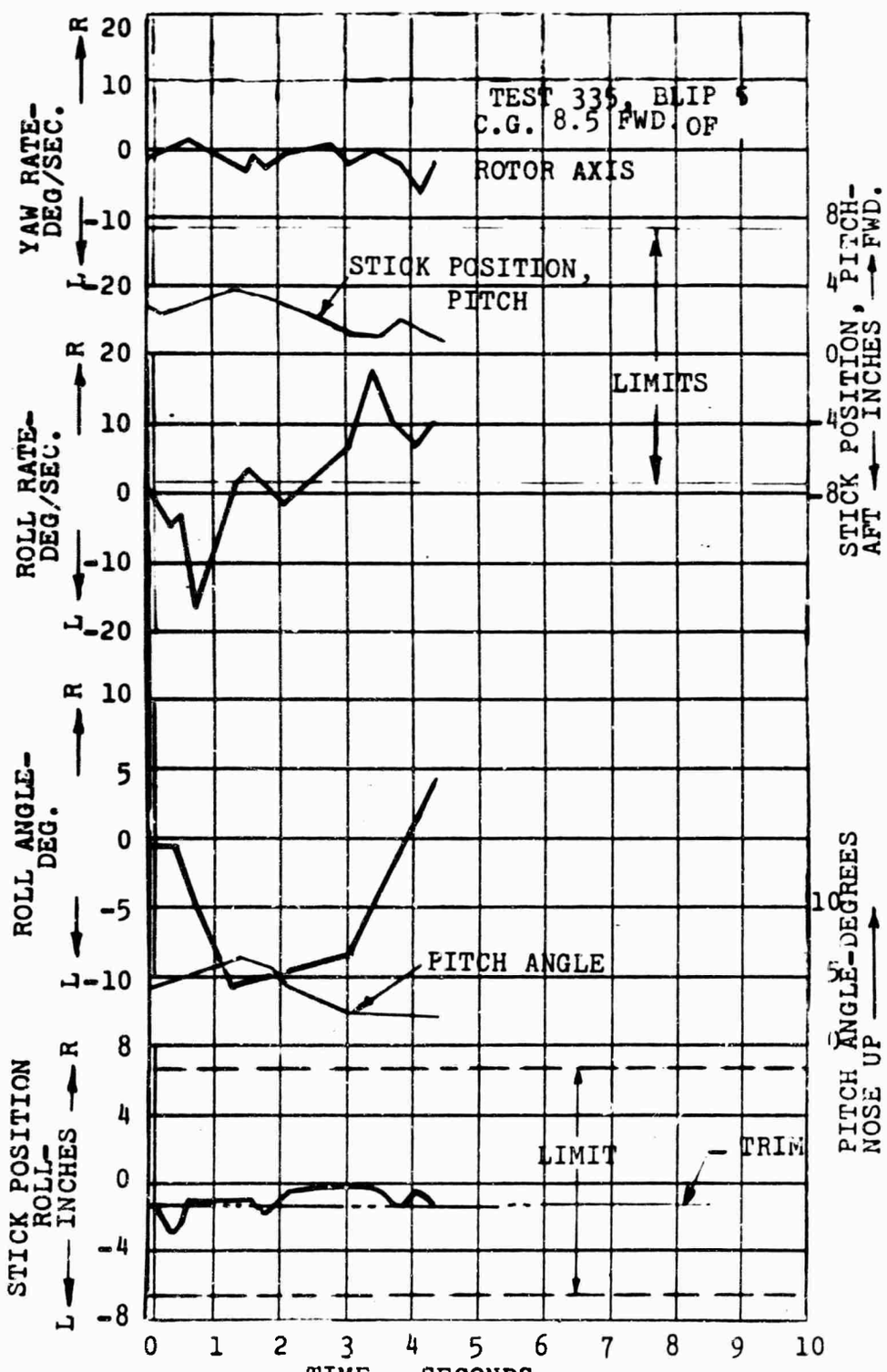


Figure 189. Roll Response in Hover - Roll Left, C.G. 8.5.

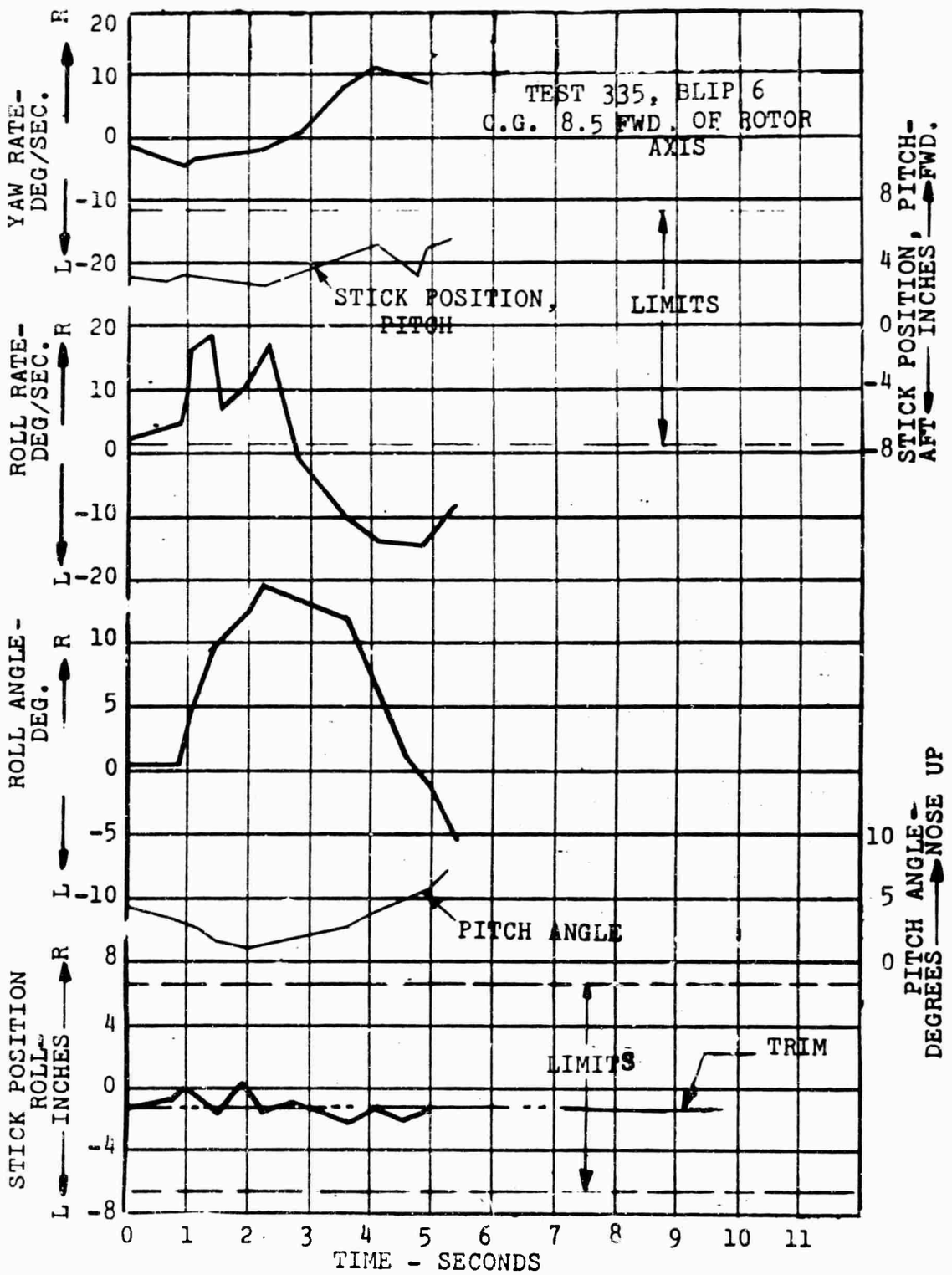


**Figure 190.** Roll Response in Hover - Roll Right, C.G. 8.5.

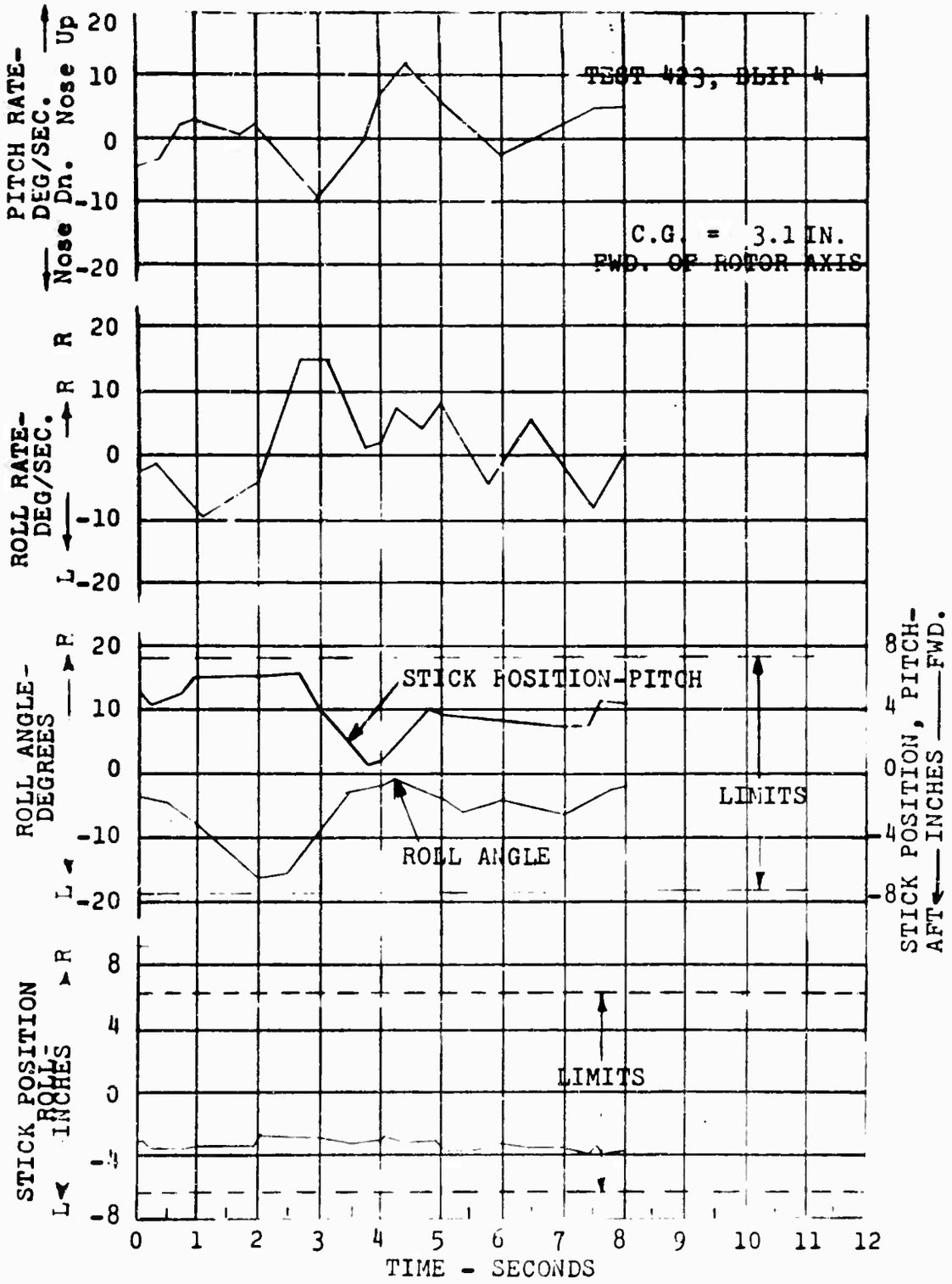


Figure 191. Roll Response in Hover - Roll Left, C.G. 3.1.

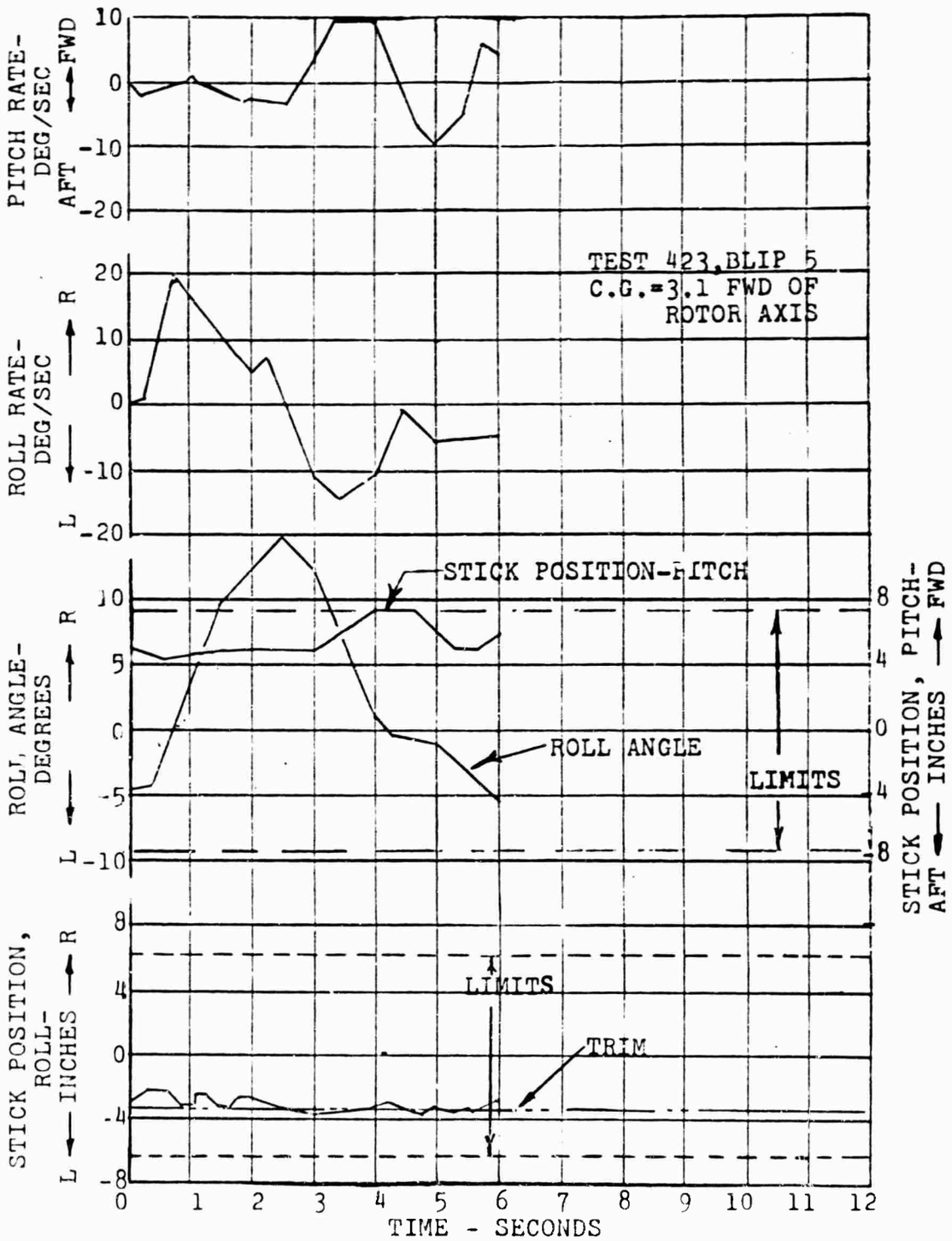


Figure 192. Roll Response in Hover - Roll Right, C.G. 3.1.

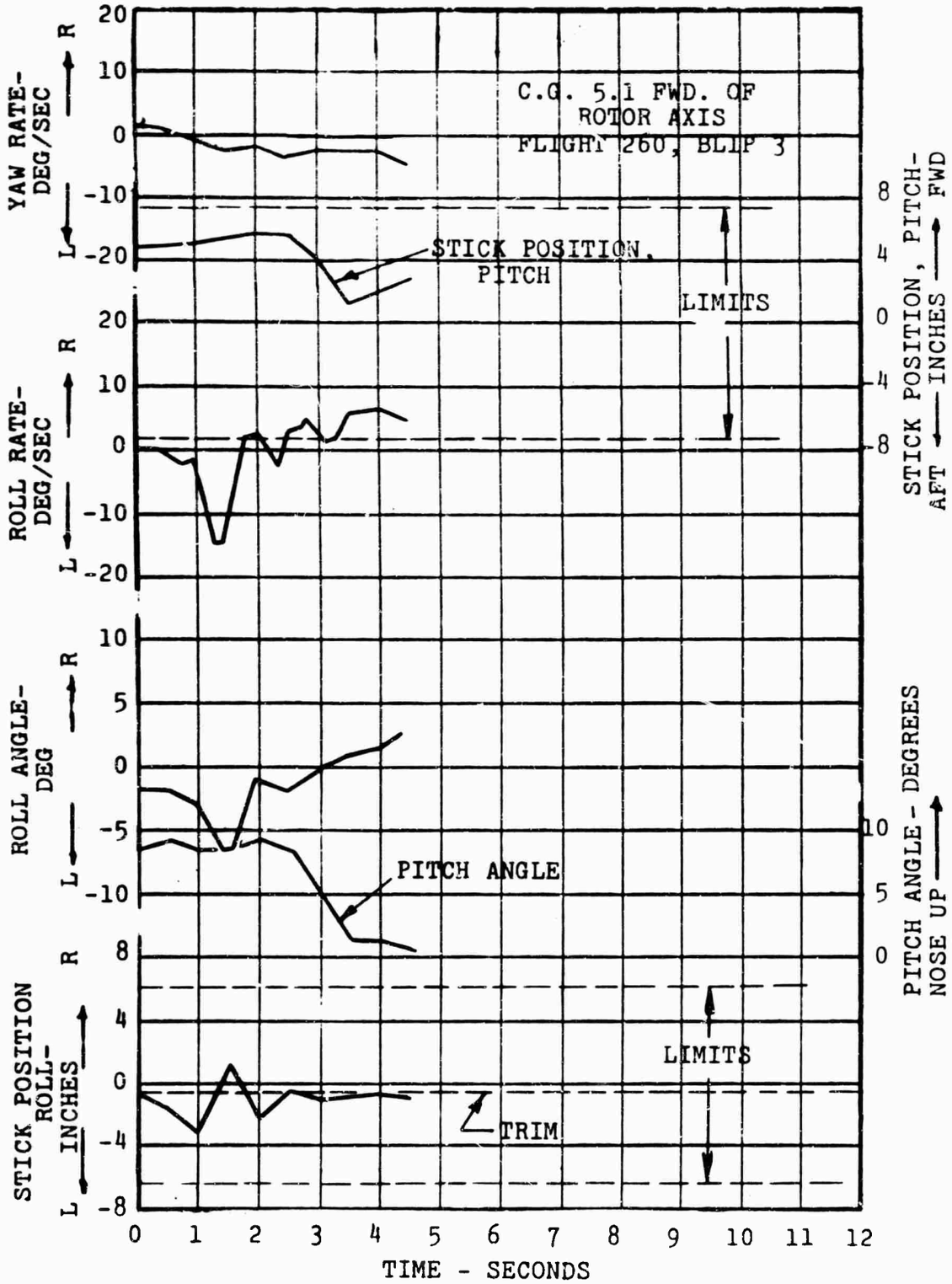


Figure 193. Roll Response in Hover - Roll Left, C.G. 5.1.

It is seen that the comparison of the test-program results with the MIL-H-8501A specification is quite satisfactory. It is evident that the control power about all axes satisfies the minimum requirements.

## ANALYSIS OF DYNAMICS AND CONTROL RESPONSE IN HOVER

### Pitch Response

A theoretical analysis of the 16H-1A control response characteristics in hover has been made. Calculated responses for the test control input conditions have been compared to the measured responses. Methods of solution of all response equations are taken from Reference 1, and the longitudinal equations of motion are given in Reference 7. On the basis of the close agreement obtained, the estimated values for control power, damping, velocity stability, and the resultant stability roots were verified. It is shown that the 16H-1A design exhibits a typical helicopter cubic characteristic equation with a short-period time constant and phugoid characteristics comparable to those of single-rotor helicopters but with a longer period. Control power exceeds the minimum MIL-H-8501A requirements.

The hover equations of motion in dimensional form, excluding the uncoupled plunging mode, are given as follows for the pitch angle and velocity degrees of freedom.

$$(X_v - mD)\, V - (mg)\, \theta = -X_\delta\, \delta(t) \tag{76}$$

$$(M_v)\, V + (M_q D - I_y D^2)\, \theta = -M_\delta\, \delta(t) \tag{77}$$

Solutions of these equations for the pitch angle response due to stick input, with zero initial conditions, yields the following third-order response with a lead time constant term.

$$\theta = \frac{K\left(D + \frac{1}{T_L}\right)\, \delta(t)}{\left(D + \frac{1}{T_{sp}}\right)\left(D^2 + 2\zeta\omega_o D + \omega_o{}^2\right)} \tag{78}$$

where $K = \dfrac{M_\delta}{I_y}$ .

The inverse lead time constant is

$$\frac{1}{T_L} = \frac{X_\delta}{m} \times \frac{M_v}{M_\delta} - \frac{X_v}{m} \tag{79}$$

and the characteristic equation is given by

$$(D + \frac{1}{T_{sp}})(D^2 + 2\zeta\omega_o D + \omega_o{}^2) = D^3 - (\frac{X_v}{m} + \frac{M_q}{I_y})\ D^2 +$$

$$(\frac{X_v}{m} \times \frac{M_q}{I_y})\ D + (\frac{gM_v}{I_y}) \qquad (80)$$

Estimates of the stability and control derivatives for hover are

$X_v$ = -5.3 lb-sec/ft
$X_\delta$ = 180 lb/in
$M_v$ = 34.4 ft-lb-sec/ft
$M_q$ = -3,840 ft-lb-sec/rad
$M_\delta$ = -1,500 ft-lb/in
$I_y$ = 11,000 slug-ft$^2$
$m$ = 186 slugs

The resulting longitudinal dynamic parameters are

$K$ = -7.80 deg/sec$^2$ per inch

$\frac{1}{T_L}$ = 0.0064 sec$^{-1}$

$\frac{1}{T_{sp}}$ = 0.622 sec$^{-1}$

$\zeta$ = -0.305

$\omega_o$ = 0.403 rad/sec

and the oscillatory mode period is found as follows

$$P = \frac{2\pi}{\omega_o \sqrt{1-\zeta^2}} \qquad (81)$$

$$= \frac{6.28}{0.403\ \sqrt{1-(0.305)^2}}$$

$$= 16.3 \text{ sec.}$$

The longitudinal control inputs and corresponding pitch angle responses for Test 335, Blips 3 and 4 (Figures 65 and 66), have been utilized for the correlation of the dynamic characteristics. In these tests, the control motions are best represented by successive pulse inputs. Impulse responses of varying magnitudes and initiation times are therefore adopted in the analysis. The basic response equation for a unit impulse input of 1 inch-second is given in degree units, in terms of the Laplace variable, as

$$\theta(s) = \frac{-7.80\ (s + .0064)}{(s+0.622)[s^2+2(-0.305)(0.403)s + (0.403)^2]}$$

The inverse transform, or time solution, is

$$\theta = 6.80\ e^{-0.622t} - 9.75\ e^{0.123t} \sin(0.385\ t + 0.77)$$

Test 335, Blip 3 (Figure 65) is adequately represented by individual inputs of 1.8 inch-second at t = 0, -0.5 inch-second at t = 1 second, and -2.0 inch-seconds at t = 2 seconds. The total response produced by the three inputs was calculated using the above solution by superimposing the individual responses weighted by their respective impulse magnitudes. The same procedure was employed for Test 335, Blip 4 (Figure 66), with impulses of -1.1 inch-seconds at t = 0, 0.4 inch-second at t = 1.5 seconds, and 1.3 inch-seconds at t = 2.5 seconds. These responses are plotted together with the test measurements, and good agreement is shown. These assumed impulse magnitudes are smaller than the integrated pulse areas shown in the actual stick motion curves in order to correct for the effects of control system elasticity present on only the early flights (see Technical Problems section).

Roll Response

Roll responses in hover are given by the data of Test 335, Blips 5 and 6, (Figure 97). From these tests and the lateral dynamic analysis at 50 knots, a lateral control power to inertia ratio of approximately 50 degrees per second per second per inch has been established. It is estimated, based on the 50-knot lateral dynamic response results, that the steady-state roll velocity per inch is approximately 39.0 degrees per second in hover. This level of initial roll acceleration and maximum roll velocity is fairly evident in the hover responses where only relatively small stick deflections from trim are required to produce momentary roll rates of 10 to 15 degrees per second.

It should be noted that strong lateral control was provided in the 16H-1A in order to insure adequate controllability in the unloaded rotor high-speed flight condition. Use of properly proportioned aileron control in conjunction with cyclic can be utilized to obtain constant lateral control power characteristics.

Yaw Response

Yaw responses in hover have been analyzed on the basis of a single-degree-of-freedom system using estimated stability and control derivatives. The measured responses are shown in Test 335, Blips 7 and 8, (Figures 194 and 195), together with the theoretically derived yaw responses which are seen to verify the estimated derivatives. From this correlation, the directional characteristics in hover indicate an initial yaw acceleration to the right of 30 degrees per second per second per inch, with a steady-state yaw rate of 188 degrees per second per inch. For yaw to the left, the initial acceleration is 14.4 degrees per second per second per inch with a steady-state yaw rate of 90.5 degrees per second per inch. The response time constant is 6.3 seconds, and the initial accelerations in both directions exceed the minimum MIL-H-8501A requirements.

The equation of motion in yaw is

$$(I_z D - N_r) \quad D\psi = N_\delta \, \delta(t) \tag{82}$$

Solving for the yaw rate response gives

$$D\psi = \frac{K \, \delta(t)}{D + \frac{1}{T}} \tag{83}$$

where $$K = \frac{N_\delta}{I_z} ,$$

and the inverse time constant is

$$\frac{1}{T} = \frac{-N_r}{I_z}$$

Estimates of the directional response parameters are

$N_r$ = -1,640 ft-lb-sec/rad
$N_\delta$ = -5,400 ft-lb/inch (right pedal)
= -2,600 ft-lb/inch (left pedal)
$I_z$ = 10,300 slug-ft$^2$

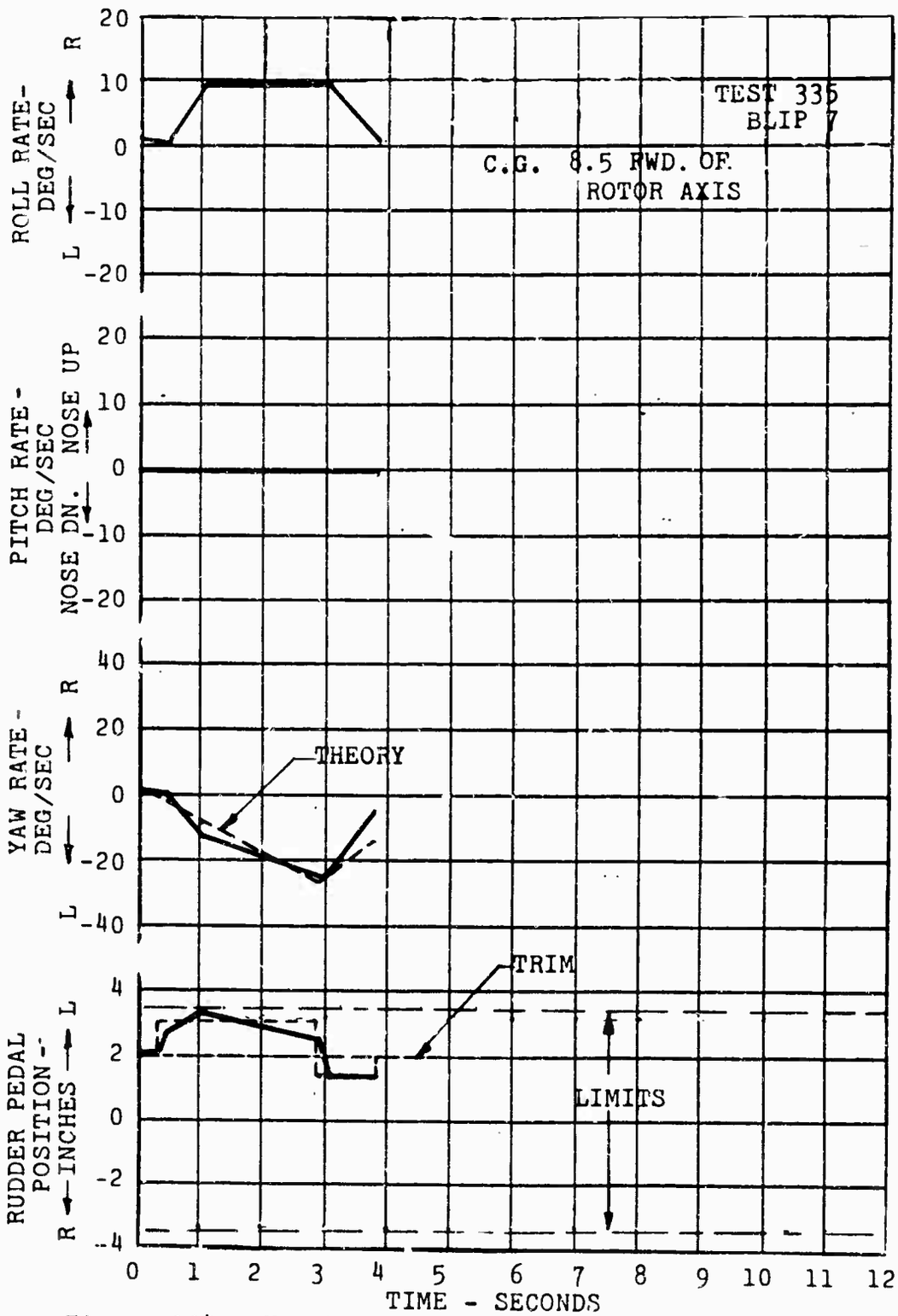


Figure 194. Yaw Response in Hover - Left Yaw, C.G. 8.5.

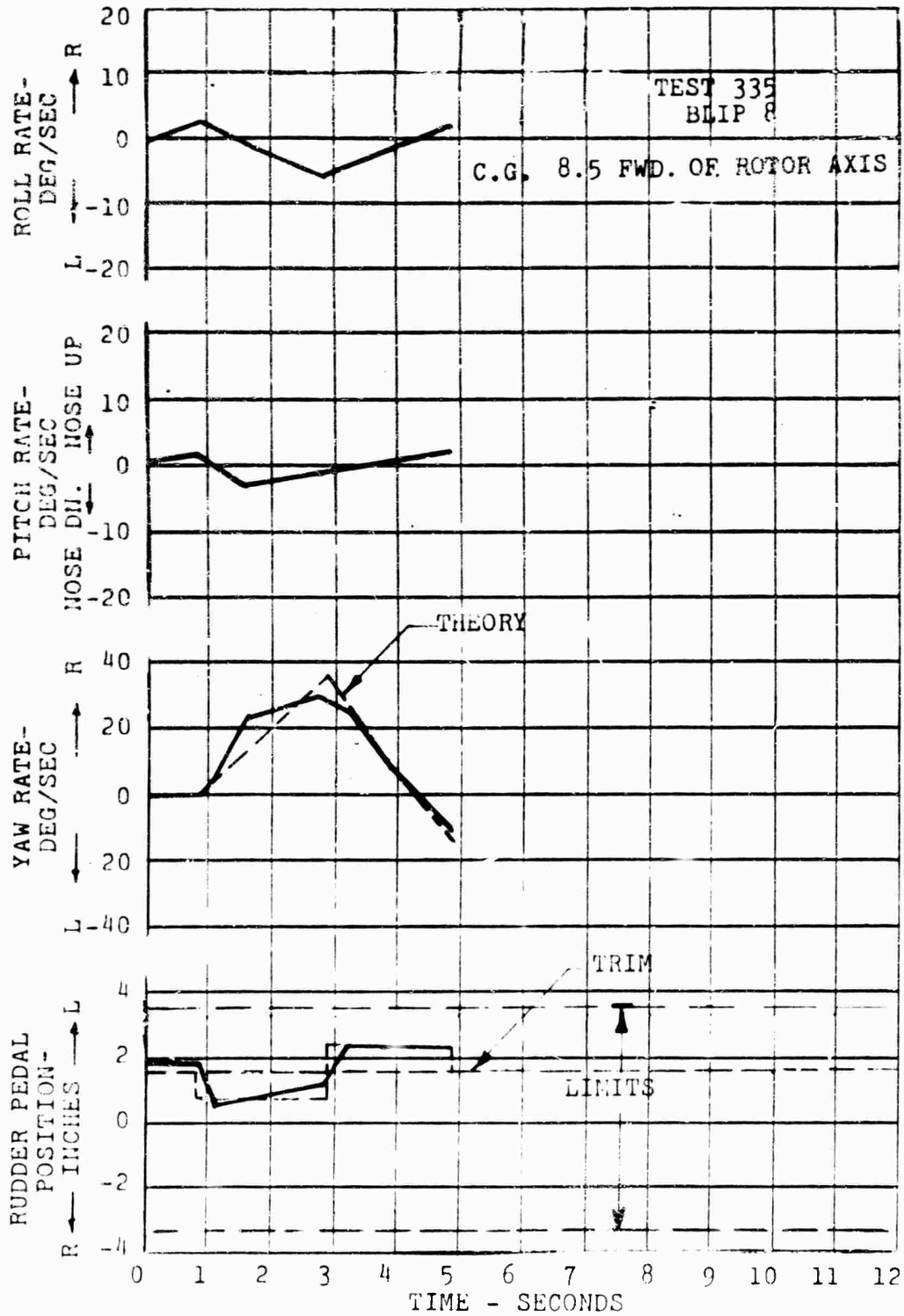


Figure 195. Yaw Response in Hover - Right Yaw, C.G. 8.5.

Applying these values yields

$$K = -30.0 \text{ deg/sec}^2 \text{ per inch (right pedal)}$$

$$= -14.4 \text{ deg/sec}^2 \text{ per inch (left pedal)}$$

$$\frac{1}{T} = 0.159 \text{ sec}^{-1}$$

An examination of the actual pedal displacement time histories in the cited tests indicates a step-input-type control motion. Consequently, consecutive step inputs have been utilized in the analysis. The Laplace transformed yaw rate response equation, in degree-per-second units, for a 1-inch step input is

$$\dot{\psi} = \frac{K}{s(s + 0.159)} \tag{84}$$

and the corresponding response solution, or inverse transform, is

$$\dot{\psi} = \frac{K}{0.159}(1 - e^{-0.159t})$$

$$= -188\ (1 - e^{-0.159t}) \quad \text{right pedal}$$

$$= -90.5\ (1 - e^{-0.159t}) \quad \text{left pedal}$$

The first solution has been applied to Test 335, Blip 8 (Figure 195), considering a -0.7-inch step at t = 0 and a 1.5-inch step initiated at t = 2 seconds. The second solution was used in Test 335, Blip 7 (Figure 194), with a 0.9-inch step at t = 0 followed by a -1.5 inch step at t = 2.5 seconds. In both responses, a satisfactory comparison is shown between test and theory.

## STATIC STABILITY

### Longitudinal

The longitudinal static stability of the 16H-1A is readily apparent in the stick position versus level flight trim speed tests (Figure 54). These data have been subjected to an analysis to establish the level of angle of attack and velocity stability available at a forward speed of 150 knots.

The overall static stability, proportional to the static margin, can be expressed in terms of the stick position with airspeed slope:

$$\frac{d\delta}{dV} = \frac{1}{-M_\delta} [M_V + CL_V (n_o - X_{CG})] \qquad (85)$$

Estimates of the above parameters for steady level flight operation at 150 knots have been made and are given as follows

$M_\delta$ = -1300 ft-lb/inch
$M_V$ = 37 ft-lb/ft/sec
$C$ = 5 feet
$L_V$ = 21 lb/ft/sec
$n_o$ = 0.54
$X_{CG}$ = 0.27

The stick position slope is then

$$\frac{d\delta}{dV} = \frac{1}{1300} [37 + 5 \times 21(0.54 - 0.27)] \qquad (86)$$

$$= 0.050 \text{ in/ft/sec}$$

$$= 0.085 \text{ in/knot}$$

This value is seen to be well represented by the slope at 150 knots of the faired curve for stick positions, thus verifying the estimated derivatives. The positive slope indicating positive overall static stability is evident throughout the operating regime above about a 70-knot forward speed.

This analysis was for test data obtained at forward center of gravity (9.6 inches). The longitudinal static stability for the aft center-of-gravity position (3.1 inches) can be evaluated by the verified approach given above. The only parameters which are center-of-gravity dependent are $M_V$ and $X_{CG}$. At the aft position, $M_V$ = 46 foot-pounds per foot per second and $X_{CG}$ = 0.37.

Thus,

$$\frac{d\delta}{dV} = \frac{1}{1300} [46 + 5 \times 21 (0.54 - 0.37)]$$

$$= 0.049 \text{ in/ft/sec}$$

$$= 0.083 \text{ in/knot}$$

The reduction in stability due to center-of-gravity shift is compensated by the increase in **velocity stability.** It should be realized that this tendency for aft center-of-gravity shift to have only minor effect on the longitudinal control position gradient is typical of helicopter characteristics (Reference 2, pages 344 and 458). At these speeds the 16H-1A unloading is such that the rotor influences govern this static stability parameter rather than the pure fixed-wing contributions.

Directional

The steady sideslip pedal position curves of Figure 103 illustrate directly the positive directional static stability of the 16H-1A at all speeds above hover. In addition, these position curves allow the computation of the static stability derivative $N_\beta$ utilizing estimated directional control power values. Control power at hover has been verified by the control response analysis and correlation given previously, and control power estimates at 50 knots are verified in the forward speed dynamic analysis in a following section of this appendix.

The steady sideslip equilibrium equation is

$$N_\beta \times \beta + N_\delta \times \delta = 0, \qquad (87)$$

giving

$$N_\beta = -\frac{d\delta}{d\beta} \times N_\delta$$

For sideslip at 50 knots, the estimated control power derivatives are

$N_\delta$ = -6,000 ft-lb/in. (right pedal)

= -4,300 ft-lb/in. (left pedal)

and from the position curve, the slopes are seen to be

$\frac{d\delta}{d\beta}$ = 0.92 in/rad (right pedal)

= 1.26 in/rad (left pedal)

Applying these measured slopes yields

$N_\beta$ = -0.92 (-6,000)

= 5,500 ft-lb/rad

and

$$N_\beta = -1.26\ (-4,300)$$

$$= 5,400\ \text{ft-lb/rad}$$

with an average value of $N_\beta = 5,450$ ft-lb/rad

At 100 knots, the estimated control power is symmetrical with a value $N_\delta = -9,800$ foot-pounds per inch. The position curve slope at this speed is

$$\frac{d\delta}{d\beta} = 2.52\ \text{in/rad}$$

giving a directional stability value of

$$N_\beta = -2.52\ (-9,800)$$

$$= 24,600\ \text{ft-lb/rad}$$

## DYNAMIC STABILITY AT 50 KNOTS

### Longitudinal

A theoretical analysis has been undertaken in order to establish the major parameters governing the longitudinal handling qualities of the 16H-1A. These results have been applied to the transient responses obtained in the test program. A sufficiently high degree of correlation is shown to verify the analysis procedures and stability estimates. It is demonstrated that at a low forward speed of 50 knots (the hover regime considered to apply up to 30 knots), the 16H-1A design exhibits a well damped short-period mode with a period of 4.8 seconds and a critical damping ratio of 0.57. The stick-fixed neutral point is at 51 percent of the mean aerodynamic chord. The control power to inertia ratio produces an initial pitch acceleration of 7.8 degrees per second per second per inch and the steady state pitch velocity is 4.7 degrees per second per inch. The pitch rate response meets the inflection point time requirements of MIL-H-8501A.

The stability-axes equations of motion in dimensional form are given as follows for the short-period control response, in which the flight speed may be considered constant.

$$[L_\alpha + (mV_o)D]\alpha - (mV_o)\,D\theta = -L_\delta\,\delta(t) \qquad (88)$$

$$(M_\alpha)\alpha + (M_qD - I_yD^2)\,\theta = -M_\delta\,\delta(t) \qquad (89)$$

Solution of these equations for the pitch angle response due to stick input, with zero initial conditions, yields the following second-order rate response with a lead time-constant term.

$$\theta = \frac{K\left(D+\frac{1}{T}\right)\delta(t)}{D\,(D^2 + 2\zeta\,\omega_o D + \omega_o{}^2)} \tag{90}$$

where $$K = \frac{M_\delta}{I_y} \tag{91}$$

(Inverse Lead Time Constant) $$\frac{1}{T} = \frac{L_\alpha}{mV_o} - \frac{M_\alpha\, L_\delta}{M_\delta\, mV_o} \tag{92}$$

(Critical Damping Ratio) $$\zeta = \frac{I_y\ \frac{L_\alpha}{mV_o} - M_q}{2\sqrt{I_y\ (-M_\alpha - M_q\ \frac{L_\alpha}{mV_o})}} \tag{93}$$

(Undamped Natural Frequency) $$\omega_o = \sqrt{\frac{-M_\alpha - M_q\ \frac{L_\alpha}{mV_o}}{I_y}} \tag{94}$$

Estimates of the stability derivatives for steady level flight at 50 knots are

$L_\alpha$ = 17,000 lb/rad
$L_\delta$ = -420 lb/inch
$M_\alpha$ = -20,000 ft-lb/rad
$M_q$ = -6,800 ft-lb-sec/rad
$M_\delta$ = -1,500 ft-lb/inch
$I_y$ = 11,000 slug-ft$^2$
$mV_o$ = 15,000 lb-sec

The resulting response parameters are

$K$ = -7.80 deg/sec$^2$ per inch
$\frac{1}{T}$ = 1.513 sec$^{-1}$
$\zeta$ = 0.570
$\omega_o$ = 1.59 rad/sec

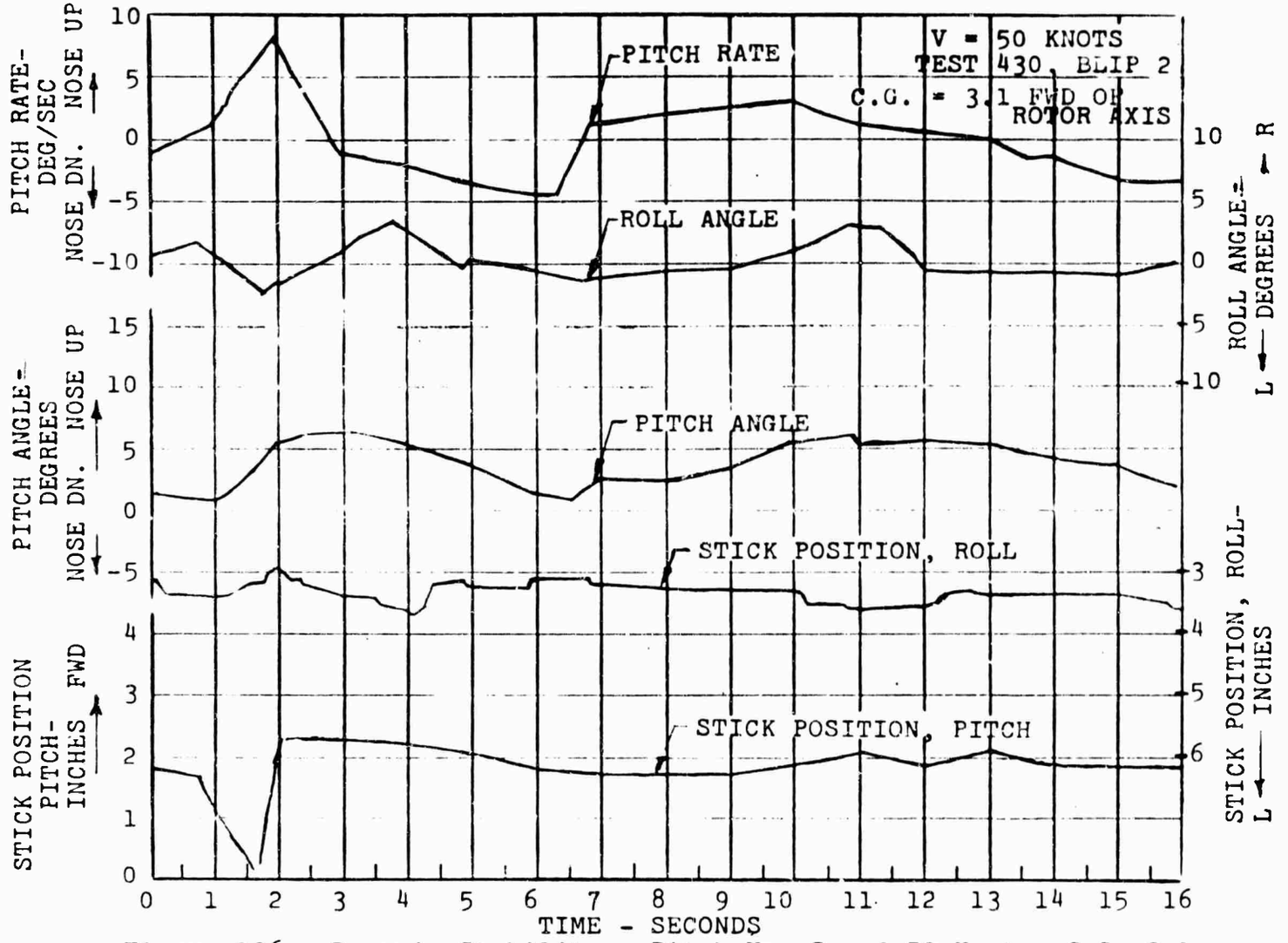


Figure 196. Dynamic Stability - Pitch Up, Speed 50 Knots, C.G. 3.1.

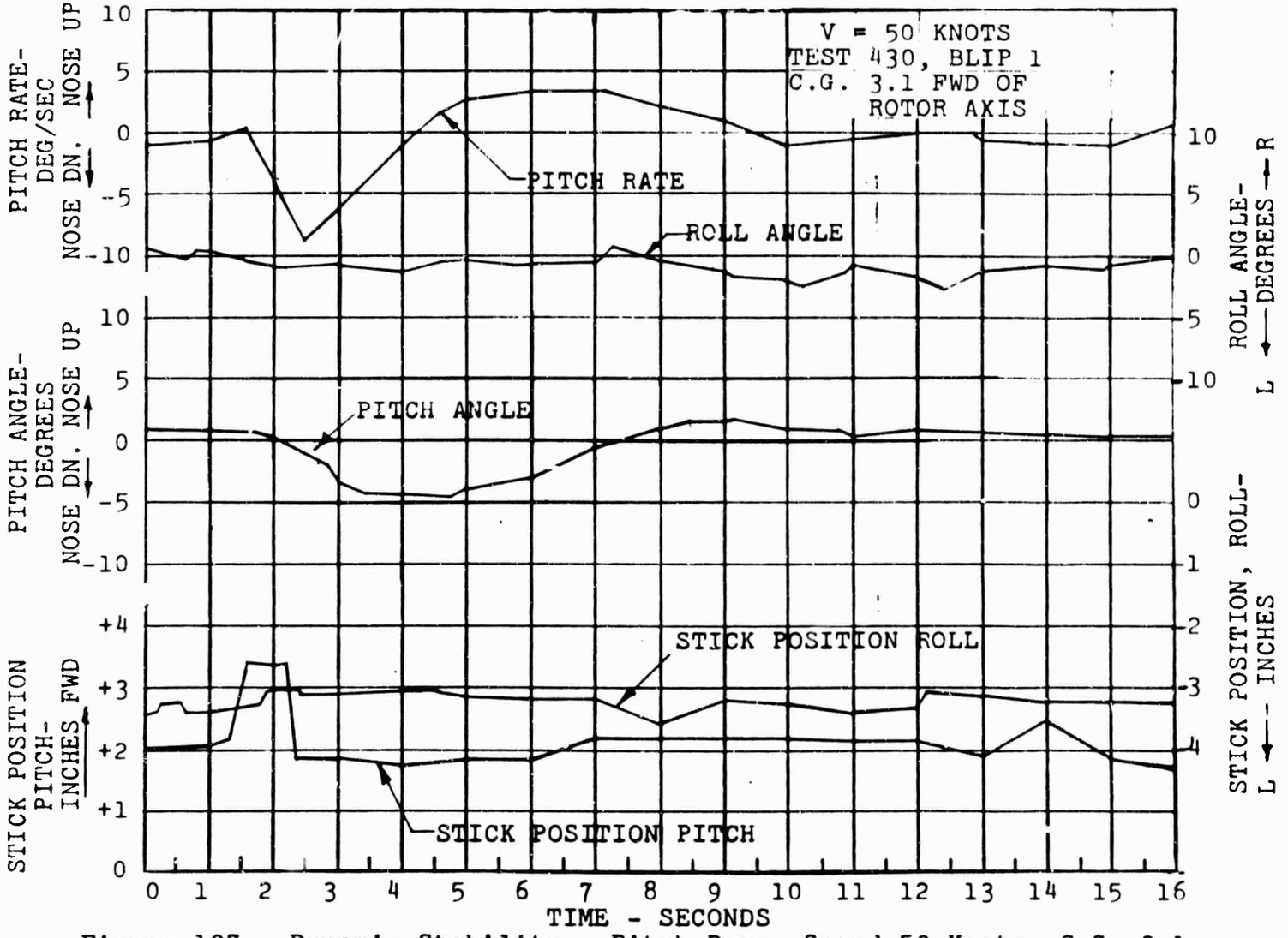


Figure 197. Dynamic Stability - Pitch Down, Speed 50 Knots, C.G. 3.1.

The longitudinal control input and pitch angle response for Test 315, Blip 5, (Figure 69), have been utilized for the correlation of the dynamic characteristics. Here, for convenience, the control input is represented by a single impulse-type input of 0.75 inch-second magnitude initiated at zero time. The pulse duration is short enough compared to the system period to allow this approach. Taking the Laplace transform of the pitch response, in degree units,

$$\theta(s) = \frac{-.75 \times 7.80\ (s + 1.513)}{s[s^2 + 2(0.57)(1.59)\ s+(1.59)^2]} \qquad (95)$$

The inverse transform, or time solution, is

$$\theta = -3.50 + 4.05e^{-0.91t} \sin(1.31\ t + 2.1) \qquad (96)$$

This response is plotted with the test measurement and shows very close agreement for the first 3.5 seconds of the transient. After this time, the relatively small corrective stick motion evident in the control trace causes the actual response to diverge toward the initial pitch attitude.

## Lateral

A theoretical analysis, similar to that of the longitudinal case, has been made for the pure roll response to lateral stick motion. In these runs, the stick was pulsed laterally in alternate directions so as to produce roll excursions which were rather quickly returned to trim. As a result, the usual attendant yaw and sideslip motions were small enough compared to the roll response to be considered negligible in the analysis.

The single-degree-of-freedom roll equation of motion is

$$(I_x D^2 - L_p D)\ \phi = L_\delta\ \delta(t) \qquad (97)$$

Solving this equation for the roll angle gives

$$\phi = \frac{K\delta(t)}{D(D+\frac{1}{T})} \qquad (98)$$

where

$$K = \frac{L_\delta}{I_x}$$

and T, the first order response time constant, is given by

$$\frac{1}{T} = \frac{L_p}{I_x}$$

The estimates of the lateral parameters at a flight speed of 50 knots are

$$I_x = 1{,}600 \text{ slug-ft}^2$$
$$L_p = -2{,}530 \text{ ft-lb-sec/rad}$$
$$L_\delta = 1{,}500 \text{ ft-lb/inch}$$

resulting in a lateral control gain and inverse time constant of

$$K = 53.8 \text{ deg/sec}^2 \text{ per inch}$$
$$\frac{1}{T} = 1.58 \text{ sec}^{-1}$$

Considering a unit impulse input of 1 inch-second, the Laplace variable response equation is

$$\phi(s) = \frac{53.8}{s(s+1.58)} \tag{99}$$

and its inverse is

$$\phi = 34.0\ (1-e^{-1.58t}) \tag{100}$$

Two lateral test responses were studied in the analysis. In Test 315, Blips 7 and 8, the former is adequately represented by a -0.26-inch-second impulse at zero time and a corrective impulse of 0.44 inch-second taking place at 1.25 seconds; the latter input is a 0.21 inch-second impulse at zero time followed by a corrective impulse of -0.28 inch-second applied at 1.25 seconds. These assumed impulse magnitudes are smaller than the integrated pulse areas shown in the actual stick motion curves in order to correct for the effects of control system elasticity present on only the early flights (see Technical Problems section). The total response due to both inputs was calculated for each case using the above solution and superimposing the individual responses weighted by their respective impulse magnitudes.

The resulting equations for both cases are:

Test 315, Blip 7 (Figure 198):

From t = 0 to t = 1.25 seconds

$$\phi = -8.84\ (1-e^{-1.58t}) \tag{101}$$

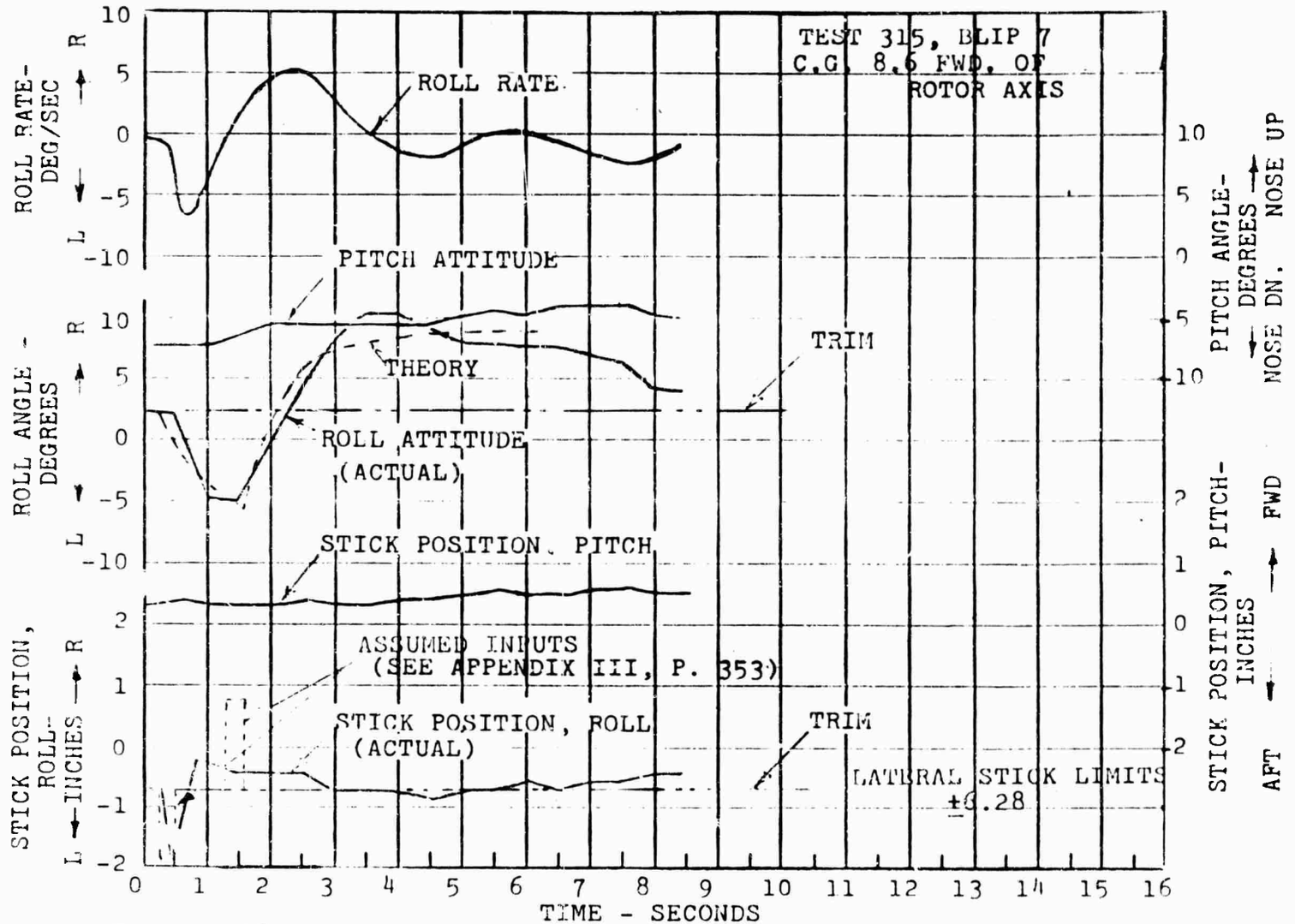


Figure 198. Dynamic Stability - Roll Left, Speed 50 Knots, C.G. 8.6.

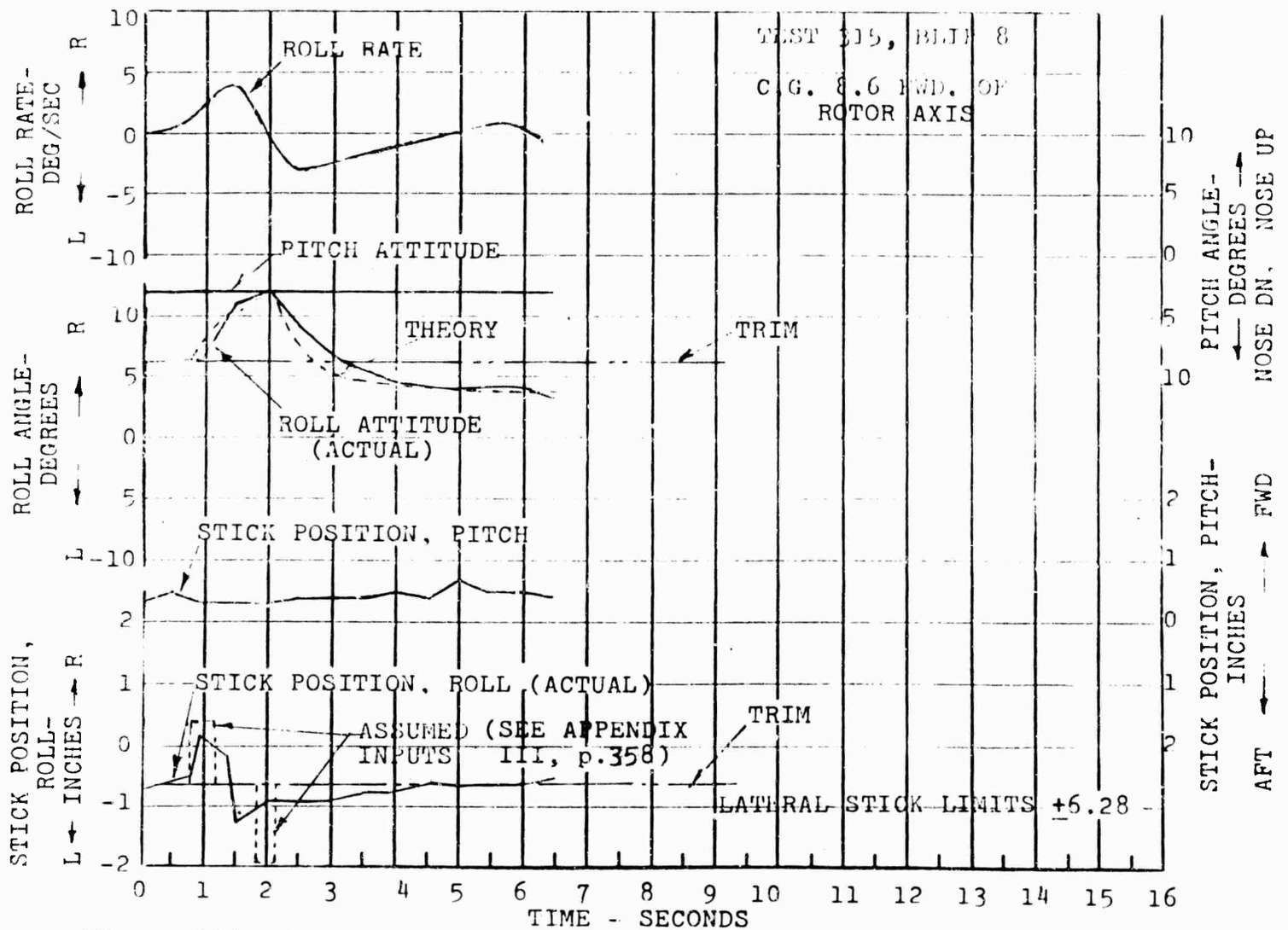


Figure 199. Dynamic Stability - Roll Right, Speed 50 Knots, C.G. 8.6.

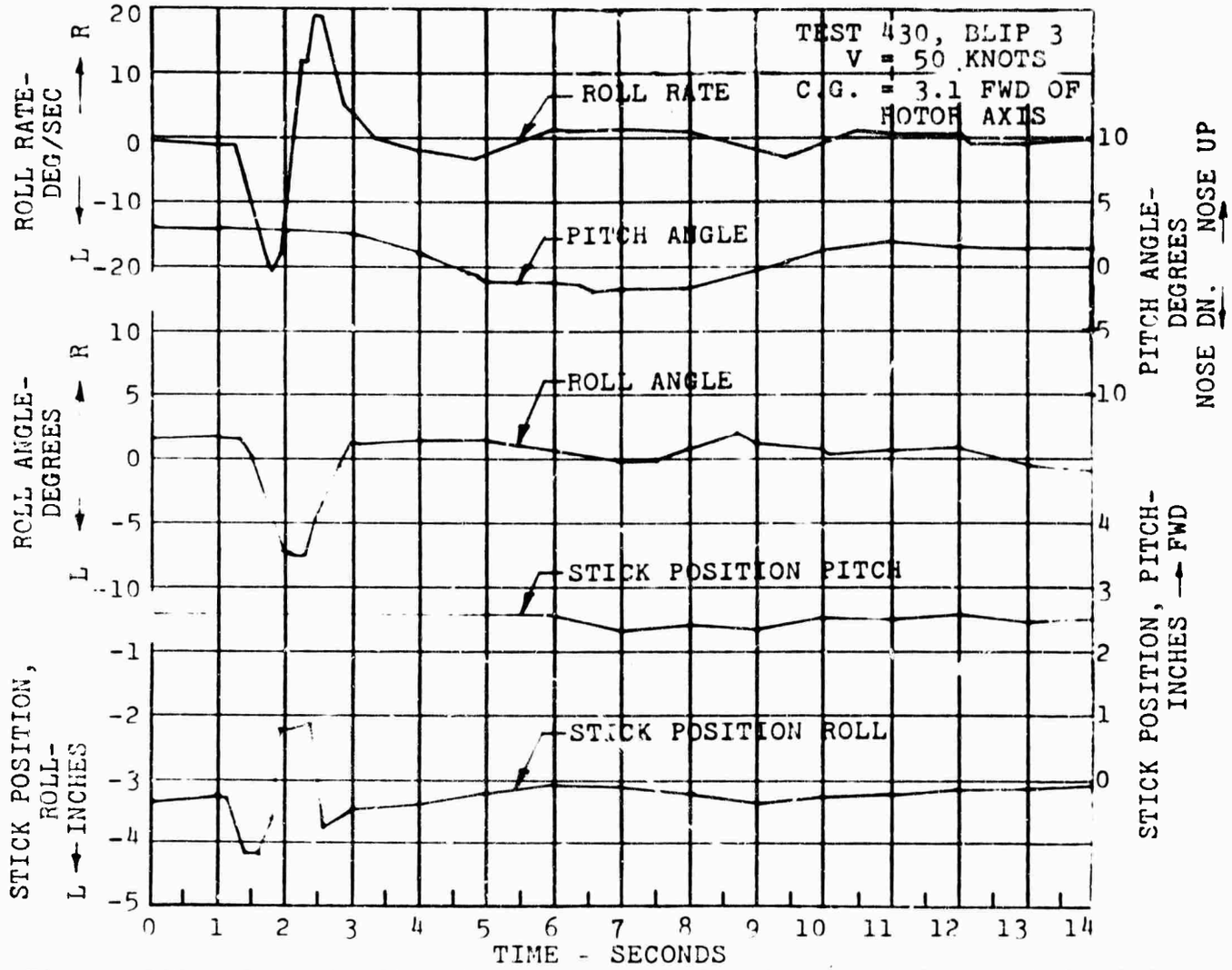


Figure 200. Dynamic Stability - Roll Left, Speed 50 Knots, C.G. 3.1.

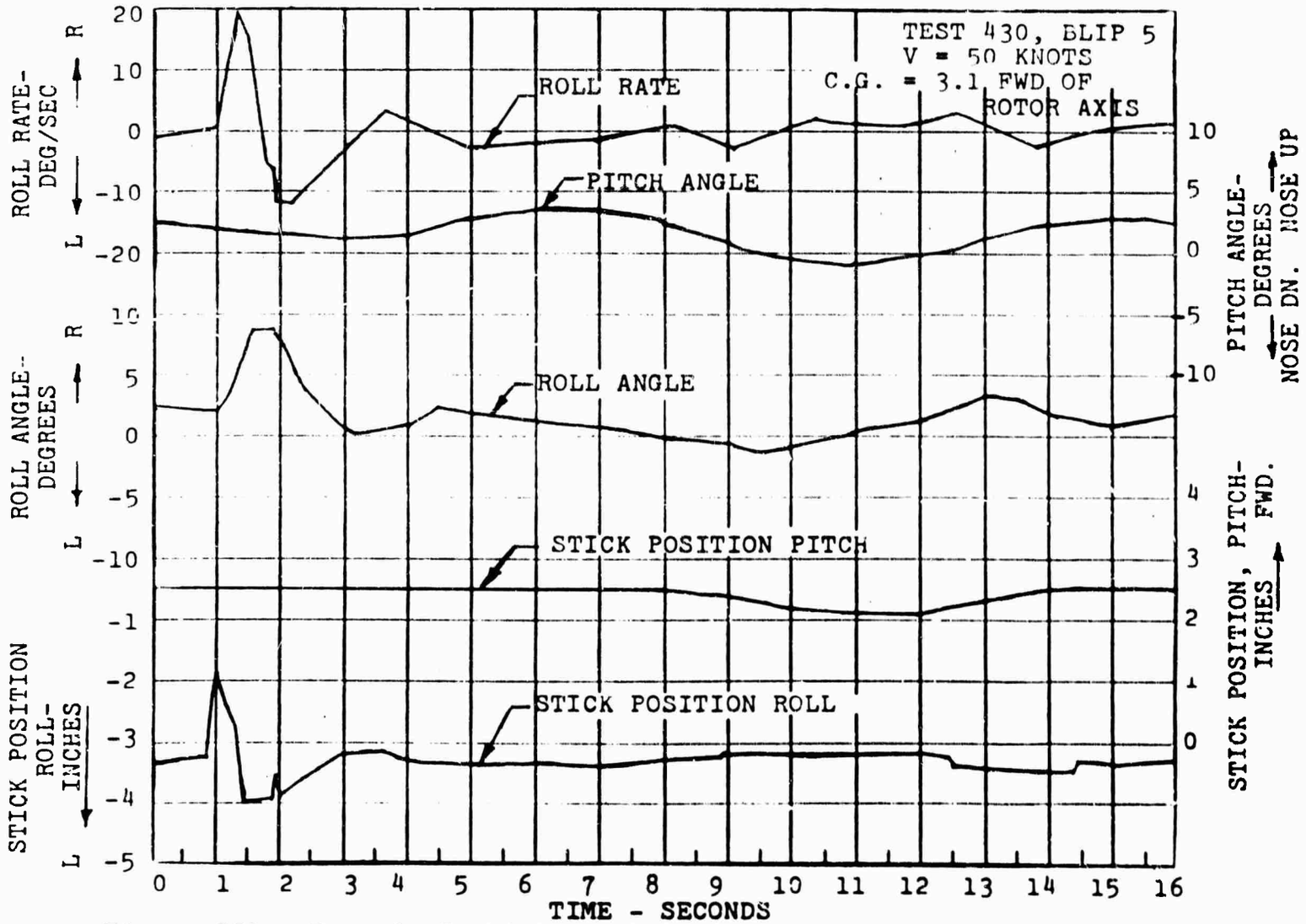


Figure 201. Dynamic Stability - Roll Right, Speed 50 Knots, C.G. 3.1.

From t = 1.25 seconds, continuous

$$\phi = 6.12\ (1-16.1\ e^{-1.58t}) \qquad (102)$$

Test 315, Blip 8 (Figure 199):

From t = 0 to t = 1.25 seconds,

$$\phi = 7.14\ (1-e^{-1.58t}) \qquad (103)$$

From t = 1.25 seconds, continuous,

$$\phi = 2.38\ (1-25.8\ e^{-1.58t}) \qquad (104)$$

These responses are included in the plots of the measured roll responses. It can be seen that correlation is satisfactory for the first 3.5 seconds in Blip 7 (Figure 192) and for more than 5 seconds in Blip 8 (Figure 199).

The observations drawn from the verified stability and control characteristics are based on the usual consideration of a 1-inch step input. The steady-state roll rate per inch of stick motion is 34.0 degrees per second. This results in a helix angle per inch of $\frac{pb}{2V} = 0.070$. In addition, the steady state is reached, essentially, in 3 time constants or

$$3T = \frac{3}{1.58} = 1.9 \text{ seconds},$$

which is a sufficiently rapid response time.

Directional

Directional dynamics have been investigated in analyses of flight test records of the directional response to input control motions. In the 50-knot response data, the aircraft was stabilized in pitch and roll so that only directional motions in which the sideslip angle is equal and opposite to yaw angle resulted. It should also be pointed out that coupled lateral-directional dynamics are minimal at 50 knots, due essentially to the favorably low level of net dihedral effect of the 16H-1A configuration.

Analyses have been performed by first determining the directional stability and control derivatives and then applying these to the aircraft equation of motion. The principal factors, control power and static stability, have been established by the data correlations given previously in this appendix.

The single degree of freedom response equation in yaw is

$$(I_z D^2 - N_r D + N_\beta)\ \psi = N_\delta\ \delta(t) \tag{105}$$

and the resulting expression for the yaw rate response to pedal displacement time function is

$$D\psi = \frac{KD\ \delta(t)}{D^2 + 2\zeta\omega_o D + \omega_o^2} \tag{106}$$

where

$$K = \frac{N_\delta}{I_z} \tag{107}$$

$$\zeta = \frac{-N_r}{2\sqrt{I_z\ N_\beta}} \tag{108}$$

$$\omega_o = \sqrt{\frac{N_\beta}{I_z}} \tag{109}$$

The stability and control derivatives, as previously obtained, are

$N_\delta$ = -6,000 ft-lb/in (right pedal)
= -4,300 ft-lb/in (left pedal)
$I_z$ = 10,300 slug-ft$^2$
$N_\beta$ = 5,450 ft-lb/rad

and the estimated directional damping is

$N_r$ = -4,600 ft-lb-sec/rad

With these parameters,

$K$ = -33.4 deg/sec$^2$ per inch (right pedal)
= -23.9 deg/sec$^2$ per inch (left pedal)
$\zeta$ = 0.307
$\omega_o$ = 0.726 rad/sec

Also, the damped natural frequency is

$$\omega = \omega_o\sqrt{1-\zeta^2} \tag{110}$$

$$= 0.726\sqrt{1-(0.307)^2}$$

$$= 0.690 \text{ rad/sec}$$

and the corresponding oscillatory period is

$$P = \frac{2\pi}{\omega} \qquad (111)$$

$$= \frac{6.28}{0.690}$$

$$= 9.10 \text{ seconds}$$

These results indicate a moderately damped long-period oscillation with high control effectiveness in yaw at low speed. At moderate and high speed, the response is of shorter period.

The control responses to be studied are the 50-knot pedal input cases for Flight 435, Blips 1 and 2, shown in Figures 202 and 203. In these plots it is seen that the control motions are pulse type. Because of the long oscillatory period compared to the actual pulse durations, an impulse approach to the theoretical response is applicable. In addition, lengthy response correlations up to 15 seconds are feasible due to the previously mentioned condition of pure yaw response.

The yaw rate response, in degrees-per-second units, for a unit impulse function (1 inch-second right and left pedal input) is given in the Laplace variable as

$$\dot{\psi}(s) = \frac{Ks}{s^2 + 2(0.307)(0.726)s + (0.726)^2} \qquad (112)$$

and the resulting response time solutions are

$$\dot{\psi} = 35.1\, e^{-0.223t} \sin (0.690t + 1.88) \qquad (113)$$

for right pedal unit impulse displacement from trim and

$$\dot{\psi} = -25.1\, e^{-0.223t} \sin (0.690t + 1.88) \qquad (114)$$

for left pedal unit impulse inputs.

Examination of the actual control pulses indicates that a representative input for Test 435, Blip 2 (Figure 203), is -0.5 inch-second and for Test 435 Blip 1 (Figure 202), is 0.7 inch-second. Use of the above solutions, weighted by their respective input magnitudes, yields the theoretical responses shown in Figures 203 and 202. The expected differences between the initial spikes because of the finite

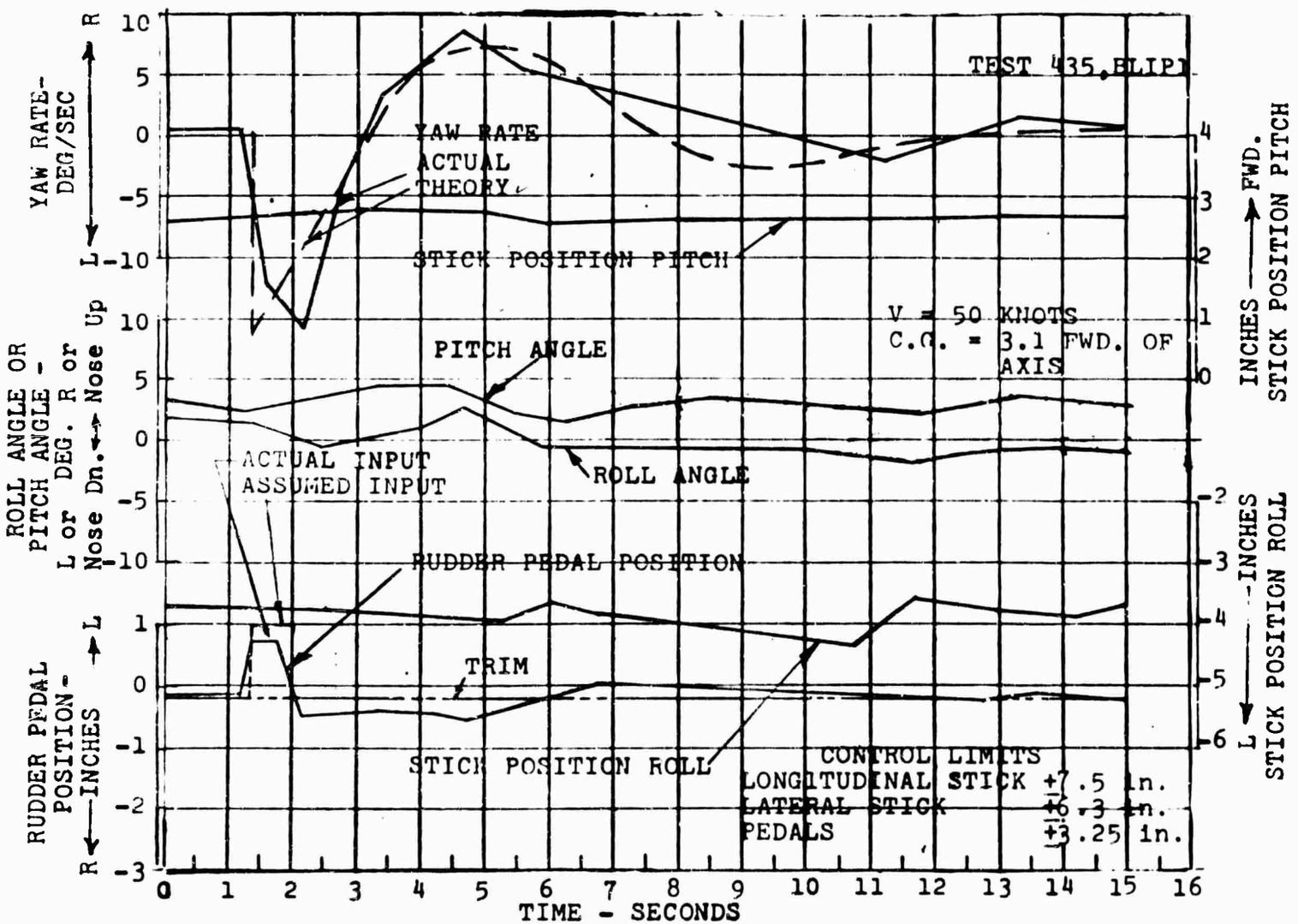


Figure 202. Dynamic Stability - Yaw Left, Speed 50 Knots, C.G. 3.1.

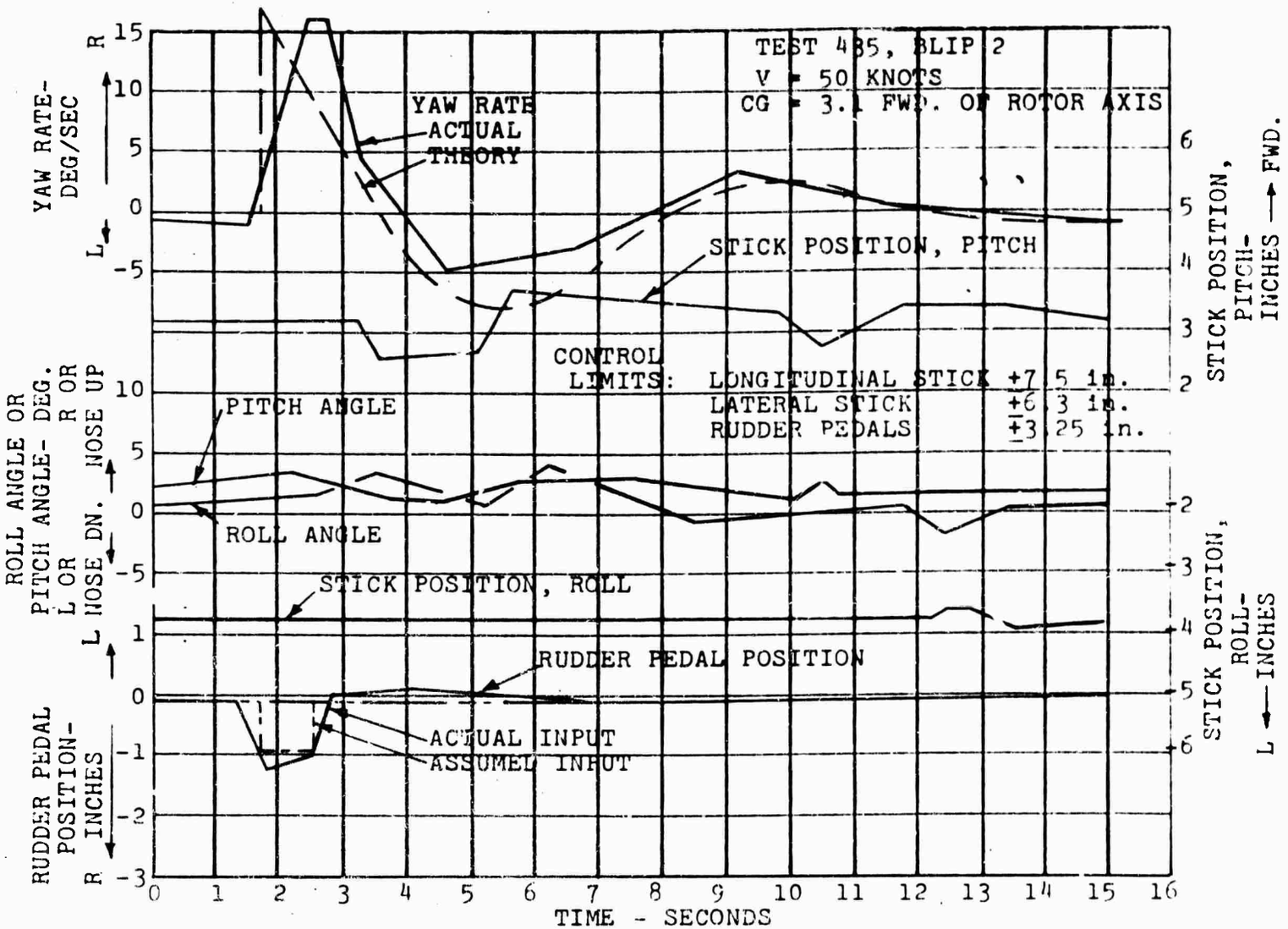


Figure 203. Dynamic Stability - Yaw Right, Speed 50 Knots, C.G. 3.1.

rate of control application required in any actual system are apparent in the comparisons between the actual and theoretical responses. Nevertheless, the response correlations are satisfactory and they substantiate the derivative evaluations as well as the corresponding directional dynamic characteristics described.

## ANALYSES OF RESULTS AT 150 KNOTS

### Longitudinal Dynamics

Control responses obtained at 150 knots have been analyzed in a similar manner to that used for the 50-knot dynamic tests presented in this appendix. Again, a sufficiently close agreement is shown so that the analysis approach and stability derivative estimates are considered verified. It is shown that the 16H-1A at 150 knots exhibits a damped short-period mode with a period of 2.0 seconds and a critical damping ratio of 0.43. The stick-fixed neutral point is at 54 percent of the mean aerodynamic chord. The control power to inertia ratio produces an initial pitch acceleration of 6.8 degrees per second per second per inch and the steady-state pitch velocity is 2.4 degrees per second per inch. The normal acceleration and pitch rate response meet the inflection point requirements of MIL-H-8501A.

The stability-axes equations of motion in dimensional form are given as follows for the short-period mode response, in which the flight speed may be considered constant.

$$[L_\alpha + (mV_o)D]\,\alpha - (mV_o)D\theta = -L_\delta\,\delta(t) \qquad (115)$$

$$(M_\alpha)\,\alpha + (M_qD - I_yD^2)\theta = -M_\delta\,\delta(t) \qquad (116)$$

Solution of these equations for the pitch angle response due to stick input, with zero initial conditions, yields the following second-order rate response with a lead time constant term.

$$\theta = \frac{K(D+\frac{1}{T})\,\delta(t)}{D(D^2 + 2\zeta\omega_o D + \omega_o{}^2)} \qquad (117)$$

where $$K = \frac{M_\delta}{I_y} \qquad (118)$$

Inverse Lead Time Constant $$\frac{1}{T} = \frac{L_\alpha}{mV_o} - \frac{M_\alpha\, L_\delta}{M_\delta\, mV_o} \qquad (119)$$

**Critical Damping Ratio**

$$\zeta = \frac{I_y \frac{L_\alpha}{mV_o} - M_q}{2\sqrt{I_y(-M_\alpha - M_q \frac{L_\alpha}{mV_o})}} \qquad (120)$$

**Undamped Natural Frequency**

$$\omega_o = \sqrt{\frac{-M_\alpha - M_q \frac{L_\alpha}{mV_o}}{I_y}} \qquad (121)$$

Estimates of the stability derivatives for steady level flight at 150 knots are

$L_\alpha$ = 76,000 lb/rad
$L_\delta$ = -1,500 lb/inch
$M_\alpha$ = -112,000 ft-lb/rad
$M_q$ = -15,600 ft-lb-sec/rad
$M_\delta$ = -1,300 ft-lb/inch
$I_y$ = 11,000 slug-ft$^2$
$mV_o$ = 47,000 lb-sec

The resulting response parameters are

$K$ = -6.78 deg/sec$^2$ per inch
$\frac{1}{T}$ = 4.37 sec$^{-1}$
$\zeta$ = 0.430
$\omega_o$ = 3.52 rad/sec

The longitudinal control inputs and pitch angle responses for Test 414, Blips 1 and 2 (Figures 204 and 71), have been utilized for the correlation of dynamic characteristics. In these tests the control inputs were (for convenience) represented by single impulse inputs initiated at zero time. They are -1 inch-second for Blip 1 (Figure 204) and -2 inch-seconds for Blip 2 (Figure 71). The actual pulse durations are fairly long compared to the system response period of 2.0 seconds. For this reason, an alternate input representation for Test 414, Blip 2, has also been considered. In this case two successive steps are used; a -1.5-inch step at t = 0 in combination with a 2.0-inch step initiated at t = 1 second.

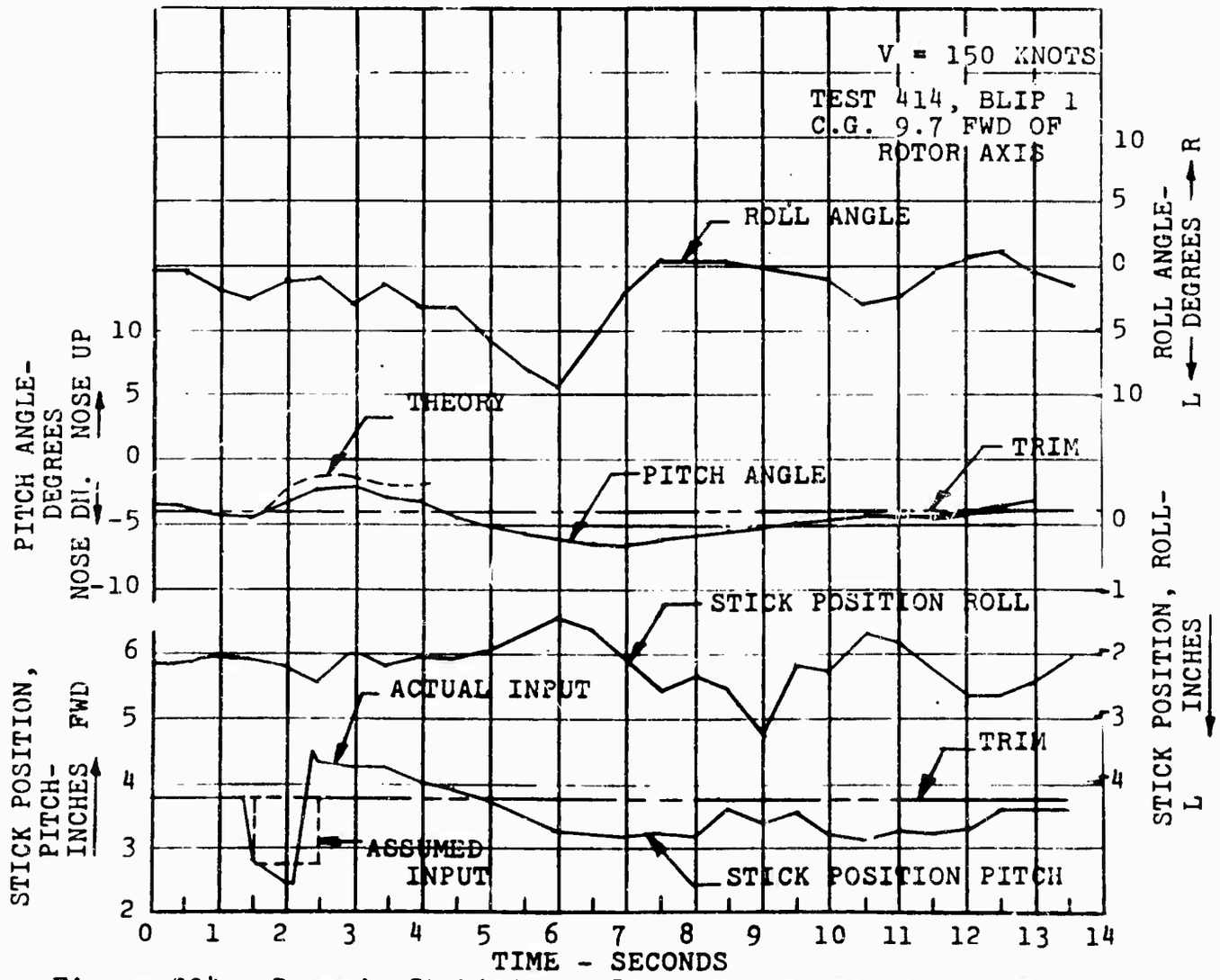


Figure 204. Dynamic Stability - Pitch Up, Speed 150 Knots, C.G. 9.7.

Considering a unit impulse input (1 inch-second), the Laplace transform of the pitch response equation, in degree units, is

$$\theta(s) = \frac{-6.78\,(s+4.37)}{s[s^2+2(0.430)(3.52)s+(3.52)^2]} \qquad (122)$$

and the inverse or time solution is

$$\theta = -2.38 + 2.58\, e^{-1.52t} \sin(3.18t+1.97) \qquad (123)$$

For a unit step function, the response equation is

$$\theta(s) = \frac{-6.78(s+4.37)}{s^2[s^2+2(0.430)(3.52)s+(3.52)^2]} \qquad (124)$$

and the corresponding time solution is

$$\theta = 0.04 - 2.38\,t - 0.74e^{-1.52t} \sin\,(3.18\,t + 3.08)$$

These solutions have been applied with the inputs described previously. They are compared to the recorded responses in Figures 204 and 71. It is seen that for the impulse-input, comparisons are satisfactory for approximately the first 3 seconds, particularly considering the corrective stick motion present in each blip, but the first portions of the pitch rates are overestimated. This is an expected result because of the pulse durations mentioned. An examination of the combination-step comparison for Test 414, Blip 2 (Figure 71), shows good correlation for the first portion of the pitch angle trace but includes an unexplainable delay in the recorded pitch angle peak of about 1 second. The overall analysis indicates that if the precise stick motion were generated as an input to the theoretical system model, the correlation accuracy would be within 1 degree throughout.

## Lateral Dynamics

A theoretical analysis of the pure lateral dynamic response similar to that for the 50-knot case has been made for the 150-knot tests. In these runs the stick was pulsed laterally in alternate directions but the attendant roll angle excursions were not rapidly attenuated, as in the 50-knot case. This occurred as a result of excitation of the Dutch roll mode which is essentially nonexistent at speeds near hover. Consequently, the consideration of the

lateral-directional system as a pure lateral one, that is, responding only in roll, applies only to the first half cycle or before sideslip and yaw rate buildup. Although this procedure does not allow verification of dihedral effect or the pure directional characteristics, it does permit evaluation of the lateral control power and damping.

The single-degree-of-freedom roll equation of motion is

$$(I_x D^2 - L_p D)\ \phi = L_\delta\ \delta(t) \tag{125}$$

where $\delta(t)$ is the lateral stick displacement from trim time function, and the remaining quantities are as defined in the nomenclature section.

Solving this equation for the roll angle yields

$$\phi = \frac{K\ \delta(t)}{D(D+\frac{1}{T})} \tag{126}$$

where

$$K = \frac{L_\delta}{I_x} \tag{127}$$

and

$$\frac{1}{T} = \frac{L_p}{I_x} \tag{128}$$

The estimates of the lateral parameters at a flight speed of 150 knots are

$$I_x = 1{,}600 \text{ slug-ft}^2$$
$$L_p = -3{,}720 \text{ ft-lb-sec/rad}$$
$$L_\delta = 1{,}000 \text{ ft-lb per inch}$$

resulting in a lateral control gain and inverse time constant of

$$K = 35.8 \text{ deg/sec}^2 \text{ per inch}$$
$$\frac{1}{T} = 2.33 \text{ sec}^{-1}$$

Considering a unit impulse input of 1 inch-second, the Laplace variable response equation is

$$\phi(s) = \frac{35.8}{s(s+2.33)} \tag{129}$$

and its inverse is

$$\phi = 15.4(1-e^{-2.33t}) \qquad (130)$$

Two lateral test responses were studied. They are Test 414, Blips 3 and 4 (Figures 98 and 99), in which the former is adequately represented by a -0.9 inch-second impulse at zero time and a corrective impulse of 1.7 inch-second taking place at 0.75 second, and the latter input is a 1.1 inch-second impulse at zero time followed by a corrective impulse of -1.1 inch-second applied at 0.5 second. The total response due to both inputs was calculated for each case using the above solution and superimposing the individual responses weighted by their respective impulse magnitudes.

These responses are shown in the plots of the measured roll responses. It is seen that the correlation is quite satisfactory for the initial roll responses.

The verified control power and damping levels indicate a steady-state roll rate of 15.4 degrees per second per inch of stick motion. In addition the corresponding helix angle or $\frac{pb}{2V}$ value for full control is 0.080, which is a favorable maneuverability level. With regard to response time, the steady state is reached, essentially, in 3 time constants or in

$$3T = \frac{3}{2.33} = 1.3 \text{ seconds} \qquad (131)$$

which is a sufficiently rapid response.

Unclassified
Security Classification

## DOCUMENT CONTROL DATA - R & D

*(Security classification of title, body of abstract and indexing annotation must be entered when the overall report is classified)*

| | |
|---|---|
| 1. ORIGINATING ACTIVITY (Corporate author)<br>Piasecki Aircraft Corporation<br>Philadelphia, Pennsylvania | 2a. REPORT SECURITY CLASSIFICATION<br>Unclassified<br>2b. GROUP |

3. REPORT TITLE

16H-1A Flight Test Research Program

4. DESCRIPTIVE NOTES (Type of report and inclusive dates)

Final Report

5. AUTHOR(S) (First name, middle initial, last name)

J. H. Goldberg
D. N. Meyers
L. V. Tompkins

| | | |
|---|---|---|
| 6. REPORT DATE<br>August 1968 | 7a. TOTAL NO. OF PAGES<br>398 | 7b. NO. OF REFS<br>10 |
| 8a. CONTRACT OR GRANT NO.<br>DA 44-177-AMC-154(T)<br>b. PROJECT NO<br>Task 1F162203A14311<br>c.<br>d. | 9a. ORIGINATOR'S REPORT NUMBER(S)<br>USAAVLABS Technical Report 67-58<br>9b. OTHER REPORT NO(S) (Any other numbers that may be assigned this report) | |

10. DISTRIBUTION STATEMENT

This document has been approved for public release and sale; its distribution is unlimited.

| | |
|---|---|
| 11. SUPPLEMENTARY NOTES | 12. SPONSORING MILITARY ACTIVITY<br>U. S. Army Aviation Materiel Laboratories<br>Fort Eustis, Virginia |

13. ABSTRACT

This report presents the results of a flight test program conducted by the Piasecki Aircraft Corporation on the Piasecki Model 16H-1A shaft-driven compound helicopter. The main components of the Model 16H-1A aircraft included: an H-21 articulated rotor, a wing with controllable flaperons and a shrouded pusher propeller. The aircraft was powered by a single T58-8 turbine engine. Aircraft performance, flying qualities, vibration and lift distibution between main rotor and wing were investigated over a level flight speed range of 0 to 167 knots and dive speeds up to 195 knots.

DD FORM 1 NOV 68 1473 REPLACES DD FORM 1473, 1 JAN 64, WHICH IS OBSOLETE FOR ARMY USE.

Unclassified
Security Classification

Unclassified
Security Classification

| 14. KEY WORDS | LINK A | | LINK B | | LINK C | |
|---|---|---|---|---|---|---|
| | ROLE | WT | ROLE | WT | ROLE | WT |
| 16H-1A | | | | | | |
| Shaft-Driven Compound Helicopter | | | | | | |
| H-21 Articulated Rotor | | | | | | |
| Controllable Flaperons | | | | | | |
| Shrouded Pusher Propeller | | | | | | |
| Flight Test | | | | | | |

Unclassified
Security Classification